PUBLICATION I

Published online 11 February 2014 *Nucleic Acids Research, 2014, Vol. 42, No. 8* ***5151–5163***
doi:10.1093/nar/gku113

Characterization of HelD, an interacting partner of RNA polymerase from *Bacillus subtilis*

Jana Wiedermannová[1,2], Petra Sudzinová[1], Tomáš Kovaľ[3], Alžbeta Rabatinová[1], Hana Šanderová[1], Olga Ramaniuk[1], Šimon Rittich[1], Jan Dohnálek[3,4], Zhihui Fu[5], Petr Halada[6], Peter Lewis[5] and Libor Krásný[1,*]

[1]Laboratory of Molecular Genetics of Bacteria, Institute of Microbiology, Academy of Sciences of the Czech Republic, Prague 14220, Czech Republic, [2]Department of Genetics and Microbiology, Faculty of Science, Charles University in Prague, Prague 12843, Czech Republic, [3]Department of Structure Analysis of Biomacromolecules, Institute of Macromolecular Chemistry, Academy of Sciences of the Czech Republic, Prague 16206, Czech Republic, [4]Laboratory of Structure and Function of Biomolecules, Institute of Biotechnology, Academy of Sciences of the Czech Republic, Prague 14220, Czech Republic, [5]School of Environmental and Life Sciences, University of Newcastle, Callaghan, NSW 2308, Australia and [6]Laboratory of Molecular Structure Characterization, Institute of Microbiology, Academy of Sciences of the Czech Republic, Prague 14220, Czech Republic

Received June 18, 2013; Revised January 14, 2014; Accepted January 16, 2014

ABSTRACT

Bacterial RNA polymerase (RNAP) is an essential multisubunit protein complex required for gene expression. Here, we characterize YvgS (HelD) from *Bacillus subtilis*, a novel binding partner of RNAP. We show that HelD interacts with RNAP-core between the secondary channel of RNAP and the alpha subunits. Importantly, we demonstrate that HelD stimulates transcription in an ATP-dependent manner by enhancing transcriptional cycling and elongation. We demonstrate that the stimulatory effect of HelD can be amplified by a small subunit of RNAP, delta. *In vivo*, HelD is not essential but it is required for timely adaptations of the cell to changing environment. In summary, this study establishes HelD as a valid component of the bacterial transcription machinery.

INTRODUCTION

RNA polymerase (RNAP) in bacteria is the key enzyme responsible for transcription of DNA into RNA. The bacterial RNAP core consists of $\alpha_2\beta\beta'\omega$ subunits and it is capable of transcription elongation but not initiation. Binding of an appropriate sigma factor to RNAP core enables the holoenzyme to recognize promoter DNA and initiate transcription (1). Unlike in gram-negative bacteria, RNAP from *Bacillus subtilis* and other gram-positive bacteria contains an additional subunit, δ. δ affects both transcription initiation and RNAP recycling, the latter depending on the ability of RNAP to be efficiently released from nucleic acids after transcription termination (2,3).

Regulation of RNAP is a complex process involving other factors besides the bona fide subunits. These factors (e.g. Gre, Nus and Rho factors) interact with RNAP and affect its function under various conditions and in various ways (4–6). Understanding the function of these factors and identification of new factors interacting with RNAP is imperative for understanding transcription and gene expression regulation.

Recently, HelD (YvgS) was identified as a binding partner of *B. subtilis* RNAP (7) and is the main copurifying band in preparations of RNAP from this organism. It is a putative helicase, and based on sequence homology, belongs to the superfamily I of DNA and RNA helicases, most closely related to HelIV helicases from gram-positive bacteria. The best characterized helicases, belonging to the same superfamily but only distantly related to HelD or HelIV, are UvrD and Rep helicases from *Escherichia coli*, or PcrA helicase from *Geobacillus stearothermophilus*. These helicases unwind DNA duplexes in an ATP-dependent manner, inchworming along the nucleic acid (8). HelD is strongly expressed during the exponential phase of growth with a further increase in expression in stationary phase (9). However, the cellular role(s) of HelD are poorly understood; it has been implicated in DNA repair and homologous recombination (10) but it has neither been characterized biochemically nor has its role(s) in transcription been investigated.

*To whom correspondence should be addressed. Tel: +420 241 063 208; Fax: +420 241 722 257; Email: krasny@biomed.cas.cz

In this study, we set out to characterize the function of HelD in transcription. We confirmed that HelD interacts with RNAP, and we identified the form of RNAP with which it interacts, and the region of RNAP to which it binds. Importantly, we found a functional link between HelD and δ and showed that these two proteins act synergistically to stimulate transcription.

MATERIALS AND METHODS

Bacterial strains and plasmids

Strains and plasmids are listed in Table 1. Competent *E. coli* cells [DH5α used for cloning or BL21 (DE3) used for overproduction of proteins] were prepared according to Hanahan (11). Competent *B. subtilis* cells were prepared as described (12).

All polymerase chain reactions (PCRs) were performed using the Expand High Fidelity System (Roche). All constructs were verified by sequencing. Wild-type *helD* was amplified by PCR from the genomic DNA of *B. subtilis* MH5636 (forward primer: 5′-caccatgaatcagcaggataagg-3′, reverse primer: 5′-tcattcagcaatctgatataag-3′), and cloned into the expression vector pET151/D-TOPO (Invitrogen) allowing in-frame fusion of a His_6 tag at the N-terminus of HelD. The resulting plasmid was named pHelD-His6 (LK800, see Table 1).

Table 1. List of strains and plasmids

Strain/plasmid	Relevant characteristics[a]	Source
B. subtilis		
MH5636	*rpoC*-His10	(13)
MGNA-A456	*helD*::MLS	(14)
LK637	*rpoC-10His, rpoE::kan*	(15)
LK782	*rpoC-10His, helD::MLS*	This work
LK1032	*rpoC-10His, rpoE::kan, helD::MLS*	This work
LK1401	*amyE::helD*-His6, *spc*	This work
BSB1	wt BaSysBio	(9)
E. coli		
LK22	BL21 pCD2/Bsu_*sigA*	(16)
RLG770	pRLG770	(17)
LK1	pRLG770 with P*veg* (−38/+1,+1G)	(18)
LK1109	pRLG770 with P*helD*	This work
LK888	pRLG770 with P*glpD*	This work
RLG7023	BL21/pFL31/*Bsu_rpoE*	(3)
LK800	BL21/pHelD-His6	This work
LK1413	pSG1721-HelD-His6	This work
pET151	pET151/D-TOPO	Invitrogen
pNG213	pETMCSIII/*His6-rpoA*	(6)
pNG490	pETMCSIII/*His6-rpoB*$_{1-608}$	(6)
pNG479	pETMCSIII/*His6-rpoB*$_{400-760}$	(6)
pNG480	pETMCSIII/*His6-rpoB*$_{750-1040}$	(6)
pNG481	pETMCSIII/*His6-rpoB*$_{950-1193}$	(6)
pNG482	pETMCSIII/*His6-rpoC*$_{1-433}$	(6)
pNG483	pETMCSIII/*His6-rpoC*$_{253-610}$	(6)
pNG484	pETMCSIII/*His6-rpoC*$_{600-915}$	(6)
pNG485	pETMCSIII/*His6-rpoC*$_{800-1199}$	(6)
pNG492	pETMCSIII/*His6-yloH* (ω_2)	(6)
pNG579	pETMCSIII/*His6-ykzG* (ω_1)	(6)
pNG613	pETMCSIII/*His6-rpoB*$_{750-846,\ 875-1040}$	(6)

[a]MLS, macrolide-lincosamide-streptogramin B resistance; kan, kanamycin; spc, spectinomycin.

The *B. subtilis helD*-null knockout strain (LK782) was prepared by transformation of *B. subtilis* strain MH5636 containing a His_{10}-tagged β' subunit (13) with chromosomal DNA from MGNA-A456, kindly provided by the National BioResource Project (Japan). A double knockout strain LK1032 (for *helD* and *rpoE* encoding the δ subunit of RNAP) was obtained by transformation of strain LK637 (15) with MGNA-A456 chromosomal DNA.

Supercoiled plasmids and linear DNA for *in vitro* transcription assays were obtained using the Wizard Midiprep Purification System (Promega) and subsequently phenol-chloroform extracted, precipitated with ethanol, and dissolved in water. The plasmids used in *in vitro* transcriptions contained promoter fragments cloned into p770 (17). Transcription terminated at a Rho-independent terminator. Linear DNA templates were prepared by PCR from the plasmid containing P*veg* (LK1). All linear templates started at −118 relative to the transcription start site. The template containing the Rho-independent terminator (at +145) ended at +255. The template without the Rho-independent terminator ended at +111. The template with the short transcribed region (Figure 6D) ended at +20.

For *in vitro* transcription assays, pRLG770 with P*veg* (−38/−1,+1G) was used (18) unless stated otherwise.

Media and growth conditions

For plasmid and protein purifications, appropriate strains were grown in Luria-Bertani (LB) medium at 37°C. For *in vivo* experiments, the cells were grown in defined 3-(N-morpholino)propanesulfonate (MOPS) - buffered medium (18) supplemented with 0.4% glucose and all 20 amino acids at 25 μg/ml.

Purification of proteins

Bacillus subtilis RNAP with a His_{10}-tagged β' subunit or His_6-HelD was purified from the strain LK782 (strain without *helD*), LK1032 (strain without *helD* and *rpoE*) or LK1401 (strain with HelD-His6). The purifications were performed as described (13). Induction of HelD-His6 in strain LK1401 was carried out at $OD_{600} = 0.5$ with 0.08% xylose for 2 h.

Plasmid pHelD-His6 was transformed into *E. coli* BL21 (DE3) and the production of HelD-His_6 induced following the addition of 1 mM IPTG for 2 h at room temperature. Cells were harvested and protein was purified by affinity chromatography as described for RNAP.

The σ^A subunit of RNAP was overproduced from the pCD2 plasmid (16) and purified as described (2).

The δ protein was purified from RLG7023 as described (3). Proteins were dialyzed against storage buffer containing 50 mM Tris–Cl, pH 8.0, 100 mM NaCl, 50% glycerol, 3 mM 2-mercaptoethanol and stored at −20° C. Proteins were visualized on NuPAGE 4-12% Bis-Tris gels (Invitrogen) with Novex Sharp Pre-Stained Protein Standard as a marker.

Determination of experimental pI

The experimental pI of HelD was determined by isoelectric focusing (IEF) using precast 5% polyacrylamide

Vertical Novex® IEF Mini Gels pH 3–10 and XCell SureLock™ mini-cell electrophoresis system (Life Technologies Corp.). IEF was performed according to the manufacturer's instructions.

Western blotting

Proteins were analyzed by sodium dodecyl sulphate-polyacrylamide gel electrophoresis (SDS-PAGE) and Coomassie blue staining (SimplyBlue, Invitrogen) and detected by Western blotting using mouse monoclonal antibodies to σ^{70} [2G10] or to the β subunit of RNAP [8RB13] (both from Santa Cruz) and secondary antibodies conjugated with horseradish peroxidase. Signal was created using SuperSignal West Femto Chemiluminiscent Substrate (Thermo Scientific) and exposing blots to photographic film.

Far western blotting

Purified proteins were biotinylated using the EZ-Link sulfo-NHS-biotinylation system (Thermo Scientific). Far western blots were performed as detailed by Yang *et al.* (6), except protein–protein interactions were detected using Horseradish peroxidase-conjugated streptavidin and the Opti4CN system (BioRad). Binding affinity to RNAP fragments was determined from digitized scans of blots using ImageJ (NIH) where maximal binding (100%) was set as the intensity of the signal of HelD bound to the $\beta'_{600–915}$ fragment. HelD binding sites on RNAP were mapped onto the *B. subtilis* RNAP homology model (19) and visualized using PyMol (Schrödinger).

Native PAGE assays

Five picomoles of RNAP and 25 pmol of HelD, T4 DNA ligase (TaKaRa) or MLV reverse transcriptase (Promega), respectively, were used. Proteins tested for mutual interactions were incubated for 15 min at 30°C in 10 µl in the storage buffer. After incubation samples were mixed with 3 µl of Native PAGE 4× Sample buffer (Invitrogen) and loaded onto the Native PAGE 4-16% Bis-Tris Gel (Invitrogen) and electrophoresed. The gels were subsequently Coomassie stained.

Enzymatic digestion for mass spectrometry

Coomassie blue-stained protein bands were excised from the gel, cut into small pieces and destained using 50 mM 4-ethylmorpholine acetate (pH 8.1) in 50% acetonitrile (MeCN). The proteins were further reduced with 30 mM tris(2-carboxyethyl)phosphine (TCEP) in 100 mM Tris–HCl (pH 8.0) at 65°C for 30 min and alkylated with 30 mM iodacetamide in 100 mM Tris–HCl (pH 8.0) for 60 min in the dark. The gel was washed with water, shrunk by dehydration in MeCN and re-swelled again in water. The supernatant was removed and the gel was partly dried in a SpeedVac concentrator. The gel pieces were then incubated overnight at 37°C in cleavage buffer containing 25 mM 4-ethylmorpholine acetate, 5% MeCN and trypsin (100 ng; Promega). The resulting peptides were extracted into 40% MeCN/0.3% trifluoroacetic acid (TFA). An aqueous 50% MeCN/0.1% TFA solution of α-cyano-4-hydroxycinnamic acid (5 mg/ml; Sigma) was used as a MALDI matrix. One microliter of the peptide mixture was deposited on the MALDI plate, allowed to air-dry at room temperature and overlaid with 0.4 µl of the matrix.

MALDI mass spectrometry and protein identification

Mass spectra were measured on an Ultraflex III MALDI-TOF instrument (Bruker Daltonics, Bremen, Germany) in the mass range of 700–4000 Da and calibrated internally using the monoisotopic $[M+H]^+$ ions of trypsin autoproteolytic fragments (842.5 and 2211.1 Da). The peak lists created using flexAnalysis 3.3 were searched using an in-house MASCOT search engine against the SwissProt 2013_09 database subset of *B. subtilis* proteins with the following search settings: peptide tolerance of 30 ppm, missed cleavage site value set to one, variable carbamidomethylation of cysteine, oxidation of methionine and protein N-term acetylation. Proteins with MOWSE scores over the threshold value of 56 calculated for the used settings were considered as being positively identified. If the score was lower or only slightly higher than the threshold value, the identity of protein candidate was confirmed by tandem mass spectrometry analysis.

ATPase activity

ATPase activity was measured by the hydrolysis of inorganic phosphate from [γ-^{32}P] ATP. The reaction mixture in 110 µl of 50 mM Tris–Cl, pH 8; 5 mM $MgCl_2$, 1 M KCl contained 550 pmol HelD or 550 pmol bovine serum albumin (BSA) or 275 pmol *Bacillus stearothermophilus* EF-Tu G-domain and 3450 pmol [γ-^{32}P] ATP (specific activity 1800 cpm/pmol). The reaction was performed at 30°C and followed kinetically for 90 min at 30°C. Aliquots of 20 µl were withdrawn at appropriate time intervals (0, 30, 60 and 90 min) and liberated Pi determined by the charcoal method (20). Five microliter of the product was spotted on Whatman 3MM filter paper, dried and scanned using a Molecular Imager_FX (Bio-Rad). The amounts were quantified with QuantityOne software (Bio-Rad). Blank samples were run simultaneously to determine background values of ATP hydrolysis. The experiments were repeated three times. The amounts of hydrolyzed ATP were calculated and plotted as the function of time.

In vitro transcription assays

Initiation competent enzyme was reconstituted using RNAP isolated from LK782 or LK1032 with a saturating concentration of σ^A in storage buffer (50 mM Tris–HCl, pH 8.0, 0.1 M NaCl, 50% glycerol) for 15 min at 30°C.

Multiple round transcription assays were carried out essentially as described by (13,18) unless stated otherwise. Briefly, reactions were carried out in 10 µl: 30 nM holoenzyme (RNAPσ^A), 2.5 nM supercoiled or 50 nM linear DNA template unless stated otherwise, transcription buffer (40 mM Tris–HCl, pH 8.0, 10 mM $MgCl_2$, 0.1 mg/ml BSA and 1 mM dithiothreitol (DTT)), 150 mM KCl

and NTPs (ATP, CTP and GTP were 200 μM; UTP was 10 μM plus 2 μM of radiolabeled [α-^{32}P]-UTP).

RNAP was reconstituted with HelD at a 1:4 ratio unless stated otherwise. The RNAP:δ ratio used in experiments where δ was added was 1:4 (saturating concentration). Reconstitution experiments were carried out in storage buffer for 15 min at 30°C. When denatured HelD was used, native HelD protein was denatured at 90°C for 5 min.

All transcription reactions were allowed to proceed for 15 min at 30°C (unless stated otherwise) and stopped with equal volumes of formamide stop solution (95% formamide, 20 mM EDTA, pH 8.0). Transcription assays on 20 nt linear templates were allowed to proceed for 30 min.

In single round transcription assays, and in the multiple round assays (Figure 6), RNAP was preincubated with plasmid DNA and HelD and δ were subsequently added and incubated for 10 min at 30°C. Reactions were carried out in transcription buffer supplemented with 150 mM KCl and started by the addition of NTPs (concentration of NTPs was the same as in multiple round *in vitro* transcription assays) together with 600 nM double-stranded DNA (dsDNA) competitor. The competitor dsDNA with a full-consensus promoter sequence (21) was used to sequester free RNAP and allow only one round of *in vitro* transcription (22). Stock dsDNA competitor was prepared by annealing equimolar amounts of complementary primers (LK 923: 5′-ccggaattcaaatatttgttgttaactcttgacaaaagtgttaaattgtgctatactgtattggttctcaagcttccg-3′ and LK 924: 5′-cggaagcttgagaaccaatacagtatagcacaatttaacacttttgtcaagagttaacaacaaatatttgaattccgg-3′) in 10 mM Tris–HCl, pH 8.0, 1 mM EDTA, 50 mM NaCl, which were denatured at 95°C for 5 min and then cooled down to 30°C (1°C per min). In negative controls, whole reaction mix with plasmid DNA and competitor dsDNA was started with RNAP to ensure that all RNAPs were sequestered by the dsDNA competitor.

In vitro transcription restart assays (Figure 5E and F) were carried out in two steps. The first 15-min step was basically the same as described above for multiple round reactions; KCl was used at 100 mM concentration. At the beginning of step II, the main compounds (water, NTPs, template DNA, δ, HelD, both δ and HelD, RNAP) were added to respective reactions in the same amounts as they were at the beginning of step I. Reactions were then allowed to proceed for another 15 min and were stopped with 10 μl of stop solution. In experiments with two templates (Figure 6A), 10 nM final concentrations of the plasmids were used.

Samples were loaded onto 7 M Urea 7% polyacrylamide gels and electrophoresed. The dried gels were scanned with a Molecular Imager_FX (BioRad). The amount of transcript (originating from the cloned promoters) was quantified with QuantityOne software (BioRad). All calculations and data fitting were carried out using SigmaPlot (Jandel Scientific).

In vivo experiments: outgrowth from the lag phase

Wild type *B. subtilis*, δ and HelD knockout, and the double knockout strains (MH5636, LK637, LK782 and LK1032, respectively) were cultivated in LB medium for 24 h at 37°C under continuous shaking to ensure entry into stationary phase and then diluted into fresh LB medium to OD_{600} = 0.03. OD_{600} was measured during outgrowth to compare the duration of the lag phase of the respective strains.

Protein sequence and domain analysis

Protein sequence searches were performed with the BLAST protein–protein service (23,24). Sequence alignments were carried out with Clustalx, using the Gonnet 250 weight matrix (25).

RESULTS

HelD copurifies with RNAP

In our preparations of *B. subtilis* RNAP by affinity chromatography, we regularly observed a major contaminating band of ~90 kDa (Figure 1A). This band did not appear in control experiments where the lysate made from *B. subtilis* cells containing no His-tagged protein was incubated with the affinity matrix, indicating that the protein does not have an intrinsic ability to bind the matrix (Figure 2A). This protein could not be removed by gel filtration and its level in the preparation decreased only after ion exchange chromatography [(26) and data

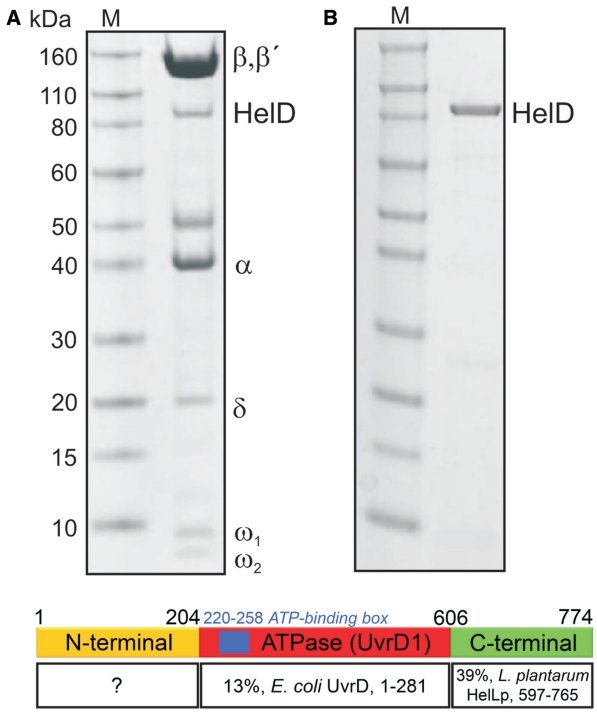

Figure 1. HelD copurifies with RNAP. (**A**) RNAP purified by Ni-affinity chromatography via the 10× N-terminal histidines on the β' subunit. Subunits of RNAP and the band corresponding to HelD are indicated. (**B**) HelD purified by Ni-affinity chromatography via the 6× N-terminal histidines. The apparent molecular weights are shown by Novex Sharp Pre-Stained Protein Standard, M. Panel C, Putative domain structure of *B. subtilis* HelD. Amino acid identity with respective protein fragments is indicated. The percent values show the level of sequence identity to the marked protein segment.

not shown]. This band was identified by MALDI mass spectrometry as the HelD protein, which was recently reported as a binding partner of RNAP (7).

The HelD protein is encoded by the *yvgS* (*helD*) gene and consists of 774 amino acids (aa). Based on its aa sequence, HelD is a putative UvrD-like helicase. Helicase from *Lactobacillus plantarum* HelLp, with a sequence identity of 39%, is the closest related protein for which any 3D structure (C-terminal domain, PDB ID 3DMN, unpublished) is available. The closest structurally related helicase of this class, UvrD from *E. coli*, for which the complete 3D structure has been determined (27), shows only 12% sequence identity with HelD. Based on domain arrangement of HelLp and UvrD and sequence comparisons of these two proteins with HelD, it is postulated that HelD comprises three domains (Figure 1C). The first, N-terminal domain (residues 1–204) may be involved in DNA binding. The second domain (205–606) contains the ATP-binding box and is related to the ATPase domain of UvrD helicase (residues 1–281 in UvrD, domain marked as UvrD1). The C-terminal domain (607–774) is related to the domain of UvrD helicase involved in DNA unwinding and shares significant similarity with the C-terminal domain of HelLp. However, in the case of UvrD this domain is formed by two distant parts of the protein chain, whereas the HelLp C-domain is formed by a single section of the protein chain. In summary, HelD is a unique protein only part of which resembles proteins characterized to date.

For further studies, we prepared recombinant HelD. The recombinant protein was purified by nickel affinity chromatography via the introduced N-terminal 6xHis tag (Figure 1B) and the experimentally determined pI of the protein under native conditions was ~7.1 (theoretical pI = 6.1). HelD was able to bind DNA (Supplementary Figure S1), and as it was predicted to be a helicase, we attempted to detect this activity in strand displacement assays. Using an array of DNA templates [5′ or 3′ overhangs, forked DNA or blunt-ended DNA; (28)] we detected no strand-displacement activity for this protein (data not shown).

Interaction of HelD with RNAP

To confirm that HelD binds to RNAP and to establish to which form (core or holoenzyme), we performed *in vivo* and *in vitro* experiments. *In vivo*, we overproduced C-terminally His-tagged HelD in *B. subtilis* cells (strain LK1401) and subsequently purified it via the His-tag. In parallel, we purified RNAP that was His-tagged at β' (MH5636) and we also performed a control purification from a strain without any His-tagged protein (BSB1). Figure 2A shows that RNAP core subunits copurified with the His-tagged HelD, and that RNAP is the main interacting partner of this protein. Western blot analysis (Figure 2B) showed that HelD interacts predominantly with the core form of RNAP as virtually no σ^A was detected.

To verify that purified HelD binds to RNAP *in vitro* we performed gel-shift experiments under native conditions in nondenaturing PAGE gels. Figure 2C lane 1 shows that HelD forms oligomers in solution as also seen by size exclusion chromatography (Supplementary Figure S2). The addition of HelD to RNAP resulted in reduced migration of RNAP, suggesting binding of HelD to

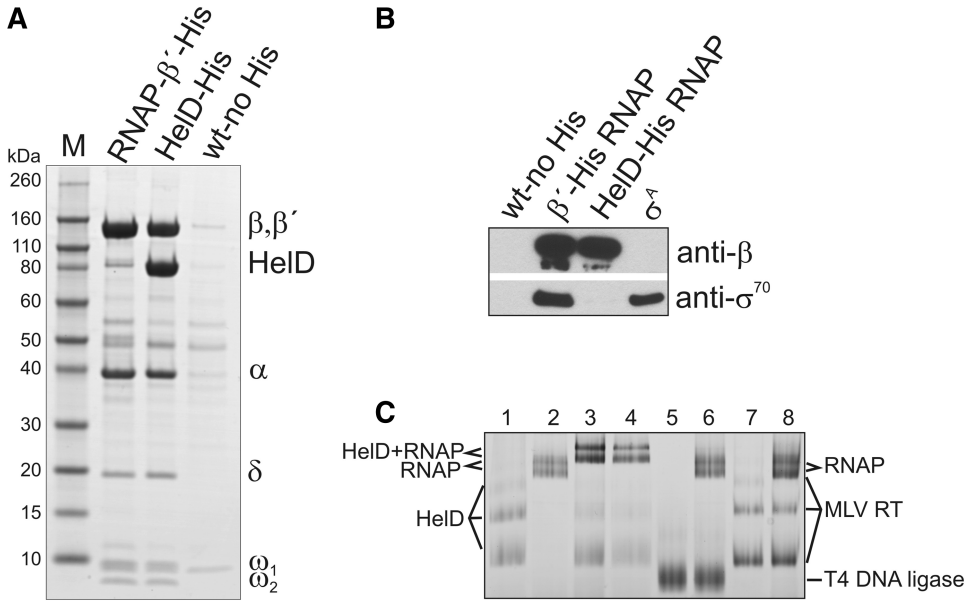

Figure 2. HelD interacts with RNAP core. (**A**) Coomassie stained gel of proteins purified by nickel affinity chromoatography. Lane 1—proteins purified from strain MH5636 containing His-tagged β' subunit of RNAP; Lane 2—proteins purified from strain LK1401 containing His-tagged HelD; Lane 3—proteins purified from strain (BSB1) without any His-tagged protein. (**B**) Western blot of the gel from (A). The antibodies used are indicated. In the last lane purified σ^A was used as a marker. (**C**) Band shift assay on native PAGE gel. RNAP was incubated with potential interacting partners: HelD, T4 DNA ligase (68 kDa), MLV reverse transcriptase (71 kDa). Samples were separated on 4–16% gradient native PAGE Bis–Tris gels. Lane 1—HelD, lane 2—RNAP, lane 3—HelD with RNAP, lane 4—DNaseI-treated HelD + DNaseI-treated RNAP, lane 5—T4 DNA ligase, lane 6—RNAP with T4 DNA ligase, lane 7—MLV reverse transcriptase, 6—RNAP with MLV reverse transcriptase. In all experiments, RNAP was prepared from the Δ*helD* strain (LK782).

RNAP (Figure 2C, lane 3). To confirm results from the gel-shift experiment, we excised the two bands predicted to be RNAP from lane 2 and lane 3 and determined the protein identity by mass spectrometry. The analysis confirmed the presence of the β, β' and α subunits as well as HelD in the bands in lane 3. It is not clear why RNAP and RNAP-HelD complexes ran as two bands on the gel (Figure 2C, lanes 2 and 3), but they appeared identical by mass spectrometry analysis, and we speculate that they may represent two conformational states of RNAP, both capable of HelD binding. We also verified by mass spectrometry that the bands in lane 1 consist of HelD (probably in different oligomeric states). As an additional control to exclude the possibility that HelD binds to RNAP via traces of DNA remaining in complex with the proteins, DNaseI was added to the RNAP and HelD preparations before the experiment and we obtained the same result (Figure 2C, lane 4). As specificity controls, we used T4 ligase and murine reverse transcriptase and neither of these proteins bound to RNAP (Figure 2C, lanes 5–8).

We conclude that HelD interacts with RNAP core *in vivo* and that purified HelD interacts directly with RNAP *in vitro*.

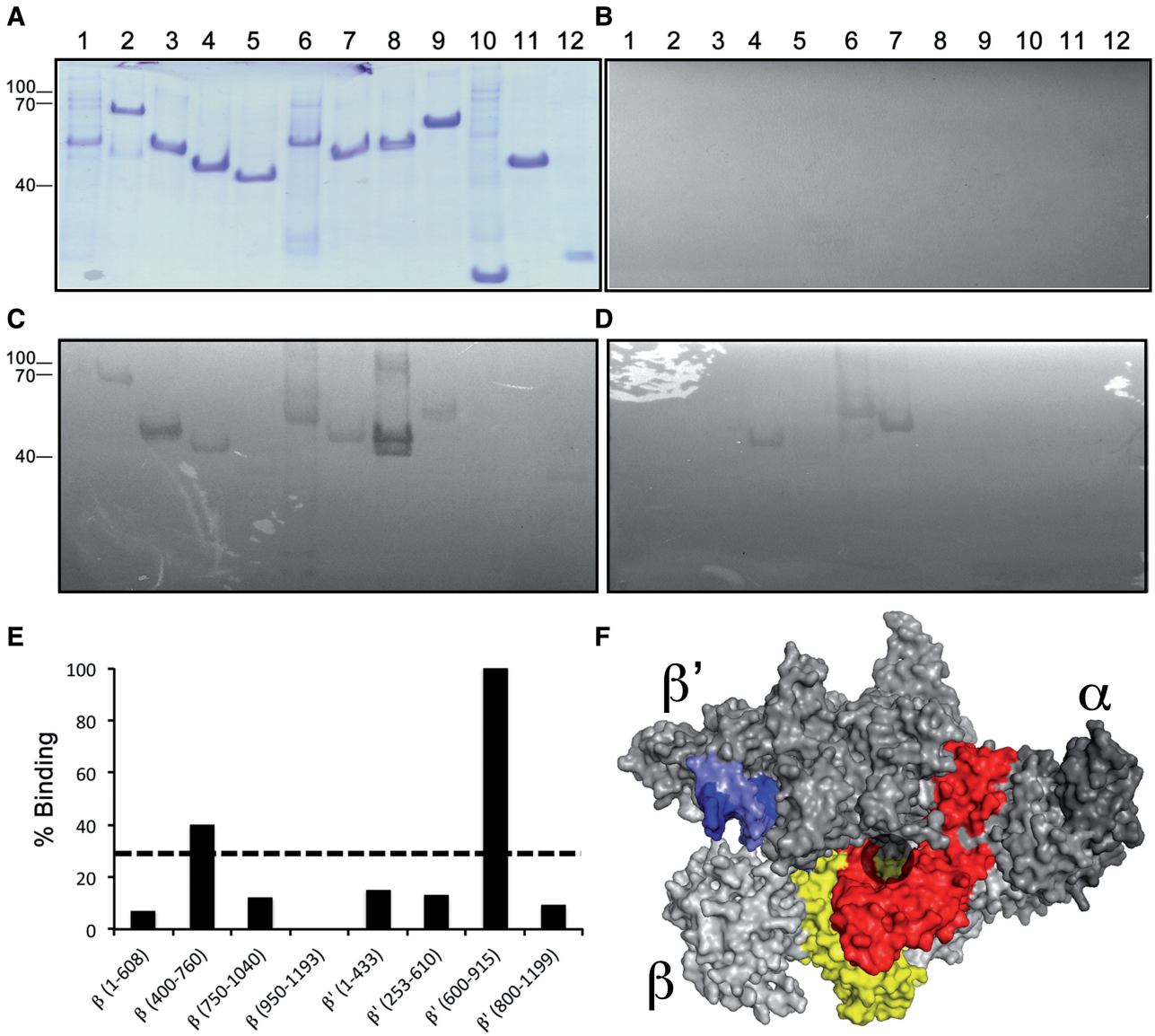

Figure 3. HelD binds on the downstream side of RNAP. (**A**) Coomassie blue stain of RNAP subunits and fragments showing approximate equal loading in all lanes. (**B**) Negative control blot containing all components except biotinylated ligand. (**C**) Blot performed using biotinylated HelD. (**D**) Control blot using biotinylated σ^A. Molecular weights (kDa) are shown down the left hand side. Lane 1—α; lane 2—β_{1-606}; lane 3—$\beta_{400-760}$; lane 4—$\beta_{750-1040}$; lane 5—$\beta_{950-1193}$; lane 6—β'_{1-433}; lane 7—$\beta'_{253-610}$; lane 8—$\beta'_{600-915}$; lane 9—$\beta'_{800-1199}$; lane 10—ω_2; lane 11—$\beta_{750-1040}$ Δflap; lane 12—ω_1. (**E**) Quantification of binding signal of HelD to β and β' fragments normalized to the strongest binding fragment, $\beta'_{600-915}$ (set at 100%). Dotted line represents 30%. (**F**) Surface rendered model of *B. subtilis* RNAP with the strongest HelD binding fragments labeled in yellow ($\beta_{400-760}$) and red ($\beta'_{600-915}$). α Subunits are shown in dark gray, β subunit in light gray and β' subunit in medium gray. DNA is shown in blue; template strand in light blue and nontemplate strand in dark blue. The approximate location of the secondary channel is indicated by the transparent gray circle.

Localization of HelD on RNAP

Next, we addressed the topology of the binding of HelD to RNAP. We used far western blot analysis using fragments of subunits of *B. subtilis* RNAP probed with biotinylated HelD (Figure 3). Controls were performed with no protein (Figure 3B) and with biotinylated σ^A that bound to the N-terminus of the β' subunit as well as the fragment of the β subunit containing the β-flap tip (Figure 3D). These data are consistent with previous far western blot results using anti-σ^A antibodies (6) and structural data (29). When using HelD as a probe, signal was observed for most of the fragments of the β and β' subunits (Figure 3C), but as shown in Figure 3E and F, it bound most strongly to two fragments that form the rim of the secondary channel by which it is believed that NTPs enter the active site (gray circle, Figure 3F). Mapping of the fragments to which HelD bound weakly enabled us to identify portions that all triangulated to the surface of RNAP close to the secondary channel (not shown) consistent with HelD forming extensive contacts with RNAP on the downstream side in close proximity to DNA (light and dark blue, Figure 3F). Assuming HelD binds on the downstream side of RNAP it is unlikely there is significant steric hindrance preventing σ from being simultaneously bound.

HelD affects transcription *in vitro*

Because HelD directly interacts with RNAP, we wished to determine whether it was important for the DNA-dependent synthesis of RNA. Therefore, we performed a panel of *in vitro* transcription experiments with RNAP purified from a HelD knockout strain, and studied the effect of addition of HelD. As a model promoter, we used P*veg*, a strong constitutive promoter that is well characterized (18). From this promoter RNAP transcribes a 145 nt transcript and transcription is terminated at a Rho-independent terminator (17,30). In *in vitro* multiple round transcription assays HelD displayed a stimulatory effect on transcription (Figure 4A, black columns; Supplementary Figure S3). However, a large stoichiometric excess of HelD over RNAP abolished transcription, possibly by nonspecific binding of HelD to DNA, resulting in the formation of transcription roadblocks (31). Negative control experiments using heat-denatured HelD failed to produce any stimulatory effect on transcription activity (Figure 4A; gray columns). We also tested the effect of HelD with two other templates containing two other promoters, P*helD* and P*glpD* (32), and we obtained similar results to those obtained with P*veg* (Supplementary Figure S3AB). Moreover the effect of HelD on transcription was salt-concentration dependent, as increasing the amount of salt in the reaction rendered the effect more pronounced (Supplementary Figure S4).

We conclude that HelD in low stoichiometric excess over RNAP stimulates transcription.

The effect of HelD is ATP-dependent

As HelD contains an ATP binding motif, we investigated whether the effect of HelD on transcription depends on ATP. First, we tested whether HelD possesses an ATPase activity. While none of the two control proteins, the GTPase domain of *B. stearothermophilus* elongation factor Tu or BSA, was able to hydrolyze ATP, HelD displayed significant ATPase activity (Figure 4B and C). This effect was independent of the presence of RNAP (data not shown). Next, we performed transcription assays with increasing concentrations of ATP either in the presence or absence of HelD. As a control, we performed the same type of experiment with increasing concentrations of CTP. When ATP or CTP concentrations were increased (from 1 to 200 μM), the other NTP concentrations were kept constant (100 μM). Figure 4D and E shows that by increasing the concentration of ATP from 1 to 20 μM (where the effect plateaued) the level of transcription increased ~6-fold in the presence of HelD. When HelD was not present, this stimulation was absent. Furthermore, increasing the CTP concentration had no significant effect on transcription either in the presence or absence of HelD. The overall higher level of transcription in the presence of HelD when CTP concentration was being varied was due to the 100 μM ATP that was present in the reaction.

We conclude that HelD is an ATPase and the stimulatory effect of HelD on transcription is ATP-dependent.

HelD and *δ* have a synergistic stimulatory effect on transcription cycling

The next question was which part of the process of RNA synthesis is affected by HelD. Even though Figure 2B shows that HelD binds to core and not holoenzyme, we wanted to test whether it has any effects on steps important for transcription initiation—RNAP association with σ^A and promoter binding. Unsurprisingly, the presence or absence of HelD had no effect either on the affinity of σ^A for RNAP or the affinity of RNAP for promoter DNA (Supplementary Figure S5A and B).

However, another putative helicase, the RapA protein of *E. coli*, has been shown to associate with RNAP and stimulate transcription by promoting cycling of RNAP by enhancing the release of RNAP from nucleic acids after termination and also by stimulating the dissociation of RNA–DNA hybrids (30). HelD and RapA are not sequence homologs; RapA belongs to the Swi2 family of helicases, but we speculated that these two proteins may be functional analogs. As the δ subunit of RNAP was previously also shown to enhance cycling of RNAP, we included δ as a positive control. We used RNAP from a double knockout strain (δ-null HelD-null, LK1032) in *in vitro* transcription assays from a P*veg*-based supercoiled template. First, we tested the effects of HelD and δ separately and observed moderate stimulatory effects for each (2-fold increase) (Figure 5A and B; multiple rounds). Surprisingly, when we combined HelD and δ together, we detected a strong increase in RNA synthesis. The ~10-fold stimulation by HelD and δ together was more than the sum of the stimulatory effects of HelD and δ alone, suggesting a synergistic effect of these proteins.

Next, we decided to directly test whether the synergistic effect of HelD and δ is due to a more efficient cycling of transcription. If this was true, then limiting transcription

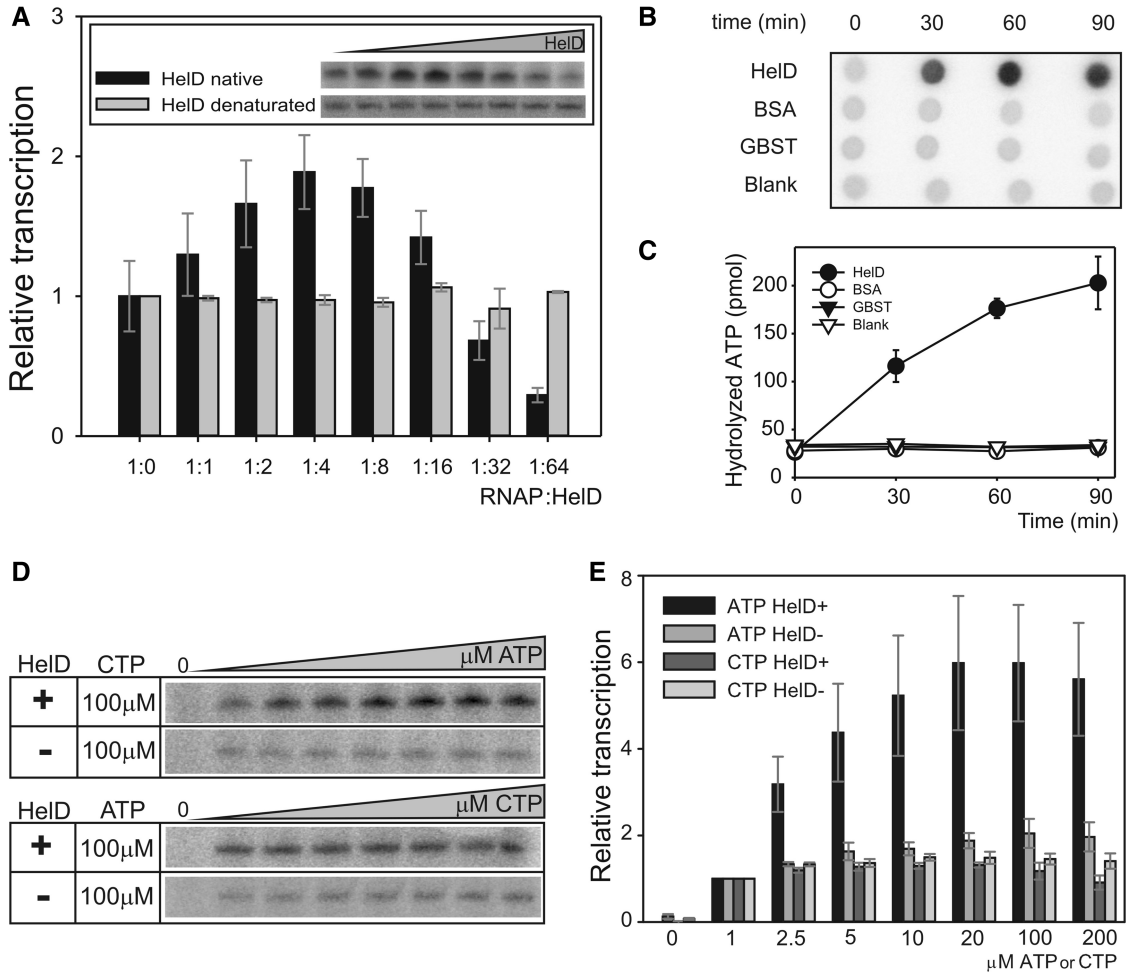

Figure 4. Effect of HelD on *in vitro* transcription. (**A**) RNAP (from HelD knockout strain LK782) was reconstituted with saturating concentrations of σ^A. Holoenzyme was incubated with increasing amounts (molar ratio from 1:0 to 1:64) of HelD (black bars) or heat denatured HelD (gray bars) and used to initiate transcription. Primary data are shown in the inserted box and show a representative experiment. The data were normalized to the 1:0 ratio set as 1. In this and the following experiments, the graphs represent data from three independent experiments ±SD. (**B**) HelD hydrolyzes ATP. Primary data show spots with hydrolyzed γ-^{32}P (for details see 'Materials and Methods' section). (**C**) Graph showing the quantification, with the symbol key presented in the graph. (**D**) The effect of HelD is ATP-dependent- representative primary data. RNAP from HelD knockout strain (LK 782) was tested in *in vitro* multiple round transcription assays in the presence/absence of HelD and increasing amounts of ATP (from 1 to 200 μM total ATP). As a control, CTP was varied. The concentration of CTP was 100 μM when [ATP] was varied and *vice versa*. (**E**) The effect of HelD is ATP-dependent quantification of the data normalized to transcription at 1 μM ATP or CTP. The color coding of the bars is defined in the graph.

to a single round should abolish the effect. As shown in Figure 5A and B, the pronounced stimulatory effect of these factors was cancelled, consistent with the stimulatory effect of HelD and δ being due to cycling of transcription.

To examine the cycling in more detail, we performed multiple round transcription experiments where we followed transcription in the presence/absence of δ, HelD or δ and HelD as a function of time. In the absence of HelD or δ, transcription stopped at about the 5-min time point. The addition of either protein modestly prolonged this time. The addition of both proteins then markedly increased the time with transcription still continuing at the final 25-min point (Figure 5C and D).

This experiment raised two principal questions: (i) Why does the cycling of transcription stop after 5 min in the absence of δ and HelD? and (ii) Why is the cycling more efficient with δ and HelD? We address these questions in the following two sections.

Transcription cycling stops because the template is not functional

There are three possibilities to explain why transcription stops after 5 min: first, depletion of NTPs prevents RNA synthesis; second, RNAP is in complex with RNA and/or DNA and inactive; third, the template DNA is not functional either because it is blocked by RNAP, or because it forms interactions with RNA [such as R-loops (33)].

To distinguish between these possibilities we allowed the *in vitro* transcription assays to proceed for 15 min without HelD and δ and then divided the mixture into several aliquots. Next, equal amounts of the main components (NTPs, template DNA, RNAP) were added as at the

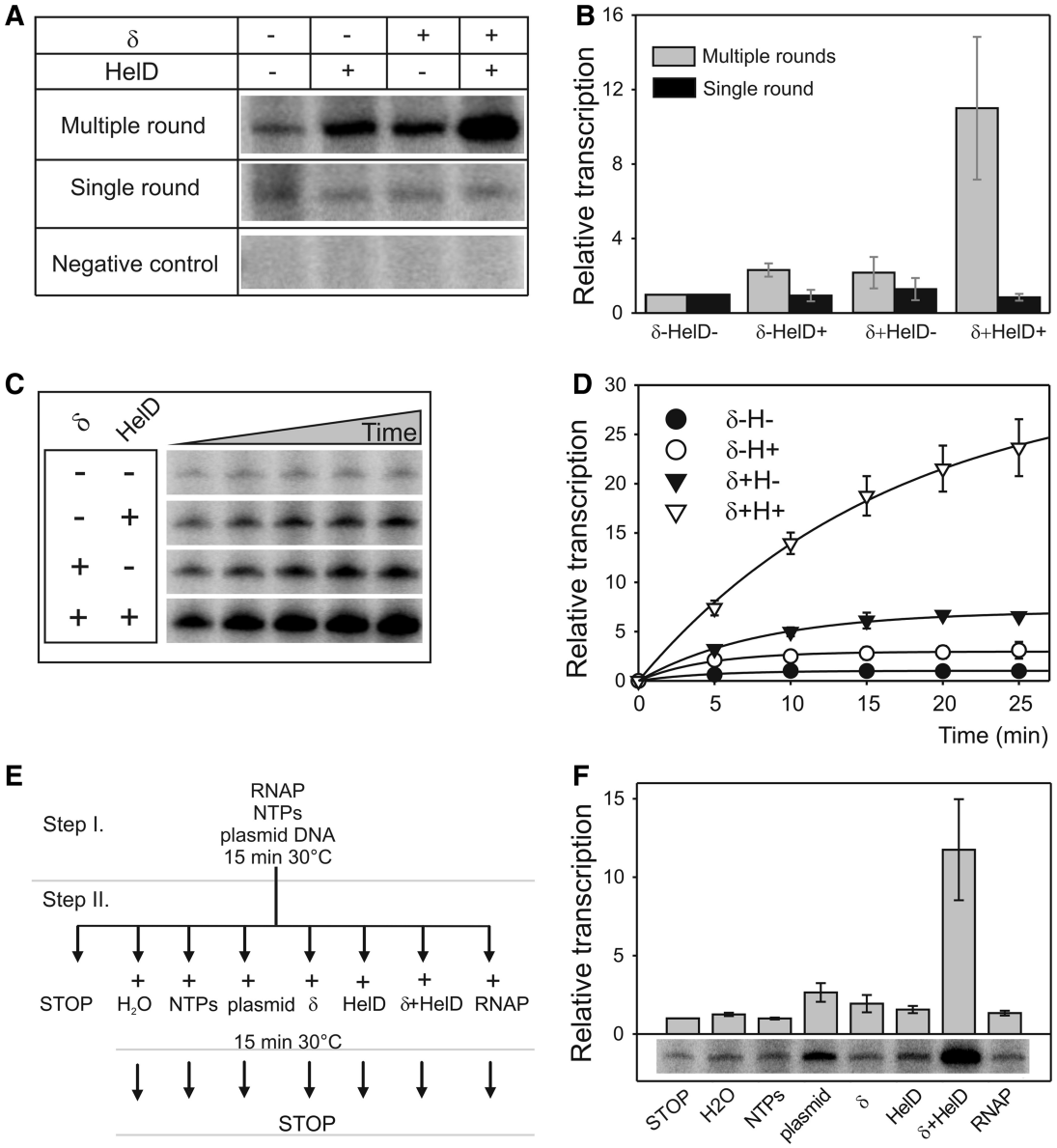

Figure 5. HelD and δ stimulate cycling of transcription. (**A**) Multiple round transcription assays were conducted in the absence of a competitor (dsDNA), whereas single round assays were conducted in its presence. In single round assays, the competitor was added to preform open complexes together with NTPs that were used to initiate transcription. The negative control shows the efficiency of the dsDNA competitor at preventing transcription of the 145-nt product when added to assay mixtures before formation of the open complex. (**B**) Quantification of data from multiple round (gray bars) and single round (black bars) transcription assays. Data from three independent experiments were quantified; the graph shows averages ±SD. (**C**) Multiple round *in vitro* transcription is limited in time—representative data. RNAP was preincubated with/without δ and/or HelD. Reactions were started at time zero by NTPs. Aliquots were withdrawn at 5, 10, 15, 20 and 25 min, respectively, and stopped by formamide stop solution. (**D**) Multiple round *in vitro* transcription is limited in time—quantification. Data were quantified from two independent experiments normalized to the value of transcription without δ and HelD after 15 min (set as 1). The bars indicate the range. (**E**) HelD and δ restart halted *in vitro* transcription—a schematic drawing of the experiment. In step I, all the indicated components of the transcription reaction were combined together and transcription reactions were allowed to proceed for 15 min. At this time point, the mixture was distributed to eight tubes containing the indicated components, and the reactions (Step II) were allowed to proceed for further 15 min. (**F**) HelD and δ restart halted *in vitro* transcription—a representative result and quantitation of the data. The quantified data were normalized to lane 1, set as 1. The graph represents data from three independent experiments ±SD.

beginning of the reaction, or HelD, δ or HelD and δ were added, and the reaction allowed to proceed for another 15 min. From the results (Figure 5E and F) we can exclude the first hypothesis: the addition of NTPs did not restart transcription (Figure 5F, lane 3). We can also exclude inactivation of all RNAP present in the experiment (second hypothesis) as addition of RNAP did not restart transcription (Figure 5F, lane 8). This is in agreement with the fact that there was 12-fold molar excess of RNAP over the template DNA already at the beginning of the reaction. Finally, the addition of plasmid DNA resulted in ~2-fold increase in transcription, suggesting it is the lack of an available template DNA that prevents further transcription (third hypothesis).

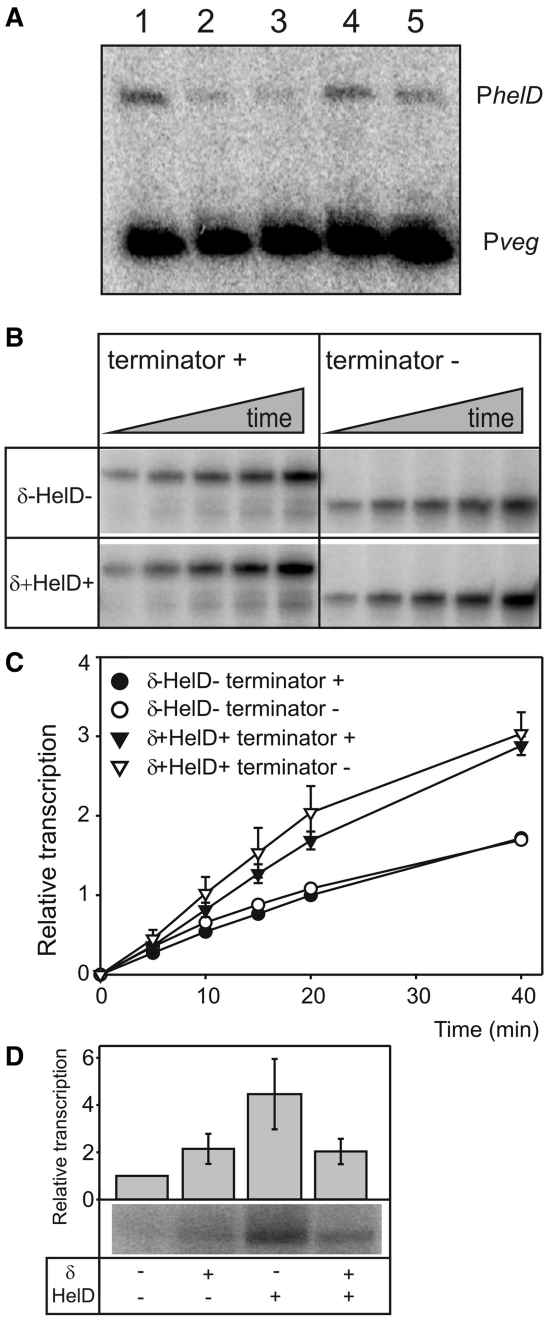

Figure 6. HelD liberates RNAP and affects elongation. (**A**) HelD liberates sequestered RNAPs—primary data. Transcription assays were performed with two supercoiled templates, either P*veg* (145-nt transcript) or P*helD* (245 nt). P*veg* was in all reactions from the beginning. P*helD* was added at the beginning (lane 1) or after 15 min (lanes 2–5) and reactions were allowed to proceed for another 15 min. RNAP contained no HelD or δ. These proteins were added after 15 min (lane 2—no protein; lane 3—δ; lane 4—HelD; lane 5—HelD+δ). (**B**) HelD and δ increase transcriptional rate on linear templates regardless of the presence/absence of a Rho-independent terminator—representative primary data. Two templates both containing the P*veg* promoter were used (see 'Materials and Methods' section for details). One template contained a Rho-independent terminator, while the other lacked this terminator. With both templates, the experiment was conducted ± HelD+δ. (**C**) Quantification of the data (plus two more repeats) from the experiment shown in (**B**). Panel (**D**), HelD stimulates transcription of 20 nt RNA. Multiple round *in vitro* transcription reactions on a linear template with a 20 bp template were performed in the presence/absence of HelD and/or δ. The radioactively labeled transcripts were resolved on 20% polyacrylamide gels. The graph shows a representative result and quantification of the data. The quantified data were normalized to lane 1, set as 1. The graph represents data from three independent experiments ± SD.

The addition of HelD or δ alone had again a moderate stimulatory effect on transcription. However, a pronounced stimulatory effect was observed on the addition of HelD and δ together (Figure 5F, lane 7). This demonstrated that the lack of transcription-competent template was not caused by, for example, degradation or irreversible alteration of DNA.

HelD and *δ* release RNAP from DNA and affect elongation

The reason for the transcriptional inactivity of the plasmid in the previous experiment could be due to the presence of stalled (nonproductive) RNAP complexes either on the P*veg* template or elsewhere on the plasmid. Another possibility is an alteration of the plasmid by transcription (e.g. a change of supercoiling), which would suggest an effect of HelD on elongation. Finally, the plasmid could be in complex with RNA (e.g. R-loops) and thus not functional in transcription. Previous experiments have already ruled out such possibilities as affecting promoter affinity (Supplementary Figure S5B) or affinity of σ^A for RNAP (Supplementary Figure S5A).

To test whether the presence of δ and HelD releases nonproductive RNAP from DNA we performed *in vitro* transcription assays with two templates producing RNAs of different length (from P*veg* and P*helD* promoters). A subsaturating concentration of RNAP (with respect to the plasmid template) was used. When both templates were added at time zero, both were transcribed by RNAP in the absence of δ and HelD (Figure 6A, lane 1). When transcription started only from P*veg*, and P*helD* was added after 15 min, free RNAP appeared to be unavailable, as only a small amount of transcript from P*helD* was generated (Figure 6A, lane 2), suggesting that RNAP may be sequestered on the P*veg* template DNA. This effect was alleviated when HelD or HelD with δ were added together with the second template (Figure 6A, lanes 4 and 5). The presence of δ and HelD enabled RNAP to be reused for transcription from both templates. We note that δ alone did not display a stimulatory effect with the P*helD* template (Figure 6A, lane 3). This could be due to an effect of δ on transcription initiation at P*helD*, as δ is known to decrease transcription from promoters that form relatively unstable open complexes (important intermediates during transcription initiation) (15).

Next, we tested whether HelD and δ were able to release RNAP from posttermination complexes as suggested for RapA (30,34). We performed *in vitro* transcription reactions with linear templates containing or lacking Rho-independent terminators. Figure 6B and C shows that the presence or absence of the terminator had no effect on the stimulatory effect of HelD and δ. Interestingly,

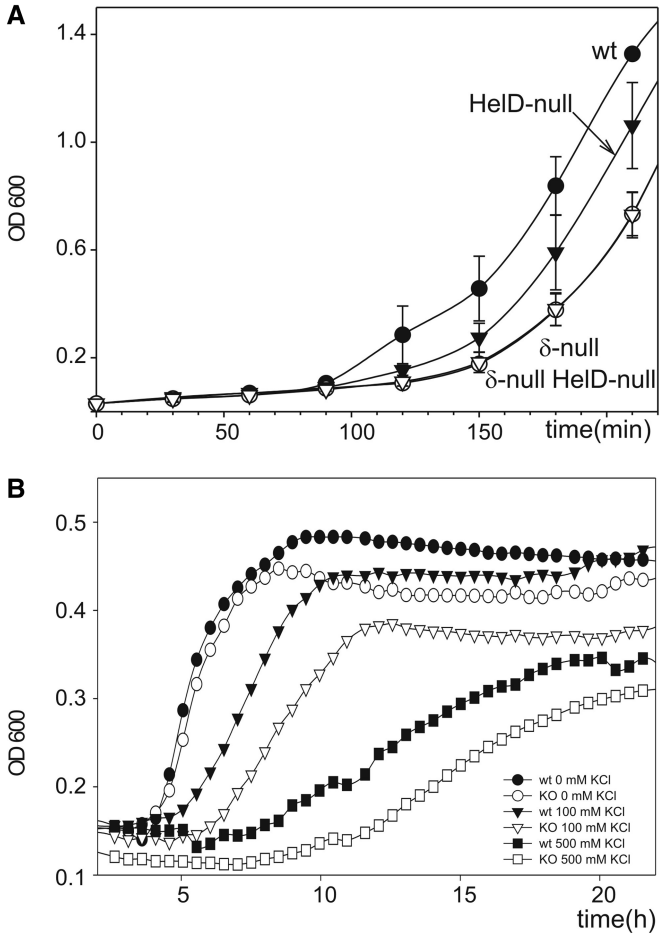

Figure 7. HelD and δ affect the growth phenotype. **(A)** wt, wild type *B. subtilis* strain (MH5636): closed circles; HelD-null (LK782): closed triangles; δ-null (LK637): open circles; δ-null HelD-null (LK1032): open triangles. The strains were grown for 24 h at 37°C. After 24 h, the cells were diluted into fresh LB medium at $OD_{600} = 0.03$ and the growth curves after the dilution are shown. (**B**) Growth in defined MOPS medium supplemented with all 20 amino acids in the presence 0, 0.5 or 1.0 M KCl as stated in the figure legend. Cells were cultivated in 1 ml of volumes at 37°C in 24-well EMSA plates in a TECAN Infinite® 200 Pro and OD 600 was measured every 10 min.

transcription did not stop on the linear templates after 5 min in the absence of these two proteins but continued throughout the duration of the experiment. However, the overall level of transcription was less in the absence of HelD and δ. We tested the effect of HelD and δ on releasing RNAP from the linear template and detected only a modest (20%) stimulation of this process (Supplementary Figure S6A and B). Hence, the main stimulatory effect of HelD on linear templates is most consistent with an effect on elongation.

To test whether the elongation effect could be due to the inability of RNAP to read through complexes of DNA with RNA, as also suggested for RapA (34), we performed experiments with a short linear DNA template where the transcribed region was only 20 nt long. This short length of transcribed template does not permit significant interactions of the nascent RNA with DNA (35). As shown in Figure 6D, HelD and δ were still capable of stimulating transcription. Interestingly, the effect of δ with HelD was decreased relative to the effect of HelD alone. A possible explanation could be a parallel negative effect of δ on, for example, the affinity of RNAP for the promoter located on this short linear DNA fragment.

We conclude that the effect of HelD in conjunction with δ on transcriptional cycling on supercoiled templates appears to be caused, at least in part, by liberating nonproductive RNAPs from complexes with DNA. A parallel stimulatory effect of HelD on the rate of elongation that is more apparent with linear templates seems to also play a role.

HelD and *δ* display similar phenotypes *in vivo*

To assess the importance of HelD for the cell, we performed phenotypic experiments, using a HelD-null strain. In comparison with wild type, no difference in growth was observed in rich (LB) or nutritionally defined media (MOPS). Similarly, no difference was observed in response to various stresses, such as heat and ethanol (data not shown). However, the mutant strain displayed a prolonged lag phase for stationary cells diluted into fresh medium. This phenotype was reminiscent of the phenotype displayed by the δ-null strain (10,15). Therefore, we directly compared wild type, δ-null, HelD-null and the double knockout strain, HelD-null and δ-null (MH5636, LK637, LK782 and LK1032, respectively). The cells were grown for 24 h and then diluted into fresh LB medium. The outgrowth from lag phase of the δ-null strain was delayed compared with wild-type cells for ~30 min, as reported previously (Figure 7A). Growth of the HelD-null strain was delayed for ~15 min and the double knockout strain displayed an identical delay to the δ-null strain. The same phenotype was observed for wild-type versus HelD-null strain in defined rich medium (MOPS supplemented with all amino acids) and in poor M9 medium (Supplementary Figure S7A). Further, we also observed a minor effect on growth in the presence of increased amounts of salt (Figure 7B and Supplementary Figure S7B). Albeit relatively small, these phenotypes were highly reproducible. We concluded that the absence of HelD decreased the ability of the cell to rapidly adapt to nutritional changes in the environment.

DISCUSSION

In this study we confirmed HelD as a new interacting partner of RNAP from *B. subtilis*, we identified that it binds to the core form of the enzyme, localized its approximate binding region on RNAP and provided insights into the role of HelD in transcription. We have shown that HelD hydrolyzes ATP independently of RNAP and stimulates transcription in an ATP-dependent manner. This differs from RapA from *E. coli* where the ATPase activity of RapA without RNAP was minimal (36).On supercoiled templates, this effect can be enhanced by an additional subunit called δ and the two proteins promote more efficient cycling of RNAP. Furthermore, HelD appears to increase the transcription rate by stimulating

elongation. Finally, we demonstrated that the absence of HelD prolongs the lag phase of growth in a similar manner as the absence of δ does. This phenotype negatively affects the ability of the cell to rapidly react to nutritional changes in the environment.

Far western blotting experiments indicate that HelD binds to RNAP core on the downstream side, in close proximity to the secondary channel (Figure 3F). Interestingly, RapA, a putative helicase that stimulates transcription in an ATP-dependent manner in *E. coli* was found to cross-link to β' and α subunits on *E. coli* RNAP (37). These results are at low resolution but they are consistent with the possibility that HelD and RapA may bind to the same region of their respective RNAPs. Future studies will have to address the exact mode of binding of these two proteins.

RapA is a putative helicase, and, similarly to HelD, no helicase activity was detected for this protein (38). Further, both HelD from *B. subtilis* and RapA of *Pseudomonas putida* (39) bind to core RNAP although RapA of *E. coli* was shown to bind to the holoenzyme containing the main sigma factor (37,39). HelD and RapA, however, belong to different protein families with no significant amino acid sequence homology. Closer sequence analysis suggests that even if both proteins use ATP-binding domains, the structures of these domains and also of the whole proteins are likely entirely unrelated. The two proteins further differ in their effects during UV-induced DNA damage when in *B. subtilis* the lack of HelD was reported to have a negative effect (10), whereas the lack of RapA had no effect in *E. coli* (37). Nevertheless, both proteins stimulate transcription in an ATP-dependent manner, and HelD can be further assisted in this function by a small subunit of RNAP, δ, which is absent from gram-negative bacteria. Interestingly, both δ and HelD are conserved in the industrially and medically important Firmicutes. The stimulatory effect of RapA was shown to be caused by enhancing of the transcriptional cycling by releasing RNAP from the DNA of posttermination complexes (30,34), and possibly also by assisting with reading through RNA–DNA hybrids (34). HelD and δ enhance the release of stalled RNAP from DNA and this, at least partially, contributes to the more efficient cycling of transcription. The character of the RNAP–DNA complexes is not apparent but it seems that it is not a posttermination complex, as the presence or absence of the terminator had no effect (Figure 6B and C). Finally, it appears that HelD may also contribute to more efficient elongation. Interestingly, the level of expression of HelD inversely correlates with the level of expression of topoisomerases TopA and TopB (9) that are known to affect transcription elongation (9,40). The elongation effect is unlikely to be due to a more efficient reading through of RNA–DNA hybrids, such as R-loops, as experiments with short transcribed regions seem to argue against this possibility. Further studies will be required to address the mechanistic details of the interplay between HelD, δ, RNAP and nucleic acids.

The phenotype of the HelD-null strain is not dramatic but it is likely that the prolonged lag phase would adversely affect the competitive fitness of the cell in nature. Further, it is possible that some other proteins, such as the PcrA helicase (7,41), may have overlapping functions with HelD and future studies will be required to decipher the role of these RNAP-associated helicases or helicase-like proteins in transcription. In conclusion, HelD is a novel type of RNAP-associated protein with an important role in transcription.

SUPPLEMENTARY DATA

Supplementary Data are available at NAR Online.

ACKNOWLEDGEMENT

The authors thank the National BioResource Project (NIG, Japan) for the *B. subtilis* HelD knockout strain MGNA-A456.

FUNDING

Czech Science Foundation [P302/11/0855, P305/12/G034, 13-16842S]; Science Foundation of Charles University [GAUK 425311]; Ministry of Education, Youth and Sports of the Czech Republic [EE2.3.30.0029]; European Regional Development Fund [BIOCEV CZ.1.05/1.1.00/02.0109]; National Health and Medical Research Council, Australia [APP1021479 to P.L.]; Operational Program Prague—Competitiveness [Project No.: CZ.2.16/3.1.00/24023 toward 'Prague Infrastructure for Structure Biology and Metabolomics']. Funding for open access charges: Czech Science Foundation [P302/11/0855, P305/12/G034, 13-16842S].

Conflict of interest statement. None declared.

REFERENCES

1. Osterberg,S., del Peso-Santos,T. and Shingler,V. (2011) Regulation of alternative sigma factor use. *Annu. Rev. Microbiol.*, **65**, 37–55.
2. Juang,Y.L. and Helmann,J.D. (1994) The delta subunit of *Bacillus subtilis* RNA polymerase. An allosteric effector of the initiation and core-recycling phases of transcription. *J. Mol. Biol.*, **239**, 1–14.
3. Lopez de Saro,F.J., Woody,A.Y. and Helmann,J.D. (1995) Structural analysis of the *Bacillus subtilis* delta factor: a protein polyanion which displaces RNA from RNA polymerase. *J. Mol. Biol.*, **252**, 189–202.
4. Epshtein,V., Dutta,D., Wade,J. and Nudler,E. (2010) An allosteric mechanism of Rho-dependent transcription termination. *Nature*, **463**, 245–249.
5. Toulme,F., Mosrin-Huaman,C., Sparkowski,J., Das,A., Leng,M. and Rahmouni,A.R. (2000) GreA and GreB proteins revive backtracked RNA polymerase *in vivo* by promoting transcript trimming. *EMBO J.*, **19**, 6853–6859.
6. Yang,X., Molimau,S., Doherty,G.P., Johnston,E.B., Marles-Wright,J., Rothnagel,R., Hankamer,B., Lewis,R.J. and Lewis,P.J. (2009) The structure of bacterial RNA polymerase in complex with the essential transcription elongation factor NusA. *EMBO Rep.*, **10**, 997–1002.
7. Delumeau,O., Lecointe,F., Muntel,J., Guillot,A., Guedon,E., Monnet,V., Hecker,M., Becher,D., Polard,P. and Noirot,P. (2011) The dynamic protein partnership of RNA polymerase in *Bacillus subtilis*. *Proteomics*, **11**, 2992–3001.

8. Yang,W. (2010) Lessons learned from UvrD helicase: mechanism for directional movement. *Annu. Rev. Biophys.*, **39**, 367–385.
9. Nicolas,P., Mader,U., Dervyn,E., Rochat,T., Leduc,A., Pigeonneau,N., Bidnenko,E., Marchadier,E., Hoebeke,M., Aymerich,S. *et al.* (2012) Condition-dependent transcriptome reveals high-level regulatory architecture in *Bacillus subtilis*. *Science*, **335**, 1103–1106.
10. Carrasco,B., Fernandez,S., Petit,M.A. and Alonso,J.C. (2001) Genetic recombination in *Bacillus subtilis* 168: effect of DeltahelD on DNA repair and homologous recombination. *J. Bacteriol.*, **183**, 5772–5777.
11. Hanahan,D. (1983) Studies on transformation of *Escherichia coli* with plasmids. *J. Mol. Biol.*, **166**, 557–580.
12. Dubnau,D. and Davidoff-Abelson,R. (1971) Fate of transforming DNA following uptake by competent Bacillus. subtilis. I. Formation and properties of the donor-recipient complex. *J. Mol. Biol.*, **56**, 209–221.
13. Qi,Y. and Hulett,F.M. (1998) PhoP-P and RNA polymerase sigmaA holoenzyme are sufficient for transcription of Pho regulon promoters in *Bacillus subtilis*: PhoP-P activator sites within the coding region stimulate transcription *in vitro*. *Mol. Microbiol.*, **28**, 1187–1197.
14. Kobayashi,K., Ehrlich,S.D., Albertini,A., Amati,G., Andersen,K.K., Arnaud,M., Asai,K., Ashikaga,S., Aymerich,S., Bessieres,P. *et al.* (2003) Essential *Bacillus subtilis* genes. *Proc. Natl Acad. Sci. USA*, **100**, 4678–4683.
15. Rabatinova,A., Sanderova,H., Matejckova,J.J., Korelusova,J., Sojka,L., Barvik,I., Papouskova,V., Sklenar,V., Zidek,L. and Krasny,L. (2013) The delta subunit of RNA polymerase is required for rapid changes in gene expression and competitive fitness of the cell. *J. Bacteriol.*, **195**, 2603–2611.
16. Chang,B.Y. and Doi,R.H. (1990) Overproduction, purification, and characterization of *Bacillus subtilis* RNA polymerase sigma A factor. *J. Bacteriol.*, **172**, 3257–3263.
17. Ross,W., Thompson,J.F., Newlands,J.T. and Gourse,R.L. (1990) *E. coli* Fis protein activates ribosomal RNA transcription *in vitro* and *in vivo*. *EMBO J.*, **9**, 3733–3742.
18. Krasny,L. and Gourse,R.L. (2004) An alternative strategy for bacterial ribosome synthesis: *Bacillus subtilis* rRNA transcription regulation. *EMBO J.*, **23**, 4473–4483.
19. Johnston,E.B., Lewis,P.J. and Griffith,R. (2009) The interaction of *Bacillus subtilis* sigmaA with RNA polymerase. *Protein Sci.*, **18**, 2287–2297.
20. Anborgh,P.H., Parmeggiani,A. and Jonak,J. (1992) Site-directed mutagenesis of elongation factor Tu. The functional and structural role of residue Cys81. *Eur. J. Biochem.*, **208**, 251–257.
21. Gaal,T., Ross,W., Estrem,S.T., Nguyen,L.H., Burgess,R.R. and Gourse,R.L. (2001) Promoter recognition and discrimination by EsigmaS RNA polymerase. *Mol. Microbiol.*, **42**, 939–954.
22. Barker,M.M., Gaal,T. and Gourse,R.L. (2001) Mechanism of regulation of transcription initiation by ppGpp. II. Models for positive control based on properties of RNAP mutants and competition for RNAP. *J. Mol. Biol.*, **305**, 689–702.
23. Camacho,C., Coulouris,G., Avagyan,V., Ma,N., Papadopoulos,J., Bealer,K. and Madden,T.L. (2008) BLAST+: architecture and applications. *BMC Bioinformatics*, **10**, 421.
24. Altschul,S.F., Gish,W., Miller,W., Myers,E.W. and Lipman,D.J. (1990) Basic local alignment search tool. *J. Mol. Biol.*, **215**, 403–410.
25. Larkin,M.A., Blackshields,G., Brown,N.P., Chenna,R., McGettigan,P.A., McWilliam,H., Valentin,F., Wallace,I.M., Wilm,A., Lopez,R. *et al.* (2007) Clustal W and Clustal X version 2.0. *Bioinformatics*, **23**, 2947–2948.
26. Anthony,L.C., Artsimovitch,I., Svetlov,V., Landick,R. and Burgess,R.R. (2000) Rapid purification of His(6)-tagged *Bacillus subtilis* core RNA polymerase. *Protein Expr. Purif.*, **19**, 350–354.
27. Lee,J.Y. and Yang,W. (2006) UvrD helicase unwinds DNA one base pair at a time by a two-part power stroke. *Cell*, **127**, 1349–1360.
28. Cao,Z. and Julin,D.A. (2009) Characterization *in vitro* and *in vivo* of the DNA helicase encoded by *Deinococcus radiodurans* locus DR1572. *DNA Repair (Amst)*, **8**, 612–619.
29. Vassylyev,D.G., Sekine,S., Laptenko,O., Lee,J., Vassylyeva,M.N., Borukhov,S. and Yokoyama,S. (2002) Crystal structure of a bacterial RNA polymerase holoenzyme at 2.6 A resolution. *Nature*, **417**, 712–719.
30. Sukhodolets,M.V., Cabrera,J.E., Zhi,H. and Jin,D.J. (2001) RapA, a bacterial homolog of SWI2/SNF2, stimulates RNA polymerase recycling in transcription. *Genes Dev.*, **15**, 3330–3341.
31. Epshtein,V., Toulme,F., Rahmouni,A.R., Borukhov,S. and Nudler,E. (2003) Transcription through the roadblocks: the role of RNA polymerase cooperation. *EMBO J.*, **22**, 4719–4727.
32. Holmberg,C. and Rutberg,B. (1991) Expression of the gene encoding glycerol-3-phosphate dehydrogenase (glpD) in *Bacillus subtilis* is controlled by antitermination. *Mol. Microbiol.*, **5**, 2891–2900.
33. Gowrishankar,J., Leela,J.K. and Anupama,K. (2013) R-loops in bacterial transcription: their causes and consequences. *Transcription*, **4**, 153–157.
34. McKinley,B.A. and Sukhodolets,M.V. (2007) Escherichia coli RNA polymerase-associated SWI/SNF protein RapA: evidence for RNA-directed binding and remodeling activity. *Nucleic Acids Res.*, **35**, 7044–7060.
35. Vassylyev,D.G., Vassylyeva,M.N., Zhang,J., Palangat,M., Artsimovitch,I. and Landick,R. (2007) Structural basis for substrate loading in bacterial RNA polymerase. *Nature*, **448**, 163–168.
36. Yawn,B., Zhang,L., Mura,C. and Sukhodolets,M.V. (2009) RapA, the SWI/SNF subunit of *Escherichia coli* RNA polymerase, promotes the release of nascent RNA from transcription complexes. *Biochemistry*, **48**, 7794–7806.
37. Sukhodolets,M.V. and Jin,D.J. (2000) Interaction between RNA polymerase and RapA, a bacterial homolog of the SWI/SNF protein family. *J. Biol. Chem.*, **275**, 22090–22097.
38. Sukhodolets,M.V. and Jin,D.J. (1998) RapA, a novel RNA polymerase-associated protein, is a bacterial homolog of SWI2/SNF2. *J. Biol. Chem.*, **273**, 7018–7023.
39. Stec-Dziedzic,E., Lyzen,R., Skarfstad,E., Shingler,V. and Szalewska-Palasz,A. (2013) Characterization of the transcriptional stimulatory properties of the Pseudomonas putida RapA protein. *Biochim. Biophys. Acta*, **1829**, 219–230.
40. Baranello,L., Kouzine,F. and Levens,D. (2013) DNA Topoisomerases: beyond the standard role. *Transcription*, **4** doi: 10.4161/trns.26598.
41. Gwynn,E.J., Smith,A.J., Guy,C.P., Savery,N.J., McGlynn,P. and Dillingham,M.S. (2013) The conserved C-terminus of the PcrA/UvrD helicase interacts directly with RNA polymerase. *PLoS One*, **8**, e78141.

Supplementary data

Characterization of HelD, an interacting partner of RNA polymerase from *Bacillus subtilis*

Jana Wiedermannová[1,2], Petra Sudzinová[1], Tomáš Kovaľ[3], Alžbeta Rabatinová[1], Hana Šanderová[1], Olga Ramaniuk[1], Šimon Rittich[1], Jan Dohnálek[3,4], Zhihui Fu[5], Petr Halada[1], Peter Lewis[5], and Libor Krásný[1]*

[1] Institute of Microbiology, Academy of Sciences of the Czech Republic, Prague, 14220, Czech Republic

[2] Faculty of Science, Charles University in Prague, Prague, 12843, Czech Republic

[3] Institute of Macromolecular Chemistry, Academy of Sciences of the Czech Republic, Prague, 16206, Czech Republic

[4] Institute of Biotechnology, Academy of Sciences of the Czech Republic, Prague, 14220, Czech Republic

[5] School of Environmental and Life Sciences, University of Newcastle, Callaghan, NSW 2308, Australia

* To whom correspondence should be addressed. Tel: +420 241 063 208; Fax: +420 241 722 257; Email: krasny@biomed.cas.cz

Material and methods

Preparation of radiolabeled DNA

Linear DNA templates were prepared with PCR from the plasmid containing P*veg* (LK1) and subsequently phenol-chloroform extracted, precipitated with ethanol, and dissolved in water. The DNA fragments used in Fig. S1 started at -118 relative to the transcription start site and ended at +55. The DNA templates used in Fig. S6 started at -118 relative to the transcription start site and ended at +255 (containing the rho-independent terminator (at +145)). The DNA fragments were radiolabeled at their 5´ends by T4 polynucleotide kinase and purified with Nucleotide removal kit (Qiagene).

Native PAGE assays

0.5-160 pmol of HelD and 0.5 or 1 pmol of 5´- radiolabeled DNA were incubated for 15 minutes at 30°C. As controls, denatured HelD (5 minutes in 95°C) or 160 pmol of BSA were used. After incubation samples were mixed with Native PAGE 4X Sample buffer (Invitrogen) and loaded onto the Native PAGE 4-16 % Bis-Tris Gel (Invitrogen) and electrophoresed. The dried gels were scanned with a Molecular Imager_FX (BioRad).

Size exclusion chromatography

Size exclusion chromatography was performed by HiLoad^{TM} Superdex 200 prep grade column and absorbance profile was collected at 280 nm for HelD.

Plasmids for *in vitro* transcription

Plasmid pRLG770 (1) was used for cloning promoter constructs used in *in vitro* multiple-round transcriptions in Fig S3. The GlpD promoter fragment was created by annealing two complementary oligonucleotides with appropriate overhangs (5‘AATTCGCTTTTAAATAAAGTAATACTATGGTATAATGGTTACAAGTA 3‘, 5‘AGCTTACTTGTAACCATTATACCATAGTATTACTTTATTTAAAAGCG3‘) and was inserted into the vector using EcoRI and HindIII restriction sites, yielding plasmid LK888. The HelD promoter region was amplified via PCR (primers: 5‘CGCGAATTC GGCTGGGGAACTCGTTCGGC3‘, 5’CCCAAGCTTCAAACATAGATGAAATACTG3‘), cleaved by EcoRI and HindIII restriction enyzmes and cloned into the same vector, yielding plasmid LK1109. All constructs were verified by DNA sequencing.

***In vitro* transcription**

In vitro transcription was done as in main paper (see Mat & Met section). The salt used was 150 mM KCl. In Fig S6 - the α^{32}P-UTP was ommited and 50 fmol of 5´ radiolabeled linear DNA was used as the template with 300 nM RNAP.

***In vivo* experiments**

Outgrowth from lag phase was conducted as in Fig 7 (shown in the main text). Media used for this experiment were MOPS supplemented with 0.4% glucose and all 20 amino acids at 25 μg/ml (2) and M9 medium supplemented with tryptophan and phenylalanin (25 μg/ml) (3).

Supplementary Figures

Figure S1.

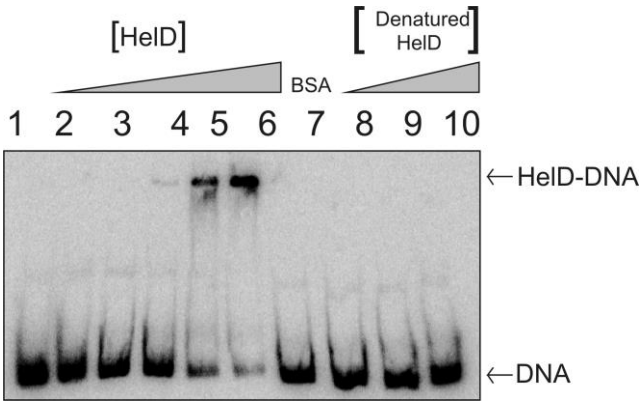

Figure S1. HelD binds to dsDNA. Radiolabeled dsDNA was incubated with increasing amounts of HelD for 15 min at 30°C and separated on 4-16% gradient native PAGE Bis-Tris gels. Lane 1 –ds DNA 0.5 pmol, lane 2-6– 0.5 pmol of dsDNA and 0.5, 1, 10, 100, 160 pmol of HelD respectively. As a control we used BSA (lane 7- 160 pmol) and HelD denatured for 5 minutes in 95°C (lane 8-10; 1, 10, 100 pmol of HelD respectively).

Figure S2.

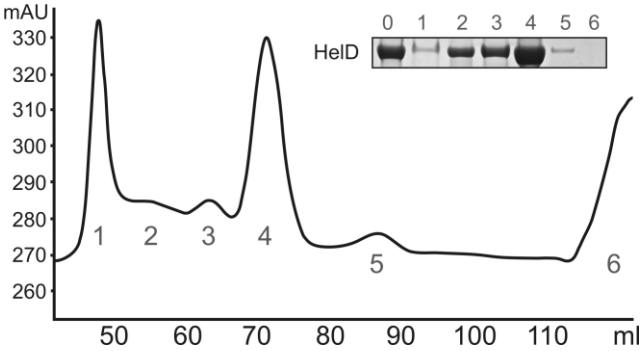

Figure S2. HelD oligomerizes. A. Size exclusion chromatography (HiLoad™ Superdex 200 prep grade column) absorbance profile collected at 280 nm for HelD. Peaks 2, 3 and 4 belong to different oligomers of HelD. B. SDS PAGE analysis of the HelD size exclusion chromatography profile. In lane 0 is the original sample of HelD loaded on the column, in lanes 1 to 6 are the concentrated peaks from the size exclusion chromatography with the corresponding numbering.

Figure S3.

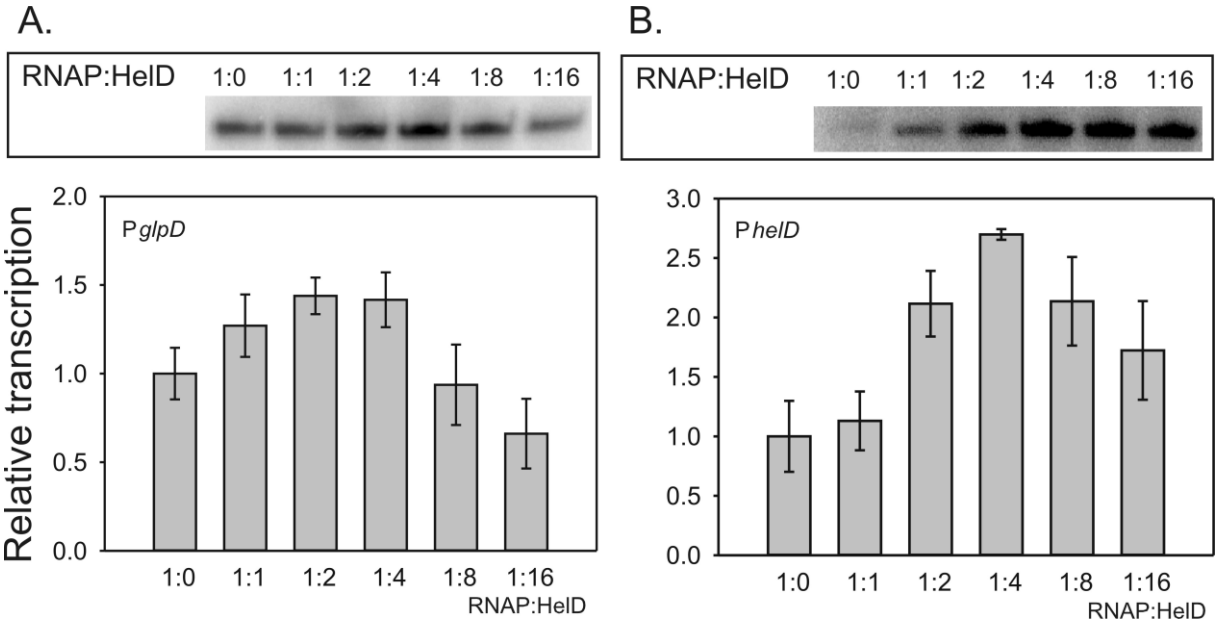

Figure S3. Effect of HelD on *in vitro* transcription. RNAP (from HelD knock out strain LK782) was reconstituted with saturating concentrations of σ^A. The holoenzyme was then incubated with increasing amounts (molar ratio from 1:0 to 1:16) of HelD and used to initiate transcription. The template plasmids with either the P*glpD* promoter LK888 (A) or P*helD* promoter LK1109 (B) were used. Primary data are shown in the upper panel and show a representative experiment. The data were normalized to the 1:0 ratio that was set as 1. Graphs represent data from three independent experiments ±SD.

Figure S4.

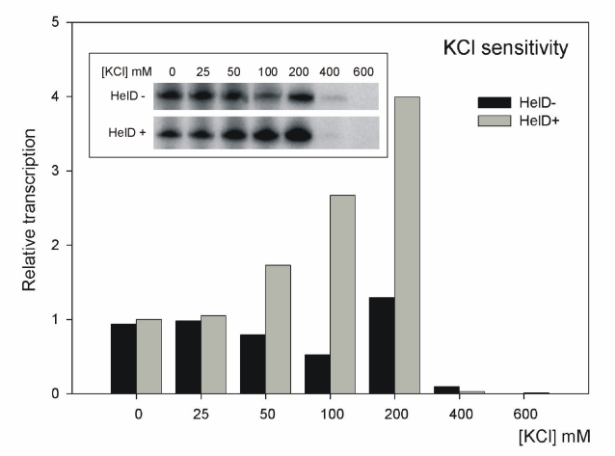

Figure S4. Effect of HelD on *in vitro* transcription is KCl- dependent.. RNAP (from HelD knock out strain LK782) was reconstituted with saturating concentrations of σ^A. The holoenzyme with or without HelD was then used to initiate transcription with increasing concentration of KCl in the reaction buffer (0-600 mM). Primary data are shown in the upper panel and show a representative experiment. The data were normalized to transcription without KCl set as 1. Experiment was repeated three times in different conditions (RNAP:HelD ratio) with the same trend.

Figure S5.

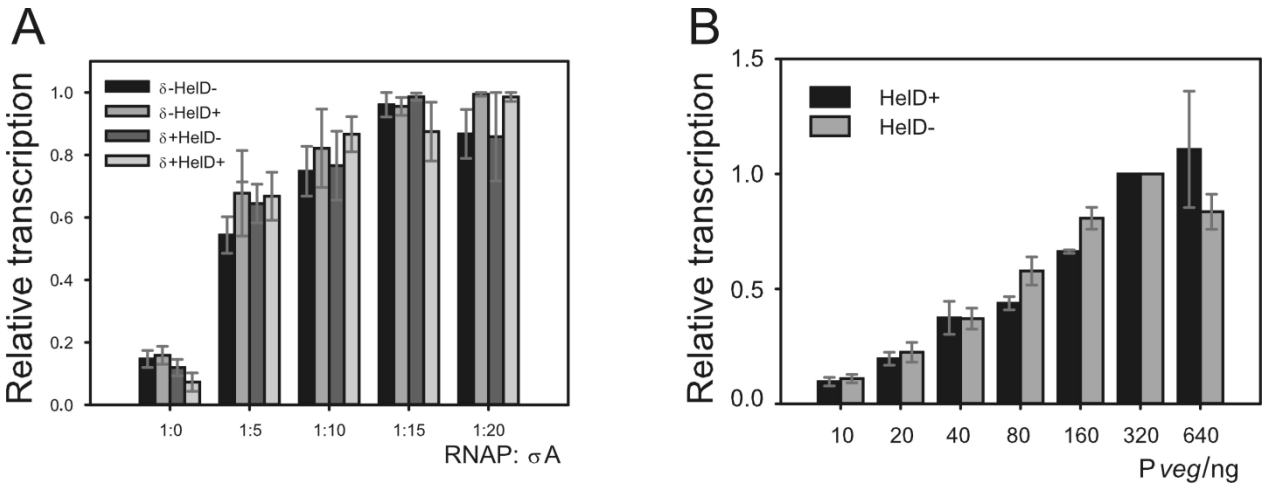

Figure S5. HelD does not affect initial steps of transcription. A. RNAP (from HelD-null δ-null strain LK1032) was reconstituted for 15 min at 30°C with increasing amounts of σ^A (molar ratio 1:0 to 1:20). The holoenzyme was subsequently reconstituted for 15 min at 30°C with δ (1:4 ratio) and/or HelD (1:4 ratio) and used to initiate transcription (proteins present in each reaction are indicated in graph legend). B. RNAP (from LK 782) either was (black bars) or was not (grey bars) reconstituted with HelD and used in transcription assays with increasing amounts of template DNA (P*veg*, 10- 640 ng). The data were normalized to the maximal value set as 1. Graphs represent data from three independent experiments ±SD.

Figure S6.

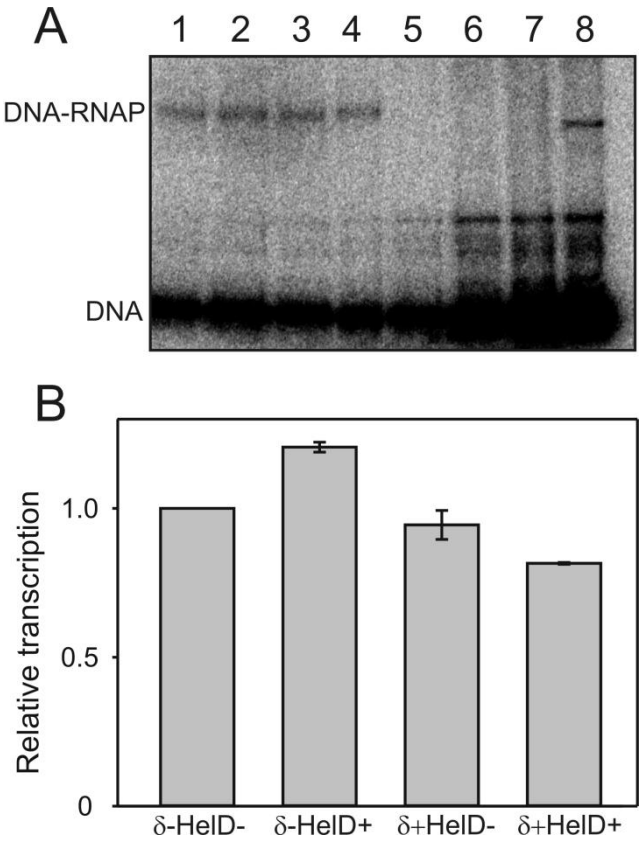

Figure S6. Effect of δ and HelD on the release of RNAP from linear template DNA after transcription. A. *In vitro* transcription was performed as described in Materials & Methods in the main paper with the following differences: α^{32}P-UTP was ommited and 50 fmol of 5´ radiolabeled linear DNA was used as the template with 300 nM RNAP. The template DNA contained the P*veg* promoter and a Rho-independetnt terminator, as used in the experiments shown in Fig.6B and C. Transcription was allowed to proceed for 15 min without δ and HelD and then dsDNA competitor (6 μM) together with δ and/or HelD were added (1:4 molar ratio; lane 1 - no protein, lane 2- HelD, lane 3 - δ, lane 4 - δ and HelD). Lane 5 shows control with the competitor DNA- when the competitor was added at the beggining of transcription, no RNAP bound to the radiolabeled DNA. Lane 6 - 100 fmol of radiolabeled DNA, lane7 - 100 fmol of radiolabeled DNA with 12 pmol HelD (this amount of HelD is too low to observe the binding of HelD to the DNA; see Fig. S1), lane 8 - 100 fmol of radiolabeled DNA with RNAP (600 fmol) before transcription. Note that the band migrates faster because the complex of RNAP-DNA lacks the transcribed RNA B. Quantification of data from lanes 1-4; the bars show the averages from two independent experiments. The error bars show the range.

Figure S7.

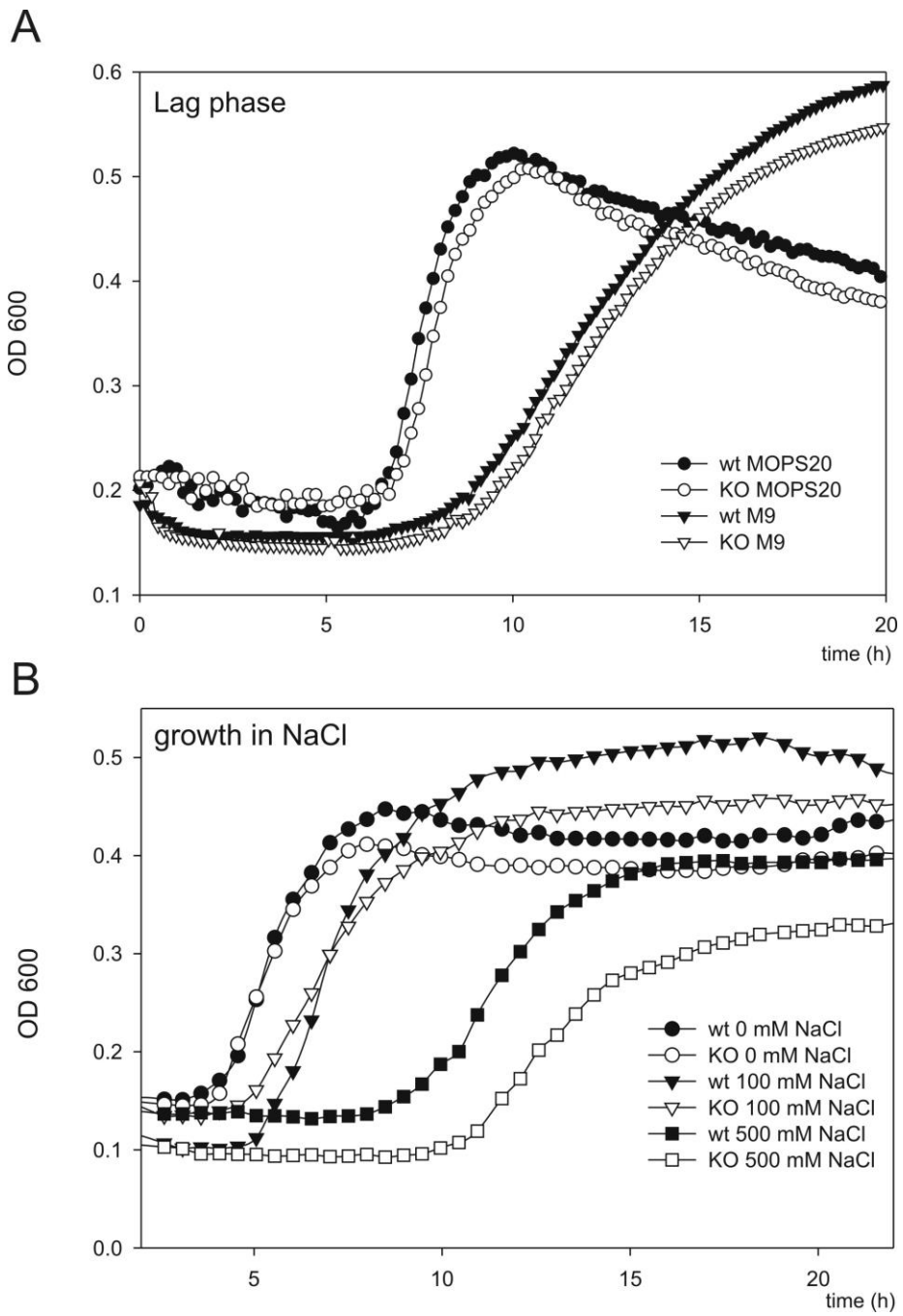

Figure S7. A. **HelD affects the growth phenotype.** A. The strains (wt, wild type *B. subtilis* strain (MH5636); HelD-null (KO; LK782)) were grown for 24 hours at 37° C in either defined MOPS medium supplemented with 0.4% glucose and all 20 amino acids at 25 μg/ml or in M9 medium supplemented with tryptophan and phenylalanine (25 μg/ml). After 24 hours, the cells were diluted into fresh medium and cultivated in 1 ml volumes at 37°C in 24-well EMSA plates in a TECAN Infinite® 200 Pro and OD 600 was measured every 10 min. B. Growth in defined MOPS medium supplemented with all 20 amino acids in the presence of various concentrations of NaCl (0, 0.5, or 1.0 M) as indicated in the figure legend.

Reference list

1. Ross,W., Thompson,J.F., Newlands,J.T. and Gourse,R.L. (1990) E.coli Fis protein activates ribosomal RNA transcription in vitro and in vivo. *EMBO J.*, **9**, 3733-3742.
2. Krasny,L. and Gourse, R.L. (2004) An alternative strategy for bacterial ribosome synthesis: Bacillus subtilis rRNA transcription regulation. EMBO J., 23, 4473-4483.
3. Harwood, C.R. and Cutting, S.M. (1990). Molecular biological methods for Bacillus: Chemically defined growth media and supplements. Wiley. Chichester, UK.

PUBLICATION II

Molecular Microbiology (2019) 111(2), 514–533

doi:10.1111/mmi.14171
First published online 11 December 2018

Spx, the central regulator of the heat and oxidative stress response in *B. subtilis*, can repress transcription of translation-related genes

Heinrich Schäfer,[1] Anja Heinz,[2] Petra Sudzinová,[3] Michelle Voß,[1] Ingo Hantke,[1] Libor Krásný [3] and Kürşad Turgay [1]*

[1] *Institute of Microbiology, Leibniz Universität Hannover, Herrenhäuser Str. 2, D-30419, Hannover, Germany.*
[2] *Institute of Biology-Microbiology, Freie Universität Berlin, Königin-Luise-Str. 12–16, D-14195, Berlin, Germany.*
[3] *Institute of Microbiology, Czech Academy of Sciences, Vídeňská 1083, 142 20, Prague, Czech Republic.*

Summary

Spx is a *Bacillus subtilis* transcription factor that interacts with the alpha subunits of RNA polymerase. It can activate the thiol stress response regulon and interfere with the activation of many developmental processes. Here, we show that Spx is a central player orchestrating the heat shock response by up-regulating relevant stress response genes as revealed by comparative transcriptomic experiments. Moreover, these experiments revealed the potential of Spx to inhibit transcription of translation-related genes. By *in vivo* and *in vitro* experiments, we confirmed that Spx can inhibit transcription from rRNA. This inhibition depended mostly on UP elements and the alpha subunits of RNA polymerase. However, the concurrent up-regulation activity of stress genes by Spx, but not the inhibition of translation related genes, was essential for mediating stress response and antibiotic tolerance under the applied stress conditions. The observed inhibitory activity might be compensated *in vivo* by additional stress response processes interfering with translation. Nevertheless, the impact of Spx on limiting translation becomes apparent under conditions with high cellular Spx levels. Interestingly, we observed a subpopulation of stationary phase cells that contains raised Spx levels, which may contribute to growth inhibition and a persister-like behaviour of this subpopulation during outgrowth.

Accepted 21 November, 2018. *For correspondence. E-mail turgay@ifmb.uni-hannover.de; Tel. +49 511 7625241; Fax +49 511 762-5287

Introduction

All cells need to monitor and maintain their protein homeostasis, which becomes particularly challenging during adverse environmental conditions that induce unfolding, misfolding or aggregation of cellular proteins. For this purpose, a cellular protein quality control system (PQS) evolved, which is conserved and present in all domains of life (Balchin *et al.*, 2016). This PQS includes chaperones which can prevent protein aggregation or facilitate the refolding of already misfolded proteins. Specific chaperone complexes can disaggregate and refold already aggregated proteins. Furthermore, potentially toxic subcellular protein aggregates can be removed from the cell by AAA+ protease complexes (Wickner *et al.*, 1999; Kirstein *et al.*, 2009; Mogk *et al.*, 2011; Kim *et al.*, 2013). Consequently, the cellular levels of most chaperones and proteases of the PQS, also known as heat shock proteins, are increased in response to a temperature upshift, but also to other stress conditions affecting protein homeostasis. Importantly, a pre-shock at elevated but not lethal temperature can provide cells with an acquired resistance to extreme and otherwise lethal temperatures in a process called priming or thermotolerance. This heat-mediated acquisition of thermotolerance appears to be conserved in all domains of life (Lindquist, 1986).

The heat shock response of the Gram-positive model organism *Bacillus subtilis* is controlled by multiple regulators (Hecker *et al.*, 1996; Elsholz *et al.*, 2017). Two heat-sensitive transcriptional repressors, HrcA and CtsR, control the expression of chaperone systems of the Hsp60 (GroESL) and Hsp40/70 (DnaKJ/GrpE) families, or the Hsp100/Clp unfoldase/protease systems ClpCP, ClpXP and ClpEP respectively (Mogk *et al.*, 1997; Krüger and Hecker, 1998; Wiegert and Schumann, 2001; Elsholz *et al.*, 2010). The membrane anchored proteases HtrA and HtrB are under transcriptional control of the CssRS

two-component system, which can respond to secretion and cell wall stress (Darmon *et al*., 2002; Rojas-Tapias and Helmann, 2018b). These stress response regulons are augmented by the activation of the general stress response controlled by the alternative sigma factor σ^B also during heat stress (Hecker *et al*., 2007).

Recently, we identified Spx, the regulator of thiol- and oxidative-stress response, which affects various regulatory pathways such as competence development (Nakano *et al*., 2001; Petersohn *et al*., 2001; Zuber, 2004), as a critical regulator for thermotolerance development and heat shock response (Runde *et al*., 2014). It should be noted that Spx was initially identified and named as suppressor of *clpP* and *clpX* and that the raised levels of Spx in *B. subtilis* strains lacking the active ClpXP protease system result also in decreased growth rate, which can be alleviated by mutations in *spx* (Nakano *et al*., 2002a; Runde *et al*., 2014).

Spx is subject to multiple stages of regulation. Its transcription is controlled by several promoters recognized by the sigma factors σ^A, σ^B, σ^M, σ^W and σ^X and regulated by the repressors PerR and YodB, thereby the transcription of *spx* is stimulated under a variety of abiotic and biotic stress conditions, including heat stress (Petersohn *et al*., 1999; Antelmann *et al*., 2000; Helmann *et al*., 2001; Leelakriangsak *et al*., 2007; Jervis *et al*., 2007; Nicolas *et al*., 2012; Rojas-Tapias and Helmann, 2018a). However, the activity of Spx is primarily controlled post-translationally through regulatory proteolysis by the ClpXP protease complex and the adaptor protein YjbH during non-stress conditions (Nakano *et al*., 2003b; Larsson *et al*., 2007; Garg *et al*., 2009).

Proteotoxic conditions such as heat and oxidative stress lead to the aggregation and inactivation of YjbH and thus increase the Spx protein level and activity (Zhang and Zuber, 2007; Engman and von Wachenfeldt, 2015). As a second layer of post-translational activity control, Spx possesses a CXXC motif that can undergo reversible cysteine oxidation and disulphide bond formation, thereby acting as a redox-sensitive switch (Nakano *et al*., 2005). The expression of some but not all genes of the Spx regulon exclusively depends on the oxidized state of Spx (Rochat *et al*., 2012; Gaballa *et al*., 2013; Rojas-Tapias and Helmann, 2018a). Spx also becomes activated upon cell wall stress via an independent mechanism by increased transcription of *spx* from a σ^M-dependent promoter and stabilization of Spx by cell wall and secretion stress dependent synthesis of the anti-adaptor protein YirB (Rojas-Tapias and Helmann, 2018a; 2018b).

Unlike most transcriptional regulators, Spx does not appear to possess DNA-binding activity on its own. Instead it directly interacts with the C-terminal domain of the RNA-polymerase (RNAP) alpha subunit (α-CTD), which itself can interact with specific UP-elements, AT-rich sequences encoded in the DNA upstream of the core promoter region (Zuber, 2004; Newberry *et al*., 2005; Reyes and Zuber, 2008; Lamour *et al*., 2009; Nakano *et al*., 2010; Delumeau *et al*., 2011; Rochat *et al*., 2012). In this complex, Spx can modulate RNAP activity and influence gene expression by (1) disrupting the binding of other transcriptional activators, e.g. ResD or ComA (Nakano *et al*., 2003b; Zhang *et al*., 2006). However, Spx can also (2) stimulate transcription from certain promoters, e.g. of the *trxA* and *trxB* genes. This stimulatory activity requires the interaction of the Spx/α-CTD complex with a *cis*-acting sequence motif associated with the UP-element upstream of the core promoter (Nakano *et al*., 2003a; Reyes and Zuber, 2008; Nakano *et al*., 2010; Rochat *et al*., 2012; Lin *et al*., 2013).

Several transcriptomic studies revealed that Spx is a global and pleiotropic regulator of the thiol-stress and oxidative stress response in *B. subtilis* (Leichert *et al*., 2003; Nakano *et al*., 2003a; Rochat *et al*., 2012; Gaballa *et al*., 2013). In addition, Rochat and co-workers applied global ChIP–chip experiments, which allowed to specifically identify the binding sites of the Spx/RNAP complex on the *B. subtilis* chromosome (Rochat *et al*., 2012). Upon heat or oxidative stress, i.a. the thioredoxin system encoded by *trxA* and *trxB*, the AAA+ ATPase *clpX*, the genes of the adaptor proteins YjbH, MecA and YpbH or the genes required for the synthesis of bacillithiol *bshA,B1,B2,C* are upregulated by Spx (Leichert *et al*., 2003; Nakano *et al*., 2003a; Rochat *et al*., 2012; Gaballa *et al*., 2013). Thus, *B. subtilis* cells lacking Spx display high sensitivity to a variety of stress conditions, including heat, oxidative stress caused by exposure to diamide or paraquat, low temperatures, salt and cell wall-active antibiotics (Petersohn *et al*., 2001; Höper *et al*., 2005; Reder *et al*., 2012; Runde *et al*., 2014; Rojas-Tapias and Helmann, 2018a).

Previously, we studied thermotolerance in *B. subtilis* and could show that the activity of Spx is directly required for the development of thermotolerance. Cells lacking Spx are unable to develop thermotolerance when primed by a mild pre-shock. Additionally, accumulation of Spx prior to stress, either by deletion of *yjbH, clpX* or *clpP* or by expression of Spx^{DD} *in trans*, resulted in a strongly increased thermoresistance phenotype and reduced cell growth (Nakano *et al*., 2002b; Runde *et al*., 2014).

By investigating the role of Spx in thermotolerance and heat stress response, we observed a specific ability of Spx to inhibit transcription of genes associated with translation such as genes encoding ribosomal proteins (r-proteins) and ribosomal RNA (rRNA). This inhibitory activity of Spx depended mostly on specific UP elements and the interaction of Spx with the alpha subunits of RNAP. Further experiments demonstrated that this specific ability of Spx is not necessary for Spx-dependent stress response, possibly because other redundant stress induced cellular systems, which also interfere with protein synthesis,

might complement this inhibitory activity. However, during specific environmental conditions such as the stationary phase, Spx reaches relatively high cellular levels in a subpopulation of cells and might contribute to a slower growth of this subpopulation during outgrowth in fresh medium. The raised Spx levels may contribute to a persister-like phenotype and support the survival of this sub-population of cells, when confronted with antibiotics or environmental stress.

Results

Microarray-based characterization of thermotolerance development

In order to characterize the development of thermotolerance in *B. subtilis*, we carried out microarray experiments of cells treated with a lethal heat shock with or without prior priming. A log-phase culture of *B. subtilis* grown at 37°C was divided and either treated with 48°C or left untreated at 37°C. After 15 min, both cultures were transferred to 53°C for another 15 min. Total RNA from all samples was prepared and analysed by microarrays directly comparing the four different conditions (Fig. 1A).

Transcriptional changes important for thermotolerance could be recognized in array 4 that compared primed (48–53°C) and non-primed (37–53°C) cells at 53°C (Fig. 1B, Tables S2 and S3). The transcripts of 334 genes were more than twofold differentially expressed. A significant portion of these differentially regulated genes are known to be under SigB (88 with 87 up-regulated, according to SubtiWiki (Michna *et al.*, 2016)) or Spx (79 with 55 up- and 24 down-regulated, as defined in previous studies (Nakano *et al.*, 2003a; Rochat *et al.*, 2012), including direct and indirect regulation control. In addition, many of the most down-regulated genes are also known to be under the control of stringent response mediated transcriptional down-regulation upon amino acid starvation (Eymann *et al.*, 2002; Kriel *et al.*, 2012; Hauryliuk *et al.*, 2015) (Fig. 1B, Tables S1–S3).

For the mild heat shock condition (37°C vs 48°C; array 3), we observed 529 genes which appear to be

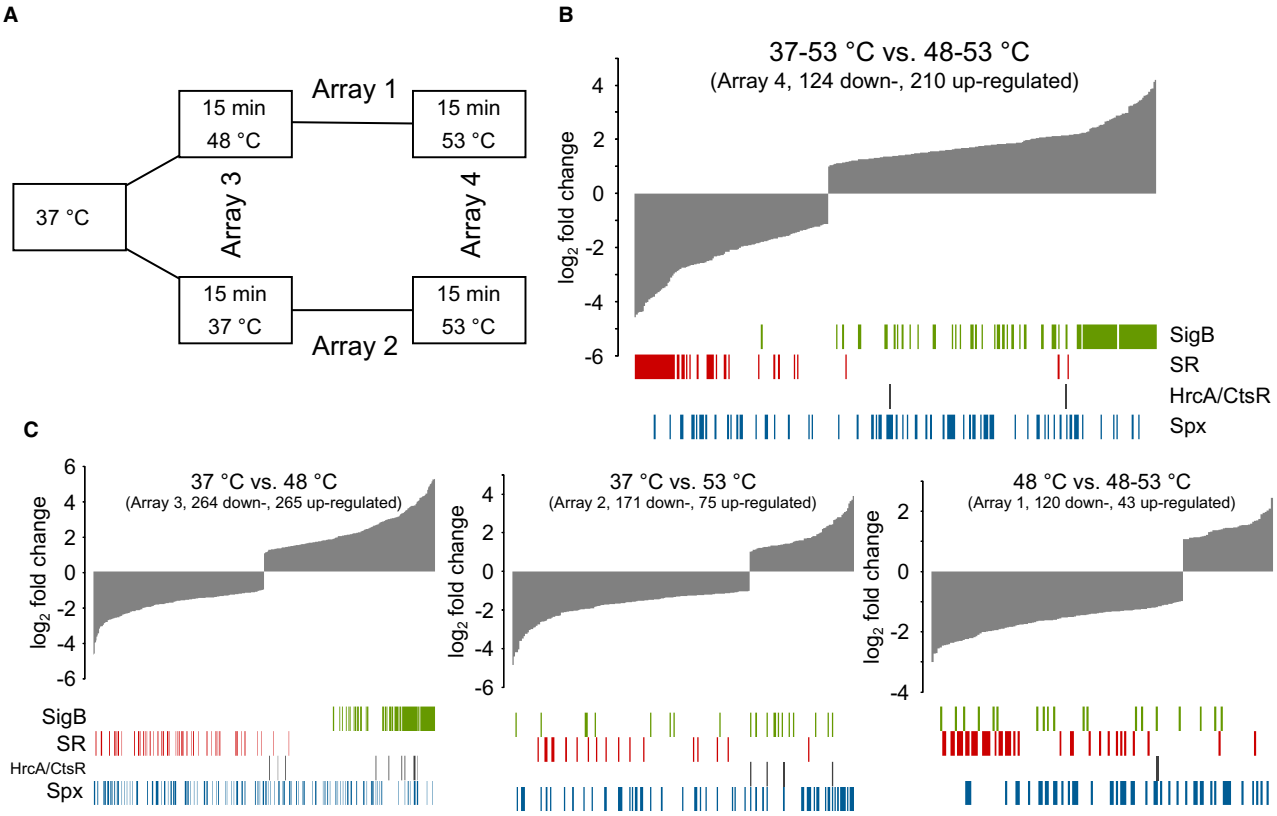

Fig. 1. Differentially regulated genes during thermotolerance.
A. Schematic representation of the thermotolerance protocol and the analysed microarrays.
B. The distribution of regulated genes in Array 4 (37–53°C vs. 48–53°C). Bar tracks indicate the number and distribution of genes of the σ^B regulon (SigB), regulated by the stringent response (SR), the HrcA and CtsR regulons (HrcA/CtsR) or the Spx regulon (Spx) as defined by (Nakano et al., 2003a; Rochat et al., 2012),
C. The distribution of arrays 1–3, representing the conditions 37°C vs. 48°C, 37°C vs. 53°C or 48°C vs. 48–53°C and bars representing the respective regulons with abbreviations as above. [Colour figure can be viewed at wileyonlinelibrary.com]

differentially regulated more than twofold. This set of genes partially overlapped with the set obtained from array 4 (Fig. 1C). Consistent with previous reports, we noticed an extensive up-regulation of genes controlled by the heat-shock regulators HrcA and CtsR as well as many genes of the general stress response regulon controlled by SigB (116 genes), (Helmann *et al*., 2001) (array 3; Fig. 1C). However, we observed relatively little additional induction for most of these genes in the microarray comparing 48°C vs 48–53°C, suggesting that these regulons were already fully induced at 48°C with little potential for further adjustments upon more severe stress conditions (Array 1; Fig. 1C).

Moreover, array 2 (37–53°C) displayed a lower induction of heat shock genes controlled by HrcA, CtsR or SigB than array 2 (37–48°C). The applied lethal heat shock conditions (Völker *et al*., 1999; Runde *et al*., 2014) most likely also contributed to the diminished ability of the cells to efficiently change their gene expression. Nevertheless, a significant number of Spx-controlled genes were differentially transcribed under these conditions.

Spx had emerged from these experiments as an important heat shock regulator (Runde *et al*., 2014), since a substantial fraction of previously identified Spx-regulated genes was observed in all investigated thermotolerance conditions (Fig. 1) (Nakano *et al*., 2003a; Rochat *et al*., 2012). While the regulons of SigB, HrcA and CtsR were almost exclusively up-regulated, the Spx regulon differed markedly from this pattern of transcriptional changes, since it exhibited both up- and down-regulation which appeared mostly equally distributed in all tested conditions (Fig. 1B and C, Tables S1 and S2). Interestingly, a Δ*spx* strain exhibited the most severe thermosensitivity phenotype assessed by growth on plates at 55°C compared to the also strongly impaired Δ*sigB* mutant strain, while both Δ*hrcA* or Δ*ctsR* were not strongly affected (Fig. S1A). In addition, Δ*sigB*, Δ*hrcA* or Δ*ctsR* strains were much less affected in thermotolerance development (Fig. S1B) compared to the previously investigated Δ*spx* (Runde *et al*., 2014), corroborating an apparent difference in the role of these heat shock transcription factors.

Taken together with our previous results showing a strong impact of Spx on the development of thermotolerance (Runde *et al*., 2014), these findings (Figs. 1 and S1, Table S1) further establish Spx as an important stress response regulator intricately involved in heat stress response.

Transcriptional changes of ΔclpX vs ΔclpX Δspx mutant that mediate thermotolerance controlled by Spx

To understand the role of Spx in thermotolerance development and the previously observed heat-resistant phenotype of the Δ*clpX* mutant strain in more detail (Runde *et al*., 2014), we carried out microarray experiments comparing Δ*clpX* vs Δ*clpX* Δ*spx* mutant cells in the absence of stress at 37°C (Fig. 2). Since Spx is stabilized in cells lacking ClpX, we compare in this experiment the transcriptome of cells containing raised Spx levels, with cells lacking Spx, allowing to track the contributions of Spx on changes in the transcriptome (Nakano *et al*., 2002b; Runde *et al*., 2014).

In total, we observed 378 differentially transcribed genes (>2-fold change, 201 up-regulated, 177 down-regulated, Fig. 2A, Table S4) in this experiment. Besides up-regulated genes encoding proteins with unknown functions, there were many up-regulated genes encoding proteins of the general and oxidative stress response, in accordance with previous observations (Nakano *et al*., 2003a; Rochat *et al*., 2012) (Fig. 2A). Notably, this included the thioredoxin-system (*trxAB*), superoxide dismutase (*sodF*) and genes required for the synthesis of bacillithiol (*bsaA, bshB2*) but also genes of the heat-shock response (*clpC*, *htpG*, *ytvA*, *lonA*). Furthermore, we noticed the up-regulation of genes that mediate resistance against heavy metals (*cadA*, *copA*) or antibiotics (*ycbJ*, *ybxI*). Some of these genes were previously described to be regulated by Spx, but other transcripts were not yet known to be Spx-regulated (Table S4) (Gaidenko *et al*., 2006; Rochat *et al*., 2012; Gaballa *et al*., 2013). Down-regulated transcription units were enriched in genes required for motility, translation or stringent response (see below) and genes of prophages (PBSX- and SPβ-prophages) (Rochat *et al*., 2012; Molière *et al*., 2016).

We observed a large overlap when comparing the regulated genes of the Δ*clpX* vs Δ*clpX* Δ*spx* microarray with Spx-regulated genes identified in (Nakano *et al*., 2003a; Rochat *et al*., 2012) (Fig. 2A, blue bars denoted 'Spx', 114 out of 378 genes). As expected, we also observed a strong overlap with the regulated genes of the heat-shock arrays (overlap with array 3: 100 genes; array 4: 93 genes, Fig. 2A) and observed a good correlation of up- and down-regulated transcripts between these datasets.

We confirmed the Spx-dependent regulation of selected genes in Δ*clpX* and Δ*clpX*Δ*spx* mutants by northern blotting (Fig. S2). However, since a Δ*clpX* deletion strain displays a considerable growth defect and a pleiotropic phenotype with both Spx dependent and independent regulated traits (Elsholz *et al*., 2017), we aimed to confirm the Spx-dependent regulation of selected genes in independent experiments by RT-qPCR (Fig. 2B–D). Therefore, we utilized the conditional induction of the stabilized Spx^{DD} variant at 37°C in the absence of stress (Fig. 2B). In a second approach, we treated wild-type or Δ*spx* mutant cells with a mild heat-shock at 50°C for 15 min, which is not yet lethal to the heat-sensitive Δ*spx* mutant strain (Fig. 2C–E). Thereby, we could confirm the Spx-dependent regulation of *trxB*, *hslO* and *ytvA*, as described

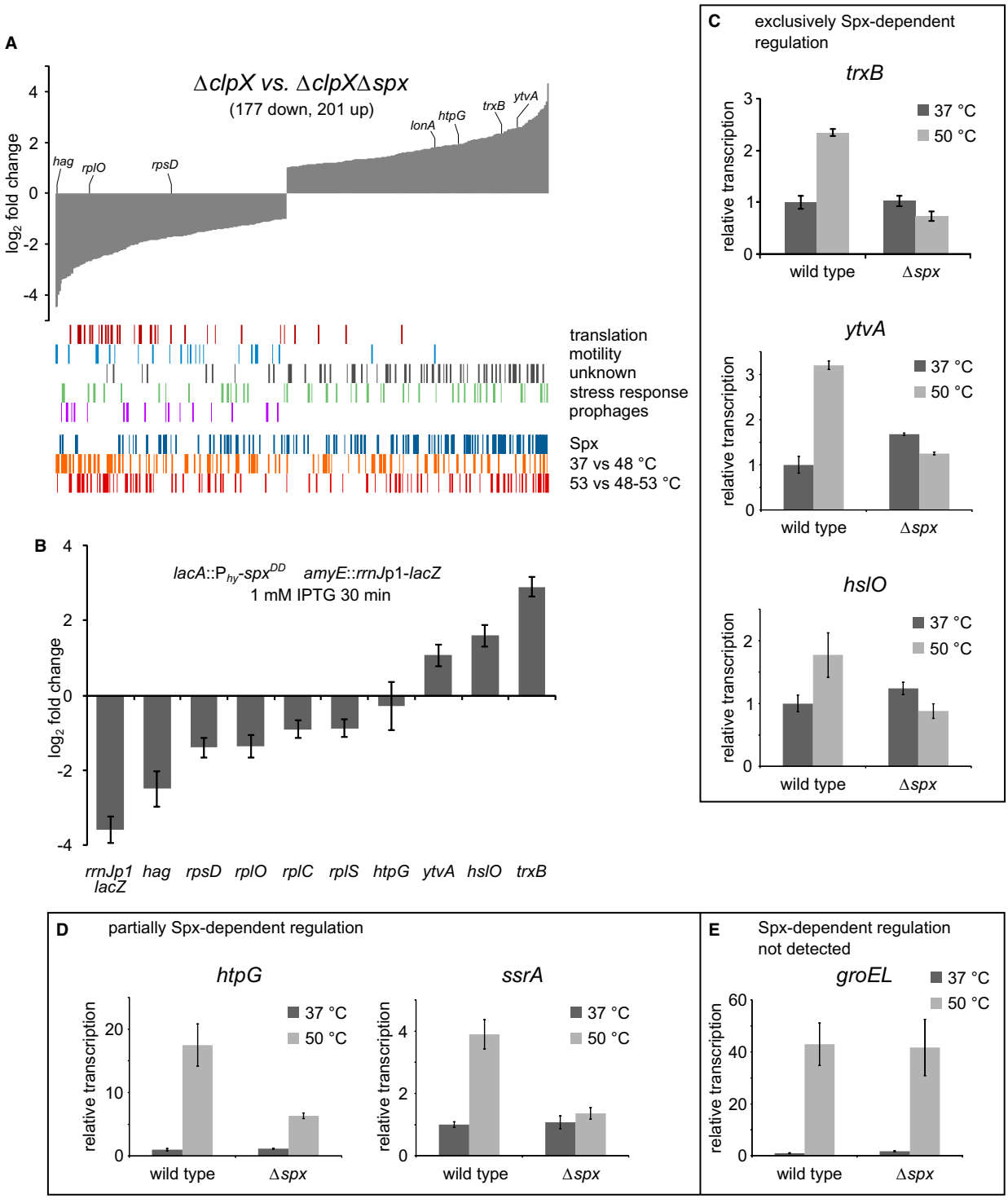

Fig. 2. Transcriptional changes mediated by Spx-accumulation under stress and non-stress conditions.
A. Differentially regulated genes of the Δ*clpX* vs. Δ*clpX*Δ*spx* microarray. Bar tracks indicate the number and distribution of regulated genes of the respective functional group (translation, motility, unknown, stress response, prophages), the overlap with the Spx-regulon (Spx) as defined by (Nakano *et al*., 2003a; Rochat *et al*., 2012) and the overlap with the arrays 3 and 4.
B. Changes in relative transcription of selected targets after treatment of a culture of P_{hy}-spx^{DD} cells (BHS225) with or without 1 mM IPTG for 30 min (to induce Spx^{DD}) as determined by RT-qPCR. Means and standard errors of three biological replicates are shown.
C–E. Relative expression changes after application of heat stress as determined by RT-qPCR. Means and standard errors of three biological replicates are shown. All strains carried *rrnJ* P1 *-lacZ* in the *amyE* site. Log-phase cultures of wild-type *rrnJ* P1-*lacZ* (BHS220) or Δ*spx rrnJ* P1-*lacZ* (BHS222) were divided and incubated at 37°C or 50°C for 15 min, then harvested. [Colour figure can be viewed at wileyonlinelibrary.com]

earlier (Nakano *et al*., 2003a; Rochat *et al*., 2012) (Fig. 2B) and observed that their heat-induced expression is completely dependent on Spx (Fig. 2C). Interestingly, *htpG*, encoding a HSP90 homolog, was up-regulated by Spx in the Δ*clpX* vs Δ*clpX* Δ*spx* microarray experiment (Table S4). It was previously observed that Spx in complex with RNAP binds to the promoter region of *htpG*, but no Spx-dependent regulation was detected (Rochat *et al*., 2012). While an up-regulation of this locus upon expression of Spx^{DD} was not observed (Fig. 2B), we noticed a clear reduction in its heat-induced expression in the Δ*spx B. subtilis* strain (Fig. 2D). These observations suggest a partial, but not exclusive Spx-dependent heat regulation of *htpG* transcription (Schulz and Schumann, 1996; Versteeg *et al*., 2003). Similar Spx-binding sites were also reported for other heat shock loci, such as *smpB-ssrA* and *groES-groEL* transcription units (Rochat *et al*., 2012). We could confirm a Spx-dependent induction of the *ssrA* gene transcription at elevated temperature but observed no Spx-dependent heat regulation of the *groEL* locus (Fig. 2D and E). Overall, we observed a strong up-regulation of genes required for stress response and down-regulation of genes active during vegetative growth.

Spx down-regulates ribosomal promoters in vivo

Interestingly, we found the majority of r-proteins to be strongly down-regulated by Spx in the Δ*clpX* vs Δ*clpX* Δ*spx* dataset (26 of 55 CDS down-regulated, with the exception of *rpmEB* being up-regulated, Fig. 3A). In addition, genes encoding subunits of RNAP (*rpoA, rpoC*) or with functions in translation elongation (*lepA*) or secretion (*secY*) were also found to be down-regulated, while genes required for rRNA and tRNA maturation (*trmB, mrnC, cspR*) were up-regulated. The same pattern of strongly down-regulated genes for ribosomal proteins and other translation related genes associated with stringent response could be clearly observed for the thermotolerance array (Array 4 Fig. 1B, Tables S1–S3).

A similar down-regulation of r-proteins and other genes associated with the RelA-dependent stringent response (Eymann *et al*., 2002) was observed for *B. subtilis* cells exposed to various stress conditions where Spx could be activated and involved in the response (Leichert *et al*., 2003; Mostertz *et al*., 2004; Rochat *et al*., 2012). Interestingly, the additional ChIP–chip experiments by

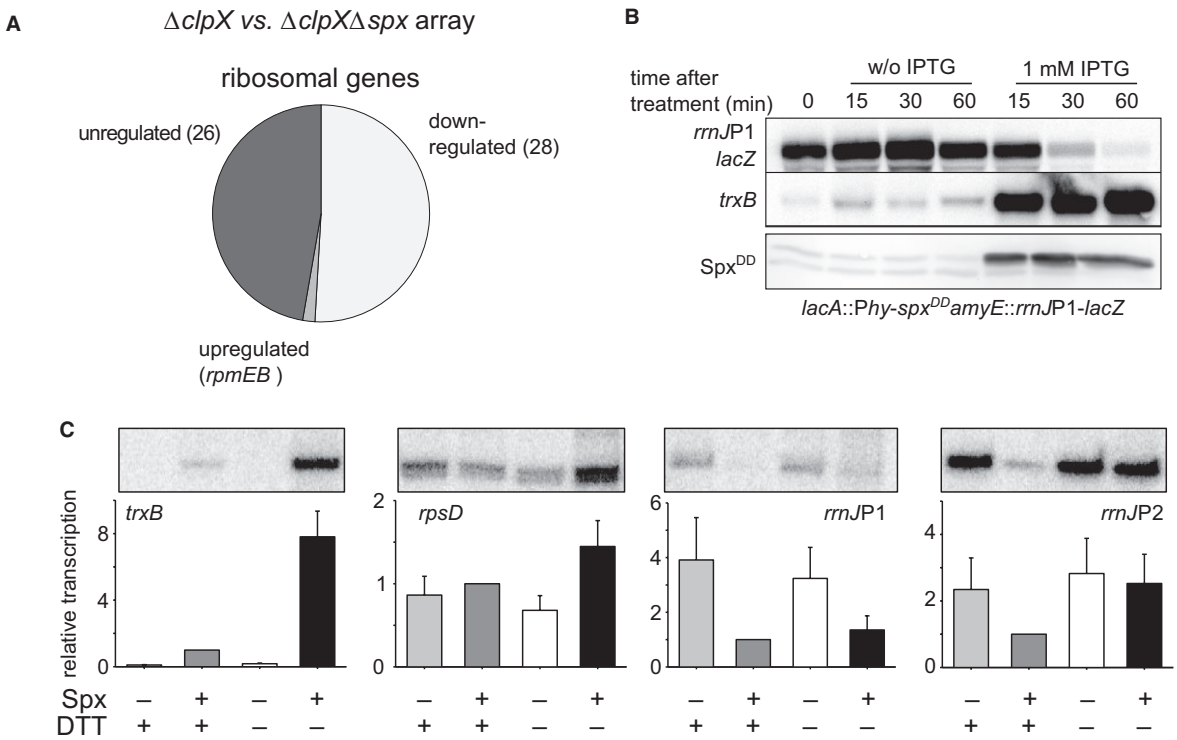

Fig. 3. Spx down-regulates transcription of ribosomal promoters *in vivo* and *in vitro*.
A. The fraction of ribosomal genes differentially regulated by Spx in the Δ*clpX* vs. Δ*clpX*Δ*spx* microarray.
B. Northern blots (*rrnJ* P1 -*lacZ*, *trxB*) and western blot (α-Spx). A mid-log culture (OD_{600} of 0.3–0.35) of BHS225 cells was divided and treated with or without 1 mM IPTG. Samples were withdrawn at the time points indicated and 2 μg total RNA or 10 μg total protein per lane were subjected to northern or western blotting.
C. *In vitro* transcription assays with *B. subtilis* RNA polymerase with or without Spx and/or dithiothreitol (DTT). The transcription rate with Spx and DTT was set to 1. Means and standard deviations of four replicates and a representative experiment are shown.

Rochat *et al.* suggest that the complex of Spx and RNAP specifically interacts with binding sites in front of the promotor regions of the *rrn* operons and other genes important for translation (such as, e.g. *rplC*, *secY*, *ssrA*, *ffh*) (Rochat *et al.*, 2012).

These observations strongly suggested that Spx may contribute to regulation of these genes. Therefore, we went on to investigate in more detail the possible role of Spx in the repression of rRNA and other translation-related genes.

In order to assess the effect of Spx on rRNA expression, we combined an array of strains carrying transcriptional *rrn-gfp* fusions in the *amyE* site (Rosenberg *et al.*, 2012) with an IPTG-inducible copy of spx^{DD} in the *lacA* site (Fig. S3A). Northern blot experiments revealed that the transcription from all tested promoters was repressed by the induction of spx^{DD} with 1 mM IPTG for 30 min (Fig. S4). Subsequently, we selected the *rrnJ-rrnW* operon as our model system. We constructed a transcriptional fusion of a 132 bp fragment carrying *rrnJ* P1, the first of the two promoters of the *rrnJ-rrnW* transcription unit (Koga *et al.*, 2006; Natori *et al.*, 2009), to the *lacZ* reporter gene (Fig. S3B, see Materials and Methods). Northern blot experiments revealed that the activity of the *rrnJ* P1 promoter was strongly decreased shortly after the induction of Spx^{DD} by the addition of IPTG. As expected, the addition of IPTG also resulted in a strong increase in the *trxB* control mRNA and an accumulation of the Spx protein, as revealed by western blotting (Fig. 3B). RT-qPCR experiments using the same strain confirmed that, after 30 min of treatment with IPTG, the transcription of the *lacZ* gene from the *rrnJ* P1 promoter and the selected transcripts of rRNA genes were strongly down-regulated. (Fig. 2B). Taken together, these results suggest that the observed down-regulation of ribosomal genes can be directly or indirectly caused by the activity of Spx.

Spx down-regulates rrnJ P1 in vitro

In order to confirm the observed *in vivo* down-regulation of the *rrnJ* P1 promoter and to assess whether this inhibition can be directly caused by Spx or requires another factor, *in vitro* transcription experiments using *B. subtilis* RNAP were carried out with either reduced (+DTT) or oxidized (–DTT) Spx (Fig. 3C). The results demonstrated that transcription from *rrnJ* P1 was inhibited upon Spx addition regardless of its oxidation state. Interestingly, transcription of *rrnJ* P2 was inhibited only by the reduced (+DTT) but not by oxidized Spx (–DTT). Transcription from the *rpsD* promoter was not strongly affected by Spx while transcription of the *trxB* promoter was significantly stimulated by oxidized Spx, as described previously (Nakano *et al.*, 2005; Rochat *et al.*, 2012). From these experiments, we conclude that Spx can directly act on the ribosomal promoters *rrnJ* P1 and *rrnJ* P2 and inhibit their transcription without the need for additional factors.

Spx-RpoA interaction and the influence of specific upstream sequences (UP-elements) are crucial for Spx-dependent regulation of the RNAP

The promoters of the *rrn* operons are well-conserved but do not contain the Spx binding motif (-45-AGCA-42) (Helmann, 1995; Reyes and Zuber, 2008; Nakano *et al.*, 2010; Rochat *et al.*, 2012). However, transcription from the *rrn*-promoters in *B. subtilis* is stimulated by contacts of α-CTD with AT-rich upstream sequences (UP-elements) (Ross *et al.*, 1993; Rao *et al.*, 1994; Krásný and Gourse, 2004; Murayama *et al.*, 2015). As the transcriptional regulation by Spx depends on its interaction with α-CTD, it was suggested that the Spx/α-CTD complex could recognize promoters by interaction with sequence motifs associated with the UP-element upstream of the core promoter (Reyes and Zuber, 2008; Nakano *et al.*, 2010). Therefore, we hypothesized that regulatory upstream sequence motifs associated with the UP-elements of *rrn*-promoters could also be required for the observed Spx-dependent transcriptional down-regulation.

To test whether there are any sequence-specific determinants for Spx-dependent repression within the upstream regulatory elements, we constructed a series of transcriptional promoter-*lacZ* fusions, each comprising the 41 bp *rrnJ* P1 core promoter and upstream sequences of variable-length. In addition, a 22 nt GC-rich sequence that is not recognized by α-CTD (denoted 'SUB' sequence, (Rao *et al.*, 1994)) and a 22 nt sequence upstream of the P_{trxB} promoter were fused to the same core promoter sequence as well (Fig. 4A). The influence of Spx^{DD} synthesis, induced *in trans*, on the *in vivo* transcription from these promoters was assessed by northern blotting and RT-qPCR (Fig. 4B and C).

In the absence of the inducer IPTG, the shorter fragments (61 nt or 41 nt) with truncated upstream elements showed a decreased promoter activity compared to the 110 nt fragment with the longest upstream region and the fusion of the SUB sequence further diminished the promoter activity (Fig. 4B and C), consistent with previous reports (Rao *et al.*, 1994; Krásný and Gourse, 2004). Upon induction of Spx^{DD}, the activity of all promoter fragments was decreased, but the magnitude of repression differed between the tested fragments. For the 110 nt fragment, the promoter activity decreased about 6–7 times, whereas for the 61 nt- or 41 nt fragments, the reduction of promoter activity was about 4–6 and 2–3 times respectively. This deletion analysis suggested a direct influence of the upstream elements on the Spx-dependent down-regulation.

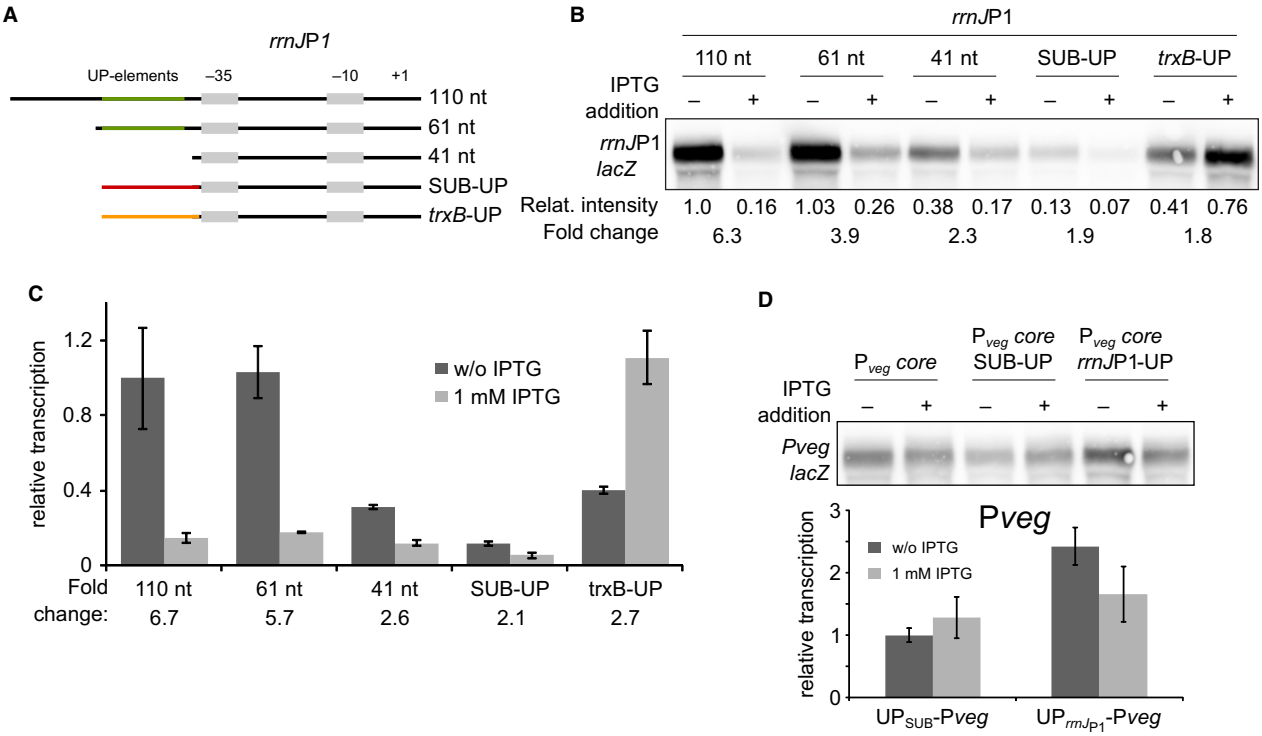

Fig. 4. UP elements are important for Spx-mediated up- and down-regulation.
A. Schematic drawing of the different *rrnJ* P1 variants with truncated or replaced upstream sequences.
B. Northern blot of BHS807 (110 nt), BHS516 (61 nt), BHS517 (41 nt), BHS601 (SUB-UP) or BHS602 (*trxB*-UP) cells treated with or without 1 mM IPTG for 30 min to induce Spx^{DD}. Relative band intensities were calculated using ImageJ, Ratios indicate the absolute value of fold change.
C. Relative transcription of *lacZ* in a similar but independent experiment as panel B. Means and standard errors of two biological replicates are shown. Ratios indicate the absolute value of fold change.
D. Northern blot of BHS573 (P*veg-lacZ*) BHS668 (SUB-P*veg-lacZ*) and BHS669 (*rrnJ* P1 UP-P*veg-lacZ*) cells treated with or without 1 mM IPTG for 30 min and relative transcription of *lacZ* in a similar but independent experiment as determined by RT-qPCR. Means and standard errors of two biological replicates are shown. [Colour figure can be viewed at wileyonlinelibrary.com]

Replacement of the upstream elements with the SUB sequence, which is not acting as an UP-element (Rao *et al.*, 1994), significantly decreased the promoter activity. However, the promoter was still repressed about two times when Spx^{DD} was synthesized *in trans* (Fig. 4B and C). This suggested that features of the core promoter might also influence the Spx-mediated down-regulation. Another possibility could be that Spx can recognize sequences within the GC-rich SUB element. However, when we fused the upstream sequences of P_{trxB} that carries known binding sites for Spx (Reyes and Zuber, 2008; Nakano *et al.*, 2010), the basal activity of the *rrnJ* P1 core promoter was significantly increased about three times and the transcript level was further raised about 2–3 times upon induction of Spx^{DD} synthesis (Fig. 4B and C), emphasizing the role of the upstream sequences for alpha-subunit-dependent activation together with Spx.

To confirm our findings, we fused the upstream elements of *rrnJ* P1 as well as the SUB sequence to the P_{veg} promoter. This promoter was previously shown to be constitutively active (Fukushima *et al.*, 2003; Sojka *et al.*, 2011; Nicolas *et al.*, 2012; Radeck *et al.*, 2013). The activity of the P_{veg} core promoter alone and the promoter with the SUB element was unchanged upon induction of Spx^{DD} synthesis (Fig. 4D). However, when the upstream sequence of the *rrnJ* P1 promoter was fused to the P_{veg} core promoter, a higher transcript level was observed, consistent with the finding that these upstream elements, containing the UP-elements, can stimulate promoter activity. Importantly, this promoter construct was sensitive to Spx and was down-regulated upon induction of Spx^{DD} synthesis, although to a lesser extent than observed for the *rrnJ* P1 promoter (Fig. 4B and C). We also confirmed by RT-qPCR measurements that the transcription of P_{veg} fused to the SUB element was not regulated by Spx^{DD} induction while P_{veg} fused to the UP-element of *rrnJ* P1 was down-regulated by Spx^{DD} (Fig. 4D).

Taken together, these experiments indicate that sequence elements upstream of the core promoter are a key factor for both positive and negative modulation of promoter activity by Spx in conjunction with the alpha

subunit of RNAP. Nevertheless, the properties of the *rrnJ* P1 core promoter also appear to influence the Spx-dependent down-regulation.

The positive and negative influence of Spx on transcription can be separated by a mutation in the alpha subunit of the RNAP

To gain insights into the mechanism of the Spx^{DD}-dependent down-regulation of *rrnJ* P1 we introduced the previously described point mutants *rpoA*Y263C or *rpoA*V260A (*cxs*-1 or *cxs*-2) into the *rpoA* gene of the *rrnJ* P1-*lacZ* reporter strain. Both mutations change the interaction surface of α-CTD with Spx and suppress the detrimental effects of Spx accumulation on growth by disturbing the interaction α-CTD-Spx required for the activity of Spx (Nakano *et al*., 2000; Nakano *et al*., 2003b). Northern blot experiments revealed that the negative regulatory impact of Spx^{DD} induction is completely suppressed in the *cxs*-1 background and almost completely suppressed in the *cxs*-2 background (Fig. 5A). This finding is in agreement with the previous reports that both mutations suppress any activity of Spx on gene expression (Nakano *et al*., 2000; Nakano *et al*., 2003b). Interestingly, only the *rpoA*Y263C (*cxs*-1) variant also abolished transcription of *trxB*. In contrast, *trxB* transcription was still activated by Spx^{DD} induction similarly to the wild-type in cells carrying the *rpoA*V260A (*cxs*-2) variant (Fig. 5A).

These experiments support the hypothesis that the tested ribosomal promoter is directly down-regulated by a repressor activity of Spx while interacting with the α-subunit. This activity is distinct from its previously described functions for (1) transcriptional repression by interfering with transcriptional activators (Nakano *et al*., 2003b) or its second observed function as (2) direct activator of the thiol stress response (Nakano *et al*., 2003a). Since both mutations (*cxs*-1 and 2) also restore growth (Fig. S6B) and viability of cells carrying P_{hy}-spx^{DD} on agar plates supplemented with IPTG (Fig. 5B), we assume that the inhibitory effects of Spx accumulation on growth could be caused rather by the depletion of rRNA than by Spx-dependent induction of the synthesis of a toxic factor, such as a toxin-antitoxin system.

Down-regulation of rrnJ P1 and r-proteins can occur in vivo in the absence of Spx

Next, we wished to determine to what extent Spx contributes to downregulation of rRNA genes during heat stress. Therefore, we analysed the transcriptional response of *rrnJ* P1 to heat stress in wild-type and Δ*spx* cells (Fig. 6A). Upon a temperature upshift from 37 to 50°C we noticed a pronounced down-regulation of *rrnJ* P1. Surprisingly, a comparable downshift was observed also in the Δ*spx* mutant. We observed this Spx-independent down-regulation of rRNA genes also during oxidative and cell wall stress (Fig. S5A and C).

Hence, we asked whether another protein might function similarly to, and substitute for, Spx in the cell. Indeed, *B. subtilis* possesses a paralog of Spx, MgsR, which modulates the expression of a sub-regulon of the general stress response controlled by σ^B. Given the high sequence similarity between MgsR and Spx, MgsR may have a similar negative regulatory activity on ribosomal promoters as observed for Spx and might be able to complement a deletion of *spx* in this regard. To test this hypothesis, we constructed and assessed the influence of Δ*mgsR* and Δ*spx* Δ*mgsR* deletion strains on heat-mediated *rrnJ* P1 transcriptional down regulation. However, despite a slightly increased transcription rate during non-stress conditions in strains with the Δ*mgsR* background, we still observed the down-regulation of *rrnJ* P1 and r-protein genes in the double deletion strain during heat stress (Fig. S5B).

Thus, we confirmed the transcriptional down-regulation of rRNA and r-proteins during severe stress conditions. However, a deletion of *spx* and/or its paralog *mgsR* did not significantly affect this down-regulation, suggesting that the Spx-dependent downregulation of rRNA expression may play a role under different conditions.

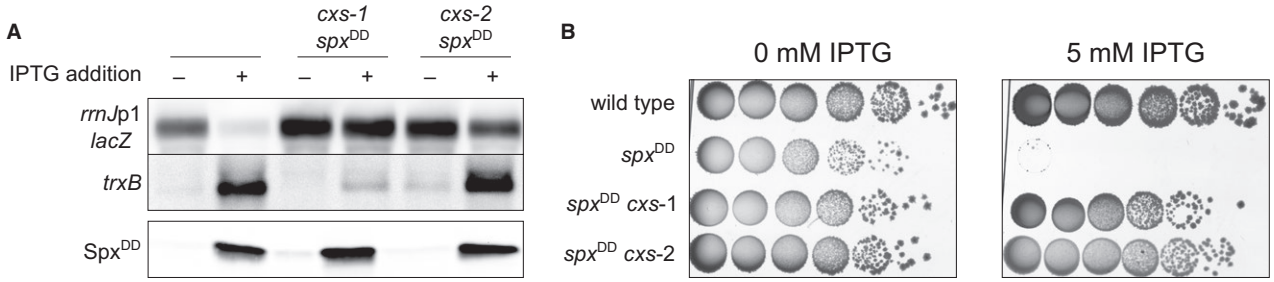

Fig. 5. The impact of *cxs* mutations in *rpoA* on Spx-mediated transcriptional regulation.
A. Northern blot (*rrnJ* P1-*lacZ, trxB*) and western blot (α-Spx) of BHS225, BHS729 and BHS730 cells. Mid-log cultures were divided and treated with or without 1 mM IPTG for 30 min. 2 µg total RNA or 10 µg protein per lane were analysed.
B. Serial dilutions of *B. subtilis* wild type, BHS225, BHS729 or BHS730 cells spotted on agar plates without (left) or with 5 mM IPTG (right).

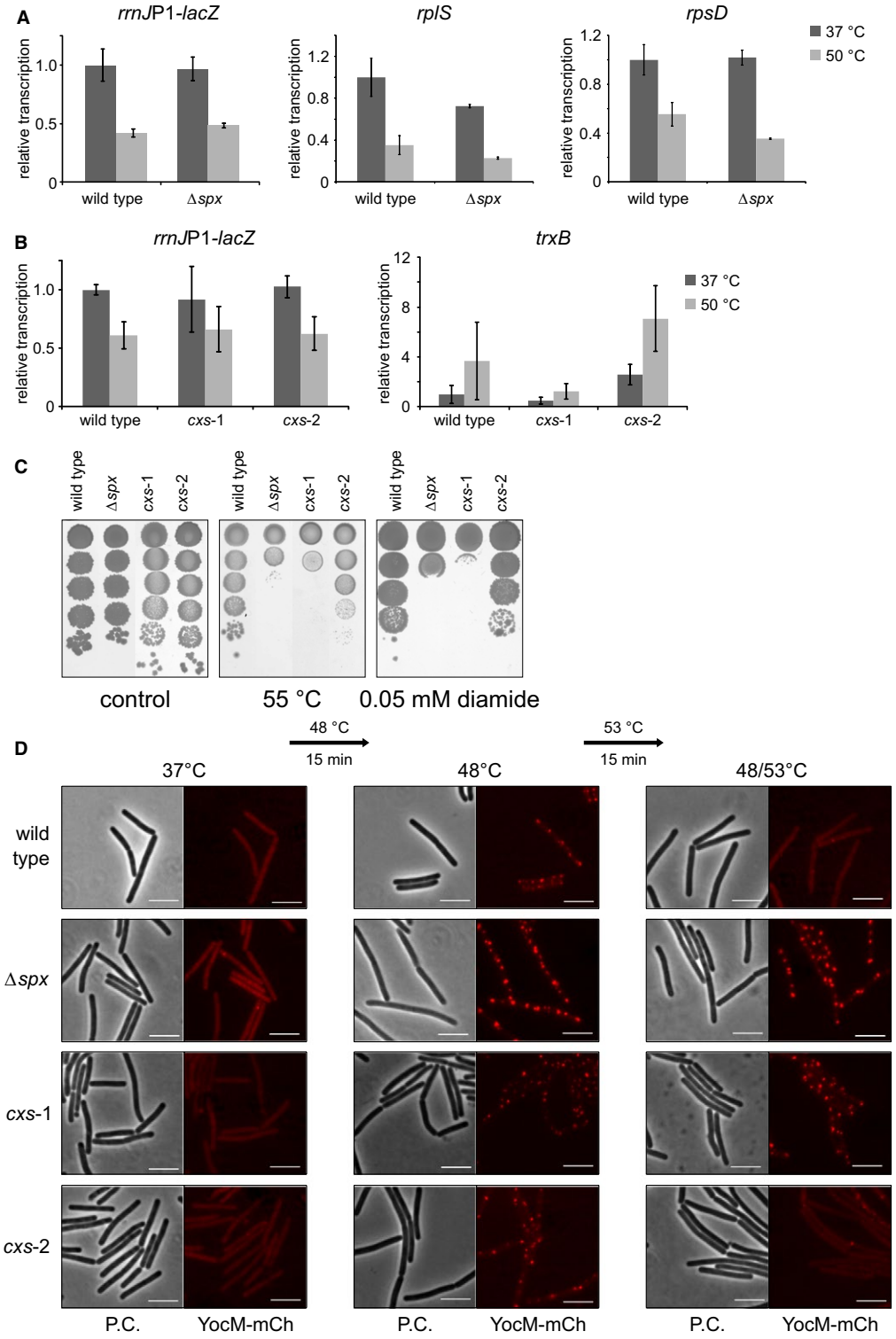

Fig. 6. Up-regulation of stress response-genes but not down-regulation of rRNA contributes to survival of stress.
A, B. Relative expression changes after application of heat stress as determined by RT-qPCR. Means and standard errors of three biological replicates are shown. All strains carried *rrnJ* P1-*lacZ* in the *amyE* site. Log-phase cultures of BHS220 (wild-type *rrnJ* P1-*lacZ*), BHS222 (Δ*spx*), BHS549 (*cxs*-1) and BHS550 (*cxs*-2) were divided and incubated at 37°C or 50°C for 15 min, then harvested.
C. Growth of wild type, Δ*spx* (BNM111), *cxs*-1 (BHS475) or *cxs*-2 cells (BHS476) on agar plates incubated ON at 37°C, 55°C or supplemented with 0.05 mM diamide and incubated at 37°C.
D. Subcellular protein aggregation of wild type, Δ*spx*, *cxs*-1 or *cxs*-2 cells carrying a YocM-mCherry fusion after heat shock. Scale bars are 5 μm. Phase contrast images (P.C.) and fluorescence images with RFP-filters (YocM-mCherry) are shown. [Colour figure can be viewed at wileyonlinelibrary.com]

Up-regulation of stress-response genes and not down-regulation of rRNA is the important activity for Spx-mediated thermoresistance in vivo

As Spx appeared to be dispensable for the stress-mediated down-regulation of rRNA genes, we explored the roles of the *cxs*-1 (Y263C) and *cxs*-2 (V260A) mutants in stress resistance and survival. We observed the strong down-regulation of *rrnJ* P1 upon heat shock, independent of Spx and regardless of the *rpoA* point mutations in the strain background (Fig. 6A and B). However, in line with the observation from Fig. 5A, the heat-induced transcription of *trxB* was abolished in the *cxs*-1 mutant (Y263C), but not in the *cxs*-2 mutant (V260A). We assayed the growth of wild-type and *rpoA* mutant cells on agar plates incubated at high temperatures or supplemented with diamide, a strong oxidizing agent (Fig. 6C). Both the Δ*spx* and the *cxs*-1 mutant exhibited a high sensitivity to both stress conditions (Nakano *et al.*, 2003a). However, the strain carrying the *cxs*-2 mutation, which still allows the upregulation of the thiol stress response, displayed only slightly reduced growth compared to the wild type under both stress conditions.

Previously, we reported that Spx protects the cells from heat-induced protein aggregates that can be visualized by fluorescence microscopy (Runde *et al.*, 2014). We developed a tool utilizing *yocM*, a member of the small heat shock proteins in *B. subtilis*, fused to the fluorescent mCherry protein, that localizes to and thus visualizes protein aggregates *in vivo* as similarly demonstrated with the sHsp-GFP fusion from *E. coli* (Lindner *et al.*, 2008; Runde *et al.*, 2014; Hantke *et al.*, 2018). Upon the non-lethal preshock, some protein aggregates were visible as fluorescent foci at the cell poles in all strains, that disappeared during prolonged heat exposure in primed wild-type cells, but not in the Δ*spx* mutant (Fig. 6C) (Runde *et al.*, 2014). Cells carrying the *cxs*-1 mutation displayed a severe protein aggregation phenotype, similar to the Δ*spx* mutant in accordance with the other observations, while cells with the *cxs*-2 mutation accumulated only slightly more protein aggregates than the wild type (Fig. 6C).

From these observations, we infer that up-regulation of stress response-genes is a crucial activity for the protective role of Spx during stress conditions and that a Spx-mediated down-regulation of rRNA is either dispensable under the tested conditions or can be complemented by other redundant different stress response mechanisms active under these conditions.

Spx-levels exhibit heterogeneity during outgrowth from the stationary phase

Finally, the possible different conditions, mentioned in the preceding paragraphs, must entail a high cellular level of Spx as the Spx-dependent inhibition of rRNA promoters was observed either upon overexpression of stabilized Spx^{DD} or in a strain where Spx was stabilized (Δ*clpX*). To identify and search for such conditions where Spx might accumulate either in all cells or in a subpopulation of cells, we investigated the cellular Spx levels during growth and stress response in a population of cells on a single-cell level. For these experiments, we utilized a recently constructed *B. subtilis* strain carrying a translational GFP-Spx fusion that retains the native transcriptional and post-translational regulation (Riley *et al.*, 2018).

We observed that upon heat or cell wall stress all the cells of an exponentially growing cell population synthesized the GFP-Spx fusion in high amounts with a broad but unimodal distribution. We also examined the different growth phases and observed for late stationary phase cells from an over-night culture that a significant number of the population displayed bright fluorescence (Fig. 7). The establishment of the Spx positive subpopulation took place late in stationary phase as Spx positive cells started to appear after 540 min of incubation (Fig. S7). This sub-population of cells with elevated Spx concentration diminished when exponential growth was resumed (time points 90, 120, 180 min in Fig. S7) after dilution into fresh medium (Figs 7 and S7). The increased fluorescence of the subpopulation was not caused by differential autofluorescence of the stationary phase cells (Fig. S7 wild-type cells lacking GFP (PY97)). Furthermore, when we correlated the cell size with the fluorescence signal we observed a strong correlation between small cell sizes, which are typical for non-growing stationary phase cells, and high levels of Spx (Fig. S7). These results suggest that Spx may contribute to the growth arrest of this distinct subpopulation, possibly also by downregulating rRNA expression. This observed heterogeneity of Spx levels in stationary phase cells could represent an additional role of Spx during outgrowth from stationary phase, where the inhibition of growth activity by Spx in these cells might play a role establishing a persister-like phenotype and support the survival of the cell population when confronted with antibiotics or environmental stress (Dubnau and Losick, 2006; Veening *et al.*, 2008; Fridman *et al.*, 2014).

Discussion

We analysed the transcriptome of *B. subtilis* cells during thermotolerance development and observed that Spx, a transcription factor interacting with the alpha-subunit of the RNA polymerase, is a central player orchestrating heat shock response. We characterized a distinct activity of Spx to inhibit transcription from specific promoters of genes related to translation. The concurrent

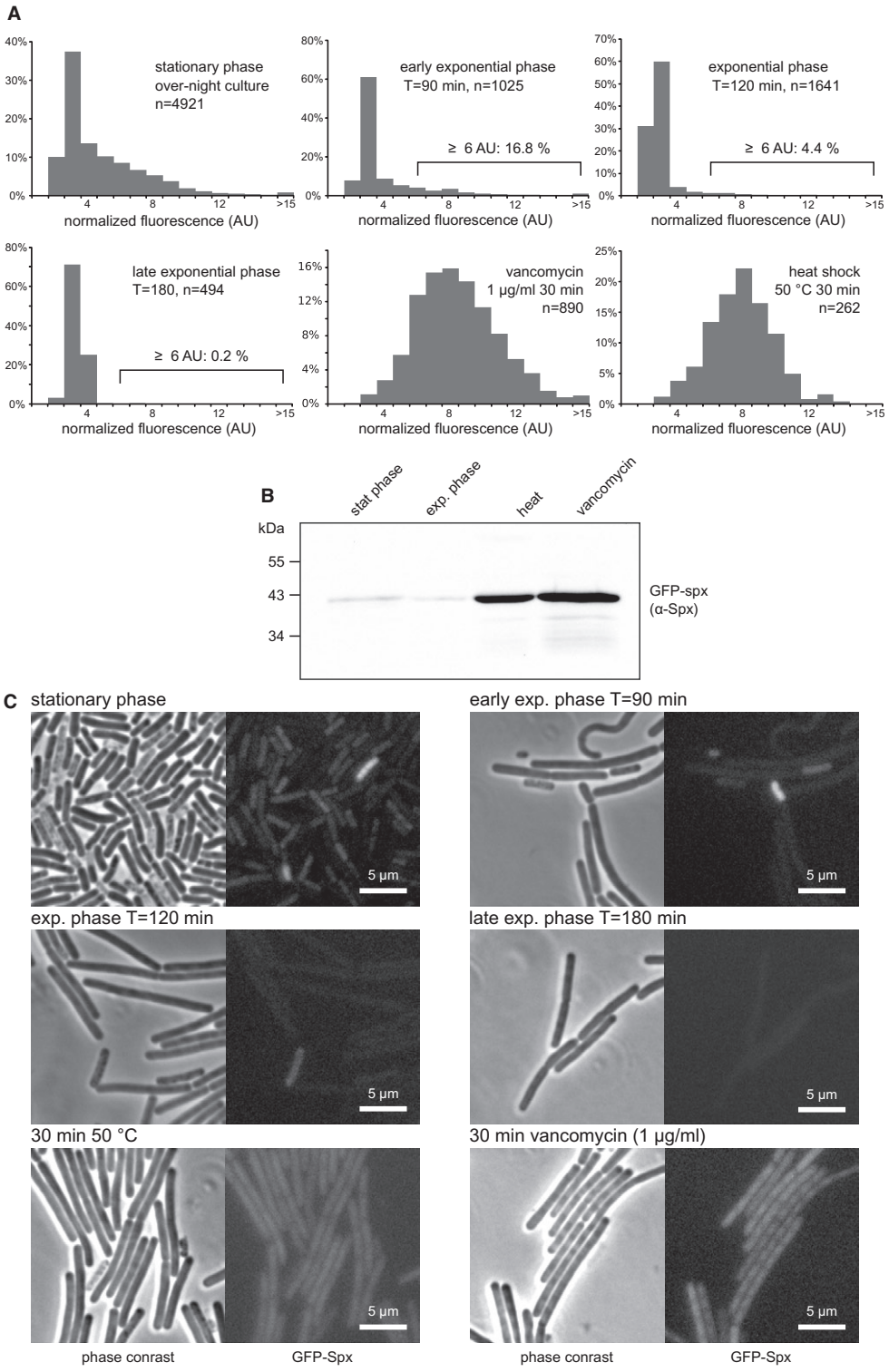

Fig. 7. Spx-activity displays heterogeneity during outgrowth from the stationary phase.
A. Histograms showing the distribution of GFP-Spx fluorescence among N single cells from different growth phases and indicated treatments.
B. Relative levels of GFP-Spx as determined by western blotting.
C. Representative images showing heterogeneous levels of GFP-Spx
in different growth phases or treatments. Scale bars are 5 µm. Phase contrast images (P.C.) and fluorescence images with GFP-filters (GFP-spx) are shown.

downregulation of translation as part of a protein folding stress response would result in a reduction in the metabolic burden accompanying protein repair mediated by the upregulated chaperone systems. However, only the concurrent up-regulation activity of stress genes by Spx is essential for mediating stress response and in a *spx* deletion mutant strain the inhibitory activity could be compensated *in vivo* by other differently acting cellular stress response processes. Nevertheless, the impact of Spx on limiting translation might become important under different conditions.

Thermotolerance development as a concerted process involving multiple regulators

The heat shock response in *B. subtilis* has been divided into different classes, which depend on the activity of different transcription factors such as SigB, and the repressors CtsR and HrcA (Hecker *et al*., 1996). Recently, Spx the transcription factor controlling thiol stress response was also identified as a heat stress sensing transcription factor (Runde *et al*., 2014). Our results (Figs 1 and 2, Tables S1, S2 and S4) and other studies suggest that Spx controls or influences the expression of heat shock proteins such as ClpC, LonA and HtpG as well as tmRNA, general stress proteins (YtkL, YraA, GabD, YfhF, YvgN) or oxidative stress response (TrxA, TrxB) (Nakano *et al*., 2003a; Rochat *et al*., 2012; Runde *et al*., 2014). It further indicates that there exists a considerable overlap between the Spx regulon and the heat shock regulons controlled by CtsR and SigB (Figs 1 and 2). However, although bindings sites for Spx near the promoters of the HrcA-controlled chaperone systems *dnaKJE* and *groESL* were reported, neither we nor others could detect an influence of Spx on the expression of these transcription units in response to heat- (Fig. 2) or oxidative stress (Rochat *et al*., 2012).

Spx-mediated down-regulation of ribosomal promoters

We showed that Spx down-regulates promoters that initiate transcription of rRNA and, to a lesser extent, promoters of ribosomal proteins (Figs 2A and B and 3A and B). This activity could be reconstituted *in vitro* and appears to be partly dependent on the state of the CXXC redox-switch of Spx in a promoter-specific manner (Fig. 3C). The inhibitory effect of Spx on *rrnJ* P1 could be reduced but not completely abolished by substitution of the UP element with a mock sequence (Fig. 4) and reconstituted on an unregulated promoter P_{veg} by fusing the UP element of a regulated promoter (Fig. 4D).

Spx was first described as an 'anti-alpha' factor as it could displace certain transcription factors and thereby interfere with their activity without sequence-specific requirements to the promoter (Nakano *et al*., 2003b). Later it was shown that Spx also has a stimulatory activity on certain promoters, which requires interactions with an upstream sequence motif and is thought to re-position the RNAP for better promoter-recognition (Nakano *et al*., 2003a; Reyes and Zuber, 2008; Nakano *et al*., 2010).

As Spx binds close to the surface of α-CTD, which contacts the upstream UP elements (Gaal *et al*., 1996; Zhang *et al*., 2006; Birch *et al*., 2017), it could act by influencing the recognition and productive interactions of α-CTD with the specific upstream sequences. The strong transcription of rRNA promoters is also dependent on these UP-elements (Fig. 4B and C) (Ross *et al*., 1993; Rao *et al*., 1994). Therefore, accumulation of Spx could lead to a down-regulation of the respective transcription units in a sequence-independent manner similar to the previously observed 'anti-alpha' activity. A specific interaction of Spx with the alpha subunit appears to be very important for the observed repressor activity of Spx, since both *rpoA* mutations *cxs*-1 and *cxs*-2 result in the alleviation of down-regulation of *rrnJ* P1 while cxs-2 can still upregulate the transcription of e.g. *trxB*.

Interestingly, SoxS, the activator of the superoxide stress response in *E. coli*, which shares no homology to Spx, can modulate RNAP holoenzyme activity with a 'pre-recruitment' mechanism by binding the DNA-recognition surface of α-CTD. SoxS then redirects RNAP to promoters that feature a degenerate 'soxbox' upstream of or within the – 35 promoter element (Griffith *et al*., 2002; Martin *et al*., 2002). Concurrently, binding of SoxS to α-CTD renders the complex unable to interact with UP elements, thereby decreasing the strong transcription of the *rrnB* P1 promoter (Shah and Wolf, 2004).

Nevertheless, the interaction and architecture of Spx/α-CTD is different from SoxS, which reprograms the up-element recognition and is therefore not directly applicable for Spx-mediated promoter regulation (Browning and Busby, 2016). A simple model in which Spx interferes like SoxS with the recognition of UP elements by α-CTD might not explain different promoter-specific *in vitro* down-regulation of oxidized or reduced form of Spx on *rrnJ* P1 and *rrnJ* P2 (Fig. 3C) or residual regulation of UP_{SUB}-*rrnJ* P1 *in vivo* (Fig. 4B and C). However, it was demonstrated that the Spx-mediated up-regulation and the sequence specific recognition and binding to promoters for different thiol-stress or redox chaperone genes is controlled by the redox state of the CXXC switch (Nakano *et al*., 2003a; Reyes and Zuber, 2008; Nakano *et al*., 2010; Lin *et al*., 2013). Therefore, it appears that Spx regulates these promoters by a not yet understood mechanism, which might require sequence-specific contact of the Spx-RNAP complex with sequences upstream of or within the core promoter as observed for the up-regulated

promoters. This hypothesis is supported by the observation of Spx-RNAP binding sites in close proximity of *rrn* promoters (Rochat *et al*., 2012).

In addition, it was recently observed that Spx interacts not only with α but also β or β′ subunits of RNAP (Birch *et al*., 2017). Such a more complex interaction or different binding mode of Spx and RNAP might also contribute to the inhibition of transcription at the *rrnJ* P1 promoter. However, mechanistic details are not yet known, and more experiments are required to fully understand the different impacts which Spx can have on RNAP activity at these different promoters. Our results reveal that the ability of the unusual transcription factor Spx to influence the RNAP activity, especially via the alpha subunit is much more versatile than expected.

It should be emphasized that the experiments employing induction of Spx^{DD} synthesis were carried out in the absence of stress. Therefore, we assume that the CxxC redox switch of Spx remains in its reduced state (Nakano *et al*., 2005; Rojas-Tapias and Helmann, 2018a). Interestingly, we observed that both the reduced and oxidized form of Spx were able to down-regulate transcription of *rrnJ* P1, while only the reduced state of Spx could down-regulate transcription of *rrnJ* P2 (Fig. 3C). These experiments suggest that the regulatory activity of Spx on *rrn* promoters might be particularly required during adverse conditions that do not involve oxidative stress.

Significance of down-regulation of ribosomal promoters for stress resistance and survival

During heat and oxidative stress, we and others observed a pronounced down-regulation of genes involved in transcription, translation and protein secretion (Figs 1B and C and 4) (Helmann *et al*., 2001; Price *et al*., 2001; Leichert *et al*., 2003; Mostertz *et al*., 2004; Chi *et al*., 2011; Rochat *et al*., 2012). We showed that Spx down-regulates the respective promoters during non-stress conditions. However, we also observed that this down-regulation occured independently of Spx during heat stress (Fig. 6A and B). Therefore, we conclude that other redundant regulatory stress responsive mechanisms must exist, that mediate the strong repression of these genes during heat or oxidative stress.

Moreover, a point mutation in *rpoA* conferring loss of Spx-mediated repression of *rrn* transcription did not affect survival or protein aggregation during heat stress (Fig. 6C and D). Thus, the up-regulation of genes of the heat and oxidative stress response (Fig. 2) appears to be the crucial activity of Spx for survival and stress resistance, while the negative impact on *rrn* transcription is dispensable for survival (Fig. 6C and D).

We believe that the herein described additional activity of Spx may impose benefits for the *B. subtilis* cell population under stress. Since the majority of total RNA synthesized during fast growth is rRNA, Spx might actively withdraw RNAP holoenzyme from the transcription of rRNA and concurrently re-deploy the complex to promoters of stress-related genes. This strategy could ensure reallocation of RNAP for a fast and efficient transcription of stress response genes during emerging stress. Furthermore, regulation of *rrn* transcription by Spx may become essential under environmental conditions not tested in this work. Finally, down-regulation of rRNA ultimately leads to a depletion of active ribosomes and the total translation capacity which diminishes the burden for protein quality control and reduces the cell growth. This would also provide tolerance to antibiotics and proteotoxic stress conditions.

An important role of Spx in antibiotic resistance especially against antibiotics interfering with cell-wall biosynthesis is already well-established (Luo and Helmann, 2012; Rojas-Tapias and Helmann, 2018a; 2018b) and we could clearly confirm the induction of Spx by vancomycin (Figs 7 and S5C). *B. subtilis* strains where Spx is stabilized due to mutations in *clpX*, *clpP* or *yjbH* are impaired in growth and a longer lag phase after inoculation can be observed. This growth impairment can be relieved by suppressor mutants appearing in *rpoA* (Fig. S6) (Nakano *et al*., 2000; 2003a; Molière *et al*., 2016). The high Spx concentration observed in the heterogenous population of stationary phase cells could also contribute to the growth inhibition of this subpopulation, most likely resulting in a longer lag phase for this sub-population. This is reminiscent of the antibiotic tolerance in type 1 persister cell formation, which could also be influenced by a variation of the lag-phase during outgrowth from the stationary phase (Balaban *et al*., 2004; Fridman *et al*., 2014). It is possible that in *B. subtilis* cell populations Spx is involved in two different processes conferring antibiotic tolerance. First through the Spx mediated stress response signalled by cell-wall stress through application of antibiotics like vancomycin, which affect cell-wall synthesis. Thereby the Spx-mediated upregulation of, e.g., redox-stress response genes might also enable a generally improved stress resistance. In a second process, a higher Spx level of a sub-population of stationary phase cells might facilitate possible persister-cell-like behaviour, which might also contribute to a raised antibiotic resistance of *B. subtilis* cells.

Redundancy in stress signal sensing, transduction and subsequent gene regulation would allow a much more robust cellular stress response. Therefore, we hypothesize, that the negative regulatory activity of Spx on *rrn* promoters may be complemented or superseded by additional stress response systems under these

conditions (Fig. 4A). In previous studies, the observed down-regulation of ribosomal RNA and proteins was frequently attributed to the (p)ppGpp-mediated stringent response. However, despite a considerable number of reports on this topic for *B. subtilis* and other organisms (Hecker *et al.*, 1989; Yang and Ishiguro, 2003; Abranches *et al.*, 2009; Fitzsimmons *et al.*, 2018), persuasive evidence for these hypotheses is scarce and molecular details on the regulation of stress-mediated (p)ppGpp-synthesis is lacking. However, the second messenger-based stringent response could act relatively fast on the protein level by shutting down translation and protecting ribosomes (Beckert *et al.*, 2017). This fast response could very well be complemented by down-regulation of the transcription of translation-related genes through (p)ppGpp induced changes in the GTP concentration (Krásný and Gourse, 2004; Kriel *et al.*, 2012) together with the here described Spx activity. A possible role of (p)ppGpp as a messenger during heat and other stress conditions in *B. subtilis* will have to be addressed in future studies.

Experimental procedures

Growth media and thermotolerance

B. subtilis strains were grown in a water bath at 37°C with orbital shaking at 200 rpm in Lysogeny Broth LB medium (5 g l^{-1} yeast extract, 10 g l^{-1} tryptone-peptone, 10 g l^{-1} NaCl). Belitzky minimal medium (Stülke *et al.*, 1993) supplemented with 0.05% yeast extract was used for experiments where diamide was added to the medium. Thermotolerance development and survival assays were performed as described previously (Runde *et al.*, 2014).

Cloning and strain construction

PCR-amplification using Phusion® high-fidelity polymerase (NEB), cloning using *E. coli* DH5α and transformation of *B. subtilis* 168 was carried out according to standard methods (Spizizen, 1958; Inoue *et al.*, 1990; Sambrook and Russell, 2001). All utilized primers are listed in Table S7. Transformants were selected on agar plates supplemented with 100 µg ml^{-1} ampicillin, 5 µg ml^{-1} chloramphenicol, 1 µg ml^{-1} erythromycin and 25 µg ml^{-1} lincomycin, 10 µg ml^{-1} kanamycin or 100 µg ml^{-1} spectinomycin when appropriate. Correct insertion of integrative plasmids into the *amyE* or *lacA* site was facilitated by digestion with *Sca*I or *Bsa*I and screening for loss of α-amylase activity.

To construct pMAD*hrcA,* flanking regions of *hrcA* were amplified using primers pMADhrcAp1-4, fused by overlap-extension PCR and cloned into the *Bam*HI/*Sal*I sites of pMAD. Transformation of this plasmid into *B. subtilis* 168 and successive recombination yielded BAH42 (Arnaud *et al.*, 2004). pBSIIE-spxDD was generated by amplification of a fragment containing Phy-*spx*^{DD} and *lacI* from pSN56 (Nakano *et al.*, 2003a) using primers p222/p223 and ligation into the *Eco*RI/*Spe*I sites of pBSIIE (Radeck *et al.*, 2013). To construct transcriptional fusions to the *lacZ* reporter gene, the respective promoter fragments were amplified from *B. subtilis* 168 genomic DNA and cloned into pDG268 (Antoniewski *et al.*, 1990). Substituted upstream elements are encoded on the 5' region of the forward-primer. To construct pDG268-Pveg, primer p445 and p446 were annealed in a 1:1 ratio and directly ligated into pDG268 digested with *Hind*III/*Eco*RI. The insert for pDG268-SUB-Pveg was created by annealing and extension of p493 and p494 in a standard PCR reaction without additional template. The insert for pDG268-rrnJ-Pveg was created by annealing and extension of p493 and p495 without additional template and a subsequent PCR reaction with p491 and p493 using the product of the first reaction as template.

The generated and used strains and plasmids are listed in Supplementary Tables S5 and S6.

In vitro transcription

His-tagged Spx was expressed from the plasmid pQE60-*spx* in *E. coli* FI1202 and purified by nickel affinity chromatography as described previously (Runde *et al.*, 2014). Purification of His-tagged *B. subtilis* RNA polymerase and *in vitro* transcription was carried out as described previously (Rochat *et al.*, 2012). Briefly, control promoters P_{trxB}, P_{rpsD} and *rrnJ* P1 P2 were PCR amplified, cloned via EcoRI and HindIII into the p770 vector (Ross *et al.*, 1990). For *in vitro* transcription reactions, plasmid DNA was linearized with EcoRI, and the restriction enzyme was inactivated at 65°C for 15 min. RNAP from the *spx*-null strain was reconstituted with saturating concentration of σ^A (ratio 1:5) in storage buffer (50 mM Tris-HCl, pH 8.0, 0.1 M NaCl, 50% (v/v) glycerol) for 15 min at 37°C. Spx either was or was not pre-incubated with 5 mM DTT for 30 min at 37°C before addition to the transcription reaction. Multiple round transcription reactions were carried out in 10 µL reaction volumes with 30 nM RNAP holoenzyme and 50 ng of linearized plasmid DNA with tested promoters. The transcription buffer contained 40 mM Tris-HCl pH 8.0, 10 mM $MgCl_2$, 1 mM DTT, 0.1 mg mL^{-1} BSA and 150 mM KCl and NTPs (ATP, CTP were at 200 µM; GTP 1300 µM; UTP was 10 µM plus 30 nM radiolabeled [α-^{32}P] UTP). All transcription reactions were allowed to proceed for 10 min at 37°C and were stopped with equal volumes of formamide stop solution (95% formamide, 20 mM EDTA, pH 8.0). Samples were loaded onto 7 M urea-7% polyacrylamide gels and electrophoresed. The dried gels were scanned with a Molecular Imager FX (Bio-Rad) and visualized and analysed using the Quantity One software (Bio-Rad). The lengths of the transcribed fragments were 233 nt (*rrnJ* P1), 148 nt (*rrnJ* P2), 216 nt (p*rpsD*) or 228 nt (p*trxB*) respectively.

Preparation of total RNA

Total RNA was prepared from cells from 15 to 25 mL cell culture using the illustra RNAspin Mini Kit (GE Healthcare). Cells were resuspended in 350 µl buffer Lysis Buffer,

supplemented with 0.2 mL zircomium/glass beads (0.1 mm dia.) and lysed by vigorously shaking the suspension on a Vortex-Genie 2 (Scientific Industries) for 2 minutes. Further steps were carried out as recommended by the manufacturer. Additionally, RNA was treated with RNase-free DNase I (NEB) for 15 min at 37°C. Integrity of the RNA was checked by native agarose gel electrophoresis or methylene blue stain of blotted samples.

Northern blotting

About 2 µg total RNA per sample was denatured for 10 min at 65°C in sample buffer (50% formamide, 20 mM MOPS pH 7.0, 50 mM sodium acetate, 19 mM EDTA, 2.2% formaldehyde, 1.5% Ficoll 70) and run on a 1.3% agarose, 6.6% formaldehyde gel in 1x MOPS buffer (20 mM MOPS pH 7.0, 50 mM sodium acetate, 10 mM EDTA) for 1.5 h at 100 V. The RNA was transferred to a positively charged nylon membrane by upwards capillary transfer overnight (~16 h) using 10x standard saline citrate buffer (10x SSC; 150 mM sodium citrate, 1.5 M sodium chloride, pH 7.0) and crosslinked to the membrane by irradiation with 120 mJ cm^{-2} in a Stratalinker UV cross-linker apparatus. The membrane was stained with methylene blue dye (0.02% methylene blue, 300 mM sodium acetate pH 5.5) to verify integrity and equal loading of the RNA, scanned and subsequently destained with 1% SDS in 0.2x SSC. Digoxygenin-labelled RNA probes were generated by *in vitro*-transcription with T7 RNA-polymerase (NEB) and labelled DIG RNA Labelling Mix (Roche) in a 20 µl reaction for 3 h at 37°C. The templates were generated by PCR with primers listed in Table S7 that carry the sequence of the T7-promoter.

Membranes were hybridized with labelled probes in hybridization buffer (5x SSC, 0.02% sodium dodecyl sulphate, 0.1% N-laurylsarcosine, 2% blocking reagent (Roche), 20 mM sodium maleate, 4 M urea, pH 7) at 68°C over night as described in (Simard *et al*., 2001). The membrane was blocked by incubation in 100 mM maleic acid pH 7.5, 150 mM NaCl, 1% w/v Blocking reagent (Roche Applied Sciences) for 1 h. Anti-digoxigenin antibodies conjugated to alkaline phosphatase (Roche Applied Sciences) were diluted 1:5000 in the same buffer and applied to the blot for 2 h with mild shaking. The membrane was washed twice for 15 min in 100 mM maleic acid pH 7.5, 150 mM NaCl and equilibrated in 100 mM Tris-HCl pH 9.5, 100 mM NaCl, 5 mM $MgCl_2$. CDP-Star solution (Tropix Inc.) was used as the substrate and signals were detected in a ChemiBIS 4.2 imaging system (DNR).

RT-qPCR

Total RNA was prepared as described above. cDNA from was synthesized from 500 ng total RNA using Protoscript® II reverse transcriptase (NEB) in a 20 µl reaction with 3.5 µM random hexamer primers for 1 h at 42°C and diluted in TE-Buffer (10 mM TRIS, 1 mM EDTA pH 8). qPCR was performed using Luna® Universal qPCR Master Mix (NEB) in a 20 µl reaction with 0.25 µM primers and cDNA equivalent to 5 ng RNA (or 0.5 ng RNA for rRNA targets). Cycling conditions were: 95°C for 60 s followed by 45 cycles of 95°C for 15 s and 60°C for 30 s. Primer efficiency was calculated using a standard curve with serial 10-fold dilutions of cDNA. 23S rRNA was used as a reference and the $2^{\Delta\Delta CT}$ Method (Livak and Schmittgen, 2001) was used to calculate relative gene expression. The primers used for RT-qPCR are listed in Table S8.

Western blotting

Samples of 10 ml were collected by centrifugation for 5 min, 4°C, washed once in buffer TE (10 mM TRIS-HCl pH 8.0, 1 mM EDTA) and resuspended in the same buffer supplemented with 0.1 mM PMSF. Lysates were prepared by sonication and cleared by centrifugation for 5 min at 11.000 × g. Western blotting was carried out with antibody sera as described previously (Molière *et al*., 2016). Signals were detected either using alkaline phosphatase (AP)-conjugated antibody or the ECF-reagent (GE healthcare) (Molière *et al*., 2016) or HRP-conjugated antibody (Mruk and Cheng, 2011). Images were acquired using the MF-ChemiBIS 4.2 imaging system (DNR Bio-Imaging Systems) or ChemoStar imaging system (Intas, Göttingen, Germany).

Growth on agar plates

Stationary-phase cultures were adjusted to an OD_{600} of 1.0 and diluted in 0.9% NaCl. 5 µl cell suspension was spotted on LB agar plates with or without IPTG or diamide as indicated. Plates were incubated overnight (18 h) at 37°C.

Microarray experiments

For thermotolerance experiments, *B. subtilis* wild-type cells were grown in LB medium at 37°C and shaking at 300 rpm to the mid-exponential phase ($OD_{600\ nm}$ 0.6) and divided in four 50 ml cultures. Two cultures were incubated for 15 min at 37 or 48°C and harvested. The other cultures were incubated for 15 min at 37 or 48°C, then incubated at 53°C for additional 15 min, harvested by centrifugation at 3860 × g for 5 min and flash-frozen in liquid nitrogen. Δ*clpX* (BNM107) cells or Δ*clpX*Δ*spx* (BNM112) cells were grown in LB medium to the mid-exponential phase at 37°C and 300 rpm, harvested by centrifugation and frozen in liquid nitrogen.

Total RNA was prepared from frozen pellets using the ® FastRNA Pro Blue Kit (Qbiogene, Inc., CA), resuspended in 100 µl DEPC treated water, treated with DNase I at 37°C for 20 min and purified by phenol/chloroform extraction and ethanol precipitation. The quality of the RNA was checked by agarose gel electrophoresis. cDNA was synthesized from 15 µg total RNA and 5 µg random hexamer primers in a 30 µl scale using SuperScript® Plus Indirect cDNA Labelling Kit (Invitrogen), purified using the Low Elution cDNA Purification Module (Invitrogen) and labelled using the Alexa Fluor® 555 and 647 Reactive Dye modules (Invitrogen) according to the manufacturer's instructions.

The labelled cDNAs were concentrated to 6 µl, mixed with 35 µl prewarmed SlideHyb Glass Array Hybridization Buffer #1 (Ambion) and applied to an oligonucleotide microarray

prepared by the Center of Applied Genomics (ICPH, UMDNJ, Newark) in a Micro-Array Hybrid Chamber (Amlab) and incubated in a water bath over night at 55°C. The array was then washed in buffer 1 (2 × SSC, 0.5% SDS), buffer 2 (0.5 × SSC, 0.5% SDS) and buffer 3 (0.5 × SSC, 0.03% SDS) for 5 min each at 55°C and then washed with buffer 4 (0.2 × SSC), buffer 5 (0.1 × SSC) and buffer 6 (0.01 × SSC) for 5 min each at room temperature. The array was read in a Genepix 4100 Laserscanner (Molecular Devices) using auto PMT and the GenePix Pro 6.1 software. The dye swap and further analysis was performed using the Acuity 4.0 software (Axon) and Microsoft Excel 2010. Functional groups and regulon annotations were inferred from subtiwiki (Michna *et al.*, 2016).The data have been deposited NCBI's Gene Expression Omnibus (Edgar *et al.*, 2002) and are accessible through GEO Series accession numbers GSE45972 and GSE50102.

Fluorescence microscopy

Cells carrying a xylose-inducible copy of a translational fusion of *yocM* with mCherry were grown in LB medium supplemented with 0.5% (w/v) xylose. Upon an OD600 of 0.4, cells were treated with a 15 min pre-shock at 48°C followed by a shift to 53°C. Strain BER550, carrying a translational *in cis* GFP-*spx* fusion was inoculated in LB medium from a stationary phase overnight culture. Cells were briefly concentrated by centrifugation at 5000 × g for 2 min. Samples of 3 µl were subjected to phase contrast or fluorescence microscopy on agarose-coated slides with a Axio Imager.Z2 (Zeiss) using the GFP or RFP filter set with a fixed exposure time of 3000 ms (Runde *et al.*, 2014). Images were obtained with an AxioCam MRm (Zeiss). Fluorescence intensity of individual cells was integrated on background-substracted images using the Fiji distribution of ImageJ (Schindelin *et al.*, 2012) and normalized to the cell area.

Acknowledgements

We want to thank Peter Zuber (Oregon Health & Science University, Portland), Sigal Ben-Yehuda (Hebrew U, Jerusalem), Ulf Gerth (U Greifswald), Javier Lopez-Garrido (UC San Diego) and Gert Bange (U Marburg) for strains and plasmids. Work in our Laboratories was supported by the Czech Science Foundation to LK (Grant No. 17-03419S), by the Deutsche Forschungsgemeinschaft (SPP1879 Tu106/8-1) and by a PhD fellowship of the Hannover School for Biomolecular Drug Research (HSBDR) to IH. The work was also supported by the Czech research infrastructure for systems biology C4SYS (project LM2015055).

Author contributions

The authors HS (i, ii, iii), AH (ii), PS (ii), MV (ii), IH (ii), LK (ii, iii), KT (i, ii, iii) have made major contributions to (i) the conception or design of the study, (ii) the acquisition, analysis, or interpretation of the data; and (iii) writing of the manuscript.

References

Abranches, J., Martinez, A.R., Kajfasz, J.K., Chávez, V., Garsin, D.A. and Lemos, J.A. (2009) The molecular alarmone (p)ppGpp mediates stress responses, vancomycin tolerance, and virulence in *Enterococcus faecalis*. *Journal of Bacteriology*, **191**, 2248–2256.

Antelmann, H., Scharf, C. and Hecker, M. (2000) Phosphate starvation-inducible proteins of *Bacillus subtilis*: proteomics and transcriptional analysis. *Journal of Bacteriology*, **182**, 4478–4490.

Antoniewski, C., Savelli, B. and Stragier, P. (1990) The spoIIJ gene, which regulates early developmental steps in *Bacillus subtilis*, belongs to a class of environmentally responsive genes. *Journal of Bacteriology*, **172**, 86–93.

Arnaud, M., Chastanet, A. and Débarbouillé, M. (2004) New vector for efficient allelic replacement in naturally nontransformable, low-GC-content, gram-positive bacteria. *Applied and Environment Microbiology*, **70**, 6887–6891.

Balaban, N.Q., Merrin, J., Chait, R., Kowalik, L. and Leibler, S. (2004) Bacterial persistence as a phenotypic switch. *Science*, **305**, 1622–1625.

Balchin, D., Hayer-Hartl, M. and Hartl, F.U. (2016) In vivo aspects of protein folding and quality control. *Science*, **353**, aac4354.

Beckert, B., Abdelshahid, M., Schäfer, H., Steinchen, W., Arenz, S., Berninghausen, O., *et al.* (2017) Structure of the *Bacillus subtilis* hibernating 100S ribosome reveals the basis for 70S dimerization. *EMBO Journal*, **36**, 2061–2072.

Birch, C.A., Davis, M.J., Mbengi, L. and Zuber, P. (2017) Exploring the amino acid residue requirements of the RNA polymerase (RNAP) α subunit C-terminal domain for productive interaction between Spx and RNAP of *Bacillus subtilis*. *Journal of Bacteriology*, **199**, e00124.

Browning, D.F. and Busby, S.J.W. (2016) Local and global regulation of transcription initiation in bacteria. *Nature Reviews Microbiology*, **14**, 638–650.

Chi, B.K., Gronau, K., Mäder, U., Hessling, B., Becher, D. and Antelmann, H. (2011) S-bacillithiolation protects against hypochlorite stress in *Bacillus subtilis* as revealed by transcriptomics and redox proteomics. *Mol Cell Proteomics MCP*, **10**(M111), 009506.

Darmon, E., Noone, D., Masson, A., Bron, S., Kuipers, O.P., Devine, K.M., et al (2002) A novel class of heat and secretion stress-responsive genes is controlled by the autoregulated CssRS two-component system of *Bacillus subtilis*. *Journal of Bacteriology*, **184**, 5661–5671.

Delumeau, O., Lecointe, F., Muntel, J., Guillot, A., Guédon, E., Monnet, V., et al. (2011) The dynamic protein partnership of RNA polymerase in *Bacillus subtilis*. *Proteomics*, **11**, 2992–3001.

Dubnau, D. and Losick, R. (2006) Bistability in bacteria. *Molecular Microbiology*, **61**, 564–572.

Edgar, R., Domrachev, M. and Lash, A.E. (2002) Gene expression omnibus: NCBI gene expression and hybridization array data repository. *Nucleic Acids Research*, **30**, 207–210.

Elsholz, A.K.W., Michalik, S., Zühlke, D., Hecker, M. and Gerth, U. (2010) CtsR, the gram-positive master regulator of protein quality control, feels the heat. *EMBO Journal*, **29**, 3621–3629.

Elsholz, A.K.W., Birk, M.S., Charpentier, E. and Turgay, K. (2017) Functional diversity of AAA+ protease complexes in *Bacillus subtilis*. *Front Mol Biosci*, **4**, 44.

Engman, J. and von Wachenfeldt, C. (2015) Regulated protein aggregation: a mechanism to control the activity of the ClpXP adaptor protein YjbH. *Molecular Microbiology*, **95**, 51–63.

Eymann, C., Homuth, G., Scharf, C. and Hecker, M. (2002) *Bacillus subtilis* functional genomics: global characterization of the stringent response by proteome and transcriptome analysis. *Journal of Bacteriology*, **184**, 2500–2520.

Fitzsimmons, L.F., Liu, L., Kim, J.-S., Jones-Carson, J. and Vázquez-Torres, A. (2018) *Salmonella* reprograms nucleotide metabolism in its adaptation to nitrosative stress. *MBio*, **9**, e00211–e00218.

Fridman, O., Goldberg, A., Ronin, I., Shoresh, N. and Balaban, N.Q. (2014) Optimization of lag time underlies antibiotic tolerance in evolved bacterial populations. *Nature*, **513**, 418–421.

Fukushima, T., Ishikawa, S., Yamamoto, H., Ogasawara, N. and Sekiguchi, J. (2003) Transcriptional, functional and cytochemical analyses of the veg gene in *Bacillus subtilis*. *Journal of Biochemistry*, **133**, 475–483.

Gaal, T., Ross, W., Blatter, E.E., Tang, H., Jia, X., Krishnan, V.V., et al. (1996) DNA-binding determinants of the alpha subunit of RNA polymerase: novel DNA-binding domain architecture. *Genes & Development*, **10**, 16–26.

Gaballa, A., Antelmann, H., Hamilton, C.J. and Helmann, J.D. (2013) Regulation of *Bacillus subtilis* bacillithiol biosynthesis operons by Spx. *Microbiology*, **159**, 2025–2035.

Gaidenko, T.A., Kim, T.-J., Weigel, A.L., Brody, M.S. and Price, C.W. (2006) The blue-light receptor YtvA acts in the environmental stress signaling pathway of *Bacillus subtilis*. *Journal of Bacteriology*, **188**, 6387–6395.

Garg, S.K., Kommineni, S., Henslee, L., Zhang, Y. and Zuber, P. (2009) The YjbH protein of *Bacillus subtilis* enhances ClpXP-catalyzed proteolysis of Spx. *Journal of Bacteriology*, **191**, 1268–1277.

Griffith, K.L., Shah, I.M., Myers, T.E., O'Neill, M.C. and Wolf, R.E. (2002) Evidence for "pre-recruitment" as a new mechanism of transcription activation in *Escherichia coli*: the large excess of SoxS binding sites per cell relative to the number of SoxS molecules per cell. *Biochemical and Biophysical Research Communications*, **291**, 979–986.

Hantke, I., Schäfer, H., Janczikowski, A. and Turgay, K. (2018) YocM a small heat shock protein can protect *Bacillus subtilis* cells during salt stress. *Molecular Microbiology*. https://doi.org/10.1111/mmi.14164

Hauryliuk, V., Atkinson, G.C., Murakami, K.S., Tenson, T. and Gerdes, K. (2015) Recent functional insights into the role of (p)ppGpp in bacterial physiology. *Nature Reviews Microbiology*, **13**, 298–309.

Hecker, M., Völker, U. and Heim, C. (1989) RelA-independent (p)ppGpp accumulation and heat shock protein induction after salt stress in *Bacillus subtilis*. *FEMS Microbiology Letters*, **58**, 125–128.

Hecker, M., Schumann, W. and Völker, U. (1996) Heat-shock and general stress response in *Bacillus subtilis*. *Molecular Microbiology*, **19**, 417–428.

Hecker, M., Pane-Farre, J. and Völker, U. (2007) SigB-dependent general stress response in *Bacillus subtilis* and related gram-positive bacteria. *Annual Review of Microbiology*, **61**, 215–236.

Helmann, J.D. (1995) Compilation and analysus of *Bacillus Subtilis* σ^A -dependent promoter sequences: evidence for extended contact between RNA polymerse and upstream promoter DNA. *Nucleic Acids Research*, **23**, 2351–2360.

Helmann, J.D., Wu, M.F., Kobel, P.A., Gamo, F.J., Wilson, M., Morshedi, M.M., et al. (2001) Global transcriptional response of *Bacillus subtilis* to heat shock. *Journal of Bacteriology*, **183**, 7318–7328.

Höper, D., Völker, U. and Hecker, M. (2005) Comprehensive characterization of the contribution of individual SigB-dependent general stress genes to stress resistance of *Bacillus subtilis*. *Journal of Bacteriology*, **187**, 2810–2826.

Inoue, H., Nojima, H. and Okayama, H. (1990) High efficiency transformation of *Escherichia coli* with plasmids. *Gene*, **96**, 23–28.

Jervis, A.J., Thackray, P.D., Houston, C.W., Horsburgh, M.J. and Moir, A. (2007) SigM-responsive genes of *Bacillus subtilis* and their promoters. *Journal of Bacteriology*, **189**, 4534–4538.

Kim, Y.E., Hipp, M.S., Bracher, A., Hayer-Hartl, M. and Hartl, F.U. (2013) Molecular chaperone functions in protein folding and proteostasis. *Annual Review of Biochemistry*, **82**, 323–355.

Kirstein, J., Molière, N., Dougan, D.A. and Turgay, K. (2009) Adapting the machine: adaptor proteins for Hsp100/Clp and AAA+ proteases. *Nature Reviews Microbiology*, **7**, 589–599.

Koga, K., Ikegami, A., Nakasone, K., Murayama, R., Akanuma, G., Natori, Y., et al. (2006) Construction of *Bacillus subtilis* strains carrying the transcriptional bgaB fusion with the promoter region of each rrn operon and their differential transcription during spore development. *Journal of General and Applied Microbiology*, **52**, 119–124.

Krásný, L. and Gourse, R.L. (2004) An alternative strategy for bacterial ribosome synthesis: *Bacillus subtilis* rRNA transcription regulation. *EMBO Journal*, **23**, 4473–4483.

Kriel, A., Bittner, A.N., Kim, S.H., Liu, K., Tehranchi, A.K., Zou, W.Y., et al. (2012) Direct regulation of GTP homeostasis by (p)ppGpp: a critical component of viability and stress resistance. *Molecular Cell*, **48**, 231–241.

Krüger, E. and Hecker, M. (1998) The first gene of the *Bacillus subtilis* clpC operon, ctsR, encodes a negative regulator of its own operon and other class III heat shock genes. *Journal of Bacteriology*, **180**, 6681–6688.

Lamour, V., Westblade, L.F., Campbell, E.A. and Darst, S.A. (2009) Crystal structure of the in vivo-assembled *Bacillus subtilis* Spx/RNA polymerase alpha subunit C-terminal domain complex. *Journal of Structural Biology*, **168**, 352–356.

Larsson, J.T., Rogstam, A. and von Wachenfeldt, C. (2007) YjbH is a novel negative effector of the disulphide stress regulator, Spx, in *Bacillus subtilis*. *Molecular Microbiology*, **66**, 669–684.

Leelakriangsak, M., Kobayashi, K. and Zuber, P. (2007) Dual negative control of spx transcription initiation from the P3 promoter by repressors PerR and YodB in *Bacillus subtilis*. *Journal of Bacteriology*, **189**, 1736–1744.

Leichert, L.I.O., Scharf, C. and Hecker, M. (2003) Global characterization of disulfide stress in *Bacillus subtilis*. *Journal of Bacteriology*, **185**, 1967–1975.

Lin, A.A., Walthers, D. and Zuber, P. (2013) Residue substitutions near the redox center of *Bacillus subtilis* Spx affect RNA polymerase interaction, redox control, and Spx-DNA contact at a conserved cis-acting element. *Journal of Bacteriology*, **195**, 3967–3978.

Lindner, A.B., Madden, R., Demarez, A., Stewart, E.J. and Taddei, F. (2008) Asymmetric segregation of protein aggregates is associated with cellular aging and rejuvenation. *Proceedings of the National Academy of Sciences*, **105**, 3076–3081.

Lindquist, S. (1986) The heat-shock response. *Annual Review of Biochemistry*, **55**, 1151–1191.

Livak, K.J. and Schmittgen, T.D. (2001) Analysis of relative gene expression data using real-time quantitative PCR and the 2(-Delta Delta C(T)) method. *Methods*, **25**, 402–408.

Luo, Y. and Helmann, J.D. (2012) Analysis of the role of *Bacillus subtilis* σ(M) in β-lactam resistance reveals an essential role for c-di-AMP in peptidoglycan homeostasis. *Molecular Microbiology*, **83**, 623–639.

Martin, R.G., Gillette, W.K., Martin, N.I. and Rosner, J.L. (2002) Complex formation between activator and RNA polymerase as the basis for transcriptional activation by MarA and SoxS in *Escherichia coli*: transcriptional activator-RNP complexes. *Molecular Microbiology*, **43**, 355–370.

Michna, R.H., Zhu, B., Mäder, U. and Stülke, J. (2016) SubtiWiki 2.0–an integrated database for the model organism *Bacillus subtilis*. *Nucleic Acids Research*, **44**, D654–D662.

Mogk, A., Homuth, G., Scholz, C., Kim, L., Schmid, F.X. and Schumann, W. (1997) The GroE chaperonin machine is a major modulator of the CIRCE heat shock regulon of *Bacillus subtilis*. *EMBO Journal*, **16**, 4579–4590.

Mogk, A., Huber, D. and Bukau, B. (2011) Integrating protein homeostasis strategies in prokaryotes. *Cold Spring Harbor Perspectives in Biology*, **3**(4), a004366–a004366.

Molière, N., Hoßmann, J., Schäfer, H. and Turgay, K. (2016) Role of Hsp100/Clp protease complexes in controlling the regulation of motility in *Bacillus subtilis*. *Frontiers in Microbiology*, **7**, 315.

Mostertz, J., Scharf, C., Hecker, M. and Homuth, G. (2004) Transcriptome and proteome analysis of *Bacillus subtilis* gene expression in response to superoxide and peroxide stress. *Microbiology*, **150**, 497–512.

Mruk, D.D. and Cheng, C.Y. (2011) Enhanced chemiluminescence (ECL) for routine immunoblotting: an inexpensive alternative to commercially available kits. *Spermatogenesis*, **1**, 121–122.

Murayama, S., Ishikawa, S., Chumsakul, O., Ogasawara, N. and Oshima, T. (2015) The role of α-CTD in the genome-wide transcriptional regulation of the *Bacillus subtilis* cells. *PLoS ONE*, **10**, e0131588.

Nakano, M.M., Zhu, Y., Liu, J., Reyes, D.Y., Yoshikawa, H. and Zuber, P. (2000) Mutations conferring amino acid residue substitutions in the carboxy-terminal domain of RNA polymerase alpha can suppress clpX and clpP with respect to developmentally regulated transcription in *Bacillus subtilis*. *Molecular Microbiology*, **37**, 869–884.

Nakano, M.M., Hajarizadeh, F., Zhu, Y. and Zuber, P. (2001) Loss-of-function mutations in yjbD result in ClpX- and ClpP-independent competence development of *Bacillus subtilis*. *Molecular Microbiology*, **42**, 383–394.

Nakano, M.M., Nakano, S. and Zuber, P. (2002a) Spx (YjbD), a negative effector of competence in *Bacillus subtilis*, enhances ClpC-MecA-ComK interaction. *Molecular Microbiology*, **44**, 1341–1349.

Nakano, S., Zheng, G., Nakano, M.M. and Zuber, P. (2002b) Multiple pathways of Spx (YjbD) proteolysis in *Bacillus subtilis*. *Journal of Bacteriology*, **184**, 3664–3670.

Nakano, S., Küster-Schöck, E., Grossman, A.D. and Zuber, P. (2003a) Spx-dependent global transcriptional control is induced by thiol-specific oxidative stress in *Bacillus subtilis*. *Proceedings of the National Academy of Sciences*, **100**, 13603–13608.

Nakano, S., Nakano, M.M., Zhang, Y., Leelakriangsak, M. and Zuber, P. (2003b) A regulatory protein that interferes with activator-stimulated transcription in bacteria. *Proceedings of the National Academy of Sciences*, **100**, 4233–4238.

Nakano, S., Erwin, K.N., Ralle, M. and Zuber, P. (2005) Redox-sensitive transcriptional control by a thiol/disulphide switch in the global regulator, Spx. *Molecular Microbiology*, **55**, 498–510.

Nakano, M.M., Lin, A., Zuber, C.S., Newberry, K.J., Brennan, R.G. and Zuber, P. (2010) Promoter recognition by a complex of Spx and the C-terminal domain of the RNA polymerase α subunit. *PLoS ONE*, **5**, e8664.

Natori, Y., Tagami, K., Murakami, K., Yoshida, S., Tanigawa, O., Moh, Y., et al. (2009) Transcription activity of individual rrn operons in *Bacillus subtilis* mutants deficient in (p)ppGpp synthetase genes, relA, yjbM, and ywaC. *Journal of Bacteriology*, **191**, 4555–4561.

Newberry, K.J., Nakano, S., Zuber, P. and Brennan, R.G. (2005) Crystal structure of the *Bacillus subtilis* anti-alpha, global transcriptional regulator, Spx, in complex with the alpha C-terminal domain of RNA polymerase. *Proceedings of the National Academy of Sciences*, **102**, 15839–15844.

Nicolas, P., Mäder, U., Dervyn, E., Rochat, T., Leduc, A., Pigeonneau, N., et al. (2012) Condition-dependent transcriptome reveals high-level regulatory architecture in *Bacillus subtilis*. *Science*, **335**, 1103–1106.

Petersohn, A., Antelmann, H., Gerth, U. and Hecker, M. (1999) Identification and transcriptional analysis of new members of the sigmaB regulon in *Bacillus subtilis*. *Microbiol Read Engl*, **145**(Pt 4), 869–880.

Petersohn, A., Brigulla, M., Haas, S., Hoheisel, J.D., Volker, U. and Hecker, M. (2001) Global analysis of the general stress response of *Bacillus subtilis*. *Journal of Bacteriology*, **183**, 5617–5631.

Price, C.W., Fawcett, P., Cérémonie, H., Su, N., Murphy, C.K. and Youngman, P. (2001) Genome-wide analysis of the general stress response in *Bacillus subtilis*. *Molecular Microbiology*, **41**, 757–774.

Radeck, J., Kraft, K., Bartels, J., Cikovic, T., Dürr, F., Emenegger, J., et al. (2013) The Bacillus BioBrick Box: generation and evaluation of essential genetic building blocks for standardized work with *Bacillus subtilis*. *Journal of Biological Engineering*, **7**, 29.

Rao, L., Ross, W., Appleman, J.A., Gaal, T., Leirmo, S., Schlax, P.J., et al. (1994) Factor independent activation of rrnB P1. An "extended" promoter with an upstream element that dramatically increases promoter strength. *Journal of Molecular Biology*, **235**, 1421–1435.

Reder, A., Hoper, D., Gerth, U. and Hecker, M. (2012) Contributions of individual B-dependent general stress genes to oxidative stress resistance of *Bacillus subtilis*. *Journal of Bacteriology*, **194**, 3601–3610.

Reyes, D.Y. and Zuber, P. (2008) Activation of transcription initiation by Spx: formation of transcription complex and identification of a Cis-acting element required for transcriptional activation. *Molecular Microbiology*, **69**, 765–779.

Riley, E.P., Trinquier, A., Reilly, M.L., Durchon, M., Perera, V.R., Pogliano, K. and Lopez-Garrido, J. (2018) Spatiotemporally regulated proteolysis to dissect the role of vegetative proteins during *Bacillus subtilis* sporulation: cell-specific requirement of σ^H and σ^A: Spatiotemporally regulated proteolysis in *Bacillus*. *Molecular Microbiology*, **108**, 45–62.

Rochat, T., Nicolas, P., Delumeau, O., Rabatinová, A., Korelusová, J., Leduc, A., et al. (2012) Genome-wide identification of genes directly regulated by the pleiotropic transcription factor Spx in *Bacillus subtilis*. *Nucleic Acids Research*, **40**, 9571–9583.

Rojas-Tapias, D.F. and Helmann, J.D. (2018a) Induction of the Spx regulon by cell wall stress reveals novel regulatory mechanisms in *Bacillus subtilis*. *Molecular Microbiology*, **107**, 659–674.

Rojas-Tapias, D.F. and Helmann, J.D. (2018b) Stabilization of *Bacillus subtilis* Spx under cell wall stress requires the anti-adaptor protein YirB. *PLoS Genetics*, **14**, e1007531.

Rosenberg, A., Sinai, L., Smith, Y. and Ben-Yehuda, S. (2012) Dynamic expression of the translational machinery during *Bacillus subtilis* life cycle at a single cell level. *PLoS ONE*, **7**, e41921.

Ross, W., Thompson, J.F., Newlands, J.T. and Gourse, R.L. (1990) *E. coli* Fis protein activates ribosomal RNA transcription in vitro and in vivo. *EMBO Journal*, **9**, 3733–3742.

Ross, W., Gosink, K., Salomon, J., Igarashi, K., Zou, C., Ishihama, A., et al. (1993) A third recognition element in bacterial promoters: DNA binding by the alpha subunit of RNA polymerase. *Science*, **262**, 1407–1413.

Runde, S., Molière, N., Heinz, A., Maisonneuve, E., Janczikowski, A., Elsholz, A.K.W., et al. (2014) The role of thiol oxidative stress response in heat-induced protein aggregate formation during thermotolerance in *B acillus subtilis*: Thiol oxidation in protein aggregate formation. *Molecular Microbiology*, **91**, 1036–1052.

Sambrook, J. and Russell, D.W. (2001) *Molecular Cloning: A Laboratory Manual*, 3rd edition. Cold Spring Harbor, NY: Cold Spring Harbor Laboratory Press.

Schindelin, J., Arganda-Carreras, I., Frise, E., Kaynig, V., Longair, M., Pietzsch, T., et al. (2012) Fiji: an open-source platform for biological-image analysis. *Nature Methods*, **9**, 676–682.

Schulz, A. and Schumann, W. (1996) hrcA, the first gene of the *Bacillus subtilis* dnaK operon encodes a negative regulator of class I heat shock genes. *Journal of Bacteriology*, **178**, 1088–1093.

Shah, I.M. and Wolf, R.E. (2004) Novel protein-protein interaction between *Escherichia coli* SoxS and the DNA binding determinant of the RNA polymerase α subunit: SoxS functions as a co-sigma factor and redeploys RNA polymerase from UP-element-containing promoters to SoxS-dependent promoters during oxidative stress. *Journal of Molecular Biology*, **343**, 513–532.

Simard, C., Lemieux, R. and Côté, S. (2001) Urea substitutes toxic formamide as destabilizing agent in nucleic acid hybridizations with RNA probes. *Electrophoresis*, **22**, 2679–2683.

Sojka, L., Kouba, T., Barvík, I., Sanderová, H., Maderová, Z., Jonák, J. and Krásny, L. (2011) Rapid changes in gene expression: DNA determinants of promoter regulation by the concentration of the transcription initiating NTP in *Bacillus subtilis*. *Nucleic Acids Research*, **39**, 4598–4611.

Spizizen, J. (1958) Transformation of biochemically deficient strains of *Bacillus subtilis* by deoxyribonucleate. *Proceedings of the National Academy of Sciences*, **44**, 1072–1078.

Stülke, J., Hanschke, R. and Hecker, M. (1993) Temporal activation of beta-glucanase synthesis in *Bacillus subtilis* is mediated by the GTP pool. *Journal of General Microbiology*, **139**, 2041–2045.

Veening, J.W., Smits, W.K. and Kuipers, O.P. (2008) Bistability, epigenetics, and bet-hedging in bacteria. *Annual Review of Microbiology*, **62**, 193–210.

Versteeg, S., Escher, A., Wende, A., Wiegert, T. and Schumann, W. (2003) Regulation of the *Bacillus subtilis* heat shock gene htpG is under positive control. *Journal of Bacteriology*, **185**, 466–474.

Völker, U., Maul, B. and Hecker, M. (1999) Expression of the sigmaB-dependent general stress regulon confers multiple stress resistance in *Bacillus subtilis*. *Journal of Bacteriology*, **181**, 3942–3948.

Wickner, S., Maurizi, M.R. and Gottesman, S. (1999) Posttranslational quality control: folding, refolding, and degrading proteins. *Science*, **286**, 1888–1893.

Wiegert, T. and Schumann, W. (2001) SsrA-mediated tagging in *Bacillus subtilis*. *Journal of Bacteriology*, **183**, 3885–3889.

Yang, X. and Ishiguro, E.E. (2003) Temperature-sensitive growth and decreased thermotolerance associated with relA mutations in *Escherichia coli*. *Journal of Bacteriology*, **185**, 5765–5771.

Zhang, Y. and Zuber, P. (2007) Requirement of the zinc-binding domain of ClpX for Spx proteolysis in *Bacillus subtilis* and effects of disulfide stress on ClpXP activity. *Journal of Bacteriology*, **189**, 7669–7680.

Zhang, Y., Nakano, S., Choi, S.-Y. and Zuber, P. (2006) Mutational analysis of the *Bacillus subtilis* RNA polymerase α C-terminal domain supports the interference model of Spx-dependent repression. *Journal of Bacteriology*, **188**, 4300–4311.

Zuber, P. (2004) Spx-RNA polymerase interaction and global transcriptional control during oxidative stress. *Journal of Bacteriology*, **186**, 1911–1918.

Supporting Information

Additional supporting information may be found online in the Supporting Information section at the end of the article.

SUPPLEMENTARY INFORMATION

Spx, the central regulator of the heat- and oxidative stress response in *B. subtilis*, can repress transcription of translation-related genes

Heinrich Schäfer, Anja Heinz, Petra Sudzinová, Michelle Voß, Ingo Hantke, Libor Krásný & Kürşad Turgay

Content

Supplementary tables

Table S1 Summary of regulated genes and their regulons

See supplementary excel data file.

Table S2 Regulated genes of the thermotolerance arrays

See supplementary excel data file.

Table S3 the most up- and down-regulated genes of array 4 (37/53 °C vs 48/53 °C)

See supplementary excel data file.

Table S4 Regulated genes in the Δc*lpX* vs Δc*lpX*Δ*spx* array

See supplementary excel data file.

Table S5 List of strains

Strain	**genotype**	**Source/construction**
B. subtilis 168	*trpC2*	(Spizizen, 1958)
B. subtilis PY79		(Youngman *et al.*, 1984)
BNM107	*trpC2* Δ*clpX::kan*	(Runde *et al.*, 2014)
BNM111	*trpC2* Δ*spx::kan*	(Runde *et al.*, 2014)
BNM112	*trpC2* Δ*spx::kan* Δ*clpX::spec*	(Runde *et al.*, 2014)
BNM810	*trpC2 amyE:: P_{hy}-spx^{DD} lacI spec*	(Runde *et al.*, 2014)
BAH34	*trpC2* ΔctsR*::kan*	This work, BHL-5 → *B. subtilis 168* (Krüger *et al.*, 2001)
BAH35	*trpC2* Δ*sigB::cat*	This work, ML-6 → *B. subtilis 168* (Igo *et al.*, 1987)
BAH42	*trpC2* Δ*hrcA*	This work, pMADΔhrcA → *B. subtilis 168*
BNM855	Δ*yjbH::spec*	(Molière *et al.*, 2016)
BHS201	*trpC2 lacA::P_{hy}-spx^{DD} lacI erm*	This work, pBSIIE-spxDD → *B. subtilis 168*
BHS220	*trpC2 amyE::RrnJP1(-107/+25)-lacZ Cm*	This work, pDG268-RrnJP1-132 → *B. subtilis 168*
BHS222	*trpC2 amyE::RrnJP1-lacZ Cm* Δ*spx::kan*	This work, BNM111 → BHS220
BHS225	*trpC2 amyE::RrnJP1-lacZ Cm lacA::P_{hy}-spx^{DD} lacI erm*	This work, BHS201 → BHS220
BHS475	*trpC2 rpoA^{Y263C}*	This work, pYZ37 → → *B. subtilis 168* (Nakano *et al.*, 2000)
BHS476	*trpC2 rpoA^{V260A}*	This work, pYZ38 → → *B. subtilis 168* (Nakano *et al.*,

		2000)
BHS516	*trpC2 amyE::RrnJP1(-59/+3)-lacZ cat*	This work, pDG268-RrnJP1-62 → *B. subtilis 168*
BHS517	*trpC2 amyE::RrnJP1(-38/+3)-lacZ cat*	This work, pDG268-RrnJP1-41 → *B. subtilis 168*
BHS549	*trpC2 rpoA^{Y263C} amyE::RrnJP1(-107/+25)-lacZ cat*	This work, BHS220 →BHS475
BHS550	*trpC2 rpoA^{V260A} amyE::RrnJP1(-107/+25)-lacZ cat*	This work, BHS220 →BHS476
BHS569	*trpC2 amyE::Pveg (-38/+1) -lacZ cat*	This work, pDG268-Pveg → *B. subtilis 168*
BHS573	*trpC2 amyE::Pveg (-38/+1) -lacZ cat lacA::P$_{hy}$-spx^{DD} lacI erm*	This work, BHS201 → BHS569
BHS591	*trpC2 amyE::RrnJP1(SUB -38/+3)-lacZ cat*	This work, pDG268-SUB-RrnJP1 → *B. subtilis 168*
BHS592	*trpC2 amyE::RrnJP1(trxB_UP -38/+3)-lacZ cat*	This work, pDG268-TRXB-RrnJP1 → *B. subtilis 168*
BHS601	*trpC2 amyE::RrnJP1(SUB -38/+3)-lacZ cat lacA::P$_{hy}$-spx^{DD} lacI erm*	This work, BHS201 → BHS591
BHS602	*trpC2 amyE::RrnJP1(trxB_UP -38/+3)-lacZ cat lacA::P$_{hy}$-spx^{DD} lacI erm*	This work, BHS201 → BHS592
BHS652	*trpC2 amyE::Pveg (SUB -38/+1) -lacZ cat*	This work, pDG268-SUB-Pveg → *B. subtilis 168*
BHS653	*trpC2 amyE::Pveg (rrnJ_UP -38/+1) -lacZ cat*	This work, pDG268-rrnJ-Pveg → *B. subtilis 168*
BHS668	*trpC2 amyE::Pveg (SUB -38/+1) -lacZ cat lacA::P$_{hy}$-spx^{DD} lacI erm*	This work, BHS201 → BHS652
BHS669	*trpC2 amyE::Pveg (rrnJ_UP -38/+1) -lacZ cat lacA::P$_{hy}$-spx^{DD} lacI erm*	This work, BHS201 → BHS653
BHS729	*trpC2 rpoA^{Y263C} amyE::RrnJP1(-107/+25)-lacZ cat lacA::P$_{hy}$-spx^{DD} lacI erm*	This work, BHS201 → BH549
BHS730	*trpC2 rpoA^{V260A} amyE::RrnJP1(-107/+25)-lacZ cat lacA::P$_{hy}$-spx^{DD} lacI erm*	This work, BHS201 → BHS550
BHS800	*trpC2 amyE::RrnJP1(-98/+3)-lacZ cat*	This work, pDG268-RrnJP1-101 → *B. subtilis 168*
BHS807	*trpC2 amyE::RrnJP1(-98/+3)-lacZ cat lacA::P$_{hy}$-spx^{DD} lacI erm*	This work, BHS201 → BHS800
BHS882	*trpC2 amyE::RrnJP1-lacZ Cm ΔmgsR::erm*	This work, BAR1 → BHS220 (Reder *et al.*, 2008)
BHS883	*trpC2 amyE::RrnJP1-lacZ Cm Δspx::kan ΔmgsR::erm*	This work, BAR1→ BHS222 (Reder *et al.*, 2008)
BHS932	*PY79 amyE::PrrnA-gfpmut2 spc lacA::P$_{hy}$-spx^{DD} lacI erm*	This work, pBSIIE-spxDD → AR13 (Rosenberg *et*

		al., 2012)
BHS933	*PY79 amyE::PrrnB-gfpmut2 spc lacA::P_{hy}-spx^{DD} lacI erm*	This work, pBSIIE-spxDD → AR14 (Rosenberg *et al.*, 2012)
BHS934	*PY79 amyE::PrrnD-gfpmut2 spc lacA::P_{hy}-spx^{DD} lacI erm*	This work, pBSIIE-spxDD → AR15 (Rosenberg *et al.*, 2012)
BHS935	*PY79 amyE::PrrnE-gfpmut2 spc lacA::P_{hy}-spx^{DD} lacI erm*	This work, pBSIIE-spxDD → AR16 (Rosenberg *et al.*, 2012)
BHS936	*PY79 amyE::PrrnO-gfpmut2 spc lacA::P_{hy}-spx^{DD} lacI erm*	This work, pBSIIE-spxDD → AR17 (Rosenberg *et al.*, 2012)
BHS937	*PY79 amyE::PrrnI-gfpmut2 spc lacA::P_{hy}-spx^{DD} lacI erm*	This work, pBSIIE-spxDD → AR18 (Rosenberg *et al.*, 2012)
BHS938	*PY79 amyE::PrrnJ-gfpmut2 spc lacA::P_{hy}-spx^{DD} lacI erm*	This work, pBSIIE-spxDD → AR19 (Rosenberg *et al.*, 2012)
BIH369	*trpC2 lacA::Pxyl yocM-mCherry erm*	(Hantke *et al.*, 2018)
BIH632	*trpC2 rpoA^{Y263C} lacA::Pxyl yocM-mCherry erm*	BIH369 →BHS475
BIH633	*trpC2 rpoA^{Y263C} lacA::Pxyl yocM-mCherry erm*	BIH369 →BHS476
BER550	PY79 *gfp-spx cat*	(Riley *et al.*, 2018)
LK1119	*rpoC-His10, spx::aphA-3*	(Rochat *et al.*, 2012)

Table S6 List of plasmids

Plasmid	**Relevant features**	**Source or cloning primers**
pYZ37	*rpoA^{Y263C}*	(Nakano *et al.*, 2000)
pYZ38	*rpoA^{V260A}*	(Nakano *et al.*, 2000)
pMADhrcA	Δ*hrcA*	pMADhrcAp1-4
pDG268-RrnJP1-132	*amyE3' cat* RrnJP1(-107/+25)-*lacZ amyE5'*	p249/p250
pDG268-RrnJP1-102	*amyE3' cat* RrnJP1(-98/+3)-*lacZ amyE5'*	p377/p616
pDG268-RrnJP1-62	*amyE3' cat* RrnJP1(-59/+3)-*lacZ amyE5'*	p377/379
pDG268-RrnJP1-41	*amyE3' cat* RrnJP1(-38/+3)-*lacZ amyE5'*	p377/378
pDG268-SUB-RrnJP1	*amyE3' cat* RrnJP1(SUB -38/+3)-*lacZ amyE5'*	p377/p463
pDG268-TRXB-RrnJP1	*amyE3' cat* RrnJP1(trxB_UP -38/+3)-*lacZ amyE5'*	p377/p464
pDG268-Pveg	*amyE3' cat* P*veg* (-38/+1)-*lacZ amyE5'*	p455/p456

pDG268-SUB-Pveg	*amyE3' cat* P*veg* (SUB-38/+1)-*lacZ amyE5'*	p493/p494
pDG268-rrnJ-Pveg	*amyE3' cat* P*veg* (trxB_UP-38/+1)-*lacZ amyE5'*	p493/p495, p491/p493
pBSIIE-spxDD	*lacA5' erm Phy-spx^{DD} lacI lacA3'*	p222/p223
P770-rrnJ P1 P2	*amp* rrnJ P1 P2 (-108/+88)	pLK2037/pLK2039
pEDJ160	*amp* p770-PtrxB	(Rochat *et al.*, 2012)
pEDJ163	*amp* p770-PrpsD	(Rochat *et al.*, 2012)
pCD2	*B. subtilis sigA*	(Chang and Doi, 1990)

Table S7 List of oligonucleotides

primer	**Sequence (5'-3')**
pMADhrcAp1	CCCCGGATCCGGATATGATCAACCGCGTGC
pMADhrcAp2	CCCCGTCGACCATCACCTCTGTTAGCACTC
pMADhrcAp3	CCCCGTCGACGCTTCAGCATGTGACTTCGG
pMADhrcAp4	CTTTGACCATGGAAGGGCG
p249_EcoRI_PrrnJ_P1_for	CCGGAATTCAAGAGCGGTATCCTCCATAG
p250_BamHI_PrrnJ_P1_rev	CGCGGATCCCGTTATCGCCTTGTTTAGCG
p377_RrnJP1_+3_rev	CGCGGATCCAACGAATAATAATATACCACC
p378_RrnJP1_-39_for	CCGGAATTCTATTGCACTATTATTTACTAGG
p379_RrnJP1_-60_for	CCGGAATTCTTAGTATTTCTTCAAAAAAACTATTGC
p616_RrnJP1_102	ATAGAATTCATCCTCCATAGGGAAAGG
p463_PrrnJ_SUB_up_for	CCGGAATTCTCGACTGCAGTGGTACCTAGGCTATTGCACTATTATTTACTAGG
p464_trxB_UP_rrnJ_core	CCGGAATTCGAATACATTTAATCGTGTTGAGCAAAAATATTGCACTATTATTTACTA
222_pDR111_for	CAGGAATTCGACTCTCTAGC
223_pDR111_rev	taACTAGTATAATGGATTTCCTTACGCG
p455_Pveg_core_for	AATTCTATTTGACAAAAATGGGCTCGTGTTGTACAATAAATGTAA
p456_Pveg_core_rev	AGCTTTACATTTATTGTACAACACGAGCCCATTTTTGTCAAATAG
491_RrnJP1_up	ataGAATTCGATGCCGCTCTTTTTAAATCCCTTAGTATTTCTTCAAAAAAA
493_Pveg_core_rev	tatAAGCTTTACATTTATTGTACAACACGAGCCCATTTTTGTCAAATA
494_SUB_UP_Pveg	ataGAATTCTCGACTGCAGTGGTACCTAGGTATTTGACAAAAATGG
495_RrnJP1_UP_Pveg	CTTAGTATTTCTTCAAAAAAATATTTGACAAAAATGGGC
LK2037/rrnJ_F	GCGAATTCAAGAGCGGTATCCTCCATAG
LK2039/rrnJP1+P2_R	GCAAGCTTGACTTTATTATTATAACTCG

Table S8 List of oligonucleotides for qPCR experiments

primer	**Sequence (5'-3')**

585_qPCR_lacZ_rev	CGTTTCACCCTGCCATAAAG
586_qPCR_lacZ_for	GGAAGATCAGGATATGTGGC
595_qPCR_rplC_for	TCCGGTAACTGTTATCGAGG
596_qPCR_rplC_rev	GACCAACTTCATACGCATCC
599_qPCR_trxB_for	CCGTGCTGTCATCATTGCTG
600_qPCR_trxB_rev	TATACGCCTTCTTCAACCGC
605_qPCR_23S_for	CTTTGATCCGGAGATTTCCG
606_qPCR_23S_rev	GTACAGAGTGTCCTACAACC
638_qPCR_rplS_for	GGTGGAATCAGCGAAACGTT
639_qPCR_rplS_rev	TAATACGAGCCGCTTTTCCG
640_qPCR_rpsD_for	GGCTCGCTATACAGGTCCAT
641_qPCR_rpsD_rev	TGCGGAATTGACGTTCGTTT
648_qPCR_ssrA_for	CGAGCTCTTCCTGACATTGC
649_qPCR_ssrA_rev	AACCCACGTCCAGAAACATC
650_qPCR_rplO_for	GTCGTGGTATTGGTTCTGGC
651_qPCR_rplO_rev	GTGACTTCCGTTCCTTCTGC
722_qPCR_ytvA_for	ATTGGCCCAAGTGAACGAAC
723_qPCR_ytvA_rev	ATCGGAAGCACTTTAACGGC
726_qPCR_hag_for	CATGCGATCCTTCAACGTGT
727_qPCR_hag_rev	TGCAGGAGTAGCTGTGTCAA
758_qPCR_groEL_for	GGTGATCGCCGTAAAGCAAT
759_qPCR_groEL_rev	TGTTTCTTCCACTTGAGCGC
762_qPCR_htpG_for	GGCATAGACACGGATGAGGA
763_qPCR_htpG_rev	GCTGTCAGGCATCGCATTTA
765_qPCR_hslO_for	ACGATGCCTGTCAGATTCCA
766_qPCR_hslO_rev	TAGTTTGGTCACGAAGCCCT

References

Chang, B.Y., and Doi, R.H. (1990) Overproduction, purification, and characterization of Bacillus subtilis RNA polymerase sigma A factor. *J Bacteriol* **172**: 3257–3263.

Hantke, I., Schäfer, H., Janczikowski, A., and Turgay, K. (2018) YocM a small heat shock protein can protect Bacillus subtilis cells during salt stress. *Mol Microbiol* .

Igo, M., Lampe, M., Ray, C., Schafer, W., Moran, C.P., and Losick, R. (1987) Genetic studies of a secondary RNA polymerase sigma factor in Bacillus subtilis. *J Bacteriol* **169**: 3464–3469.

Krüger, E., Zühlke, D., Witt, E., Ludwig, H., and Hecker, M. (2001) Clp-mediated proteolysis in Gram-positive bacteria is autoregulated by the stability of a repressor. *EMBO J* **20**: 852–863.

Molière, N., Hoßmann, J., Schäfer, H., and Turgay, K. (2016) Role of Hsp100/Clp Protease Complexes in Controlling the Regulation of Motility in Bacillus subtilis. *Front*

Microbiol **7** http://journal.frontiersin.org/Article/10.3389/fmicb.2016.00315/abstract. Accessed February 1, 2018.

Nakano, M.M., Zhu, Y., Liu, J., Reyes, D.Y., Yoshikawa, H., and Zuber, P. (2000) Mutations conferring amino acid residue substitutions in the carboxy-terminal domain of RNA polymerase alpha can suppress clpX and clpP with respect to developmentally regulated transcription in Bacillus subtilis. *Mol Microbiol* **37**: 869–884.

Reder, A., Höper, D., Weinberg, C., Gerth, U., Fraunholz, M., and Hecker, M. (2008) The Spx paralogue MgsR (YqgZ) controls a subregulon within the general stress response of Bacillus subtilis. *Mol Microbiol* **69**: 1104–1120.

Riley, E.P., Trinquier, A., Reilly, M.L., Durchon, M., Perera, V.R., Pogliano, K., and Lopez-Garrido, J. (2018) Spatiotemporally regulated proteolysis to dissect the role of vegetative proteins during *Bacillus subtilis* sporulation: cell-specific requirement of σ^{H} and σ^{A}: Spatiotemporally regulated proteolysis in *Bacillus*. *Mol Microbiol* **108**: 45–62.

Rochat, T., Nicolas, P., Delumeau, O., Rabatinová, A., Korelusová, J., Leduc, A., *et al.* (2012) Genome-wide identification of genes directly regulated by the pleiotropic transcription factor Spx in Bacillus subtilis. *Nucleic Acids Res* **40**: 9571–9583.

Rosenberg, A., Sinai, L., Smith, Y., and Ben-Yehuda, S. (2012) Dynamic Expression of the Translational Machinery during Bacillus subtilis Life Cycle at a Single Cell Level. *PLoS ONE* **7**: e41921.

Runde, S., Molière, N., Heinz, A., Maisonneuve, E., Janczikowski, A., Elsholz, A.K.W., *et al.* (2014) The role of thiol oxidative stress response in heat-induced protein aggregate formation during thermotolerance in *B acillus subtilis*: Thiol oxidation in protein aggregate formation. *Mol Microbiol* **91**: 1036–1052.

Spizizen, J. (1958) TRANSFORMATION OF BIOCHEMICALLY DEFICIENT STRAINS OF BACILLUS SUBTILIS BY DEOXYRIBONUCLEATE. *Proc Natl Acad Sci U S A* **44**: 1072–1078.

Youngman, P., Perkins, J.B., and Losick, R. (1984) A novel method for the rapid cloning in Escherichia coli of Bacillus subtilis chromosomal DNA adjacent to Tn917 insertions. *Mol Gen Genet* **195**: 424–433.

Supplementary Figures

Figure S1: Growth and survival of strains with deletions of individual heat shock regulators.

A: Growth of *B. subtilis* wild type, Δ*sigB*, Δ*ctsR*, Δ*hrcA* or Δ*spx* cells spotted on agar plates at 37 °C (left) or 55 °C (right) over night. **B:** Survival of wild type (black lines) and mutant strains Δ*sigB*, Δ*ctsR*, or Δ*hrcA* (red lines) during thermotolerance. Solid lines: 15 min pre-shock at 48 °C, dashed lines: no pre-shock. Means of normalized

log10 colony forming units and standard errors of 3 (mutants) or 48 (wild type) biological replicates are shown.

Figure S2: Relative levels of selected transcripts in mutant strains with increased or decreased Spx levels.

Samples of exponentially growing Δ*clpX or* Δ*spx*Δ*clpX* cells were subjected to western or northern blotting.

Figure S3: Genetic organisation of the transcriptional promoter fusions.

Transcriptional *rrn-gfp* fusions **(A)** or *rrnJ-lacZ* fusions **(B)** were integrated into the *amyE* locus. The Digoxigenin-11-UTP labelled RNA probe binds within the *gfp* or *lacZ* mRNA.

Figure S4: Spx acts similarly on all *rrn*-promoters

Northern blots of *rrn-gfp* transcripts. Mid-log cultures (OD_{600} of 0.3-0.35) of BHS923 - BHS938 cells, carrying transcriptional fusions of 7 *rrn* promoters to *gfp*, were divided and treated with or without 1 mM IPTG. Samples were withdrawn after 30 min and 2 µg total RNA per lane were subjected to northern blotting. The relative position of the 16 S and 23 S band is indicated.

Figure S5: Relative transcription of selected targets during oxidative stress and in Δ*spx*Δ*mgsR* mutant cells

Relative expression changes as determined by RT-qPCR. Means and standard errors of three biological replicates are shown. All strains carried *rrnJ* P1 -*lacZ* in the *amyE* site. **A:** Log-phase cultures of BHS220 (wild type *rrnJ* P1-*lacZ*) and BHS222 (Δ*spx rrnJ* P1-*lacZ*) were grown in minimal medium, divided and supplemented with or without 1 mM diamide for 15 min, then harvested. **B:** Log-phase cultures of BHS220 (wild type *rrnJ* P1-*lacZ*), BHS222 (Δ*spx rrnJ* P1-*lacZ*), BHS882 (Δ*mgsR rrnJ*

P1-*lacZ*) and BHS883 (Δ*spx* Δ*mgsR rrnJ* P1-*lacZ*) were divided and incubated at 37 °C or 50 °C for 15 min, then harvested. C: Northern blot showing the *rrnJ* P1-*lacZ* and *trxB* transcript. Log-phase cultures of BHS220 (wild type *rrnJ* P1-*lacZ*), BHS549 (*cxs*-1) and BHS550 (*cxs*-2) were divided and treated with or without 1 µg/mL vancomycin for 15 min and then harvested.

Figure S6: Impaired growth of strains synthesizing Spx^{DD} *in trans*

A: Growth of BHS148 (*amyE::Phy-spx^{DD}*) cells in LB medium. The mid-log culture was divided and supplemented with (red bar) or without (black bar) 1 mM IPTG. **B:** Growth of BHS148 (*amyE::Phy-spx^{DD}*), BHS535 (*amyE::Phy-spx^{DD} rpoA^{Y263C}*) and BHS536 (*amyE::Phy-spx^{DD} rpoA^{V260A}*) cells with (squares and dashed lines) or without (diamonds and solid lines) 1 mM IPTG added from the start.

Figure S7: Distribution of GFP-Spx fluorescence and cell size

Scatter plots and histograms showing the distribution and the relationship of GFP-Spx fluorescence and cell area among single cells of the experiment shown in Fig. 7.

Figure S1

A

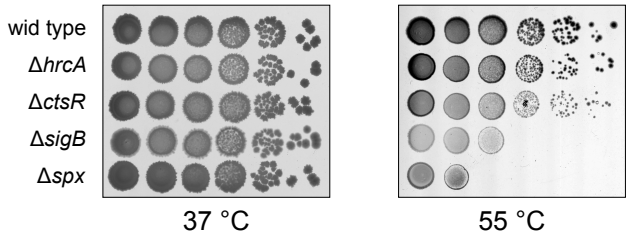
wid type
ΔhrcA
ΔctsR
ΔsigB
Δspx
37 °C
55 °C

B

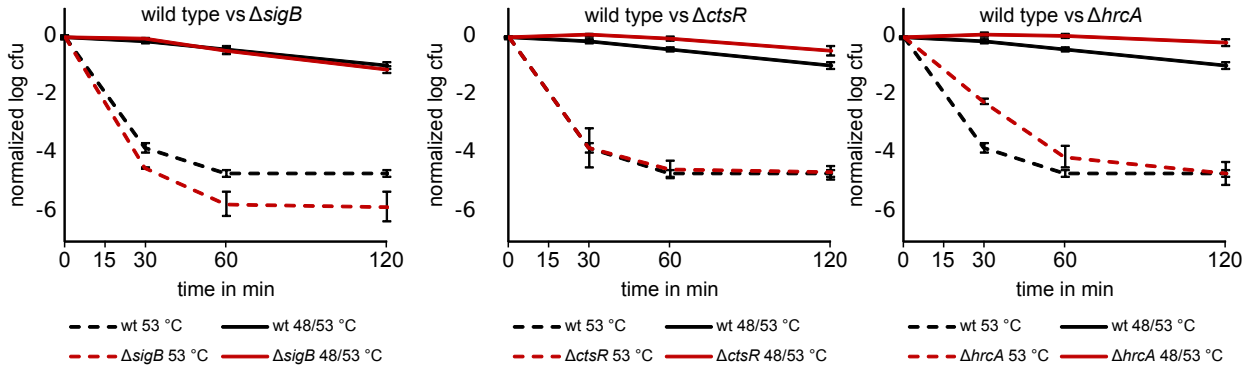
wild type vs ΔsigB
wild type vs ΔctsR
wild type vs ΔhrcA
normalized log cfu
0
-2
-4
-6
0 15 30 60 120
time in min
wt 53 °C
wt 48/53 °C
ΔsigB 53 °C
ΔsigB 48/53 °C
ΔctsR 53 °C
ΔctsR 48/53 °C
ΔhrcA 53 °C
ΔhrcA 48/53 °C

Figure S2

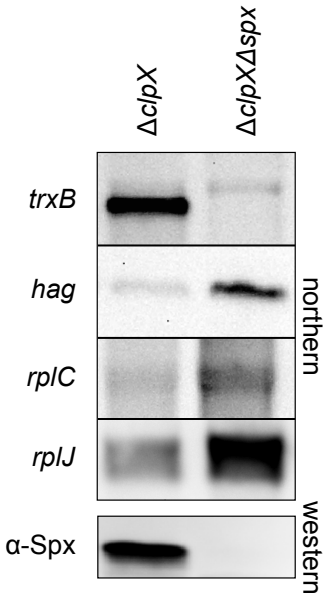

Figure S3

A

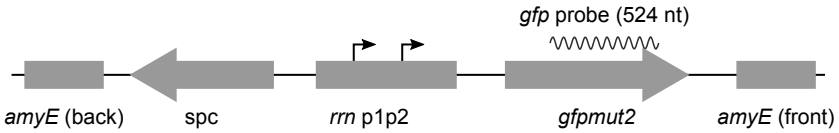
gfp probe (524 nt)
amyE (back)
spc
rrn p1p2
gfpmut2
amyE (front)

B

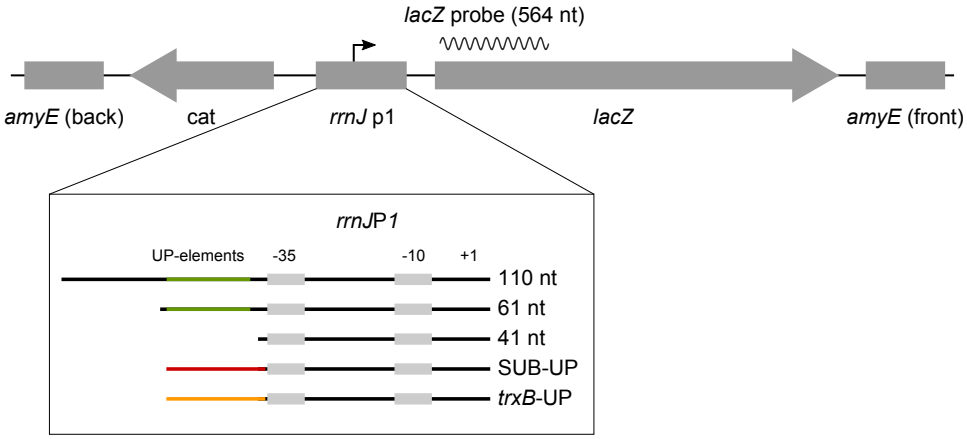
lacZ probe (564 nt)
amyE (back)
cat
rrnJ p1
lacZ
amyE (front)
rrnJP1
UP-elements
-35
-10
+1
110 nt
61 nt
41 nt
SUB-UP
trxB-UP

Figure S4

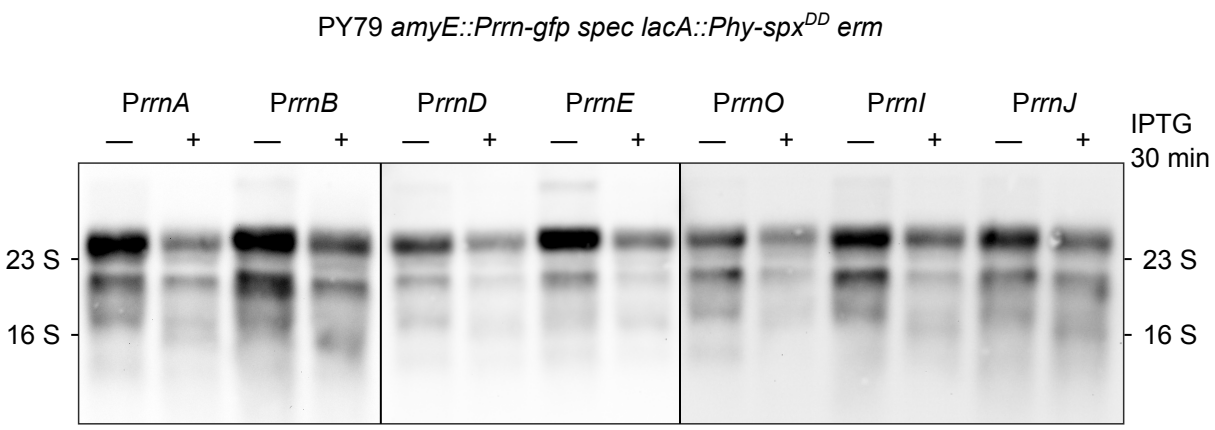
PY79 amyE::Prrn-gfp spec lacA::Phy-spx^DD erm
PrrnA
PrrnB
PrrnD
PrrnE
PrrnO
PrrnI
PrrnJ
— + — + — + — + — + — + — +
IPTG
30 min
23 S
16 S
23 S
16 S

Figure S5

A

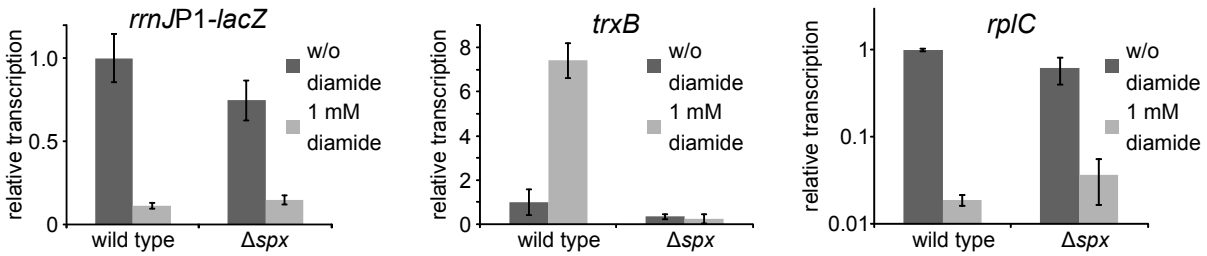

B

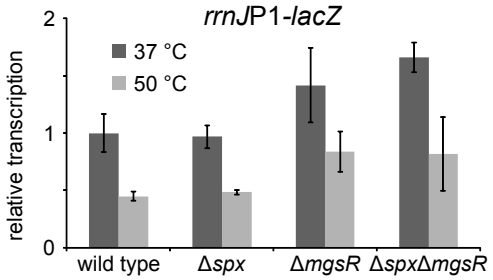

C

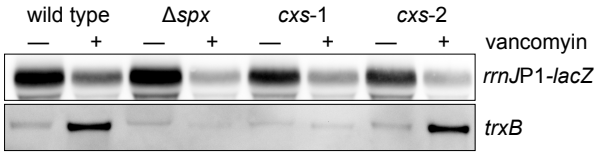

Figure S6

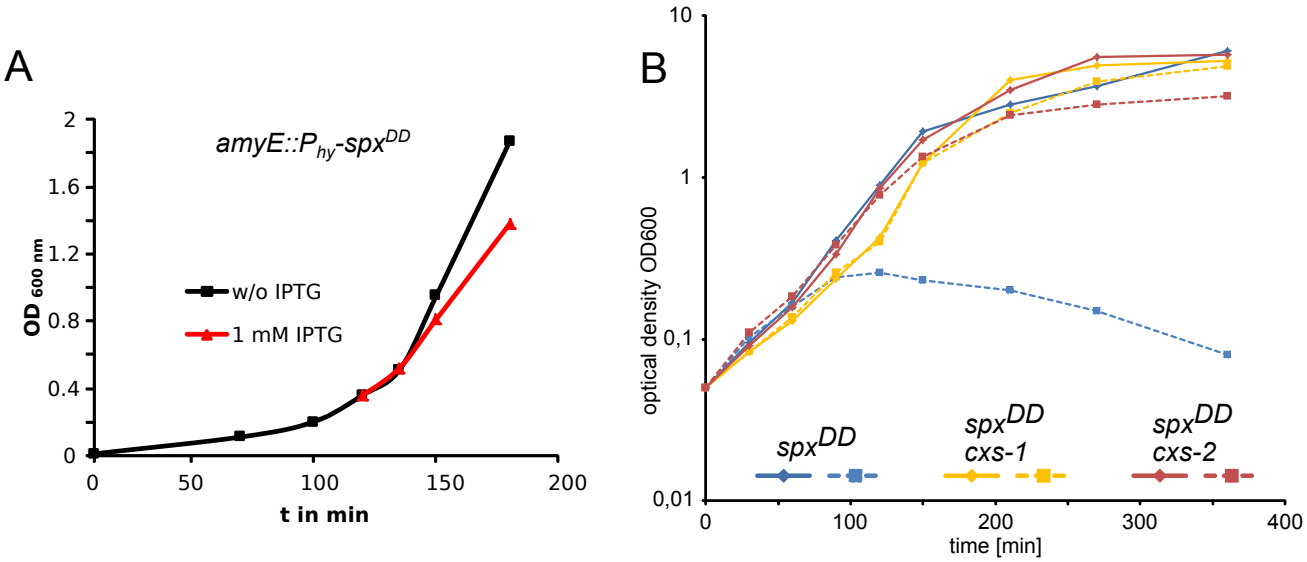
A
amyE::P_hy-spx^DD
w/o IPTG
1 mM IPTG
OD 600 nm
t in min
B
optical density OD600
time [min]
spx^DD
spx^DD cxs-1
spx^DD cxs-2

Figure S7

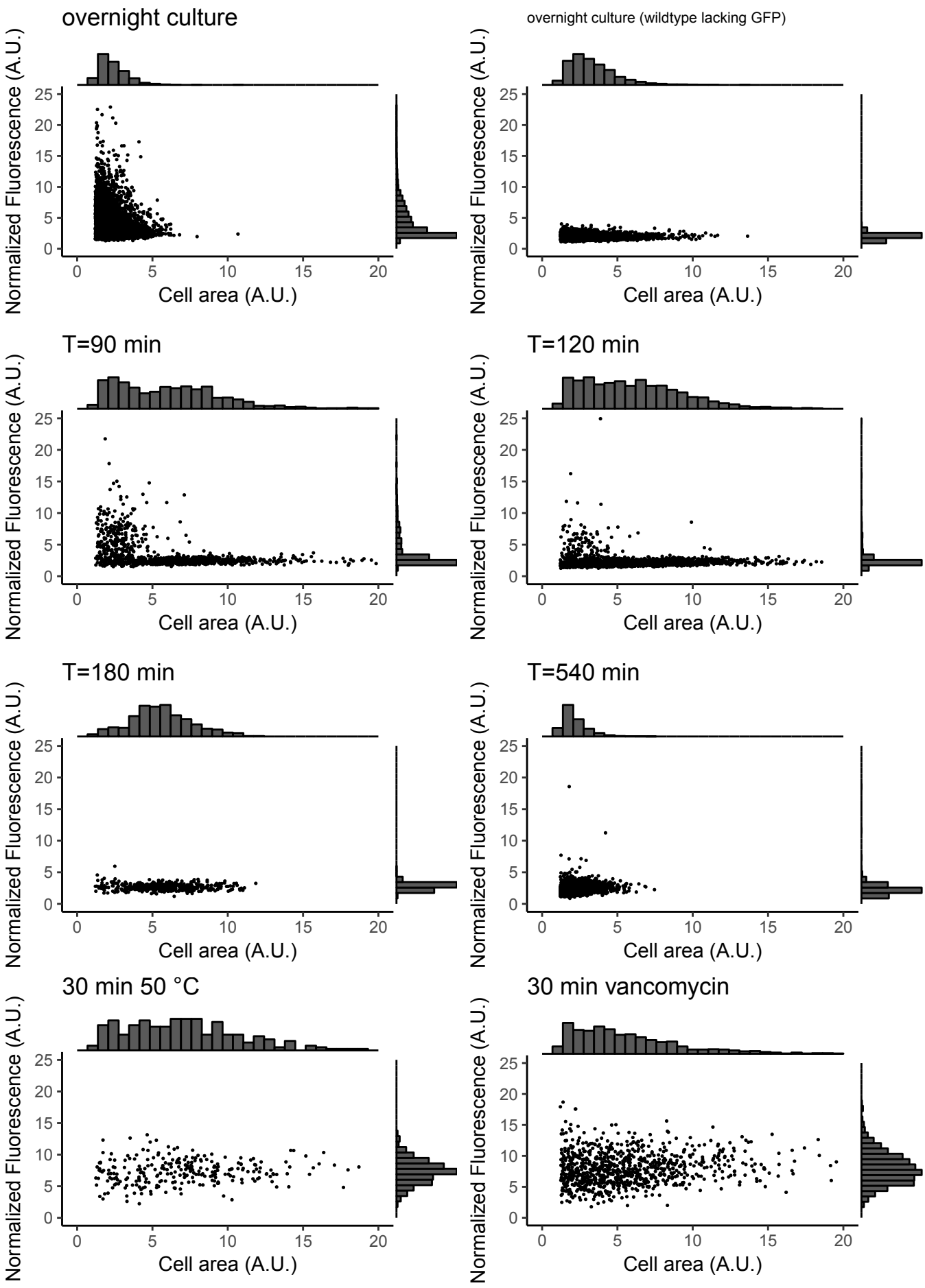
overnight culture
overnight culture (wildtype lacking GFP)
T=90 min
T=120 min
T=180 min
T=540 min
30 min 50 °C
30 min vancomycin
Normalized Fluorescence (A.U.)
Cell area (A.U.)
0
5
10
15
20
25

PUBLICATION III

FEBS Letters

FEBS PRESS science publishing by scientists

Domain structure of HelD, an interaction partner of *Bacillus subtilis* RNA polymerase

Tomáš Koval'[1], Petra Sudzinová[2], Terézia Perháčová[1], Mária Trundová[1], Tereza Skálová[1], Karla Fejfarová[1], Hana Šanderová[2], Libor Krásný[2], Jarmila Dušková[1] and Jan Dohnálek[1]

1 Laboratory of Structure and Function of Biomolecules, Institute of Biotechnology of the Czech Academy of Sciences, v. v. i., Biocev, Vestec, Czech Republic

2 Laboratory of Microbial Genetics and Gene Expression, Institute of Microbiology of the Czech Academy of Sciences, v. v. i., Praha 4, Czech Republic

Correspondence

J. Dohnálek, Laboratory of Structure and Function of Biomolecules, Institute of Biotechnology of the Czech Academy of Sciences, v. v. i., Biocev, Průmyslová 595, 25250 Vestec, Czech Republic

Tel: +420 325 873 758

E-mail: dohnalek@ibt.cas.cz

Website: http://www.ibt.cas.cz/vyzkum/laboratore/laborator-struktury-a-funkce-biomolekul/

Tomáš Koval' and Petra Sudzinová contributed equally

Terézia Perháčová died on 27 August 2017.

(Received 14 December 2018, revised 29 March 2019, accepted 1 April 2019, available online 23 April 2019)

doi:10.1002/1873-3468.13385

Edited by Stuart Ferguson

The HelD is a helicase-like protein binding to *Bacillus subtilis* RNA polymerase (RNAP), stimulating transcription in an ATP-dependent manner. Here, our small angle X-ray scattering data bring the first insights into the HelD structure: HelD is compact in shape and undergoes a conformational change upon substrate analog binding. Furthermore, the HelD domain structure is delineated, and a partial model of HelD is presented. In addition, the unique N-terminal domain of HelD is characterized as essential for its transcription-related function but not for ATPase activity, DNA binding, or binding to RNAP. The study provides a topological basis for further studies of the role of HelD in transcription.

Keywords: *Bacillus subtilis*; HelD; RNAP; SAXS

Bacteria are the dominant form of life on Earth. They inhabit every possible niche and excel at adaptation. Adaptation depends on changes in gene expression. The first step in gene expression is transcription of genetic information from DNA into RNA. The key enzyme of this process in bacteria is a multisubunit enzyme—DNA-dependent RNA polymerase (RNAP). The activity of RNAP has to be tightly regulated. This is mediated by various factors, such as small molecules including nucleoside triphosphates (NTPs) [1,2] and ppGpp [3], by small RNAs, like 6S and Ms1 RNA [4,5], and by numerous proteins [6–8].

Previously, we and others identified a new interaction partner of RNAP in *Bacillus subtilis*, a helicase-like protein termed HelD (~ 90 kDa) [9,10]. HelD belongs to the UvrD helicase family and, based on a previous bioinformatics analysis, consists of three

Abbreviations

AMP-PNP, adenosine 5′-(β,γ-imido)triphosphate; MBP, maltose binding protein; R_g, radius of gyration; SAXS, small-angle X-ray scattering; SEC, size-exclusion chromatography; SEC-SAXS, size-exclusion chromatography in line with small-angle X-ray scattering; TCEP, tris(2-carboxyethyl)phosphine.

domains: (a) the N-terminal domain, which bears no homology to other known helicases, (b) the ATPase domain, and (c) the C-terminal domain. Other helicases from this protein family (superfamily 1, SF1) are capable of unwinding DNA in either 3′-5′ (SF1A subfamily) or 5′-3′ (SF1B subfamily) translocation direction. Structural experiments with the SF1 family helicases indicate that these enzymes are monomers [11]. The most thoroughly studied helicases are PcrA from gram-positive bacteria and UvrD from gram-negative bacteria that share the same domain organization [12–15]. To the contrary, the predicted domain structure of HelD is different and the sequence identity is low (12% between HelD and UvrD). Nevertheless, UvrD is a protein with known 3D structure that is most related to HelD. UvrD's ATP-ase and 'C-terminal' domains are similar to HelD but with different topology; importantly, the DNA-binding domain of UvrD is not present in HelD.

The *Escherichia coli* protein RapA, involved in the release of stalled transcription complexes by backward translocation, represents the only related protein (sequence identity to HelD 21.0%), for which coordinates of the complex with RNAP are available (PDB ID 4S20) [16]. The domain structure of RapA resembles that of UvrD (N-terminal domain, ATPase domains) but with different chain topology [17].

Previously, we showed that HelD binds to RNAP and stimulates its activity in an ATP-dependent manner by stimulating transcriptional cycling and elongation [9]. Also, HelD was reported to be involved in DNA repair and homologous recombination [18] and amyloid-like fibrils formation [19]. A strain lacking the HelD-encoding gene displays prolonged lag phase [9]. Nevertheless, the specific role(s) and structure of HelD are still unknown.

Here, we extend the knowledge on HelD by characterizing its shape by small angle X-ray scattering (SAXS), by analysis of its domain structure, and by studies of the importance of the unique N-terminal domain of HelD for binding to DNA and to RNAP and for the activity of the protein.

Materials and methods

Preparation of protein samples and complexes

Bacillus subtilis HelD

The HelD from *B. subtilis* was expressed from pHelD-His6 (LK800, Table 1) in *E. coli* BL21 (DE3). The construct contained a 6xHis tag at the N-terminus cleavable by TEV protease. Details of the cloning, expression, and purification procedures are in [9].

Table 1. Bacterial strains and plasmids used in this study

Strain	Description	Source
LK782	Bsu RNAP *rpoC*-10xHis, *helD::MLS*	Wiedermannová *et al.* [9]
LK22	pCD2/Bsu_sigA; BL21 (DE3)	Chang and Doi [21]
LK800	pHelD-His6; BL21 (DE3)	Wiedermannová *et al.* [9]
HelDΔN	MBP-HelDΔN, Lemo21 (DE3)	This work
Plasmid		
pRLG7558	p770 with P*veg* (−38/+1, +1G)	Krasny and Gourse [1]
pLK28	p770 with *rrn*B P1 (−248/+8)	Krasný *et al.* [22]

Bacillus subtilis HelDΔN

The truncated version of HelD (HelDΔN, residues 204–774) lacking the N-terminal domain was expressed in *E. coli* using pET28-MBP-TEV, a gift from Zita Balklava & Thomas Wassmer (Addgene plasmid # 69929; http://n2t.net/addgene:69929; RRID:Addgene_69929) [20]. HelDΔN was prepared in fusion with maltose binding protein (MBP) and His-tag at the N-terminus. MBP is cleavable from the construct using TEV protease. HelDΔN expression was induced with 1 mM IPTG in *E. coli* Lemo21 (DE3) cells (New England Biolabs, Ipswich, MA, USA) grown in Power broth (Molecular Dimensions, Newmarket, UK). HelDΔN was purified using Ni-NTA affinity chromatography and size-exclusion chromatography. For details, see Supporting Information.

TEV digestion

Except for samples for SAXS experiments, both HelD and HelDΔN were treated with TEV protease. TEV cleavage was performed in 50 mM Tris/HCl, pH 7.5, 100 mM NaCl, 0.5 mM TCEP, 0.5 mM dithiothreitol (DTT), 1 mM EDTA, and 5% (v/v) glycerol at 37 °C for 1 h. Both samples were then run on charged HisTrap™ FF (1 mL) columns (GE-Healthcare, Chicago, IL, USA) using an ÄKTA purifier and the proteins were in the flow-through fraction. Samples were analyzed using SDS/PAGE (Fig. S1).

Bacillus subtilis RNA polymerase

RNAPΔHelD was produced using a strain lacking HelD (LK782, Table 1). Expression and purification were done according to Ref. [9] with the addition of size-exclusion chromatography (SEC) performed using an ÄKTA purifier, a Superose 6 10/300 GL column (GE Healthcare),

and 100 mM Na/K phosphate buffer, pH 7.5 supplemented with 50 mM NaCl, 0.5 mM TCEP, and 3% (v/v) glycerol.

SAXS data collection

Size-exclusion chromatography in line with small-angle X-ray scattering (SEC-SAXS) were used to analyze HelD in solution −/+ an ATP analog. HelD (10 mg·mL^{-1}) in the presence of 10 mM adenosine 5′-(β,γ-imido)triphosphate (AMP-PNP), a non-hydrolysable analog of ATP, was applied to a Superdex 200 10/300 GL column (GE Healthcare) at a flow rate of 0.5 mL·min^{-1}. HelD without AMP-PNP (19 mg·mL^{-1}) was applied to a Superose 6 10/300 GL column (GE Healthcare) at a flow rate of 0.4 mL·min^{-1}. Both samples were applied using an FPLC Agilent BioInert system with an autosampler. Buffer containing 100 mM Na/K phosphate pH 7.5, 50 mM NaCl, 0.5 mM TCEP, and 3% (v/v) glycerol was used for HelD without AMP-PNP. For HelD with bound AMP-PNP, 50 mM Tris pH 7.5, 50 mM NaCl, 5 mM $MgCl_2$, 0.5 mM TCEP, and 3% (v/v) glycerol was used. SAXS data were collected on the eluted fractions at beam line P12 of the synchrotron radiation source PetraIII in Hamburg [23] using a Pilatus 2M detector (Dectris, Baden-Daettwil, Switzerland) at sample to detector distance 3 m, λ = 1.24 Å, exposure time per image 0.995 s, at 20 °C. Quality of SAXS data and the SEC profiles are shown in Supporting Information (Figs S2–S4).

SAXS data analysis and *ab initio* model calculations

The SEC-SAXS data were processed using ATSAS version 2.8.2 with help of versions 2.7.2 (stable version of DAMMIF) and 2.8.3 [24]. Analysis of the resulting *ab initio* models, generation of three-dimensional molecular envelopes, fitting with protein structures, and generation of the graphics were performed with the UCSF CHIMERA package [25]. SEC-SAXS frames were merged in interval selected by R_g value, omitting frames of low quality (Fig. S2). The selected intervals were: for HelD:AMP-PNP, frames 1268–1331 as body and 1420–1569 as solvent; for HelD, frames 2443–2448 and 895–1027, 2807–2980 as solvent. Solvent-subtracted merged SAXS curves, Guinier plot, Kratky plot, and distance distribution function are shown in Figs S3 and S4. R_g, D_{max}, and molecular weight estimated from SAXS data are shown in Table 2.

Sequence analysis

Multiple and pairwise sequence alignments were performed using the Clustal Omega server [27], MUSCLE v3.8.31 [28], and GeneDoc [29]. Manual editing of sequence alignments was done in GeneDoc. Structure-based sequence alignments were calculated using the Secondary structure matching algorithm of the PDBeFold server (http://www.ebi.ac.uk/msd-srv/ssm/) [30] and processed using GeneDoc and MUSCLE.

Molecular modeling

Generation of the partial HelD model was based on the coordinates of the C-terminal domain of the putative DNA helicase from *Lactobacillus plantarum* (LpCter, PDB ID 3DMN, unpublished). Alternative conformations and ligands were removed from the model. Two positions of the domain in each of the structures of helicase UvrD from *E. coli* (PDB ID 2IS4) [15] and of protein RapA from *E. coli* (PDB ID 4S20) [16] were found using the PDBeFold server with multiple hits option and standard parameters. For each target structure, the first 20 matches were analyzed and assigned to two categories: (a) putative 1A domain and (b) C-terminal domain (putative 2A domain). Alignments of the full sequences of UvrD, RapA, and HelD, and of sequences of individual domains of these proteins with the addition of LpCter provided information on localization of both domains in the HelD sequence. These results together with structural alignments of 3D structures of the full proteins and of individual domains were used as a basis for assembling the model of the recurring domains in HelD. On the basis of a higher sequence similarity between HelD and UvrD (as opposed to RapA) in the interdomain region, the mutual position of the putative 1A and C-terminal (putative 2A) domains was defined as in UvrD.

The C-terminal domain (putative 2A) of HelD could be reliably modeled with LpCter (100% coverage, 40% identity). Unreliable parts of the 3D model of the putative 1A domain similar to LpCter (as judged by agreement

Table 2. Results of SAXS data processing. The individual columns correspond to samples of HelD and complexes HelD:AMP-PNP. The parameters (excluding DAMMIF values) were calculated using PRIMUS [26]. R_g is radius of gyration calculated from the Guinier plot (Figs S2–S4). D_{max} is the estimated maximum size of the particle (Fig. S2)

	HelD	HelD:AMP-PNP
I(0) [a.u.] (from Guinier)	3920.3	1588.9
R_g [Å] (from Guinier)	35.0	36.2
Guinier analysis fidelity [%]	72	87
I(0) [a.u.] (from P(r))	3913	1590
R_g [Å] (from P(r))	35.0	36.3
D_{max} [Å]	113.8	115.1
Porod volume [Å^3] (from P(r))	144	167
MW from sequence [kDa]	90	90
MW from DAMMIF [kDa]	107	90
MW from Porod [kDa]	90	104

between UvrD, RapA, and LpCter) were deleted. Secondary structure prediction for HelD was calculated using Jpred4 [31]. The multiple structure-based sequence alignment of the putative 1A and C-terminal (putative 2A) domains of the known structures was aligned against the sequence of HelD to satisfy the results of the secondary structure prediction. A satisfactory alignment was used to assign sequence to the model of the putative 1A domain of HelD. The assembled model of both domains of HelD was energy minimized using the Yasara server [32].

In vitro transcription assays

Transcription experiments were performed with the *B. subtilis* RNAP core lacking HelD (isolated from the strain LK782) reconstituted with saturating concentration of σ^A (ratio 1 : 5, strain LK22, [21]) and HelD/HelDΔN (ratio 1 : 4) in storage buffer (50 mM Tris-HCl, pH 8.0, 0.1 M NaCl, 50% (v/v) glycerol, 3 mM β-mercaptoethanol) for 15 min at 30 °C. Multiple round transcription reactions were carried out in 10 μL reaction volumes with 30 nM RNAP holoenzyme and 100 ng of supercoiled plasmid DNA containing *B. subtilis rrn*B P1 promoter [22]. The transcription buffer contained 40 mM Tris-HCl pH 8.0, 10 mM $MgCl_2$, 1 mM DTT, 0.1 mg·mL^{-1} BSA, 150 mM KCl, and NTPs (ATP, CTP were at 200 μM; GTP 1300 μM; UTP was 10 μM plus 2 μM radiolabeled [α-^{32}P]UTP). All transcription reactions were allowed to proceed for 15 min at 30 °C and were stopped with equal volumes of formamide stop solution (95% formamide, 20 mM EDTA, pH 8.0). Samples were loaded onto 7 M urea-7% polyacrylamide gels and electrophoresed. The dried gels were scanned with a Molecular Imager FX (Bio-Rad, Hercules, CA, USA) and visualized and analyzed using the QUANTITY ONE software (Bio-Rad).

Analysis of the formation of RNAP:HelD/HelDΔN complexes

To analyze the association of HelDΔN with RNAP *in vitro*, we performed gel-shift experiments under native conditions in non-denaturing PAGE gel. Full-length HelD was used as a positive control. Both HelD and HelDΔN were treated using TEV protease prior to experiments (Fig. S1). For the gel-shift assay, RNAP was mixed with either HelD or HelDΔN at molar ratio 1 : 1 and 1 : 2 and left in the dark at room temperature for 1 h. This incubation was performed in 100 mM Na/K phosphate buffer, pH 7.5, with 100 mM NaCl, 0.5 mM TCEP, and 3% (v/v) glycerol. The gel-shift assay was performed using an XCell SureLock™ mini-cell electrophoresis system, polyacrylamide NuPAGE® 7% Tris-acetate gel, Novex™ Tris-Glycine Native Sample Buffer, and Novex™ Tris-Glycine Native Running Buffer (ThermoFisher Scientific, Waltham, MA, USA). Electrophoresis was done according to the manufacturer's instructions.

ATPase activity of HelD and HelDΔN

ATPase activity of both full-length HelD and of the truncated construct HelDΔN was tested using samples treated with TEV protease. Reactions were carried out at 25 °C for 30 min. Mixtures (100 μL) contained 10 μg of protein and 10 mM of ATP in 50 mM Tris pH 7.5, 50 mM NaCl, and 5 mM $MgCl_2$. The amount of released phosphate was analyzed according to the modified molybdenum blue method [33] by spectrophotometry at λ = 850 nm using a microplate reader CLARIOstar (BMG LABTECH, Ortenberg, Germany).

DNA binding assay

Preparation of radiolabeled DNA

The DNA primer LK999 5′-GCGCTACGGCGTTTCACTTC-3′ was radiolabeled at the 5′ end by T4 polynucleotide kinase and purified with Nucleotide removal kit (Qiagene, Venlo, Netherlands). A DNA fragment was prepared with PCR from the plasmid containing P*veg* (pRLG7558) using the ^{32}P-labeled primer LK999 and primer LK1000 5′-CCACCTGACGTCTAAGAAACC-3′. The DNA fragment started at −118 relative to the transcription start site and ended at +55.

Native PAGE assays

About 0.5 pmol of 5′-radiolabeled DNA and HelD/HelDΔN at ratios 1 : 10, 1 : 20, 1 : 100, 1 : 400, and 1 : 800 were incubated for 15 min at 30 °C in buffer containing 50 mM Tris-HCl, pH 8.0, 0.1 M NaCl, 50% (v/v) glycerol, 3 mM β-mercaptoethanol. Final concentrations in the 10 μL reactions were 0.05 μM for DNA and up to 40 μM for proteins, respectively. As controls, denatured HelD/HelDΔN (5 min at 95 °C) at ratios 1 : 10, 1 : 100, 1 : 400, and 1 : 800 was used. After incubation, samples were mixed with Native PAGE 4X Sample buffer (Invitrogen, Waltham, MA, USA), loaded onto the Native PAGE 4–16% Bis-Tris Gel (Invitrogen), and electrophoresed. The dried gels were scanned with a Molecular Imager_FX (BioRad).

Results

HelD shape

To provide structural information for HelD, we performed numerous crystallization experiments with the protein and its complex with RNAP, all without success (data not shown). Therefore, we performed SAXS experiments. SAXS data were obtained for HelD and HelD in complex with AMP-PNP (an ATP analog used to mimic the ATP-bound state) in the SEC-SAXS mode. The average R_g values corresponded to the size of a monomer of HelD (Table 2).

Domain structure and modeling of HelD fragment

To get better insights into the domain structure of HelD, we performed sequence analysis and 3D modeling of (or parts of) HelD. We used sequences and structures of related proteins RapA, UvrD, and the C-terminal fragment of the *Lactobacillus plantarum* HelD homolog (LpCter), displaying the Rossman fold (Pfam, http://pfam.xfam.org) [34]. SF1 helicases, such as UvrD, typically consist of two domains divided into four subdomains: 1A, 1B, 2A, 2B. The domain structure of UvrD is shown in Fig. 1A. The following analysis starts with the C-terminal domain (of HelD) and continues toward the N-terminus.

As the starting point, we used LpCter and created its 3D superpositions with RapA and UvrD (Fig. 1B, C) using SSM (secondary structure matching). The 3D structure of LpCter superposed with 2A domains in both RapA and UvrD all showing Rossman fold (r.m.s.d. 2.8 Å on 109 C^{α} atoms of RapA and 1.8 Å on 152 C^{α} atoms of UvrD, sequence identity 11.9% and 23.0%, respectively). This Rossman fold was also identified at a second location, in domains 1A (r.m.s.d of C^{α} coordinates 3.0 Å for 113 residues of RapA and 2.5 Å for 109 residues of UvrD, sequence identity 11.5% and 9.2%, respectively). The fit of LpCter with domain 2A was better than the fit with domain 1A. Therefore, we propose to name the C-terminal domain of HelD as putative 2A and an internal part of HelD as putative 1A (Fig. 2).

Given the sequence similarity between RapA, UvrD, *L. plantarum* HelD, and *B. subtilis* HelD (illustrated in Fig. S5), it was possible to create a limited model of HelD consisting of two Rossman fold domains: the putative domain 1A and the C-terminal domain which corresponded to domain 2A (Fig. 1D). This partial HelD model, based on the coordinates of UvrD (PDB ID 2IS4) and LpCter (PDB ID 3DMN), was further used for interpretation of the SAXS data.

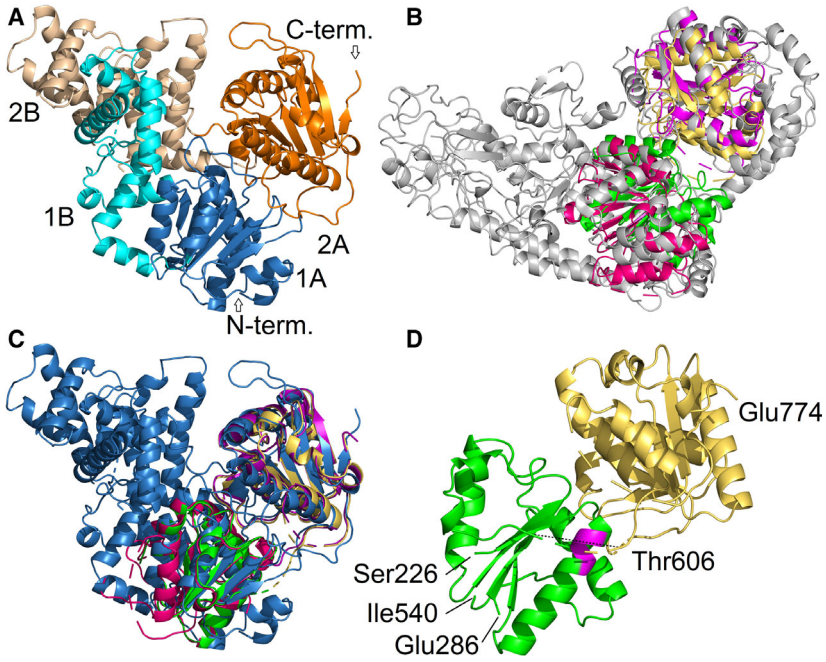

Fig. 1. Typical domain organization of SF1 helicases and structural alignments of UvrD and RapA with partial model of HelD. All protein chains are shown as cartoons with secondary structure elements. (A) Domain structure of UvrD from *Escherichia coli*. Domain 1A is colored dark blue, domain 1B light blue, domain 2A orange, and domain 2B pale yellow. Domains are marked. The N- and C-termini of UvrD in the structure are marked (protein chain continues with the C-terminal extension). (B) *E. coli* RapA (gray) with the best superposition of LpCter on the internal ATPase domain (hot pink), on the C-terminal domain (magenta), and the partial model of HelD—internal ATPase domain (putative 1A) in green and the C-terminal domain (putative 2A) in yellow. (C) *E. coli* UvrD with the best superposition of LpCter on the internal ATPase domain (hot pink), on the C-terminal domain (magenta), and the partial model of HelD—internal ATPase domain (putative 1A) in green and the C-terminal domain (putative 2A) in yellow. (D) Partial HelD model of the internal ATPase domain (putative 1A, green) and of the C-terminal domain (putative 2A, yellow) based on the coordinates of UvrD and RapA. Black dashed line—residues missing from the model in the linker region between the two domains. The typical ATP-binding site residues in the ATPase domain are colored in magenta (residues GSGK of the ATP-binding box, see Supplementary material Fig. S5, residues 236–239 and Fig. 2 for the placement of the ATP-binding box).

The remaining parts of HelD are the HelD-specific and N-terminal domains. In the linear aa sequence, the HelD-specific domain is inserted into the putative domain 1A. No 3D structures of these domains or their homologs exist.

The above described results suggested division of the HelD protein into four structurally compact parts of which one (putative domain 1A) is divided in the sequence in two parts (by the HelD-specific domain) and the other domains are continuous: N-terminal (residues 1–203, MNQQ…HHSD), putative 1A—part 1 (residues 204–~292, TQMK…EQAT), HelD-specific domain (~293–~539, FQEY…KNTK), putative 1A—part 2 (~540–606, IKHL…LKRT), and the C-terminal (putative 2A)

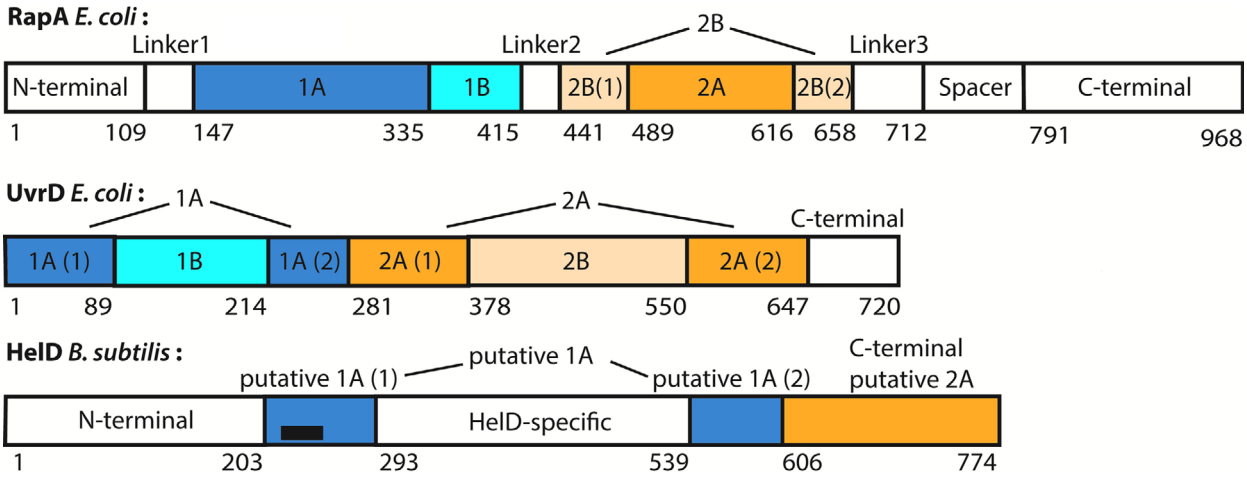

Fig. 2. Comparison of domain structure of RapA and UvrD from *Escherichia coli* and HelD from *Bacillus subtilis*. Residue numbers delimiting selected domains are shown. The black bar represents the estimated ATP-binding box, residues 220–258 in HelD.

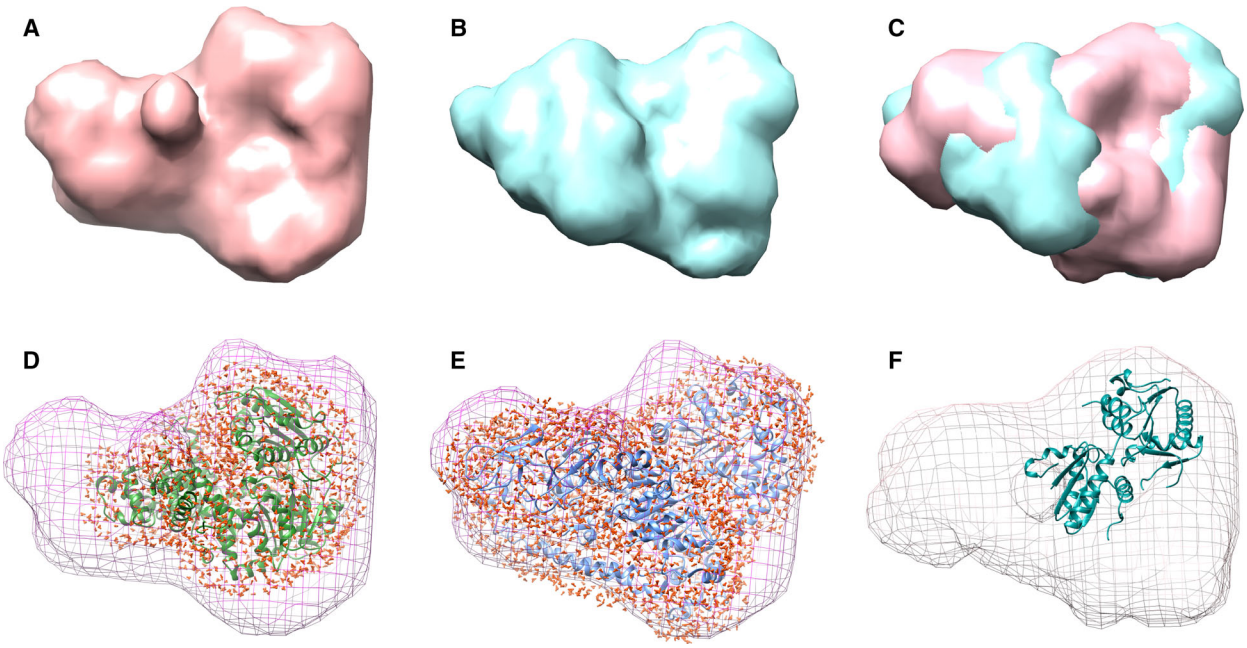

Fig. 3. Small-angle X-ray scattering-based molecular envelopes for *Bacillus subtilis* HelD. (A) HelD with AMP-PNP. (B) HelD—without AMP-PNP in the presence of 100 mM PO_4 ions. (C) Optimized fit of envelopes of HelD in the presence (pink) and absence (cyan) of AMP-PNP. (D) Fit of the solvated structure of *Escherichia coli* UvrD in the envelope of HelD:AMP-PNP. (E) Fit of the solvated structure of RapA in the envelope of HelD:AMP-PNP. (F) Partial model of HelD fitted into the SAXS envelope of HelD:AMP-PNP; the approximate position is based on the fit of UvrD and RapA in panels D and E, respectively.

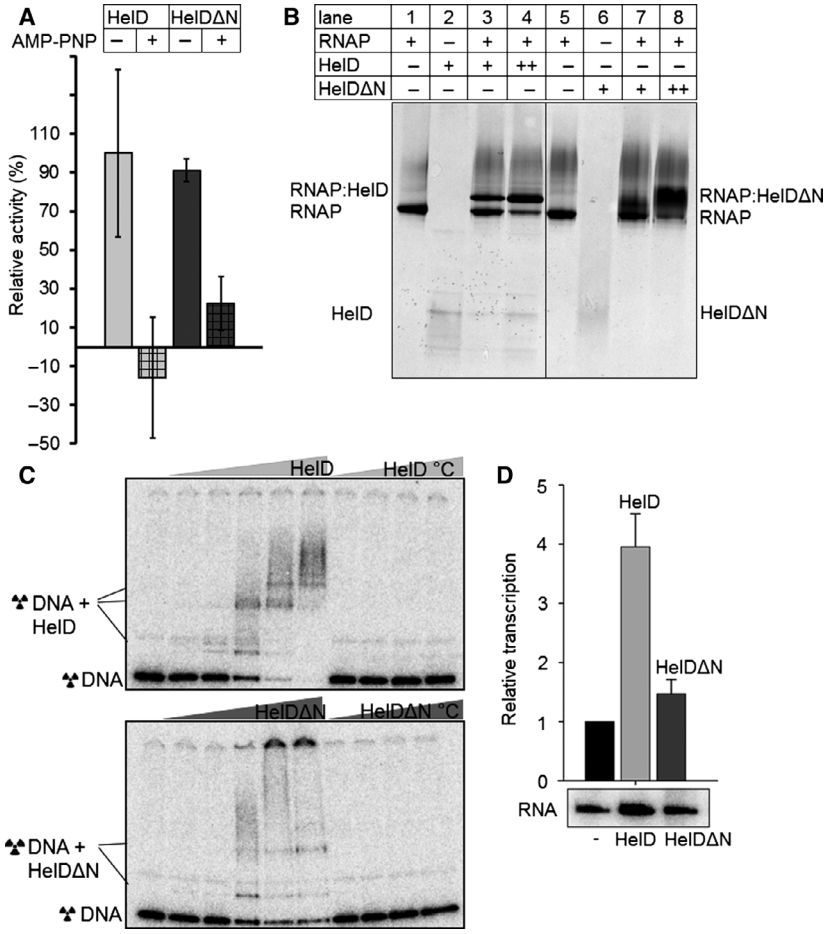

Fig. 4. Truncated HelDΔN lacking the N-terminal domain has still the ATPase activity and ability to form complex with RNAP and bind DNA but cannot stimulate transcription. (A) HelDΔN has the same ATPase activity as full-length HelD. The ATPase assay was done in the absence (indicated by –) and presence (indicated by +) of AMP-PNP as competitive inhibitor, in triplicates. Activity is quantified using the amount of PO_4 (in μmol) released from ATP by 1 μmol of the enzyme at 25 °C in 1 min. (B) Gel-shift assay under native conditions using non-denaturing PAGE. Lanes 1 and 5, RNAP expressed in the strain of *Bacillus subtilis* lacking the ability to produce HelD (LK782, Table 1); lane 2, HelD; lanes 3 and 4, RNAP mixed and incubated with HelD at molar ratios of 1 : 1 and 1 : 2, respectively; lane 6, HelDΔN; lanes 7 and 8, RNAP mixed and incubated with HelDΔN at molar ratios 1 : 1 and 1 : 2. (C) HelD and HelDΔN interact with radiolabeled DNA. DNA was prepared by PCR and the ratios of DNA: HelD/HelDΔN were 1 : 10, 1 : 20, 1 : 100, 1 : 400, and 1 : 800. As a control, the same ratios of heat-denaturated HelD/HelDΔN (with the exception of 1 : 20) were used (marked by symbol °C). (D) The N-terminal domain of HelD is required for stimulation of transcription. Multiple round transcriptions were performed with *B. subtilis* RNAPσ^A from a plasmid containing the *B. subtilis rrn*B P1 promoter. Transcription in the presence of HelD or HelDΔN is indicated; transcription in the absence of any factor is marked as (–) and was set as 1. The experiment was performed three times, the bars show the average values and the error bars ±SD. While the full-length HelD showed stimulation of transcription as we reported previously [9], the stimulation level with the HelDΔN product was significantly lower—close to the background level without HelD.

domain (607–774, YRST. . .QIAE). The suggested domain structure of HelD and its comparison with the domain structures of RapA and UvrD are shown in Fig. 2.

Subsequently, the SAXS-based *ab initio* shape calculations provided sets of three-dimensional models, which could be represented by average models of HelD shown in Fig. 3A–C. The optimized alignments between the SAXS models and monomers of UvrD and RapA (Fig. 3D,E) revealed that the AMP-PNP-bound HelD acquired a different conformation with the overall shape similar to its distant homologs. Based on the fit of UvrD and RapA in the HelD envelopes, an approximate position of the partial HelD model can be estimated (Fig. 3F).

N-terminal domain of HelD

Motivated by the sequence analysis, we decided to provide data for the unique N-terminal domain. We designed a construct of HelD lacking this domain,

hereafter called HelDΔN (residues 204–774). This truncated version of HelD was recombinantly produced in, and purified from *E. coli*, and subsequently used to address the role(s) of this part of the protein in the activity of HelD and its interactions with RNAP. First, we tested whether the enzymatic activity of HelD was still intact: HelDΔN maintained its ATPase activity at a level comparable to full-length HelD (Fig. 4A). Second, we investigated the importance of the N-terminal domain for the interaction with RNAP. Figure 4B shows that truncated HelD associated with the RNAP core similarly as HelD. As HelD was previously shown to interact rather nonspecifically with DNA [9], we compared HelDΔN with full-length HelD in their ability to bind DNA. Figure 4C shows that even in the absence of the N-terminal domain HelD still interacted with DNA although less strongly than full-length HelD. Finally, we tested the ability of the truncated protein to enhance transcription *in vitro*. Multiple round transcription assays revealed that the N-terminal domain was essential for the stimulatory effect of HelD (Fig. 4D).

Discussion

In this study, we obtained the first insights into the structure–function relationship of the RNAP-associated protein HelD. We characterized its overall 3D shape and a conformational change induced by ATP. Importantly, we described the domain structure of HelD and partially characterized the role of its unique N-terminal domain.

The shape of AMP-PNP-bound HelD differs from that of the unliganded form and approximately resembles the observed crystal structures of *E. coli* UvrD and RNAP-bound RapA. HelD without AMP-PNP likely represents a structurally distinct form. Even if limited by the low resolution of the current SAXS results, the observed changes suggest that, upon ATP binding/cleavage, HelD undergoes a pronounced conformational change (data for isolated HelD in solution). This conformational change is supported by the observed substantial increase in the thermal stabilization of HelD upon AMP-PNP binding (change of T_m from 51 °C to 62 °C, Fig. S6). Similar to HelD, a conformational change (rotation of the 2B subdomain) was observed for UvrD upon binding of nucleotide or/and DNA [35]. The observed change of HelD conformation can also be reminiscent of, for example, the translation elongation factor Tu (EF-Tu) where the binding of GTP or GDP radically affects the conformation, and in the absence of either molecule the protein collapses [36].

The structure of HelD can be newly dissected into the N-terminal domain (residues 1–203), the putative 1A domain, topologically split into two parts (204–~292 and ~540–606), the HelD-specific domain inserted in between them (293–~539), and the C-terminal (putative 2A) domain (607–774). The putative 1A domain and the C-terminal domain together form the ATPase unit. The overall organization of the protein is different from UvrD and RapA. The role of the ATPase unit most likely lies in securing the transfer of the ATP-driven conformational changes (confirmed by our SAXS results). Our results show that the N-terminal domain of HelD appears to be essential for its transcription-related function but not for ATPase activity, DNA binding, or binding to RNAP. This domain is instrumental for the HelD function by a yet unknown molecular mechanism.

Further studies will focus on explaining the role of the N-terminal domain, the structure and function of the HelD-specific domain, and elucidation of the exact mechanistic details of the ATP-driven action of HelD.

Acknowledgements

This work was supported by CSF (grants no. 15-05228S and 19-12956S), by the projects CIISB4-HEALTH (CZ.02.1.01/0.0/0.0/16_013/0001776), BIOCEV (CZ.1.05/1.1.00/02.0109), and ELIBIO (CZ.02.1.01/0.0/0.0/15_003/0000447) from the ERDF, institutional support (RVO 86652036), and MEYS support for CMS-Biocev (LM2015043). We thank J. Vohradsky for providing access to Molecular Imager FX Scanner, supported by the Czech research infrastructure for systems biology C4SYS (LM2015055).

Author contributions

LK and JDo designed research. TK, PS, HS, TP, and MT prepared samples and performed experiments. TK designed, performed, and analyzed SAXS experiments. TS performed computational modeling and analysis. KF performed sequence-structure analysis and stability calculations. JDu secured laboratory background. JDo performed sequence-structure analysis, modeling, and data interpretation. TK, PS, HS, LK, and JDo discussed results and wrote the manuscript.

References

1 Krásný L and Gourse RL (2004) An alternative strategy for bacterial ribosome synthesis: *Bacillus subtilis* rRNA transcription regulation. *EMBO J* **23**, 4473–4483.

2 Murray HD, Schneider D and Gourse RL (2003) Control of rRNA expression by small molecules is dynamic and nonredundant. *Mol Cell* **12**, 125–134.
3 Hauryliuk V, Atkinson GC, Murakami KS, Tenson T and Gerdes K (2015) Recent functional insights into the role of (p)ppGpp in bacterial physiology. *Nat Rev Microbiol* **13**, 298–309.
4 Steuten B, Hoch PG, Damm K, Schneider S, Köhler K, Wagner R and Hartmann RK (2014) Regulation of transcription by 6S RNAs. *RNA Biol* **11**, 508–521.
5 Hnilicová J, Jirát Matějčková J, Šiková M, Pospíšil J, Halada P, Pánek J and Krásný L (2014) Ms1, a novel sRNA interacting with the RNA polymerase core in mycobacteria. *Nucleic Acids Res* **42**, 11763–11776.
6 Borukhov S, Lee J and Laptenko O (2004) Bacterial transcription elongation factors: new insights into molecular mechanism of action. *Mol Microbiol* **55**, 1315–1324.
7 Brantl S and Licht A (2010) Characterisation of *Bacillus subtilis* transcriptional regulators involved in metabolic processes. *Curr Protein Pept Sci* **11**, 274–291.
8 Weiss A and Shaw LN (2015) Small things considered: the small accessory subunits of RNA polymerase in Gram-positive bacteria. *FEMS Microbiol Rev* **5**, 541–554.
9 Wiedermannová J, Sudzinová P, Koval' T, Rabatinová A, Šanderová H, Ramaniuk O, Rittich Š, Dohnálek J, Fu Z, Halada P *et al*. (2014) Characterization of HelD, an interacting partner of RNA polymerase from *Bacillus subtilis*. *Nucleic Acids Res* **42**, 5151–5163.
10 Delumeau O, Lecointe F, Muntel J, Guillot A, Guédon E, Monnet V, Hecker M, Becher D, Polard P and Noirot P (2011) The dynamic protein partnership of RNA polymerase in *Bacillus subtilis*. *Proteomics* **11**, 2992–3001.
11 Singleton MR, Dillingham MS and Wigley DB (2007) Structure and mechanism of helicases and nucleic acid translocases. *Annu Rev Biochem* **76**, 23–50.
12 Petit MA, Dervyn E, Rose M, Entian KD, McGovern S, Ehrlich SD and Bruand C (1998) PcrA is an essential DNA helicase of *Bacillus subtilis* fulfilling functions both in repair and rolling-circle replication. *Mol Microbiol* **29**, 261–273.
13 Epshtein V, Kamarthapu V, McGary K, Svetlov V, Ueberheide B, Proshkin S, Mironov A and Nudler E (2014) UvrD facilitates DNA repair by pulling RNA polymerase backwards. *Nature* **505**, 372–377.
14 Gwynn EJ, Smith AJ, Guy CP, Savery NJ, McGlynn P and Dillingham MS (2013) The conserved C-terminus of the PcrA/UvrD helicase interacts directly with RNA polymerase. *PLoS ONE* **8**, e78141.
15 Lee JY and Yang W (2006) UvrD helicase unwinds DNA one base pair at a time by a two-part power stroke. *Cell* **127**, 1349–1360.
16 Liu B, Zuo Y and Steitz TA (2015) Structural basis for transcription reactivation by RapA. *Proc Natl Acad Sci USA* **112**, 2006–2010.
17 Shaw G, Gan J, Zhou YN, Zhi H, Subburaman P, Zhang R, Joachimiak A, Jin DJ and Ji W (2008) Structure of RapA, a Swi2/Snf2 protein that recycles RNA polymerase during transcription. *Structure* **16**, 1417–1427.
18 Carrasco BA, Ndez SF, Petit M-A and Alonso JC (2001) Genetic recombination in *Bacillus subtilis* 168: Effect of Δ*helD* on DNA repair and homologous recombination. *J Bacteriol* **183**, 5772–5777.
19 Kaur G, Kapoor S and Thakur KG (2018) *Bacillus subtilis* HelD, an RNA polymerase interacting helicase, forms amyloid-like fibrils. *Front Microbiol* **9**, 1934.
20 Currinn H, Guscott B, Balklava Z, Rothnie A and Wassmer T (2015) APP controls the formation of PI (3,5)P vesicles through its binding of the PIKfyve complex. *Cell Mol Life Sci* **73**, 393–408.
21 Chang BY and Doi RH (1990) Overproduction, purification, and characterization of *Bacillus subtilis* RNA polymerase sigma A factor. *J Bacteriol* **172**, 3257–3263.
22 Krásný L, Tiserová H, Jonák J, Rejman D and Sanderová H (2008) The identity of the transcription + 1 position is crucial for changes in gene expression in response to amino acid starvation in *Bacillus subtilis*. *Mol Microbiol* **69**, 42–54.
23 Blanchet CE, Spilotros A, Schwemmer F, Graewert MA, Kikhney A, Jeffries CM, Franke D, Mark D, Zengerle R, Cipriani F *et al*. (2015) Versatile sample environments and automation for biological solution X-ray scattering experiments at the P12 beamline (PETRA III, DESY). *J Appl Crystallogr* **48**, 431–443.
24 Franke D, Petoukhov MV, Konarev PV, Panjkovich A, Tuukkanen A, Mertens HDT, Kikhney AG, Hajizadeh NR, Franklin JM, Jeffries CM *et al*. (2017) ATSAS 2.8: a comprehensive data analysis suite for small-angle scattering from macromolecular solutions. *J Appl Cryst* **50**, 1212–1225.
25 Pettersen EF, Goddard TD, Huang CC, Couch GS, Greenblatt DM, Meng EC and Ferrin TE (2004) UCSF Chimera – a visualization system for exploratory research and analysis. *J Comput Chem* **25**, 1605–1612.
26 Konarev VP, Volkov VV, Sokolova AV, Koch MHJ and Svergun DI (2003) PRIMUS: a Windows PC-based system for small-angle scattering data analysis. *J Appl Cryst* **36**, 1277–1282.
27 Sievers F, Wilm A, Dineen D, Gibson TJ, Karplus K, Li W, Lopez R, McWilliam H, Remmert M, Söding J *et al*. (2011) Fast, scalable generation of high-quality protein multiple sequence alignments using Clustal Omega. *Mol Syst Biol* **7**, 539.
28 Edgar RC (2004) MUSCLE: multiple sequence alignment with high accuracy and high throughput. *Nucleic Acids Res* **32**, 1792–1797.

29 Nicholas KB, Nicholas HB Jr & Deerfield DW II (1997) GeneDoc: Analysis and visualization of genetic variation. *EMBNEW.NEWS* **4**, 14.
30 Krissinel E and Henrick K (2004) Secondary-structure matching (SSM), a new tool for fast protein structure alignment in three dimensions. *Acta Crystallogr D* **60**, 2256–2268.
31 Drozdetskiy A, Cole C, Procter J and Barton GJ (2015) JPred4: a protein secondary structure prediction server. *Nucl Acids Res* **43**, W389–W394.
32 Krieger E, Joo K, Lee J, Lee J, Raman S, Thompson J, Tyka M, Baker D and Karplus K (2009) Improving physical realism, stereochemistry, and side-chain accuracy in homology modeling: four approaches that performed well in CASP8. *Proteins* **77** (Suppl. 9), 114–122.
33 He Z and Honeycutt WC (2005) A modified molybdenum blue method for orthophosphate determination suitable for investigating enzymatic hydrolysis of organic phosphates. *Communicat Soil Sci Plant Analysis* **36**, 1373–1383.
34 Finn RD, Coggill P, Eberhardt RY, Eddy SR, Mistry J, Mitchell AL, Potter SC, Punta M, Qureshi M, Sangrador-Vegas A *et al.* (2016) The Pfam protein families database: towards a more sustainable future. *Nucleic Acids Res* **44**, D279–D285.
35 Jia H, Korolev S, Niedziela-Majka A, Maluf NK, Gauss GH, Myong S, Ha T, Waksman G and Lohman TM (2011) Rotation of the 2B sub-domain of *E. coli* UvrD helicase/translocase coupled to nucleotide and DNA binding. *J Mol Biol* **411**, 633–648.
36 Lai J, Ghaemi Z and Luthey-Schulten Z (2017) The conformational change in elongation factor Tu involves separation of its domains. *Biochemistry* **56**, 5972–5979.

Supporting information

Additional supporting information may be found online in the Supporting Information section at the end of the article.

Fig. S1. SDS-PAGE analysis of HelD and HelDΔN after TEV digestion.

Fig. S2. SEC-SAXS profiles for HelD.

Fig. S3. Basic SAXS plots for uninhibited HelD in phosphate buffer.

Fig. S4. Basic SAXS plots for HelD with AMP-PNP.

Fig. S5. Sequence alignment of HelD from *B. subtilis* and *L. plantarum* with sequence-based placement of the structurally superimposed ATPase and C-terminal domains.

Fig. S6. Thermal stability of HelD with and without AMP-PNP measured by differential scanning fluorimetry.

Supplementary data for

Domain structure of HelD, an interaction partner of *Bacillus subtilis* RNA polymerase

by Tomáš Kovaľ, Petra Sudzinová, Terézia Perháčová, Mária Trundová, Tereza Skálová, Karla Fejfarová, Hana Šanderová, Libor Krásný, Jarmila Dušková, and Jan Dohnálek

Supplementary Materials and Methods

Cloning, expression and purification of HelDΔN

HelDΔN insert was amplified by PCR from the genomic DNA of *B. subtilis* MH5636 using forward primer:
5'-TTCCAGGGCGCTAGCGGATCCACCCAAATGAAAAACATCGTG-3' and reverse primer: 5'-CAGGTTTTCTTCTCGAGAAGCTTCA TTCAGCAATCTGAT-3'. It was cloned into pET28bMBP vector using CyClone Ligase-free Cloning Kit (Jena Bioscience) according to manufacturer's instructions. Schematically, the sequence of the vector product is:
MVPHHHHHHSRAWRHPQFGGHHHHHH – MaltoseBindingProtein – ENLYFQGASGS – **HelDΔN** (construct abbreviated as MBP-HelDΔN)**.** The TEV protease cleavage site is underlined. Abbreviation of the protein of interest is written in bold.

Competent *E. coli* Lemo21 (DE3) cells (New England Biolabs) were transformed using the heat shock method (30 min on ice, 50 s at 42 °C, 2 min on ice) and afterwards incubated for 1 h in the Power broth (PB) (Molecular Dimensions) medium. Selection was done using LB agar plates supplemented with chloramphenicol at the concentration of 30 μg/mL, kanamycin at 50 μg/mL, and 1% (w/v) glucose. LB agar plates were incubated at 37 °C overnight. Level of expression was analyzed for several randomly selected colonies. For the expression of the protein for further experiments an overnight culture (PB medium with 30 μg/mL chloramphenicol, 50 μg/mL kanamycin, and 1% (w/v) glucose, 37 °C and 250 rpm overnight) was diluted at 1:100 ratio in fresh PB medium supplemented with 30 μg/mL chloramphenicol and 25 μg/mL kanamycin. The cells were grown to the OD_{600} of 0.6 at 37 °C, 250 rpm and then protein expression was induced by adding IPTG to a final concentration of 1 mM. After induction, cells were cultivated overnight at 25 °C and 250 rpm. Cells were harvested by centrifugation at 3000 x g, 4 °C for 30 min. Cell pellets were stored at –80 °C.

Cell pellets were thawed and resuspended in 5 mL per 1 g of wet cells in the lysis buffer (50 mM Tris pH 7.5, 500 mM NaCl, 15 mM imidazole, 0.5% (v/v) TWEEN 20, 0.5 mg/mL lysozyme, 20 μg/mL DNaseI from bovine pancreas, and 0.5 mL of Protease Inhibitor Cocktail per 10 g of wet weight). Cells were incubated in the lysis buffer on ice with gentle steering for 30 min. Lysate was afterwards treated by sonication (15 cycles lasting 15 s with 40 s cooling period; 200 W). Cell debris were removed by centrifugation at 30000 x g, 4 °C for 30 min. Supernatant was filtered using 0.22 μm filter. The first purification step of MBP-HelDΔN was Ni-NTA affinity chromatography using an ÄKTA purifier, a HisTrap™ FF (1 mL) column (GE-Healthcare), equilibration buffer (50 mM Tris pH 7.5 500 mM NaCl, 15

mM imidazole, and 5% (v/v) glycerol) and elution buffer (50 mM Tris pH 7.5, 500 mM NaCl, 500 mM imidazole, and 5% (v/v) glycerol). MBP-HelDΔN was eluted in a continuous rising gradient of the elution buffer from 0% to 100% over 20 column volumes. The second purification step was size exclusion chromatography using an ÄKTA purifier, a Superdex 200 10/300 GL column (GE Healthcare) and buffer composed of 50 mM Tris pH 7.5, 100 mM NaCl, 0.5 mM TCEP, and 5% (v/v) glycerol. Unless stated otherwise, all chemicals were purchased from Sigma-Aldrich.

Supplementary figures

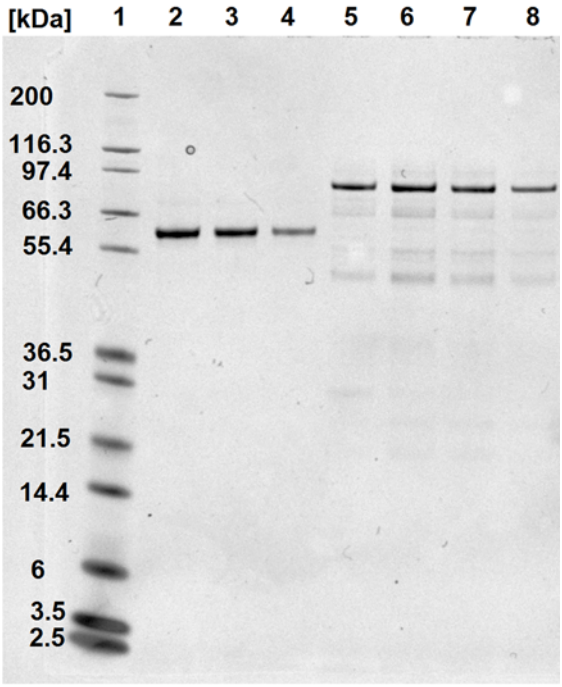

Fig. S1. SDS-PAGE analysis of HelD and HelDΔN after TEV digestion. Lane 1, Mark12™ Unstained Standard (Thermo Fisher Scientific); lanes 2-4, flow-through fractions containing HelDΔN; lanes 5-8, flow-through fractions containing HelD.

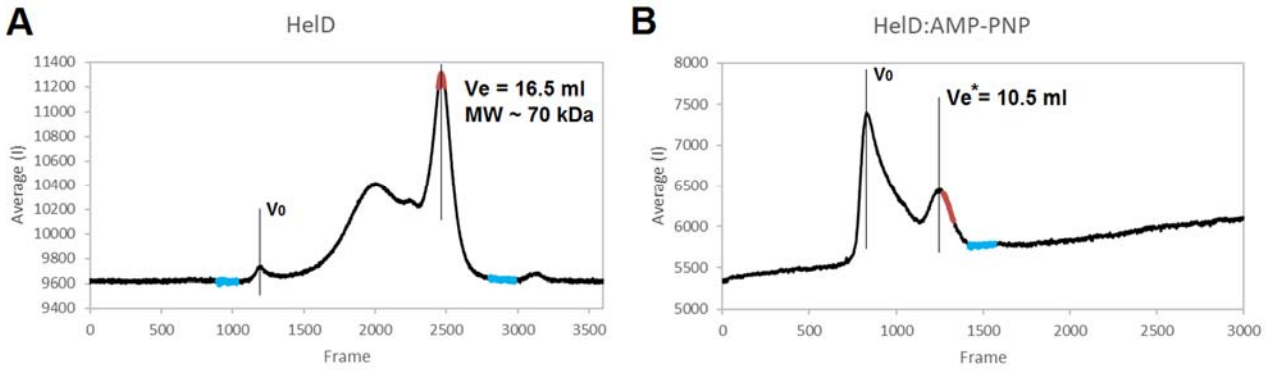

Fig. S2. SEC-SAXS profiles for HelD. Average intensity of SAXS signal *vs.* SAXS frame number is shown. For merged files and subsequent computations, the red regions were selected as body signal and the cyan regions were selected as solvent signal. Exclusion volume of the column and elution volume of the selected data region for each protein/complex are marked. (A) Data for the HelD in phosphate buffer. (B) Data for HelD inhibited with AMP-PNP. * MW cannot be estimated due to column damage.

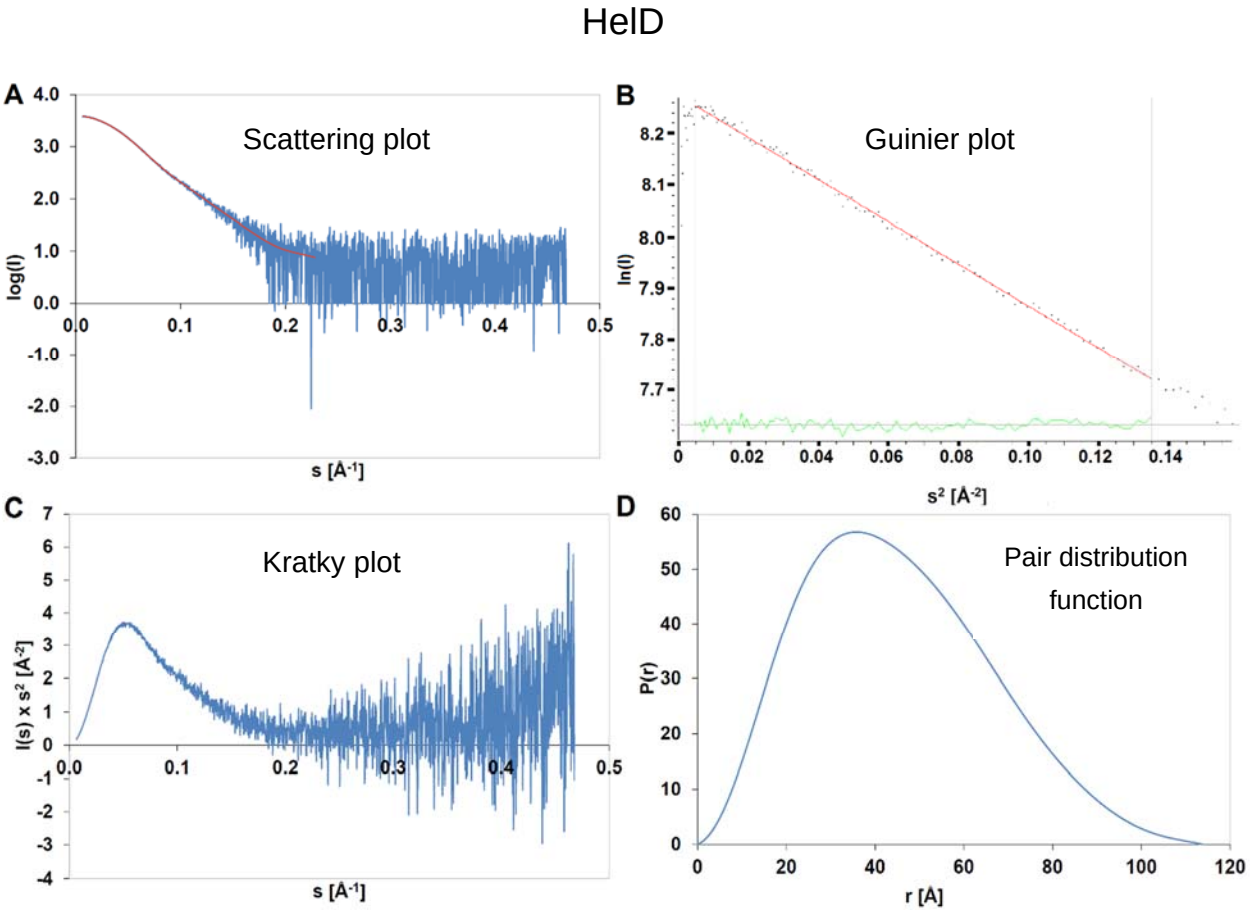

Fig. S3. Basic SAXS plots for uninhibited HelD in phosphate buffer. (A) Scattering plot (blue) and its fit with DAMMIN *ab initio* model (red). (B) Guinier plot. (C) Kratky plot. (D) Pair distribution function.

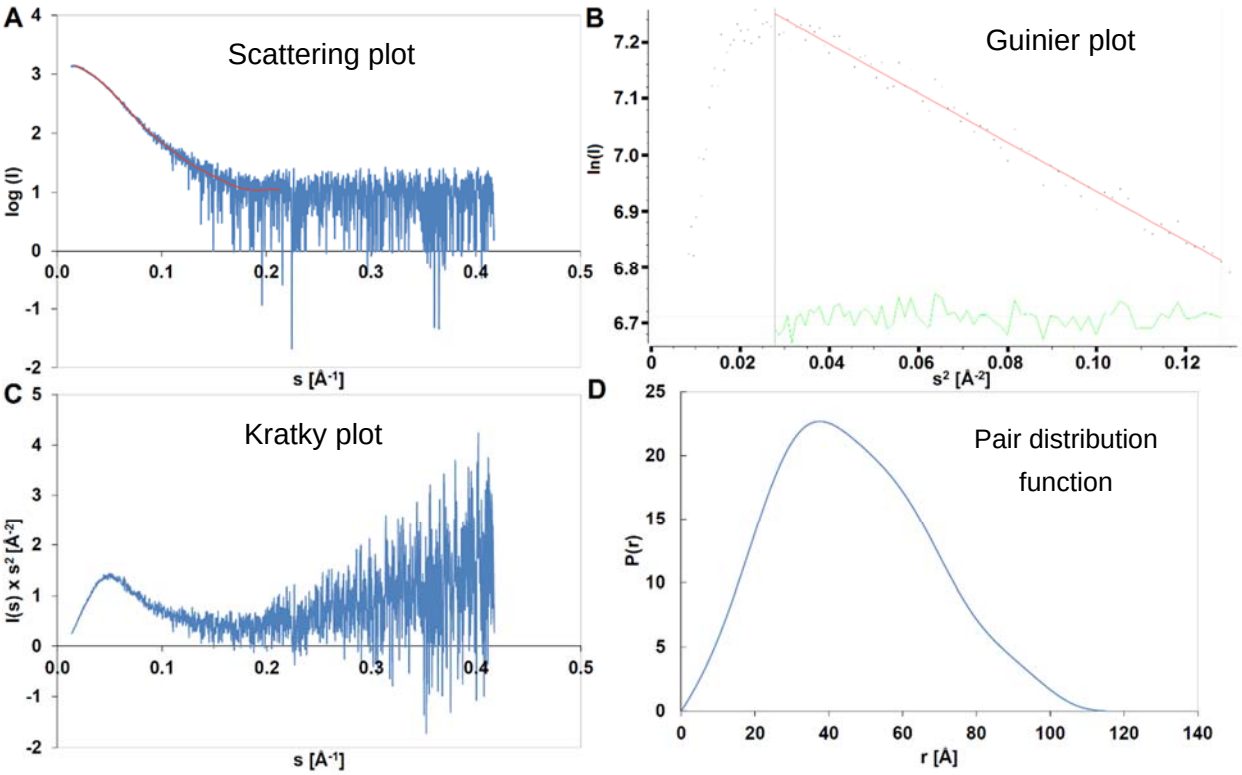

Fig. S4. Basic SAXS plots for HelD with AMP-PNP. (A) Scattering plot (blue) and its fit with DAMMIN *ab initio* model (red). (B) Guinier plot. (C) Kratky plot. (D) Pair distribution function.

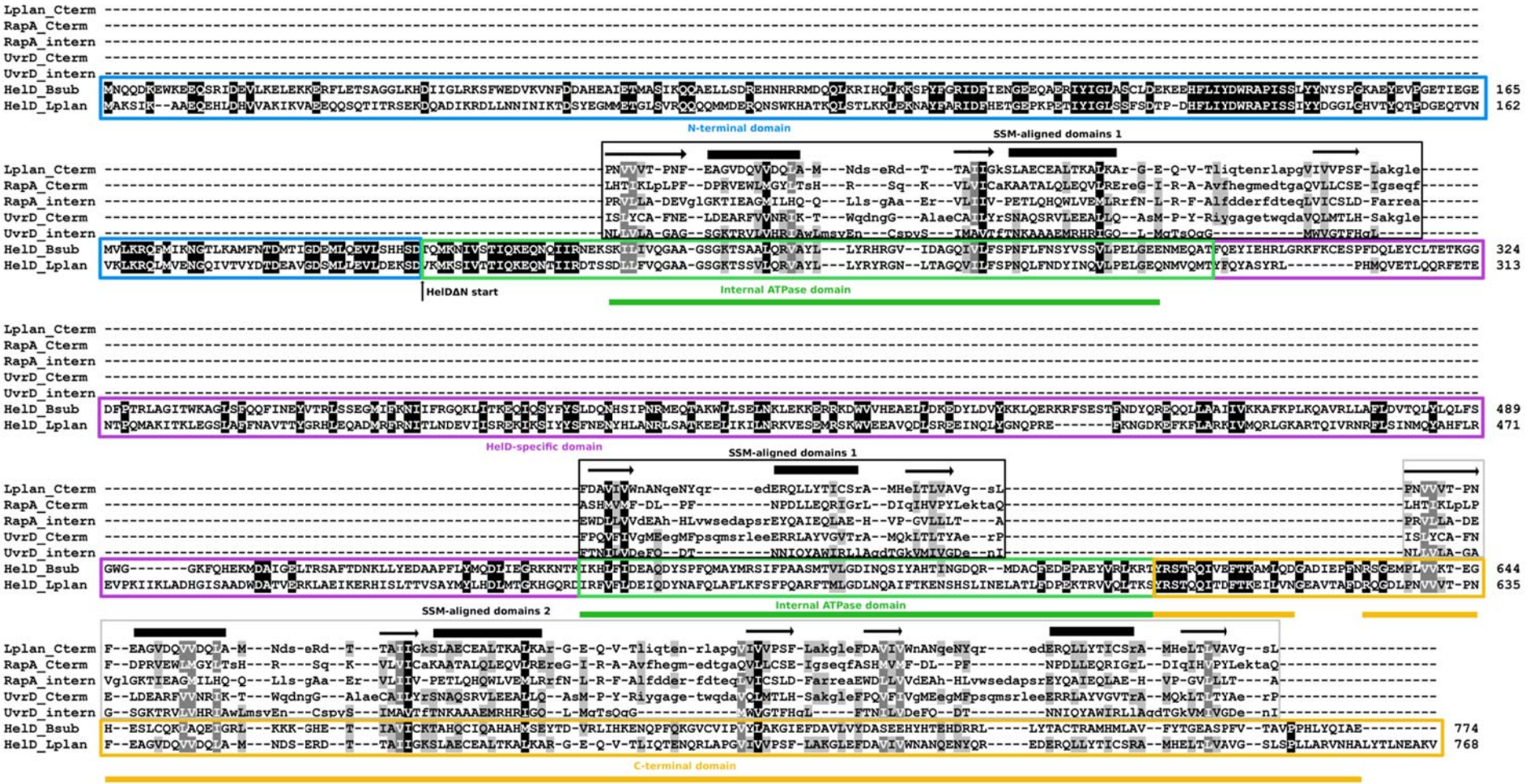
Lplan_Cterm
RapA_Cterm
RapA_intern
UvrD_Cterm
UvrD_intern
HelD_Bsub
HelD_Lplan
N-terminal domain
SSM-aligned domains 1
HelDΔN start
Internal ATPase domain
HelD-specific domain
SSM-aligned domains 2
C-terminal domain

Fig. S5. Sequence alignment of HelD from *B. subitlis* and *L. plantarum* with sequence-based placement of the structurally superimposed ATPase and C-terminal domains. Sequences from the following organisms and proteins were used: *L. plantarum* (Lplan) HelD, *E. coli* RapA (RapA), *E. coli* UvrD (UvrD), and *B. subtilis* HelD (HelD_Bsub). Domains and protein parts: C-terminal domain (Cterm), internal ATPase domain (intern). Division of *B. subtilis* and *L. plantarum* HelD is marked by color frames and corresponding titles. Internal ATPase domains and C-terminal domains of structures of related proteins were superimposed with use of the Secondary structure matching (SSM) algorithm and two occurrences of similar domains in the HelD sequence are shown. Secondary structure elements of the internal ATPase domain of UvrD are indicated by arrows (β-sheet) and bars (α-helix) above the sequences. Sequence similarity is indicated in the blocks with SSM-aligned domains by background in shades of gray; in the remaining parts identities are marked by black background. The starting residue of the HelDΔN product is marked by an arrow. The region of HelD covered by the model is marked with color bars below the sequences according to the domain structure.

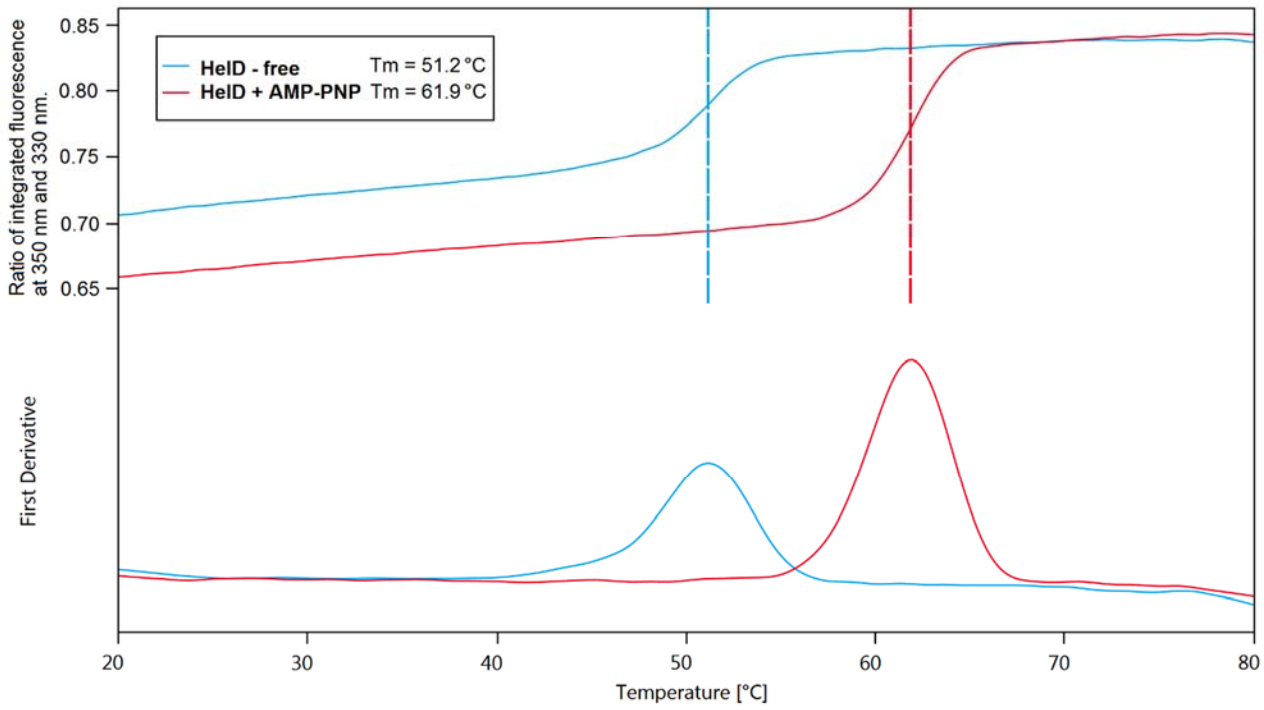

Fig. S6. Thermal stability of HelD with and without AMP-PNP measured by differential scanning fluorimetry. Melting temperature increases by about 11 °C upon AMP-PNP binding (red curve). Measurements were performed using a Prometheus NT.48 (Nanotemper) with protein concentration 1.5 mg/ml in 40 mM Tris-HCl pH 8.0, 10 mM MgCl2, 1 mM DTT, and 150 mM KCl. Measurements were done in temperature range 20-80 °C with rate of temperature increase 2 °C per min.

PUBLICATION IV

PLOS GENETICS

RESEARCH ARTICLE

The alarmones (p)ppGpp are part of the heat shock response of *Bacillus subtilis*

Heinrich Schäfer[1,2], Bertrand Beckert[3], Christian K. Frese[2], Wieland Steinchen[4], Aaron M. Nuss[5], Michael Beckstette[5], Ingo Hantke[1], Kristina Driller[2], Petra Sudzinová[6], Libor Krásný[6], Volkhard Kaever[7], Petra Dersch[5,8], Gert Bange[4]*, Daniel N. Wilson[3]*, Kürşad Turgay[1,2]*

1 Institute of Microbiology, Leibniz Universität Hannover, Hannover, Germany, **2** Max Planck Unit for the Science of Pathogens, Berlin, Germany, **3** Institute for Biochemistry and Molecular Biology, University of Hamburg, Hamburg, Germany, **4** Philipps-University Marburg, Center for Synthetic Microbiology (SYNMIKRO) and Department of Chemistry, Marburg, Germany, **5** Department of Molecular Infection Biology, Helmholtz Centre for Infection Research, Braunschweig, Germany, **6** Institute of Microbiology, Czech Academy of Sciences, Prague, Czech Republic, **7** Hannover Medical School, Research Core Unit Metabolomics, Hannover, Germany, **8** Institute of Infectiology, University of Münster, Münster, Germany

* gert.bange@synmikro.uni-marburg.de (GB); daniel.wilson@chemie.uni-hamburg.de (DNW); turgay@mpusp.mpg.de (KT)

Citation: Schäfer H, Beckert B, Frese CK, Steinchen W, Nuss AM, Beckstette M, et al. (2020) The alarmones (p)ppGpp are part of the heat shock response of *Bacillus subtilis*. PLoS Genet 16(3): e1008275. https://doi.org/10.1371/journal.pgen.1008275

Editor: Jue D. Wang, University of Wisconsin-Madison, UNITED STATES

Received: June 21, 2019

Accepted: February 26, 2020

Published: March 16, 2020

Data Availability Statement: All RNA-seq files are available from the GEO database (accession number GSE125467). The mass spectrometry proteomics data have been deposited to the ProteomeXchange Consortium via the PRIDE partner repository with the dataset identifier PXD015416. All other relevant data are within the manuscript and its Supporting Information files.

Funding: This work was supported by Czech Science Foundation Grant No. 19-12956S (to LK), by the Czech research infrastructure for systems

Abstract

Bacillus subtilis cells are well suited to study how bacteria sense and adapt to proteotoxic stress such as heat, since temperature fluctuations are a major challenge to soil-dwelling bacteria. Here, we show that the alarmones (p)ppGpp, well known second messengers of nutrient starvation, are also involved in the heat stress response as well as the development of thermo-resistance. Upon heat-shock, intracellular levels of (p)ppGpp rise in a rapid but transient manner. The heat-induced (p)ppGpp is primarily produced by the ribosome-associated alarmone synthetase Rel, while the small alarmone synthetases RelP and RelQ seem not to be involved. Furthermore, our study shows that the generated (p)ppGpp pulse primarily acts at the level of translation, and only specific genes are regulated at the transcriptional level. These include the down-regulation of some translation-related genes and the up-regulation of *hpf*, encoding the ribosome-protecting hibernation-promoting factor. In addition, the alarmones appear to interact with the activity of the stress transcription factor Spx during heat stress. Taken together, our study suggests that (p)ppGpp modulates the translational capacity at elevated temperatures and thereby allows *B. subtilis* cells to respond to proteotoxic stress, not only by raising the cellular repair capacity, but also by decreasing translation to concurrently reduce the protein load on the cellular protein quality control system.

Author summary

We observed that the second messenger (p)ppGpp, known to be synthesized by the ribosome-associated Rel synthetase upon nutrient starvation during the stringent response, is also intricately involved in the stress response of *B. subtilis* cells and can act as a pleiotropic regulator during the adaptation to heat stress. (p)ppGpp can slow down and modulate

biology C4SYS (project LM2015055). This research was supported by grants from the Deutsche Forschungsgemeinschaft (SPP 1879 to KT, GB, and DNW) and by funding from the Max Planck Society (to CKF, and KT). The funders had no role in study design, data collection and analysis, decision to publish, or preparation of the manuscript.

Competing interests: The authors have declared that no competing interests exist.

translation and is, together with the transcriptional stress regulator Spx, partially involved in the transcriptional down-regulation of the translation machinery. The stress-induced elevation of cellular (p)ppGpp levels confers increased stress tolerance and facilitates an improved protein homeostasis by modulating translation and reducing the load on the protein quality control system.

Introduction

Bacteria have evolved complex and diverse regulatory networks to sense and respond to changes in the environment, which can include physical stresses or nutrient limitation [1]. The universally conserved protein quality control system comprises a conserved set of chaperones and proteases that monitor and maintain protein homeostasis. Various physical stresses, such as heat stress, favor the unfolding and aggregation of cellular proteins, which can be sensed by heat shock response systems, allowing an appropriate cellular stress response. The response to such protein unfolding stresses includes the induction of the expression of genes encoding chaperones and proteases of the quality control system, also known as heat shock proteins, and is usually very fast (less than 2–5 min) [2–7].

Interestingly, in *B*. *subtilis* cells, a short exposure to a raised but non-lethal temperature induces thermotolerance, an acquired resistance to otherwise lethal temperatures [8,9]. Investigating the adaptation to such adverse conditions, also known as priming, allows the molecular mechanisms and interplay of the various cellular processes involved in the cellular stress and heat shock response to be studied [8,9]. In *B*. *subtilis*, the heat shock response is orchestrated by multiple transcriptional regulators, including the heat-sensitive repressors HrcA & CtsR, which control the expression of the protein quality control system and other general stress genes [10–13]. The general stress response, activated by the alternative sigma factor σ^B, is controlled by a complex regulatory network that integrates diverse stress and starvation signals, including heat [14]. In addition, Spx is a central regulator of the heat and thiol stress response, which is important for the development of thermotolerance. Spx activates the expression of many genes of the heat shock response, including *clpX*, *htpG* and genes of the oxidative and thiol stress response such as thioredoxin [9,15–18]. Interestingly, Spx can also mediate the inhibition of cell growth by the concurrent transcriptional down-regulation of many translation-related genes [17].

Another fast-acting bacterial stress response system is the stringent response (SR), which is mediated by the second messenger alarmones (p)ppGpp [19]. The synthesis and hydrolysis of (p)ppGpp is catalyzed by RelA/SpoT homologs (RSH) which contain N-terminal synthetase and hydrolase domains (bifunctional Rel or SpoT subgroup), or an active synthetase and an inactive hydrolase domain (RelA subgroup) together with additional regulatory domains at the C-terminus [20]. RSH can therefore direct both synthesis and, in the case of Rel, hydrolysis of (p)ppGpp. The enzyme activity of RelA or Rel is stimulated by association with uncharged tRNAs and the ribosome, thereby mediating (p)ppGpp synthesis upon amino acid starvation [21–25]. In addition to this long multi-domain RSH form, monofunctional small alarmone synthetases (SAS) or small alarmone hydrolases (SAH) with single synthetase or hydrolase domains are present in many bacteria [26]. In *B*. *subtilis*, alarmone levels are controlled by Rel (often referred to as RelA), a bifunctional, RSH-type synthetase/hydrolase as well as two SAS proteins RelP (SasA, YwaC) and RelQ (SasB, YjbM) [27–29].

The synthesis and hydrolysis of (p)ppGpp allows the activation or repression of different cellular pathways by modulating various enzyme activities involved in GTP homeostasis,

replication, transcription and translation, not only in response to amino acid starvation, but also to various other signals or stresses. It was observed for different bacteria that additional and diverse starvation or stress signals can activate the SR via interacting proteins or metabolites that bind and modulate the activity of RSH-type enzymes, or by transcriptional or post-translational regulation of monofunctional SAS [30,31]. *B. subtilis* and related Firmicutes lack a DksA homolog and a direct binding site for (p)ppGpp on RNA polymerase (RNAP) which mediate positive and negative stringent regulation in *E. coli* and other proteobacteria. Instead, in *B. subtilis* (p)ppGpp can exert transcriptional regulation via a drop in GTP levels caused by the direct inhibition of multiple enzymes of the GTP synthesis pathway [32,33]. Thus, transcription of ribosomal RNA (rRNA) and ribosomal protein (r-protein) genes from promoters that initiate transcription with GTP is strongly reduced, while in turn promoters that initiate with ATP are activated [34,35]. In addition, the global regulator and repressor CodY is activated by GTP via an allosteric binding site, and therefore amino acid biosynthesis genes and other pathways are de-repressed upon a drop of the cellular GTP level during the SR [36,37]. Beyond its impact on transcription, (p)ppGpp can modulate ribosome assembly, translation initiation and elongation by binding, for example, to the translation initiation factor IF-2 and other ribosome-associated GTPases [38–44]. With its ability to inhibit translation and growth, the SR was also implicated in persister cell formation and development of antibiotic tolerance [45]. In addition, (p)ppGpp is required for virulence as well as survival of pathogens during infection [19,46].

During exposure to heat and oxidative stress, we and others previously observed in *B. subtilis* a pronounced down-regulation of rRNA and r-protein genes that resembled the pattern of the SR [16–18,47]. Thus, we hypothesized that the alarmone (p)ppGpp and the SR-like response could be part of the heat shock response of *B. subtilis*. Therefore, we investigated the role of the SR and its intricate and mutual involvement with the cellular stress response under various proteotoxic stress conditions, including various heat shock conditions [9,48].

Consistent with our hypothesis, we could demonstrate that the cellular level of (p)ppGpp was increased upon heat shock, as well as upon salt and oxidative stress. In addition, raised alarmone levels conferred increased stress tolerance and a (p)ppGpp^0 strain appeared more stress sensitive. The presence of the bifunctional Rel was necessary and sufficient for the observed stress induced increase of (p)ppGpp. Overall (p)ppGpp appeared to play only a minor more complementary role for the heat mediated adjustments of transcription. However, we observed a prominent and instantaneous effect of the cellular alarmone (p)ppGpp levels on limiting and modulating translation by reducing the protein load on the quality control system during heat stress and concurrently allowing the expression of heat shock genes. Thereby the fast reallocation of cellular resources to raise the cellular repair capacity controlled by the other known regulators of the heat shock response could be facilitated.

Results and discussion

Regimes for monitoring of heat shock stress response in *B. subtilis*

In this study, we investigated the stress response of *B. subtilis* by application of different, but related, heat shock conditions: (i) growth and heat shock at 50 ˚C, a temperature that is non-lethal for *B. subtilis* but already induces a significant heat shock response with a raised expression of chaperones and proteases, (ii) resistance to severe heat shock by measuring the survival of exponentially growing cells exposed to a severe, lethal heat shock at 53 ˚C, which can also be considered a measure for thermoresistance (37/53 ˚C) (Fig 1A), and (iii) the development of thermotolerance by measuring the survival of exponentially growing cells primed by a mild pre-shock for 15 min at 48 ˚C before their exposure to the severe heat shock at 53 ˚C (48/53

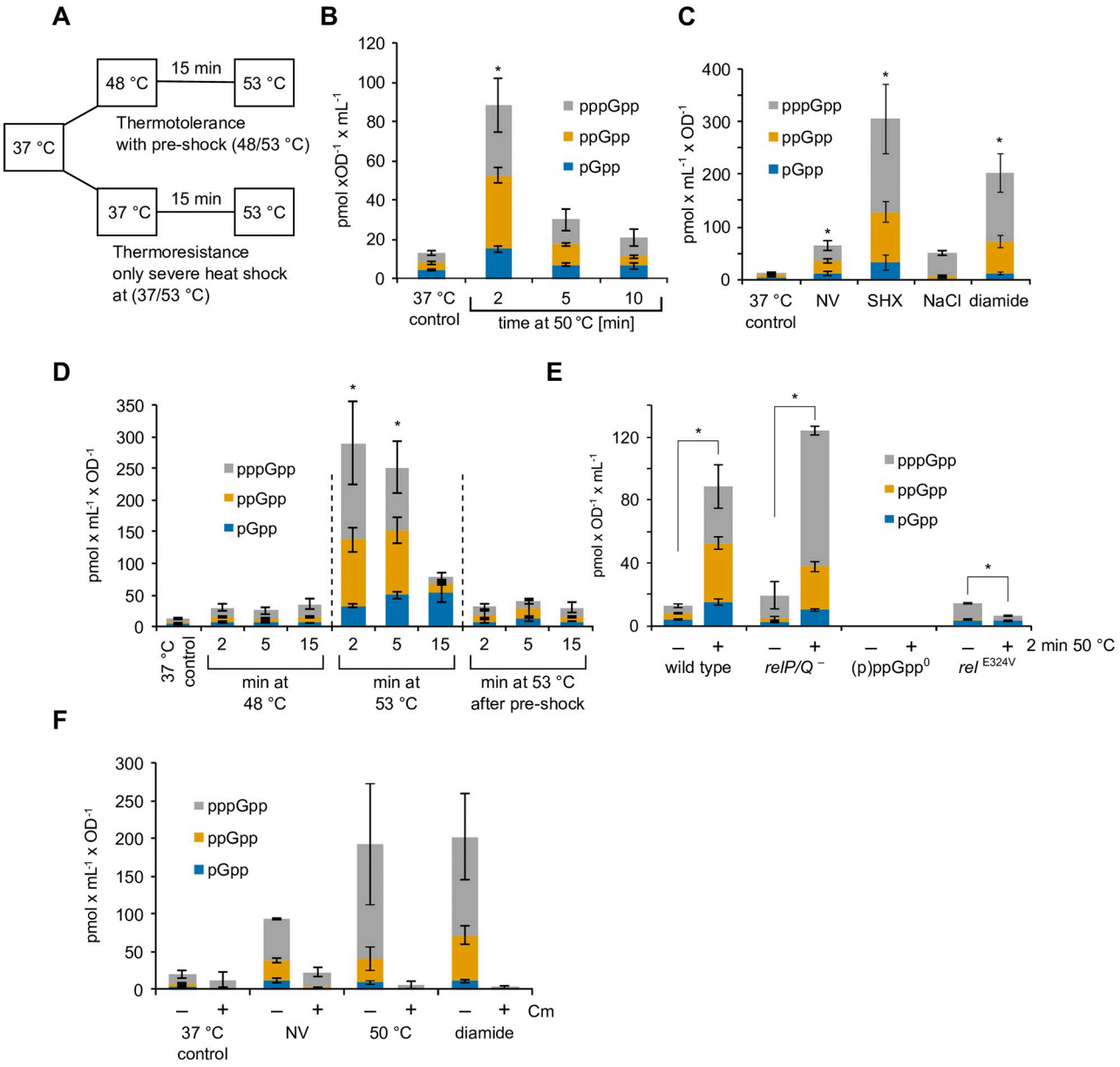

Fig 1. (p)ppGpp levels are increased by heat shock and stress. (A) Outline of the thermotolerance protocol. A culture of cells growing exponentially at 37 ˚C is divided and incubated at 48 ˚C or left at 37 ˚C. After 15 min, both cultures are shifted to 53 ˚C. **(B-F)** Levels of pGpp, ppGpp and pppGpp under different conditions. Asterisks (*) indicate significance ($p_{adj.} \leq 0.05$) of combined pGpp, ppGpp and pppGpp levels according to the Kruskal-Wallis and Dunn-Bonferroni test. **(B)** Cells were grown in minimal medium to OD_{600} of 0.4 and transferred to 50 ˚C. Means and and standard error of mean (SEM) of four independent experiments are shown. **(C)** Cells were grown in minimal medium to the mid-exponential phase (OD_{600} ~ 0.4) and treated with DL-norvaline (NV; 0.5 mg ml^{-1}), serine hydroxamate (SHX; 5 μg ml^{-1}), NaCl (6%) or diamide (0.5 mM) for 10 min. Means and SEM of three to four independent experiments are shown. **(D)** Wild type cells were grown at 37 ˚C and shifted to 48 ˚C for 15 min (pre-shock), then to 53 ˚C or directly to 53 ˚C. Samples were taken at 2, 5 and 15 min. Means and SEM of four independent experiments are shown. **(E)** Wild type cells or strains with mutations in (p)ppGpp synthetases (*relP/Q* ˚: BHS204, *rel*^{E324V}: BHS709; (p)ppGpp˚: BHS214) were treated with or without heat shock at 50 ˚C for 2 min. Means and SEM of three to six independent experiments are shown. No alarmone peaks were detected in the (p)ppGpp˚ mutant (lower limit of quantification: 0.26 pmol x mL^{-1} x OD^{-1}). Asterisks (*) indicate significant changes ($p \leq 0.05$) of combined pGpp, ppGpp and pppGpp levels according to Welch's *t*-test. **(F)** The influence of chloramphenicol on alarmone accumulation during stress. Cells were grown in minimal medium and treated with DL-norvaline (0.5 mg ml^{-1}) for 10 min, heat shock at 50 ˚C for 2 min or diamide (1 mM) for 10 min. Chloramphenicol (Cm, 25 μg ml^{-1}) was added at the same time to one part. Means and SEM of two independent experiments are shown.

https://doi.org/10.1371/journal.pgen.1008275.g001

˚C) (Fig 1A). We experimentally established that 55 ˚C was an appropriate temperature to examine the impact of severe heat on *B*. *subtilis* cells growing on agar plates. In addition to exposure to these various heat conditions, we also examined other potentially proteotoxic stresses, such as salt and oxidative stress [9,17,48].

Cellular (p)ppGpp levels increase during heat shock exposure

To investigate the impact of heat on the SR, we first assessed the intracellular levels of the alarmones pGpp, ppGpp and pppGpp ((p)ppGpp) during the heat shock response at 50 ˚C. We consider the sum of the cellular concentration of these three alarmones as a measure of the total (p)ppGpp alarmones concentration. Cells were grown at 37 ˚C in minimal medium to an optical density at 600 nm (OD_{600nm}) of 0.4, and subsequently treated with a single, non-lethal temperature upshift to 50 ˚C in order to induce the heat shock response. After 2, 5 and 10 minutes of incubation at 50 ˚C, the intracellular levels of the alarmones were examined by liquid chromatography coupled mass spectrometry (LC-MS) (see Methods) (Fig 1) [49].

Already after 2 minutes, the alarmone levels increased approx. seven-fold (from 13 to 88 pmol OD^{-1} ml^{-1}) (Fig 1B), which is in a similar range to that observed upon amino acid starvation induced by DL-norvaline (NV) (Fig 1C). In addition, significantly increased (p)ppGpp levels could be observed upon treatment with serine hydroxamate (SHX), salt stress induced by 6% (w/v) NaCl or 0.5 mM diamide, a strong oxidant of thiol groups (Fig 1C) [50,51]. It should be noted that (p)ppGpp levels increased only transiently during heat shock and returned to almost basal levels after 10 minutes (Fig 1B). Thus, we conclude that exposure to a non-lethal heat shock at 50 ˚C elicits a fast, but transient, increase of the (p)ppGpp alarmone levels.

We also assessed the levels of the alarmones under thermoresistance conditions (37/53 ˚C) and after priming (48 ˚C) under thermotolerance conditions (48/53 ˚C) (Fig 1A and 1D). We observed transiently increased (p)ppGpp levels (Fig 1D), however, the alarmone levels were particularly high during the severe heat shock shift at 37/53 ˚C (about 25-fold increase) and the induction was lower both for the 37/48 ˚C or 48/53 ˚C conditions (about 2–3 fold increase) (Fig 1D). The priming at 48˚C appear to limit the alarmone synthesis of thermotolerant cells, when subsequently exposed to the lethal heat shock at 53 ˚C (Fig 1D).

The synthesis of (p)ppGpp that occurs during activation of the SR e.g. by treatment with serine hydroxamate or DL-norvaline, is in *B*. *subtilis* accompanied by a rapid decrease in the cellular GTP level [33], which we also observed after exposure to salt or diamide (S1A Fig). Interestingly, we did not observe a reduction in the GTP level after exposure to 50 ˚C (S1A Fig). The GTP level was at a relatively high level (S1B Fig) during temperature upshifts of 37/48 ˚C, 37/53 ˚C and 48/53 ˚C. However, after 15 min exposure to the raised temperature, the GTP level decreased in all temperature upshifts (S1B Fig).

Taken together, we observed that exposure to heat shock elicits a fast, but only transient, increase of the (p)ppGpp alarmones, which did not immediately affect the cellular GTP levels, which control the transcriptional response [33]. Therefore, it seems that alarmone levels might exhibit a graded response to heat exposure and temperature levels.

Rel activity is the main source for (p)ppGpp synthesis during stress response

Next, we aimed to identify the source of (p)ppGpp during the heat stress response. To this end, strains with mutations that disrupt the (p)ppGpp synthetase activity of the proteins encoded by *relP* and *relQ* (*relP/Q*$^{-}$ strain) or *rel* (*rel*^{E324V}; inactive synthetase) were assayed for (p)ppGpp accumulation and GTP levels upon heat shock at 50 ˚C for 2 min (Fig 1E and S1C Fig). As a control, the (p)ppGpp accumulation was also measured in a (p)ppGpp˚ strain

bearing inactivating mutations in all three alarmone synthetase genes (*relP*^{E154V}, *relQ*^{E139V} and Δ*rel*) (Figs 1E and 2E). In addition, the (p)ppGpp-dependent transcription of *hpf* was employed as an additional read-out for the activation of the SR (S1D Fig) [52,53]. As expected, alarmone nucleotides were not detected in the (p)ppGpp˚ mutant under any conditions [28] (Fig 1E). We observed that upon heat exposure, the *relP/Q*$^{-}$ (*relP*^{E154V}, *relQ*^{E139V}) strain also exhibited accumulation of (p)ppGpp (Fig 1E) and up-regulation of the *hpf* transcript similar to wild type cells (S1D Fig), indicating that the activity of RelP and RelQ is dispensable for (p)ppGpp production during heat stress. By contrast, the *rel*^{E324V} strain accumulated only small amounts of (p)ppGpp, with even lower levels after a brief heat exposure to heat (Fig 1E). Consistently, up-regulation of the *hpf* transcript in response to stress was also impaired in the *rel*^{E324V} strain (S1D Fig). Together, these results strongly suggest that the activity of Rel is the main source of (p)ppGpp during heat stress.

Activation of Rel during amino acid starvation requires the presence of uncharged tRNA and its association with the ribosome [21,22]. Early experiments by Cashel demonstrated that (p)ppGpp accumulation upon starvation for amino acids was almost completely suppressed in the presence of the translation inhibitor chloramphenicol, which indicated a connection between Rel activation and translation [54]. Interestingly, we also observed the same suppression of alarmone accumulation also upon heat and diamide treatment (Fig 1F). These experiments indicate that heat and oxidative stress mediated signal to activate Rel synthetase activity could be similar to the tRNA mediated signal activating the ribosome associated Rel upon amino acid starvation [19,20,54].

B. subtilis cells lacking (p)ppGpp are more sensitive to stress

To assess the importance of alarmone production for cellular survival under heat stress, we monitored growth of wild type, (p)ppGpp˚, *relP/Q*$^{-}$ (*relP*^{E154V}, *relQ*^{E139V}) and *rel*^{E324V} *B. subtilis* strains at 37 ˚C and 55 ˚C on agar plates (Fig 2A and 2B). As expected, no obvious growth defect was observed for any of the strains at 37 ˚C. While the survival of the cells from the *relP/Q*—strain at 55 ˚C was identical to that of the wild type strain, strong growth defects were evident for the cells of the (p)ppGpp˚ and *rel*^{E324V} strains at 55 ˚C. These findings suggested that production of (p)ppGpp by Rel, but not RelP/Q, is critical for survival of *B. subtilis* cells under heat stress. Such severe growth defects were observed for both the (p)ppGpp˚ and *rel*^{E324V} strains not only under heat-, but also under oxidative- and salt stress, whereas the growth behavior of the *relP/Q*$^{-}$ strain again resembled the wild type strain under the same conditions (Fig 2C and 2D). Collectively, these findings suggest that production of (p)ppGpp by Rel is critical for survival of *B. subtilis* cells, not only under heat stress, but also conditions of oxidative and salt stress.

High cellular (p)ppGpp levels confer elevated heat stress resistance

Next, we asked whether (p)ppGpp levels influence thermotolerance development and survival. To do this, we utilized the (p)ppGpp˚ strain, which cannot synthesize (p)ppGpp (Fig 1E) as well as a Δ*rel* strain that exhibits constantly raised (p)ppGpp (Fig 2F) with concomitantly lowered GTP levels (S2A Fig). Rel is the only alarmone hydrolase in *B. subtilis* and the increased high (p)ppGpp levels in cells of *B. subtilis* Δ*rel* strain cause also an overall decrease in the growth rate (Fig 2F, S2A and S2B Fig), consistent with previous reports [28,29].

In the thermoresistance (37/53 ˚C) and thermotolerance (48/53 ˚C) experiments we observed that, unlike the cells of wild type, (p)ppGpp˚ or the Δ*relP* and Δ*relQ* cells strains (Fig 2G and 2H, S2C and S2D Fig), the Δ*rel* strain exhibited strongly increased thermoresistance, which was apparent from the high number of Δ*rel* cells still able to form colonies after the

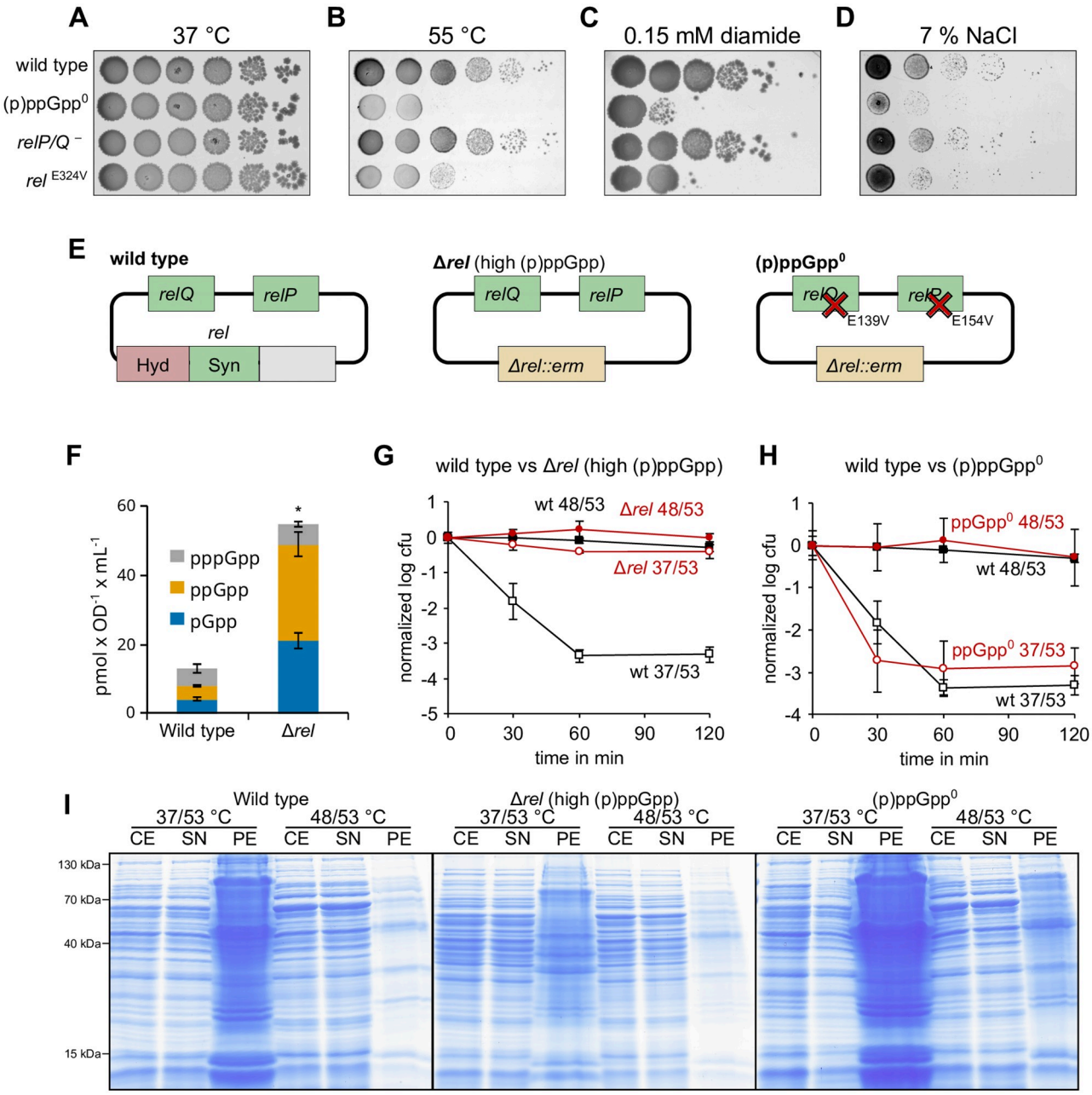

Fig 2. Increased (p)ppGpp levels confer high heat stress resistance. (A-D) Growth of strains with mutations in (p)ppGpp synthetases (*relP/Q*$^{-}$: BHS204, *rel*^{E324V}: BHS709; (p)ppGpp^{0}: BHS214) on agar plates at 37 ˚C, during heat stress (55 ˚C), oxidative stress (0.1 mM diamide) or salt stress (total concentration of 7% (w/v) NaCl) over night. **(E)** Outline of the genotypes and the (p)ppGpp synthesis capabilities of the assessed wild type, Δ*rel* (BHS126 and BHS368) and (p)ppGpp^{0} (BHS214 and BHS319) strains. **(F)** Cellular alarmone levels of wild type and Δ*rel* strain. Asterisks indicate significant changes ($p \leq 0.05$) of combined pGpp, ppGpp and pppGpp levels according to Welch's *t*-test. Means and SEM of three independent experiments are shown. **(G/H)** Thermotolerance and survival of wild type (black lines) and mutant strain (red lines) at 53 ˚C. Means and SEM of at least three independent experiments are shown. Open symbols: no pre-shock, closed symbols: 15 min pre-shock at 48 ˚C. (I) Accumulation of protein aggregates during heat stress at 53 ˚C without (37/53 ˚C) or with (48/53 ˚C) pre-shock. Exponentially growing cells of the indicated strains were shifted to 48 ˚C or left untreated for 15 min, then shifted to 53 ˚C for another 15 min. CE: cell extract, SN: supernatant, PE: pellet (aggregated protein fraction).

https://doi.org/10.1371/journal.pgen.1008275.g002

otherwise lethal heat shock (Fig 2G). Consistently, we also observed a strong reduction in protein aggregation during the 37/53 ˚C heat shock for the Δ*rel* strain, while the (p)ppGpp˚ strain exhibited more protein aggregation when exposed to the 37/53 ˚C heat shock (Fig 2I).

To investigate whether the increased heat resistance of the Δ*rel* strain was caused by the elevated levels of the alarmone (p)ppGpp, rather than the absence of the Rel protein, we expressed a truncated form of the *E. coli* RelA (*RelA*$_{hyper}$) that exhibits constitutive and hyperactive alarmone synthetase activity *in trans* in wild type *B. subtilis* cells [55,56]. As a control, we also expressed a truncated form of the *E. coli* RelA (*RelA*$_{inactive}$) that has no alarmone synthetase activity [55,56]. In a second approach, we examined *B. subtilis* Rel variants inactive in either the synthetase (Rel^{E324V}) or hydrolase (Rel$^{H77A/D78A}$) expressed *in trans* in the *B. subtilis* (p)ppGpp˚ strain.

Expression of *E. coli* RelA$_{hyper}$ or hydrolase-inactive *B. subtilis* Rel$^{H77A/D78A}$ *in trans* resulted in increased alarmone levels (S3A Fig) and conferred high thermoresistance (S3B and S3C Fig), as observed for the *B. subtilis* Δ*rel* strain (Fig 2G). By contrast, *B. subtilis* (p)ppGpp˚ strains expressing *E. coli* RelA$_{inactive}$ or the *B. subtilis* synthetase-inactive Rel^{E324V} *in trans* displayed neither increased alarmone levels (S3A Fig), nor increased survival to severe heat stress (S3D and S3E Fig). This suggests that the increased alarmone levels, independent of the synthetase, are responsible for the thermoresistance phenotype in *B. subtilis*.

The role of cellular GTP levels during heat stress

High (p)ppGpp levels during the SR lead in *B. subtilis* to a decrease in the cellular GTP level and this decrease is known to be intricately involved in causing the transcriptional changes during the SR [33,34] (S1, S2A and S3A Figs). To examine, whether the resistance to heat stress observed in the Δ*rel* strain could be mediated simply by lowering the cellular GTP level, wild type cells were treated with decoyinine, an inhibitor of GMP synthetase, which decreases the cellular GTP level (> 3-fold) without increasing (p)ppGpp levels [57,58]. Treatment with 50 μg ml^{-1} decoyinine showed no effect, while addition of 250 μg/ml decoyinine resulted in a partially increased thermoresistance. (S4 Fig). However, further increased decoyinine concentrations reduced (400 μg/ml), or even abolished (1000 μg/ml) both thermoresistance and thermotolerance development (S4 Fig). These experiments suggest that the decoyinine-mediated lowered cellular GTP level, which is a prerequisite for the reprogramming of the transcriptome during SR [33,34,59], can elicit heat resistance only to a limited extent. However, the observed effect of decoyinine on thermoresistance was weaker in comparison to the effect of raised (p)ppGpp levels (Fig 2F and 2G and S3 Fig).

From these observations, we infer that raised (p)ppGpp levels are sufficient to confer increased stress resistance and reduced levels of heat-induced protein aggregates. However, the SR-mediated drop in the cellular GTP level [33] was not observed during the heat shock response (S1 Fig) and an artificial reduction of the cellular GTP level by decoyinine had only a moderate effect on thermoresistance and could even abolish thermotolerance (S4 Fig).

Therefore, we went on and investigated the transcriptome, translation and proteome at raised temperatures and in the absence and presence of (p)ppGpp.

Transcriptome changes in the presence and absence of (p)ppGpp at raised temperatures

We performed global RNA-seq experiments to compare the transcriptome changes between *B. subtilis* wild type, Δ*rel* and (p)ppGpp˚ strains under exponential growth (37 ˚C) after heat shock (15 min 48 ˚C) as well as the thermotolerance conditions 37/53 ˚C and 48/53 ˚C (Fig 1A) in wild type cells. Since down-regulation of "stable" rRNA is a hallmark of the SR, we

introduced a previously established chromosomal *rrnJ*p1-*lacZ* fusion into the tested strains, which allowed us to follow the activity of this rRNA promoter with RNA-seq and RT-qPCR experiments in these *B*. *subtilis* strains [17].

Thereby we were able to gain insights into (i) the strong phenotype associated with a *rel* deletion especially when compared with the (p)ppGpp° *B*. *subtilis* strain (Fig 3A and 3B) and compare it to the (ii) transcriptome changes of wild type cells during thermotolerance 37 vs 48/53 ˚C (Fig 3C and 3D). At the same time (iii) the transcription pattern of all gene sets of interest could be compared and inspected for all the tested conditions and introduced mutations (Fig 4, S5, S6 and S7 Figs). In addition, we used RT-qPCR experiments to validate our RNA-seq experiment and to investigate different conditions such as growth at 50 ˚C.

Stringent response. First, we analyzed the transcriptomic data from the exponentially growing wild type, (p)ppGpp° and Δ*rel* strains (Fig 3A and 3B, S1, S2 and S3 Datasets). By comparing Δ*rel* cells, which exhibit constitutively high alarmone levels (Fig 2F), with (p)ppGpp° cells, 682 genes were found to be regulated by (p)ppGpp (Fig 3A) and we observed a good correlation with RT-qPCR experiments of selected regulated genes (S5A Fig). We noticed a broad down-regulation of many translation-related genes including the *rrnJ*p1-*lacZ* reporter as well as an extensive de-repression of CodY-controlled amino acid synthesis genes (e.g. *ilvB* (Fig 3A and 3B, S5B and S6 Figs)), both of which are characteristic for the SR in accordance with previous transcriptomic studies [37,53,60,61]. Furthermore, a strong decrease in the transcription of CcpA-regulated genes required for the utilization of alternative carbon sources was observed (e.g. *rbsC* (Fig 3A and 3B, S5B and S6 Figs)). Interestingly, the transcription of many heat shock genes was decreased in Δ*rel* cells (e.g. *dnaK* and *clpE* (S5B Fig)). In contrast, we noticed increased transcript levels of many general stress genes of the SigB regulon (e.g. *ssrA*, *dps*, *gsiB*, *ysnF*) in the absence of stress at 37 ˚C Δ*rel* cells (Fig 3B and S5B Fig). Notably, the transcript level of *hpf* (*yvyD*), encoding the hibernation promoting factor Hpf, was increased by raised (p)ppGpp levels (24-fold up-regulated, (S5A and S5B Fig)), confirming that the increased transcription of *hpf* can be considered as a reporter for the activation of the SR [52,53].

The heat-induced (p)ppGpp pulse mediates only minor transcriptional changes. After having established that alarmones can play a protective role during the heat shock response, we sought to assess the role of (p)ppGpp in transcriptional changes during heat exposure. To this end, we analyzed the thermoresistance (37/53 ˚C) and thermotolerance (48˚/53 ˚C) conditions (Figs 1A, 3C and 3D) [9,17] in wild type cells and investigated the wild type, (p)ppGpp° and Δ*rel* strains also at 48 ˚C, of the same RNA-seq experiment. Overall, we detected only small changes when comparing the transcriptome of wild type cells and (p)ppGpp° cells at 37 ˚C and 48 ˚C, indicating that the majority of transcriptional changes of the heat stress response are mediated independently of (p)ppGpp (Fig 4A and 4B). Thermotolerant wild type cells (48/53 ˚C) exhibited a comprehensive down-regulation of translation-related genes including the *rrnJ*p1-*lacZ* reporter that was, to a lesser extent, also observed in the mild pre-shock (48 ˚C) and severe heat shock (37/53 ˚C) conditions (Figs 3 and 4, S5 and S6 Figs), in agreement with previous observations [17]. Importantly, the heat-mediated down-regulation of *rrnJ*p1-*lacZ* appeared to be partially (p)ppGpp-dependent and was therefore less pronounced in the (p)ppGpp° strain (Fig 4C and 4D). Independent RT-qPCR experiments confirmed this observation. The requirement of (p)ppGpp for repression of *rrnJ*p1 under heat stress became even more apparent when the 50 ˚C heat shock condition was examined (S7A Fig).

By contrast, the heat-mediated down-regulation of many ribosomal protein genes and other translation-related genes appeared to also occur in the absence of (p)ppGpp, indicating a more complex and (p)ppGpp-independent control of the transcription of these genes (Fig 4C). Furthermore, while an extensive de-repression of the CodY regulon could be observed in Δ*rel*

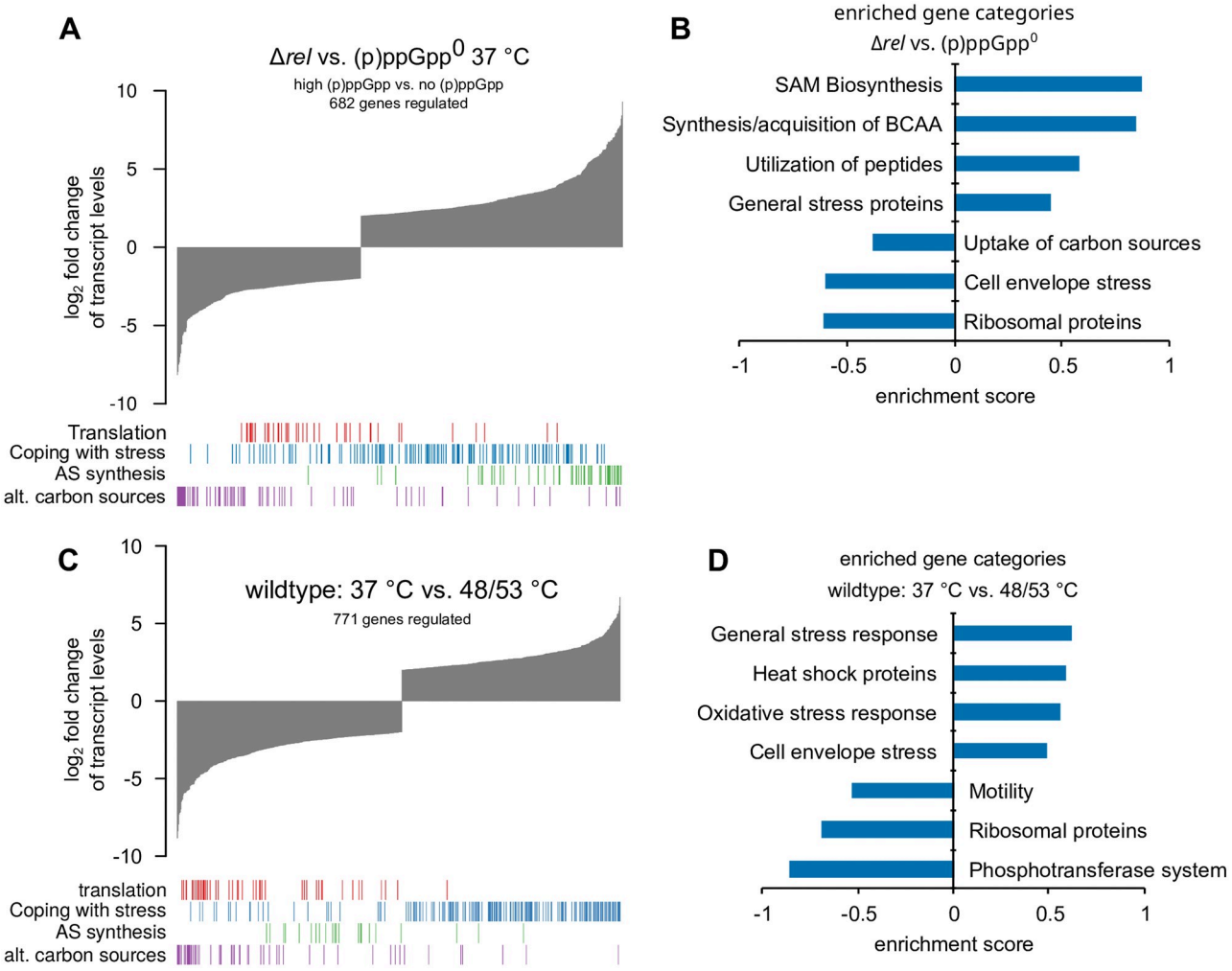

Fig 3. (p)ppGpp- mediated global changes in the transcriptome. (A) Global differences in gene expression in Δ*rel* versus (p)ppGpp˚ strains. Bar tracks indicate the distribution of genes in the respective functional groups. **(B)** Selected category results of the gene set enrichment analysis from regulated transcripts in Δ*rel* vs. (p)ppGpp˚ cells. Positive/negative enrichment scores represent enrichment in the up- or down-regulated genes. **(C)** Global differences in gene expression in exponentially growing (37 ˚C) or thermotolerant (48/53 ˚C) wild type cells. Bar tracks indicate the distribution of genes in the respective functional groups. **(D)** Selected category results of the gene set enrichment analysis from regulated transcripts in unstressed (37 ˚C) or thermotolerant (48/53 ˚C) wild type cells. Positive/negative enrichment scores represent enrichment in the up- or down-regulated genes.

https://doi.org/10.1371/journal.pgen.1008275.g003

cells as a hallmark of the SR, no increased transcription of CodY-regulated genes was observed in any of the heat shock conditions tested (S6 and S7B Figs), which could be explained by the unchanged GTP level in heat shocked cells (S1 Fig).

The transcript level of the genes encoding conserved chaperones and proteases of the heat shock response regulon were strongly up-regulated upon all temperature up-shifts, independently of the presence or absence of (p)ppGpp (S6 and S7C Figs). Interestingly, additional RT-qPCR experiments performed with RNA from 50 ˚C heat shock-treated cells revealed that the heat-induced expression of some SigB-regulated genes was impaired in the (p)ppGpp˚ background, e.g. *ssrA* (approx. 2-fold lower expression in (p)ppGpp˚ cells at 50 ˚C) and *dps* (approx. 3-fold lower expression), indicating a possible functional connection between the SR and the general stress response (S7C and S7D Fig) [62,63]. However, the majority of genes of the SigB regulon were found to be induced in the (p)ppGpp˚ strain similarly to wild type cells at 48 ˚C (S6 Fig).

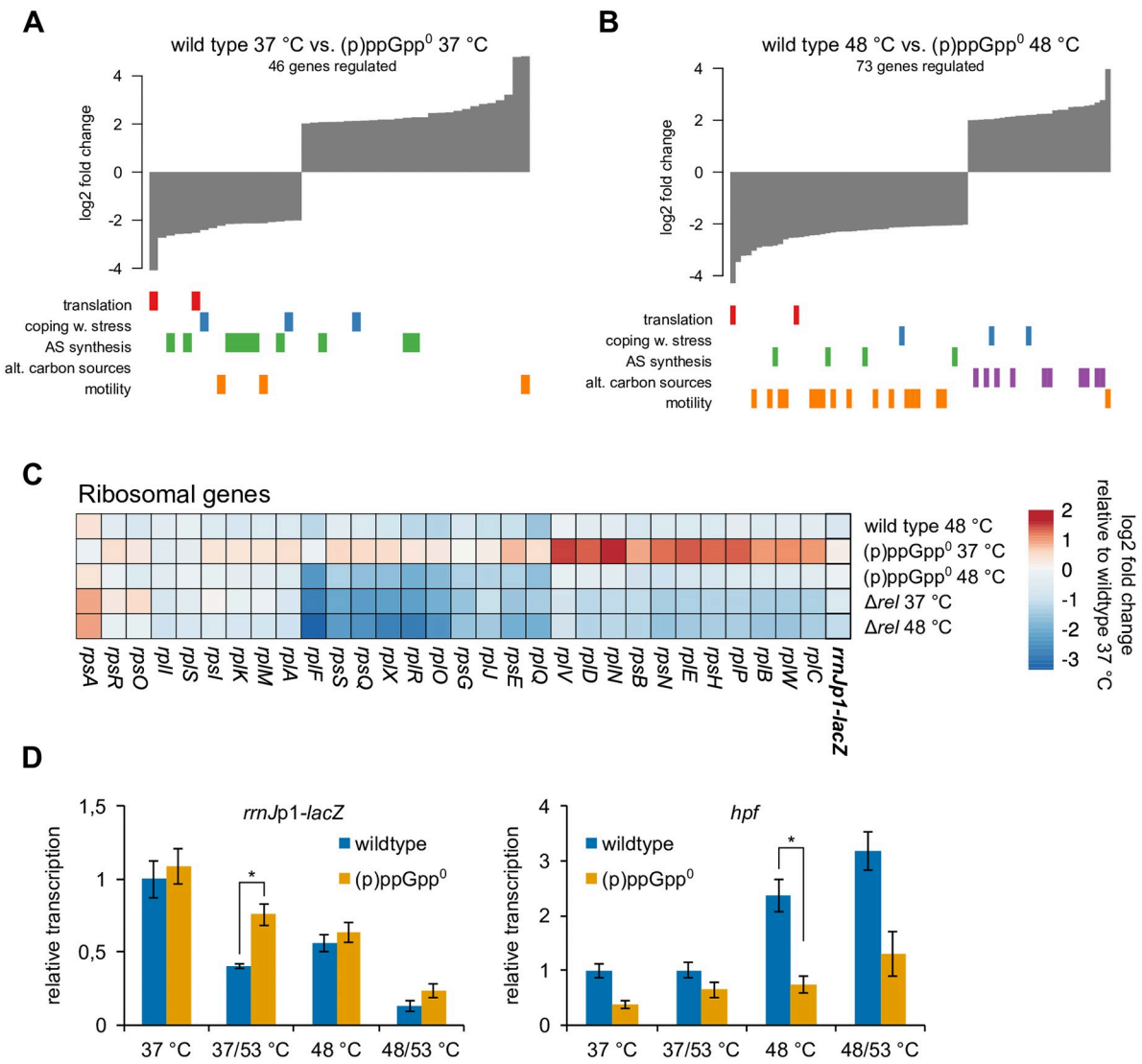

Fig 4. (p)ppGpp mediated transcriptional changes during heat stress. (A/B) Global differences in gene expression in wild type versus (p)ppGpp˚ strains at 37 ˚C or 48 ˚C, respectively. Bar tracks indicate the distribution of genes in the respective functional groups. **(C)** Heatmap showing expression changes of selected transcripts during mild heat stress in wild type, (p)ppGpp˚ or Δ*rel* cells. Values represent $\log_2$ fold changes of transcript levels relative to wild type cells at 37 ˚C. **(D)** Relative changes in the transcription of selected genes during heat shock in wild type and (p)ppGpp˚ strains determined by RT-qPCR. Means and SEM of three replicates are shown. Asterisks indicate significance ($p \leq 0.05$) according to Welch's *t*-test.

https://doi.org/10.1371/journal.pgen.1008275.g004

Notably, the heat-induced expression of *hpf*, which is positively regulated by the SR (S5A Fig), was lower in the (p)ppGpp˚ strain compared to wild type cells during heat stress (Fig 4D and S7A Fig). Furthermore, while CcpA-regulated genes were repressed in wild type and (p)ppGpp˚ cells under heat shock conditions (Fig 3 and S6 Fig), some genes (e.g. *rbsD*, *ganP*, *licH*) were less down-regulated or even induced at 48 ˚C in the (p)ppGpp˚ strain (Fig 4B). In contrast, motility-genes were particularly strongly down-regulated by heat in the (p)ppGpp˚ mutant (Fig 4B, S5 and S6 Figs), while the down-regulation of these genes appeared not to be significant in wild type cells at 48 ˚C (median 1.14-fold change, S6 Fig) [64].

Taken together, (p)ppGpp has a small but noticeable impact on the transcriptome during heat stress. The heat-mediated up-regulation of *hpf* and the down-regulation of *rrnJp1-lacZ*

appear to be dependent on (p)ppGpp. However, the overall induction of the heat shock response as well as the strong repression of many ribosomal protein genes observed during heat stress appear to be mostly independent of alarmones. The induction of the CodY regulon, a hallmark of SR, was also not much effected during heat stress, most likely because the heat mediated transient increase of (p)ppGpp might not be sufficient to lower the cellular GTP level for the subsequent remodeling of the transcriptome known from the fully induced SR [60].

It should be noted that when designing the RNA-seq experiment, we choose 48 ˚C as a simple heat shock condition for the mutant strains since it resembled the thermotolerance protocol (Fig 1A) and the condition of previously published microarrays [17]. However, many phenotypes of Spx and (p)ppGpp could be observed best upon a stronger, but non-lethal, heat shock at 50 ˚C [17], which we could assess by RT-qPCR. We also observed that, while wildtype cells treated with 37/53 ˚C exhibit a strong increase of (p)ppGpp within the first minutes of stress (Fig 1D), the examination of cellular physiology under these lethal conditions might be influenced by the apparent reduction of viability of about one order of magnitude (Fig 2G) [9,17].

Complementary roles of Spx and stringent response during heat shock

Previously, we reported that Spx, a central regulator of the heat- and oxidative stress response, can down-regulate the transcription of translation-related genes and rRNA [17]. However, an *spx* deletion strain was not impaired in the heat-mediated down-regulation of these genes [17]. Here, we noticed a detectable, albeit limited, involvement of the SR in the transcriptional down-regulation of specific genes during heat stress (*rrnJ*p1-*lacZ*), suggesting an intricate regulation of these genes by different factors. To test for such a concurrent and complementary transcriptional regulation by Spx and (p)ppGpp, a *B*. *subtilis* strain combining a *spx* deletion with the (p)ppGpp˚ mutations was constructed. Down-regulation of *rrnJ*p1-*lacZ* upon heat shock appear to largely depend on (p)ppGpp (Fig 5A), however Spx can also repress this promoter also in the absence of (p)ppGpp (S9B Fig) [17]. Interestingly, this (p)ppGpp˚ Δ*spx* strain also displayed a slow growth phenotype at 37 ˚C and a more severe growth defect at 50 ˚C compared to the strains with single deletions of (p)ppGpp˚ or Δ*spx* (Fig 5B and S8B Fig). These findings suggest a possible genetic interaction of the SR and the *spx* regulon under heat stress conditions. Consistently, the (p)ppGpp˚ Δ*spx* strain accumulated more heat-induced protein aggregates at 50 ˚C than cells lacking either (p)ppGpp or *spx* (S8C Fig). However, the transcription of selected r-protein genes was also down-regulated in the (p)ppGpp˚ Δ*spx* strain (S8A Fig), suggesting additional factors beyond Spx and (p)ppGpp, that can also influence the promoter and/or the stability of these transcripts.

When mutations in *rpoA* were introduced in the (p)ppGpp˚ strain that abolish Spx-mediated up- and down-regulation (*cxs*-1/*rpoA*^{Y263C}), or interfere only with Spx-mediated repression of rRNA while still allowing up-regulation of redox chaperones (*cxs*-2 / *rpoA*$^{V26\circ A}$) [17], only the (p)ppGpp˚ *cxs*-1 strain displayed a severe growth defect as observed for the (p)ppGpp ˚ Δ*spx* strain (S8B Fig). This experiment suggests that the Spx-mediated up-regulation of stress response genes, and not the ability to down-regulate translation-related genes, is required for efficient growth in the (p)ppGpp˚ background. Notably, (p)ppGpp is sufficient for the down-regulation of translation-related genes during norvaline-induced amino acid limitation, while Spx is dispensable for this process (S9A Fig). Conversely, Spx can act on rRNA promoters independently of (p)ppGpp *in vivo* (S9B Fig) [17]. In addition, *in vitro* transcription experiments with purified Spx and RNAP gave no indications that ppGpp could directly influence Spx mediated transcriptional activation or inhibition of RNAP (S9C Fig). Furthermore, Spx-

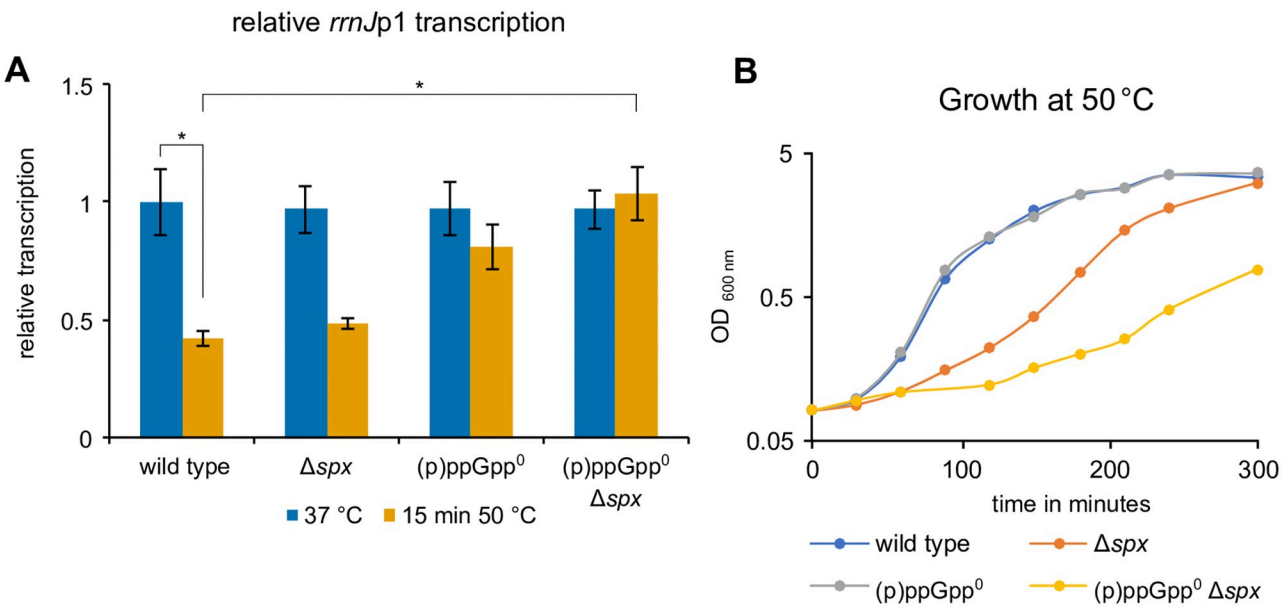

Fig 5. Complementary roles of (p)ppGpp and Spx under heat stress. (A) Heat mediated down-regulation *of rrnJ*p1-*lacZ* transcription in wild type (BHS220), Δ*spx* (BHS222), (p)ppGpp° (BHS319) and Δ*spx* (p)ppGpp° (BHS766) strains as determined by RT-qPCR. Means and SEM of three independent experiments are shown. Asterisks indicate significance ($p \leq 0.05$) according to Welch's *t*-test. **(B)** Growth of the same strains in LB medium at 50 °C.

https://doi.org/10.1371/journal.pgen.1008275.g005

dependent stress response genes (e.g. *trxB*, *clpX*) are not up-regulated in the Δ*rel* strain (S3 Dataset), suggesting that Spx is not activated by (p)ppGpp *in vivo*.

Together, these experiments suggest a complex interplay between Spx and (p)ppGpp during the heat shock response and that the activity of at least either Spx or (p)ppGpp is important for efficient growth during heat stress. However, the inhibitory activity of Spx on translation-related genes appears to be dispensable for stress tolerance and many r-protein genes were down-regulated during heat stress even in the absence of both Spx and (p)ppGpp.

The observation that transcription of *spx* is also activated by (p)ppGpp via CodY in *Enterococcus faecalis* and that *rel* transcription is activated by the disulfide-stress regulator σ^R in *Streptomyces coelicolor* points toward a possible functional connection of these two regulators [65,66].

(p)ppGpp regulates translation during heat stress

Upon heat shock, we observed raised levels of (p)ppGpp, but not the transcriptional reprogramming triggered by lowered GTP levels (Figs 3 and 4, S6 and S7 Figs). Therefore, we wanted to determine the impact of (p)ppGpp on translation during heat stress. To this end, a method for pulse-labeling newly synthesized nascent peptide chains using puromycin was utilized to estimate protein synthesis rates (see Methods, S10 Fig) [67]. As expected, expressing the small alarmone synthetase *relP* (*ywaC) in trans*, results in accumulation of high (p)ppGpp levels, which concurrently lead to a strong decrease in translation rate, indicating that translation is inhibited in these cells (S10D and S10E Fig) [39,53,68].

When we examined the translation rate in cells, we observed that the Δ*rel* strain always exhibited a lower translation rate compared to wild type cells at 37˚C (Fig 6A and 6B), consistent with its raised (p)ppGpp levels and the observed "stringent" phenotype of this strain. The difference between wild type and Δ*rel* strain diminished upon exposure to higher

temperatures, possibly influenced also by stress induced raised levels of the alarmone in wild type cells at these higher temperatures. By contrast, the "relaxed" (p)ppGpp° strain always exhibited higher translation rates (Fig 6A and 6B), indicating a more deregulated translation compared to wild type or Δ*rel* strains. During the non-lethal 50 °C heat shock, translation rates transiently increased in all strains (Fig 6A). Nevertheless, the (p)ppGpp° strain still displayed significantly higher translation rates compared to wild type and the Δ*rel B. subtilis* strains (Fig 6A and 6B). The observed influence of (p)ppGpp on translation suggests that the most important impact of (p)ppGpp under heat stress appears not to be its effect on transcription (Fig 4 and S5 Fig), but the direct modulation of translation (Fig 6), possibly by directly interfering with the activity of different translational GTPases [39,40,68,69].

Down-regulation of translation accompanied by slower growth that increases thermoresistance can also be observed in cells with defective ribosomes, lacking e.g. the ribosomal protein L11 (RplK). RplK is not essential, however the Δ*rplK* strain exhibits severe translation defects and a strongly reduced growth rate (S11 Fig), despite its inability to synthesize (p)ppGpp [70]. Such a *B. subtilis* Δ*rplK* strain exhibits increased heat stress tolerance similar to Δ*rel* cells (S11 Fig). This observation suggests that a reduced translation rate caused by a defective ribosome is sufficient to increase survival under heat stress, even in the absence of the alarmone. In summary, these observations indicate that the intracellular (p)ppGpp second messenger can immediately modulate translation during heat stress and that the reduction of the protein synthesis rate *per se* can promote increased stress tolerance.

Changes in protein levels mediated by heat shock and (p)ppGpp

The observation that (p)ppGpp appears to directly regulate translation under heat stress prompted us to also examine the effect of the alarmones and heat on changes in the proteome. Therefore, we employed mass spectrometry for a proteome-wide identification and quantification of cellular proteins from stressed (15 min 50 °C) and unstressed (37 °C) wild type, (p)ppGpp° and Δ*rel* cells. In total, we quantified 2641 proteins which were identified with at least two peptides in all conditions (S4 and S5 Datasets, S12 and S13 Figs). Under heat stress (50 °C), a pronounced increase of heat-specific stress response proteins, e.g. ClpC or GroEL, was observed in all strains, indicating that the translational capacity is sufficient to promote the synthesis of heat shock proteins in wild type, and even in the Δ*rel* strains where the translation rate is reduced (Fig 6C and S12 Fig).

In contrast, the heat mediated synthesis of SigB-controlled general stress proteins was reduced in (p)ppGpp° cells, whereas their levels were increased in the Δ*rel* strain, which corroborates the regulatory connection between alarmone synthesis and the general stress response already observed in the RNA-seq experiment (Fig 6C and S12 Fig).

Abundant ribosomal proteins represent a large proportion of the cellular protein mass in wild type and (p)ppGpp° cells, however their levels were strongly decreased in Δ*rel* cells in accordance with the constitutive stringent regulation observed in this strain (Fig 6C, S12 and S13 Figs). Interestingly, the levels of many r-proteins appear to be reduced upon heat stress in wild type but not in (p)ppGpp° cells (Fig 6C and S12 Fig), which supports an alarmone dependent post-translational control mechanism of the abundance of these translation-related proteins.

When comparing the proteomes of Δ*rel* cells with wild type cells under unstressed conditions, we observed large-scale changes that resembled in many ways the results obtained by RNA-seq (S13 Fig). In contrast, the differences in the proteome between wild type and (p)ppGpp° cells were comparatively smaller at both 37 °C and 50 °C (S13 Fig). Importantly, a gene set enrichment analysis of the differentially regulated proteins from wild type or (p)ppGpp° at

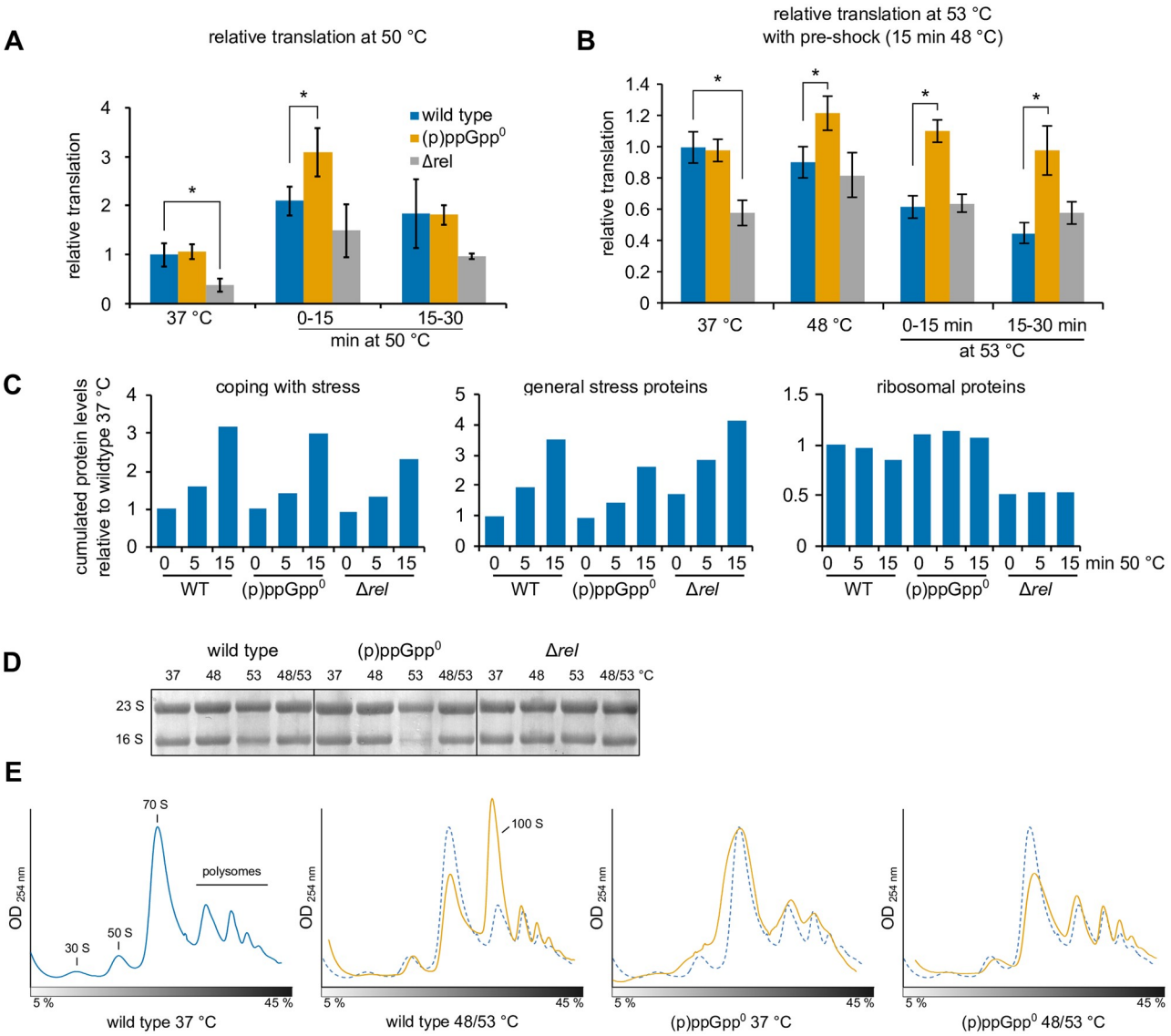

Fig 6. (p)ppGpp modulates translation during stress response. (A/ B) Relative translation (estimated from puromycin incorporation) of wild type, (p)ppGpp˚ (BHS214) and Δ*rel* (BHS126) strains during heat stress **(A)** at 50 ˚C or **(B)** at 48 ˚C or 48/53 ˚C. 1 μg ml^{-1} puromycin was added for 15 min to the medium directly after (0–15 min) or 15 min after shifting the sample to the indicated temperatures. Means and SEM of four independent experiments are shown. Asterisks indicate significance ($p \leq 0.05$) relative to wild type according to Welch's *t*-test. **(C)** Relative cumulated protein levels of selected categories of wild type, (p)ppGpp0 and Δ*rel* strains during heat stress. Categories were inferred from SubtiWiki. The relative abundances of all proteins of the respective category were cumulated and normalized to the control condition (wild type 37 ˚C). **(D)** Methylene blue stained membranes showing the integrity or degradation of rRNA after severe heat stress (53 ˚C). Wild type, (p)ppGpp˚ (BHS214) or Δ*rel* (BHS126) cells were heat-shocked at 48 ˚C, 53 ˚C or 48/53 ˚C for 15 min each. 2 μg total RNA was separated on denaturing agarose gels and blotted on nylon membranes. **(E)** Sucrose gradient profiles of extracts from untreated (37 ˚C) or thermotolerant (48/53 ˚C for 15 min each) wild type or (p)ppGpp˚ (BHS214) cells. The dashed blue line of untreated wild type cells is shown for reference.

https://doi.org/10.1371/journal.pgen.1008275.g006

37 ˚C or 50 ˚C revealed only few enriched functional categories (S5 Dataset). These observations suggest, that (p)ppGpp is involved in the regulation of the total translation capacity.

In summary, although (p)ppGpp may be involved in post-transcriptional regulation of some proteins, it appears that the alarmones assist in the development of stress tolerance by controlling global changes in translation rate. However, we observed a (p)ppGpp-dependent regulation of specific protein classes of the proteome. (Fig 6C). Notably we observed a

reduction of r- proteins depending on the alarmone and a relative increase in chaperone levels during heat shock independent of the alarmone (Fig 6C, S12 and S13 Figs). Since we observed the heat mediated induction of chaperones even in the *rel* strain with its constantly elevated (p)ppGpp levels and a slowed down translation, we suspect the possibility of a mechanism allowing the specific translation of chaperones, albeit the generally slowed down translation.

In addition to this protective function, (p)ppGpp, which is synthesized only as a pulse by Rel during relatively uninhibited growth at 50 ˚C, could modulate or inhibit translation, presumably by directly interfering with translation factors [38,39,41,69]. A set of interesting *in vitro* experiments suggested a modulating effect of ppGpp and (p)ppGpp on IF2 and translation initiation, which also depended on specific structured elements of translated mRNA, allowing translation of specific mRNA's in the presence of alarmones [41]. These experiments indicate a specific ability of alarmones, interacting with IF2, to limit translation in general, while possibly still allowing the expression of specific genes necessary for stress resistance [41].

(p)ppGpp is required for ribosome integrity and 100S formation during heat stress

Treatment with a lethal temperature shift (37/53 ˚C) without pre-shock resulted in a strong decrease in translation efficiency in wild type and (p)ppGpp˚ strains. Interestingly, translation was strongly decreased in (p)ppGpp˚ cells at 37/53 ˚C, while wild type cells still maintained active translation under these conditions (S14A Fig). The lowered translation activity in (p)ppGpp˚ cells appears to be accompanied by a strong reduction of the levels of cellular 16S rRNA during this severe heat shock (Fig 6D). This could indicate a defect in 16S rRNA maturation and the assembly and/or activity of the small ribosomal subunit, which would be consistent with the observed heat sensitivity of the *B*. *subtilis* (p)ppGpp˚ strain (Fig 2A and 2B). In contrast, the translation in Δ*rel* cells appeared to be transiently increased in comparison to the wild type and (p)ppGpp˚ strains (S14A Fig), in agreement with the observed high heat-resistance of this strain to the otherwise lethal heat shock, which negatively affects the growth of the more sensitive wild type and (p)ppGpp˚ strain (Fig 2G).

The (p)ppGpp˚ strain also failed to induce expression of the *hpf* gene during heat stress and did not accumulate the Hpf protein (Fig 4D and S14B Fig). Thus, the formation of 100S disomes upon heat stress, which was clearly visible in the ribosome profiles of wild type and Δ*rel* cells (especially under thermotolerance conditions) was abolished in the (p)ppGpp˚ strain where only polysomes could be detected similarly as in Δ*hpf* cells (Fig 6E and S14C Fig) [71]. However, the apparent decrease in the 16S rRNA observed under severe stress conditions was not prevented by *in trans* expression of Hpf (S14D Fig) and overexpression of Hpf could not rescue the heat-sensitive phenotype of (p)ppGpp˚ strains (S14E Fig). Also, the addition of translation-inhibiting antibiotics could not rescue this phenotype, indicating that inhibition of translation *per se* is not sufficient to protect ribosomes during severe heat stress (S14F Fig).

It was recently observed in *B*. *subtilis* that tRNA maturation defects could lead to an inhibition of rRNA processing and 30S assembly via the synthesis of (p)ppGpp [72], supporting a role of the alarmone in ribosome maturation.

Taken together, these observations indicate that (p)ppGpp is also required for the integrity of the ribosomal subunits and the formation of 100S particles under heat stress. These observations might be important to understand possible stress signaling pathways and also the protective effects of (p)ppGpp on translation under proteotoxic stress conditions.

The activation of the stringent response during heat stress

The results presented here clearly reveal that (p)ppGpp accumulates rapidly during heat and other environmental stresses (Fig 1). In addition, strains unable to synthesize (p)ppGpp are rendered sensitive to high temperatures and accumulate more heat-induced protein aggregates (Fig 2A–2D, 2H and 2I). Interestingly, (p)ppGpp synthesis and heat tolerance are solely dependent on the synthetase activity of Rel, indicating that this enzyme is responsible for the synthesis of (p)ppGpp under these conditions (Figs 1E and 2A–2D).

Similarly to heat stress, disulfide or salt stress can also lead to inactivation, unfolding and aggregation of proteins [48,73]. It is possible that protein aggregation or inactivation could be involved in the signal for the stress-mediated activation of Rel, since proteotoxic and oxidative stress can result in the inactivation of enzymes and may impair uptake or biosynthesis of certain amino acids [51,74–76].

The transcriptional and translational heat shock response, which usually depends on sensing temperature indirectly or directly by cellular protein unfolding is in the range of 2–5 min [5,6]. Since the protein unfolding precedes the transcriptional or translational response, one can estimate that cellular protein unfolding upon sudden proteotoxic stress happen faster than 2–3 min. This is also consistent with the observation of the *in vivo* formation of subcellular protein aggregates, which are preceded by unfolding and misfolding events, can already be observed about 2 min after heat shock [7]. The relatively fast and transient kinetics of heat induced alarmone synthesis (Fig 1) would therefore be consistent with the time frame known from general heat mediated protein misfolding and the unfolding or misfolding of specific stress-sensor proteins during heat stress.

Our experiments demonstrate that Rel activation during heat- or oxidative stress can be inhibited by chloramphenicol, similarly as during amino acid starvation (Fig 1F and S1E Fig). Therefore, the underlying activation mechanisms during environmental stress likely share some similarities to the well-studied SR-activation upon amino acid deprivation and may also involve the sensing of uncharged tRNA on the ribosome [21,22,74,77].

The stress induced depletion of amino acids can result in the accumulation of uncharged tRNA, which serves as a signal to activate Rel. In addition, tRNAs and proteins of the translational machinery are prone to oxidation or modification upon stress, leading to translation stalling, which can also elicit the SR [78]. For example, oxidation of tRNAs at a conserved 4-thiouridine residue reduced the affinity for their cognate aminoacyl-tRNA synthetase, which was found to be the basis for the activation of the SR upon UV-exposure in *S. enterica* [79].

It is very likely that the heat stress signal is first sensed via unfolded proteins which might then be transmitted by specific tRNA to Rel on the ribosome by the various discussed possibilities. However, it cannot be excluded that e.g. Rel itself can act as a heat stress sensing protein on the ribosome, or that a heat stress sensing protein that interacts with Rel could be involved, as for example suggested for competence development in *B. subtilis* [80]. Clearly, more experiments are required to identify the molecular mechanism underlying the activation of Rel and the control of the SR during heat stress in *B. subtilis*.

The role of (p)ppGpp and SigB upon heat stress

Both the transcriptomic and the proteomic datasets also indicate a possible activation of the SigB-dependent general stress response by (p)ppGpp during stress- and non-stress conditions (Figs 3B and 6C, S5B, S7, S12 and S13 Figs). SigB becomes activated by decreased GTP levels as elicited by decoyinine [62,63]. In addition, a requirement of L11, which is necessary for Rel synthetase activity, and Obg, a ribosome-associated GTPase that interacts with (p)ppGpp, for the activation of SigB upon physical stress and an interaction of Obg with components of the

SigB regulatory cascade was reported, suggesting an intricate connection between the ribosome, Rel and the activation of the general stress response [62,70,81].

The role of the SR during the heat stress response

Taken together, our data suggest a model in which cells respond to heat-mediated protein unfolding and aggregation, not only by raising the repair capacity, but also by decreasing translation to concurrently reduce the load on the cellular protein quality control systems (Fig 7).

Upon heat shock, Rel is activated and rapidly synthesizes alarmones. The second messenger (p)ppGpp can then directly control the activity of translation factors and may thereby mediate a fast and immediate response to modulate translation during stress. At the same time (p)ppGpp might play a significant role in maintaining and protecting active ribosomes, which might involve modulating translation already at the ribosome assembly stage. The readjustments of translation could then allow an efficient reallocation of cellular resources to the synthesis of stress response proteins and concurrently minimize the load on the protein quality control systems, thus contributing to protein homeostasis [3,82,83]. The unfolded protein response to misbalances in protein homeostasis in the endoplasmic reticulum of eukaryotic cells is a well-studied and analogous stress response mechanism where the up-regulation of chaperones is also coupled to the concurrent down-regulation of translation, albeit by different mechanisms [3,84].

It should be noted that lowering the cellular GTP level by treatment with decoyinine also resulted in a limited increase of thermoresistance in the absence of elevated alarmone levels. Similarly, it was reported that mutant strains of *Lactococcus lactis* with constitutively lowered GTP levels also exhibited increased stress tolerance [85]. These observations suggest, that a decrease in the cellular GTP concentration alone can reproduce many effects on the cellular physiology that can also be observed in the presence of (p)ppGpp. However, the heat stress resistance conferred by increased (p)ppGpp levels appeared to be stronger than observed upon decoyinine treatment, which could indicate that certain processes important for stress resistance are predominantly controlled by (p)ppGpp directly. Clearly, more work is required to

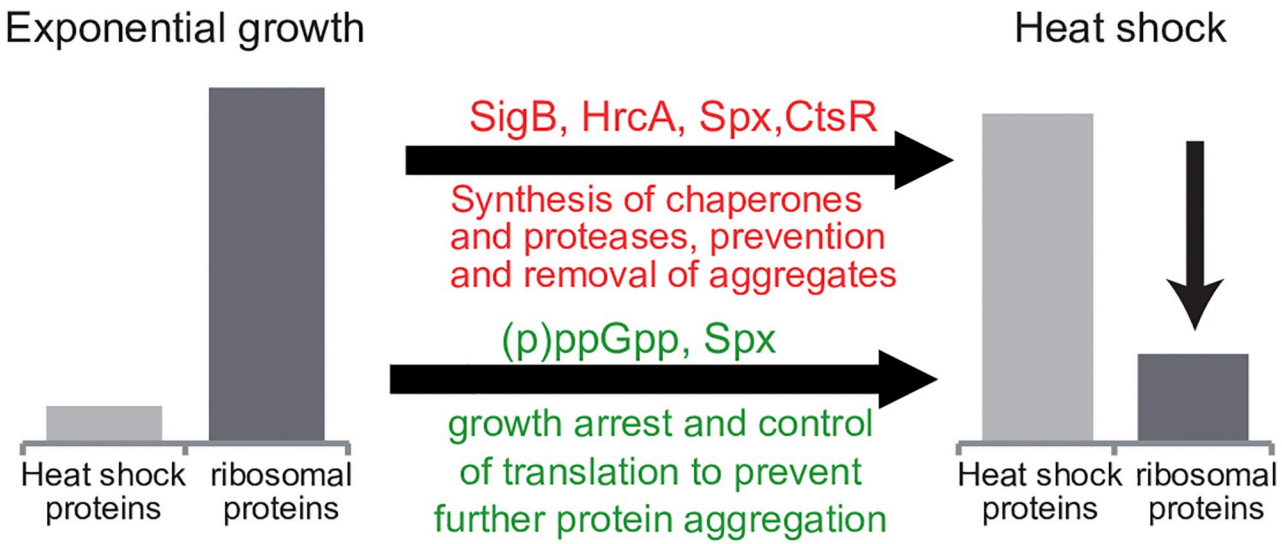

Fig 7. The role of the stringent response in the heat shock response. Model of the role of the stringent response in the regulatory network of the heat shock response.

https://doi.org/10.1371/journal.pgen.1008275.g007

identify and characterize the cellular targets of (p)ppGpp and to examine the differential roles of GTP and (p)ppGpp during thermotolerance development.

Interestingly, accumulation of (p)ppGpp upon heat or oxidative stress and its importance for stress resistance has also been reported in other *Firmicutes* and also *Proteobacteria* that differ widely in terms of (p)ppGpp signaling [49,74,77,86,87]. Accumulation of (p)ppGpp was shown to protect cells from salt or osmotic stress [85,88]. Conversely, the lack of (p)ppGpp is known to render cells sensitive to heat or oxidative stress [74,89,90], suggesting that activation of the SR, allowing the fast down-regulation of translation, is an important and conserved part of the response to environmental stress in bacteria. It is interesting to note that the SR was also implicated in *B. subtilis* competence development, facilitating a cellular state where cells cease to divide, and most transcription and translation is strongly down-regulated (also referred to as the K-state). In these cells, only competence proteins, together with DNA repair and recombination genes, are expressed, allowing the uptake and possible utilization of homologous DNA in this specific cellular state of a subpopulation of stationary phase cells [80]. Bacterial cells thus appear to utilize the (p)ppGpp second messengers, which can interfere directly with basic cellular processes such as translation, replication and growth, as an important part of different regulatory networks, facilitating and allowing the survival of bacterial cells in fast changing environments with limited nutrient availability and exposure to various stress conditions.

Methods

Construction of strains and plasmids

Strains, plasmids and primers are listed in S1 Table. PCR-amplification and molecular cloning using *E. coli* DH5α as host was carried out according to standard protocols [91]. Point mutations were introduced via overlap-extension PCR. To generate pBSII-spxDD-spec, a fragment carrying spx^{DD}, *lacI* and the spectinomycin resistance cassette was amplified from pSN56 [15] with primers p289/p223 and ligated using *Spe*I/*Nsi*I sites into the pBSIIE backbone amplified with primers p203/p288. Integrative plasmids were linearized by digestion with *Sca*I or *Bsa*I prior to transformation. Point mutations in the *rel* gene were first cloned in the pMAD vector and then re-amplified for cloning into pDR111.

Transformation of *B. subtilis* strains, the generation of scarless mutations using the pMAD system and the introduction of *cxs-1/2* mutations in *rpoA* was carried out as described previously [92–94]. Mutants were selected on 100 μg ml^{-1} spectinomycin, 10 μg ml^{-1} kanamycin, 1 μg ml^{-1} erythromycin, 25 μg ml^{-1} lincomycin or 5 μg ml^{-1} chloramphenicol, respectively. To obtain the (p)ppGpp° strain (BHS214), markerless $relP^{E154V}$ and $relQ^{E139V}$ mutations were introduced into *B. subtilis 168* cells by successive transformation and recombination of plasmids pMAD-$relP^{E154V}$ and pMAD-$relQ^{E139V}$, yielding strain BHS204. Next, a PCR amplified fragment carrying *rel*::*erm* [27] and flanking homologous regions was transformed to generate BHS214. Since the (p)ppGpp° strain fails to develop natural competence, additional mutations were introduced in BHS204 and transformed with a PCR-amplified *rel*::*erm* fragment or BHS214 genomic DNA in a second step.

Growth conditions

B. subtilis strains were grown in LB medium (5 g L^{-1} yeast extract, 10 g L^{-1} tryptone-peptone, 10 g L^{-1} NaCl) or minimal medium [95] supplemented with 0.5% casamino acids in water baths with 200 rpm orbital shaking at the desired temperatures. 1 mM IPTG or 0.4% xylose was supplemented if required.

Survival and viability assays

The assays for thermotolerance development, survival and preparation of protein aggregate are described previously [9]. 1 mM IPTG was added to induce expression of recombinant proteins 30 min before the division of the culture. The influence of decoyinine on thermotolerance was tested in 1.5 mL tubes in a ThermoMixer (Eppendorf). Detection of aggregates by fluorescence microscopy was described previously in [48]. Spot colony formation assays were carried out as described previously and incubated at the indicated temperatures [17].

Transcription analysis

Strains were grown in LB and treated as indicated. Samples of 15–25 mL were harvested by centrifugation for 3 min at 3,860 x g at 4 ˚C and frozen in liquid nitrogen. Isolation of total RNA, treatment with DNase I (NEB) and quality control by native agarose gel electrophoresis, methylene blue staining and northern blotting was described previously [17]. Northern blotting, hybridization with DIG-labeled RNA probes and detection was carried out as described previously [17]. Primers for the synthesis of probes are listed in S1 Table. Reverse transcription and qPCR were carried out as described previously [17]. The primers are listed in S1 Table. 23 S rRNA was used as a reference.

RNA sequencing

Cells of BHS220, BHS319 and BHS368 were grown in 150 mL LB medium in 500 mL flasks in water baths at 37 ˚C and 200 rpm. In the mid-exponential phase ($OD_{600\ nm}$ ~ 0.4), the culture was divided and shifted to 48 ˚C or left at 37 ˚C. After 15 min, samples were withdrawn and both cultures were shifted to 53 ˚C for another 15 min and harvested. Cells from 25 mL medium were pelleted by centrifugation for 3 min at 3,860 x g and 4 ˚C and flash-frozen in liquid nitrogen. RNA was prepared the using phenol/trizol method as described in [96] and treated with TURBO DNase (Invitrogen). RNA quality was assessed on a Bioanalyzer 2100 System (Agilent).

rRNA depletion from total RNA using MICROBExpress (Ambion), treatment with tobacco acid pyrophosphatase (TAP) for +TAP libraries, library preparation, Illumina sequencing and quality control of the sequencing output was carried out as described previously [97]. Reads were mapped to the *Bacillus subtils* 168 genome with insertion of *rrnJp1-lacZ* in the *amyE* site (strain BHS220, *amyE*::*rrnJp1-lacZ cat*) using Bowtie2 (version 2.1.0) reads [98] with default parameters and filtered for uniquely mapped reads using SAMtools [99]. The DEseq2 package with default parameters was used for the detection of differentially expressed genes from raw count data of triplicate experiments [100]. Expression changes were considered significant if differentially regulated by at least 4-fold (p-value ≤ 0.05). The data have been deposited in NCBI's Gene Expression Omnibus and are accessible through GEO Series accession number GSE125467 [101]. Transcription start sites were annotated from the comparison of rRNA-depleted, tobacco acid pyrophosphatase (TAP) treated libraries that allow adaptor-ligation to 5' primary transcripts and libraries, where TAP treatment was omitted using the TSSpredator v1.06 software [102] in the "more sensitive" parameter preset and manually reviewed.

In vitro transcription

In vitro transcription assays using purified *B*. *subtilis* RNA polymerase and Spx protein was carried out as described previously [17].

Fluorescence microscopy

Strain BIH369 (*lacA*::*Pxyl-yocM-mCherry erm*) was grown in LB medium + 0.5% xylose. The culture was divided in the mid-exponential phase, supplemented with puromycin for 15 min and subjected to fluorescence microscopy in a Axio Imager.Z2 (Zeiss) microscope using the RFP filter set [17].

SDS PAGE and western blotting

Strains were grown in LB medium and treated as indicated, harvested by centrifugation for 5 min at 3,860 x g at 4 ˚C, washed in TE buffer (10 mM TRIS-HCl, 1 mM EDTA, pH 8.0) and disrupted by sonication in TE supplemented with 1 mM PMSF. Equal amounts of protein were separated by SDS-PAGE and stained with coomassie or subjected to western blotting [103–105]. For signal detection, polyclonal α-Hpf antibody (1:5,000) [71] or monoclonal anti-puromycin antibody (1:10,000, Merck) and HRP-conjugated anti-mouse or anti-rabbit antibodies (1:10,000, Roth) were used in conjunction with the ECL-system as described previously [17]. Images were acquired using a ChemoStar Imaging System (Intas, Göttingen, Germany).

Translation rate analysis

Puromycin becomes covalently incorporated into nascent peptide chains, which can be used as readout for the rate of translation [67,106,107]. We verified that low puromycin concentrations (1 μg mL^{-1}) do not perturb growth or lead to the accumulation of misfolded proteins in cellular protein aggregates, which can be visualized as using the previously established YocM-mCherrry fusion protein (S10A–S10C Fig) [48,108]. Strains were grown in LB medium and treated as indicated. For *in vivo* labeling, 10 mL medium were separated, supplemented with 1 μg mL^{-1} puromycin (Roth) and incubated for 15 min at the same conditions. Then, samples were supplemented with 25 μg mL^{-1} chloramphenicol, harvested by centrifugation for 5 min at 3,860 x g at 4 ˚C, washed in TE buffer (10 mM TRIS-HCl, 1 mM EDTA, pH 8.0) and disrupted by sonication in TE supplemented with 1 mM PMSF. Equal amounts of protein were directly spotted on nitrocellulose membranes (5 μg) or subjected to SDS-PAGE and western blotting [91]. Puromycin-signals were detected using monoclonal anti-puromycin antibody (1:10,000, Merck), HRP-conjugated anti-mouse antibody (1:10,000, Roth) and the ECL-system in a ChemoStar imaging system (Intas, Göttingen, Germany). Signals were analyzed using Fiji distribution of ImageJ [109].

Sucrose density gradient centrifugation analysis

Early exponential phase cultures of *B. subtilis* strains grown in LB medium were treated with heat shock at 48 ˚C or 48 ˚C/53 ˚C for 15 min each. Samples of 50 mL were supplemented with 50 μg mL^{-1} chloramphenicol to stall translation and harvested by centrifugation at 4,000 x g for 10 min at 4 ˚C. Cells were resuspended in 25 mM HEPES-KOH, pH 7.5, 150 mM KOAc, 25 mM $Mg(OAc)_2$, 1 mM dithiothreitol (DTT), n-Decyl–β–D-thiomaltopyranoside (DTM), 5% (w/v) sucrose) and lysed by sonication. The lysate was cleared by centrifugation at 16,000 x g for 15 min at 4 ˚C. 10 OD_{260} units were loaded on a 10 mL 5–45% (w/v) sucrose gradient prepared in the same buffer, run in a SW-40 Ti rotor (Beckman Coulter) at 57,471 x g for 16.5 h and analyzed using a Gradient Station (Biocomp) with an Econo UV Monitor (Bio-Rad).

Quantification of nucleotides

Cells were grown in minimal medium supplemented with 0.5% casamino acids to support the growth of (p)ppGpp deficient strains [60] and treated as indicated. Samples of 2 mL were removed, supplemented with 75 μL 100% formic acid and incubated on ice for 30 min.

Extraction of nucleotides was carried out as described in [110] and detected by HPLC-ESI-MS/MS on a QTRAP 5500 instrument. Analytes were separated on a Hypercarb column (30 x 4.6 mm, 5 μm particle size) in a linear gradient of solvent A (10 mM ammonium acetate pH 10) and solvent B (acetonitrile) at a flow rate of 0.6 mL/min from 96% A + 4% B (0 min) to 40% A + 60% B (8 min) into the ESI ion source at 4.5 kV in positive ion mode. Tenofovir was used as internal standard. pGpp and pppGpp standards were synthesized *in vitro* from ATP and GTP or GMP as described previously [111]. ppGpp was purchased from Trilink Biotechnologies.

Identification and quantification of proteins by mass spectrometry

Strains were grown in LB medium at 37 ˚C and 200 rpm to the mid-exponential phase (OD_{600nm} 0.4) and transferred to a 50 ˚C water bath. Samples were taken at before, 5 min and 15 min after the temperature shift and washed three times in 50 mM HEPES pH 8, 150 mM NaCl. Three biological replicates were analyzed. All samples were subjected to SP3 sample preparation [112]. Briefly, to each sample 4x lysis buffer was added (4% SDS, 40 mM TCEP, 160 mM chloroacetamide, 200 mM HEPES pH 8) and proteins were denatured, reduced and alkylated during incubation at 95 ˚C for 5 minutes. 0.8 μL Benzonase (NEB) was added and samples were incubated at 37 ˚C for 30 minutes. Ten μg of a 1:1 mixture of hydrophilic and hydrophobic carboxyl-coated paramagnetic beads (SeraMag, #24152105050250 and #44152105050250, GE Healtcare) were added for each μg of protein. Protein binding was induced by addition of acetonitrile to a final concentration of 50% (v/v). Samples were incubated for 10 minutes at room temperature. The tubes were placed on a magnetic rack and beads were allowed to settle for three minutes. The supernatant was discarded and beads were rinsed three times with 200 μL of 80% ethanol without removing the tubes from the rack. Beads were resuspended in digestion buffer containing 50 mM triethylammonium bicarbonate and both Trypsin (Serva) and Lys-C (Wako) in a 1:50 enzyme to protein ratio. Protein digestion was carried out for 14 hours at 37˚C in a PCR cycler. Afterwards the supernatant was recovered and 1 μL was used to perform peptide quantification using a quantitative colorimetric peptide assay (Pierce, #23275) following the manufacturer's instructions.

TMT 11plex (Pierce, #A37725) was used for peptide multiplexing and quantification. Briefly, equal amounts of peptides were dried down in a vacuum concentrator and resuspended in 50 mM HEPES pH 8.5. Additionally, 10% from each sample was pooled to create a common sample as internal standard. TMT reagents were allowed to equilibrate to room temperature for 30 minutes and were dissolved in anhydrous acetonitrile to a final concentration of 59 mM. To each sample TMT was added to a final concentration of 11.8 mM and tubes were incubated at 25˚C for 60 minutes with mixing at 500 rpm on a ThermoMixer. Labeling was quenched by addition of hydroxylamine to a final concentration of 0.4%. Samples were mixed, desalted using solid phase extraction (Seppak 1cc/50mg, Waters), dried down in a vacuum concentrator and resuspended in 20 μL 2% acetonitrile. Basic reversed phase fractionation was performed on a quaternary Agilent 1290 Infinity II UPLC system equipped with a Kinetex Evo-C18 column (150 x 2.1 mm, 2.6μm, 100 Å, Phenomenex) that was operated at 40 ˚C. Solvent A consisted of water, solvent B consisted of 100% acetonitrile, and solvent C consisted of 25 mM ammonium bicarbonate. Fractionation was carried out at a constant flow rate of 100 μl/min using a linear gradient from 2–25% acetonitrile within 50 minutes, followed by column washing and equilibration. Over the whole gradient solvent C was kept constant at 10%. In total 32 fractions were collected in conical 96well plates. The organic solvent was removed in a vacuum concentrator for one hour and fractions were combined into 8 final samples. Peptides were acidified with formic acid, desalted using OASIS HLB 96well cartridges

(Waters, #186001828BA), dried down and resuspended in 2% acetonitrile, 0.1% trifluoroacetic acid (TFA) prior MS analysis.

All samples were analyzed on a Q-Exactive HF (Thermo Scientific) that was coupled to a 3000 RSLC nano UPLC (Thermo Scientific). Samples were loaded on a pepmap trap cartridge (300 μm i.d. x 5 mm, C18, Thermo) with 2% acetonitrile, 0.1% TFA at a flow rate of 20 μL/min. Peptides were separated over a 50 cm analytical column (Picofrit, 360 μm O.D., 75 μm I.D., 10 μm tip opening, non-coated, New Objective) that was packed in-house with Poroshell 120 EC-C18, 2.7 μm (Agilent). Solvent A consists of 0.1% formic acid in water. Elution was carried out at a constant flow rate of 250 nL/min using a 180 minute method: 8–33% solvent B (0.1% formic acid in 80% acetonitrile) within 120 minutes, 33–48% solvent B within 25 minutes, 48–98% buffer B within 1 minute, followed by column washing and equilibration. Data acquisition on the Q-Exactive HF was carried out using a data-dependent method in positive ion mode. MS survey scans were acquired from 375–1500 m/z in profile mode at a resolution of 120,000. AGC target was set to 3e6 charges at a maximum injection time of 60 ms. The ten most abundant peptides were isolated within a 0.7 m/z window offset by +0.1 m/z and subjected to HCD fragmentation at a normalized collision energy of 32%. The MS2 AGC target was set to 2e5 charges, allowing a maximum injection time of 78 ms. Product ions were detected in the Orbitrap at a resolution of 45,000. Precursors were dynamically excluded for 30 s.

Raw files were processed with Proteome Discoverer 2.3 (Thermo Scientific). Briefly, peak lists were extracted from raw files and searched using SEQUEST HT against a Uniprot bacillus subtilis database (version 190614, taxonomy ID 224308) and a database containing sequences of common contaminants (derived from Maxquant v.1.6.0.1). Trypsin/p was set as enzyme specificity, allowing a maximum of two missed cleavages. The minimum peptide length was set to 7 amino acids. Carbamidomethylation on cysteine was set as fixed modification. Protein N-terminal acetylation, oxidation of methionine, and TMT on lysines and peptide n-termini were allowed as variable modifications. Mass tolerances for MS1 and MS2 were set to 10 ppm and 0.02 Da, respectively. Peptide-spectrum-matches (PSMs) were filtered to a 1% FDR level using Percolator employing a target/decoy approach. Only rank 1 peptides were allowed. TMT reporter ion intensities were quantified within 20 ppm windows and quan value correction was used to correct for reagent isotope impurities. Only unique peptides were used for protein quantification. PSM with a co-isolation value of >50% were rejected. Further data processing was carried out in R and Perseus (v. 1.6.2.3). Only proteins identified with at least two peptides were included in the analysis. All contaminant proteins and proteins that have not been quantified in all 18 samples were filtered out. A three step normalization procedure was applied. First, the sum of the reporter ion intensities for each TMT channel was normalized to the average grand total to correct for mixing errors. Next, the common internal standard in each TMT 11plex set was used for internal reference scaling [113] in order to correct for batch effects. Afterwards the data was normalized applying trimmed mean of M values (TMM) using the edgeR package. Statistical analysis was performed using two-sample t-tests and multiple sample ANOVA tests. Resulting p-values were corrected for multiple testing using a permutation-based FDR approach or by the method of Benjamini-Hochberg. The mass spectrometry proteomics data have been deposited to the ProteomeXchange Consortium via the PRIDE [114] partner repository with the dataset identifier PXD015416.

Gene set enrichment analysis

A gene set enrichment analysis (GSEA) of the significantly regulated genes or proteins was carried out on the Category (SW1 to SW4) and regulon datasets provided by SubtiWiki (http://subtiwiki.uni-goettingen.de/v3/category/) [115]. The GNU R software v. 3.5.1 [116] and the

clusterProfiler library v. 3.10.1 [117] was used. P values were adjusted according to the Benjamini-Hochberg (BH) method and $P_{adjust} \leq 0.05$ was set as significance threshold.

Supporting information

S1 Fig. Alarmone and GTP levels during stress and starvation. (A) Means and SEM of GTP after the application of different stress conditions. Sample sizes and treatments are the same as in Fig 1A and 1B. NV: DL-norvaline, SHX: serine hydroxamate. Asterisks (*) indicate significance ($p_{adj.} \leq 0.05$) of combined pGpp, ppGpp and pppGpp levels according to the Kruskal-Wallis and Dunn-Bonferroni test. (B) Levels of GTP during thermotolerance development. Wild type cells were grown at 37 ˚C and shifted to 48 ˚C for 15 min (pre-shock), then to 53 ˚C or directly to 53 ˚C. Samples were taken at 2, 5 and 15 min. Means and SEM of four independent experiments are shown. All changes are not significant ($p \leq 0.05$) according to the Kruskal-Wallis test. (C) Means and SEM of GTP levels in wild type cells or strains with mutations in (p)ppGpp synthetases (*relP/Q*$^{-}$: BHS204, *rel*^{E324V} (inactive synthetase): BHS709; (p)ppGpp˚: BHS214) treated with heat stress (2 min 50 ˚C) or left untreated at 37 ˚C. Sample sizes are the same as in Fig 1E. Asterisks indicate significant changes ($p \leq 0.05$) according to Welch's *t*-test. (D) Relative changes in the transcription of *hpf* during heat shock in the same strains (15 min 50 ˚C). Means and SEM of three independent experiments are shown. Asterisks (*) indicate significant changes ($p_{adj.} \leq 0.05$) according to the Kruskal-Wallis and Dunn-Bonferroni test. (E) The influence of chloramphenicol on GTP levels during stress. Sample sizes and treatments are the same as in Fig 1F. Asterisks indicate significant changes ($p \leq 0.05$) according to Welch's *t*-test.
(TIFF)

S2 Fig. Phenotype of single deletions of (p)ppGpp synthetase genes. (A) Cellular GTP levels in wild type or Δ*rel*: (BHS126) strains. **(B)** Growth of strains with mutations or deletions in (p)ppGpp metabolizing enzymes in rich LB medium. Δ*rel*: BHS126, (p)ppGpp˚: BHS214. **(C/D)** Survival of wild type (black lines) and mutant strains (Δ*relQ*: BHS127 or Δ*relP*: BHS128) red lines at 53 ˚C with (48/53 ˚C) or without (37/53 ˚C) pre-shock. Means and SEM of at least three independent experiments are shown. Open symbols: no pre-shock, closed symbols: 15 min pre-shock at 48 ˚C. **(E)** Growth of wild type, (p)ppGpp˚ cells (BHS214) or strains with deletions in *relQ* (BHS127) or *relP* (BHS128) on agar plates at 37 ˚C, during heat stress (55 ˚C) or oxidative stress (0.2 mM diamide).
(TIFF)

S3 Fig. Thermotolerance and survival of strains expressing *rel* variants *in trans*. (A) Levels of alarmones in strains expressing hyperactive or inactive variants of *B.s. rel* (E324V: inactive synthetase, E77A/D78A: inactive hydrolase) or *E.c. relA*. Cells were treated with 1 mM IPTG for 15 min. Asterisks indicate significant changes ($p \leq 0.05$) of combined alarmone levels according to Welch's *t*-test. **(B-E)** Survival of wild type (black lines) and mutant strains (red lines) at 53 ˚C without pre-shock (37/53 ˚C; open symbols) or with pre-shock (15 min 48 ˚C/53 ˚C; closed symbols). Means and SEM of at least three independent experiments are shown. Strains were supplemented with 1 mM IPTG 15 min prior to 48 ˚C temperature shift. **(B)** Expression of a truncated, hyperactive *E. coli relA* variant (designated $relA_{hyper}$). **(C)** Expression of *B.s. rel* with inactive hydrolase domain (E77A D78A) in the (p)ppGpp˚ strain. **(D)** Expression of a truncated, inactive *E. coli relA* variant ($relA_{inactive}$). (E) Expression of *B.s. rel* with inactive synthetase domain (E324V) in the (p)ppGpp˚ strain.
(TIFF)

S4 Fig. Thermotolerance and survival of strains expressing treated with decoyinine. Thermotolerance development and survival of wild type cells treated with decoyinine (red lines) or left untreated (black lines).
Means and SEM of at least three independent experiments are shown. Strains were supplemented with 50, 250, 400 or 1000 μg ml^{-1} decoyinine 15 min before heat treatment. Open symbols: no pre-shock, closed symbols: 15 min pre-shock at 48 ˚C. n.d.: not determined, no cfu could be detected from 100 μl cell culture.
(TIFF)

S5 Fig. Transcriptional changes mediated by changed (p)ppGpp levels or heat stress. (A) Comparison of the relative transcription changes of selected genes in, Δrel and (p)ppGpp0 strains during exponential growth at 37 ˚C as determined by RNA-seq or RT-qPCR from independent experiments. Means and SEM of three replicates are shown. **(B)** Heatmap showing the expression changes of selected transcripts in wild type, (p)ppGpp˚ or Δ*rel* strains. Values represent normalized log_2 scaled read counts centered on the mean expression level of each transcript. **(C/D)** The distributions of all up- and down-regulated genes in wild type cells (BHS220) heat shocked at 48 ˚C or 53 ˚C versus unstressed cells are shown. Bar tracks indicate the distribution of the respective functional groups.
(TIFF)

S6 Fig. Up- or down-regulation of regulons or gene categories. Points in the scatterplot represent log2-transformed up- or down-regulation of individual genes of the respective regulons relative to wild type cells at 37 ˚C. Blue/gray color indicates transcriptional changes above/below the significance threshold (see Materials and Methods). Horizontal bars represent the median expression changes of the whole gene set.
(TIFF)

S7 Fig. (p)ppGpp mediated transcriptional changes during heat stress. (A) Relative changes in the transcription of selected genes known to controlled by the stringent response during heat shock in wild type and (p)ppGpp˚ strains determined by RT-qPCR. Means and SEM of three replicates are shown. Asterisks indicate significance ($p \leq 0.05$) according to Welch's t-test. **(B/C)** Heatmap showing expression changes of selected transcripts during mild heat stress in wild type, (p)ppGpp˚ or Δ*rel* cells. Values represent log_2 fold changes of transcript levels relative to wild type cells at 37 ˚C. **(D)** Relative changes in the transcription of selected stress response genes during heat shock in wild type and (p)ppGpp˚ strains determined by RT-qPCR. Means and SEM of three replicates are shown. Asterisks indicate significance ($p \leq 0.05$) according to Welch's t-test.
(TIFF)

S8 Fig. Phenotypes of (p)ppGpp˚, Δ*spx* and (p)ppGpp˚ Δ*spx* strains. (A) RT-qPCR experiment showing the relative transcription of *rplC* and *rplO* in wild type (BHS220), Δ*spx* (BHS222), (p)ppGpp˚ (BHS319) or (p)ppGpp˚ Δ*spx* (BHS766) cells treated with or heat stress at 50 ˚C for 15 min. Means and SEM of three replicates are shown. Asterisks indicate significant changes ($p \leq 0.05$) of transcript levels according to Welch's *t*-test. **(B)** Growth of wild type, Δ*spx*, (p)ppGpp˚ or (p)ppGpp˚ Δ*spx* cells in LB medium at 37 ˚C (left) as well as growth of wild type, (p)ppGpp˚, *cxs*-1, *cxs*-2, (p)ppGpp˚ cxs-1 or (p)ppGpp˚ cxs-2 cells in LB medium at 50 ˚C (right). **(C)** The fraction of aggregated proteins (left) or soluble proteins (right) in wild type, Δ*spx* (BHS014), (p)ppGpp˚ (BHS214) or (p)ppGpp˚ Δ*spx* (BHS766) cells treated with or heat stress at 50 ˚C for 15 min.
(TIF)

S9 Fig. (p)ppGpp and Spx act independently. (A) Northern and western blot of wild type, Δ*spx* (BHS014) or (p)ppGpp° (BHS214) strains treated with or without DL-norvaline. Cells were grown in minimal medium supplemented with 0.5% casamino acids to OD_{600} 0.4. The medium was removed by centrifugation and the cells were resuspended in fresh medium with casamino acids (—) or 0.5 mg/ml DL-norvaline (+) and grown for 30 min. **(B)** Relative transcription of *rrnJp1-lacZ* with or without expression of spx^{DD} with 1 mM IPTG for 30 min in the wild type or (p)ppGpp° background as determined by RT-qPCR. Means and SEM of three replicates are shown. Asterisks indicate significant changes ($p \leq 0.05$) of transcript levels according to Welch's *t*-test. **(C)** *In vitro* transcription experiments with selected promoters in the presence or absence of Spx or ppGpp under reducing (+ DTT) or oxidizing (- DTT) conditions. Means and SEM of three replicates and a representative autoradiogram are shown.
(TIFF)

S10 Fig. Puromyin labels nascent proteins and does not disturb protein homeostasis at low concentration. (A) Accumulation of subcellular protein aggregates (fluorescent spots) after the addition of puromycin visualized by YocM-mCherry. BIH369 cells were grown in LB + 0.5% xylose and treated with 1, 10 or 25 μg ml^{-1} puromycin or left untreated for 15 min. Phase contrast images (P.C.) and fluorescence images with RFP-filters (YocM-mCherry) are shown. **(B)** The effect of puromycin on growth. Wild type cells were grown in LB to the mid-exponential phase (OD_{600} 0.4) and supplemented with puromycin at the indicated concentrations. **(C)** Dot blot or western blot of puromycin-labeled proteins. Exponentially growing cells grown in LB were treated with the indicated concentrations of puromycin for 15 min. **(D)** Outline of the genotypes of the RIK1066 strain, carrying an inducible copy of *relP* in the (p)ppGpp° background. **(E)** Relative puromycin incorporation in RIK1066 cells treated with or without 1 mM IPTG. Cells were incubated with 1 mg ml^{-1} puromycin for 15 min added directly to the medium after the addition of IPTG (0–15 min) or after 15 min (15–30 min), then harvested. One representative experiment and means and SEM from the quantification of three independent experiments are shown. Asterisks indicate significance ($p \leq 0.05$) according to Welch's *t*-test.
(TIFF)

S11 Fig. Growth and thermotolerance development of Δ*rplK* cells. (A) Growth of wild type and Δ*rplK* (BHS859) cells. **(B)** Relative translation rates of wild type and Δ*rplK* (BHS859) cells at 37 ˚C. **(C)** Thermotolerance development and thermoresistance of Δ*rplK* (BHS859) cells. Means and standard error of three biological replicates are shown.
(TIFF)

S12 Fig. The influence of (p)ppGpp on individual protein levels upon heat treatment. Levels of individual proteins in wild type and mutant strains with or without heat treatment (50 ˚C for 5 min or 15 min at 50 ˚C) relative to unstressed wild type cells. Means and standard error of three biological replicates are shown.
(TIFF)

S13 Fig. Global changes in the proteome mediated by heat shock or (p)ppGpp. The distributions of all up- and down-regulated in wild type or mutant cells with or without heat treatment (15 min 50 ˚C). Bar tracks indicate the distribution of the respective functional groups.
(TIFF)

S14 Fig. The role of (p)ppGpp and Hpf on ribosome integrity and 100S formation. (A) Relative translation (puromycin incorporation) of wild type, (p)ppGpp° (BHS214) and Δ*rel* (BHS126) strains during heat stress at 53 ˚C. 1 μg ml^{-1} puromycin was added for 15 min to the

medium directly after (sample "0–15 min") or 15 min (sample "15–30 min") after the temperature upshift. Means and SEM of three independent experiments are shown. Asterisks indicate significance ($p \leq 0.05$) according to Welch's *t*-test. **(B)** Western blot showing Hpf levels during thermotolerance development in wild type, (p)ppGpp° (BHS214) or Δ*rel* (BHS126) strains. Cells were heat shocked for 15 min each at the indicated temperature(s). **(C)** Sucrose gradient profiles of extracts from untreated (37 °C) or thermotolerant (48/53 °C for 15 min each) Δ*hpf* (BHS008) or Δ*rel* (BHS126) cells. The dashed blue line of untreated wild type cells is shown for reference. **(D)** Methylene blue stained membranes showing the integrity or degradation of rRNA. Wild type, (p)ppGpp° (BHS214) Δ*hpf* (BHS008) or (p)ppGpp° P_{spac}-*hpf* (BHS626) cells were treated with or without heat shock at 53 °C for 15 min. 1 mM IPTG was added to the strains to induce the expression of *hpf* 15 min prior to heat shock. 2 μg total RNA was separated on denaturing agarose gels and blotted on nylon membranes. **(E)** Wild type, (p)ppGpp° (BHS214) (p)ppGpp° P_{spac}-*rel* (BHS622) or (p)ppGpp° P_{spac}-*hpf* (BHS626) were spotted on agar plates supplemented with 1 mM IPTG and incubated over night at 37 °C or 55 °C. **(F)** rRNA degradation after severe heat stress (53 °C) in wild type or (p)ppGpp° (BHS214) cells left untreated or treated with 5 μg ml^{-1} chloramphenicol or 100 μg ml^{-1} spectinomycin 15 min prior to the application of stress. 2 μg total RNA was separated on denaturing agarose gels and blotted on nylon membranes.
(TIFF)

S1 Table. List of strains, plasmids and oligonucleotides. This table lists all *B. subtilis* strains, plasmids and oligonucleotides used in this study.
(DOCX)

S1 Dataset. List of identified transcription start sites. In this dataset, all identified transcriptional start sites and their classification is shown.
(XLSX)

S2 Dataset. Results of the gene set enrichment analysis. This dataset lists all enriched functional categories and regulons for each condition in separate sheets.
(XLSX)

S3 Dataset. List of differentially expressed genes. Global gene expression changes for all conditions are listed in separate sheets.
(XLSX)

S4 Dataset. List of differentially regulated proteins. Changes in the cellular levels of individual proteins in the examined strains and heat shock conditions.
(XLSX)

S5 Dataset. Enrichment analysis for differentially expressed proteins. This dataset lists all enriched functional categories and regulons for all differentially expressed proteins of S4 Dataset.
(XLSX)

Acknowledgments

We thank Dr. Laurent Jannière (French National Centre for Scientific Research, Paris, France) and the National BioResource Project (National Institute of Genetics, Japan) for providing strains and plasmids.

Author Contributions

Conceptualization: Heinrich Schäfer, Bertrand Beckert, Christian K. Frese, Wieland Steinchen, Aaron M. Nuss, Ingo Hantke, Kristina Driller, Petra Dersch, Gert Bange, Daniel N. Wilson, Kürşad Turgay.

Data curation: Heinrich Schäfer, Bertrand Beckert, Christian K. Frese, Aaron M. Nuss, Michael Beckstette, Petra Sudzinová, Volkhard Kaever.

Formal analysis: Heinrich Schäfer, Bertrand Beckert, Christian K. Frese, Michael Beckstette, Volkhard Kaever, Kürşad Turgay.

Funding acquisition: Libor Krásný, Volkhard Kaever, Petra Dersch, Gert Bange, Daniel N. Wilson, Kürşad Turgay.

Investigation: Heinrich Schäfer, Bertrand Beckert, Christian K. Frese, Wieland Steinchen, Aaron M. Nuss, Michael Beckstette, Ingo Hantke, Kristina Driller, Petra Sudzinová, Volkhard Kaever, Petra Dersch, Gert Bange, Daniel N. Wilson, Kürşad Turgay.

Methodology: Bertrand Beckert, Christian K. Frese, Volkhard Kaever, Petra Dersch.

Project administration: Libor Krásný, Volkhard Kaever, Petra Dersch, Gert Bange, Daniel N. Wilson, Kürşad Turgay.

Resources: Wieland Steinchen.

Software: Michael Beckstette.

Supervision: Libor Krásný, Volkhard Kaever, Petra Dersch, Gert Bange, Daniel N. Wilson, Kürşad Turgay.

Validation: Heinrich Schäfer, Christian K. Frese, Michael Beckstette, Petra Sudzinová, Volkhard Kaever, Petra Dersch, Daniel N. Wilson.

Visualization: Heinrich Schäfer, Bertrand Beckert, Christian K. Frese, Ingo Hantke, Kristina Driller.

Writing – original draft: Heinrich Schäfer, Daniel N. Wilson, Kürşad Turgay.

Writing – review & editing: Bertrand Beckert, Christian K. Frese, Wieland Steinchen, Kristina Driller, Petra Sudzinová, Libor Krásný, Petra Dersch, Gert Bange.

References

1. Storz G, Hengge R, American Society for Microbiology, editors. Bacterial stress responses. 2nd ed. Washington, DC: ASM Press; 2011.
2. Mogk A, Huber D, Bukau B. Integrating protein homeostasis strategies in prokaryotes. Cold Spring Harb Perspect Biol. 2011; 3. https://doi.org/10.1101/cshperspect.a004366 PMID: 21441580
3. Hartl FU, Bracher A, Hayer-Hartl M. Molecular chaperones in protein folding and proteostasis. Nature. 2011; 475: 324–332. https://doi.org/10.1038/nature10317 PMID: 21776078
4. Lindquist S. The Heat-Shock Response. Annual Review of Biochemistry. 1986; 55: 1151–1191. https://doi.org/10.1146/annurev.bi.55.070186.005443 PMID: 2427013
5. Lim B, Gross CA. Cellular Response to Heat Shock and Cold Shock. In: Storz G, Hengge R, editors. Bacterial stress responses 2nd edition. Washington, DC: ASM press, American Society for Microbiology; 2010. pp. 93–114.
6. Helmann JD, Wu MF, Kobel PA, Gamo FJ, Wilson M, Morshedi MM, et al. Global transcriptional response of Bacillus subtilis to heat shock. J Bacteriol. 2001; 183: 7318–7328. https://doi.org/10.1128/JB.183.24.7318-7328.2001 PMID: 11717291
7. Winkler J, Seybert A, Konig L, Pruggnaller S, Haselmann U, Sourjik V, et al. Quantitative and spatio-temporal features of protein aggregation in Escherichia coli and consequences on protein quality

control and cellular ageing. EMBO J. 2010; 29: 910–23. https://doi.org/10.1038/emboj.2009.412 PMID: 20094032

8. Völker U, Mach H, Schmid R, Hecker M. Stress proteins and cross-protection by heat shock and salt stress in Bacillus subtilis. J Gen Microbiol. 1992; 138: 2125–2135. https://doi.org/10.1099/00221287-138-10-2125 PMID: 1362210

9. Runde S, Molière N, Heinz A, Maisonneuve E, Janczikowski A, Elsholz AKW, et al. The role of thiol oxidative stress response in heat-induced protein aggregate formation during thermotolerance in *B acillus subtilis*: Thiol oxidation in protein aggregate formation. Molecular Microbiology. 2014; 91: 1036–1052.

10. Hecker M, Schumann W, Völker U. Heat-shock and general stress response in *Bacillus subtilis*. Molecular microbiology. 1996; 19: 417–428. https://doi.org/10.1046/j.1365-2958.1996.396932.x PMID: 8830234

11. Mogk A, Homuth G, Scholz C, Kim L, Schmid FX, Schumann W. The GroE chaperonin machine is a major modulator of the CIRCE heat shock regulon of *Bacillus subtilis*. EMBO J. 1997; 16: 4579–4590. https://doi.org/10.1093/emboj/16.15.4579 PMID: 9303302

12. Krüger E, Hecker M. The first gene of the *Bacillus subtilis* clpC operon, ctsR, encodes a negative regulator of its own operon and other class III heat shock genes. J Bacteriol. 1998; 180: 6681–6688. PMID: 9852015

13. Elsholz AKW, Michalik S, Zühlke D, Hecker M, Gerth U. CtsR, the Gram-positive master regulator of protein quality control, feels the heat. The EMBO Journal. 2010; 29: 3621–3629. https://doi.org/10.1038/emboj.2010.228 PMID: 20852588

14. Hecker M, Pané-Farré J, Völker U. SigB-Dependent General Stress Response in *Bacillus subtilis* and Related Gram-Positive Bacteria. Annual Review of Microbiology. 2007; 61: 215–236. https://doi.org/10.1146/annurev.micro.61.080706.093445 PMID: 18035607

15. Nakano S, Küster-Schöck E, Grossman AD, Zuber P. Spx-dependent global transcriptional control is induced by thiol-specific oxidative stress in *Bacillus subtilis*. Proc Natl Acad Sci USA. 2003; 100: 13603–13608. https://doi.org/10.1073/pnas.2235180100 PMID: 14597697

16. Rochat T, Nicolas P, Delumeau O, Rabatinová A, Korelusová J, Leduc A, et al. Genome-wide identification of genes directly regulated by the pleiotropic transcription factor Spx in *Bacillus subtilis*. Nucleic Acids Res. 2012; 40: 9571–9583. https://doi.org/10.1093/nar/gks755 PMID: 22904090

17. Schäfer H, Heinz A, Sudzinová P, Voß M, Hantke I, Krásný L, et al. Spx, the central regulator of the heat and oxidative stress response in *B. subtilis*, can repress transcription of translation-related genes. Mol Microbiol. 2019; 111: 514–533. https://doi.org/10.1111/mmi.14171 PMID: 30480837

18. Leichert LIO, Scharf C, Hecker M. Global characterization of disulfide stress in *Bacillus subtilis*. J Bacteriol. 2003; 185: 1967–1975. https://doi.org/10.1128/JB.185.6.1967-1975.2003 PMID: 12618461

19. Potrykus K, Cashel M. (p)ppGpp: still magical? Annu Rev Microbiol. 2008; 62: 35–51. https://doi.org/10.1146/annurev.micro.62.081307.162903 PMID: 18454629

20. Hauryliuk V, Atkinson GC, Murakami KS, Tenson T, Gerdes K. Recent functional insights into the role of (p)ppGpp in bacterial physiology. Nat Rev Microbiol. 2015; 13: 298–309. https://doi.org/10.1038/nrmicro3448 PMID: 25853779

21. Haseltine WA, Block R. Synthesis of guanosine tetra- and pentaphosphate requires the presence of a codon-specific, uncharged transfer ribonucleic acid in the acceptor site of ribosomes. Proc Natl Acad Sci USA. 1973; 70: 1564–1568. https://doi.org/10.1073/pnas.70.5.1564 PMID: 4576025

22. Wendrich TM, Blaha G, Wilson DN, Marahiel MA, Nierhaus KH. Dissection of the Mechanism for the Stringent Factor RelA. Molecular Cell. 2002; 10: 779–788. https://doi.org/10.1016/s1097-2765(02)00656-1 PMID: 12419222

23. Arenz S, Abdelshahid M, Sohmen D, Payoe R, Starosta AL, Berninghausen O, et al. The stringent factor RelA adopts an open conformation on the ribosome to stimulate ppGpp synthesis. Nucleic Acids Res. 2016; 44: 6471–6481. https://doi.org/10.1093/nar/gkw470 PMID: 27226493

24. Brown A, Fernández IS, Gordiyenko Y, Ramakrishnan V. Ribosome-dependent activation of stringent control. Nature. 2016; 534: 277–280. https://doi.org/10.1038/nature17675 PMID: 27279228

25. Loveland AB, Bah E, Madireddy R, Zhang Y, Brilot AF, Grigorieff N, et al. Ribosome•RelA structures reveal the mechanism of stringent response activation. Elife. 2016; 5. https://doi.org/10.7554/eLife.17029 PMID: 27434674

26. Atkinson GC, Tenson T, Hauryliuk V. The RelA/SpoT Homolog (RSH) Superfamily: Distribution and Functional Evolution of ppGpp Synthetases and Hydrolases across the Tree of Life. Stiller JW, editor. PLoS ONE. 2011; 6: e23479. https://doi.org/10.1371/journal.pone.0023479 PMID: 21858139

27. Wendrich TM, Marahiel MA. Cloning and characterization of a relA/spoT homologue from *Bacillus subtilis*. Mol Microbiol. 1997; 26: 65–79. https://doi.org/10.1046/j.1365-2958.1997.5511919.x PMID: 9383190

28. Nanamiya H, Kasai K, Nozawa A, Yun C-S, Narisawa T, Murakami K, et al. Identification and functional analysis of novel (p)ppGpp synthetase genes in *Bacillus subtilis*. Mol Microbiol. 2008; 67: 291–304. https://doi.org/10.1111/j.1365-2958.2007.06018.x PMID: 18067544

29. Srivatsan A, Han Y, Peng J, Tehranchi AK, Gibbs R, Wang JD, et al. High-precision, whole-genome sequencing of laboratory strains facilitates genetic studies. PLoS Genet. 2008; 4: e1000139. https://doi.org/10.1371/journal.pgen.1000139 PMID: 18670626

30. Boutte CC, Crosson S. Bacterial lifestyle shapes stringent response activation. Trends Microbiol. 2013; 21: 174–180. https://doi.org/10.1016/j.tim.2013.01.002 PMID: 23419217

31. Irving SE, Corrigan RM. Triggering the stringent response: signals responsible for activating (p)ppGpp synthesis in bacteria. Microbiology. 2018; 164: 268–276. https://doi.org/10.1099/mic.0.000621 PMID: 29493495

32. Lopez JM, Dromerick A, Freese E. Response of guanosine 5'-triphosphate concentration to nutritional changes and its significance for *Bacillus subtilis* sporulation. J Bacteriol. 1981; 146: 605–613. PMID: 6111556

33. Kriel A, Bittner AN, Kim SH, Liu K, Tehranchi AK, Zou WY, et al. Direct regulation of GTP homeostasis by (p)ppGpp: a critical component of viability and stress resistance. Mol Cell. 2012; 48: 231–241. https://doi.org/10.1016/j.molcel.2012.08.009 PMID: 22981860

34. Krásný L, Gourse RL. An alternative strategy for bacterial ribosome synthesis: *Bacillus subtilis* rRNA transcription regulation. EMBO J. 2004; 23: 4473–4483. https://doi.org/10.1038/sj.emboj.7600423 PMID: 15496987

35. Krásný L, Tišerová H, Jonák J, Rejman D, Šanderová H. The identity of the transcription +1 position is crucial for changes in gene expression in response to amino acid starvation in *Bacillus subtilis*. Molecular Microbiology. 2008; 69: 42–54. https://doi.org/10.1111/j.1365-2958.2008.06256.x PMID: 18433449

36. Geiger T, Wolz C. Intersection of the stringent response and the CodY regulon in low GC Gram-positive bacteria. Int J Med Microbiol. 2014; 304: 150–155. https://doi.org/10.1016/j.ijmm.2013.11.013 PMID: 24462007

37. Ratnayake-Lecamwasam M, Serror P, Wong KW, Sonenshein AL. *Bacillus subtilis* CodY represses early-stationary-phase genes by sensing GTP levels. Genes Dev. 2001; 15: 1093–1103. https://doi.org/10.1101/gad.874201 PMID: 11331605

38. Milon P, Tischenko E, Tomsic J, Caserta E, Folkers G, La Teana A, et al. The nucleotide-binding site of bacterial translation initiation factor 2 (IF2) as a metabolic sensor. Proc Natl Acad Sci USA. 2006; 103: 13962–13967. https://doi.org/10.1073/pnas.0606384103 PMID: 16968770

39. Corrigan RM, Bellows LE, Wood A, Gründling A. ppGpp negatively impacts ribosome assembly affecting growth and antimicrobial tolerance in Gram-positive bacteria. Proc Natl Acad Sci USA. 2016; 113: E1710–1719. https://doi.org/10.1073/pnas.1522179113 PMID: 26951678

40. Steinchen W, Bange G. The magic dance of the alarmones (p)ppGpp: The structural biology of the alarmones (p)ppGpp. Molecular Microbiology. 2016; 101: 531–544.

41. Vinogradova DS, Zegarra V, Maksimova E, Nakamoto JA, Kasatsky P, Paleskava A, et al. How the initiating ribosome copes with ppGpp to translate mRNAs. PLoS Biol. 2020; 18: e3000593. https://doi.org/10.1371/journal.pbio.3000593 PMID: 31995552

42. Kanjee U, Ogata K, Houry WA. Direct binding targets of the stringent response alarmone (p)ppGpp: Protein targets of ppGpp. Molecular Microbiology. 2012; 85: 1029–1043. https://doi.org/10.1111/j.1365-2958.2012.08177.x PMID: 22812515

43. Zhang Y, Zborníková E, Rejman D, Gerdes K. Novel (p)ppGpp Binding and Metabolizing Proteins of *Escherichia coli*. MBio. 2018; 9. https://doi.org/10.1128/mBio.02188-17 PMID: 29511080

44. Wang B, Dai P, Ding D, Del Rosario A, Grant RA, Pentelute BL, et al. Affinity-based capture and identification of protein effectors of the growth regulator ppGpp. Nat Chem Biol. 2019; 15: 141–150. https://doi.org/10.1038/s41589-018-0183-4 PMID: 30559427

45. Bokinsky G, Baidoo EEK, Akella S, Burd H, Weaver D, Alonso-Gutierrez J, et al. HipA-triggered growth arrest and β-lactam tolerance in Escherichia coli are mediated by RelA-dependent ppGpp synthesis. J Bacteriol. 2013; 195: 3173–3182. https://doi.org/10.1128/JB.02210-12 PMID: 23667235

46. Dalebroux ZD, Swanson MS. ppGpp: magic beyond RNA polymerase. Nat Rev Microbiol. 2012; 10: 203–212. https://doi.org/10.1038/nrmicro2720 PMID: 22337166

47. Mostertz J, Scharf C, Hecker M, Homuth G. Transcriptome and proteome analysis of *Bacillus subtilis* gene expression in response to superoxide and peroxide stress. Microbiology (Reading, Engl). 2004; 150: 497–512.

48. Hantke I, Schäfer H, Janczikowski A, Turgay K. YocM a small heat shock protein can protect *Bacillus subtilis* cells during salt stress. Mol Microbiol. 2019; 111: 423–440. https://doi.org/10.1111/mmi.14164 PMID: 30431188

49. Gaca AO, Kudrin P, Colomer-Winter C, Beljantseva J, Liu K, Anderson B, et al. From (p)ppGpp to (pp)pGpp: Characterization of Regulatory Effects of pGpp Synthesized by the Small Alarmone Synthetase of *Enterococcus faecalis*. J Bacteriol. 2015; 197: 2908–2919. https://doi.org/10.1128/JB.00324-15 PMID: 26124242

50. Hecker M, Völker U, Heim C. RelA-independent (p)ppGpp accumulation and heat shock protein induction after salt stress in *Bacillus subtilis*. FEMS Microbiology Letters. 1989; 58: 125–128. https://doi.org/10.1111/j.1574-6968.1989.tb03031.x

51. Pöther D-C, Liebeke M, Hochgräfe F, Antelmann H, Becher D, Lalk M, et al. Diamide triggers mainly S Thiolations in the cytoplasmic proteomes of *Bacillus subtilis* and *Staphylococcus aureus*. J Bacteriol. 2009; 191: 7520–7530. https://doi.org/10.1128/JB.00937-09 PMID: 19837798

52. Drzewiecki K, Eymann C, Mittenhuber G, Hecker M. The yvyD gene of *Bacillus subtilis* is under dual control of sigmaB and sigmaH. J Bacteriol. 1998; 180: 6674–6680. PMID: 9852014

53. Tagami K, Nanamiya H, Kazo Y, Maehashi M, Suzuki S, Namba E, et al. Expression of a small (p)ppGpp synthetase, YwaC, in the (p)ppGpp(0) mutant of *Bacillus subtilis* triggers YvyD-dependent dimerization of ribosome. Microbiologyopen. 2012; 1: 115–134. https://doi.org/10.1002/mbo3.16 PMID: 22950019

54. Cashel M. The Control of Ribonucleic Acid Synthesis in Escherichia coli : IV. RELEVANCE OF UNUSUAL PHOSPHORYLATED COMPOUNDS FROM AMINO ACID-STARVED STRINGENT STRAINS. Journal of Biological Chemistry. 1969; 244: 3133–3141. PMID: 4893338

55. Schreiber G, Metzger S, Aizenman E, Roza S, Cashel M, Glaser G. Overexpression of the relA gene in *Escherichia coli*. J Biol Chem. 1991; 266: 3760–3767. PMID: 1899866

56. Nouri H, Monnier A-F, Fossum-Raunehaug S, Maciag-Dorszynska M, Cabin-Flaman A, Képès F, et al. Multiple links connect central carbon metabolism to DNA replication initiation and elongation in *Bacillus subtilis*. DNA Res. 2018. https://doi.org/10.1093/dnares/dsy031 PMID: 30256918

57. Lopez JM, Marks CL, Freese E. The decrease of guanine nucleotides initiates sporulation of *Bacillus subtilis*. Biochim Biophys Acta. 1979; 587: 238–252. https://doi.org/10.1016/0304-4165(79)90357-x PMID: 114234

58. Tojo S, Satomura T, Kumamoto K, Hirooka K, Fujita Y. Molecular Mechanisms Underlying the Positive Stringent Response of the *Bacillus subtilis* ilv-leu Operon, Involved in the Biosynthesis of Branched-Chain Amino Acids. J Bacteriol. 2008; 190: 6134–6147. https://doi.org/10.1128/JB.00606-08 PMID: 18641142

59. Tojo S, Kumamoto K, Hirooka K, Fujita Y. Heavy involvement of stringent transcription control depending on the adenine or guanine species of the transcription initiation site in glucose and pyruvate metabolism in *Bacillus subtilis*. J Bacteriol. 2010; 192: 1573–1585. https://doi.org/10.1128/JB.01394-09 PMID: 20081037

60. Kriel A, Brinsmade SR, Tse JL, Tehranchi AK, Bittner AN, Sonenshein AL, et al. GTP Dysregulation in *Bacillus subtilis* Cells Lacking (p)ppGpp Results in Phenotypic Amino Acid Auxotrophy and Failure To Adapt to Nutrient Downshift and Regulate Biosynthesis Genes. Journal of Bacteriology. 2014; 196: 189–201. https://doi.org/10.1128/JB.00918-13 PMID: 24163341

61. Eymann C, Homuth G, Scharf C, Hecker M. *Bacillus subtilis* functional genomics: global characterization of the stringent response by proteome and transcriptome analysis. J Bacteriol. 2002; 184: 2500–2520. https://doi.org/10.1128/JB.184.9.2500-2520.2002 PMID: 11948165

62. Zhang S, Haldenwang WG. RelA is a component of the nutritional stress activation pathway of the *Bacillus subtilis* transcription factor sigma B. J Bacteriol. 2003; 185: 5714–5721. https://doi.org/10.1128/JB.185.19.5714-5721.2003 PMID: 13129942

63. Zhang S, Haldenwang WG. Contributions of ATP, GTP, and redox state to nutritional stress activation of the *Bacillus subtilis* sigmaB transcription factor. J Bacteriol. 2005; 187: 7554–7560. https://doi.org/10.1128/JB.187.22.7554-7560.2005 PMID: 16267279

64. Molière N, Hoßmann J, Schäfer H, Turgay K. Role of Hsp100/Clp Protease Complexes in Controlling the Regulation of Motility in *Bacillus subtilis*. Front Microbiol. 2016; 7: 315. https://doi.org/10.3389/fmicb.2016.00315 PMID: 27014237

65. Paget MSB, Molle V, Cohen G, Aharonowitz Y, Buttner MJ. Defining the disulphide stress response in Streptomyces coelicolor A3(2): identification of the sigmaR regulon. Molecular Microbiology. 2001; 42: 1007–1020. https://doi.org/10.1046/j.1365-2958.2001.02675.x PMID: 11737643

66. Gaca AO, Abranches J, Kajfasz JK, Lemos JA. Global transcriptional analysis of the stringent response in *Enterococcus faecalis*. Microbiology (Reading, Engl). 2012; 158: 1994–2004.

67. Schmidt EK, Clavarino G, Ceppi M, Pierre P. SUnSET, a nonradioactive method to monitor protein synthesis. Nat Methods. 2009; 6: 275–277. https://doi.org/10.1038/nmeth.1314 PMID: 19305406

68. Svitil AL, Cashel M, Zyskind JW. Guanosine tetraphosphate inhibits protein synthesis *in vivo*. A possible protective mechanism for starvation stress in *Escherichia coli*. J Biol Chem. 1993; 268: 2307–2311. PMID: 8428905

69. Diez S, Ryu J, Caban K, Gonzalez RL, Dworkin J. (p)ppGpp directly regulates translation initiation during entry into quiescence. bioRxiv. 2019; 807917. https://doi.org/10.1101/807917

70. Zhang S, Scott JM, Haldenwang WG. Loss of ribosomal protein L11 blocks stress activation of the *Bacillus subtilis* transcription factor sigma(B). J Bacteriol. 2001; 183: 2316–2321. https://doi.org/10.1128/JB.183.7.2316-2321.2001 PMID: 11244072

71. Beckert B, Abdelshahid M, Schäfer H, Steinchen W, Arenz S, Berninghausen O, et al. Structure of the *Bacillus subtilis* hibernating 100S ribosome reveals the basis for 70S dimerization. EMBO J. 2017; 36: 2061–2072. https://doi.org/10.15252/embj.201696189 PMID: 28468753

72. Trinquier A, Ulmer JE, Gilet L, Figaro S, Hammann P, Kuhn L, et al. tRNA Maturation Defects Lead to Inhibition of rRNA Processing via Synthesis of pppGpp. Molecular Cell. 2019; 0. https://doi.org/10.1016/j.molcel.2019.03.030 PMID: 31003868

73. Engman J, von Wachenfeldt C. Regulated protein aggregation: a mechanism to control the activity of the ClpXP adaptor protein YjbH. Mol Microbiol. 2015; 95: 51–63. https://doi.org/10.1111/mmi.12842 PMID: 25353645

74. Fitzsimmons LF, Liu L, Kim J-S, Jones-Carson J, Vázquez-Torres A. *Salmonella* Reprograms Nucleotide Metabolism in Its Adaptation to Nitrosative Stress. Aballay A, editor. mBio. 2018; 9: e00211–18. https://doi.org/10.1128/mBio.00211-18 PMID: 29487237

75. Hyduke DR, Jarboe LR, Tran LM, Chou KJY, Liao JC. Integrated network analysis identifies nitric oxide response networks and dihydroxyacid dehydratase as a crucial target in Escherichia coli. Proceedings of the National Academy of Sciences. 2007; 104: 8484–8489. https://doi.org/10.1073/pnas.0610888104 PMID: 17494765

76. Richardson AR, Payne EC, Younger N, Karlinsey JE, Thomas VC, Becker LA, et al. Multiple Targets of Nitric Oxide in the Tricarboxylic Acid Cycle of Salmonella enterica Serovar Typhimurium. Cell Host & Microbe. 2011; 10: 33–43. https://doi.org/10.1016/j.chom.2011.06.004 PMID: 21767810

77. Gallant J, Palmer L, Pao CC. Anomalous synthesis of ppGpp in growing cells. Cell. 1977; 11: 181–185. https://doi.org/10.1016/0092-8674(77)90329-4 PMID: 326415

78. Katz A, Orellana O. Protein Synthesis and the Stress Response. In: Biyani M, editor. Cell-Free Protein Synthesis. InTech; 2012.

79. Kramer GF, Baker JC, Ames BN. Near-UV stress in Salmonella typhimurium: 4-thiouridine in tRNA, ppGpp, and ApppGpp as components of an adaptive response. J Bacteriol. 1988; 170: 2344–2351. https://doi.org/10.1128/jb.170.5.2344-2351.1988 PMID: 3283108

80. Hahn J, Tanner AW, Carabetta VJ, Cristea IM, Dubnau D. ComGA-RelA interaction and persistence in the *Bacillus subtilis* K-state. Mol Microbiol. 2015; 97: 454–471. https://doi.org/10.1111/mmi.13040 PMID: 25899641

81. Scott JM, Haldenwang WG. Obg, an essential GTP binding protein of *Bacillus subtilis*, is necessary for stress activation of transcription factor sigma(B). J Bacteriol. 1999; 181: 4653–4660. PMID: 10419966

82. Bruel N, Castanié-Cornet M-P, Cirinesi A-M, Koningstein G, Georgopoulos C, Luirink J, et al. Hsp33 controls elongation factor-Tu stability and allows *Escherichia coli* growth in the absence of the major DnaK and trigger factor chaperones. J Biol Chem. 2012; 287: 44435–44446. https://doi.org/10.1074/jbc.M112.418525 PMID: 23148222

83. Maaβ S, Wachlin G, Bernhardt J, Eymann C, Fromion V, Riedel K, et al. Highly precise quantification of protein molecules per cell during stress and starvation responses in *Bacillus subtilis*. Mol Cell Proteomics. 2014; 13: 2260–2276. https://doi.org/10.1074/mcp.M113.035741 PMID: 24878497

84. Walter P, Ron D. The unfolded protein response: from stress pathway to homeostatic regulation. Science. 2011; 334: 1081–1086. https://doi.org/10.1126/science.1209038 PMID: 22116877

85. Rallu F, Gruss A, Ehrlich SD, Maguin E. Acid- and multistress-resistant mutants of *Lactococcus lactis*: identification of intracellular stress signals. Molecular Microbiology. 2000; 35: 517–528. https://doi.org/10.1046/j.1365-2958.2000.01711.x PMID: 10672175

86. VanBogelen RA, Kelley PM, Neidhardt FC. Differential induction of heat shock, SOS, and oxidation stress regulons and accumulation of nucleotides in *Escherichia coli*. J Bacteriol. 1987; 169: 26–32. https://doi.org/10.1128/jb.169.1.26-32.1987 PMID: 3539918

87. Abranches J, Martinez AR, Kajfasz JK, Chávez V, Garsin DA, Lemos JA. The molecular alarmone (p)ppGpp mediates stress responses, vancomycin tolerance, and virulence in *Enterococcus faecalis*. J Bacteriol. 2009; 191: 2248–2256. https://doi.org/10.1128/JB.01726-08 PMID: 19168608

88. Okada Y, Makino S, Tobe T, Okada N, Yamazaki S. Cloning of rel from Listeria monocytogenes as an osmotolerance involvement gene. Appl Environ Microbiol. 2002; 68: 1541–1547. https://doi.org/10.1128/AEM.68.4.1541-1547.2002 PMID: 11916666

89. Yang X, Ishiguro EE. Temperature-Sensitive Growth and Decreased Thermotolerance Associated with relA Mutations in *Escherichia coli*. J Bacteriol. 2003; 185: 5765–5771. https://doi.org/10.1128/JB.185.19.5765-5771.2003 PMID: 13129947

90. Khakimova M, Ahlgren HG, Harrison JJ, English AM, Nguyen D. The stringent response controls catalases in Pseudomonas aeruginosa and is required for hydrogen peroxide and antibiotic tolerance. J Bacteriol. 2013; 195: 2011–2020. https://doi.org/10.1128/JB.02061-12 PMID: 23457248

91. Sambrook J, Russell DW. Molecular cloning: a laboratory manual. 3rd ed. Cold Spring Harbor, N.Y: Cold Spring Harbor Laboratory Press; 2001.

92. Spizizen J. TRANSFORMATION OF BIOCHEMICALLY DEFICIENT STRAINS OF BACILLUS SUBTILIS BY DEOXYRIBONUCLEATE. Proc Natl Acad Sci USA. 1958; 44: 1072–1078. https://doi.org/10.1073/pnas.44.10.1072 PMID: 16590310

93. Nakano MM, Zhu Y, Liu J, Reyes DY, Yoshikawa H, Zuber P. Mutations conferring amino acid residue substitutions in the carboxy-terminal domain of RNA polymerase alpha can suppress clpX and clpP with respect to developmentally regulated transcription in *Bacillus subtilis*. Mol Microbiol. 2000; 37: 869–884. https://doi.org/10.1046/j.1365-2958.2000.02052.x PMID: 10972808

94. Arnaud M, Chastanet A, Débarbouillé M. New vector for efficient allelic replacement in naturally nontransformable, low-GC-content, gram-positive bacteria. Appl Environ Microbiol. 2004; 70: 6887–6891. https://doi.org/10.1128/AEM.70.11.6887-6891.2004 PMID: 15528558

95. Stülke J, Hanschke R, Hecker M. Temporal activation of beta-glucanase synthesis in *Bacillus subtilis* is mediated by the GTP pool. J Gen Microbiol. 1993; 139: 2041–2045. https://doi.org/10.1099/00221287-139-9-2041 PMID: 8245830

96. Lamy M-C, Zouine M, Fert J, Vergassola M, Couve E, Pellegrini E, et al. CovS/CovR of group B streptococcus: a two-component global regulatory system involved in virulence: The CovS/CovR regulatory system of Streptococcus agalactiae. Molecular Microbiology. 2004; 54: 1250–1268. https://doi.org/10.1111/j.1365-2958.2004.04365.x PMID: 15554966

97. Nuss AM, Heroven AK, Waldmann B, Reinkensmeier J, Jarek M, Beckstette M, et al. Transcriptomic Profiling of Yersinia pseudotuberculosis Reveals Reprogramming of the Crp Regulon by Temperature and Uncovers Crp as a Master Regulator of Small RNAs. Sharma CM, editor. Genet PLoS. 2015; 11: e1005087. https://doi.org/10.1371/journal.pgen.1005087 PMID: 25816203

98. Langmead B, Salzberg SL. Fast gapped-read alignment with Bowtie 2. Nat Methods. 2012; 9: 357–359. https://doi.org/10.1038/nmeth.1923 PMID: 22388286

99. Li H, Handsaker B, Wysoker A, Fennell T, Ruan J, Homer N, et al. The Sequence Alignment/Map format and SAMtools. Bioinformatics. 2009; 25: 2078–2079. https://doi.org/10.1093/bioinformatics/btp352 PMID: 19505943

100. Anders S, Huber W. Differential expression analysis for sequence count data. Genome Biol. 2010; 11: R106. https://doi.org/10.1186/gb-2010-11-10-r106 PMID: 20979621

101. Edgar R, Domrachev M, Lash AE. Gene Expression Omnibus: NCBI gene expression and hybridization array data repository. Nucleic Acids Res. 2002; 30: 207–210. https://doi.org/10.1093/nar/30.1.207 PMID: 11752295

102. Dugar G, Herbig A, Förstner KU, Heidrich N, Reinhardt R, Nieselt K, et al. High-Resolution Transcriptome Maps Reveal Strain-Specific Regulatory Features of Multiple Campylobacter jejuni Isolates. Hughes D, editor. PLoS Genetics. 2013; 9: e1003495. https://doi.org/10.1371/journal.pgen.1003495 PMID: 23696746

103. Towbin H, Staehelin T, Gordon J. Electrophoretic transfer of proteins from polyacrylamide gels to nitrocellulose sheets: procedure and some applications. Proc Natl Acad Sci USA. 1979; 76: 4350–4354. https://doi.org/10.1073/pnas.76.9.4350 PMID: 388439

104. Laemmli UK. Cleavage of structural proteins during the assembly of the head of bacteriophage T4. Nature. 1970; 227: 680–685. https://doi.org/10.1038/227680a0 PMID: 5432063

105. Neuhoff V, Arold N, Taube D, Ehrhardt W. Improved staining of proteins in polyacrylamide gels including isoelectric focusing gels with clear background at nanogram sensitivity using Coomassie Brilliant Blue G-250 and R-250. Electrophoresis. 1988; 9: 255–262. https://doi.org/10.1002/elps.1150090603 PMID: 2466658

106. Yarmolinsky MB, Haba GL. INHIBITION BY PUROMYCIN OF AMINO ACID INCORPORATION INTO PROTEIN. Proc Natl Acad Sci USA. 1959; 45: 1721–1729. https://doi.org/10.1073/pnas.45.12.1721 PMID: 16590564

107. Nathans D. PUROMYCIN INHIBITION OF PROTEIN SYNTHESIS: INCORPORATION OF PUROMYCIN INTO PEPTIDE CHAINS. Proc Natl Acad Sci USA. 1964; 51: 585–592. https://doi.org/10.1073/pnas.51.4.585 PMID: 14166766

108. Krüger E, Witt E, Ohlmeier S, Hanschke R, Hecker M. The clp proteases of *Bacillus subtilis* are directly involved in degradation of misfolded proteins. J Bacteriol. 2000; 182: 3259–3265. https://doi.org/10.1128/jb.182.11.3259-3265.2000 PMID: 10809708

109. Schindelin J, Arganda-Carreras I, Frise E, Kaynig V, Longair M, Pietzsch T, et al. Fiji: an open-source platform for biological-image analysis. Nat Methods. 2012; 9: 676–682. https://doi.org/10.1038/nmeth.2019 PMID: 22743772

110. Ihara Y, Ohta H, Masuda S. A highly sensitive quantification method for the accumulation of alarmone ppGpp in Arabidopsis thaliana using UPLC-ESI-qMS/MS. J Plant Res. 2015; 128: 511–518. https://doi.org/10.1007/s10265-015-0711-1 PMID: 25752614

111. Steinchen W, Schuhmacher JS, Altegoer F, Fage CD, Srinivasan V, Linne U, et al. Catalytic mechanism and allosteric regulation of an oligomeric (p)ppGpp synthetase by an alarmone. Proc Natl Acad Sci USA. 2015; 112: 13348–13353. https://doi.org/10.1073/pnas.1505271112 PMID: 26460002

112. Hughes CS, Moggridge S, Müller T, Sorensen PH, Morin GB, Krijgsveld J. Single-pot, solid-phase-enhanced sample preparation for proteomics experiments. Nat Protoc. 2019; 14: 68–85. https://doi.org/10.1038/s41596-018-0082-x PMID: 30464214

113. Plubell DL, Wilmarth PA, Zhao Y, Fenton AM, Minnier J, Reddy AP, et al. Extended Multiplexing of Tandem Mass Tags (TMT) Labeling Reveals Age and High Fat Diet Specific Proteome Changes in Mouse Epididymal Adipose Tissue. Mol Cell Proteomics. 2017; 16: 873–890. https://doi.org/10.1074/mcp.M116.065524 PMID: 28325852

114. Perez-Riverol Y, Csordas A, Bai J, Bernal-Llinares M, Hewapathirana S, Kundu DJ, et al. The PRIDE database and related tools and resources in 2019: improving support for quantification data. Nucleic Acids Res. 2019; 47: D442–D450. https://doi.org/10.1093/nar/gky1106 PMID: 30395289

115. Zhu B, Stülke J. SubtiWiki in 2018: from genes and proteins to functional network annotation of the model organism *Bacillus subtilis*. Nucleic Acids Research. 2018; 46: D743–D748. https://doi.org/10.1093/nar/gkx908 PMID: 29788229

116. R Core Team. R: A Language and Environment for Statistical Computing. Vienna, Austria: R Foundation for Statistical Computing; 2018. https://www.R-project.org/

117. Yu G, Wang L-G, Han Y, He Q-Y. clusterProfiler: an R Package for Comparing Biological Themes Among Gene Clusters. OMICS: A Journal of Integrative Biology. 2012; 16: 284–287. https://doi.org/10.1089/omi.2011.0118 PMID: 22455463

PUBLICATION V

Article

SOURCE DATA | TRANSPARENT PROCESS

THE EMBO JOURNAL

The torpedo effect in *Bacillus subtilis*: RNase J1 resolves stalled transcription complexes

Michaela Šiková[1,†], Jana Wiedermannová[1,†], Martin Převorovský[2], Ivan Barvík[3], Petra Sudzinová[1], Olga Kofroňová[1], Oldřich Benada[1], Hana Šanderová[1], Ciarán Condon[4] & Libor Krásný[1,*]

Abstract

RNase J1 is the major 5′-to-3′ bacterial exoribonuclease. We demonstrate that in its absence, RNA polymerases (RNAPs) are redistributed on DNA, with increased RNAP occupancy on some genes without a parallel increase in transcriptional output. This suggests that some of these RNAPs represent stalled, non-transcribing complexes. We show that RNase J1 is able to resolve these stalled RNAP complexes by a "torpedo" mechanism, whereby RNase J1 degrades the nascent RNA and causes the transcription complex to disassemble upon collision with RNAP. A heterologous enzyme, yeast Xrn1 (5′-to-3′ exonuclease), is less efficient than RNase J1 in resolving stalled *Bacillus subtilis* RNAP, suggesting that the effect is RNase-specific. Our results thus reveal a novel general principle, whereby an RNase can participate in genome-wide surveillance of stalled RNAP complexes, preventing potentially deleterious transcription–replication collisions.

Keywords RNAP; RNase J1; stalling; torpedo; transcription–replication collision
Subject Categories DNA Replication, Recombination & Repair; Microbiology, Virology & Host Pathogen Interaction; Transcription
DOI 10.15252/embj.2019102500 | Received 17 May 2019 | Revised 26 November 2019 | Accepted 27 November 2019 | Published online 16 December 2019
The EMBO Journal (2020) 39: e102500

See also: **V Svetlov & E Nudler** (February 2020)

Introduction

Ribonucleic acids (RNAs) are indispensable for living organisms. They are transcribed from DNA and function as templates for translation into proteins, while also serving regulatory, catalytic, and structural roles (Jimenez *et al*, 2015; Radhakrishnan & Green, 2016; Gimpel & Brantl, 2017; Sikova *et al*, 2018). The amount of any RNA in the cell is determined by the ratio between its synthesis and degradation rates (Arraiano *et al*, 2010).

Synthesis of RNA in bacteria is dependent on RNA polymerase (RNAP) that recognizes promoter DNA sequences where transcription begins (Ruff *et al*, 2015). After initiation, RNAP forms the elongation complex (EC) and proceeds in a step-wise manner, functioning as a Brownian ratchet (Bar-Nahum *et al*, 2005). During elongation, RNAP may encounter obstacles, such as thymidine dimers or DNA-binding proteins that make it pause or even backtrack, and subsequently stall (He & Zalkin, 1992; Tornaletti & Hanawalt, 1999; Kireeva & Kashlev, 2009). These stalled complexes can be resolved by various factors that either allow RNAP to proceed with transcription or liberate RNAP from the stalled complex (Toulme *et al*, 2000; Peters *et al*, 2009; Epshtein *et al*, 2014; Fan *et al*, 2016). These factors include (i) the termination factor Rho (Epshtein *et al*, 2010), (ii) the transcription–repair coupling factor, Mfd, that recognizes stalled RNAPs and which recruits UvrA to initiate nucleotide excision repair (Le *et al*, 2018), and (iii) GreA, a translation elongation factor that induces hydrolysis of RNA by RNAP in backtracked complexes (Kusuya *et al*, 2011). These factors are vital for physiologically appropriate gene expression as well as for genome integrity (Nadkarni *et al*, 2016). At the ends of genes, transcription is terminated in a manner dependent on RNA hairpins and/or auxiliary proteins such as Rho (Larson *et al*, 2008; Epshtein *et al*, 2010).

Degradation of RNA is carried out by various ribonucleases (RNases) that can cleave RNA either endo- or exonucleolytically. Exoribonucleases can function either in the 3′-to-5′ or in the 5′-to-3′ direction (Lehnik-Habrink *et al*, 2012). Until relatively recently, 5′-to-3′ exoribonucleases were believed to be exclusively eukaryotic. However, a bacterial 5′-to-3′ exoribonuclease, RNase J1, was discovered in the model soil-dwelling organism *Bacillus subtilis* (Mathy *et al*, 2007) and shown to be widespread in bacteria and archaea (Phung *et al*, 2013; Condon *et al*, 2018). RNase J1 is a member of the β-lactamase family of ribonucleases that also possesses endoribonucleolytic activity, at least *in vitro* (Even *et al*, 2005). In *B. subtilis*, RNase J1 associates with its paralog RNase J2 in the cell and although these two RNases act synergistically, formation of this complex is not necessary for its enzymatic activity (Mathy *et al*, 2010). RNase J1 is not essential, but its depletion results in significant changes in the transcriptome (Durand *et al*, 2012).

1 Institute of Microbiology of the Czech Academy of Sciences, Prague 4, Czech Republic
2 Department of Cell Biology, Faculty of Science, Charles University, Prague, Czech Republic
3 Division of Biomolecular Physics, Institute of Physics, Charles University, Prague 2, Czech Republic
4 UMR8261, CNRS, Université de Paris, Institut de Biologie Physico-Chimique, Paris, France
*Corresponding author. Tel: +420 241063208; E-mail: krasny@biomed.cas.cz
†These authors contributed equally to this work

Here, using the *B. subtilis* model system, we describe a new phenomenon, the ability of RNase J1 to disassemble stalled transcription complexes, preventing transcription–replication collisions. Our initial goal was to determine the effect of the absence of RNase J1 on the transcriptome using an *rnjA* (encodes RNase J1) deletion strain, as previously this effect had been determined with a strain that allowed only incomplete depletion of this enzyme (Durand *et al*, 2012). We performed RNAseq and ChIPseq experiments and detected massive changes both in the levels of individual transcripts and in the distribution of DNA occupancy by RNAP, where RNAP accumulated on genes that have low transcript levels, suggesting the presence of stalled transcription complexes. Subsequently, we demonstrated that RNase J1 is close to, and physically linked to, RNAP through RNA in the cell. We present a model supported by experimental evidence in which RNase J1 resolves stalled RNAP complexes by degrading nascent RNA and disassembling the stalled complex after colliding with it, thereby likely acting as a "torpedo" in a manner analogous to a particular mode of eukaryotic transcription termination (Luo & Bentley, 2004).

Results

The absence of RNase J1 affects the transcriptome and DNA occupancy by RNAP

To characterize the global effects of a complete absence of RNase J1, we first created a *B. subtilis* 168 tryptophan prototrophic strain (BaSysBio; Nicolas *et al*, 2012) with a deletion of the *rnjA* gene. As previously reported for *rnjA* deletions, this strain displayed a markedly decreased growth rate (Fig EV1A) and altered cell morphology (Figaro *et al*, 2013; Cascante-Estepa *et al*, 2016)—both with respect to cell shape and length (Fig EV1B; see Fig EV1C for distribution of non-spiral cell lengths). We also measured the overall RNA synthesis rate, and, in agreement with the decreased growth rate of the Δ*rnjA* mutant, it displayed a strongly decreased RNA synthesis rate (Fig EV1D).

Next, using RNAseq we determined the effects of the absence of RNase J1 on individual gene expression. The Δ*rnjA* mutant showed altered RNA levels for 1,740 genes (at least a twofold difference), of which 879 were upregulated (↑) and 861 were downregulated (↓) with respect to wt (Tables EV1 and EV2). Thirteen selected differentially expressed genes were validated by RT–qPCR (Appendix Fig S1). The similar distribution of up- and downregulated mRNAs applied to five out of six major gene ontology categories; the exceptions were mRNAs from prophages and mobile genetic elements where the gene expression was preferentially downregulated (Appendix Fig S2). Among the most upregulated mRNAs was *mreBH* (~ 16× ↑) that encodes a protein whose physiologically correct level is required for cell shape determination (Kawai *et al*, 2009). We have shown previously that the upregulation of the *mreBH* mRNA is primarily due to the strong stabilization of a non-functional degradation intermediate whose 5′ end lies within the *mreBH* ORF (Durand *et al*, 2012). The perturbed expression of this and several other mRNAs encoding proteins involved in cell-wall synthesis possibly explains, at least in part, the "spiral" phenotype [see (Figaro *et al*, 2013)].

Several alternative sigma factor-encoding mRNAs, especially *sigD* [~ 8× ↓] but also *sigB*, *sigM*, *sigW*, *sigX*, and *sigY* were downregulated in cells lacking RNase J1 (Fig 1C and D). While most of the upregulated mRNAs are likely due to the direct stabilization of either full-length mRNAs or long degradation intermediates (Durand *et al*, 2012), we anticipate that most of the downregulated mRNAs are due to indirect transcription effects. This is because stabilizing effects of RNase J1 5′-to-3′ exoribonuclease activity, the primary *in vivo* activity of this enzyme, are expected to be rare (if any). The downregulation of *sigD* expression likely explains the loss of motility as expression of the flagellar machinery is controlled by this sigma factor (Mirel *et al*, 1992). The long filaments of the Δ*rnjA* strain might be related to downregulation of the gene responsible for cell separation—*cwlS* (~ 18× ↓; Fukushima *et al*, 2006).

A comparison with the previously reported transcriptome data based on the depletion strain (Durand *et al*, 2012) revealed that the effect of the complete absence of RNase J1 significantly overlapped with the effect of its depletion. The depletion strain displayed changes in RNA accumulation of 1,261 genes (at least a twofold difference). 239 out of the 385 downregulated mRNAs (62%) in the RNase J1 depletion strain were also downregulated in the RNase J1 null strain. 504 out of the 876 upregulated mRNAs (58%) in the RNase J1 depletion strain were also upregulated in the RNase J1 null strain (Fig EV2). Nevertheless, using the deletion strain we identified ~ 1,000 new genes whose expression was affected by RNase J1 (Table EV3).

To see whether we could correlate the changes in gene expression with RNAP occupancy of the affected genes, we conducted ChIPseq experiments, comparing wt and RNase J1-null strains, where we sequenced the DNA associated with RNAP in the cell. Surprisingly, we observed a major redistribution of RNAPs over the genome. Figure 1A and B shows an overall comparison of the RNAseq and ChIPseq data for wt and Δ*rnjA*.

For comparisons of RNAseq and ChIPseq data, we had anticipated and subsequently detected two types of effects: (i) correlated effects—the more or less occupied a gene with RNAP, the higher or lower the respective RNA level (classes I and II, showing transcriptional up or down effects, respectively), and (ii) effects where genes with increased RNA levels in the mutant displayed unchanged or possibly decreased occupancy with RNAP, reflecting an increased stability of these RNAs because they are direct targets of RNase J1 (class III, representing primarily post-transcriptional effects). Indeed, the averaged effects of the *rnjA* deletion on both RNA abundance (RNAseq) and DNA occupancy with RNAP (ChIPseq) showed mRNAs belonging to these three classes (Fig 2).

Remarkably, we also detected another effect—a reciprocal phenomenon to class III, i.e., an increased RNAP occupancy and an equal or decreased mRNA level (Fig 2). This occurred especially in the case of genes with less abundant transcripts, although some genes, such as *veg* (Lei *et al*, 2013), with highly abundant transcripts were identified as well (Fig EV3, class IV). These genes were shifted to the right (in the ChIPseq dimension) in the graph in Fig 1, unlike highly expressed genes in the upper part of the graph. The increased occupancy of RNAP within these genes without a parallel RNA output suggests the presence of non-productive or stalled elongation complexes. Genes of classes I–IV represented three quarters of all *B. subtilis* genes; a quarter of all genes was relatively unaffected or not detected by RNAseq (Fig 2). The list of genes sorted according to classes I–IV is provided in Table EV4. Examples of individual genes from these classes are shown in Fig EV3. Validations of the ChIPseq data (by qPCR) are shown in Appendix Fig S3.

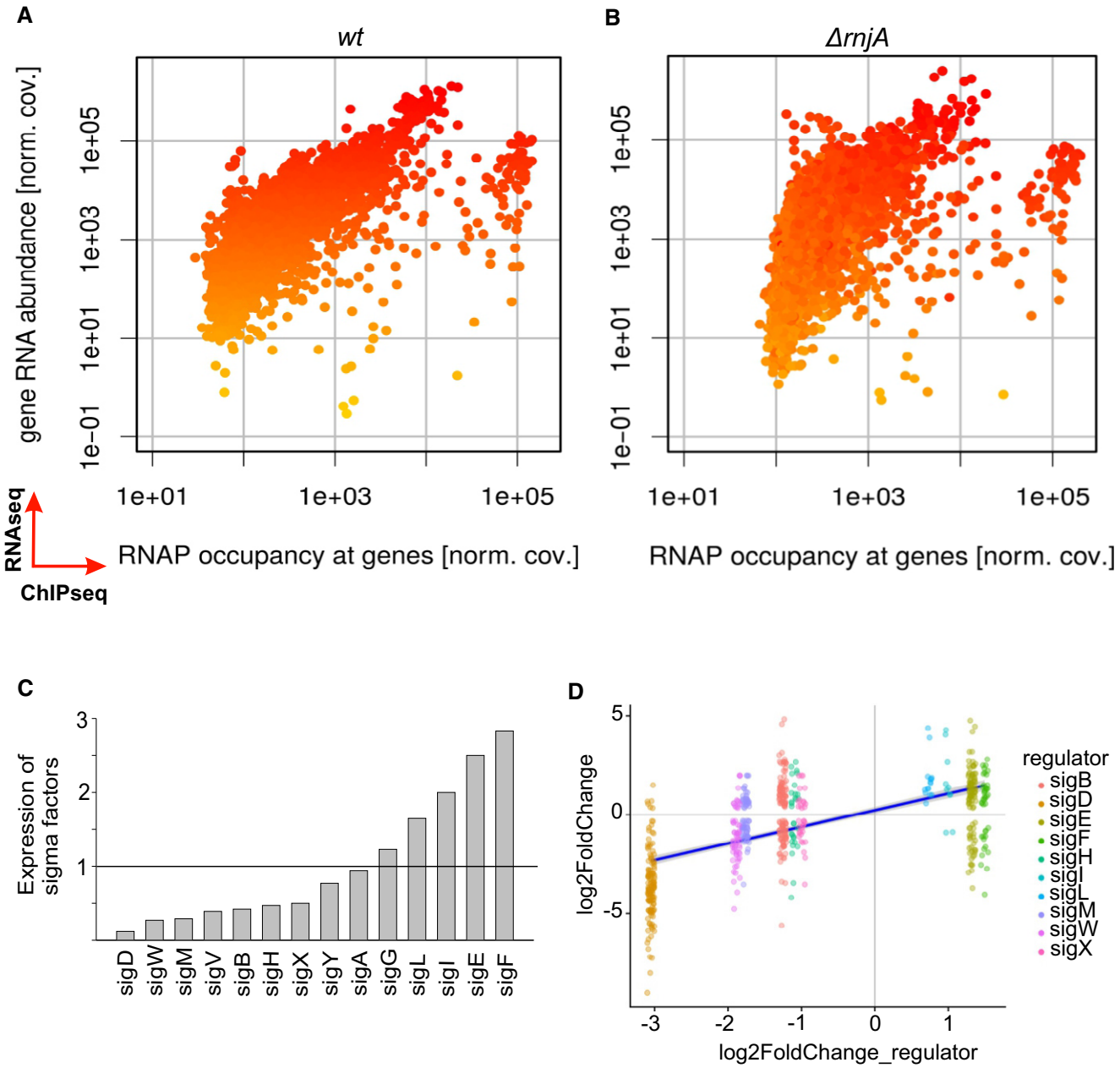

Figure 1. Global changes in Δ*rnjA* compared to wt.

A, B Comparisons of RNAseq and ChIPseq data. Wt strain (A) and Δ*rnjA* (B). The *x*-axis shows the relative RNAP occupancy at a given gene (normalized ChIPseq coverage). The *y*-axis shows the relative abundance of the transcript (normalized RNAseq coverage; each dot is one gene). The genes are color-coded, ranging from yellow (low RNA abundance) to red (high RNA abundance) in wt. The Δ*rnjA* strain has higher RNAP occupancy mainly among the genes with less abundant transcripts. The color coding in (B) reveals no dramatic overall changes in the vertical direction (RNA abundance). If anything, some of the low abundance transcripts decreased further in level in the mutant strain. The main difference (mostly among the low abundance transcripts) is their shift in the horizontal direction to the right (toward higher occupancy with RNAP). Data represent mean values of three independent experiments.

C Relative expression of all sigma factors in wt (LK1371) vs. Δ*rnjA* (LK1381). Wt levels of each sigma factor were set as 1 (indicated with the horizontal line).

D Sigma-dependent genes and correlation with expression of sigma factors (significantly changed) in Δ*rnjA* (LK1381). The most downregulated sigma factor was *sigD*, and almost all *sigD*-dependent genes were downregulated. A similar trend is visible for the rest of sigma factors and their respective dependent genes. The *x*-axis shows expression of each sigma factor, and the *y*-axis shows expression of genes for each sigma regulon. The violet (dark blue) line: regression line.

Source data are available online for this figure.

We checked whether the increased occupancy of DNA with RNAP on class IV genes might be explained by an elevated concentration of RNAP in the mutant; we determined the level of RNAP in both wt and Δ*rnjA* cells. In fact, we detected a lower level of RNAP in cells lacking RNase J1 (Fig EV4A–C). This correlated with the decreased levels of transcripts of the *rpoA*, *rpoB*, and *rpoC* RNAP

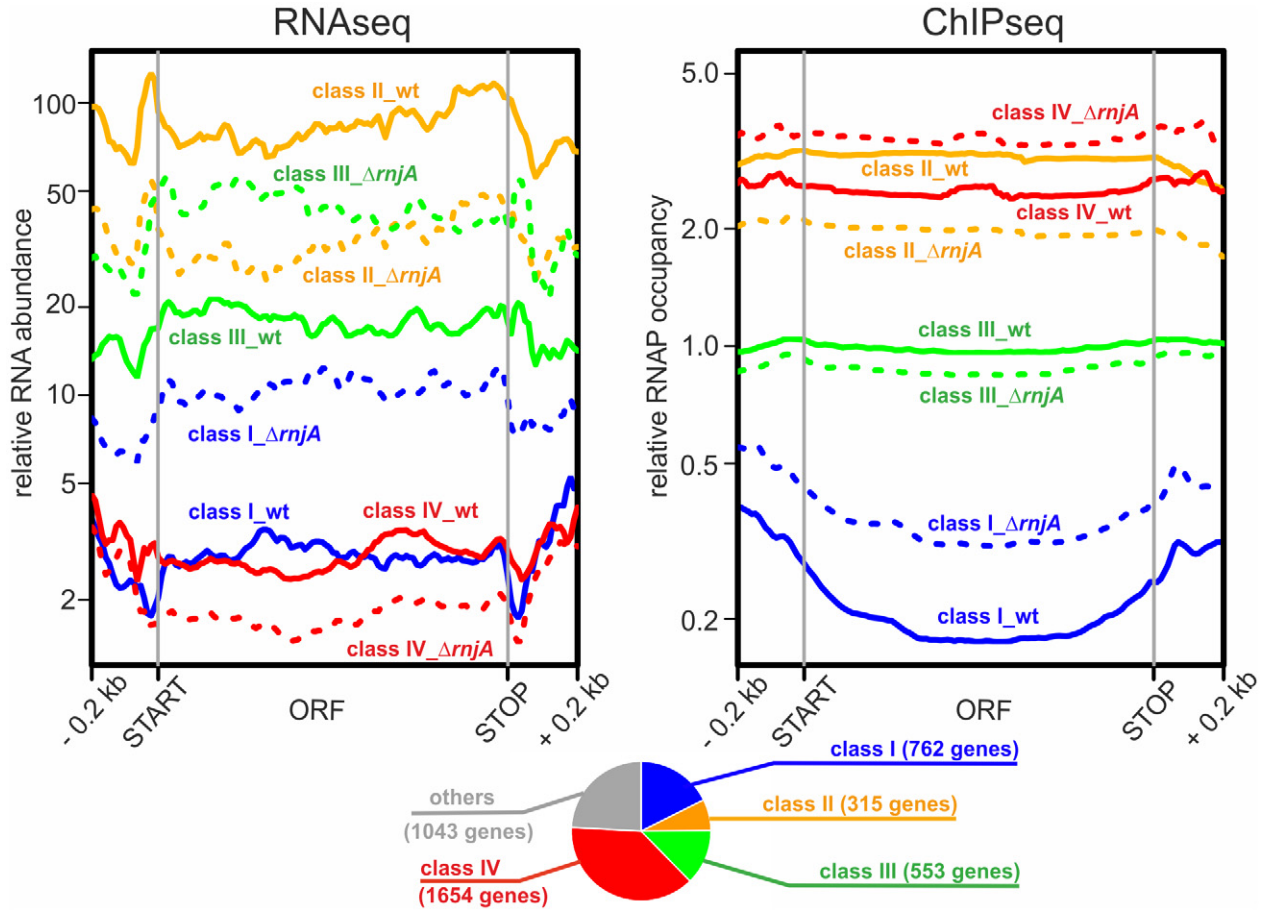

Figure 2. Class I, II, III, and IV genes.

Average gene profiles of normalized RNAseq and RNAP ChIPseq coverages from wt (solid lines) and Δ*rnjA* (dashed lines) strains were plotted for gene classes I–IV (n = 762, 315, 553, and 1,654 genes, respectively). Open reading frames were rescaled to 1 kb; upstream and downstream regions of 0.2 kb were also included in the plots. Data represent mean values of three independent experiments. For the definition of class I–IV genes, see text and Materials and Methods section "Gene classification (classes I–IV)". The pie chart shows the overall distribution of classes I–IV and other genes.

Source data are available online for this figure.

subunit-encoding genes, observed in the RNAseq experiments (Fig EV4D). Thus, the redistribution of RNAP over the genome in the *rnjA* mutant was not due to an increased abundance of RNAP.

These results prompted the following question: Could RNase J1 directly affect gene occupancy by RNAP? A possible scenario was that it might contribute to removing stalled RNAP complexes from the DNA. Hence, in the absence of RNase J1, the occupancy of some genes with RNAP would increase as they would contain more stalled RNAPs. To remove these stalled RNAPs, we speculated that RNase J1 might act on the RNA extruding from RNAP and degrade it in the 5′-to-3′ direction. Upon encountering RNAP, the resulting interaction would cause the transcription complex to disassemble.

RNase J1 and RNAP co-localize *in vivo* and are associated through RNA

If our hypothesis is correct, it would require RNase J1 and RNAP to interact in the cell. However, RNase J1 has been reported to be localized either in the polar regions of the cell (Cascante-Estepa *et al*, 2016) or associated with ribosomes (Even *et al*, 2005), and generally not present around/in the nucleoid. To resolve this issue, we used super-resolution microscopy (SIM) and strain bearing RNase J1-GFP and RNAP-mCherry. Figure 3A shows that RNase J1 was present in other regions of the cell besides the poles. Moreover, the strong overlap of the two fluorophores, especially on the periphery of the nucleoid, supports the idea that these two enzymes could encounter each other in the cell. To view a larger number of cells, see Appendix Fig S4.

To test more directly whether RNase J1 is associated with RNAP, we pulled down RNase J1 via a His-tag and used an antibody against the β subunit of RNAP to detect its presence in complex with RNase J1. Figure 3B shows that RNase J1 associates with RNAP in both exponential and stationary phases (lanes 1 and 2), although we retrieved larger amounts of RNase J1 in the latter. In a reciprocal experiment with His-tagged RNAP, we detected RNase J1 in stationary phase only (lane 4). In a control (using a strain without His-tagged proteins), neither RNase J1 nor RNAP was detected (lanes 7 and 8).

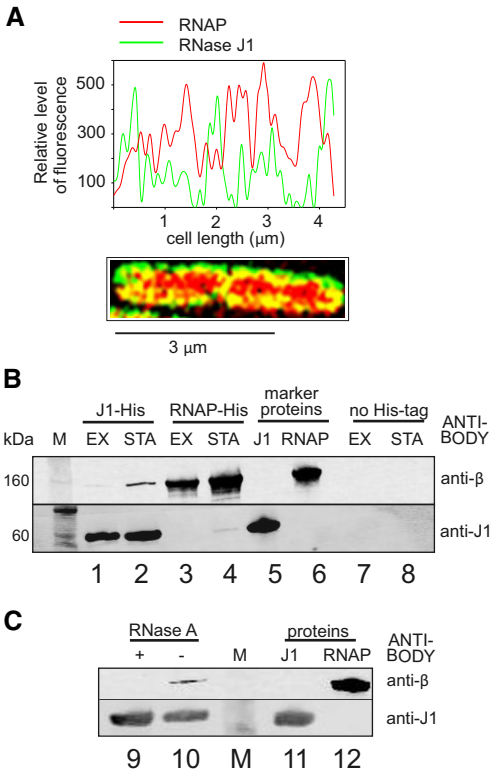

Figure 3. RNAP and RNase J1 may interact in the cell.

A SIM of exponential *Bacillus subtilis* cells. RNase J1 was fused to GFP (green), RNAP to mCherry (red). The graph shows relative fluorescence intensities at the cell midsection (along the long axis); SIM of the cell is below. Yellow indicates colocalization of the two proteins.

B Pull-down with RNase J1-8xHis tag and RNAP-10xHis tag and detection of the proteins with antibodies. Lanes 1 and 2—RNase J1-8xHis was used to pull down RNAP; lanes 3 and 4—RNAP-10xHis was used to pull down RNase J1; lanes 5 and 6—purified proteins were used as markers; lanes 7 and 8—strains without His-tagged proteins were used as negative controls to demonstrate the specificity of the interaction. M, molecular size marker; EX, exponential phase; STA, stationary phase.

C Pull-down with RNase J1-8xHis tag from stationary phase cells—the same conditions as in (B). The samples then either were (lane 9) or were not (lane 10) treated with RNase A to detect whether the interaction was via RNA. Lanes 11 and 12—purified proteins were used as markers. The experiment was performed three times (biological replicates) with the same result.

Source data are available online for this figure.

We next asked whether the observed complexes between RNase J1 and RNAP represented a direct protein–protein interaction, or whether this association depended on RNA. Figure 3C shows that RNase A treatment abolished the association (lanes 9 and 10), suggesting that RNase J1 and RNAP were linked via RNA.

RNase J1 dissociates transcription elongation complexes

To address directly whether RNase J1 is able to resolve stalled transcription complexes, we set up an *in vitro* system with purified components (Fig 4A). We assembled *B. subtilis* RNAP transcription elongation complex on a DNA scaffold with a 30-nt RNA. The complex was attached to streptavidin beads via biotinylated DNA. Then, we utilized the enzymatic activity of RNAP to label the RNA with three consecutive Us (encoded in the DNA), by adding radioactive UTP to the complex (Fig 4B). Subsequently, we washed off the unincorporated UTP and added either RNase J1 or RNase R, a 3′-to-5′ exoribonuclease, as a negative control. Figure 4B (lane 2) shows that RNase J1 was able to degrade the extruding RNA up to RNAP, leaving 17–18 nt long stubs, consistent with the length of the RNA channel that protects the exiting RNA (~ 16 nt; Fig EV5A). Importantly, smaller RNA fragments, 1–5 nt in length, also appeared in the gel. RNase J1 is known to have processive 5′ exoribonuclease activity until RNA fragments are chewed down to < 5 nts in size, after which the enzyme behaves distributively (Dorleans *et al*, 2011). The fragments released in the *in vitro* degradation assay thus correspond to the expected sizes of the distributive products of RNA digestion by RNase J1, after the RNA was released from RNAP into the buffer. That these short RNA products are no longer associated with RNAP was confirmed by showing that they disappeared upon washing the beads after RNase J1 treatment (lane 6). The 17–18 nt long fragments, however, remained tightly associated with the beads after the wash step showing they were still in complex with RNAP and suggesting that not all RNAP complexes reached by RNase J1 release their RNAs immediately.

The 3′ exoribonuclease RNase R was unable to digest the RNA, as expected, since the 3′ RNA end is protected inside RNAP (Fig 4B, lane 3). This control was important to show that no free RNA was present in the reaction and that the complexes did not spontaneously dissociate during the incubation period. Lanes 4 and 5 show reactions where the elongation complexes were heat-denatured prior to nuclease treatment to show the patterns of free RNA digested with the two RNases. As expected, no 17–18 nt long fragments were detected with either RNase J1 or RNase R. Rather, the 1–5 nt distributive products of RNase J1 digestion were observed. The experiments clearly show that RNase J1 can digest RNA in stalled transcription complexes until it reaches RNAP and then trigger the release of the 17–18 nt RNA stub to digest it further to 1–5 nt end products.

Next, we wished to determine to what extent the effect of RNase J1 was specific. We assembled elongation complexes and treated them with either RNase J1 or the eukaryotic 5′-to-3′ exoribonuclease Xrn1 (Sun *et al*, 2013). Figure 5A–C shows that RNase J1 was significantly more efficient at degrading full-length RNA than Xrn1, which was stopped more frequently by RNAP, as indicated by the greater quantities of RNA stubs still associated with RNAP. We also note that Xrn1-generated stubs were more diverse than RNase J1-generated stubs (Fig 5A—asterisks), likely reflecting differences in the behavior of these two RNases as they approach RNAP (Fig EV5B and C).

As in the previous experiments we used the degradation of RNA in its entirety as an indirect indicator that the EC had been dissociated, we asked whether RNase J1 truly dissociates RNAP from DNA. We assembled ECs as in the previous experiment and challenged them either with buffer (mock treatment), RNase J1, or Xrn1. By Western blotting with anti-β (subunit of RNAP) antibody, we then detected the amounts of RNAP retained on beads (in complex with DNA) and released in the buffer (dissociated). Figure 6A shows that RNase J1 was able to dislodge RNAP from DNA and was more efficient in this regard than Xrn1, consistent with the results from the previous experiment.

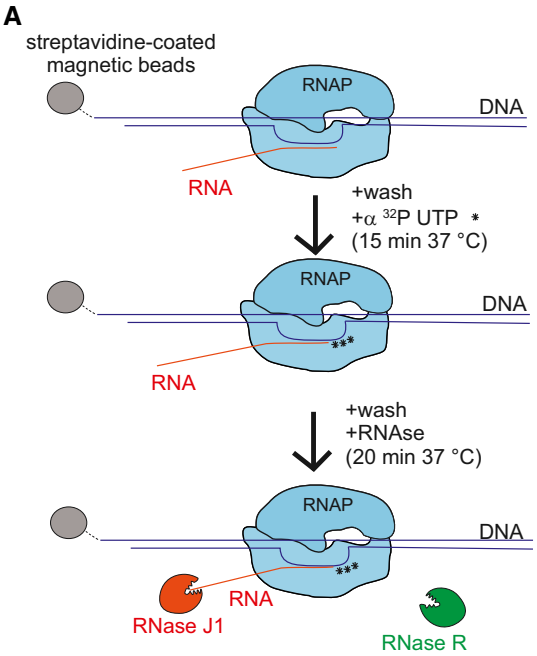

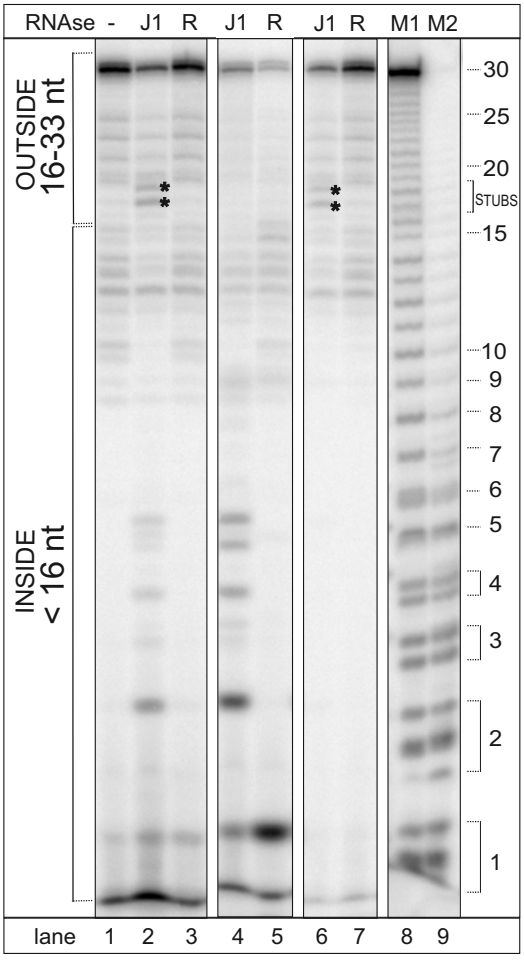

Figure 4. RNase J1 disassembles stalled transcription complexes (TC).

A Schematic representation of the flow of the experiment. TCs were assembled on DNA-RNA scaffolds (DNA was biotinylated); RNA was labeled at 3′ with radioactive UTPs (asterisks). The RNA length (including label) was 33 nt.

B Representative primary data—polyacrylamide gel (the experiment was performed 3× with the same results). Lane 1, the full-length (33 nt) labeled RNA; lane 2, the same as lane 1 but it included also incubation with RNase J1 (J1), 17–18 nt long fragments (RNase J1 stopped by RNAP; indicated with asterisks) and < 5 nt fragments (RNA released from TC into buffer—indicative of TC disassembly) are shown; lane 3, the same as lane 1 but included also incubation with RNase R (R); lanes 4 and 5, TCs were denatured by heat prior to RNase addition to demonstrate the activity and cleavage patterns of both enzymes; lanes 6 and 7, the same as lanes 2 and 3 but the buffer was washed off (TCs were retained by streptavidin beads) to demonstrate which RNA fragments were associated with TC; lanes 8 and 9 (M1, M2) Mw marker generated by treating the 30 nt RNA with alkali and formamide (M1—4-min treatment, M2—7-min treatment). As reported in Costanzo *et al* (2016) (and references therein), the cleavage by alkali or formamide leaves the phosphate group of the attacked phosphodiester bond bound at 3′, initially in the 2′,3′ cyclic form (upper band in the band couples). This successively opens (lower band in the band couples) yielding a double-banded pattern for short oligoribonucleotides.

Source data are available online for this figure.

To further pursue the question of specificity, we asked whether RNase J1 and Xrn1 would function similarly with RNAP from *Escherichia coli*. We performed the same experiments as in Fig 5 and obtained similar results (Fig 6B and C), suggesting that the effects of these two RNases are relatively non-specific with respect to RNAP.

Finally, we tested whether ε (encoded by *rpoY*), a small, non-essential subunit of *B. subtilis* RNAP, which is organized in a two-gene operon with *rnjA* (Keller *et al*, 2014), had an effect on dissociation of ECs in the *in vitro* assay, but did not detect any impact (data not shown).

Effect of Rho

Of the factors involved in the resolution of stalled RNAP complexes, Rho was significantly downregulated in Δ*rnjA* (Fig 7B). A decreased level of Rho could conceivably contribute to the observed effect found in class IV genes. Another factor whose activity significantly changed (fivefold ↑) was HelD. HelD is a helicase-like protein that associates with RNAP and helps with transcription recycling, possibly helping with RNAP release from DNA (Wiedermannova *et al*, 2014). This increased expression may help the cell to compensate for the absence of RNase J1. To address a possible role for Rho or HelD, we compared wt cells with single and double deletion mutants in RNase J1 and Rho or HelD under normal conditions and after UV irradiation. UV irradiation increases RNAP stalling as it creates changes in DNA (e.g., cyclobutane pyrimidine dimers and 6,4 pyrimidine–pyrimidones; Goodsell, 2001) that form obstacles to transcription. Consistent with the role of RNase J1 in disassembly of stalled RNAP complexes, the Δ*rnjA* mutant displayed increased sensitivity to UV irradiation compared to wt although the result was not statistically significant ($P = 0.06$; Fig 7). Interestingly, the absence of neither Rho nor HelD alone negatively impacted cell viability in response

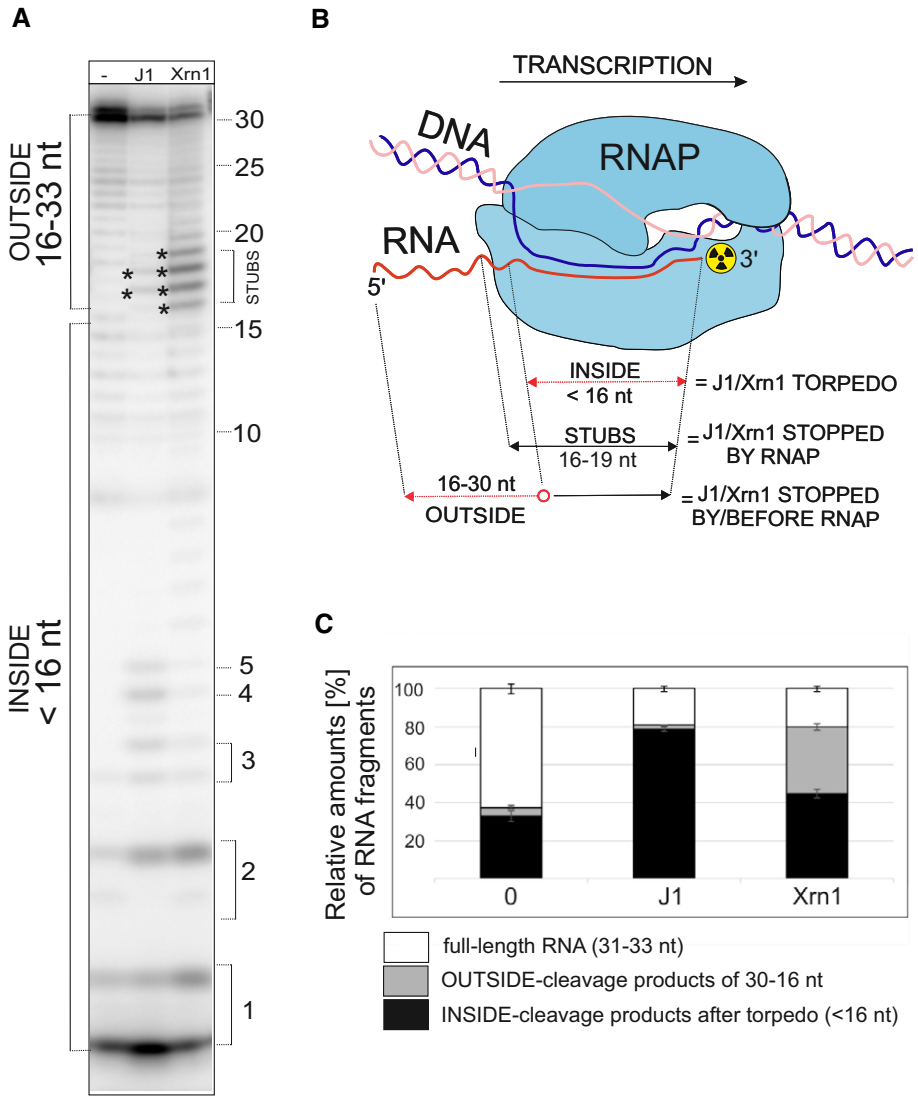

Figure 5. The effect of RNase J1 on TC is RNase-specific.

A Primary data—polyacrylamide gel—a representative result. The experimental setup was the same as in Fig 4. For the description of bands/fragments, see next panel legend. Asterisks indicate STUBS (16–19 nt).

B A schematic representation of quantitation of fragments. OUTSIDE (16–30 nt) are RNA fragments that originated by digestion of the full-length RNA by RNases that were stopped either before reaching or at the point of reaching RNAP; STUBS (16–19 nt) are RNA fragments that originated by digestion of the full-length RNA that were stopped at the point of reaching RNAP; INSIDE (< 16 nt) are RNA fragments (oligonucleotides) that could be only generated after the disassembly of the complex by the torpedo mechanism. The red color indicates parts of RNA that were digested.

C Quantitation of three independent experiments. "Full length"indicates the remaining undigested RNA. "OUTSIDE" and "INSIDE" are fragments as explained in (B) and indicated in (A). The bars represent 100% (all fragments). The black-gray-white boxes indicate the percentage of each fragment group (in %). The error bars indicate ± SEM for each group of fragments calculated from three biological replicates.

Source data are available online for this figure.

to UV treatment. In combination with the Δ*rnjA* mutation, the absence of Rho, but not HelD, appeared to lead to a further exacerbation of the UV-sensitive phenotype (Fig 7).

Discussion

In this study, we have characterized the effect of the absence of *B. subtilis* RNase J1 on the transcriptome and DNA occupancy with RNAP. Moreover, we identified a novel concept linking RNA transcription and degradation: a 5′-to-3′ exoribonuclease (RNase J1 in *B. subtilis*), in addition to its canonical role in mRNA turnover, helps disassemble stalled transcription complexes, thereby contributing to the smooth functioning of the transcription machinery, and preventing transcription–replication collisions (Fig 8). Parallels can be drawn to the effects of prokaryotic RNA/DNA translocases such as Rho and Mfd, and even more closely to eukaryotic 5′-to-3′ exonucleases (see the second part of Discussion).

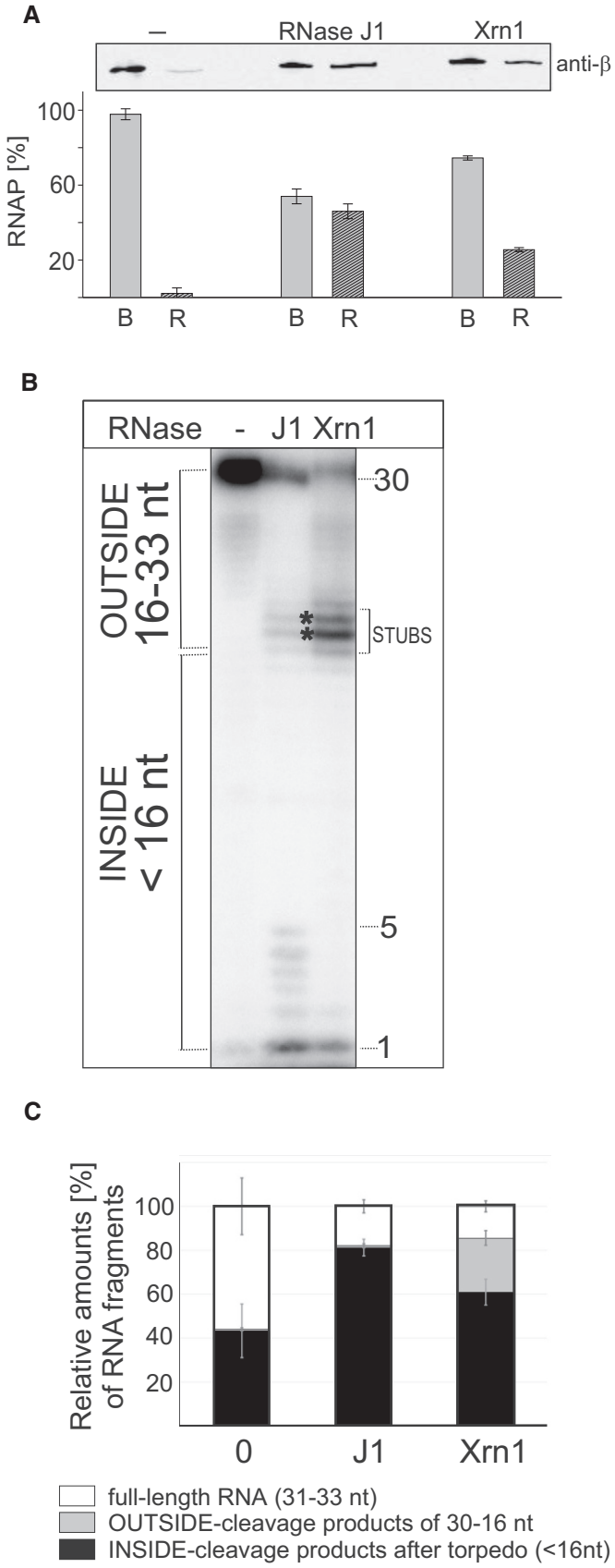

Figure 6. RNase J1 specifically dissociates RNAP from DNA in stalled TCs.

A TCs were assembled on DNA-RNA scaffolds (DNA was biotinylated and attached to streptavidin-coated magnetic beads); TCs were then divided into three tubes and challenged with buffer ("–", mock treatment) or RNase J1 of Xrn1. Dissociation of RNAP from DNA was monitored by detecting RNAP with anti-β antibody in two fractions: B—beads (RNAP still bound to DNA) and R—released (free in buffer). The gel strip shows representative primary data (Western blot). The graph shows averages (the bars) of two experiments (biological replicates), and the error bars show the range. The combined signal for B+R for each treatment was set as 100%.

B Primary data—polyacrylamide gel. The experimental setup was the same as in Fig 5 but with RNAP from *Escherichia coli*. Lane 1, the full-length (33 nt) labeled RNA; lane 2, the same as lane 1 but it included also incubation with RNase J1 (J1); lane 3, the same as lane 1 but included also incubation with Xrn1.

C Quantitation of three independent experiments. "Full length" indicates the remaining undigested RNA. "OUTSIDE" and "INSIDE" are fragments as explained in Fig 5. The bars represent 100% (all fragments). The black-gray-white boxes indicate the percentage of each fragment group (in %). The error bars indicate ± SEM for each group of fragments.

Source data are available online for this figure.

Effect of the absence of RNase J1 on the transcriptome

More than one-third of all genes were affected in the *B. subtilis* Δ*rnjA* mutant compared to wt, a moderately more pronounced effect than the one observed previously with an RNase J1 depletion strain (1,740 vs. 1,261 affected genes; Durand *et al*, 2012). In our previous study with an RNase J1-depletion strain, we showed that most upregulated mRNAs were due to an increase in RNA stability, as one would expect for a loss of RNase activity, while most down-regulated RNAs predicted to be due to indirect transcriptional effects (Durand *et al*, 2012). Although more genes belonged to class I (showing transcriptional up effects) than class III (post-transcriptional up effects) in this study (Fig 2), some class I genes could have both increased transcription levels and increased stability. It is also important to note that "upregulated" mRNAs may not necessarily result in upregulated protein levels. In many cases, only non-functional RNA fragments, corresponding to the 3′ products of endonucleolytic cleavages that are normally degraded by RNase J1, are overexpressed (Durand *et al*, 2012). Since the RNAseq reads were averaged over the whole open reading frame, if the degradation intermediate was reasonably long, it would result in an "overexpressed" candidate mRNA but not in more protein. For the following discussion, we will therefore only consider upregulated mRNA candidates whose full-length, and presumably functional, mRNAs accumulate.

Transcription and translation machineries

We detected lower amounts of mRNAs encoding the core RNAP subunits (α, β, β′), which may be correlated with the slower growth rate of the Δ*rnjA* mutant. We did not detect a difference in the amount of the primary sigma factor mRNA, sigA (Nicolas *et al*, 2012; Ramaniuk *et al*, 2017). However, we observed differences (in both directions) for most alternative sigma factors (Fig 1C). Sigma factors involved in sporulation were generally upregulated as was the master regulator for entry into sporulation, *spo0A* (Molle *et al*, 2003). It should be noted, however, that the Δ*rnjA* mutant fails to sporulate (Figaro *et al*, 2013). On the other side of the spectrum, SigD, required for the motility of the cell (Helmann *et al*, 1988;

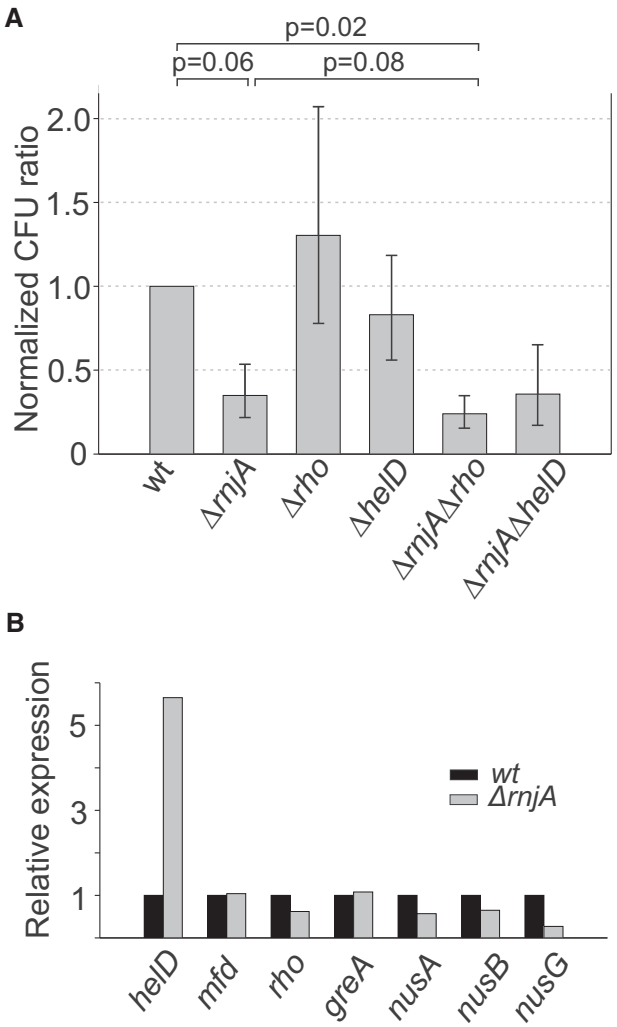

Figure 7. Effect of RNase J1, Rho, and HelD in UV sensitivity assays.

A Exponential cells of indicated strains (below the bars) were plated onto LB agar and either were or were not UV-irradiated. After overnight incubation, CFU were counted. UV sensitivity of the mutant strains (KO) was then calculated as the ratio between irradiated vs. non-irradiated cells and normalized to this ratio from the wt strain. As a consequence, the wt ratio is 1. The experiment was conducted 4× (biological replicates), and the bars show the geometric mean. The *P*-values, shown above the bars, were computed using two-tailed unpaired *t*-test for logarithms of the ratios. The error bars show ± SEM (computed on the log scale).

B Relative expression (mRNA) of helD, mfd, rho, greA, nusA, nusB, and nusG in the Δ*rnjA* strain [normalized to wt (set as 1)].

Source data are available online for this figure.

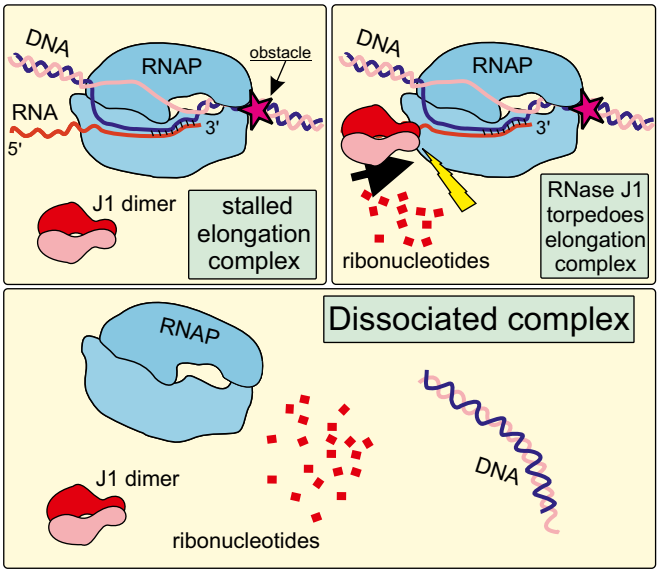

Figure 8. Model of RNase J1 functioning as the torpedo, dissociating stalled complexes of RNAP from DNA.

RNase J1 is depicted as a dimer. RNase J1, after the nascent transcript has been endonucleolytically cleaved, degrades RNA in the 5′-to-3′ direction. Upon encounter with RNAP, conformational changes are induced, likely resulting in dissociation of the complex, and liberating RNAP from DNA thereby removing obstacles potentially causing transcription–replication clashes.

Serizawa *et al*, 2004; Cozy & Kearns, 2010), was the most downregulated sigma factor, followed by extracytoplasmic function sigma factors, SigW (Turner & Helmann, 2000; Zweers *et al*, 2012) and SigM (Jervis *et al*, 2007; Eiamphungporn & Helmann, 2008). The upregulation/downregulation of sigma factors correlated to various degrees with upregulation/downregulation of the genes in their respective regulons, with the best correlation observed for SigD (Fig 1D). In general, the altered expression of sigma factors, especially those that were downregulated, appears to have contributed to the shaping of the transcriptome in the mutant strain. Interestingly, transcription elongation factors that stimulate pausing, NusA and NusG (Ma *et al*, 2015; Yakhnin *et al*, 2016), were downregulated (Fig 7B), which might be beneficial for the cell in light of the already high number of RNAPs stalled over the genome.

Many mRNAs transcribed from genes encoding the translation machinery were also downregulated, especially translation elongation factors (Appendix Fig S6), including tufA, encoding the most abundant protein in exponentially growing cells (Krasny *et al*, 2000). This might reflect the decreased growth rate of the Δ*rnjA* strain and may result in an increased stalling of ribosomes which could in turn increase stalling of RNAPs through uncoupling of the transcription–translation machineries (Nudler, 2012; Buskirk & Green, 2017).

RNases

Out of 22 RNases, half of them changed gene expression in the *rnjA* mutant. mRNAs for six RNases were upregulated (including *rny*, *yhaM*) and five RNases were downregulated. Of the upregulated RNases, RNase Y (*rny*) is a key RNase that is involved in maturation of RNase P RNA, small cytoplasmic RNA, and many mRNAs (Durand *et al*, 2012; Gilet *et al*, 2015). Upregulation of these RNases may be the result of the cell attempting to increase RNA turnover in the absence of RNase J1. The most downregulated RNase was *rnhB*, encoding RNase HII which is responsible for removing incorporated rNMP from DNA strand during replication (Randall *et al*, 2017). An absence of this RNase increases mutation rate in *B. subtilis* (Schroeder *et al*, 2017) and this could cause replication pausing, leading to replication–transcription collisions. Overall, alteration of expression of these RNases suggests that some of the effects of the

absence of RNase J1 on RNA accumulation may be indirect, mediated by other RNases.

DNA repair and replication

A number of proteins involved in DNA repair were upregulated in the mutant strain (23 genes Table EV5), which may, at least in part, stem from feedback mechanisms increasing the amount of these proteins to help the cell cope with increased number of transcription–replication collisions with mutagenic/DNA damaging effects. These upregulated genes included genes for mismatch repair *mutS, mutL* (Liu *et al*, 2016; LeBlanc *et al*, 2018), nucleotide excision repair *pcrA* (Sanders *et al*, 2017), base excision repair *mutM, mutT, ung*, processing of abasic sites *yqfS, exoA, yshC* (Lenhart *et al*, 2012), and genes for restart after replication–transcription collision *addA, addB, recA* (Shepanek *et al*, 1989; Krajewski *et al*, 2014). Interestingly, genes involved in DNA repair after UV damage (UvrABC; Lenhart *et al*, 2012) were either unchanged or upregulated.

Genes involved in DNA replication were either up- or downregulated (see Table EV6). Conceivably, this imbalance in their expression could have contributed to the slow growth of the RNase J1-null strain. Interestingly, ts (thermosensitive) mutants in the downregulated mRNAs DnaE/G/C form long filaments similar to the phenotype observed in the Δ*rnjA* strain (Janniere *et al*, 2007; Figaro *et al*, 2013). This phenotype is induced, e.g., when perturbations in DNA chain elongation lead to the generation of ssDNA.

RNase J1 and its role in disassembly of transcription complexes

The ChIPseq experiments revealed that genes, especially those with relatively low expression, displayed increased accumulation of RNAP in the Δ*rnjA* mutant, without a concomitant increase in RNA levels. This indicates an increase in the number of stalled RNAP complexes at these loci. Such complexes create obstacles for the replication machinery, and their collision may result in mutations in DNA and have an adverse effect on genome integrity. Pausing and stalling of RNAP is widespread and affects gene expression (Kang *et al*, 2019). The observed accumulation of RNAP on weakly transcribed genes is consistent with the finding that trailing RNAPs on heavily transcribed genes help the translocation of leading RNAPs, allowing them transcribe through regions that are more pause-prone, or through possible obstacles on the DNA. On weakly transcribed genes, this phenomenon is absent (Epshtein & Nudler, 2003) and correlates with increased accumulation of RNAP on these genes in the absence of RNase J1.

Collectively, the experiments presented in this study reveal that RNase J1 is present in the cell in the vicinity of DNA, associates with RNAP, and is able to disassemble stalled transcription complexes.

Transcription and translation are often coupled when the leading ribosome helps push RNAP forward (Kohler *et al*, 2017). However, if these two processes become uncoupled, RNAP may be more prone to pausing and possibly backtracking, remaining in an inactive form (Zhang *et al*, 2014). RNase J1 access to primary transcripts is known to be inhibited by the presence of the 5′ triphosphate group (Mathy *et al*, 2007). We envision that either deprotection of the 5′ end by RNA pyrophosphohydrolase (RppH) activity (Hsieh *et al*, 2013; Frindert *et al*, 2018) or prior endonucleolytic cleavage allows RNase J1 access to the mRNA to degrade it to the outer edge of the RNA exit channel. Subsequently, the remaining part of RNA, initially protected by RNAP, becomes available for degradation by action of RNase J1. The action may be mediated by the "torpedo" effect. The torpedo effect was first described in eukaryotes, and it is mediated by the 5′-to-3′ exonucleases Rat1/Xrn2 or CPSF-73 acting on eukaryotic RNAP II to terminate its transcription (Kim *et al*, 2004; Yang *et al*, 2009; Pearson & Moore, 2013; Baejen *et al*, 2017). This occurs after the nascent RNA has been cleaved at the polyadenylation signal when RNAP continues synthesizing non-coding RNA and needs to be stopped. The mechanistic details of the torpedo effect are poorly understood. We do not know whether RNase J1 first dissociates RNAP and then degrades the RNA, or if it degrades the RNA first, which would cause collapse of the transcription bubble and subsequent dissociation of RNAP. Alternatively, shortening the RNA may induce backtracking and destabilize the complex, resulting in its disassembly. However, the fact that Xrn1 was also capable of shortening RNA to the RNAP-protected stubs but unable to degrade the remaining RNA as efficiently as RNase J1 argues against this possibility.

We also considered the possibility that the endoribonuclease activity of RNase J1 might contribute to the results observed in this study, but a number of arguments favor the idea that the torpedo effect is primarily related to its 5′-exoribonuclease activity. First, while RNase J1 does have endoribonuclease activity *in vitro,* it is primarily thought to act as an exoribonuclease *in vivo.* Indeed, most of the endonucleolytic cleavage sites previously ascribed to RNase J1 *in vivo* are now thought to be performed by RNase Y, which has a similar specificity (Condon, 2010). The enzyme's preference for exonucleolytic activity has been further confirmed by the crystal structure of RNase J1 bound to RNA (Dorleans *et al*, 2011). While RNA can easily be threaded through an entry channel to reach the catalytic site in exonucleolytic mode, endonucleolytic cleavage requires dissociation of dimers and then additional separation of the β-CASP from the β-lactamase domain to allow the RNA to lie across the catalytic site. This likely explains why endonuclease activity is only observed in the presence of a large excess of enzyme over RNA, i.e., by simple probability, only a few isolated RNase J1 molecules are likely to be in a conformation capable of performing endonucleolytic cleavage. Lastly, RNase J1 acts more processively as an exoribonuclease with increasing length of RNA (Dorleans *et al*, 2011). Thus, if RNase J1 were to first shorten the RNA endonucleolytically before acting as an exoribonuclease in our torpedo assay, this would likely decrease the efficiency of degradation of the short RNA (< 5 nts) buried within RNAP and an underestimate the torpedo effect.

The length of the stubs and the path of RNA in RNase J1 and RNAP (Fig EV5A and B) suggest that RNase J1 and RNAP are likely in contact at this point in the process. The region on the surface of RNAP around the RNA exit channel contains elements important for the stability of RNAP complexes. These elements include the ω subunit (Weiss & Shaw, 2015) and the β-flap helix that interacts also with other proteins, such as NusA (Twist *et al*, 2011; Tagami *et al*, 2014; Ma *et al*, 2015; Guo *et al*, 2018). Whether and how RNase J1 interacts with these elements is currently unknown, and the details of the RNase J1-RNAP contacts will be studied in future experiments.

Regardless of the mechanistic details, it appears that the efficiency of the effect is RNase-specific as RNase J1 and Xrn1 acted with different efficiencies to provoke the release of the RNA and dissociate the EC. Therefore, different 5′-to-3′ RNases likely

possess different abilities to disassemble stalled transcription complexes. This is consistent with the previously reported observation that yeast Rat1/Rai1 does not terminate *E. coli* RNAP, probably due to the divergent structure of the yeast enzyme (Park *et al*, 2015). In contrast, the effect does not appear to discriminate between *E. coli* and *B. subtilis* RNAPs as both RNase J1 and Xrn1 exerted similar effects on complexes assembled with these enzymes. We stress, however, that despite the large phylogenetic distance between these two species, the relevant regions (RNA exit channel region) in β and β′ are highly homologous. It is possible that more divergent RNAPs, such as single-peptide enzymes (e.g., *E. coli* T7 phage RNAP) may behave differently toward RNase "torpedoes".

Other prokaryotic proteins that function in a "torpedo"-like manner are Rho and Mfd. These factors are ATP-dependent (Epshtein *et al*, 2010; Le *et al*, 2018). Their mechanisms of dissociating the transcription complex differ from each other and are likely also different from that of RNase J1. Rho was reported to decrease non-specific, pervasive transcription (Bidnenko *et al*, 2017), and its mRNA level was decreased in the Δ*rnjA* strain. We tested the effect of its absence in UV sensitivity assay. While deletion of the *rho* gene alone had no negative effect, deletion of *rho* and *rnjA* appeared to exacerbate the phenotype, consistent with the hypothesis that these two proteins function in an analogous manner, but in different pathways. We compared RNAseq data from a *B. subtilis* Δ*rho* strain (Nicolas *et al*, 2012) with our RNAseq data from Δ*rnjA*, focusing on class IV genes. Appendix Fig S5 reveals virtually no correlation between these two datasets, indicating that RNase J1 and Rho act on different sets of genes.

5′-to-3′ exoribonucleases are widely present in eukaryotes where transcription and replication also clash (Hamperl & Cimprich, 2016). Therefore, we envision that in eukaryotic cells 5′-to-3′ exoribonucleases may also be involved in the resolution of stalled RNAP complexes to prevent transcription–replication clashes that could result in mutations in DNA with undesirable consequences. This could be linked to diseases, such as polyglutamine diseases (neurodegenerative diseases) where, e.g., 5′-to-3′ exoribonuclease Xrn1 is sequestered and inactive in nuclear inclusions, a characteristic of the pathological state of the cell (Mori *et al*, 2018).

Materials and Methods

Cloning and strain construction

To prepare a Δ*rnjA* strain in a widely used *B. subtilis* genetic background, chromosomal DNA from a Δ*rnjA* strain (LK1191 = CCB434 in Figaro *et al*, 2013) was transformed into *B. subtilis* BaSysBio (Nicolas *et al*, 2012), yielding strain LK1381. Strains Δ*rnjA* Δ*rho* (LK2082) and Δ*rnjA* Δ*helD* (LK2336) were prepared with transformation of chromosomal DNA from the Δ*rnjA* strain (LK1190) into *B. subtilis* Δ*rho* (LK2058) (Bidnenko *et al*, 2017) or Δ*helD* (LK2329) strain (Wiedermannova *et al*, 2014).

To prepare a strain for pull-out experiments, RNase J1 was first amplified by PCR from gDNA of *B. subtilis* (LK566) and primers #1647/#1648 with Expand High Fidelity PCR System (Roche) and ligated into the expression vector pMUTIN4 (LK957) encoding a N-terminal 8xHis-tag via HindIII (Takara) and BamHI (Takara) restriction sites and transformed into *E. coli* DH5α (RLG6911), yielding strain LK1647. The plasmid was isolated with Wizard Plus Midipreps DNA purification system (Promega), verified by sequencing, and transformed into *B. subtilis* BaSysBio, resulting in strain LK1651.

To prepare strains for super-resolution microscopy (SIM), chromosomal DNA from *B. subtilis* expressing GFP-RNase J1 (LK1728 = 3,565 in Hunt *et al*, 2006) and plasmid from *E. coli* mCherry-RNAP (LK2320 = pNG622 in Doherty *et al*, 2010), a gift from P. Lewis] were transformed into *B. subtilis* BaSysBio.

For a complete list of strains (and their sources), see Table EV7.

Media and antibiotics

All experiments were performed in the rich LB medium, unless indicated otherwise. When required, the medium was supplemented with antibiotics: ampicillin 100 μg/ml (for *E. coli*), kanamycin 5 μg/ml, lincomycin 12.5 μg/ml, erythromycin 0.5 μg/ml, chloramphenicol 5 μg/ml, spectinomycin 100 μg/ml, and phleomycin 2 μg/ml (for *B. subtilis*). The expression of GFP and mCherry fusion proteins was induced with 0.5% xylose (final concentration).

^{3}H incorporation

This experiment was conducted as described previously (Panova *et al*, 2015). Wt and Δ*rnjA* strains were grown in defined MOPS medium to OD_{600} 0.3 (early exponential phase). RNA in cells was labeled with ^{3}H-uridine (1 μCi/ml), and cold uridine was added to a final concentration of 100 μM. At 0, 10, 20, 30, 40, 50, and 60 min, 100 μl and 250 μl of cells were withdrawn to measure cell density and determine ^{3}H incorporation, respectively. The 250 μl of cells was mixed with 1 ml of 10% trichloroacetic acid (TCA) and kept on ice for at least 1 h. Thereafter, each sample was vacuum-filtered and washed twice with 1 ml of 10% TCA and three times with 1 ml of ethanol. The filters were dried, scintillation liquid was added, and the radioactivity was measured. The signal was normalized to cell density.

Scanning electron microscopy

Exponential cultures of *B. subtilis* WT and Δ*rnjA* strains (OD_{600} 0.5) were prefixed with 1.5% glutaraldehyde for 1 h at room temperature. The cells were then washed with cacodylate buffer (Thermo Fisher Scientific) and fixed with 3% glutaraldehyde in cacodylate buffer overnight at 4°C. The extensively washed cells were allowed to sediment overnight at 4°C onto poly-L-lysine-treated circular glass coverslips. The coverslips were dehydrated in a graded ethanol series (25, 50, 75, 90, 96, 100, and 100%) followed by absolute acetone and critical point dried in a K850 Critical Point Dryer (Quorum Technologies Ltd, Ringmer, UK). The dried samples were sputter-coated with 3 nm of platinum in a Q150T Turbo-Pumped Sputter Coater (Quorum Technologies Ltd, Ringmer, UK). The final samples were examined in a FEI Nova NanoSEM scanning electron microscope (FEI, Brno, Czech Republic) at 5 kV using ETD, CBS, and TLD detectors.

Pull-down of RNase J1 and RNAP and Western blotting

Bacillus subtilis RNAP with a His_{10}-tagged β′ subunit (LK1275) or His_8-RNase J1 (LK1651) was pulled out from exponential and stationary phase cells (EXP, OD_{600} 0.5; STA OD_{600} ~ 3; 2 h after entry into STA) via Ni-NTA beads. RNase A (200 ng/ml) was or was not

added to the lysates. To determine the amount of RNAP, exponentially growing *wt* and Δ*rnjA* cells were sonicated and 5 μg of proteins was analyzed by sodium dodecyl sulphate–polyacrylamide gel electrophoresis (SDS–PAGE) and detected by Western blotting using mouse monoclonal antibodies against the β subunit of RNA polymerase (clone name 8RB13) or rabbit polyclonal antibodies against RNase J1 and secondary antibodies conjugated with a fluorophore dye [WesternBright™ MCF-IR, Advansta, 700 nm anti-rabbit (RNase J1) or 800 nm anti-mouse (RNAP) antibody], and the interactions were quantified with an Odyssey reader (LI-COR Biosciences).

Purification of proteins

Bacillus subtilis RNAP from wild-type strain with a His_{10}-tagged β′ subunit (LK1275), σ^A (LK1365), and RNase J1 was purified. The purification of RNAP was performed as described previously (Qi & Hulett, 1998), and σ^A was purified as described previously (Chang & Doi, 1990; Juang & Helmann, 1994). Purification of RNase J1 was performed as in Condon *et al* (2008).

Super-resolution microscopy

One milliliter of exponentially growing cells (OD_{600} 0.5) with GFP-RNase J1 and mCherry-RNAP (LK2328) was washed and resuspended in 1× PBS. To measure the cell length, exponentially growing wt and Δ*rnjA* cells (OD_{600} 0.5) were incubated with membrane dye NileRed (5 μg/ml, Sigma-Aldrich) for 10 min at RT, washed, and resuspended in 1× PBS. Strains were analyzed with super-resolution microscopy DeltaVision OMX™ equipped with a 60 × 1.42, PlanApo N, oil immersion objective, and softWoRx™ Imaging Workstation software. GFP-tagged proteins were imaged using 488 nm excitation; mCherry-RNAP and NileRed were imaged using 568 nm excitation. 3D-SIM resolution in XY was 130 ± 5 nm; 3D-SIM resolution in Z was 340 ± 10 nm. Cell length was analyzed with Fiji ImageJ.

Chromatin immunoprecipitation, ChIPseq, and qPCR validation

Bacillus subtilis wt (LK1371) and Δ*rnjA* (LK1381) cells were grown at 37°C in LB to exponential phase (OD_{600} 0.4–0.5). The culture was crosslinked with formaldehyde at a final concentration of 1% (30 min, 37°C). Then, 150 mM glycine was added and the cultures were incubated for additional 5 min at 37°C to stop the crosslinking process. Subsequently, cells were collected by centrifugation, washed with lysis buffer A (20 mM Tris–HCl, 150 mM NaCl, pH 8), resuspended in lysis buffer B (50 mM HEPES, 150 mM NaCl, 1 mM EDTA, 1% Triton X-100, 0.1% natrium deoxycholate, protease inhibitor cocktail, Calbiochem), and sonicated to obtain 200–500 bp long DNA fragments. Concentrations of proteins were measured with the Bradford method (Bradford, 1976). 20 μl of DynaBeads protein A (Thermo Fisher Scientific) was incubated with 3 μg of antibody against the β subunit of RNAP (8RB13, Santa Cruz) for 2 h at 4°C. Cell lysates (1 mg of proteins) were then mixed with the complex of antibody-DynaBeads and incubated overnight at 4°C. The beads were then washed 2× with lysis buffer B, 2× with lysis buffer 500 (50 mM HEPES, 1 mM EDTA, 500 mM NaCl, 1% Triton X-100, 0.1% natrium deoxycholate, pH 7.6), 1× with LiCl buffer (10 mM Tris–HCl, 1 mM EDTA, 250 mM LiCl, 1% Triton X-100, 1% natrium deoxycholate, pH 8), and 1× with TE buffer (10 mM Tris–HCl, 1 mM EDTA, pH 8). DNA–protein complexes were eluted from the beads with elution buffer (50 mM Tris–HCl, 10 mM EDTA, 1% SDS, pH 8) for 10 min at 65°C, dissociated at 65°C for 6 h in the presence of 200 mM NaCl and treated with 20 μg of proteinase K for 30 min at 37°C. Finally, DNA was purified by QIAquick Nucleotide Removal Kit (QIAGEN). Sequencing libraries were prepared in EMBL Heidelberg with NEBNext ChIP-Seq Library Prep Master Mix Set for Illumina (BioLabs) according to the manufacturer's instructions. Pooled barcoded libraries (two samples in biological triplicates) were sequenced in a single lane at Illumina HiSeq 2000 in the 50 bp single-end regime at EMBL Genomics Core Facility (Heidelberg, Germany). Read quality and potential adapter contamination were checked with FastQC v0.11.8 (https://www.bioinformatics.babraham.ac.uk/projects/fastqc/). Reads were aligned to the *B. subtilis* subsp. *subtilis* strain 168 genome (NCBI Nucleotide acc. no. NC_000964) using HISAT 2.0.5 (Kim *et al*, 2015)] and SAMtools 1.4 (Li *et al*, 2009). Only uniquely mapped reads (MAPQ ≥ 10) were kept. Alignment quality was checked visually using IGV 2.6.3 (Thorvaldsdottir *et al*, 2013). Read statistics for each sample can be found in Table EV8. Using deepTools 3.3.0 (Ramirez *et al*, 2016), sample data were first normalized to library size; then, IP sample coverage was normalized to the corresponding input samples, and finally, mean coverage from the three independent replicates was calculated. Per-gene coverage values were then obtained using genome annotation obtained from NCBI (GCF_000009045.1; downloaded 15/Nov/2015), and coverage for each gene was also normalized to gene length. The ChIPseq data are available from the ArrayExpress database (www.ebi.ac.uk/arrayexpress) under accession number E-MTAB-5659. The scripts used for ChIPseq data processing and analysis are available from https://github.com/mprevorovsky/krasny-torpedo. To validate the ChIPseq data, we used quantitative PCR (qPCR) in a LightCycler 480 System (Roche Applied Science) containing LightCycler® 480 SYBR Green I Master and 0.5 μM primers (each). Primers were designed with Primer3 software, and their sequences are in Table EV7. The data were normalized to input.

RNAseq and RT–qPCR validation

Two milliliters of exponentially growing cells [wt (LK1371), Δ*rnjA* (LK1381); OD_{600} 0.5] was treated with RNAprotect Bacteria Reagent (QIAGEN), pelleted, and immediately frozen. RNA was isolated with RNeasy Mini Kit (QIAGEN). Finally, RNA was DNase-treated (TURBO DNA-free Kit, Ambion). Five micrograms of total RNA was rRNA-depleted with Ribo-Zero Magnetic Kit; Gram-positive bacteria (Epicentre) and strand-specific libraries were then prepared with Illumina compatible NEXTflex Rapid Directional RNA-Seq Kit (Bioo Scientific) according to the manufacturer′s instructions. Pooled barcoded library (two samples in biological triplicates) was sequenced in a single lane at Illumina HiSeq 2000 in 50 bp single-end regime at EMBL Genomics Core Facility (Heidelberg, Germany). Read quality and potential adapter contamination were checked with FastQC v0.11.8 (https://www.bioinformatics.babraham.ac.uk/projects/fastqc/). Reads were aligned to the *B. subtilis* subsp. *subtilis* strain 168 genome (NCBI Nucleotide acc. no. NC_000964) using HISAT 2.0.5 (Kim *et al*, 2015) and SAMtools 1.4 (Li *et al*, 2009). Only uniquely mapped reads (MAPQ ≥ 10) were kept. Alignment quality was checked visually using IGV 2.6.3 (Thorvaldsdottir *et al*, 2013). Reads mapping to 30 ribosomal RNA genes (BSU_rRNA_1 –

BSU_rRNA_30) amounted to only < 0.14% of total reads for each genotype, confirming a high efficiency of rRNA depletion. Read statistics for each sample can be found in Table EV8. Using deepTools 3.3.0. (Ramirez *et al*, 2016), sample data were first normalized to library size, and mean coverage from the three independent replicates was calculated. Per-gene coverage values were then obtained using genome annotation obtained from NCBI (GCF_000009045.1; downloaded 15/Nov/2015), and coverage for each gene was also normalized to gene length. The analysis of differential gene expression was performed using unnormalized BAM files and the GenomicAlignments and DESeq2 packages in R/Bioconductor, with FDR set to 0.05 (Love *et al*, 2014). RNAseq data are available in the ArrayExpress database (www.ebi.ac.uk/arrayexpress) under accession number E-MTAB-5660. The scripts used for RNAseq data processing and analysis are available from https://github.com/mprevorovsky/krasny-torpedo. Gene Ontology terms are according to SubtiWiki (Zhu and Stulke, 2018). For Figs 1C, D, 7B, EV3, and EV4 and Appendix Figs S1 and S5, the log2(fold change) gene expression values determined by DESeq2 are shown. Since DESeq2 only reports wt-normalized relative expression values, normalized gene coverage values determined by deepTools are shown in Figs 1A and B, and 2 to visualize gene expression levels separately for wt and the *rnjA* mutant. The two methods of calculating gene expression levels were in good agreement (Pearson's $R = 0.95$). Validation of RNAseq data: First, new RNA purifications were performed under identical conditions as those for RNAseq experiments. Prior to RNA extraction, recovery marker RNA was added [a fragment of 16S rRNA from *M. smegmatis* (amplified by primers #1281 and #1282, see Table EV7)] and total RNA was then extracted. 2 μg of total RNA was reverse-transcribed to cDNA with reverse transcriptase (SuperScript™ III Reverse Transcriptase, Invitrogen). This was followed by qPCR, as described for ChIPseq validation. The data were then normalized to the recovery marker and the amount of cells.

Gene classification (classes I–IV)

Based on comparisons of mean normalized RNAP occupancy (ChIPseq) and transcript differential expression (DESeq2 results) between the *rnjA* mutant (Δ*rnjA*) and wt, 3,288 *B. subtilis* genes were assigned into four classes (I–IV). Class I: ≥ 120% RNAP occupancy and significantly upregulated in the *rnjA* mutant; class II: 0–80% RNAP occupancy and significantly downregulated in the *rnjA* mutant; class III: 0–120% RNAP occupancy in wt and significantly upregulated in the *rnjA* mutant; and class IV: ≥ 120% RNAP occupancy, and no significant change or significantly downregulated in the *rnjA* mutant. Average gene analyses of ChIPseq and RNAseq coverage for each class were performed using deepTools 3.3.0. (Ramirez *et al*, 2016).

In vitro effect of RNases J1/R/Xrn1 on elongation complexes

Transcription-competent ECs, containing a fully complementary transcription bubble, were assembled with wild-type RNA polymerase (RNAP) from *B. subtilis* (LK1275) as described before (Komissarova *et al*, 2003). DNA and RNA oligonucleotides were purchased and are listed in Table EV7. The RNA (#-pRNA) was monophosphorylated at the 5′ end by the manufacturer. A twofold molar excess of RNA was mixed with template DNA (#632) in water and annealed in a cycler (45°C 2 min, 42–27°C: T decreasing by 3°C every 2 min, 25°C 10 min). RNAP (2 pmol per sample) was incubated with a twofold molar excess of the annealed hybrid in 10 μl of reaction buffer (40 mM Tris–HCl pH 8.0, 10 mM $MgCl_2$, 1 mM dithiothreitol) for 15 min at room temperature while shaking. A fourfold molar excess of non-template DNA (#631), containing biotin at the 5′-end, was added, and the mixture was incubated at 37°C for 10 min.

Streptavidin-coated magnetic beads (25 μl per sample; Sigma S-2415) were washed with 500 μl of binding buffer (20 mM Tris, pH 8.0, 0.15 M NaCl) and resuspended in the same volume of fresh binding buffer. Assembled elongation complexes were then mixed with washed beads, and this was followed by incubation for 30 min at RT with continuous gentle shaking. Unbound complexes were removed by subsequent washing with 500 μl of binding buffer, 500 μl of washing buffer (20 mM Tris–HCl pH 8.0, 0.5 M NaCl, 2 mM $MgCl_2$, 1 mM dithiothreitol), and 500 μl of reaction buffer (Dengl & Cramer, 2009). Beads were resuspended in 10 μl of reaction buffer with 150 mM final concentration of KCl and 0.1 mg/ml BSA. RNA in the elongation complex was labeled at the 3′-end by RNAP (*E. coli* (BioLabs) or *B. subtilis*) activity by adding 0.1 μl of [α^{32}P] UTP (10 mCi/ml) per reaction, followed by incubation at 37 °C for 15 min. Unincorporated nucleotides were washed off by applying 500 μl of reaction buffer, two times 500 μl of washing buffer. Beads with bound ECs were resuspended in RNAse R reaction buffer (20 mM Tris–HCl, pH 7.0; 100 mM KCl, 1.1 mM $MgCl_2$), and 80 pmol of RNase J1 or 1U of RNase Xrn1 (New England Biolabs) or 1U of RNase R (Epicentre Biotechnologies) was added to the reaction. Samples were incubated for 20 min at 37°C. When indicated, samples were denatured for 3 min in 95°C and cooled down prior to the addition of RNases, or the cleavage products were washed off with 500 μl of binding buffer and 2 × 500 μl of washing buffer and resuspended in 10 μl of RNase R buffer after the cleavage. All the reactions were stopped by adding 10 μl of 2× loading buffer [95% formamide and 20 mM EDTA (pH 8.0)].

The RNA ladder was generated as follows: We phosphorylated a 30 nt RNA (the same as #-pRNA but without the 5′ phosphate) with ^{32}P by T4 polynucleotide kinase following the manufacturer's instructions. This RNA was then subjected to alkaline hydrolysis (15 μl reaction containing: 1 μg of yeast RNA, 0.1–1 μg of radiolabeled RNA, 1× alkaline hydrolysis buffer: 50 mM sodium carbonate pH 9.2; 1 mM EDTA; incubated at 95°C for 4 or 7 min, and then, equal amounts of 2× loading buffer [95% formamide and 20 mM EDTA (pH 8.0)] were added.

Samples were resolved on 20% polyacrylamide sequencing gels, and radioactively labeled RNA was detected by exposing the gels to a storage phosphor screen (Fujifilm) overnight. Scanning of the storage screens was done with a Molecular Imager FX (Bio-Rad). In quantitative analyses, background of the appropriate lane was subtracted from the specific signal.

RNAP release assay

Transcription elongation complexes were assembled, and the reaction conditions were as described in the previous *in vitro* experiment. TCs were bound to magnetic streptavidin-coated beads, divided into three tubes, and treated with either buffer (mock treatment) or 80 pmol RNase J1 or 1 U Xrn1 (New England Biolabs) for

20 min at 37°C. The bound (in complex with DNA) and released (free in buffer) RNAPs were separated by using a DYNAL Invitrogen bead separation device. Subsequently, the fractions were analyzed with SDS–PAGE, and RNAPs were detected by Western blotting using mouse monoclonal antibodies against the β subunit of RNA polymerase (clone name 8RB13) and secondary antibodies conjugated with a fluorophore dye (WesternBrightTM MCF-IR, Advansta, 800 nm anti-mouse antibody) and scanned with an Odyssey reader (LI-COR Biosciences). The analysis was done with the Quantity One software (Bio-Rad). The experiment was conducted in two biological replicates.

In silico models

Figures were created using the ICM Molsoft software package (ICM Molsoft (http://www.molsoft.com/icm_browser.html). The PDB codes are in the Figure legends.

UV sensitivity phenotype

Exponential cells of wt (LK1371), Δ*rnjA* (LK1381), Δ*rho* (LK2058), Δ*helD* (LK2329), Δ*rnjA*Δ*rho* (LK2082), and Δ*rnjA*Δ*helD* (LK2336) strains (OD_{600} ~ 0.5) were serially diluted (10-fold dilutions) and plated (100 µl) on duplicate LB agar plates (two sets of plates) without antibiotics. One set of plates was irradiated by UVT-20M (Herolab) at 312 nm for 15 s (0.12 W/cm^2); the other set was not irradiated. Plates were incubated at 37°C overnight. Plates were then analyzed: Colony-forming units (CFU) were counted. UV sensitivity of the mutant strains (KO) was then calculated as the ratio between irradiated vs. non-irradiated cells and normalized to this ratio from the wt strain. As a consequence, the wt ratio is 1. The experiment was conducted 4× (biological replicates). All analyses were done on the log scale. The *P*-values were computed using two-tailed unpaired *t*-test.

Data availability

The datasets produced in this study are available in the following databases:

- RNAseq data: E-MTAB-5660 (www.ebi.ac.uk/arrayexpressexperiments/E-MTAB-5660)
- ChIPseq data: E-MTAB-5659 (www.ebi.ac.uk/arrayexpressexperiments/E-MTAB-5659)

Expanded View for this article is available online.

Acknowledgements
We would like to acknowledge the Czech Science Foundation—originally by grant P305/12/G034 and subsequently by 19-12956S (to LK); Czech Research Infrastructure for Systems Biology C4SYS (project LM2015055); Light Microscopy Core Facility, IMG ASCR, Prague, Czech Republic (MEYS, LM2015062), OPPK (CZ.2.16/3.1.00/21547), and LO1419; and electron microscopy facility (LO1509, Ministry of Education, Youth, and Sports of the Czech Republic). MP was supported by Charles University grants PRIMUS/MED/26 and UNCE 204013. CC was supported by the Agence Nationale de la Recherche (ARNr-QC) and the Labex (Dynamo) program. The authors thank Dr. M. Modrák for the discussion on statistical analyses.

Author contributions
CC and LK conceptualized the study and designed the experiments. MŠ, JW, MP, PS, OB, OK, and HŠ performed the experiments. MŠ, MP, and LK analyzed the data. IB performed *in silico* modeling. LK and CC wrote the manuscript; all the other authors contributed to the final revised version.

Conflict of interest
The authors declare that they have no conflict of interest.

References

Arraiano CM, Andrade JM, Domingues S, Guinote IB, Malecki M, Matos RG, Moreira RN, Pobre V, Reis FP, Saramago M *et al* (2010) The critical role of RNA processing and degradation in the control of gene expression. *FEMS Microbiol Rev* 34: 883 – 923

Baejen C, Andreani J, Torkler P, Battaglia S, Schwalb B, Lidschreiber M, Maier KC, Boltendahl A, Rus P, Esslinger S *et al* (2017) Genome-wide analysis of RNA polymerase II termination at protein-coding genes. *Mol Cell* 66: 38 – 49 e36

Bar-Nahum G, Epshtein V, Ruckenstein AE, Rafikov R, Mustaev A, Nudler E (2005) A ratchet mechanism of transcription elongation and its control. *Cell* 120: 183 – 193

Bidnenko V, Nicolas P, Grylak-Mielnicka A, Delumeau O, Auger S, Aucouturier A, Guerin C, Repoila F, Bardowski J, Aymerich S *et al* (2017) Termination factor Rho: from the control of pervasive transcription to cell fate determination in *Bacillus subtilis*. *PLoS Genet* 13: e1006909

Bradford MM (1976) A rapid and sensitive method for the quantitation of microgram quantities of protein utilizing the principle of protein-dye binding. *Anal Biochem* 72: 248 – 254

Buskirk AR, Green R (2017) Ribosome pausing, arrest and rescue in bacteria and eukaryotes. *Philos Trans R Soc Lond B Biol Sci* 372: 20160183

Cascante-Estepa N, Gunka K, Stulke J (2016) Localization of components of the RNA-degrading machine in *Bacillus subtilis*. *Front Microbiol* 7: 1492

Chang BY, Doi RH (1990) Overproduction, purification, and characterization of *Bacillus subtilis* RNA polymerase sigma A factor. *J Bacteriol* 172: 3257 – 3263

Condon C, Pellegrini O, Mathy N, Benard L, Redko Y, Oussenko IA, Deikus G, Bechhofer DH (2008) Assay of *Bacillus subtilis* ribonucleases *in vitro*. *Methods Enzymol* 447: 277 – 308

Condon C (2010) What is the role of RNase J in mRNA turnover? *RNA Biol* 7: 316 – 321

Condon C, Piton J, Braun F (2018) Distribution of the ribosome associated endonuclease Rae1 and the potential role of conserved amino acids in codon recognition. *RNA Biol* 15: 683 – 688

Costanzo G, Pino S, Timperio AM, Sponer JE, Sponer J, Novakova O, Sedo O, Zdrahal Z, Di Mauro E (2016) Non-enzymatic oligomerization of 3′, 5′ cyclic AMP. *PLoS One* 11: e0165723

Cozy LM, Kearns DB (2010) Gene position in a long operon governs motility development in *Bacillus subtilis*. *Mol Microbiol* 76: 273 – 285

Dengl S, Cramer P (2009) Torpedo nuclease Rat1 is insufficient to terminate RNA polymerase II *in vitro*. *J Biol Chem* 284: 21270 – 21279

Doherty GP, Fogg MJ, Wilkinson AJ, Lewis PJ (2010) Small subunits of RNA polymerase: localization, levels and implications for core enzyme composition. *Microbiology* 156: 3532 – 3543

Dorleans A, Li de la Sierra-Gallay I, Piton J, Zig L, Gilet L, Putzer H, Condon C (2011) Molecular basis for the recognition and cleavage of RNA by the bifunctional 5′-3′ exo/endoribonuclease RNase J. *Structure* 19: 1252 – 1261

Durand S, Gilet L, Bessieres P, Nicolas P, Condon C (2012) Three essential ribonucleases-RNase Y, J1, and III-control the abundance of a majority of *Bacillus subtilis* mRNAs. *PLoS Genet* 8: e1002520

Eiamphungporn W, Helmann JD (2008) The *Bacillus subtilis* sigma(M) regulon and its contribution to cell envelope stress responses. *Mol Microbiol* 67: 830 – 848

Epshtein V, Nudler E (2003) Cooperation between RNA polymerase molecules in transcription elongation. *Science* 300: 801 – 805

Epshtein V, Dutta D, Wade J, Nudler E (2010) An allosteric mechanism of Rho-dependent transcription termination. *Nature* 463: 245 – 249

Epshtein V, Kamarthapu V, McGary K, Svetlov V, Ueberheide B, Proshkin S, Mironov A, Nudler E (2014) UvrD facilitates DNA repair by pulling RNA polymerase backwards. *Nature* 505: 372 – 377

Even S, Pellegrini O, Zig L, Labas V, Vinh J, Brechemmier-Baey D, Putzer H (2005) Ribonucleases J1 and J2: two novel endoribonucleases in *B. subtilis* with functional homology to *E. coli* RNase E. *Nucleic Acids Res* 33: 2141 – 2152

Fan J, Leroux-Coyau M, Savery NJ, Strick TR (2016) Reconstruction of bacterial transcription-coupled repair at single-molecule resolution. *Nature* 536: 234 – 237

Figaro S, Durand S, Gilet L, Cayet N, Sachse M, Condon C (2013) *Bacillus subtilis* mutants with knockouts of the genes encoding ribonucleases RNase Y and RNase J1 are viable, with major defects in cell morphology, sporulation, and competence. *J Bacteriol* 195: 2340 – 2348

Frindert J, Zhang Y, Nubel G, Kahloon M, Kolmar L, Hotz-Wagenblatt A, Burhenne J, Haefeli WE, Jaschke A (2018) Identification, biosynthesis, and decapping of NAD-capped RNAs in *B. subtilis*. *Cell Rep* 24: 1890 – 1901 e1898

Fukushima T, Afkham A, Kurosawa S, Tanabe T, Yamamoto H, Sekiguchi J (2006) A new D, L-endopeptidase gene product, YojL (renamed CwlS), plays a role in cell separation with LytE and LytF in *Bacillus subtilis*. *J Bacteriol* 188: 5541 – 5550

Gilet L, DiChiara JM, Figaro S, Bechhofer DH, Condon C (2015) Small stable RNA maturation and turnover in *Bacillus subtilis*. *Mol Microbiol* 95: 270 – 282

Gimpel M, Brantl S (2017) Dual-function small regulatory RNAs in bacteria. *Mol Microbiol* 103: 387 – 397

Goodsell DS (2001) The molecular perspective: ultraviolet light and pyrimidine dimers. *Oncologist* 6: 298 – 299

Guo X, Myasnikov AG, Chen J, Crucifix C, Papai G, Takacs M, Schultz P, Weixlbaumer A (2018) Structural basis for NusA stabilized transcriptional pausing. *Mol Cell* 69: 816 – 827 e814

Hamperl S, Cimprich KA (2016) Conflict resolution in the genome: how transcription and replication make it work. *Cell* 167: 1455 – 1467

He B, Zalkin H (1992) Repression of *Escherichia coli* purB is by a transcriptional roadblock mechanism. *J Bacteriol* 174: 7121 – 7127

Helmann JD, Masiarz FR, Chamberlin MJ (1988) Isolation and characterization of the *Bacillus subtilis* sigma 28 factor. *J Bacteriol* 170: 1560 – 1567

Hsieh PK, Richards J, Liu Q, Belasco JG (2013) Specificity of RppH-dependent RNA degradation in *Bacillus subtilis*. *Proc Natl Acad Sci USA* 110: 8864 – 8869

Hunt A, Rawlins JP, Thomaides HB, Errington J (2006) Functional analysis of 11 putative essential genes in *Bacillus subtilis*. *Microbiology* 152: 2895 – 2907

Janniere L, Canceill D, Suski C, Kanga S, Dalmais B, Lestini R, Monnier AF, Chapuis J, Bolotin A, Titok M *et al* (2007) Genetic evidence for a link between glycolysis and DNA replication. *PLoS One* 2: e447

Jervis AJ, Thackray PD, Houston CW, Horsburgh MJ, Moir A (2007) SigM-responsive genes of *Bacillus subtilis* and their promoters. *J Bacteriol* 189: 4534 – 4538

Jimenez RM, Polanco JA, Luptak A (2015) Chemistry and biology of self-cleaving ribozymes. *Trends Biochem Sci* 40: 648 – 661

Juang YL, Helmann JD (1994) A promoter melting region in the primary sigma factor of *Bacillus subtilis*. Identification of functionally important aromatic amino acids. *J Mol Biol* 235: 1470 – 1488

Kang JY, Mishanina TV, Landick R, Darst SA (2019) Mechanisms of transcriptional pausing in bacteria. *J Mol Biol* 431: 4007 – 4029

Kawai Y, Asai K, Errington J (2009) Partial functional redundancy of MreB isoforms, MreB, Mbl and MreBH, in cell morphogenesis of *Bacillus subtilis*. *Mol Microbiol* 73: 719 – 731

Keller AN, Yang X, Wiedermannova J, Delumeau O, Krasny L, Lewis PJ (2014) epsilon, a new subunit of RNA polymerase found in gram-positive bacteria. *J Bacteriol* 196: 3622 – 3632

Kim M, Krogan NJ, Vasiljeva L, Rando OJ, Nedea E, Greenblatt JF, Buratowski S (2004) The yeast Rat1 exonuclease promotes transcription termination by RNA polymerase II. *Nature* 432: 517 – 522

Kim D, Langmead B, Salzberg SL (2015) HISAT: a fast spliced aligner with low memory requirements. *Nat Methods* 12: 357 – 360

Kireeva ML, Kashlev M (2009) Mechanism of sequence-specific pausing of bacterial RNA polymerase. *Proc Natl Acad Sci USA* 106: 8900 – 8905

Kohler R, Mooney RA, Mills DJ, Landick R, Cramer P (2017) Architecture of a transcribing-translating expressome. *Science* 356: 194 – 197

Komissarova N, Kireeva ML, Becker J, Sidorenkov I, Kashlev M (2003) Engineering of elongation complexes of bacterial and yeast RNA polymerases. *Methods Enzymol* 371: 233 – 251

Krajewski WW, Fu X, Wilkinson M, Cronin NB, Dillingham MS, Wigley DB (2014) Structural basis for translocation by AddAB helicase-nuclease and its arrest at chi sites. *Nature* 508: 416 – 419

Krasny L, Vacik T, Fucik V, Jonak J (2000) Cloning and characterization of the str operon and elongation factor Tu expression in Bacillus stearothermophilus. *J Bacteriol* 182: 6114 – 6122

Kusuya Y, Kurokawa K, Ishikawa S, Ogasawara N, Oshima T (2011) Transcription factor GreA contributes to resolving promoter-proximal pausing of RNA polymerase in *Bacillus subtilis* cells. *J Bacteriol* 193: 3090 – 3099

Larson MH, Greenleaf WJ, Landick R, Block SM (2008) Applied force reveals mechanistic and energetic details of transcription termination. *Cell* 132: 971 – 982

Le TT, Yang Y, Tan C, Suhanovsky MM, Fulbright RM Jr, Inman JT, Li M, Lee J, Perelman S, Roberts JW *et al* (2018) Mfd dynamically regulates transcription via a release and catch-up mechanism. *Cell* 172: 344 – 357 e315

LeBlanc SJ, Gauer JW, Hao P, Case BC, Hingorani MM, Weninger KR, Erie DA (2018) Coordinated protein and DNA conformational changes govern mismatch repair initiation by MutS. *Nucleic Acids Res* 46: 10782 – 10795

Lehnik-Habrink M, Lewis RJ, Mader U, Stulke J (2012) RNA degradation in *Bacillus subtilis*: an interplay of essential endo- and exoribonucleases. *Mol Microbiol* 84: 1005 – 1017

Lei Y, Oshima T, Ogasawara N, Ishikawa S (2013) Functional analysis of the protein Veg, which stimulates biofilm formation in *Bacillus subtilis*. *J Bacteriol* 195: 1697 – 1705

Lenhart JS, Schroeder JW, Walsh BW, Simmons LA (2012) DNA repair and genome maintenance in *Bacillus subtilis*. *Microbiol Mol Biol Reu* 76: 530 – 564

Li H, Handsaker B, Wysoker A, Fennell T, Ruan J, Homer N, Marth G, Abecasis G, Durbin R Genome Project Data Processing (2009) The sequence alignment/map format and SAMtools. *Bioinformatics* 25: 2078 – 2079

Liu J, Hanne J, Britton BM, Bennett J, Kim D, Lee JB, Fishel R (2016) Cascading MutS and MutL sliding clamps control DNA diffusion to activate mismatch repair. *Nature* 539: 583 – 587

Love MI, Huber W, Anders S (2014) Moderated estimation of fold change and dispersion for RNA-seq data with DESeq2. *Genome Biol* 15: 550

Luo W, Bentley D (2004) A ribonucleolytic rat torpedoes RNA polymerase II. *Cell* 119: 911 – 914

Ma C, Mobli M, Yang X, Keller AN, King GF, Lewis PJ (2015) RNA polymerase-induced remodelling of NusA produces a pause enhancement complex. *Nucleic Acids Res* 43: 2829 – 2840

Mathy N, Benard L, Pellegrini O, Daou R, Wen T, Condon C (2007) 5′-to-3′ exoribonuclease activity in bacteria: role of RNase J1 in rRNA maturation and 5′ stability of mRNA. *Cell* 129: 681 – 692

Mathy N, Hebert A, Mervelet P, Benard L, Dorleans A, Li de la Sierra-Gallay I, Noirot P, Putzer H, Condon C (2010) *Bacillus subtilis* ribonucleases J1 and J2 form a complex with altered enzyme behaviour. *Mol Microbiol* 75: 489 – 498

Mirel DB, Lustre VM, Chamberlin MJ (1992) An operon of *Bacillus subtilis* motility genes transcribed by the sigma D form of RNA polymerase. *J Bacteriol* 174: 4197 – 4204

Molle V, Fujita M, Jensen ST, Eichenberger P, Gonzalez-Pastor JE, Liu JS, Losick R (2003) The Spo0A regulon of *Bacillus subtilis*. *Mol Microbiol* 50: 1683 – 1701

Mori F, Tanji K, Miki Y, Toyoshima Y, Sasaki H, Yoshida M, Kakita A, Takahashi H, Wakabayashi K (2018) Immunohistochemical localization of exoribonucleases (DIS3L2 and XRN1) in intranuclear inclusion body disease. *Neurosci Lett* 662: 389 – 394

Nadkarni A, Burns JA, Gandolfi A, Chowdhury MA, Cartularo L, Berens C, Geacintov NE, Scicchitano DA (2016) Nucleotide excision repair and transcription-coupled DNA repair Abrogate the impact of DNA damage on transcription. *J Biol Chem* 291: 848 – 861

Nicolas P, Mader U, Dervyn E, Rochat T, Leduc A, Pigeonneau N, Bidnenko E, Marchadier E, Hoebeke M, Aymerich S *et al* (2012) Condition-dependent transcriptome reveals high-level regulatory architecture in *Bacillus subtilis*. *Science* 335: 1103 – 1106

Nudler E (2012) RNA polymerase backtracking in gene regulation and genome instability. *Cell* 149: 1438 – 1445

Panova N, Zborníková E, Šimák O, Pohl R, Kolář M, Bogdanová K, Večeřová R, Seydlová G, Fišer R, Hadravová R *et al* (2015) Insights into the mechanism of action of bactericidal lipophosphonoxins. *PLoS One* 10: e0145918

Park J, Kang M, Kim M (2015) Unraveling the mechanistic features of RNA polymerase II termination by the 5′-3′ exoribonuclease Rat1. *Nucleic Acids Res* 43: 2625 – 2637

Pearson EL, Moore CL (2013) Dismantling promoter-driven RNA polymerase II transcription complexes *in vitro* by the termination factor Rat1. *J Biol Chem* 288: 19750 – 19759

Peters JM, Mooney RA, Kuan PF, Rowland JL, Keles S, Landick R (2009) Rho directs widespread termination of intragenic and stable RNA transcription. *Proc Natl Acad Sci USA* 106: 15406 – 15411

Phung DK, Rinaldi D, Langendijk-Genevaux PS, Quentin Y, Carpousis AJ, Clouet-d'Orval B (2013) Archaeal beta-CASP ribonucleases of the aCPSF1 family are orthologs of the eukaryal CPSF-73 factor. *Nucleic Acids Res* 41: 1091 – 1103

Qi Y, Hulett FM (1998) PhoP-P and RNA polymerase sigmaA holoenzyme are sufficient for transcription of Pho regulon promoters in *Bacillus subtilis*: PhoP-P activator sites within the coding region stimulate transcription *in vitro*. *Mol Microbiol* 28: 1187 – 1197

Radhakrishnan A, Green R (2016) Connections underlying translation and mRNA stability. *J Mol Biol* 428: 3558 – 3564

Ramaniuk O, Cerny M, Krasny L, Vohradsky J (2017) Kinetic modelling and meta-analysis of the *B. subtilis* SigA regulatory network during spore germination and outgrowth. *Biochim Biophys Acta Gene Regul Mech* 1860: 894 – 904

Ramirez F, Ryan DP, Gruning B, Bhardwaj V, Kilpert F, Richter AS, Heyne S, Dundar F, Manke T (2016) deepTools2: a next generation web server for deep-sequencing data analysis. *Nucleic Acids Res* 44: W160 – W165

Randall JR, Hirst WG, Simmons LA (2017) Substrate specificity for bacterial RNase HII and HIII is influenced by metal availability. *J Bacteriol* 200: e00401-17

Ruff EF, Record MT Jr, Artsimovitch I (2015) Initial events in bacterial transcription initiation. *Biomolecules* 5: 1035 – 1062

Sanders K, Lin CL, Smith AJ, Cronin N, Fisher G, Eftychidis V, McGlynn P, Savery NJ, Wigley DB, Dillingham MS (2017) The structure and function of an RNA polymerase interaction domain in the PcrA/UvrD helicase. *Nucleic Acids Res* 45: 3875 – 3887

Schroeder JW, Randall JR, Hirst WG, O'Donnell ME, Simmons LA (2017) Mutagenic cost of ribonucleotides in bacterial DNA. *Proc Natl Acad Sci USA* 114: 11733 – 11738

Serizawa M, Yamamoto H, Yamaguchi H, Fujita Y, Kobayashi K, Ogasawara N, Sekiguchi J (2004) Systematic analysis of SigD-regulated genes in *Bacillus subtilis* by DNA microarray and Northern blotting analyses. *Gene* 329: 125 – 136

Shepanek NA, Smith RF, Tyer ZE, Royall GD, Allen KS (1989) Behavioral and neuroanatomical sequelae of prenatal naloxone administration in the rat. *Neurotoxicol Teratol* 11: 441 – 446

Sikova M, Janouskova M, Ramaniuk O, Palenikova P, Pospisil J, Bartl P, Suder A, Pajer P, Kubickova P, Pavlis O *et al* (2018) Ms1 RNA increases the amount of RNA polymerase in *Mycobacterium smegmatis*. *Mol Microbiol* 111: 354 – 372

Sun M, Schwalb B, Pirkl N, Maier KC, Schenk A, Failmezger H, Tresch A, Cramer P (2013) Global analysis of eukaryotic mRNA degradation reveals Xrn1-dependent buffering of transcript levels. *Mol Cell* 52: 52 – 62

Tagami S, Sekine S, Minakhin L, Esyunina D, Akasaka R, Shirouzu M, Kulbachinskiy A, Severinov K, Yokoyama S (2014) Structural basis for promoter specificity switching of RNA polymerase by a phage factor. *Genes Dev* 28: 521 – 531

Thorvaldsdottir H, Robinson JT, Mesirov JP (2013) Integrative Genomics Viewer (IGV): high-performance genomics data visualization and exploration. *Brief Bioinform* 14: 178 – 192

Tornaletti S, Hanawalt PC (1999) Effect of DNA lesions on transcription elongation. *Biochimie* 81: 139 – 146

Toulme F, Mosrin-Huaman C, Sparkowski J, Das A, Leng M, Rahmouni AR (2000) GreA and GreB proteins revive backtracked RNA polymerase *in vivo* by promoting transcript trimming. *EMBO J* 19: 6853 – 6859

Turner MS, Helmann JD (2000) Mutations in multidrug efflux homologs, sugar isomerases, and antimicrobial biosynthesis genes differentially elevate activity of the sigma(X) and sigma(W) factors in *Bacillus subtilis*. *J Bacteriol* 182: 5202 – 5210

Twist KA, Campbell EA, Deighan P, Nechaev S, Jain V, Geiduschek EP, Hochschild A, Darst SA (2011) Crystal structure of the bacteriophage T4 late-transcription coactivator gp33 with the beta-subunit flap domain of *Escherichia coli* RNA polymerase. *Proc Natl Acad Sci USA* 108: 19961 – 19966

Weiss A, Shaw LN (2015) Small things considered: the small accessory subunits of RNA polymerase in Gram-positive bacteria. *FEMS Microbiol Rev* 39: 541 – 554

Wiedermannova J, Sudzinova P, Koval T, Rabatinova A, Sanderova H, Ramaniuk O, Rittich S, Dohnalek J, Fu Z, Halada P *et al* (2014)

Characterization of HelD, an interacting partner of RNA polymerase from *Bacillus subtilis*. *Nucleic Acids Res* 42: 5151 – 5163

Yakhnin AV, Murakami KS, Babitzke P (2016) NusG is a sequence-specific RNA polymerase pause factor that binds to the non-template DNA within the paused transcription bubble. *J Biol Chem* 291: 5299 – 5308

Yang XC, Sullivan KD, Marzluff WF, Dominski Z (2009) Studies of the 5′ exonuclease and endonuclease activities of CPSF-73 in histone pre-mRNA processing. *Mol Cell Biol* 29: 31 – 42

Zhang Y, Mooney RA, Grass JA, Sivaramakrishnan P, Herman C, Landick R, Wang JD (2014) DksA guards elongating RNA polymerase against ribosome-stalling-induced arrest. *Mol Cell* 53: 766 – 778

Zhu B, Stulke J (2018) SubtiWiki in 2018: from genes and proteins to functional network annotation of the model organism Bacillus subtilis. *Nucleic Acids Res* 46: D743 – D748

Zweers JC, Nicolas P, Wiegert T, van Dijl JM, Denham EL (2012) Definition of the sigma(W) regulon of *Bacillus subtilis* in the absence of stress. *PLoS One* 7: e48471

Expanded View Figures

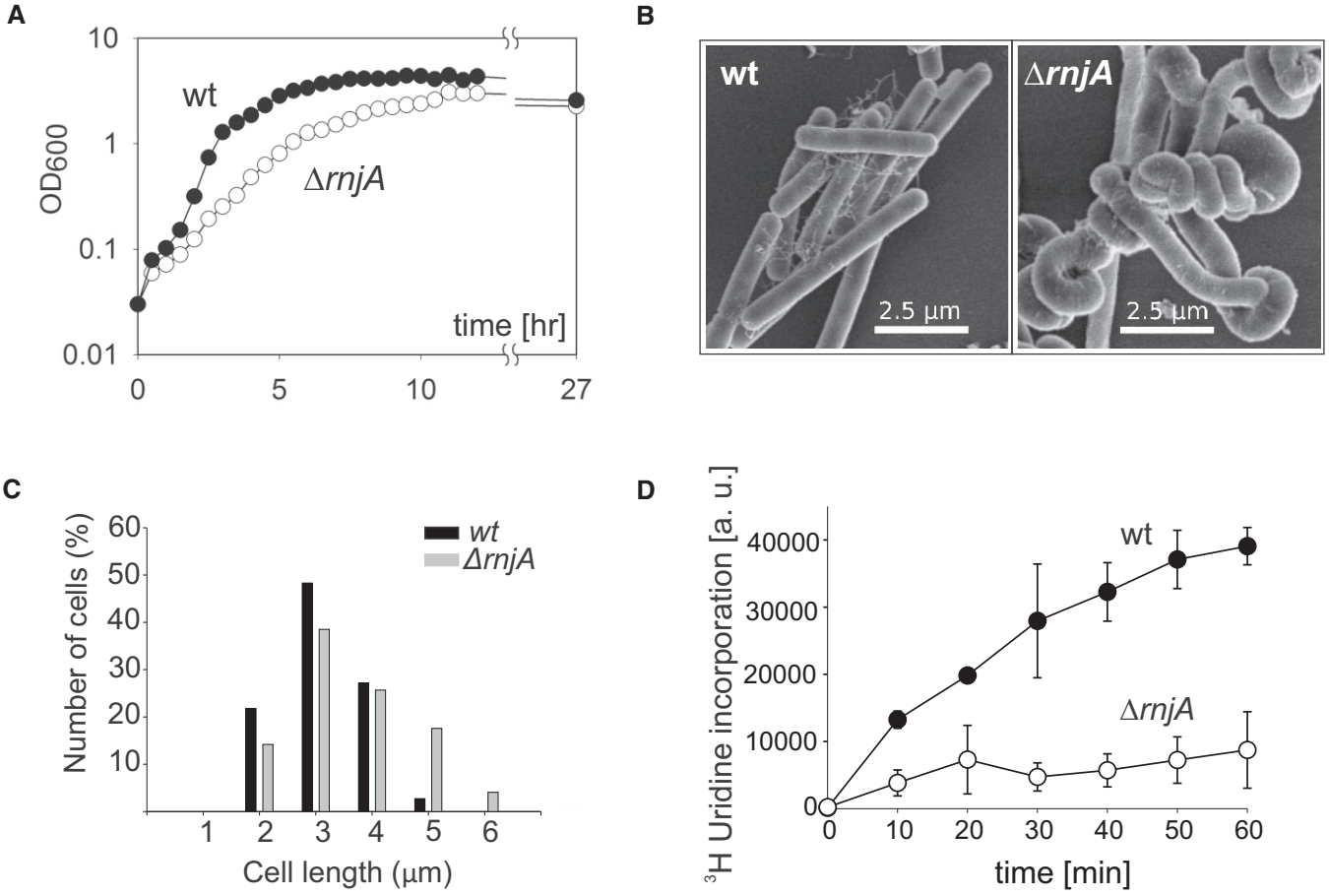

Figure EV1. Phenotypic characterization of the Δ*rnjA* strain.

A Growth of *Bacillus subtilis* wt (LK1371) and *ΔrnjA* (LK1381) strains in LB medium at 37°C.

B Morphology of wt (LK1371) and *ΔrnjA* (LK1381) strains as captured by electron microscopy of exponential phase cells (OD_{600} 0.5).

C Quantification of cells length of exponentially growing (OD_{600} 0.5) wt (LK1371) and *ΔrnjA* (LK1381) cells stained with a membrane dye (NileRed, Sigma-Aldrich). The analysis was performed on two sets consisting of 100 cells each. Due to technical considerations, the length of only non-spiral cells was measured. The length of the cells was analyzed by Fiji ImageJ.

D Total RNA synthesis wt (LK1371) and *ΔrnjA* (LK1381) strains normalized to cell density (OD_{600}). The data points are averages from two independent experiments (each done in technical duplicates); the error bars show the range.

Source data are available online for this figure.

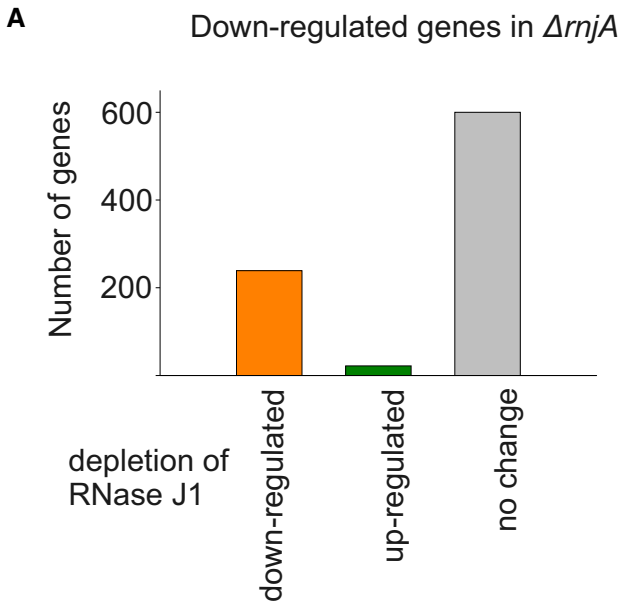

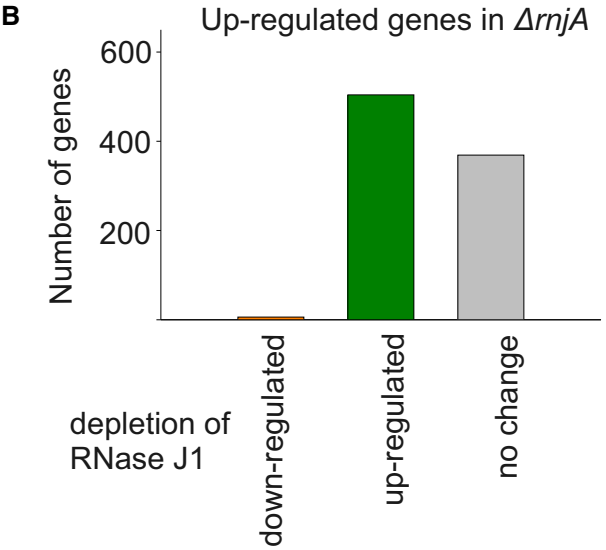

Figure EV2. Comparison of differentially regulated genes in RNase J1 depletion vs. deletion strains.

A Comparison of all downregulated genes in the Δ*rnjA* (LK1381) strain with the RNase J1-depleted strain (Durand *et al*, 2012). A small number of genes from depletion strain had opposite expression patterns. One-third of genes had the same expression pattern. Data from Table EV1 and Durand *et al* (2012).

B Comparison of all upregulated genes in the Δ*rnjA* (LK1381) strain with the RNase J1-depleted strain. A majority of genes had the same expression pattern; only six genes had opposite expression patterns. Data from Table EV2 and Durand *et al* (2012).

Source data are available online for this figure.

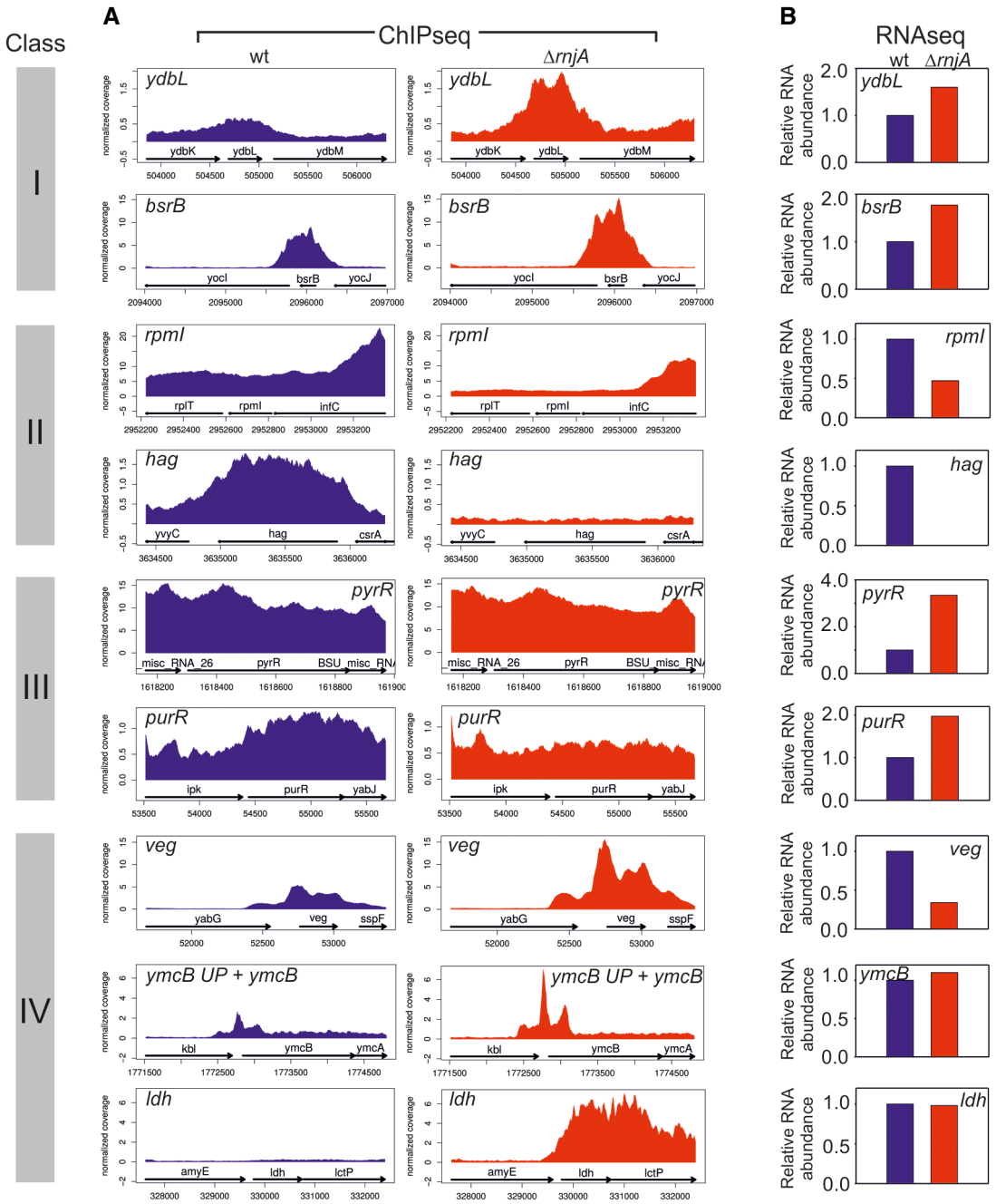

Figure EV3. Detailed comparisons of the RNAseq and ChIPseq data for selected genes.

A RNAP occupancy at selected genes (gene names indicated) in wt (blue) and Δ*rnjA* (red) strains. *ymcB* UP—5′ untranslated region (UTR) of the *ymcB* gene. Data represent mean of normalized RNAP coverage from three independent ChIPseq experiments.

B RNA abundance data for genes shown in (A). The genes are grouped into classes (indicated with colored bars with roman numerals) according to trends they displayed between wt and Δ*rnjA* with respect to gene occupancy and relative expression. Class I: Increased gene occupancy in Δ*rnjA* is accompanied by increased gene expression; class II: decreased gene occupancy in Δ*rnjA* is accompanied by decreased gene expression; class III: decreased or equal gene occupancy in Δ*rnjA* is accompanied by increased gene expression; and class IV: increased gene occupancy in Δ*rnjA* is accompanied by decreased or equal gene expression. The relative RNA level in wt was set as 1. Data represent mean of normalized read coverage from three independent RNAseq experiments.

Source data are available online for this figure.

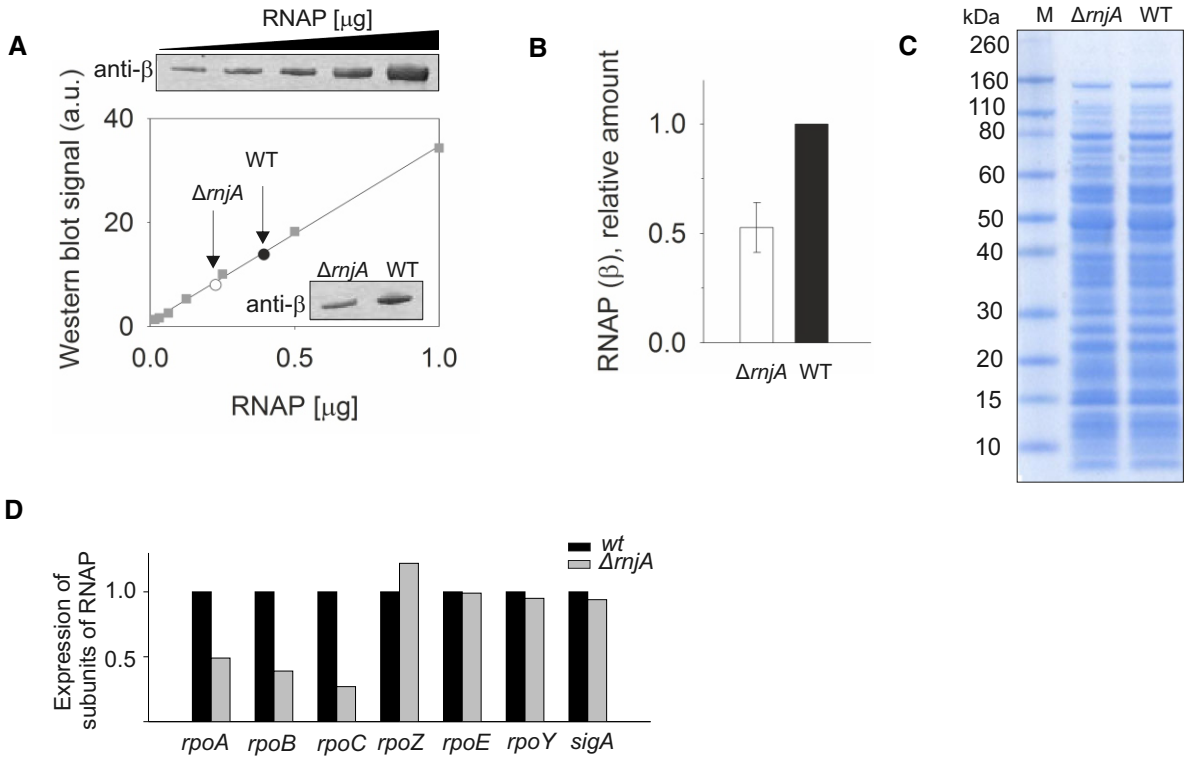

Figure EV4. Amount of RNAP in wt and Δ*rnjA* strains.

A Determination of the amount of RNAP in wt (black circle) and Δ*rnjA* (open circle) strains by Western blotting with monoclonal antibody against the β subunit of RNAP. The data for the calibration curve (squares) are shown above the graph; the data for the two strains are in the inset.

B Quantitation of the data shown in (A). The amount of RNAP in wt was set as 1. The experiment was performed three times on three different days. The bars show the average, the error bars ± SD.

C The amounts of cell lysates used to determine relative amounts of β. 5 μg of total protein was loaded per lane.

D Relative mRNA levels of three main RNAP subunits in wt [black bars, set as 1 (LK1371)] and Δ*rnjA* (gray bars; LK1381) strains. The main RNAP subunits (*rpoA*, *rpoB*, *rpoC*) had lower expression compared to wt. The expression of small subunits (ω, δ and ε) and *sigA* was unchanged.

Source data are available online for this figure.

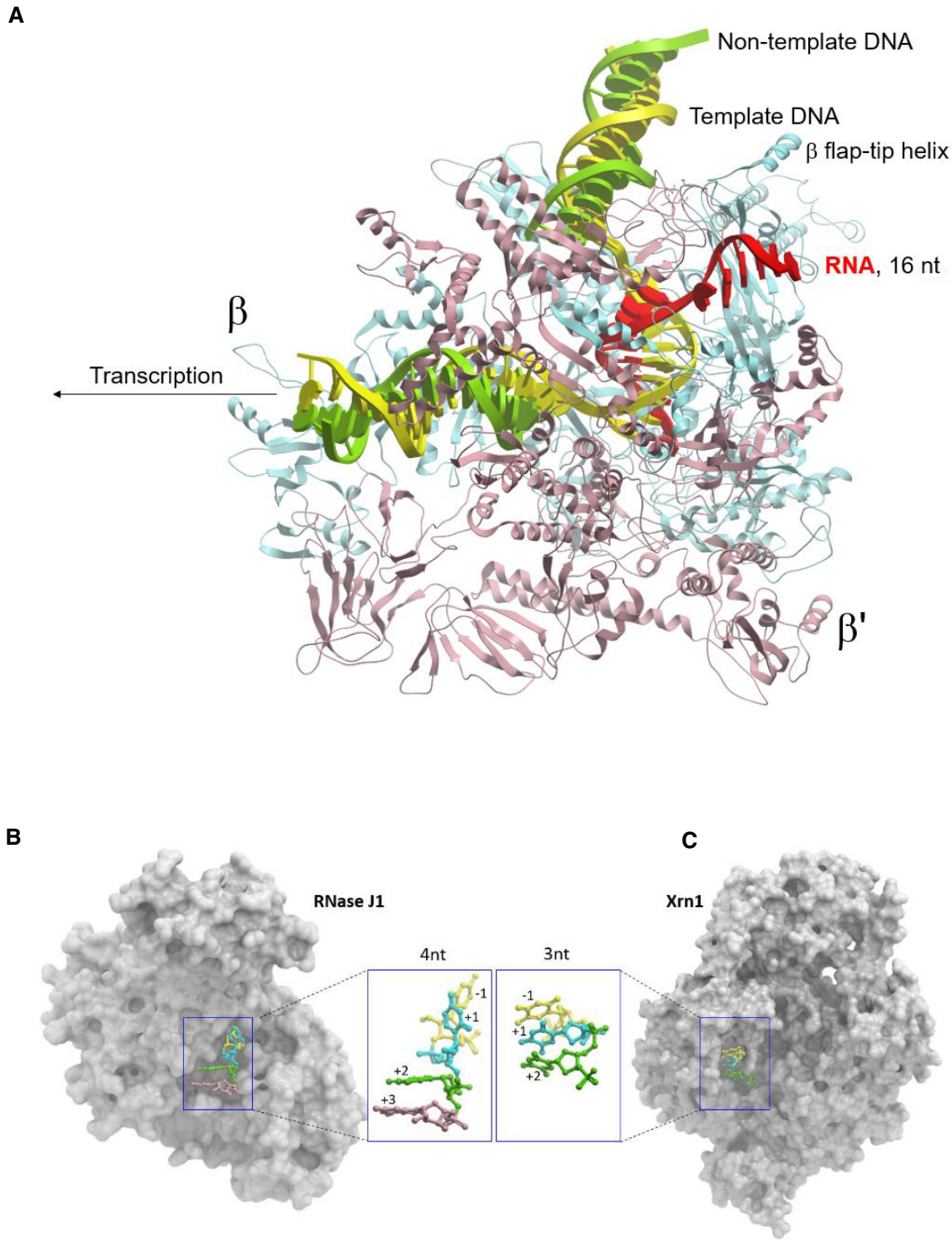

Figure EV5. Paths of RNA in RNAP, RNase J1, and Xrn1.

A Overall view of RNAP-16nt-mRNA (PDB id: 6flq). RNAP and bound nucleic acids are shown as cartoon (β—blue, β′—salmon, template DNA—yellow, non-template DNA—green, mRNA—red).

B Overall view of RNaseJ1-4nt-RNA substrate complex (PDB id: 3t3o).

C Overall view of Xrn1-3nt-RNA substrate complex (PDB id: 2y35). RNaseJ1/Xrn1 are shown as surface representation. The nucleic acid substrates are shown in ball and stick format. The carbon atoms of individual nucleotides are colored relative to the position of the scissile bond: yellow (−1), cyan (+1), green (+2), and pink (+3).

APPENDIX

TITLE:

The Torpedo Effect in *Bacillus subtilis*: RNase J1 Resolves Stalled Transcription Complexes

Michaela Šiková[1#], Jana Wiedermannová[1#], Martin Převorovský[2], Ivan Barvík[3], Petra Sudzinová[1], Olga Kofroňová[1], Oldřich Benada[1], Hana Šanderová[1], Ciarán Condon[4], Libor Krásný[1]*

[1] *Institute of Microbiology of the Czech Academy of Sciences, CZ-142 20 Prague 4, Czech Republic;*
[2] *Department of Cell Biology, Faculty of Science, Charles University, Viničná 7, 128 43 Prague, Czech Republic*
[3] *Division of Biomolecular Physics, Institute of Physics, Faculty of Mathematics and Physics, Charles University in Prague, Ke Karlovu 5, 121 16 Prague 2, Czech Republic*
[4] *UMR 8261 (CNRS-Univ. Paris Diderot, Sorbonne Paris Cité), Institut de Biologie Physico-Chimique, 13 rue Pierre et Marie Curie, 75005 Paris, France.*

[#] These authors contributed equally.
* Correspondence: krasny@biomed.cas.cz

Contents

Figure S1. RT-qPCR validation of RNAseq data.

Expression of selected genes was analyzed by RT-qPCR in wt (LK1371) and *ΔrnjA* (LK1381) strains. New RNA purifications were performed, different from those used in RNAseq experiments. The upper panel for each gene represents RNAseq values (dark colors), the bottom panel represents RT-qPCR values (light colors). Wt – blue and light blue, *ΔrnjA* – red and light red. The RNA level in wt was set as 1. The average value represents four biological replicates, error bars ±SEM.

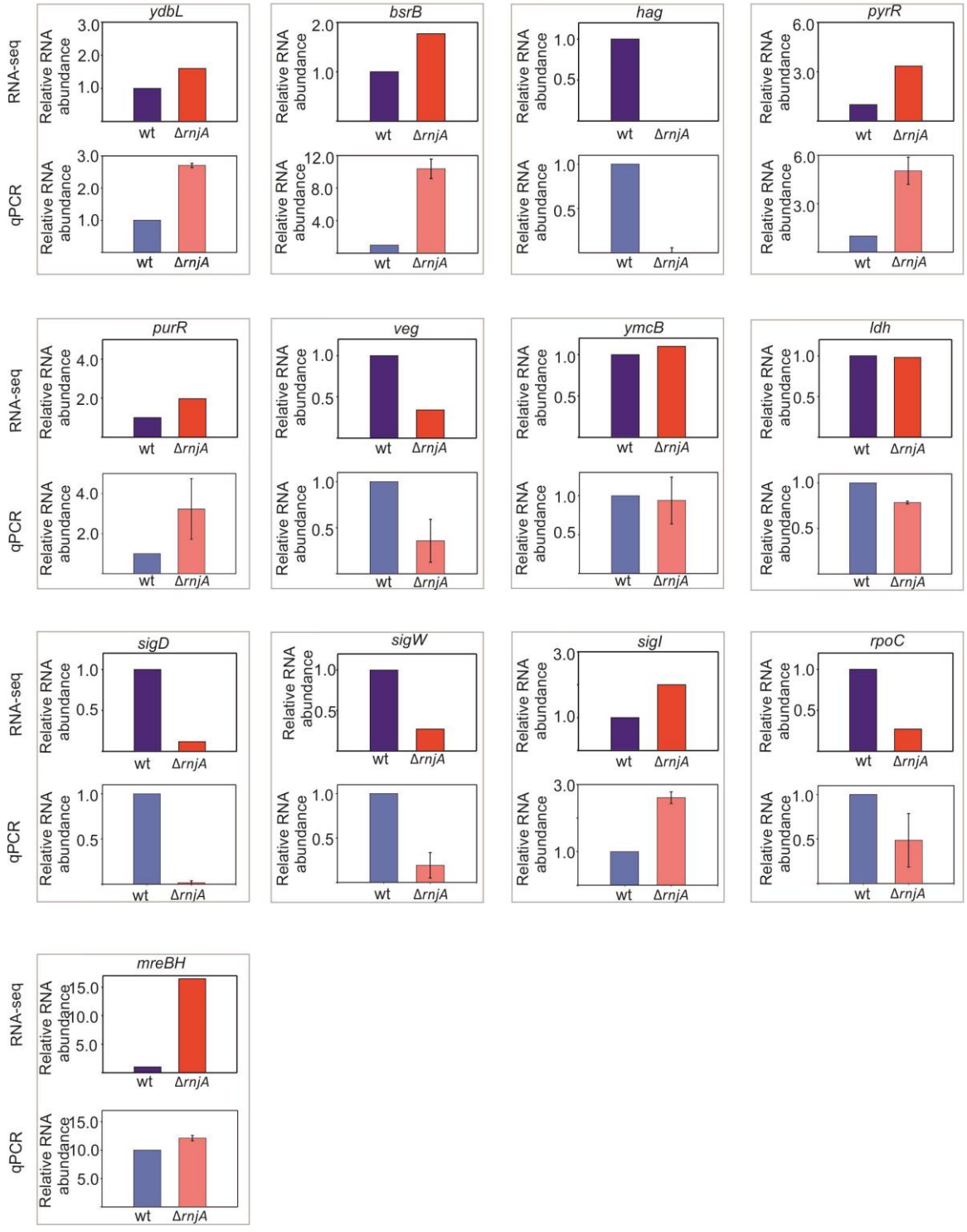

Figure S2. Gene ontology categories of differentially regulated genes in the Δ*rnjA* strain.

Comparison of up- and down-regulated genes of the *ΔrnjA* (LK1381) strain categorized into six main ontology categories according to (Zhu and Stulke, 2018). Green bars: upregulated genes, orange bars: down-regulated genes; grey bars: no differences between *wt* (LK1371) and *ΔrnjA* (LK1381) strain.

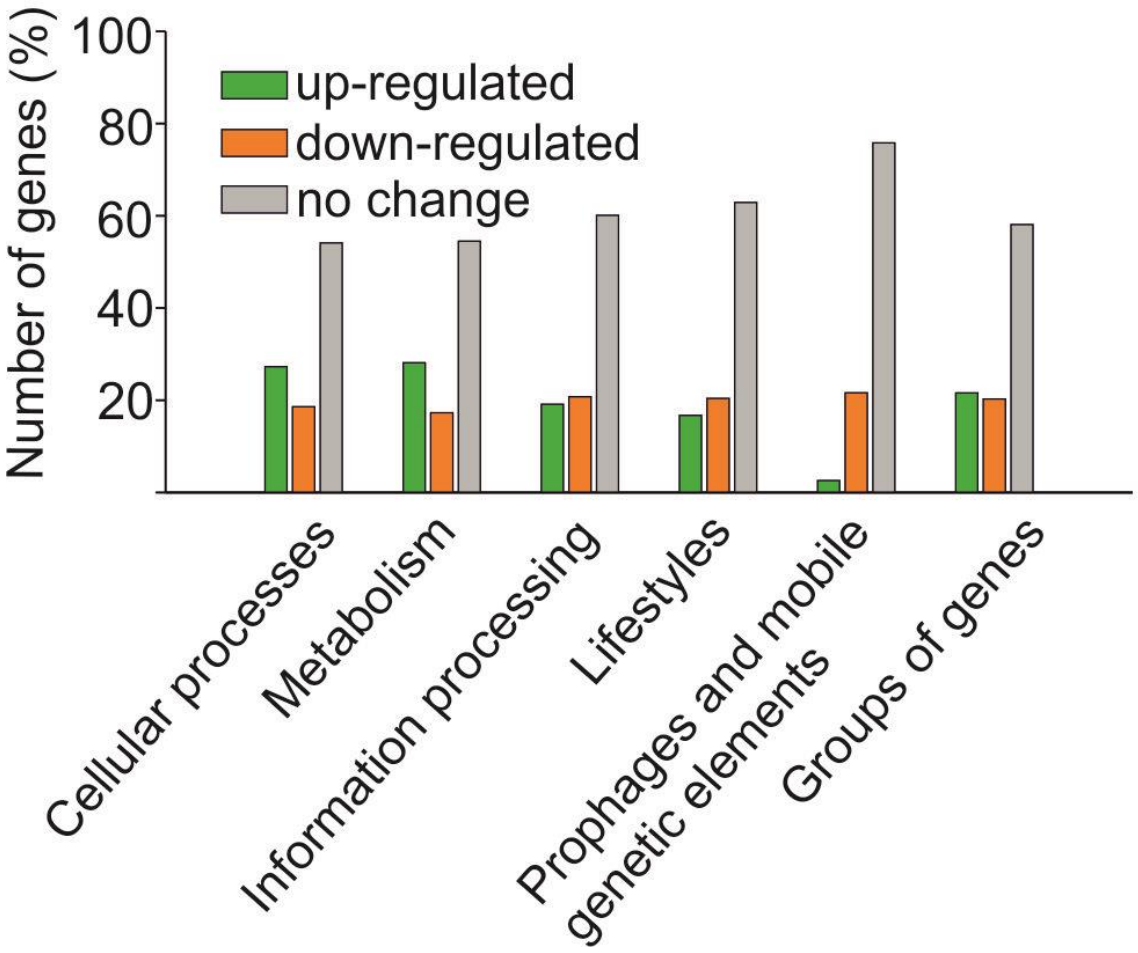

Figure S3. qPCR validation of ChIPseq data.

RNAP occupancy on selected genes was analyzed by qPCR of immunoprecipitated DNA (for details on immunoprecipitation see the Materials and Methods section). Primers used in the validation are in the Key Resources Table. PCR conditions are described in the Materials and Methods section. Wt was set as 1. The average value (ratio of Δ*rnjA* to wt) represents three biological replicates (new immunoprecipitations of DNA, different from those used for ChIPseq, were performed), error bars indicate ±SD.

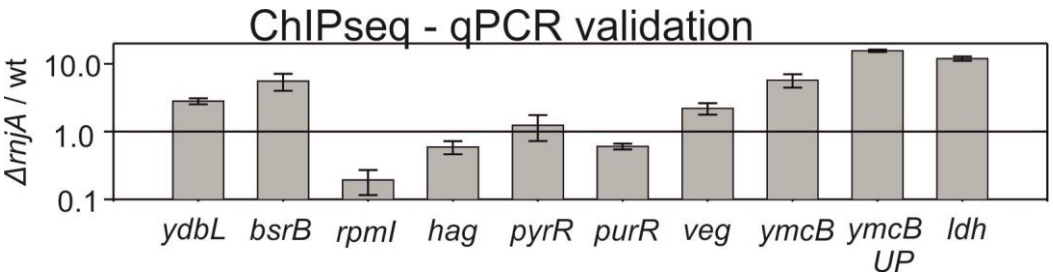

Figure S4. Super-resolution microscopy of LK2328.

Structured illumination microscopy (SIM) of exponentially growing cells of *Bacillus subtilis*, containing RNase J1 fused to GFP (green fluorescent protein) and RNAP to mCherry (red) [strain LK2328]. The scale bar below the Figure represents 3 μM.

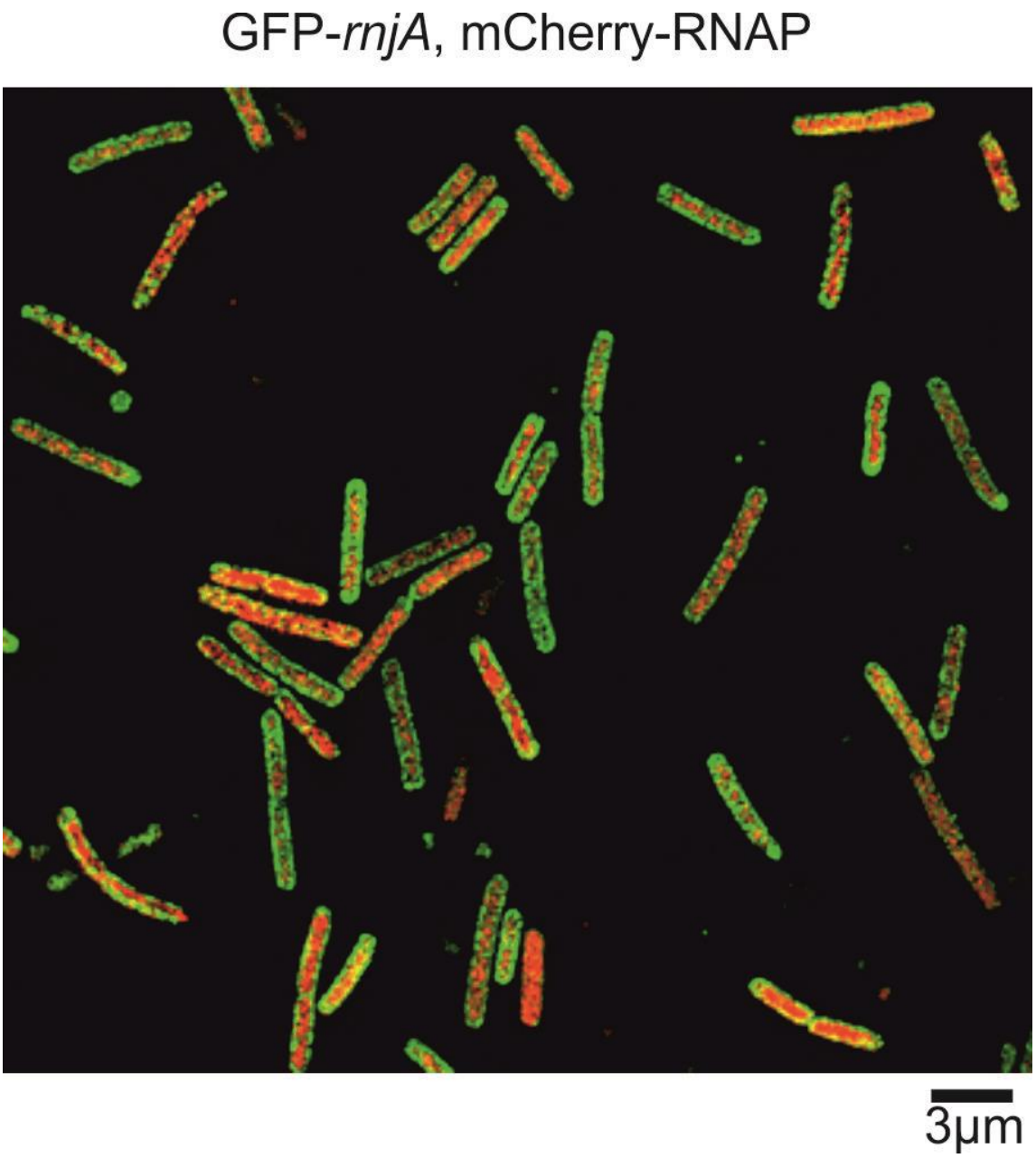

Figure S5. Effects of the absence of Rho or RNase J1 on RNA accumulation: a correlation.

Correlations are shown for relative gene expression values between the Δ*rho* mutant [expressed as log2 fold change vs wt; data taken from (Nicolas et al., 2012)] and relative gene expression values for the Δ*rnjA* mutant [expressed as log2 fold change vs wt]. Only class IV genes for which expression data were available from both Δ*rnjA* and Δ*rho* mutants were used in this comparison (1609 out of 1654 class IV genes).

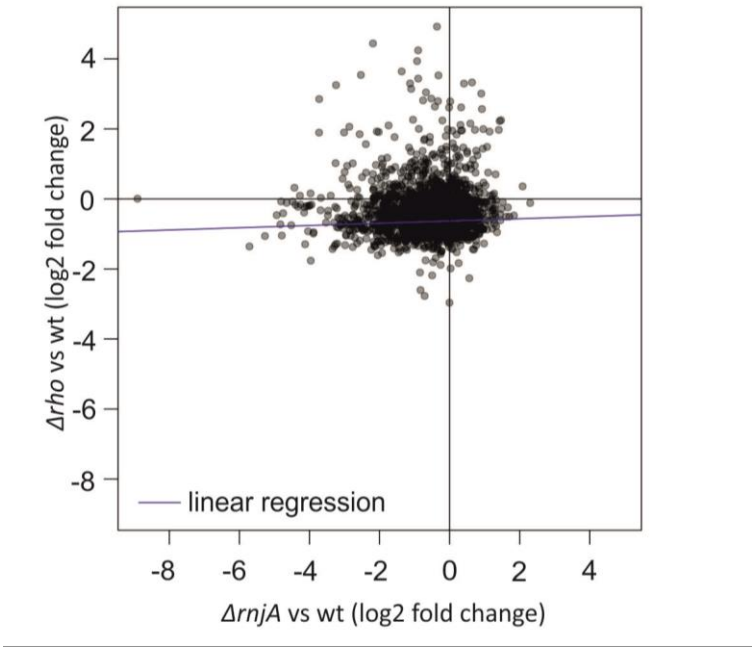

Figure S6. mRNA levels of protein translation factors in Δ*rnjA* compared to wt.

Relative expression of protein translation genes (mRNA levels) in the Δ*rnjA* strain (normalized to wt [set as 1]).

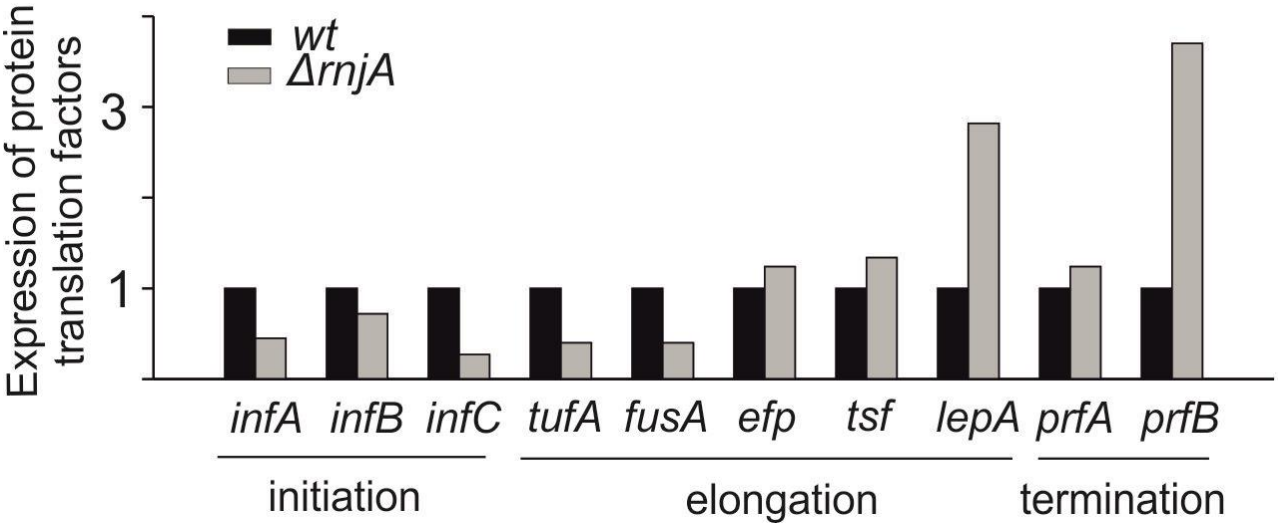

Supplemental References

Durand, S., Gilet, L., Bessieres, P., Nicolas, P., and Condon, C. (2012). Three essential ribonucleases-RNase Y, J1, and III-control the abundance of a majority of Bacillus subtilis mRNAs. PLoS Genet *8*, e1002520.

Nicolas, P., Mader, U., Dervyn, E., Rochat, T., Leduc, A., Pigeonneau, N., Bidnenko, E., Marchadier, E., Hoebeke, M., Aymerich, S., Becher, D., Bisicchia, P., Botella, E., Delumeau, O., Doherty, G., Denham, E. L., Fogg, M. J. Fromion, V., Goelzer, A., Hansen, A.*et al.* (2012). Condition-dependent transcriptome reveals high-level regulatory architecture in Bacillus subtilis. Science *335*, 1103-1106.

Zhu, B., and Stulke, J. (2018). SubtiWiki in 2018: from genes and proteins to functional network annotation of the model organism Bacillus subtilis. Nucleic Acids Res *46*, D743-D748.

PUBLICATION VI

Peer review information: *Nature Communications* thanks Elizabeth Campbell and Yu Zhang for their contribution to the peer review of this work. Peer reviewer reports are available.

Mycobacterial HelD is a nucleic acids-clearing factor for RNA polymerase

Tomáš Kouba[1*#], Tomáš Koval'[2*], Petra Sudzinová[3*], Jiří Pospíšil[3], Barbora Brezovská[3], Jarmila Hnilicová[3], Hana Šanderová[3], Martina Janoušková[3], Michaela Šiková[3], Petr Halada[3], Michal Sýkora[4], Ivan Barvík[5], Jiří Nováček[6], Mária Trundová[2], Jarmila Dušková[2], Tereza Skálová[2], URee Chon[7], Katsuhiko S. Murakami[7], Jan Dohnálek[2#], Libor Krásný[3#]

[1] EMBL Grenoble, 71 Avenue des Martyrs, France

[2] Institute of Biotechnology of the Czech Academy of Sciences, Centre BIOCEV, Průmyslová 595, 252 50 Vestec, Czech Republic

[3] Institute of Microbiology of the Czech Academy of Sciences, Prague, Czech Republic

[4] Institute of Molecular Genetics of the Czech Academy of Sciences, Prague, Czech Republic

[5] Charles University, Faculty of Mathematics and Physics, Institute of Physics, Prague, Czech Republic

[6] CEITEC, Masaryk University, Brno, Czech Republic

[7] Department of Biochemistry and Molecular Biology, The Center for RNA Molecular Biology, Pennsylvania State University, University Park, PA 16802, USA

*These authors contributed equally

#Corresponding authors: tkouba@embl.fr, dohnalek@ibt.cas.cz, krasny@biomed.cas.cz

Abstract

RNA synthesis is central to life, and RNA polymerase (RNAP) depends on accessory factors for recovery from stalled states and adaption to environmental changes. Here we investigated the mechanism by which a helicase-like factor HelD recycles RNAP. We report a cryo-EM structure of a complex between the *Mycobacterium smegmatis* RNAP and HelD. The crescent-shaped HelD simultaneously penetrates deep into two RNAP channels that are responsible for nucleic acids binding and substrate delivery to the active site, thereby locking RNAP in an inactive state. We show that HelD prevents non-specific interactions between RNAP and DNA and dissociates stalled transcription elongation complexes. The liberated RNAP can either stay dormant, sequestered by HelD, or upon HelD release, restart transcription. Our results provide insights into the architecture and regulation of the highly medically-relevant mycobacterial transcription machinery and define HelD as a clearing factor that releases RNAP from nonfunctional complexes with nucleic acids.

Introduction

A smoothly functioning transcription machinery is essential for maintaining the physiologically relevant levels of gene products and adequate changes in transcription are necessary for cell survival when the environment changes. In bacteria, transcription is executed by a single enzyme, DNA-dependent RNA polymerase (RNAP; composition of the core enzyme: $\alpha_2\beta\beta'\omega$[1]). The RNAP core is capable of transcription elongation and termination but not initiation. To initiate, a σ factor is required to form a holoenzyme that recognizes specific DNA sequences, promoters[2]. RNAP holoenzymes can contain various σ

49 factors that allow interaction with diverse promoter sequences. The primary σ factor is
50 termed σ^{70} in *E. coli* and σ^{A} in most other species.

51 The two largest subunits, β and β', held together by the α dimer, form a crab claw-
52 like structure (Figure 1a), each subunit protruding into a pincer (the respective parts are
53 called the β-protrusion and β-lobe [β-domain 1 and 2] and the β'-clamp). Subunits β and β'
54 then form three channels[3]. The opening between the β/β' pincers forms the primary
55 channel where nucleic acids bind. The primary channel is separated by the bridge helix (BH;
56 in β') from the secondary channel, through which nucleoside triphosphates or other
57 substrates[4] access the active site (AS) that is positioned at the junction of the two channels.
58 Next to the BH the trigger loop (TL, in β') is found; these two elements participate in the
59 nucleotide addition cycle. Finally, the RNA exit channel lies on the opposite side of the RNAP
60 core where nascent RNA passes between the base of the β-flap and the β'-lid. In the RNAP
61 elongation complex (*Thermus thermophilus*, PDB ID 2O5J[5]), the downstream DNA (dwDNA)
62 enters the complex through a cleft between the β'-clamp, β'-jaw and β-lobe; the template
63 strand then reaches the AS around the BH, and the DNA/RNA hybrid is held between β'-
64 rudder, β'-lid and β-protrusion.

65 Besides the RNAP subunits that are conserved in all bacteria some species contain
66 additional subunits, such as δ and ε that are present in *Firmicutes*[6,7]. In addition, the
67 regulation of the transcription machinery depends on concerted activities of RNAP and
68 numerous transcription factors, such as RbpA in mycobacteria[8].

69 Another transcription factor is HelD[9], a protein similar to SF1 helicases[10] that
70 associates with the RNAP core in the model gram-positive bacterium *Bacillus subtilis* (*Bsu*)
71 where it was shown to be involved in transcriptional recycling[11]. *Bsu* HelD binds and

hydrolyzes ATP and this is accompanied by conformational changes in the protein as demonstrated by SAXS experiments[12]. The absence of HelD from *Bsu* cells results in prolonged lag phase during outgrowth of stationary phase cells when diluted into fresh medium[11]. Overexpression of HelD then accelerates spore formation[13]. However, the structure of HelD, its binding mode to RNAP, and mechanistic details of its function are unknown.

Here, we present structural data for HelD from *Mycobacterium smegmatis* (*Msm*) in complex with the RNAP core and provide insights into its function. We solved the 3D structures of three complexes of *Msm* RNAP and HelD by cryogenic electron microscopy (cryo-EM). The structures represent a so far unknown type of interaction between an RNAP and a protein. The structures suggested the possibility of simultaneous binding of HelD and σ^A to RNAP and by immunoprecipitation experiments we detected this transitional complex in the cell. Next, we provide biochemical evidence showing that in addition to being able to hydrolyze ATP, HelD can also hydrolyze GTP. Finally, we demonstrate that HelD can both prevent binding of the RNAP core to non-specific DNA and actively remove RNAP from stalled elongation complexes. Together, the results provide the basis for defining the role of HelD in the transcriptional cycle.

Results

Cryo-EM of *Msm* RNAP-HelD complex

Our long-term attempts to crystalize *Bsu* HelD, RNAP core, or their complex failed; our cryo-EM experiments with the *Bsu* RNAP core were not successful; also, our recent SAXS-based data for the *Bsu* HelD-RNAP complex were not fully conclusive. However, in co-immunoprecipitation experiments with *Msm* RNAP we identified MSMEG_2174, a potential homolog of *Bsu* HelD (Supplementary Figure 1). We also solved the X-ray crystal structure of *Bsu* HelD C-terminal domain (CTD), which was then used as a guide for building the model of *Msm* HelD.

We reconstituted a complex of the *Msm* RNAP core and *Msm* HelD from purified recombinant proteins (Supplementary Figure 2), and froze an isolated homogenous fraction of the complex on cryo-EM grids. We collected multiple preliminary cryo-EM datasets, which allowed us to optimize the cryo-EM conditions for high-resolution three-dimensional (3D) single-particle reconstructions (Supplementary Figures 3, 4, 5 and 6). We identified two major 3D classes (State I and State II, Supplementary Figure 4) at overall resolution ~3.1 Å (plus one subclass at ~3.6 Å), visualising almost the complete structure of HelD bound to the RNAP core in two conformations (Figure 1b,c, Supplementary Movies 1,2), and one minor class (State III; Supplementary Figure 4), at ~3.5 Å, which delineates only two domains of HelD binding to the RNAP core (Figure 1d, Supplementary Movie 3).

The structures of States I and II share the same overall fold of HelD, with a crescent-like shape (Figure 1b,c). The main body of the crescent is sitting in between the β-lobe, the cleft/jaw and the funnel/secondary channel of the β' subunit, burying about 774 and 2,608 $Å^2$ in State I and 1,490 and 3,623 $Å^2$ in State II of binding surface area of β and β' subunits,

112 respectively[14]. One end of the crescent protrudes deep into the primary channel, and the
113 other end into the secondary channel of the RNAP core. Indeed, to be able to reach both
114 RNAP channels simultaneously, the HelD protein is markedly elongated, around 200 Å along
115 the outer edge of the virtual crescent, and the two ends of the HelD protein are separated
116 by ~75 Å (State II; Figure 1c).

117 The HelD protein itself is divided into six structured domains (Figure 1e-h), several of
118 which possess unique, so far unknown folds. Interestingly, the 1A domain is composed of
119 two parts (1A-1 and 1A-2) that are separated in the primary amino acid sequence by the
120 intervening HelD-specific domain. According to the position of the HelD domains within the
121 primary channel (PCh) and active site (AS), we name State I: PCh-engaged, State II: PCh-
122 engaged and AS-interfering, and State III: PCh dis-engaged and AS-interfering (Figure 1b-d).

123 **The HelD N-terminal domain inserts into the RNAP secondary channel**

124 The *Msm* N-terminal domain (HelD/1-144) forms an antiparallel α-helical coiled-coil (NCC)
125 (HelD/1-69) followed by, and packed against the four-β-strand globular (NG) domain
126 (HelD/70-144), which contains an additional prominent protruding loop (NG-loop, residues
127 HelD/88-103; Figure 1e-h and Figure 2a,b). The overall N-terminal domain structure is
128 analogous to the archetypal fold interacting with the secondary channel of RNAP present in
129 transcription factors such as GreA or ppGpp cofactor DksA[15-17]. Indeed, the HelD N-terminal
130 domain interacts tightly with the secondary channel, burying ~1,790 $Å^2$ of interaction
131 surface, contributing largely to the HelD-RNAP interaction. Several specific hydrogen bonds
132 and salt bridges (Supplementary Table 1) are formed between the N-terminal domain and
133 the secondary channel, and particularly the NG-loop specifically recognises the tip of the
134 coiled-coil (CC) motif of the β'-funnel (Figure 2a).

The topology of the *Msm* HelD NCC is conserved in comparison with other secondary channel-interacting transcription factors (Supplementary Figure 8); however, in contrast to the known structures of such complexes, the *Msm* HelD NCC is shorter and its tip does not reach into the AS (Supplementary Figure 8). Indeed, a large part of the NCC is extensively packed with the NG-domain into a common hydrophobic core, thereby preventing the NCC to bind further towards the AS. The HelD NCC tip is positioned at the level of the RNAP AS β' bridge helix (β'-BH), ~10-12 Å away from Mg^{2+} metal A (MgA) of the AS, and as a result, it constitutes one wall of the secondary channel pore leading to the AS. The pore itself is approximately ~11 Å wide (Figure 2b) and this would still allow nucleoside triphosphate (NTP) passage into the AS. On the other hand, the NCC-domain restricts the conformational freedom and induces folding of the AS trigger loop (β'-TL, β'/1009-1028). This would likely interfere with the nucleotide addition cycle.

Another difference with respect to GreA family transcription factors is that the HelD NCC tip does not contain the conserved DXX(E/D)[18-20] motif (Supplementary Figure 8), and it is, therefore, unlikely that the *Msm* HelD N-terminal domain possesses a Gre factor-like endonuclease activity.

The NTPase unit of HelD is positioned in the vicinity of the downstream section of the primary channel

The presented structure confirms our previous prediction[12] that HelD, similarly to SF1 helicases, RapA and UvrD, contains a conserved Rossmann fold 1A-2A heterodimer. Domain 1A is formed by two subdomains 1A-1 and 1A-2 separated in amino acid sequence by the HelD-specific part (Figure 1e). 1A-1 is connected with the N-terminal domain by the NG

linker (HelD/145-173), which orders only in State I. 1A-2 is then followed by 2A (Figure 1e,f,g and 2c).

The 1A domain docks on the β-lobe where it induces small changes in domain orientation and conformation and it prolongs the wall of the downstream section of the primary channel along the axis of the virtual dwDNA (Figure 2c). The 1A domain buries an area of 725 $Å^2$ of the interaction surface of the β-lobe, and the binding also involves ordering of the β-turn β/209-212 and many hydrogen bonds and salt bridges (Supplementary Table 2). In addition, the extension of the 1A domain (HelD/504-521) is clamped in between the prominent β-turn β/184-187 of the β-lobe and the tip of the β'-jaw, further securing the 1A domain in its place (Figure 2c).

The 1A-2A heterodimer establishes the canonical tertiary structure to form an NTP-binding pocket. Conserved residues of motifs Q, I, II, ~III, IIIa, Va, and VI are then likely involved in NTP binding[21] (Figure 2d), while residues typical for DNA binding (in SF1 helicases) are missing. However, the base type specificity is not obvious from the structural data and, therefore, we measured nucleoside triphosphate hydrolysis activity of the isolated HelD protein. HelD showed strong hydrolysis activity of purine base nucleoside triphosphates but no activity towards a pyrimidine-containing counterpart (Figure 2e, Supplementary Figure 9f).

We also added ATP or non-hydrolysable ATP analogue to the HelD-RNAP complex, but we were not able to visualize any NTP-bound state by cryo-EM. Indeed, the orientations of conserved HelD/Tyr589 and Arg/590 of motif IIIa, which are supposed to stack and coordinate the base and phosphate groups in the canonical ATP-bound state[22], are incompatible with NTP binding in the HelD NTP-free states (States I and II; Supplementary

Figure 9a). Notably, helix α3 of the ordered NG-linker in State I covers the putative NTP-binding pocket and partially obstructs the site entrance (Supplementary Figure 9a). However, the entire linker can become disordered as seen in State II (Supplementary Figure 10h), which is probably more compatible with NTP binding (see details below).

The superposition of HelD 1A-2A with similar structures of UvrD (PDB ID 2IS4) (Supplementary Figure 9b,c), PcrA (PDB ID 3PJR), AdnA/B (PDB ID 6PPR) and RapA (PDB ID 6BOG) confirms that the Rossmann fold domains are packed in the canonical mutual orientation. However, unlike in *bona fide* SF1 helicases[21] where ssDNA is bound in the interface cleft of the dimer by conserved motifs Ia, Ic, IV, and V (Supplementary Figure 9b,c), these motifs are not conserved in HelD. Instead, HelD contains proline-rich loops in place of these motifs and a large negatively charged surface patch in the equivalent areas (Supplementary Figure 9 d,e). Similarly, the ssDNA-binding motifs are not conserved in RapA, a functional homolog of HelD and a helicase-like protein involved in recycling of RNAP. RapA, however, binds differently to RNAP than HelD[23].

The *Msm* HelD-specific domain is inserted into the downstream section of the RNAP primary channel

The HelD-specific insertion domain is composed of the clamp-opening domain (CO-domain, HelD/261-447) and the primary channel loop (PCh-loop, HelD/448-503) (Figure 1e, 3b,c,d,e). The CO-domain is an extended, mostly α-helical, and so far undescribed fold with no structural homologs (Supplementary Figure 7b). On one side, the CO-domain packs against the 1A domain helix α19 and β-turn HelD/561-564. Additionally, the CO-1A interaction is stabilised by the CO-linker (HelD/259-275), which connects the two domains. In State I, the other side of the CO-domain, the CO-tip, butts against the three-stranded sheet of the β'

non-conserved domain (β'-NCD) and an α-helix (β'/122-133) of the β'-clamp just preceding it (Figure 3a,b,d). The only significant ordered part of the PCh-loop in State I, the protruding helix α16 (HelD/451-468), is erected against the β' three-stranded sheet (β'/1164-1210) and the α16 tip locks behind the helix-turn-helix motif β'/271-304 by HelD/Tyr466. Altogether, the α16 interaction with the β'-clamp might be helping the CO-domain insertion into the primary channel. In State II, the CO-domain fold alters and the PCh-loop completely refolds. The CO-domain tip shifts towards the β' clamp coiled-coil domain (β'-CC) domain and reaches the peptide β'/387-389 of the rudder (Figure 3c,e). The PCh-loop protruding helix α16 refolds (α16 register slightly shifts towards the C-terminus of HelD) and dis-engages with the β' three-stranded sheet (β'/1164-1210), and the whole PCh-loop orders towards the AS (see next section). Correspondingly, the two insertion modes of the CO-domain and PCh-loop into the primary channel force the β'-clamp domain to swing out into two distinct positions (see details below).

The HelD PCh-loop is able to fold into the RNAP active site

In the cryo-EM map of the AS-interfering State II, high-resolution density is present for the entire register of the PCh-loop, which is folded in the AS cavity of RNAP (Figure 3c,f,g and Supplementary Figure 5c). The folding of the PCh-loop in-between the walls of the AS chamber is also compatible with the regular open form of the RNAP core as observed in State III.

In comparison to State I, in State II the protruding helix α16 refolds, the helix register shifts to residues 455-472, and together with a newly folded helix α17 (HelD/495-500) they tightly pack with the second half of the β'-BH (Figure 3g). In detail, BH β'/Arg874 and 875 sandwich α16 HelD/Tyr466 and, cooperatively, BH β'/Tyr871 stacks on HelD/Phe502 and is

226 inserted into a hydrophobic pocket formed by HelD/Tyr466, Ala467, Val470, and Leu498.
227 The rest of the PCh-loop (HelD/473-494) specifically wedges into the AS cavity
228 (Supplementary Table 3), towards the AS aspartate triad and MgA. Notably, there are four
229 acidic residues (482-DDED-485) at the very tip of the PCh-loop and the HelD/481-483
230 peptide folds along the AS β-strand β'/537-544, such that HelD/Asp483 is in contact with
231 MgA and HelD/Asp482 in its near proximity (Figure 3f and Supplementary Figure 5c).
232 HelD/Asp482 interacts with β'/Arg500, HelD/Glu484 stabilizes the loop in the active site by
233 interaction with β/His1026, and HelD/Asp485 contributes to the AS-interfering loop stability
234 by a salt bridge with the side chain of HelD/Arg477. Two other motifs support formation of
235 the PCh-loop structure in the RNAP AS – a small hydrophobic core formed by the
236 HelD/Val475, Leu480, and Leu488 side chains and an intra-chain ion-pair HelD/Arg477-
237 Asp491, with HelD/Arg477 leaning against β/Pro483.

238 As a result of the PCh-loop folding into the primary channel and HelD NCC folding in
239 the secondary channel, the NCC tip and the tip of the PCh-loop are brought close together
240 (the shortest distance between the two tips is about 17 Å). This also restricts the trigger
241 loop, which is, therefore, partially folded in the space between the BH, HelD α2 and α17, the
242 peptide between α17 and α18, and the peptide of β/Ile182-Glu187. In summary, the PCh-
243 loop seems to interfere with the AS cavity so that it is not compatible with the NTP addition
244 cycle. Moreover, the superposition with the structure of *Thermus thermophilus* (*Tt*) RNAP EC
245 (PDB ID 2O5J; Figure 3h,i) suggests that the whole PCh-loop would be in steric clash with the
246 dwDNA duplex and the RNA/DNA hybrid in the AS as far as position -2. A parallel can be
247 drawn between the presence of the PCh-loop in State II and the so called DNA-mimicking

loop of PolI[24], which also occupies the AS chamber and the surroundings of the AS and is sterically incompatible with the presence of the DNA transcription bubble in RNAP.

Global domain changes of RNAP upon HelD binding

Superposition based on the β-core region (β/430-738) of the *Msm* RNAP core (PDB ID 6F6W), elongation complex (EC, model based on PDB ID 2O5J) and States I-III enables analyses of global differences of the three observed structural states (Supplementary Figure 10). The interaction of the HelD N-terminal domain with the secondary channel and its influence on the rest of the complex remains very similar in all the States. This interaction thus might be the initial one through which HelD starts its association with RNAP. Furthermore, this interaction seems sufficient to alter the position of the β'-jaw/cleft and β-lobe (Supplementary Figure 10g) which may weaken interaction with dwDNA, reminiscent of TraR (a distant DksA homolog) binding to *E. coli* RNAP[25].

The main change between the States is the interplay between the refolding of the PCh-loop and the CO-domain position in the primary channel. In State III, solely the PCh–loop's tight contact with the AS stabilizes a very open form of RNAP (Supplementary Figure 10a,b,f), ~33 Å at the narrowest point of the primary channel (measured by the distance of the C^{α} atoms of β/Lys273 and β'/Lys123), comparable to the structures of two previously identified conformations of very open forms of *Msm* RNAP core and holoenzyme, termed Core2 and Holo2 (32.2 and 33.6 Å, respectively)[1]. In State I, the PCh–loop's interaction with β' helix-turn-helix and three-stranded sheet, and the CO-domain insertion into the primary channel make the opening of the RNAP clamp (~35 Å; Supplementary Figure 10a,b) slightly wider than the already widely open forms of the Lipiarmycin-[26] (PDB ID 6FBV) and Fidaxomicin-locked[27] (PDB ID 6C06) RNAPs (34.2 and 33.6 Å, respectively[1]). In State II

(Supplementary Figure 10e), while the CO-domain still inserted, the PCh-loop abolishes the β' contact and folds in the AS instead, and this forces the β'-clamp (β'/1-406) to rotate with respect to the remaining parts of the complex so that the β'-NCD CC tip opens further away from the juxtaposed β-lobe but at the same time the β'-rudder, β'-CC and adjacent secondary elements move about 11 Å closer to the tip of the HelD CO-domain. The RNAP clamp is, therefore, splayed by 45 Å (Supplementary Figure 10b). This clamp opening together with the tight interaction of the PCh-loop with the AS is not compatible with nucleic acids binding.

The next major differences are the β-lobe and CO-domain adjustments upon change of the 1A-2A heterodimer (Supplementary Figure 10e). The mutual orientation of 1A and 2A domains between States I and II is almost preserved, although with much poorer density for 2A in State II. This most likely stems from the more pronounced mobility of 2A, possibly linked with the lack of stabilization by the unfolded NG-linker in State II. The 2A relaxation allows movement of 1A in respect to the N-terminal domain (~3° difference measured by HelD α1 and α5) and a concomitant shift of both the β-lobe and CO-domain (Supplementary Figure 10e). In detail, this global change is accompanied by a shift and changes in the secondary structure of HelD/230-252 within the 1A domain (largest shift about 9.3 Å for Val245). Helix α6 is extended and helix α7 is formed in State II (Supplementary Figure 7a) and 1A-extension shifted. State I interactions between α6 and the NTPase site, and α6 and the NG-linker that are NTP-binding prohibitive, are broken in State II and the NTPase site of HelD becomes wide open (NTP-binding permissive; Supplementary Figure 10h). Although this change makes the NTPase site accessible for NTPs, additional conformational changes are still required for NTP accommodation.

Finally, HelD binding in States I and II also leads to opening of the RNA exit channel between the β-flap and β'-lid and β'-Zn-finger by about 15 Å and 21 Å, respectively (Supplementary Figure 10c,d). State III keeps the channel still rather open by about 12 Å. This is expected to contribute to RNA release.

HelD clears the RNAP primary channel

The position of the HelD CO-domain in the primary channel of RNAP suggests that HelD may prevent non-specific interactions between the RNAP core and DNA. To test this, we performed electrophoretic mobility shift assay (EMSA) with RNAP and a fragment of mycobacterial DNA in the presence/absence of HelD. Figures 4a, b, and c show that HelD significantly abolishes the nonspecific binding of the RNAP core to DNA.

Moreover, we speculated that HelD might not only prevent DNA binding, but also actively disassemble stalled ECs. Stalled ECs (due to *e. g.* damaged DNA) are obstacles for both the coupled transcription-translation machinery[28,29] and also for replication[30], with potentially deleterious consequences if not removed. To test the ability of HelD to rescue stalled RNAP, we assembled ECs with the RNAP core on a DNA-RNA scaffold and challenged them with HelD in the presence/absence of NTPs (Figure 4d). HelD then, relative to mock treatment, was able to disassemble stalled ECs (Figure 4e). This process, interestingly, appeared to be independent of ATP or GTP.

312 **HelD, σ^A and RbpA can simultaneously bind RNAP core**

313 Analysis of States I-III suggested the possibility of simultaneous binding of HelD, σ^A and RbpA
314 to RNAP. Modelling of hypothetical complexes of RNAP-HelD with σ^A and RbpA then
315 confirmed that relatively small changes in conformations of these proteins could allow their
316 simultaneous binding to RNAP in States I-III (Supplementary Figure 11 and Discussion).
317 Therefore, we tested experimentally whether the HelD-RNAP complex is compatible with
318 the presence of other factors. Indeed, immunoprecipitation (IP) and Western blot
319 experiments with FLAG-tagged *Msm* RNAP revealed the presence of HelD and σ^A (Figure
320 4f,g); FLAG-tagged *Msm* σ^A pulled down the RNAP core and HelD; FLAG-tagged HelD pulled
321 down the RNAP core and σ^A. These results suggested but not proved that HelD, σ^A, and
322 RNAP are together in one complex. Alternatively, HelD and σ^A could bind each other
323 independently of RNAP. To decide between the two possibilities, we first pulled down FLAG-
324 tagged HelD and associated proteins and from this mixture we subsequently pulled down σ^A
325 (with antibody against σ^A) and associated proteins. Supplementary Figure 12 shows the
326 presence of HelD and RNAP in the second pull-down, demonstrating that all these proteins
327 (RNAP, σ^A, HelD) can coexist in one complex. Additionally, RbpA, albeit in low amounts, was
328 also present in the HelD-immunoprecipitated complex and RbpA-FLAG pulled down RNAP
329 with σ^A and HelD (Supplementary Figure 13). We then confirmed the interactions between
330 the RNAP core, σ^A, RbpA, and HelD by *in vitro* EMSA (Figure 4h).

331

Discussion

This study describes a structurally unique complex between *Msm* RNAP and the HelD protein, defines its DNA-clearing activity, and outlines its role in transcription.

Comparison of *M. smegmatis* and *B. subtilis* HelD

Previous biochemical studies used HelD from *Bsu*, which is only 21 % identical with the *Msm* homolog. Selected sequence homologs of *Msm* HelD are shown in Supplementary Figure 14, revealing two main differences between *Msm* (*Actinobacteria*) and *Bsu* (*Firmicutes*). The first marked difference is the absence of ~30 aa from the N-terminal NCC-domain region in *Msm* HelD. This is consistent with the *Bsu* HelD NCC-domain protruding much deeper into the RNAP secondary channel and even overlapping with the AS (See accompanying papers Newing e*t al.,* 2020; Pei *et al.,* 2020). The other difference is in the HelD-specific region where *Bsu* HelD completely lacks the PCh-loop. On the other hand, the organisation of the 1A-1 and 1A-2 split followed by the complete 2A domain is maintained (Figure 1e,f,g).

Interestingly, *Msm* HelD, σ^A, and RbpA can co-occur on RNAP (Figures 4h and Supplementary Figure 11-13) and we infer that the RNAP-σ^A-RbpA-HelD complex thus likely represents one of the possible transitional states in the transcriptional cycle. This differs from *Bsu* where simultaneous HelD and σ^A binding has not been detected[11]. Regardless of the exact mutual positions of σ^A, RbpA and HelD, RNAP must subsequently assume a conformation that is compatible with promoter DNA binding and transcription initiation.

Model of the HelD role in transcription

Based on the structural and functional data we propose a role for *Msm* HelD in transcription (a model is shown in Figure 5). We envisage that upon transcription termination when RNAP fails to dissociate from nucleic acids[31], or in the event of stalled elongation, *Msm* HelD first interacts with RNAP by its N-terminal domain, likely competing for binding to the secondary channel with GreA-like factors. This initial HelD binding induces changes in β-lobe and β'-jaw/cleft (Supplementary Figure 10g), possibly leading to destabilisation of dwDNA in the primary channel. The trigger loop is conformationally locked. Subsequently, the CO-domain and PCh-loop approach the primary channel. The PCh-loop, which is probably flexible in the RNAP-unbound state, folds partially upon binding RNAP (captured in State I) and then it penetrates deep into the primary channel, fully folds, and binds to the AS (captured in States II and III). The CO-domain interactions with β'-clamp then secure the primary channel wide open (Supplementary Figure 10a,b). At the same time, the RNA exit channel dilates (Supplementary Figure 10c,d). All these processes lead to the release of any contents of the AS (compare states within Supplementary Figure 10a).

We note that neither HelD loading onto RNAP nor RNAP clamp opening nor EC disassembly are dependent on NTP hydrolysis. Energy from NTP hydrolysis is probably required to release HelD from its tight contact with RNAP. Free energy corresponding to ATP hydrolysis under physiological conditions in cells is around –50 kJ/mol[32]. This is comparable to the estimated desolvation energy of the HelD-RNAP core interaction of –33.5 kJ/mol ($\Delta^{i}G$) for State I and –57 kJ/mol for State II. However, States I and II are not fully compatible with canonical NTP binding in the HelD NTPase unit. It remains to be answered which structural changes are required to actually enable NTP binding and hydrolysis.

To summarize, HelD clears RNAP of nucleic acids; this likely happens in non-functional (e. g. stalled) transcription complexes or post-termination. This may contribute to the smooth functioning of the transcription machinery. Furthermore, it is conceivable that HelD may also function similarly to 6S RNA[33] or Ms1[34], which keep RNAP in an inactive state under growth-unfavourable conditions. This stored RNAP then accelerates restart of gene expression when conditions improve.

Finally, the RNAP-inactivating ability of HelD might be utilized in development of specific antibacterial compounds that would stabilize the non-productive HelD-RNAP complex, shifting the equilibrium of RNAP states towards effective transcription inhibition, as seen *e.g.* in the action of Fidaxomicin towards *M. tuberculosis* RNAP in complex with RbpA[27].

Methods

Bacterial strains, plasmids, and oligonucleotides.

Bacterial strains and plasmids are listed in Supplementary Table 4. DNA oligonucleotides are listed in Supplementary Table 5.

Strain construction - σ^A and RbpA

σ^A (*MSMEG_2758*) and *rbpA* (*MSMEG_3858*) genes were amplified from genomic DNA by PCR with Phusion High-Fidelity DNA Polymerase (NEB) with primers #1155 + #1156 (σ^A) and #1182 + #1183 (RbpA) and *Msm* chromosomal DNA as the template, cloned into pET22b via *NdeI*/*XhoI* restriction sites and verified by sequencing. Resulting plasmids were transformed into expression *Eco* BL21(DE3) strain resulting in strains LK1740 (σ^A) and LK1254 (RbpA).

Strain construction - HelD

Plasmid encoding the N-terminally His-tagged *Msm* HelD protein was prepared by the *GeneArt® Plasmid* Construction Service (Thermofisher). Gene construct for HelD expression was designed by codon-optimized back translation of gene MSMEG_2174 from *Msm* (*strain*

ATCC 700084 / mc^2 155) with cleavage site for TEV protease placed at the 5' end. This synthetized gene was cloned into the Champion™ pET302/NT-His expression vector (Thermofisher) *via EcoRI* and *XhoI* restriction sites. Resulting protein thus has 6xHis tag at its N-terminus which is cleavable by TEV protease (protein construct starts with sequence MHHHHHHVNSLEENLYFQG followed by the second amino acid of gene *MSMEG_2174*.

Strain construction - HelD-FLAG, σ^A-FLAG and RbpA-FLAG

The genes coding for the HelD-FLAG, σ^A-FLAG and RbpA-FLAG proteins were amplified by PCR using Q5® High-Fidelity DNA Polymerase (NEB) with primers #3130 + #3131 (HelD), #2339 + #2340 (σ^A) and #2894 + #3093 (RbpA) and *Msm* chromosomal DNA as the template. The C-terminal 1x FLAG-tags (DYKDDDDK) were encoded within the reverse PCR primers for all genes. Subsequently, the genes were inserted into integrative plasmid pTetInt[35] via *NdeI*/*HindIII* restriction sites. The constructs were verified by sequencing. Resulting plasmids were transformed into *Msm* mc^2 155 (wt, LK865) cells by electroporation resulting in strains LK2590 (HelD-FLAG), LK2073 (σ^A-FLAG) and LK2541 (RbpA-FLAG).

Growth conditions

Msm strains - mc^2 155 (wt, LK865), σ^A-FLAG (LK2373), RNAP-FLAG (LK1468), HelD-FLAG (LK2590), and RbpA-FLAG (LK2541) were grown at 37 °C in Middlebrook 7H9 medium with 0.2 % glycerol and 0.05 % Tween 80 and harvested in exponential phase (OD_{600} ~0.5; 6 h of cultivation) or early stationary phase (OD_{600} ~2.5–3.0, 24 h of cultivation) unless stated otherwise. When required, media were supplemented with kanamycin (20 μg/ml). Expression of HelD-FLAG in exponential phase was induced by anhydrotetracycline (1 ng/ml) at 3 h of cultivation. The cells were then grown for additional 3 h. Expressions of σ^A-FLAG, RbpA-FLAG, and HelD-FLAG in stationary phase were induced by anhydrotetracycline (10 ng/ml) at 8 h of cultivation. The cells were then cultivated for additional 16 h.

***Msm* RNAP core purification for cryo-EM**

Eco strain BL21(DE3) was transformed with pRMS4 (*kanR*) plasmid derivative encoding *Msm* subunits ω, α, and β-β´ fusion with C-terminal His8 tag in one operon from T7 promoter. Expression cultures were incubated at 37 °C and shaken at 250 rpm until OD_{600} ~0.8, expression was induced with 500 μM isopropyl β-D-thiogalactoside (IPTG) at 17 °C for 16 h. Cells were lysed using sonication by Sonic Dismembrator Model 705 (Fisher

Scientific) in a lysis buffer containing 50 mM NaH_2PO_4/Na_2HPO_4 pH 8 (4 °C), 300 mM NaCl, 2.5 mM $MgCl_2$, 30 mM imidazole, 5 mM β-mercaptoethanol, EDTA-free protease inhibitor cocktail (Roche), RNase A (Sigma), DNase I (Sigma) and Lysozyme (Sigma). Clarified lysate was loaded onto a HisTrap FF Crude column (GE Healthcare) and proteins were eluted with a linear gradient of imidazole to the final concentration of 400 mM over 20 column volumes. The *Msm* RNAP core elution fractions were pooled and dialyzed to 20 mM Tris-HCl pH 8 (4 °C), 1 M NaCl, 5 % (v/v) glycerol and 4 mM dithiothreitol (DTT) for 20 h. The protein was further polished on XK 26/70 Superose 6 pg column (GE Healthcare) equilibrated in 20 mM Tris-HCl pH 8 (4 °C), 300 mM NaCl, 5 % (v/v) glycerol and 4 mM DTT. The *Msm* RNAP core final fractions were eluted at 6 µM concentration, aliquoted, flash-frozen in liquid nitrogen and then stored at –80 °C.

Msm HelD protein purification for cryo-EM

Eco strain Lemo 21 (DE3) was transformed with pET302/NT-His (*cmlR* and *ampR*) plasmid derivative encoding the *Msm* HelD protein fusion with N-terminal 6xHis tag under the control of the T7 promoter. Expression cultures were incubated at 37 °C and shaken at 250 rpm until OD_{600} ~0.8, expression was induced with 500 µM IPTG at 17 °C for 16 h. Cells were lysed using sonication by Sonic Dismembrator Model 705 (Fisher Scientific) in a lysis buffer containing 50 mM Tris-HCl pH 7.5 (4 °C), 400 mM NaCl, 30 mM imidazole, 0.2 % Tween20, 2 mM β-mercaptoethanol, EDTA-free protease inhibitor cocktail (Roche), RNase A (Sigma), DNase I (Sigma) and Lysozyme (Sigma). Clarified lysate was loaded onto a HisTrap FF Crude column (GE Healthcare) and proteins were eluted with a linear gradient of imidazole to the final concentration of 400 mM over 20 column volumes. Fractions containing HelD protein were pooled and dialyzed for 20 h against the dialysis buffer containing 20 mM Tris-HCl, pH 7.5 (4 °C), 500 mM NaCl, 1 mM DTT together with TEV protease at a TEV protease:HelD ratio 1:20.

The protein was then concentrated to ~15 A_{280} units and further purified using size-exclusion chromatography using a Superdex 75 column (GE Healthcare) equilibrated in 20 mM Tris-HCl, pH 7.5 (4 °C), 200 mM NaCl and 1 mM DTT. The HelD protein was eluted at ~160 µM concentration, aliquoted, flash-frozen in liquid nitrogen and then stored at –80 °C.

In vitro HelD-RNAP complex reconstitution for cryo-EM

To assemble the HelD-RNAP complex, the individual proteins were mixed at a molar ratio of 3:1. The *in vitro* reconstitutions were carried out at 4 °C, and the reconstitution mixture was incubated for 15 min. 50 µl of the reconstitution mixture was injected onto a Superose 6 Increase 3.2/300 column (GE Healthcare) equilibrated in 20 mM Tris-HCl, pH 7.8 (4 °C), 150 mM NaCl, 10 mM $MgCl_2$ and 1 mM DTT. 50-µl fractions were collected and the protein was eluted at ~1 µM concentration.

Electron microscopy

Complexes were diluted to ~850 nM and aliquots of 3 µl were applied to Quantifoil R1.2/1.3 or R2/2 Au 300 mesh grids, immediately blotted for 2 s and plunged into liquid ethane using an FEI Vitrobot IV (4 °C, 100 % humidity).

The grids were loaded into an FEI Titan Krios electron microscope at the European Synchrotron Radiation Facility (ESRF) (beamline CM01, ESRF) or CEITEC (Masaryk University, Brno), operated at an accelerating voltage of 300 keV and equipped with a post-GIF K2 Summit direct electron camera (Gatan) operated in counting mode. Cryo-EM data was acquired using EPU software (FEI) at a nominal magnification of x165,000, with a pixel size of 0.8311 and 0.840 Å per pixel. Movies of a total fluence of ~40-50 electrons per $Å^2$ were collected at ~1 $e^-/Å^2$ per frame. A total number of 15,177 movies were acquired at a defocus range from −0.7 to −3.3 µm (Supplementary Table 6).

Cryo-EM image processing

All movie frames from three datasets were aligned and dose-weighted using the MotionCor2 program (Supplementary Figure 3a) and then used for contrast transfer function parameter calculation with Gctf[36]. Initially, particles were selected without a template by Gautomatch (provided by Dr. Kai Zhang, http://www.mrc-lmb.cam.ac.uk/kzhang) from a small portion of the data set (~200 movies). This initial small dataset was subjected to reference-free 2D-classification using RELION 3.0[37]. Eight representative classes of different views were selected from the two-dimensional averages and used as reference for automatic particle picking for the dataset I by RELION. WARP[38] was used for particle picking for datasets II and III.

The resulting particles were iteratively subjected to two rounds of 2D-classification (Supplementary Figure 3b) at 3x and 2x binned a pixel size. Particles in classes with poor structural features were removed. Particles from dataset I and II were globally refined to estimate the pixel size matching[39] and particles from dataset II were estimated to match the common pixel size 0.8311 Å per pixel. Particles from all datasets were pooled (~1,560 k), 2x binned and subjected to three-dimensional classifications with image alignment (Supplementary Figure 4). The first round of 3D-classification was restricted to ten classes and performed using *Msm* RNAP core (PDB ID 6F6W) as a 60 Å low-pass filtered initial

model. Classification was done during three rounds of 25 iterations each, using regularization parameter T = 4. During the second and third round, local angular searches were performed at 3.5° and 1.8° to clearly separate structural species. The three most abundant and defined 3D-classes were re-extracted at the pixel size of 0.8311 Å per pixel and 3D auto-refined using respective masks in RELION 3.0 (Supplementary Figure 4). The results of the 3D auto-refinement were used for per particle CTF refinement in RELION 3.1[40] and further 3D auto-refined. Further 3D classification was applied on class 1 and 3 (corresponding to States I and III, respectively), but no better defined 3D classes were identified. The 3D reconstruction of class 2 (corresponding to State II) was further focus 3D auto-refined on the RNAP core region. The 3D reconstruction of class 2 was also 3D focus classified on the region of the HelD-specific domain and a more defined class was identified and 3D auto-refined separately. The final cryo-EM density maps were generated by the post-processing feature in RELION and sharpened or blurred into MTZ format using CCP-EM[41]. The resolutions of the cryo-EM density maps were estimated at the 0.143 gold standard Fourier Shell Correlation (FSC) cut off (Supplementary Figure 3d). A local resolution (Supplementary Figure 5a) was calculated using RELION and reference-based local amplitude scaling was performed by LocScale[42]. The directional resolution anisotropy (Supplementary Figure 6) was quantified by the 3D FSC algorithm[43].

Cryo-EM model building and refinement

Atomic models of *Msm* RNAP protein parts (Figure 1b-d) were generated according to the known structure of the *Msm* RNAP core (PDB entry 6F6W). The whole RNAP core was first rigid-body fitted into the cryo-EM density by Molrep[44] and individual sub-domains fits were optimized using the Jigglefit tool[45] in Coot[46] and best fits were chosen according to a correlation coefficient in the JiggleFit tool. The crystal structure of the *Bsu* HelD-2A domain (Supplementary Figure 9g) was first rigid-body fitted into the cryo-EM density by Molrep[44] and then manually adapted in Coot. Parts of the HelD main chain were first traced into the cryo-EM density by Buccaneer[47] and Mainmast[48]. The rest of the HelD protein was built *de-novo* in Coot[46]. The cryo-EM atomic-models of HelD-RNAP complexes were then iteratively improved by manual building in Coot and refinement and validation with Phenix real-space refinement[49]. The atomic models were validated with the Phenix validation tool (Supplementary Table 6) and the model resolution was estimated at the 0.5 FSC cut-off.

Structures were analyzed and Figures were prepared using the following software packages: PyMOL (Schrödinger, Inc.) with APBS plugin[50], USCF Chimera[51], CCP4mg[52], PDBePISA server[53].

X-ray crystal structure determination of the *Bsu* HelD C-terminal domain

DNA sequence encoding the C-terminal domain of HelD (from residue 608 to 774) was amplified by PCR and cloned into pET15b vector by *NdeI* and *BamHI* restriction sites to make an N-terminal His6-tagged protein. Bacterial culture containing BL21(DE3) RIPL codon-plus cells transformed with a pET15b–HelD-CTD vector was grown at 37 °C in LB medium supplemented with 100 μg/ml ampicillin, protein expression was induced with 0.5 mM IPTG at OD_{600} = 0.5, and incubated for additional 3 h to allow protein expression. Cells were harvested by centrifugation and lysed by sonication in lysis buffer (50 mM Tris-HCl, pH 8.0 at 4 °C, 200 mM NaCl, 5 % glycerol, 2 mM β-mercaptoethanol, 2 mM phenylmethylsulfonyl fluoride, PMSF). The lysate was clarified by centrifugation and HelD-CTD was purified by Ni-NTA, Q-sepharose and Heparin-column chromatography. Fractions containing HelD-CTD were concentrated using VivaSpin concentrators until 10 mg/ml in crystallization buffer (10 mM Tris-HCl, pH 8 at 4 °C, 50 mM NaCl, 1 % glycerol, 0.1 mM EDTA, 1 mM DTT).

Crystallization condition of HelD-CTD was screened by using JCSG+ screen (Molecular Dimensions) and crystals were obtained in crystallization solution (0.1 M Na/K phosphate, pH 6.2, 0.2 M NaCl, 50 % PEG200) at 22 °C. X-ray crystallographic data were collected at the Penn State X-ray Crystallography Facility and the data were processed with HKL2000[54]. For Sulfur single-wavelength anomalous dispersion phasing, 10 S atom positions were identified and the initial phase and density-modified map were calculated by AutoSol followed by automated model building by AutoBuild in the program Phenix[49]. Iterative refinement by Phenix and model building using Coot[46] improved the map and model. Finally, water molecules were added to the model. The data statistics and X-ray structure parameters are shown in Supplementary Table 7.

Protein purification for biochemical assays - *Msm* RNAP core

Strain of *Eco* containing plasmid with subunits of the RNAP core (LK1853[1]) was grown to the exponential phase (OD_{600} ~ 0.5). Expression of RNAP was induced with 500 µM IPTG for 4 h at room temperature. Cells were harvested by centrifugation, washed, resuspended in P buffer (300 mM NaCl, 50 mM Na_2HPO_4, 5 % glycerol, 3 mM β-mercaptoethanol) and disrupted by sonication. Cell debris was removed by centrifugation and supernatant was mixed with 1 ml Ni-NTA Agarose (Qiagen) and incubated for 90 minutes at 4 °C with gentle shaking. Ni-NTA Agarose with bound RNAP was loaded on a Poly-Prep® Chromatography Column (BIO-RAD), washed with P buffer and, subsequently, washed with P buffer with 30 mM imidazole. The proteins were eluted with P buffer containing 400 mM imidazole and fractions containing RNAP were pooled and dialyzed against storage buffer (50 mM Tris–HCl, pH 8.0, 100 mM NaCl, 50 % glycerol, 3 mM β-mercaptoethanol). The RNAP protein was stored at –20 °C.

Protein purification for biochemical assays - *Msm* σ^A

Expression strain of *Eco* containing plasmid with gene of σ^A (LK1740) was grown at 37 °C until OD_{600} reached ~0.5; expression of σ^A was induced with 300 µM IPTG at room temperature for 3 h. Isolation of σ^A was done in the same way as RNAP purification with the exception of 50 mM imidazole added to the P buffer before resuspending the cells. Instead of the purification in a column, batch purification and centrifugation were used to separate the matrix and the eluate.

Protein purification for biochemical assays - *Msm* RbpA

The expression and purification of RbpA (LK1254, this work) were done in the same way as for RNAP except when OD_{600} reached ~0.5, the expression was induced with 800 µM IPTG at room temperature for 3 h.

Protein purification for biochemical assays - *Msm* HelD

Msm HelD was prepared as described previously, in the paragraph about purification of proteins for cryo-EM experiments.

585 Purity of all purified proteins was checked by SDS-PAGE gel.

586 **_Msm_ HelD ATP, GTP and CTP hydrolysis assay**

587 Hydrolysis of ATP, GTP and CTP (Sigma-Aldrich) by *Msm* HelD was measured in a total
588 volume of 50 µl reaction mixture which contained 10 mM substrate, 10 µg of *Msm* HelD and
589 reaction buffer composed of 50 mM Tris-HCl, pH 7.5, 50 mM NaCl, 5 mM $MgCl_2$. Incubation
590 was carried out at 37 °C for 30 min. The amount of released phosphate was analyzed
591 spectrophotometrically at λ = 850 nm according to a modified molybdenum blue method[55]
592 using a microplate reader Clariostar (BMG LABTECH, Ortenberg, Germany). Briefly, the
593 reaction was stopped by adding 62 µl of reagent A (0.1 M L-ascorbic acid, 0.5 M Cl_3CCOOH).
594 After thorough mixing, 12.5 µl of reagent B (10 mM $(NH_4)_6Mo_7O_{24}$) and 32 µl of reagent C
595 (0.1 M sodium citrate, 0.2 M $NaAsO_2$, 10 % acetic acid) was added. All enzymatic reactions
596 were performed in triplicates with separate background readings for each condition.

597 **DNA-Protein interaction analysis *in vitro***

598 DNA-Protein interactions were analyzed on 4-16% Bis-Tris native gels (Thermo Fisher
599 Scientific, cat. No. BN1002BOX) by Electrophoretic Mobility Shift Assay (EMSA). DNA
600 fragment was amplified by Expand High Fidelity PCR System (Roche, cat. No. 11732650001)
601 using #1101 and #1146 primers and *Msm* chromosomal DNA. The resulting 304 bp long PCR
602 fragment was excised and purified from agarose gel. Binding reactions were performed in
603 1xSTB buffer (50 mM Tris-HCl pH 8.0; 5 mM $Mg(C_2H_3O_2)_2$; 100 µM DTT; 50 mM KCl; 50 µg/ml
604 BSA) that contained RNAP (25 pmol), HelD (125 pmol) and DNA (0.2 pmol). First, RNAP was
605 pre-incubated in the presence or absence of HelD (at 37 °C, 45 min). Subsequently, DNA was
606 added and samples were incubated at 37 °C for additional 45 min. Then, NativePage buffer
607 (Invitrogen, cat. No. BN2003) was added and samples were loaded on native gel.
608 Electrophoresis was run in cold room (4 °C). Finally, the gel was stained with DNA stain
609 GelRed nucleic acid stain (Biotium, cat. No. 41003) in 1xTBS for 25 minutes and images were
610 taken with an Ingenius UV-light camera (Syngen). Unbound DNA was quantified by the
611 Quantity One software (BIO-RAD). The gel was subsequently stained with Simply Blue
612 (Invitrogen, cat. No. LC6060) for protein visualization.

613

Protein-Protein interaction analysis *in vitro*

Protein-Protein interactions were analyzed on 7 % Tris-acetate native gels (Thermo Fisher Scientific, cat. No. EA0355BOX) by EMSA. Binding reaction was done in 20 µl of 1xSTB buffer containing RNAP (25 pmol), HelD (125 pmol), σ^A (1,250 pmol) and RbpA (1,250 pmol) - protein combinations in reactions are specified in the Figure 4 legend. First, RNAP was reconstituted with/without HelD (at 37 °C, 45 min). Then RbpA and/or σ^A were added, followed by additional incubation at 37 °C for 45 min. 20 µl of Native Tris-Glycine buffer (Invitrogen, cat. No. LC2673) was added and 20 µl of the mixture was then loaded on a native gel. Electrophoresis was run in cold room (4 °C). Subsequently, for protein visualization, the gels were stained with Simply Blue. The identity of proteins in each band was determined by MALDI mass spectrometric identification.

Disassembly of elongation complexes

Elongation complexes (ECs), containing a transcription bubble, were assembled with the *Msm* RNAP core, based on a previously described assay[56]. Briefly, DNA and RNA oligonucleotides were purchased and are the same as in Table EV7 in [57]. The RNA (LK-pRNA) was monophosphorylated at the 5' end by the manufacturer. A 2-fold molar excess of RNA was mixed with template DNA (LK632) in water and annealed in a cycler (45 °C for 2 min, 42-27 °C: temperature was decreasing by 3 °C every 2 min, 25 °C for 10 min). RNAP (32 pmol per sample) was incubated with 4 pmol of the annealed hybrid in 10 µl of reaction buffer (40 mM Tris-HCl, pH 8.0, 10 mM $MgCl_2$, 1 mM DTT) for 15 min at room temperature with gentle shaking. 8 pmol of non-template DNA (LK631) containing biotin at the 5´ end was added and the mixture was incubated at 37 °C for 10 min.

Streptavidin-coated magnetic beads (25 µl per sample; Sigma S-2415) were washed with 500 µl of binding buffer (20 mM Tris-HCl, pH 8.0, 0.15 M NaCl) and resuspended in the same volume of fresh binding buffer. Assembled elongation complexes were then mixed with washed beads. ECs and beads were incubated together for 30 min at RT (room temperature) with continuous gentle shaking. Unbound complexes were removed by subsequent washing with 500 µl of binding buffer, 500 µl of washing buffer (20 mM Tris-HCl pH 8.0, 0.5 M NaCl, 2 mM $MgCl_2$, 1 mM DTT) and 500 µl of reaction buffer[58]. Beads were resuspended in reaction buffer with 100 mM final concentration of KCl, with or without GTP or ATP (final

concentration 200 µM) in a total volume of 5 µl. HelD in 2-fold ratio over RNAP (64 pmol per sample) or heat-inactivated HelD (5 min at 95 °C) or buffer were added to the final reaction volume of 10 µl. Reactions proceeded for 20 min at 37 °C. The bound (in complex with EC) and released (free in buffer) RNAPs were separated by using a DYNAL Invitrogen bead separation device. Subsequently, the fractions containing released RNAPs were spotted directly on nitrocellulose membrane. RNAPs were detected by Western blotting using mouse monoclonal antibodies against the β subunit of RNAP (clone name 8RB13, dilution 1:1000) and secondary antibodies conjugated with a fluorophore dye (WesternBrightTM MCF-IR, Advansta, 800 nm anti-mouse antibody, dilution 1:10 000) and scanned with an Odyssey reader (LI-COR Biosciences). The analysis was done with the Quantity One software (BIO-RAD). The experiment was conducted in five biological replicates.

Immunoprecipitation

150 ml of *Msm* exponential (Supplementary Figure 12) and 100 ml of stationary phase (Figure 4f and Supplementary Figures 1 and 13) cells were pelleted and resuspended in 4 ml of Lysis buffer (20 mM Tris-HCl, pH 8, 150 mM KCl, 1 mM $MgCl_2$) with 1 mM DTT, 0.5 mM PMSF and Sigma protease inhibitor cocktail P8849 (5 µl/ml), sonicated 15 × 10 s with 1 min pauses on ice and centrifuged. 1 ml of stationary and 1.5 ml of exponential phase cells lysates were incubated over night at 4 °C with 25 µl of ANTI-FLAG® M2 Affinity Agarose Gel (Sigma, A2220). Agarose gel beads with the captured protein complexes were washed 4x with 0.5 ml 20 mM Tris-HCl, pH 8, 150 mM KCl, 1 mM $MgCl_2$. FLAG-tagged proteins were eluted by 60 µl of 3x FLAG® Peptide (Sigma F4799) (diluted in Tris-buffered saline (TBS) to a final concentration of 150 ng/ml). Proteins were resolved on sodium dodecylsulphate-polyacrylamide gel electrophoresis (SDS-PAGE) and Simply Blue-stained (SimplyBlue, Invitrogen) or analyzed by Western blotting.

Double pull-down

Eluted proteins from the first immunoprecipitation (ANTI-FLAG, see above) from lysates of the HelD-FLAG culture from exponential phase were incubated (O/N, 4 °C) with 5 µg of σ^A or IgG antibodies (negative control), respectively, bound to 20 µl of Protein G-plus Agarose (Santa Cruz Biotechnology, Cat. No. sc-2002), and then 4x washed with 1 ml Lysis buffer. Finally, proteins were analyzed by SDS-PAGE and Western blot.

Western blotting

Proteins were resolved by SDS-PAGE and detected by Western blotting using mouse monoclonal antibodies against σ^{70}/σ^{A} (clone name 2G10, Biolegend, cat. No. 663208, dilution 1:1000), against the β subunit of RNAP (clone name 8RB13, Biolegend, cat. No. 663903, dilution 1:1000), monoclonal anti-FLAG (clone M2, Sigma cat. No. F1804, dilution 1:1000), and anti-mouse secondary antibodies conjugated with HRP (Sigma, cat. No. A7058, dilution 1:80 000). Subsequently, the blot was incubated for 5 min with SuperSignal™ West Pico PLUS Chemiluminiscent substrate (Thermo scientific, cat. No. 34577), exposed on film and developed.

Trypsin digestion and MALDI mass spectrometric identification

Simply Blue-stained protein bands were cut out from gels, chopped into small pieces and destained using 50 mM 4-ethylmorpholine acetate (pH 8.1) in 50 % acetonitrile (MeCN). The gel pieces were then washed with water, reduced in size by dehydration in MeCN and partly dried in a SpeedVac concentrator. The proteins were digested overnight at 37 °C using sequencing grade trypsin (100 ng; Promega) in a buffer containing 25 mM 4-ethylmorpholine acetate and 5 % MeCN. The resulting peptides were extracted with 40 % MeCN/0.2 % TFA (trifluoroacetic acid).

For MALDI MS analysis, 0.5 µl of each peptide mixture was deposited on the MALDI plate, air-dried at room temperature, and overlaid with 0.5 µl of the matrix solution (α-cyano-4-hydroxycinnamic acid in 50% acetonitrile/0.1 % TFA; 5 mg/ml, Sigma). Peptide mass maps of proteins in Figure 4f and Supplementary Figure 1 were measured using an Autoflex Speed MALDI-TOF instrument (Bruker Daltonics, Billerica, USA) in a mass range of 700-4,000 Da and calibrated externally using a PepMix II standard (Bruker Daltonics). For protein identification, MS spectra were searched against NCBIprot_20190611 database subset of bacterial proteins using the in-house MASCOT v.2.6 search engine with the following settings: peptide tolerance of 20 ppm, missed cleavage site set to one and variable oxidation of methionine. The spectra of proteins in Figure 4h were acquired on a 15T Solarix XR FT-ICR mass spectrometer (Bruker Daltonics) in a mass range of 500-6,000 Da and calibrated internally using peptide masses of *Msm* RpoB and RpoC proteins. The peak lists generated using DataAnalysis 5.0 program were searched against UniProtKB database of *Msm* proteins using the

in-house MASCOT engine with the following settings: peptide tolerance of 3 ppm, missed cleavage site set to two variable and oxidation of methionine.

Data Availability

All source data used for statistics and plots are available in the Source Data file. Other data are available from the corresponding authors. Co-ordinates and structure factors or maps have been deposited in the wwwPDB or EMDB:

Bsu HelD C-terminal domain (X-ray) PDB ID 6VSX [https://doi.org/10.2210/pdb6VSX/pdb]

Msm HelD-RNAP complex State I (cryoEM) EMD-10996
[https://www.ebi.ac.uk/pdbe/entry/emdb/EMD-10996] , PDB ID 6YXU
[https://doi.org/10.2210/pdb6YXU/pdb]

Msm HelD-RNAP complex State II (cryoEM) EMD-11004
[https://www.ebi.ac.uk/pdbe/entry/emdb/EMD-11004] , PDB ID 6YYS
[https://doi.org/10.2210/pdb6YYS/pdb]

Msm HelD-RNAP complex State III (cryoEM) EMD-11026
[https://www.ebi.ac.uk/pdbe/entry/emdb/EMD-11026] , PDB ID 6Z11
[https://doi.org/10.2210/pdb6Z11/pdb]

References

1 Kouba, T. *et al.* The Core and Holoenzyme Forms of RNA Polymerase from Mycobacterium smegmatis. *J Bacteriol* **201**, doi:10.1128/JB.00583-18 (2019).

2 Paget, M. S. Bacterial Sigma Factors and Anti-Sigma Factors: Structure, Function and Distribution. *Biomolecules* **5**, 1245-1265, doi:10.3390/biom5031245 (2015).

3 Lee, J. & Borukhov, S. Bacterial RNA Polymerase-DNA Interaction-The Driving Force of Gene Expression and the Target for Drug Action. *Front Mol Biosci* **3**, 73, doi:10.3389/fmolb.2016.00073 (2016).

4 Barvik, I., Rejman, D., Panova, N., Sanderova, H. & Krasny, L. Non-canonical transcription initiation: the expanding universe of transcription initiating substrates. *FEMS Microbiol Rev* **41**, 131-138, doi:10.1093/femsre/fuw041 (2017).

5 Vassylyev, D. G., Vassylyeva, M. N., Perederina, A., Tahirov, T. H. & Artsimovitch, I. Structural basis for transcription elongation by bacterial RNA polymerase. *Nature* **448**, 157-162, doi:10.1038/nature05932 (2007).

6 Lopez de Saro, F. J., Yoshikawa, N. & Helmann, J. D. Expression, abundance, and RNA polymerase binding properties of the delta factor of Bacillus subtilis. *J Biol Chem* **274**, 15953-15958, doi:10.1074/jbc.274.22.15953 (1999).

7 Keller, A. N. *et al.* epsilon, a new subunit of RNA polymerase found in gram-positive bacteria. *J Bacteriol* **196**, 3622-3632, doi:10.1128/JB.02020-14 (2014).

8 Jensen, D., Manzano, A. R., Rammohan, J., Stallings, C. L. & Galburt, E. A. CarD and RbpA modify the kinetics of initial transcription and slow promoter escape of the Mycobacterium tuberculosis RNA polymerase. *Nucleic Acids Res* **47**, 6685-6698, doi:10.1093/nar/gkz449 (2019).

9 Delumeau, O. *et al.* The dynamic protein partnership of RNA polymerase in Bacillus subtilis. *Proteomics* **11**, 2992-3001, doi:10.1002/pmic.201000790 (2011).

10 Fairman-Williams, M. E., Guenther, U. P. & Jankowsky, E. SF1 and SF2 helicases: family matters. *Curr Opin Struct Biol* **20**, 313-324, doi:10.1016/j.sbi.2010.03.011 (2010).

11 Wiedermannova, J. *et al.* Characterization of HelD, an interacting partner of RNA polymerase from Bacillus subtilis. *Nucleic Acids Res* **42**, 5151-5163, doi:10.1093/nar/gku113 (2014).

12 Koval, T. *et al.* Domain structure of HelD, an interaction partner of Bacillus subtilis RNA polymerase. *FEBS Lett* **593**, 996-1005, doi:10.1002/1873-3468.13385 (2019).

13 Meeske, A. J. *et al.* High-Throughput Genetic Screens Identify a Large and Diverse Collection of New Sporulation Genes in Bacillus subtilis. *PLoS Biol* **14**, e1002341, doi:10.1371/journal.pbio.1002341 (2016).

14 Krissinel, E. & Henrick, K. Inference of macromolecular assemblies from crystalline state. *J Mol Biol* **372**, 774-797, doi:10.1016/j.jmb.2007.05.022 (2007).

15 Ross, W. *et al.* ppGpp Binding to a Site at the RNAP-DksA Interface Accounts for Its Dramatic Effects on Transcription Initiation during the Stringent Response. *Mol Cell* **62**, 811-823, doi:10.1016/j.molcel.2016.04.029 (2016).

16 Molodtsov, V. *et al.* Allosteric Effector ppGpp Potentiates the Inhibition of Transcript Initiation by DksA. *Mol Cell* **69**, 828-839 e825, doi:10.1016/j.molcel.2018.01.035 (2018).

17 Abdelkareem, M. *et al.* Structural Basis of Transcription: RNA Polymerase Backtracking and Its Reactivation. *Mol Cell* **75**, 298-309 e294, doi:10.1016/j.molcel.2019.04.029 (2019).
18 Laptenko, O., Lee, J., Lomakin, I. & Borukhov, S. Transcript cleavage factors GreA and GreB act as transient catalytic components of RNA polymerase. *EMBO J* **22**, 6322-6334, doi:10.1093/emboj/cdg610 (2003).
19 Perederina, A. *et al.* Regulation through the secondary channel--structural framework for ppGpp-DksA synergism during transcription. *Cell* **118**, 297-309, doi:10.1016/j.cell.2004.06.030 (2004).
20 Sosunova, E. *et al.* Donation of catalytic residues to RNA polymerase active center by transcription factor Gre. *Proc Natl Acad Sci U S A* **100**, 15469-15474, doi:10.1073/pnas.2536698100 (2003).
21 Raney, K. D., Byrd, A. K. & Aarattuthodiyil, S. Structure and Mechanisms of SF1 DNA Helicases. *Adv Exp Med Biol* **973**, E1, doi:10.1007/978-1-4614-5037-5_14 (2013).
22 Lee, J. Y. & Yang, W. UvrD helicase unwinds DNA one base pair at a time by a two-part power stroke. *Cell* **127**, 1349-1360, doi:10.1016/j.cell.2006.10.049 (2006).
23 Liu, B., Zuo, Y. & Steitz, T. A. Structural basis for transcription reactivation by RapA. *Proc Natl Acad Sci U S A* **112**, 2006-2010, doi:10.1073/pnas.1417152112 (2015).
24 Tafur, L. *et al.* Molecular Structures of Transcribing RNA Polymerase I. *Mol Cell* **64**, 1135-1143, doi:10.1016/j.molcel.2016.11.013 (2016).
25 Chen, J. *et al.* Stepwise Promoter Melting by Bacterial RNA Polymerase. *Mol Cell* **78**, 275-288 e276, doi:10.1016/j.molcel.2020.02.017 (2020).
26 Lin, W. *et al.* Structural Basis of Transcription Inhibition by Fidaxomicin (Lipiarmycin A3). *Mol Cell* **70**, 60-71 e15, doi:10.1016/j.molcel.2018.02.026 (2018).
27 Boyaci, H. *et al.* Fidaxomicin jams Mycobacterium tuberculosis RNA polymerase motions needed for initiation via RbpA contacts. *Elife* **7**, doi:10.7554/eLife.34823 (2018).
28 Kohler, R., Mooney, R. A., Mills, D. J., Landick, R. & Cramer, P. Architecture of a transcribing-translating expressome. *Science* **356**, 194-197, doi:10.1126/science.aal3059 (2017).
29 Pani, B. & Nudler, E. Mechanistic insights into transcription coupled DNA repair. *DNA Repair (Amst)* **56**, 42-50, doi:10.1016/j.dnarep.2017.06.006 (2017).
30 Lang, K. S. & Merrikh, H. The Clash of Macromolecular Titans: Replication-Transcription Conflicts in Bacteria. *Annu Rev Microbiol* **72**, 71-88, doi:10.1146/annurev-micro-090817-062514 (2018).
31 Harden, T. T. *et al.* Alternative transcription cycle for bacterial RNA polymerase. *Nat Commun* **11**, 448, doi:10.1038/s41467-019-14208-9 (2020).
32 Tran, Q. H. & Unden, G. Changes in the proton potential and the cellular energetics of Escherichia coli during growth by aerobic and anaerobic respiration or by fermentation. *Eur J Biochem* **251**, 538-543, doi:10.1046/j.1432-1327.1998.2510538.x (1998).
33 Chen, J. *et al.* 6S RNA Mimics B-Form DNA to Regulate Escherichia coli RNA Polymerase. *Mol Cell* **68**, 388-397 e386, doi:10.1016/j.molcel.2017.09.006 (2017).
34 Hnilicova, J. *et al.* Ms1, a novel sRNA interacting with the RNA polymerase core in mycobacteria. *Nucleic Acids Res* **42**, 11763-11776, doi:10.1093/nar/gku793 (2014).

35 Choudhary, E., Thakur, P., Pareek, M. & Agarwal, N. Gene silencing by CRISPR interference in mycobacteria. *Nat Commun* **6**, 6267, doi:10.1038/ncomms7267 (2015).

36 Zhang, K. Gctf: Real-time CTF determination and correction. *J Struct Biol* **193**, 1-12, doi:10.1016/j.jsb.2015.11.003 (2016).

37 Zivanov, J. *et al.* New tools for automated high-resolution cryo-EM structure determination in RELION-3. *Elife* **7**, doi:10.7554/eLife.42166 (2018).

38 Tegunov, D. & Cramer, P. Real-time cryo-electron microscopy data preprocessing with Warp. *Nat Methods* **16**, 1146-1152, doi:10.1038/s41592-019-0580-y (2019).

39 Wilkinson, M. E., Kumar, A. & Casanal, A. Methods for merging data sets in electron cryo-microscopy. *Acta Crystallogr D Struct Biol* **75**, 782-791, doi:10.1107/S2059798319010519 (2019).

40 Zivanov, J., Nakane, T. & Scheres, S. H. W. Estimation of high-order aberrations and anisotropic magnification from cryo-EM data sets in RELION-3.1. *IUCrJ* **7**, 253-267, doi:10.1107/S2052252520000081 (2020).

41 Burnley, T., Palmer, C. M. & Winn, M. Recent developments in the CCP-EM software suite. *Acta Crystallogr D Struct Biol* **73**, 469-477, doi:10.1107/S2059798317007859 (2017).

42 Jakobi, A. J., Wilmanns, M. & Sachse, C. Model-based local density sharpening of cryo-EM maps. *Elife* **6**, doi:10.7554/eLife.27131 (2017).

43 Tan, Y. Z. *et al.* Addressing preferred specimen orientation in single-particle cryo-EM through tilting. *Nat Methods* **14**, 793-796, doi:10.1038/nmeth.4347 (2017).

44 Vagin, A. & Teplyakov, A. Molecular replacement with MOLREP. *Acta Crystallogr D Biol Crystallogr* **66**, 22-25, doi:10.1107/S0907444909042589 (2010).

45 Brown, A. *et al.* Tools for macromolecular model building and refinement into electron cryo-microscopy reconstructions. *Acta Crystallogr D Biol Crystallogr* **71**, 136-153, doi:10.1107/S1399004714021683 (2015).

46 Emsley, P. & Cowtan, K. Coot: model-building tools for molecular graphics. *Acta Crystallogr D Biol Crystallogr* **60**, 2126-2132, doi:S0907444904019158 doi:10.1107/S0907444904019158 (2004).

47 Cowtan, K. The Buccaneer software for automated model building. 1. Tracing protein chains. *Acta crystallographica. Section D, Biological crystallography* **62**, 1002-1011, doi:10.1107/S0907444906022116 (2006).

48 Terashi, G. & Kihara, D. De novo main-chain modeling for EM maps using MAINMAST. *Nat Commun* **9**, 1618, doi:10.1038/s41467-018-04053-7 (2018).

49 Afonine, P. V. *et al.* Real-space refinement in PHENIX for cryo-EM and crystallography. *Acta Crystallogr D Struct Biol* **74**, 531-544, doi:10.1107/S2059798318006551 (2018).

50 Jurrus, E. *et al.* Improvements to the APBS biomolecular solvation software suite. *Protein Sci* **27**, 112-128, doi:10.1002/pro.3280 (2018).

51 Pettersen, E. F. *et al.* UCSF Chimera--a visualization system for exploratory research and analysis. *J Comput Chem* **25**, 1605-1612, doi:10.1002/jcc.20084 (2004).

52 McNicholas, S., Potterton, E., Wilson, K. S. & Noble, M. E. Presenting your structures: the CCP4mg molecular-graphics software. *Acta Crystallogr D Biol Crystallogr* **67**, 386-394, doi:10.1107/S0907444911007281 (2011).

53 Schlee, S. *et al.* Prediction of quaternary structure by analysis of hot spot residues in protein-protein interfaces: the case of anthranilate phosphoribosyltransferases. *Proteins* **87**, 815-825, doi:10.1002/prot.25744 (2019).
54 Otwinowski, Z. & Minor, W. Processing of X-ray diffraction data collected in oscillation mode. *Methods Enzymol* **276**, 307-326 (1997).
55 He, Z. & Honeycutt, C. W. A Modified Molybdenum Blue Method for Orthophosphate Determination Suitable for Investigating Enzymatic Hydrolysis of Organic Phosphates. *Communications in Soil Science and Plant Analysis* **36**, 1373-1383, doi:10.1081/CSS-200056954 (2005).
56 Komissarova, N., Kireeva, M. L., Becker, J., Sidorenkov, I. & Kashlev, M. Engineering of elongation complexes of bacterial and yeast RNA polymerases. *Methods Enzymol* **371**, 233-251, doi:10.1016/S0076-6879(03)71017-9 (2003).
57 Sikova, M. *et al.* The torpedo effect in Bacillus subtilis: RNase J1 resolves stalled transcription complexes. *EMBO J* **39**, e102500, doi:10.15252/embj.2019102500 (2020).
58 Deng, Z. *et al.* Yin Yang 1 regulates the transcriptional activity of androgen receptor. *Oncogene* **28**, 3746-3757, doi:10.1038/onc.2009.231 (2009).

Acknowledgments

We thank the ESRF (especially Michael Hons), IBS and EMBL for access to the ESRF Krios beamline CM01; the CEITEC and the Czech Infrastructure for Integrative Structural Biology (CIISB) for access to the CEITEC Krios microscope and to the CMS facilities at BIOCEV (project LM2015043 by MEYS). This work was supported by 20-12109S (to LK and JD) and 20-07473S (to JH) from the Czech Science Foundation, NIH grant R35 GM131860 to KM, and by the Academy of Sciences of the Czech Republic (RVO: 86652036), MEYS (CZ.1.05/1.1.00/02.0109), European Regional Development Fund (Project CIISB4HEALTH, No. CZ.02.1.01/0.0/0.0/16_013/0001776 and ELIBIO, No. CZ.02.1.01/0.0/0.0/15_003/0000447), T Kou. holds a fellowship from the EMBL Interdisciplinary Postdocs (EI3POD) initiative co-funded by Marie Skłodowska-Curie grant agreement No. 664726.

Author contributions

JD and LK conceived and supervised the project. TKou, TKov, MT, and JDu expressed and purified proteins for cryo-EM, TKou prepared cryoEM grids, collected cryoEM data together with JN, performed image processing and 3D reconstruction, and built initial models together with JDo. KSM and UC solved the *Bsu* HelD CTD. MJ, JH, BB, MŠ, JP, PS, and HŠ did cloning, protein purifications and IPs. PH identified proteins by mass spectrometry. JP and PS performed DNA binding experiments. MT, JDu, and TKov performed NTP hydrolysis experiments. TKou, TKov and JDo built and refined atomic models and created figures. IB and MS performed *in silico* modelling. TKou, TKov, JDo and LK wrote the manuscript with input from IB. TS performed initial modelling and comparative analysis.

Competing interests

The authors declare no competing interests.

Figure legends

Figure 1: Cryo-EM structures of *Msm* HelD-RNAP complexes.

a, Description of *Msm* RNAP core (PDB ID 6F6W) subunits and domains; RNAP subunits are color-coded according to the inset legend**. b, c and d**, Atomic model surface representation of three identified *Msm* HelD-RNAP complexes: State I – PCh-engaged, State II – PCh-engaged AS-interfering and State III – PCh-dis-engaged AS-interfering. When fully ordered in State I and II (b and c), the HelD protein [color-coded as in (e)] forms a crescent-like shape, ends of which protrude to the primary and secondary channels of the RNAP core. The partly ordered HelD protein in State III (d) vacates most of the RNAP primary channel. **e**, Schematic linear representation of the domain structure of the HelD protein. The 1A domain (two shades of yellow) is split in aa sequence into two parts, separated by a large HelD-specific insertion (hues of blue and orange). The nucleotide-binding motifs are marked as vertical thick black lines. Aa numbering (*Msm*) is shown below. **f, g and h**, Three states of HelD as observed in (b**,** c and d) color-coded according to the domain structure (e); secondary structure elements are marked as in Supplementary Figure 7a.

Figure 2: The HelD N-terminal domain inserts into the RNAP secondary channel; domains 1A-2A comprise the NTPase unit.

a and **b,** Ribbon (State I) and surface (State II) representation of the HelD N-terminal domain interaction with the secondary channel of RNAP core (grey). The HelD coiled-coil domain (NCC-domain, firebrick) and the distinct loop (NG-loop, red) of the HelD globular domain (NG-domain, salmon) are inserted between β'-funnel, shelf and jaw. The NCC-domain reaches only the boundary line of the β' bridge helix (β'-BH, cyan) and leaves a passageway to the RNAP core active site (MgA, magenta sphere). The HelD NCC also restricts the trigger loop (TL, yellow) movement. The linker (NG-linker, violet) connects the N-terminal domain with domain 1A-1. **c**, The two *Msm* HelD Rossman fold domains (1A yellow and 2A green) form a canonical NTPase unit heterodimer with respect to structurally described SF1 helicases. Domain 1A tightly packs with β-lobe (dark grey) and its extension (brown) is clamped in-between one β-turn (β/184-187) of β-lobe and the tip of the β' subunit jaw (light grey). **d**, Model of ATP binding to the conserved nucleotide-binding site of motifs Q (blue), I (brown), II (pink), ~III (orange), IIIa (red), Va (pale green) and VI (deep blue). ATP (green) and Mg^{2+} (magenta sphere) are added based on superposition with the ternary complex of UvrD (PDB ID 2IS4). **e**, HelD exhibits ATPase and GTPase activities but does not hydrolyse CTP. The apparent negative value of CTP hydrolysis was caused by high background readings. The bars show mean values, the error bars indicate ±SD and the individual symbols represent values from three independent replicates. The data were analysed and the graphics created with GraphPad Prism 7.02.

Figure 3: The *Msm* HelD-specific domain interactions with the RNAP primary channel.

a, Surface of the *Msm* RNAP core (PDB ID 6F6W), color-coded as in Fig. 1a with description of individual domains and functional parts. **b** and **c,** Surface representation of States I and II of the *Msm* HelD-RNAP complex with RNAP color-coding as in (a) and marked domain names; HelD color-coding as in Fig. 1e. **d** and **e,** Ribbon representation of the HelD-specific domain inserting into the RNAP primary channel in State I (d) and State II (e). In State I (d), the clamp-opening (CO, blue) HelD-specific domain is projected from the HelD 1A domain (yellow) towards the β'-clamp (grey). At one end, the CO is bonded to the 1A domain by the CO-linker (cyan), and stabilised by β-turn 561-563 and α19 (yellow). On the other end, the CO-domain tip abuts towards the β'-NCD three-stranded sheet. Concomitantly, the HelD helix α16 (part of peptide HelD/449-473, orange) butts against the β'/1164-1210 three-stranded sheet. The connection between α16 and the 1A-extension is disordered (dotted line). In State II (e), The CO interaction with the 1A domain remains similar to State I (d). The CO-domain tip, however, shifts towards the β'-rudder (green) and β'/122-133 α-helix. Concomitantly, the HelD PCh-loop (orange) folds towards the active site (MgA, magenta sphere) and folds back towards the 1A-extension (brick) and 1A domain. **f**, The PCh-loop folds into the RNAP active site. The HelD loop 473-494 and the two adjacent α-helices (α16 and α17, orange) fold alongside the RNAP bridge helix (BH, cyan) towards the RNAP active site and HelD/Asp482 directly contacts the MgA (magenta sphere, details in inset, coordination of MgA is marked with blue dotted lines). The RNAP trigger loop (TL, yellow) is restricted and folded between the HelD PCh-loop helix α17, the HelD NCC-domain (ruby), β'-BH and the β-core domain (dark grey). **g**, Detail of the β'-BH interaction with HelD α16 and α17. BH β'/Arg874 and 875 sandwich HelD/Tyr466, and β'/Tyr871 stacks on HelD/Phe502. The stacking interactions are marked with yellow dotted lines. **h** and **i**, The HelD PCh-loop binding in the active site chamber is mutually exclusive with the presence of the transcription bubble. Two perpendicular views of superposition of the *Tt* RNAP elongation complex (PDB ID 2O5J, pale colors) and HelD State II (solid colors) are shown. The folded TL in pre-translocated EC would sterically clash with the HelD NCC-domain. The HelD PCh-loop tip would sterically clash with RNA/DNA hybrid at positions +1 to –2, and the HelD α16 and α17 helices would clash with downstream DNA duplex. Color code as in (f), template DNA in pink, non-template DNA in grey, product RNA and incoming NTP at position +1 in green.

Figure 4: Binding of *Msm* HelD to RNAP and its effects on DNA-RNAP interactions.

a, DNA binding to RNAP - EMSA - binding of 300 bp DNA to the *Msm* RNAP core and the effect of HelD. **b,** the same gel as above but stained for proteins. The dotted line shows where the gel was electronically assembled. **c**, quantitation of EMSA – the bars here (the amount of unshifted DNA) and in (e) are mean values from at least three independent experiments, the error bars show ±SD, the individual symbols show values of individual independent replicates. The leftmost bars were set as 1 and the other values within each graph were normalized relative to this bar. The turquoise bars here and in (e) indicate the addition of HelD. **d**, EC disassembly - scheme: ECs were assembled on DNA:RNA scaffolds and challenged with HelD and/or NTPs. RNAP released into buffer was quantitated by Western dot blots. **e**, Quantitation of EC disassembly from five independent experiments. Representative primary data are shown below the graph. Presence/absence of individual components is indicated. +° indicates heat-inactivated HelD. The statistical significance in (e) for the indicated combinations was $p<0.05$ (one-sided Student's t-test; exact p values are

written in the graph). **f**, Representative SDS PAGE of immunoprecipitations of *Msm* RNAP (β), σ^A, and HelD. All proteins were FLAG fusions, the antibody was anti-FLAG. Wt, a strain without any FLAG fusion. The identity of the bands was confirmed by mass spectrometry. IP, immunoprecipitation; M, markers. The experiment (biological replicates) was performed 3x with the same result. **g**, Representative Western blot of IPs of FLAG-tagged *Msm* RNAP (β), σ^A, and HelD. Antibodies against RNAP β and σ^A were used to detect the presence of proteins in complexes. M, marker – purified σ^A. The experiment was performed twice with the same result. **h**, *In vitro* protein interactions - EMSA. Proteins were detected by Simply blue SafeStain. In all cases, RNAP was first reconstituted with HelD and then with RbpA and/or σ^A. A small, but reproducible shift was observed after addition of both RbpA and σ^A to RNAP-HelD, indicating the presence of all proteins in one complex. Numbered arrows indicate complexes with different protein composition (determined by mass spectrometry). In some cases, complexes with different protein composition displayed the same migration in the gel: 1. RNAP, RNAP-RbpA; RNAP-σ^A; 2. RNAP-HelD, RNAP-HelD-RbpA; 3. RNAP-HelD-σ^A; 4. RNAP-HelD-σ^A-RbpA. The experiment (biological replicates) was performed 3x with the same result.

Figure 5: A model of the HelD functioning in RNAP recycling.

a, When EC stalls, it needs to be disassembled. **b** The HelD N-terminal domain (pink) first approaches the RNAP secondary channel and then induces changes in RNAP likely destabilising the RNAP-dwDNA interaction. **c**, Subsequent interactions of the HelD PCh-loop (orange) and the whole HelD-specific domain (cyan) in the RNAP primary channel open the RNAP cleft, widen the RNA exit channel and mechanically interfere with dwDNA. **d**, An even broader cleft/RNA exit opening together with the PCh-loop intervening deep in the AS (MgA, magenta sphere) displace dwDNA and the RNA/DNA hybrid from the active site cavity. **e**, The HelD-RNAP nucleic acid-free complex binds σ^A factor and RbpA, and all factors can bind RNAP core simultaneously. **f**, The complex binds to DNA promoter via the σ^A factor with concomitant displacement of HelD from RNAP by an unknown mechanism, possibly dependent on NTP hydrolysis by HelD and a new round of σ^A-dependent transcription cycle can initiate.

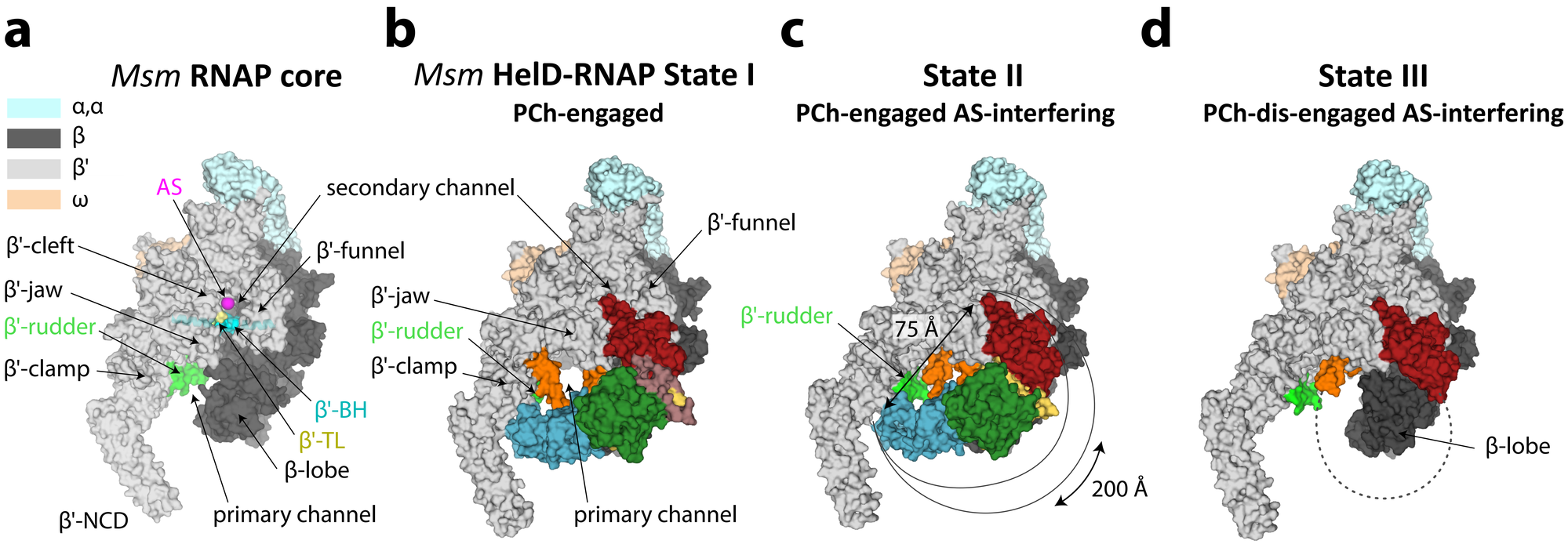
a
Msm RNAP core
α,α
β
β'
ω
AS
secondary channel
β'-cleft
β'-funnel
β'-jaw
β'-rudder
β'-clamp
β'-BH
β'-TL
β-lobe
β'-NCD
primary channel
b
Msm HelD-RNAP State I
PCh-engaged
β'-funnel
β'-jaw
β'-rudder
β'-clamp
primary channel
c
State II
PCh-engaged AS-interfering
β'-rudder
75 Å
200 Å
d
State III
PCh-dis-engaged AS-interfering
β-lobe

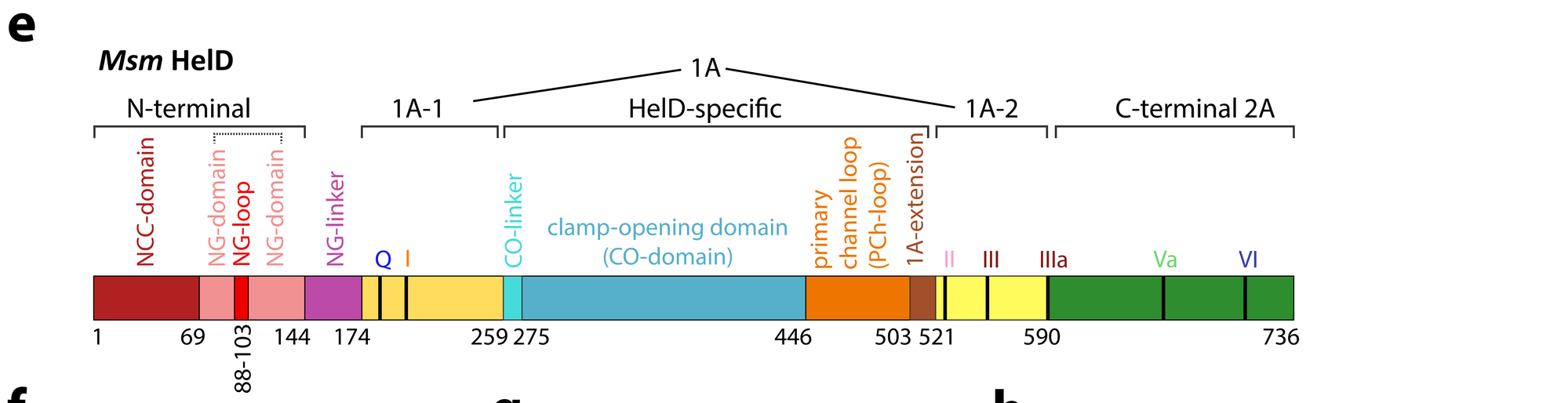
e
Msm HelD
1A
N-terminal
1A-1
HelD-specific
1A-2
C-terminal 2A
NCC-domain
NG-domain
NG-loop
NG-domain
NG-linker
Q
I
CO-linker
clamp-opening domain
(CO-domain)
primary
channel loop
(PCh-loop)
1A-extension
II
III
IIIa
Va
VI
1
69
88-103
144
174
259
275
446
503
521
590
736

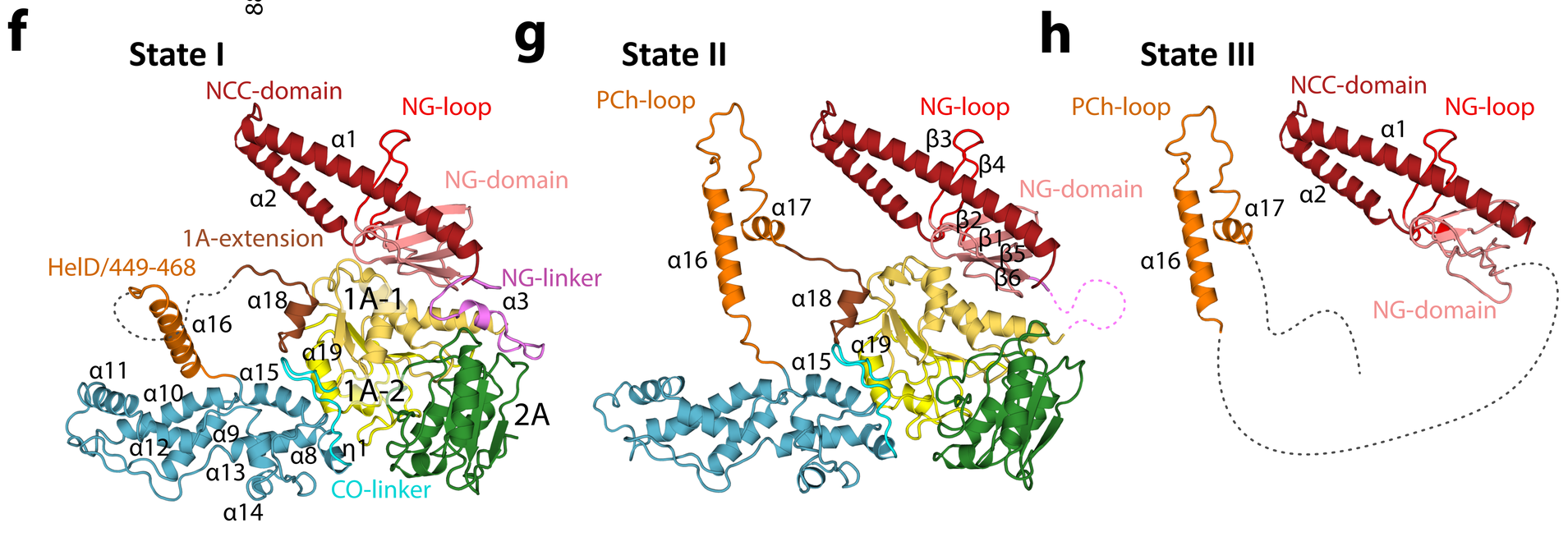
f
State I
NCC-domain
NG-loop
α1
NG-domain
α2
1A-extension
HelD/449-468
NG-linker
α18
1A-1
α3
α16
α19
α11
α15
1A-2
2A
α10
α9
α12
α8
η1
α13
CO-linker
α14
g
State II
PCh-loop
NG-loop
β3
β4
NG-domain
α17
β2
β1
β5
β6
α16
α18
α19
α15
h
State III
NCC-domain
NG-loop
PCh-loop
α1
α17
α2
α16
NG-domain

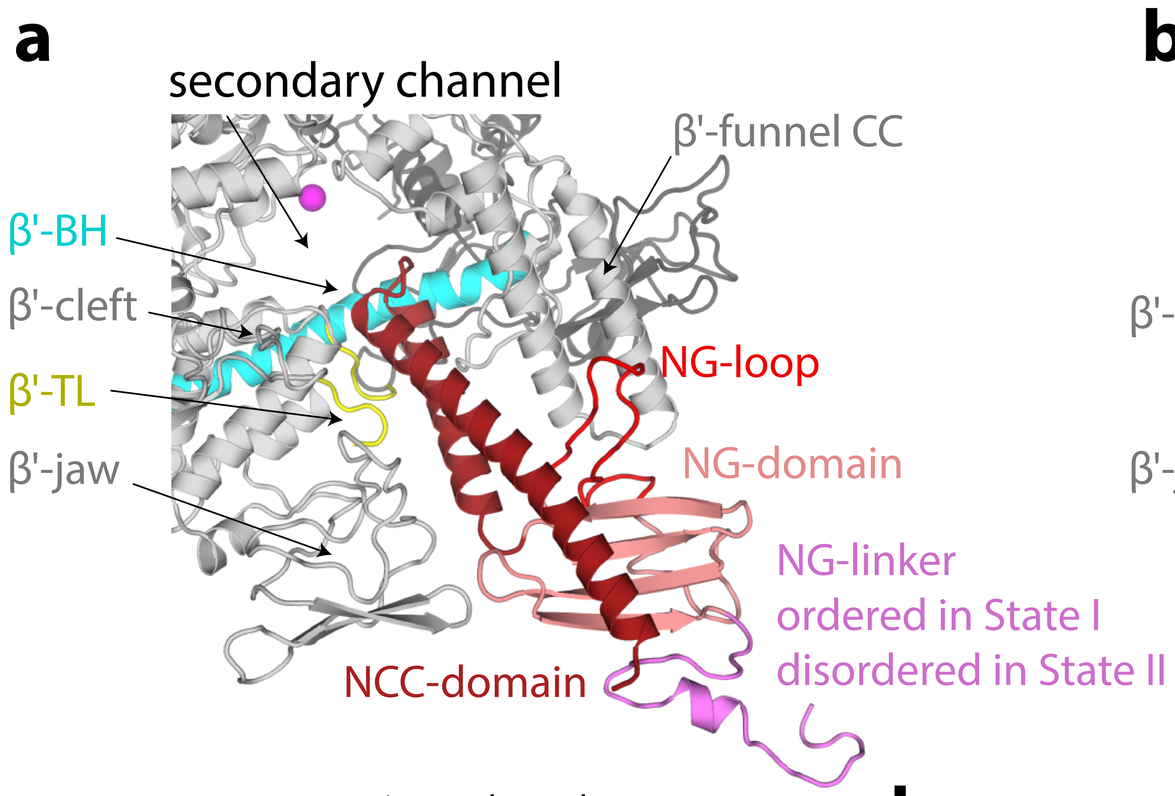
a
secondary channel
β'-funnel CC
β'-BH
β'-cleft
β'-TL
β'-jaw
NG-loop
NG-domain
NG-linker
ordered in State I
disordered in State II
NCC-domain

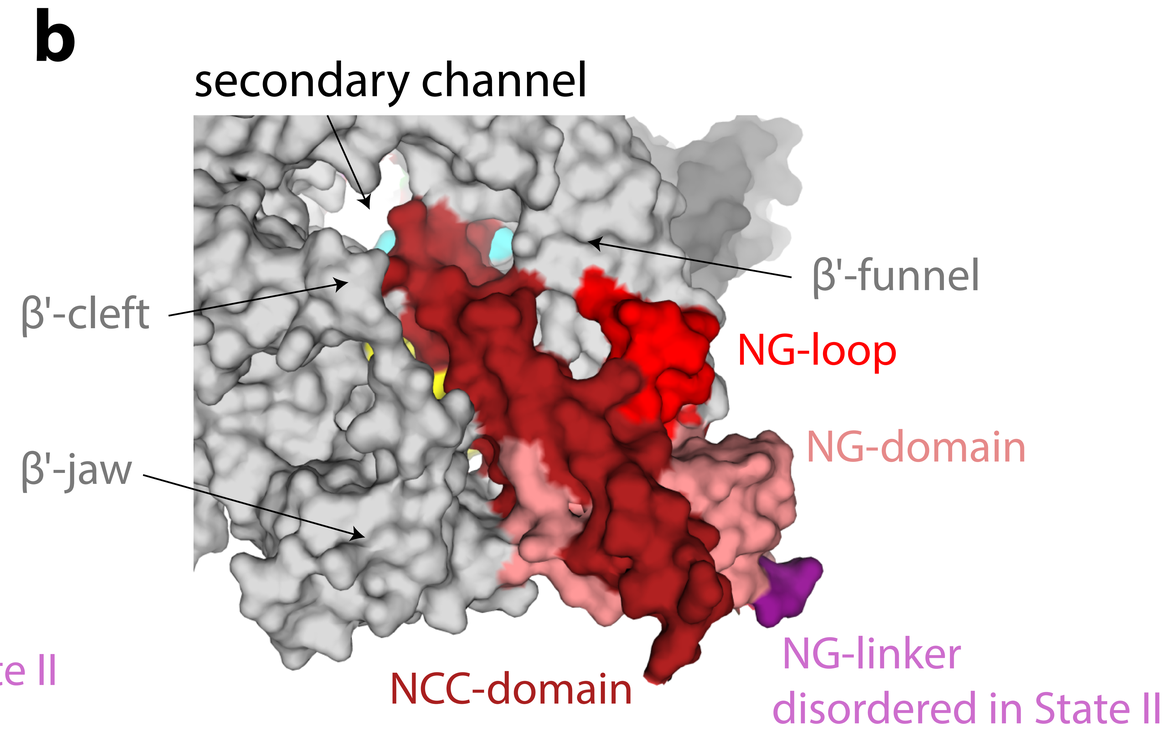
b
secondary channel
β'-cleft
β'-jaw
β'-funnel
NG-loop
NG-domain
NG-linker
disordered in State II
NCC-domain

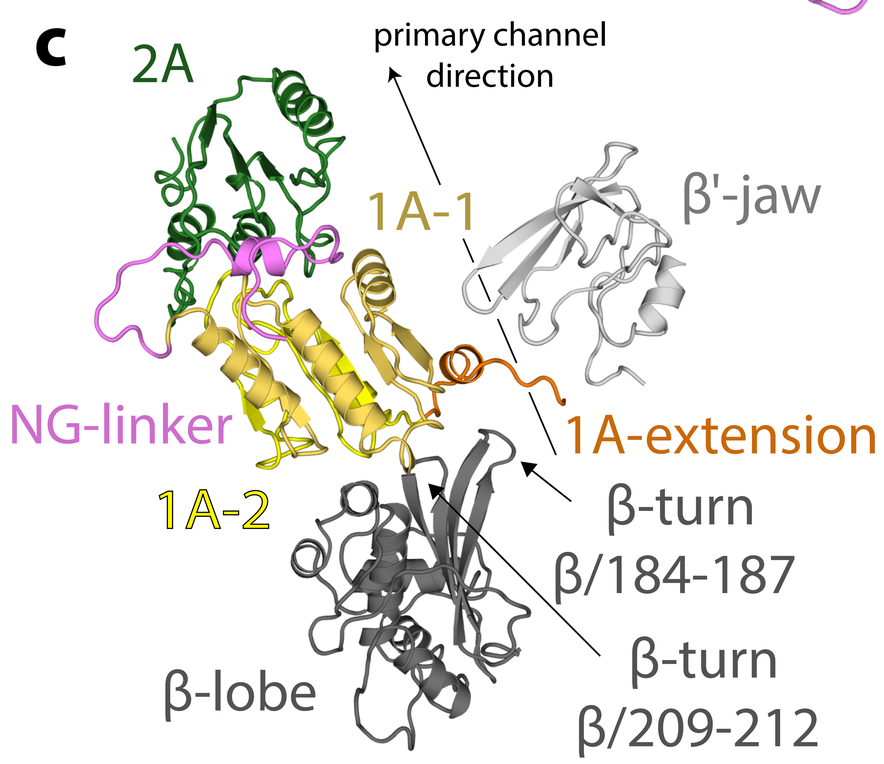
c
2A
primary channel
direction
1A-1
β'-jaw
NG-linker
1A-extension
1A-2
β-turn
β/184-187
β-lobe
β-turn
β/209-212

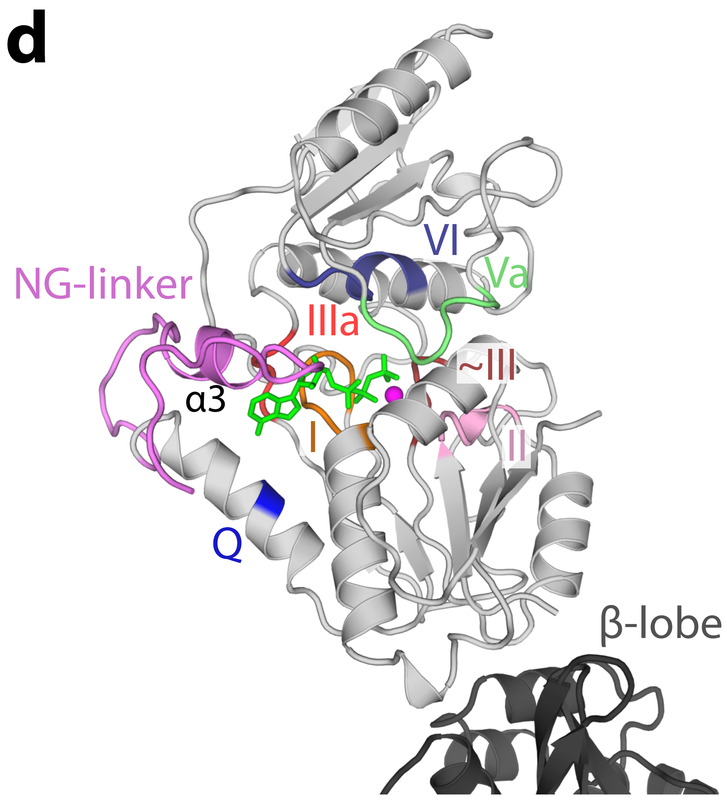
d
NG-linker
VI
Va
IIIa
~III
α3
I
II
Q
β-lobe

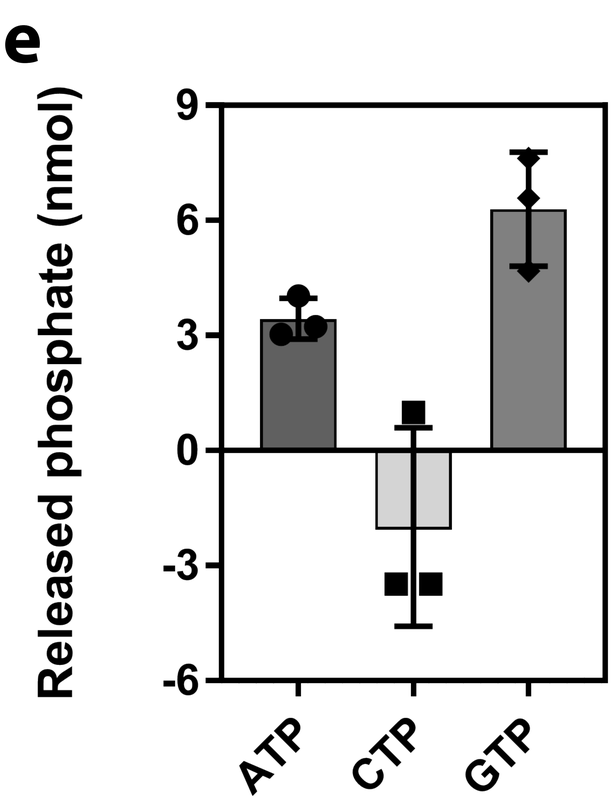
e
Released phosphate (nmol)
9
6
3
0
-3
-6
ATP
CTP
GTP

a

Msm **RNAP core**

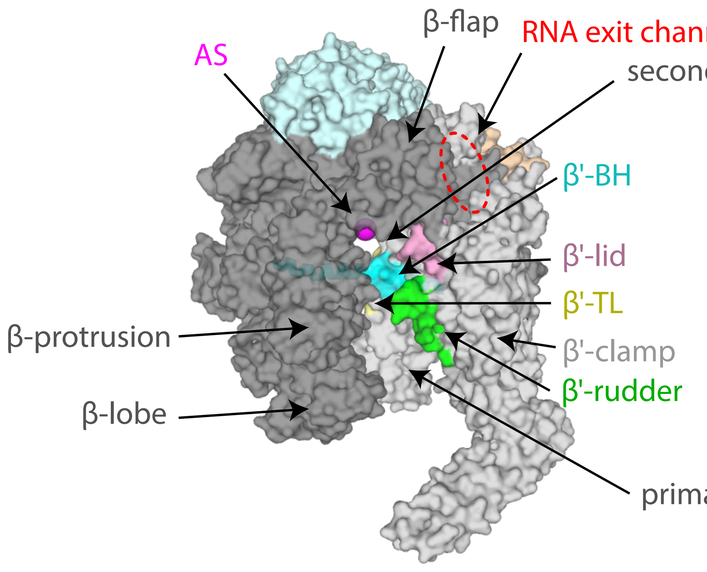

b

Msm **HelD-RNAP State I**

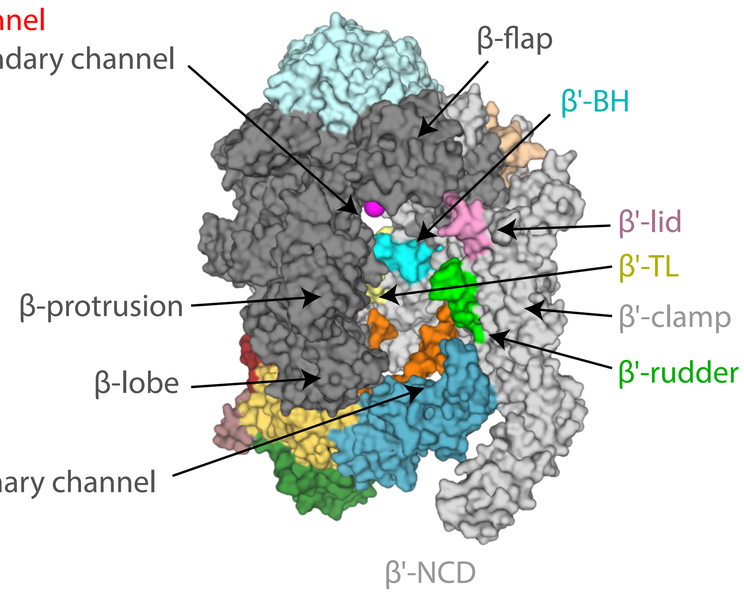

c

State II

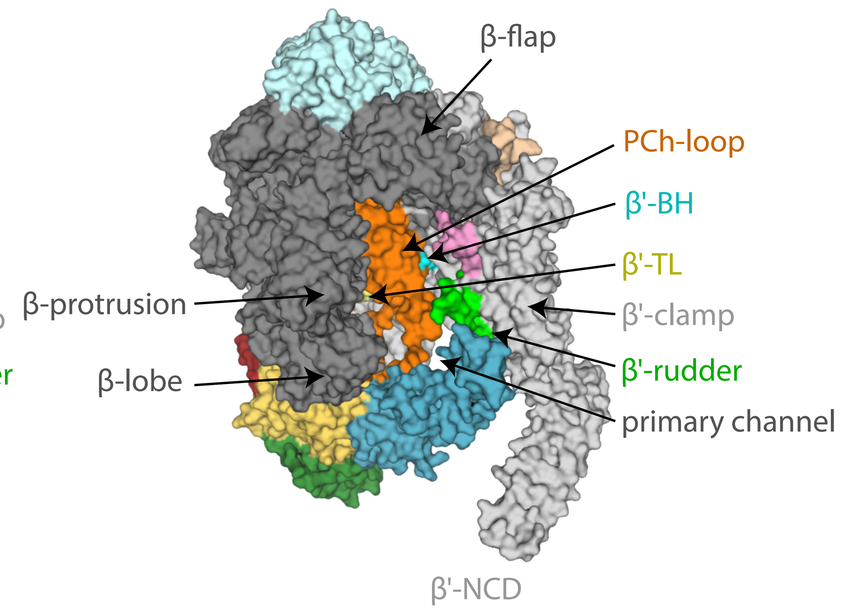

d

State I

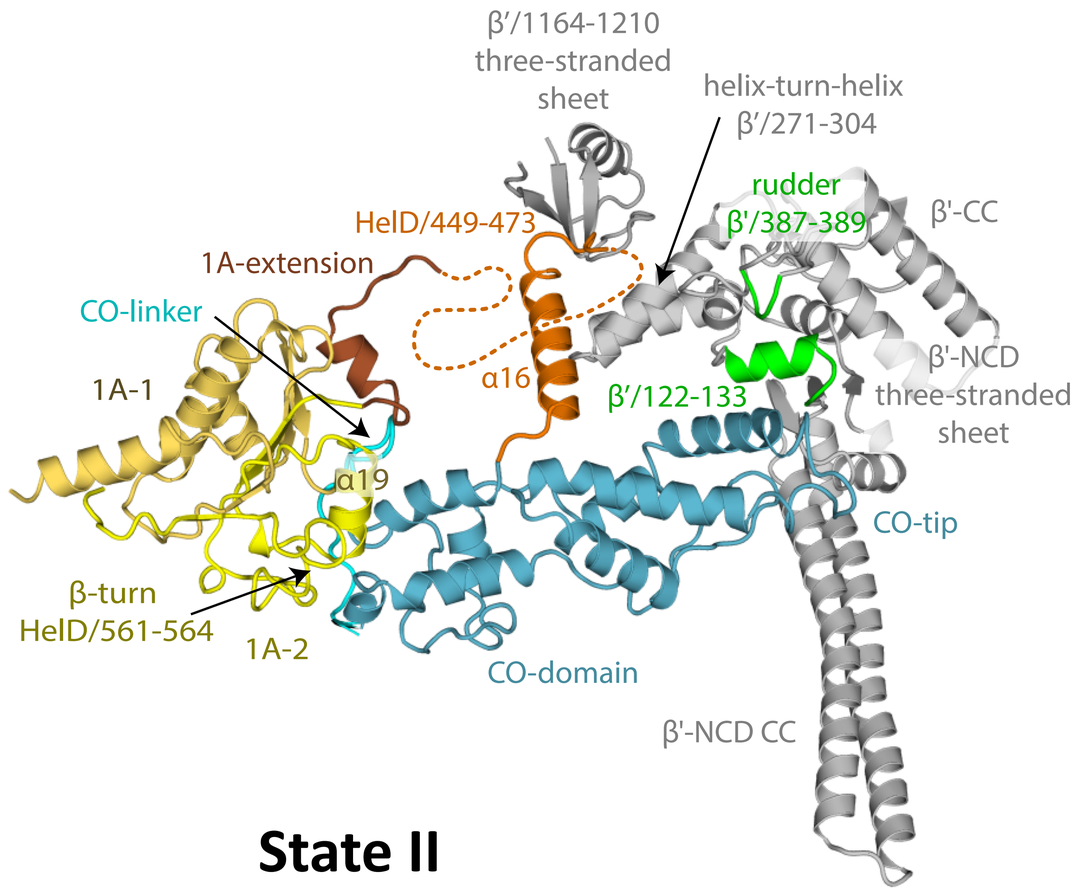

e

State II

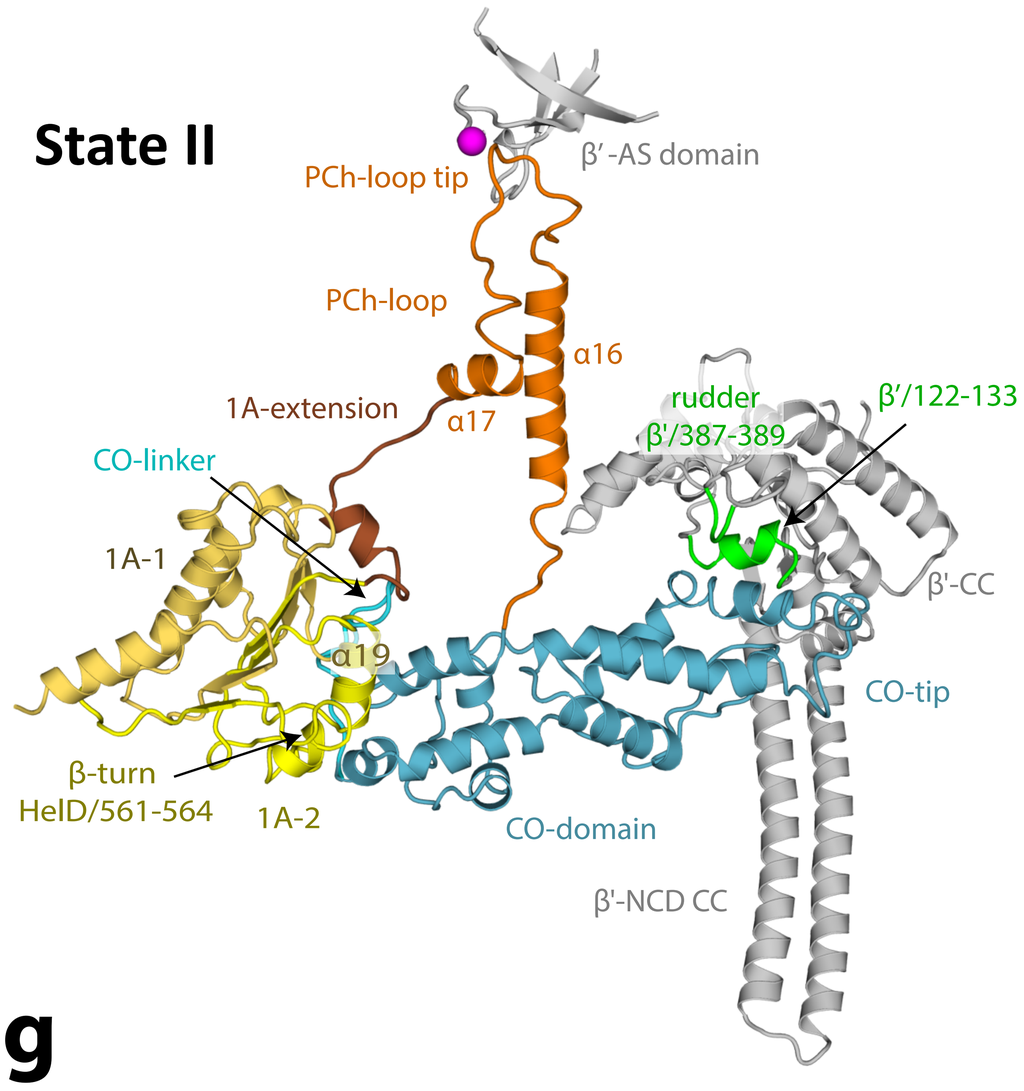

f

State II

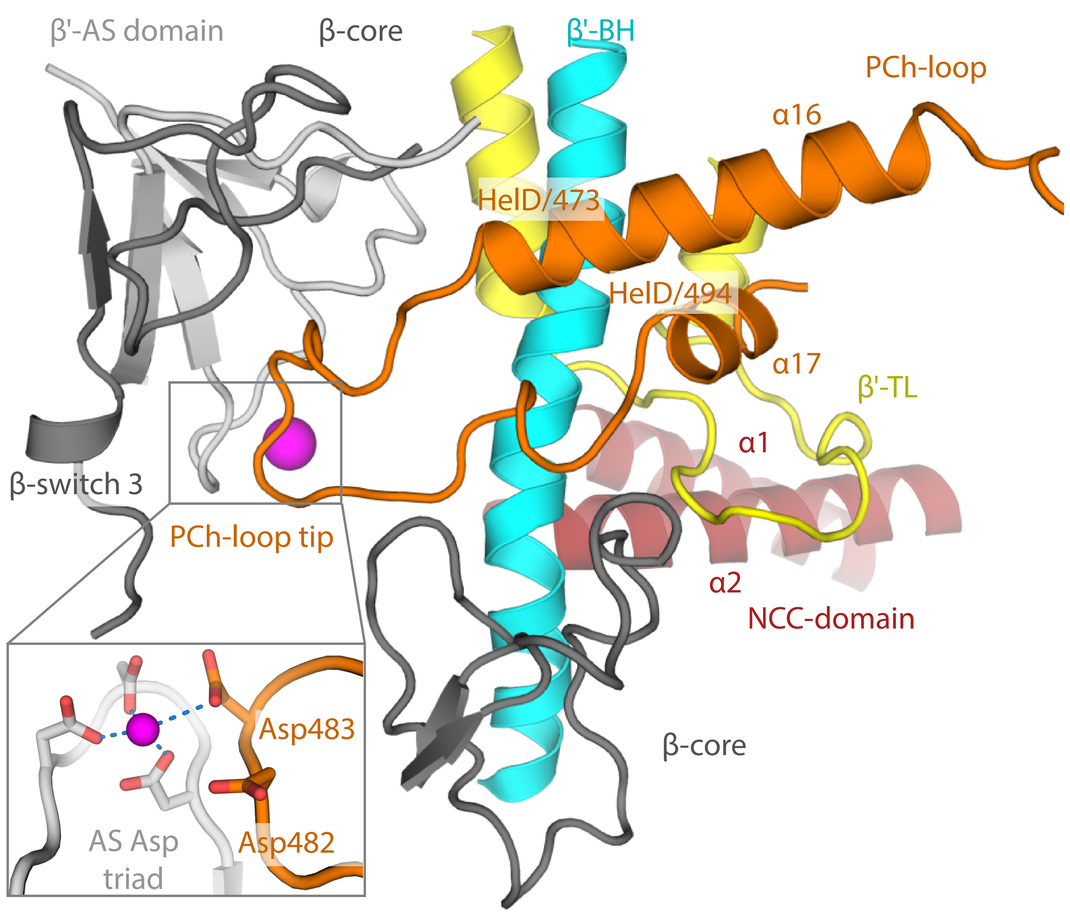

g

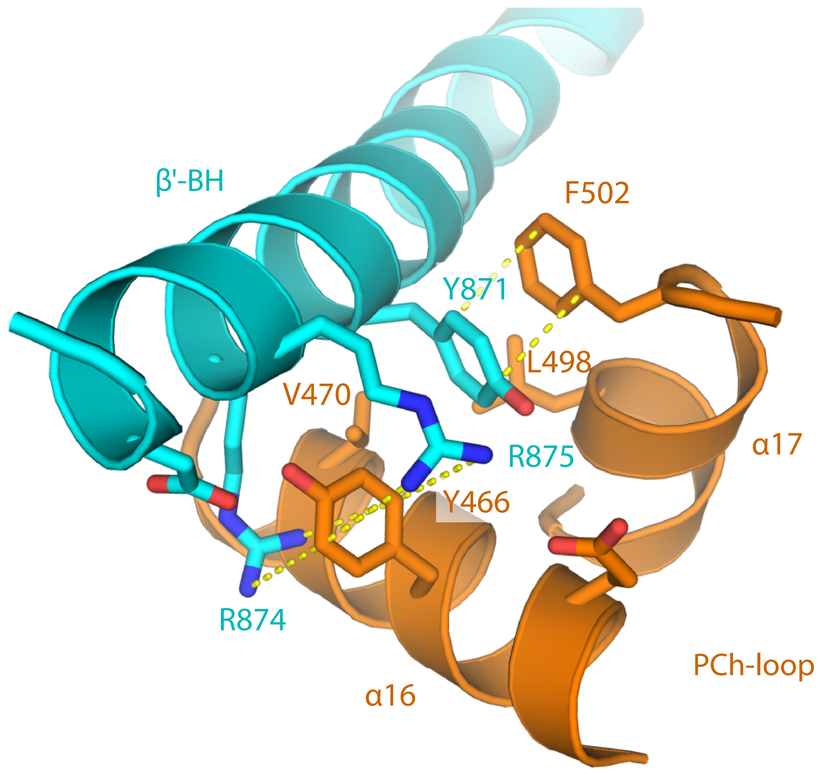

h

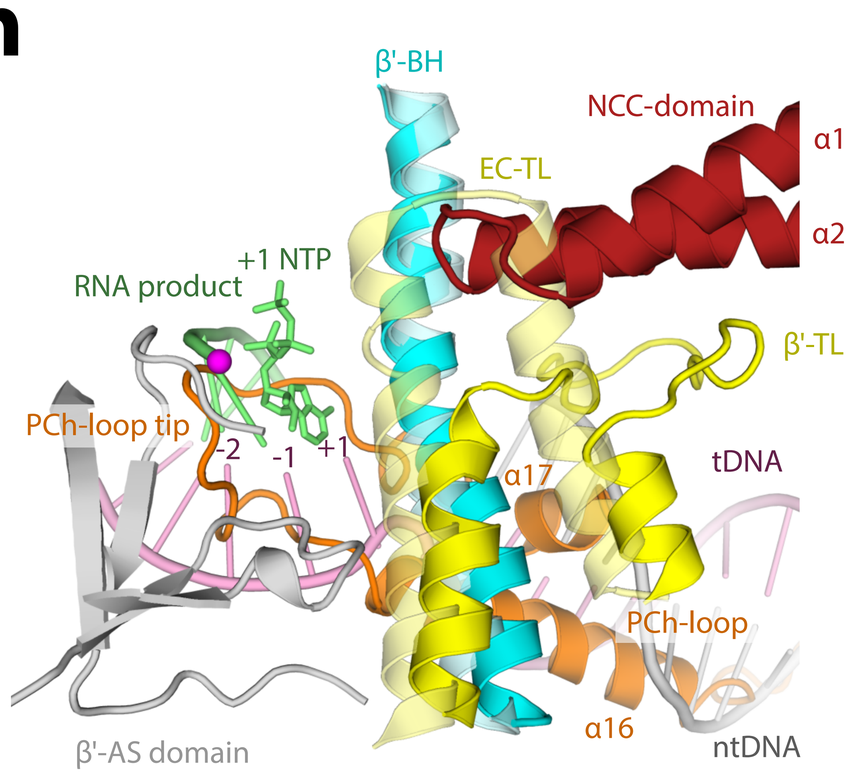

90°

i

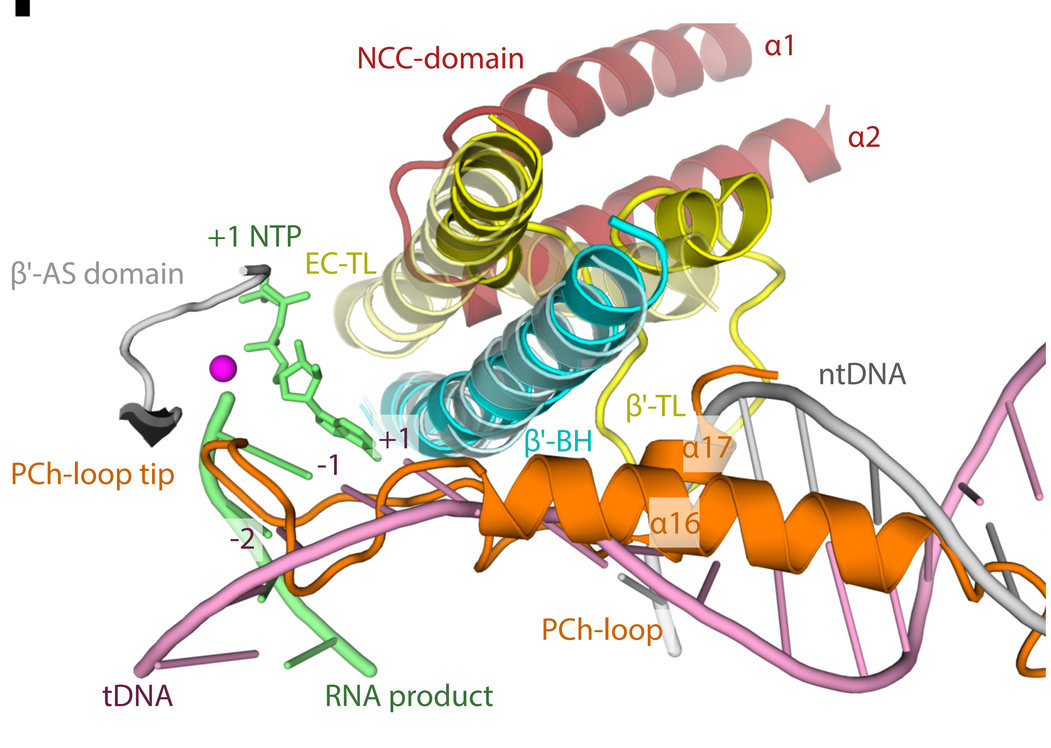

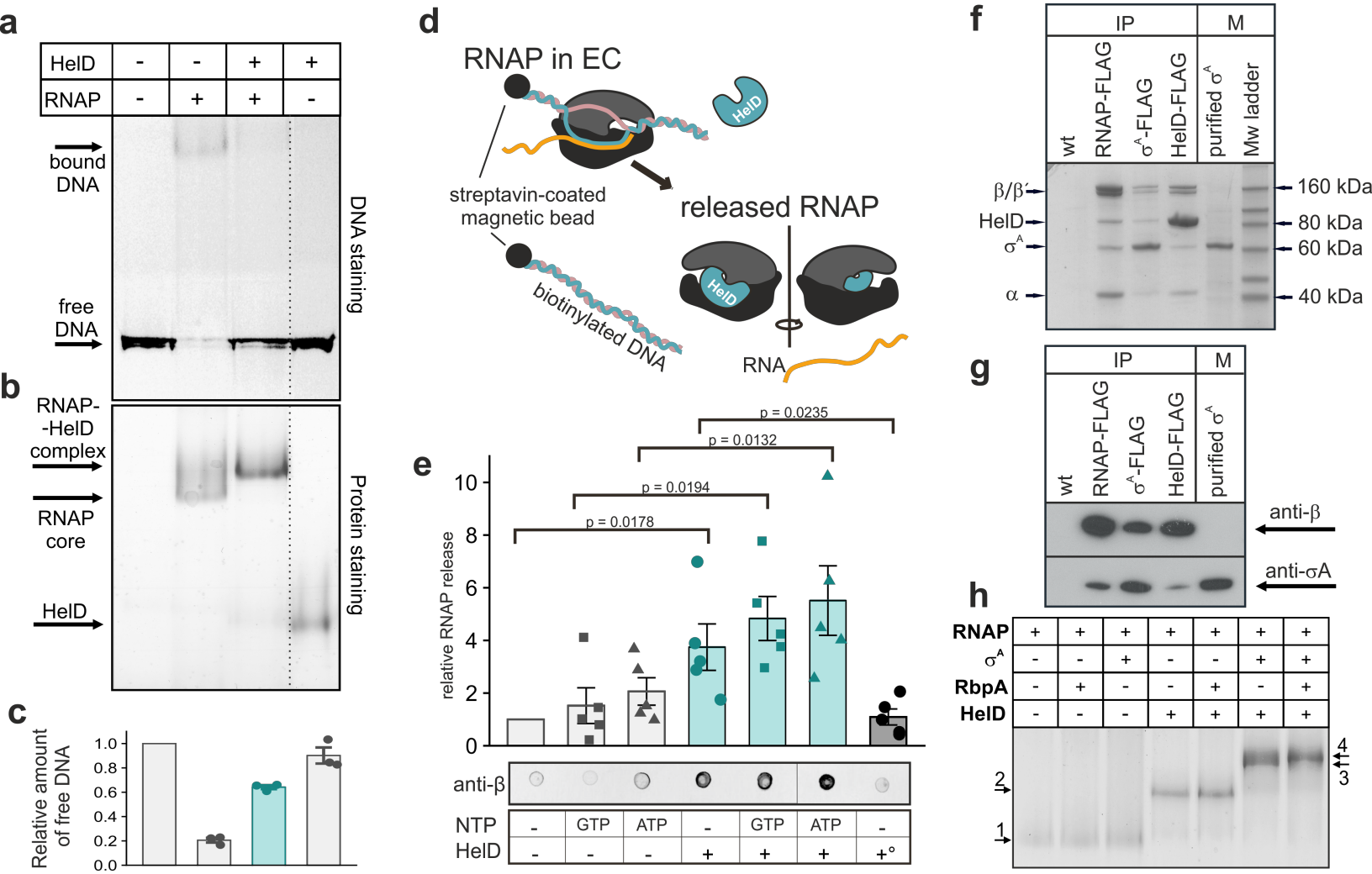
a
HelD - - + +
RNAP - + + -
bound DNA
free DNA
DNA staining
b
RNAP--HelD complex
RNAP core
HelD
Protein staining
c
Relative amount of free DNA
1.0
0.8
0.6
0.4
0.2
0.0
d
RNAP in EC
HelD
streptavin-coated magnetic bead
biotinylated DNA
released RNAP
RNA
e
relative RNAP release
p = 0.0178
p = 0.0194
p = 0.0132
p = 0.0235
anti-β
NTP - GTP ATP - GTP ATP -
HelD - - - + + + +°
f
IP
M
wt
RNAP-FLAG
σA-FLAG
HelD-FLAG
purified σA
Mw ladder
β/β´
HelD
σA
α
160 kDa
80 kDa
60 kDa
40 kDa
g
IP
M
wt
RNAP-FLAG
σA-FLAG
HelD-FLAG
purified σA
anti-β
anti-σA
h
RNAP + + + + + + +
σA - - + - - + +
RbpA - + - - + - +
HelD - - - + + + +
1
2
3
4

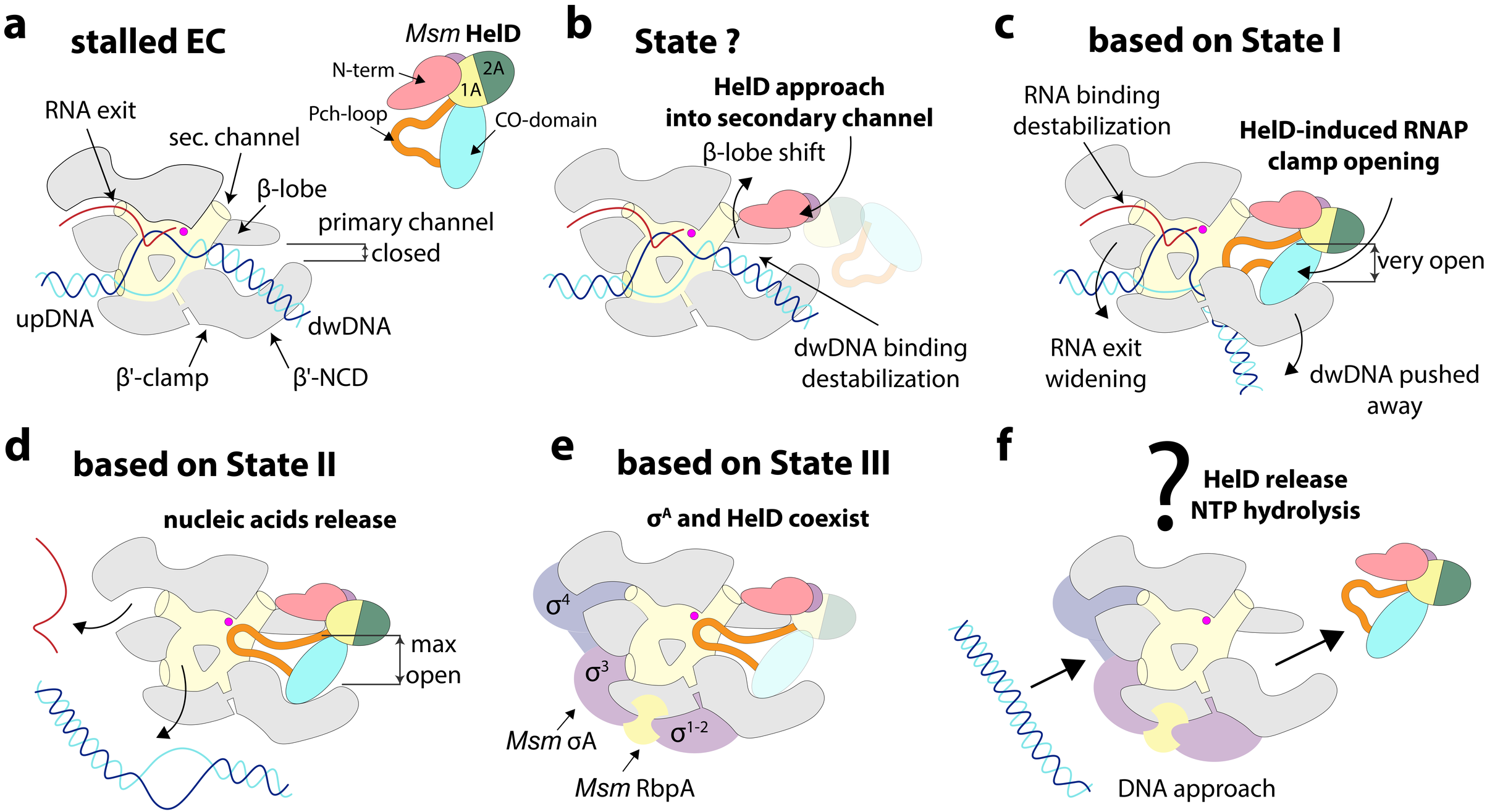
a
stalled EC
Msm HelD
N-term
2A
1A
Pch-loop
CO-domain
RNA exit
sec. channel
β-lobe
primary channel
closed
upDNA
dwDNA
β'-clamp
β'-NCD
b
State ?
HelD approach
into secondary channel
β-lobe shift
dwDNA binding
destabilization
c
based on State I
RNA binding
destabilization
HelD-induced RNAP
clamp opening
very open
RNA exit
widening
dwDNA pushed
away
d
based on State II
nucleic acids release
max
open
e
based on State III
σA and HelD coexist
σ4
σ3
σ1-2
Msm σA
Msm RbpA
f
?
HelD release
NTP hydrolysis
DNA approach

Supplementary information to

Mycobacterial HelD is a nucleic acids-clearing factor for RNA polymerase

Tomáš Kouba[1*#], Tomáš Koval'[2*], Petra Sudzinová[3*], Jiří Pospíšil[3], Barbora Brezovská[3], Jarmila Hnilicová[3], Hana Šanderová[3], Martina Janoušková[3], Michaela Šiková[3], Petr Halada[3], Michal Sýkora[4], Ivan Barvík[5], Jiří Nováček[6], Mária Trundová[2], Jarmila Dušková[2], Tereza Skálová[2], URee Chon[7], Katsuhiko S. Murakami[7], Jan Dohnálek[2#], Libor Krásný[3#]

[1] EMBL Grenoble, 71 Avenue des Martyrs, France

[2] Institute of Biotechnology of the Czech Academy of Sciences, Centre BIOCEV, Průmyslová 595, 252 50 Vestec, Czech Republic

[3] Institute of Microbiology of the Czech Academy of Sciences, Prague, Czech Republic

[4] Institute of Molecular Genetics of the Czech Academy of Sciences, Prague, Czech Republic

[5] Charles University, Faculty of Mathematics and Physics, Institute of Physics, Prague, Czech Republic

[6] CEITEC, Masaryk University, Brno, Czech Republic

[7] Department of Biochemistry and Molecular Biology, The Center for RNA Molecular Biology, Pennsylvania State University, University Park, PA 16802, USA

*These authors contributed equally to this work

#Corresponding authors: tkouba@embl.fr, dohnalek@ibt.cas.cz, krasny@biomed.cas.cz

This file includes:

Supplementary Figures 1 to 14

Supplementary Tables 1 to 7

Supplementary References

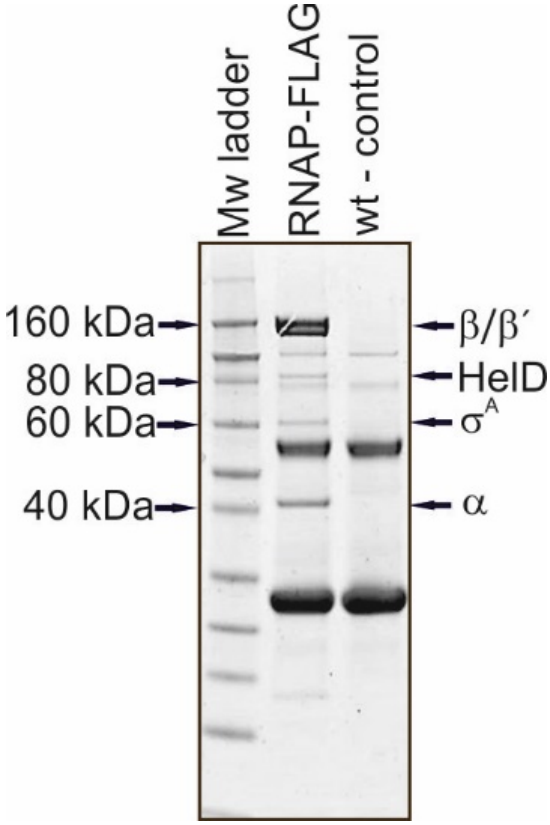

Supplementary Figure 1: *Msm* HelD is in complex with RNAP.

SDS-PAGE of IPs of RNAP-FLAG from *Msm* (RNAP-FLAG, strain LK1468; wt, strain LK865). The gel shows boiled ANTI-FLAG M2 agarose with bound proteins. The identities of the pulled-down proteins are indicated with arrows (determined by mass spectrometry). Wt – control, a strain without any FLAG-fusion. The experiment was performed 3x (biological replicates) with the same result. Mw, molecular weight marker. The two prominent un-marked bands correspond to heavy and light antibody chains, respectively.

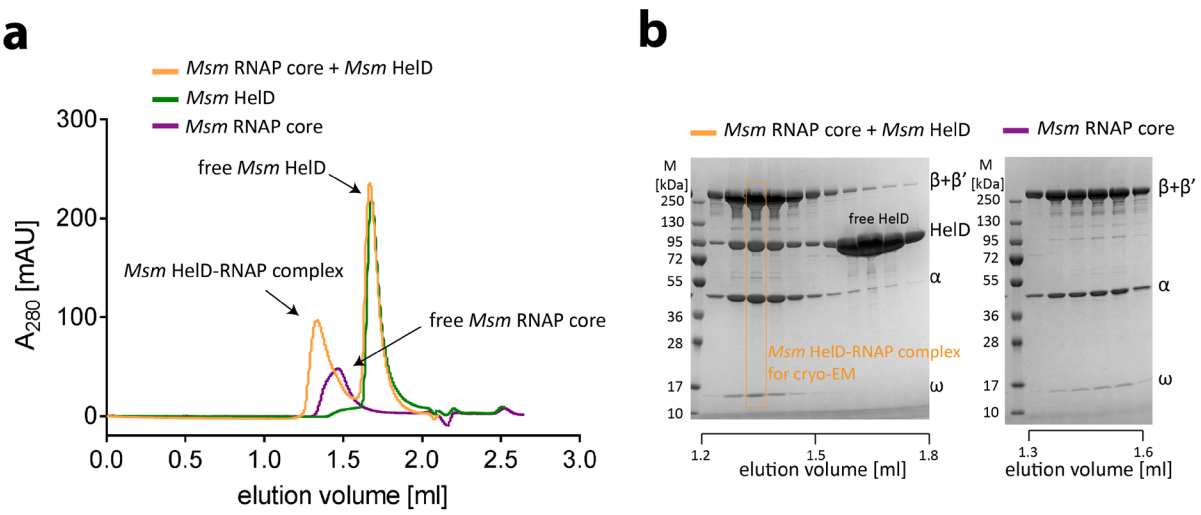

Supplementary Figure 2: Reconstitution of *Msm* HelD-RNAP complex.

a, Size-exclusion chromatography (SEC) analysis of RNAP core alone (purple line) and HelD protein alone (green line). SEC analysis of protein sample after reconstitution of RNAP core with HelD protein at a 1:3 ratio (yellow line). The first yellow peak (from left) is the *Msm* HelD-RNAP complex, the second yellow peak is excess of free HelD protein. The data were analysed and the graphics created with GraphPad Prism 7.02.

b, SDS-PAGE analysis of the *Msm* HelD-RNAP complex and the *Msm* RNAP core. 40 µg protein samples of fractions of *Msm* HelD-RNAP complex and RNAP core alone were loaded onto analytical SDS-PAGE. Fractions are indicated by the elution volume. The first lane contains the molecular weight marker.

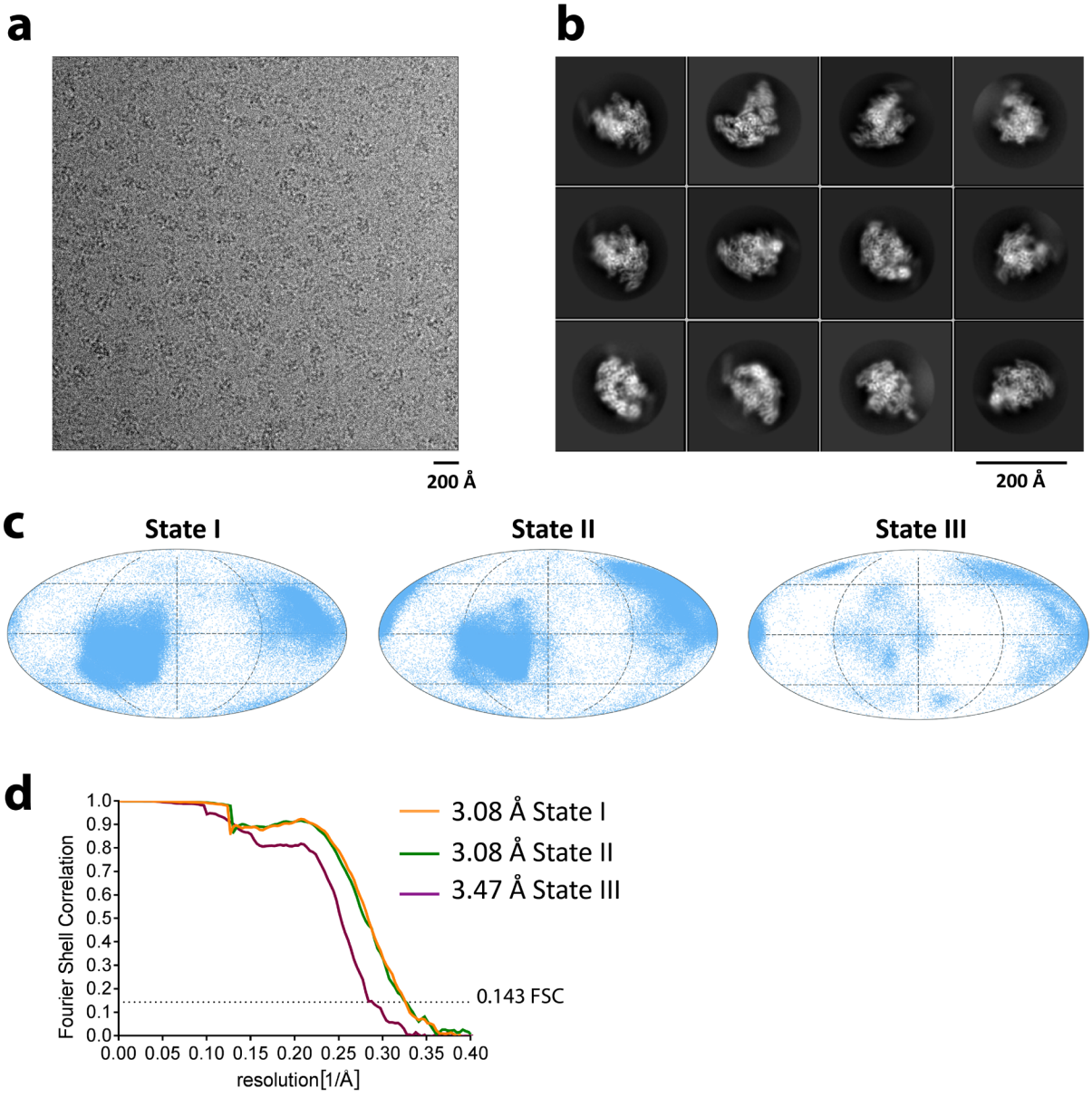

Supplementary Figure 3: Cryogenic electron microscopy of *Msm* HelD-RNAP complex.

a, Representative micrograph of *Msm* HelD-RNAP complex in free-standing ice after MotionCor2[1] correction at defocus of ~2.5 µm.

b, 2D-class averages of the *Msm* HelD-RNAP complex.

c, Angular distribution for particle projections of the *Msm* HelD-RNAP complex State I, II and III respectively, visualized on a globe-like plane. The data were analysed and the graphics created with cryoEF[2].

d, Fourier shell correlation (FSC) curves for *Msm* HelD-RNAP complex State I (yellow), II (green) and III (purple), respectively. The plot of the FSC between two independently refined half-maps shows the overall resolution of the two maps as indicated by the gold standard FSC 0.143 cut-off criteria[3]. The data were analysed and the graphics created with GraphPad Prism 7.02.

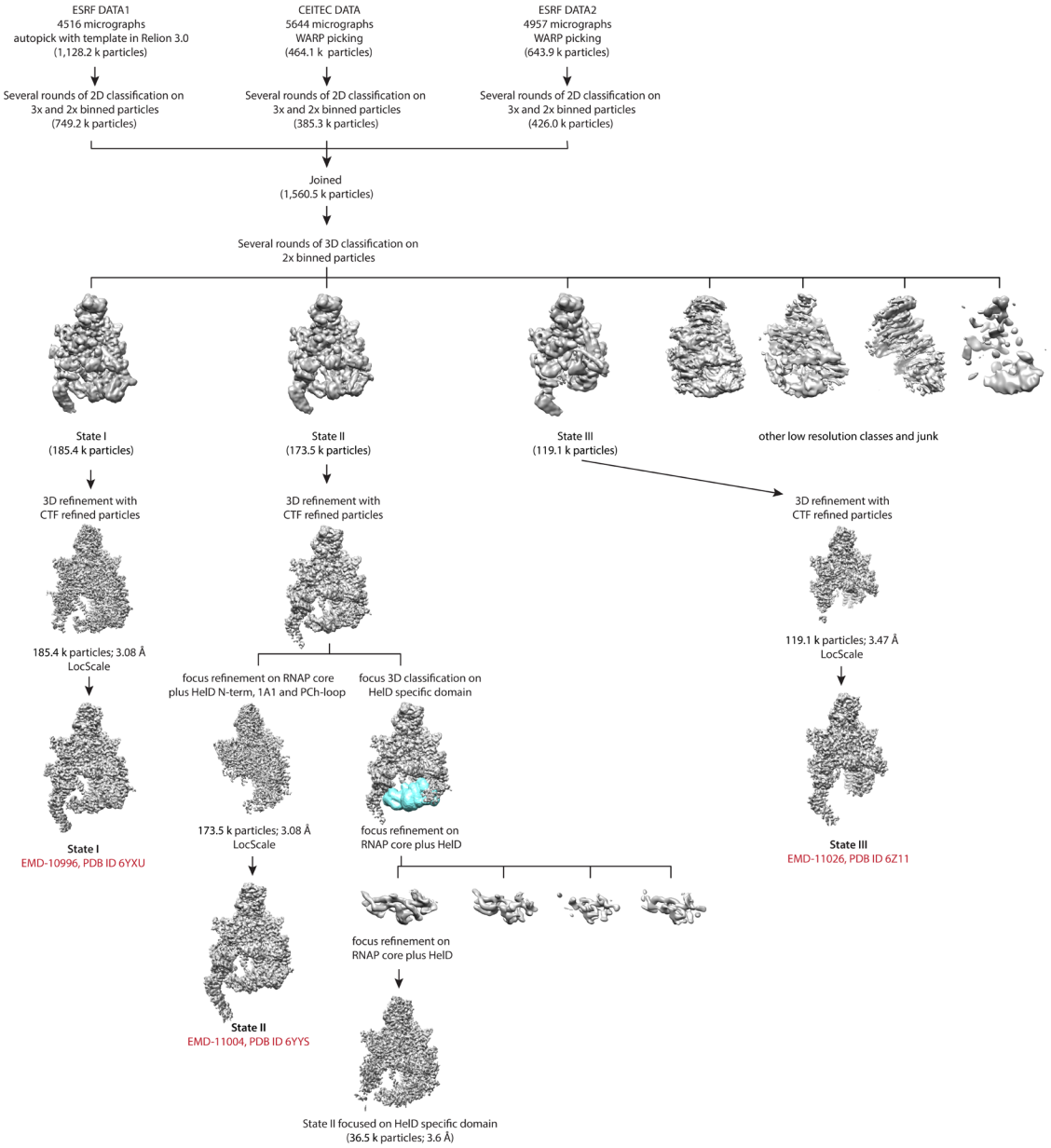

Supplementary Figure 4: Cryo-EM data 3D classification and refinement scheme.

Summary of the cryo-EM 3D classification and refinement scheme of the *Msm* HelD-RNAP complex. Initially, three different datasets were processed individually to the level of 2D classification. 2D classes with well-defined secondary structure features were merged (1,560.5k particles). The merged particles were classified into ten 3D classes with angular assignment. Incomplete, low resolution, and damaged particle classes were excluded from further data analyses. The three most prominent 3D classes of the *Msm* HelD-RNAP complex were refined, and subsequently filtered by LocScale[4], corresponding to State I, II and III. The State II class was focus-refined around the region of the RNAP core and the HelD N-terminal and 1A domain and PCh-loop. In parallel, a round of focus classification was performed on the region of the HelD 1A and HelD-specific domains using corresponding mask (cyan) in order to get a better defined map for model building of the latter region. Atomic resolution cryo-EM maps were refined and post-processed with their respective masks in RELION 3.0[5,6].

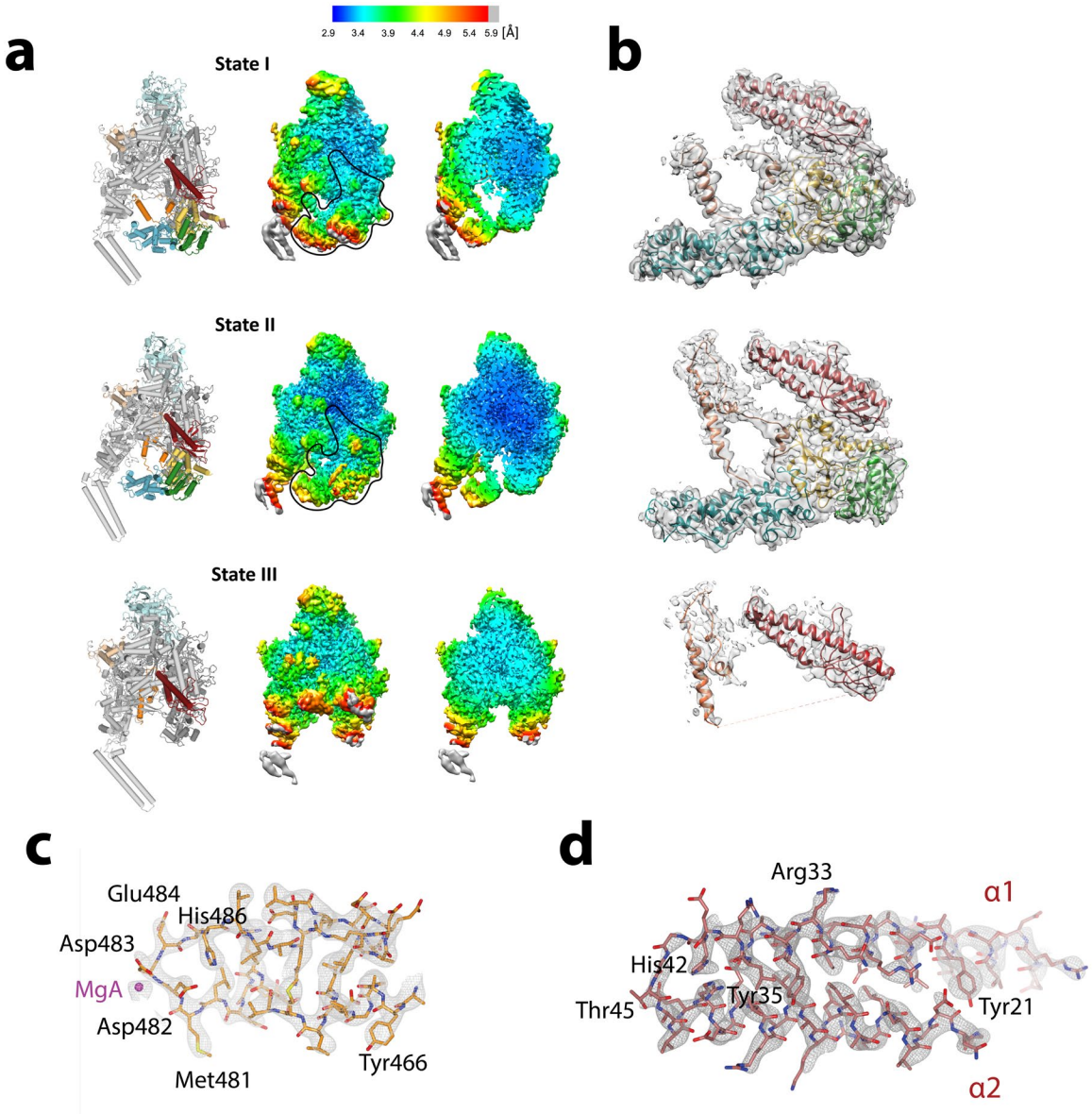

Supplementary Figure 5: Local resolution and cryo-EM density maps of the *Msm* HelD-RNAP complexes.

a, Cylinder model (**left**) and distribution of local resolution of the *Msm* HelD-RNAP State I, II and III, respectively. Surface (**middle**) and slice (**right**) representation. The black line in the middle panels delineates HelD in State I or II. Maps are colored according to the local resolution calculated within the RELION software package. Resolution is as indicated in the color bar. Graphics created with Pymol (Schrödinger, Inc.) and Chimera[7].

b, LocScale filtered cryo-EM density map for the *Msm* HelD protein in State I, II and III, respectively. Color coded as in Figure 1e. Graphics created with Chimera[7].

c, LocScale filtered cryo-EM density for the HelD PCh-loop tip, MgA is shown as magenta sphere. Carved with a 1.75 Å clip radius around the atomic model in CCP4mg[8].

d, LocScale filtered cryo-EM density for the N-terminal CC-domain of HelD carved with a 1.75 Å clip radius around the atomic model in CCP4mg[8].

a

State I

Sphericity = 0.938 out of 1. Global resolution = 3.02 Å.

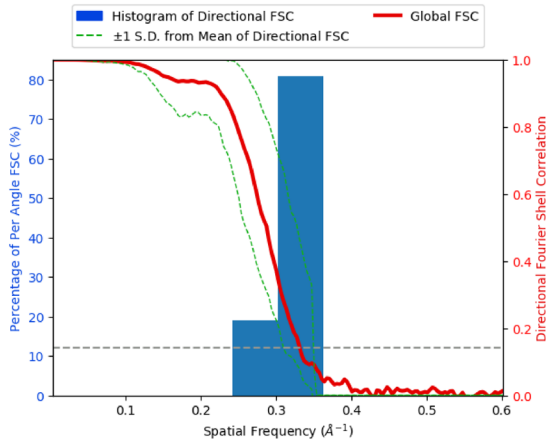

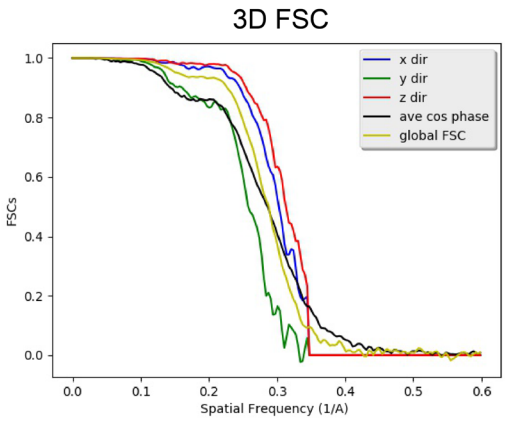

b

State II

Sphericity = 0.919 out of 1. Global resolution = 3.05 Å.

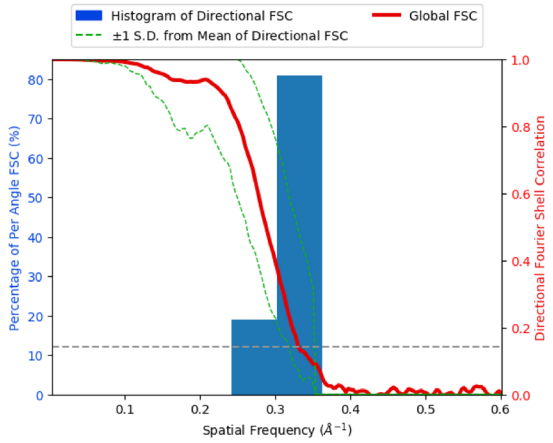

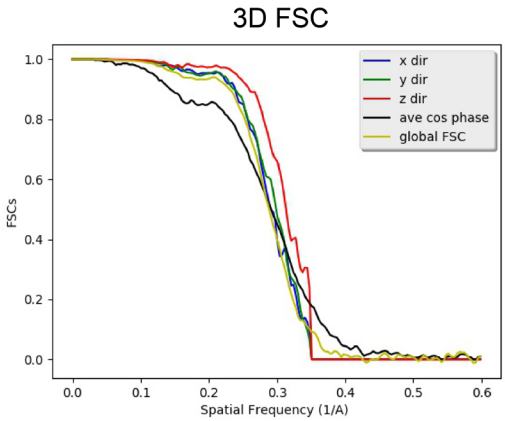

c

State III

Sphericity = 0.916 out of 1. Global resolution = 3.44 Å.

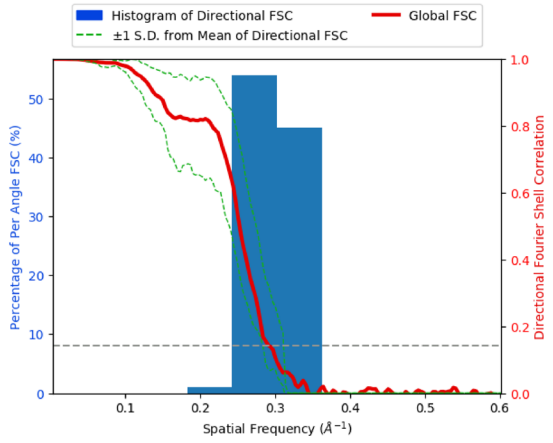

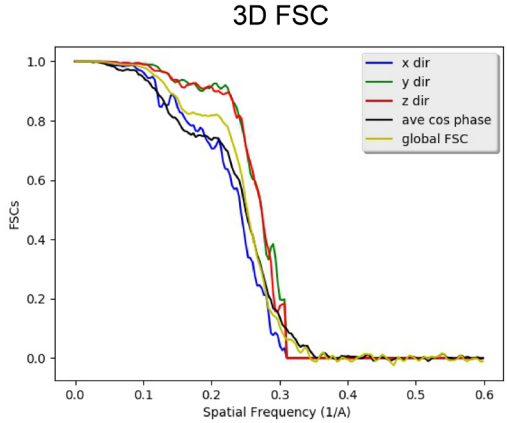

Supplementary Figure 6: 3D FSC analysis of HelD-RNAP complexes cryo-EM maps.

a, **b**, **c** Directional FSC analysis[9] (right) and 3D FSC analysis[9] (left) of HelD-RNAP in State I, II, and III, respectively. (**right**) Plots of the global half-map FSC (solid red line, right axis) together with the spread of directional resolution values defined by ±1σ from the mean (area encompassed by dotted green lines) and a histogram of Directional FSC (blue bars, left axis). (**left**) Directional FSC analysis in x (blue), y (green) and z (red) direction compared to the global (yellow) FSC analysis. The analysis was performed with the 3DFSC server v. 3.0[9].

a

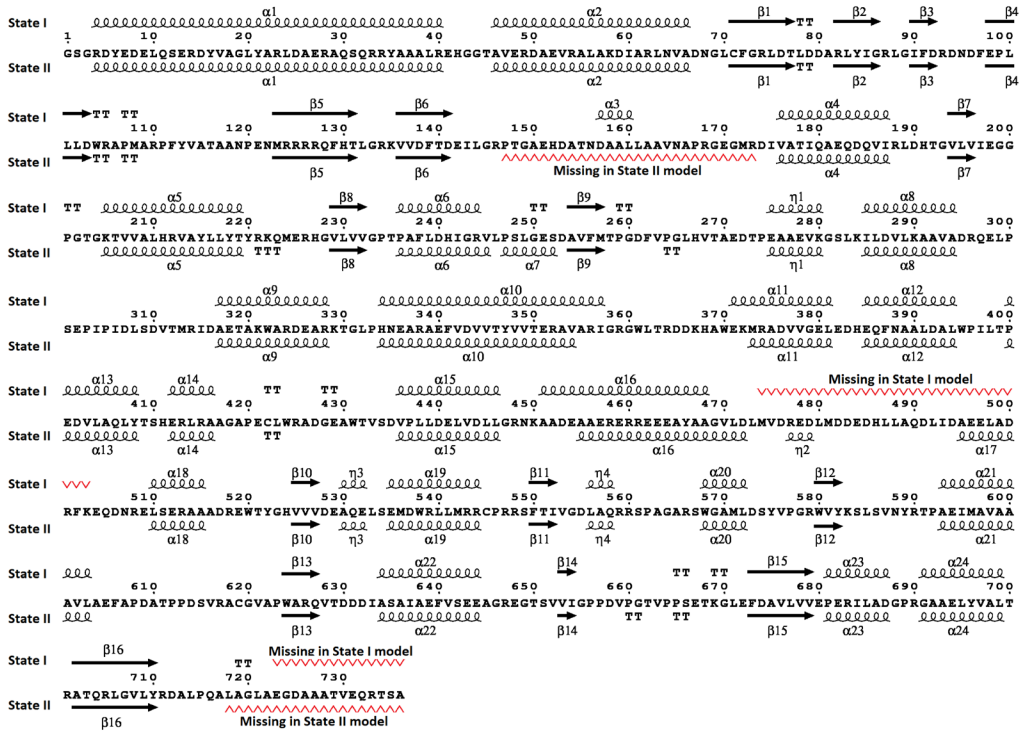

b

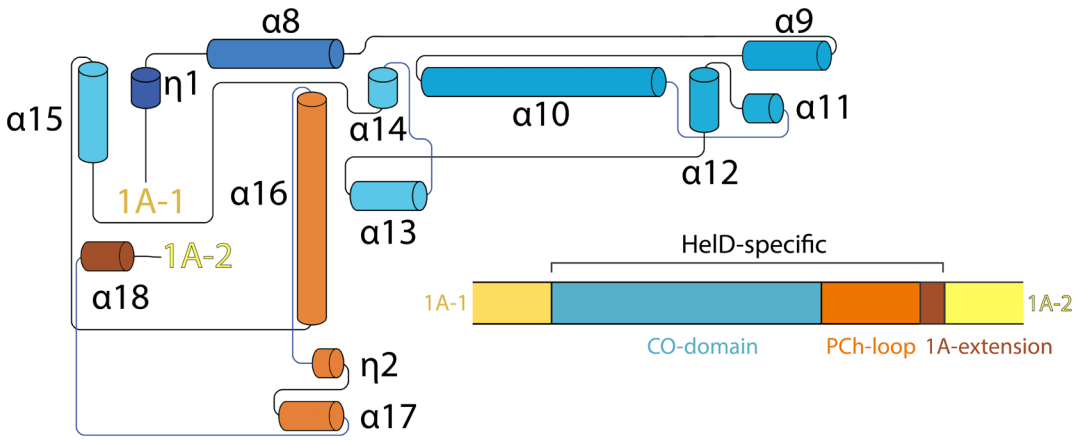

Supplementary Figure 7: Secondary structure assignment of HelD protein.

a, State I (**top**) and State II (**bottom**) secondary structure elements marked along the *Msm* HelD amino acid sequence. Some regions (red marking) are not folded in one or the other State, α7 exists in State II only, α16 has a shifted register. The graphics was created using ESPript 3.0[10].

b, Topology of the new fold of the HelD-specific domain (no structural homolog identified). The graphics was created using PDBsum server[11].

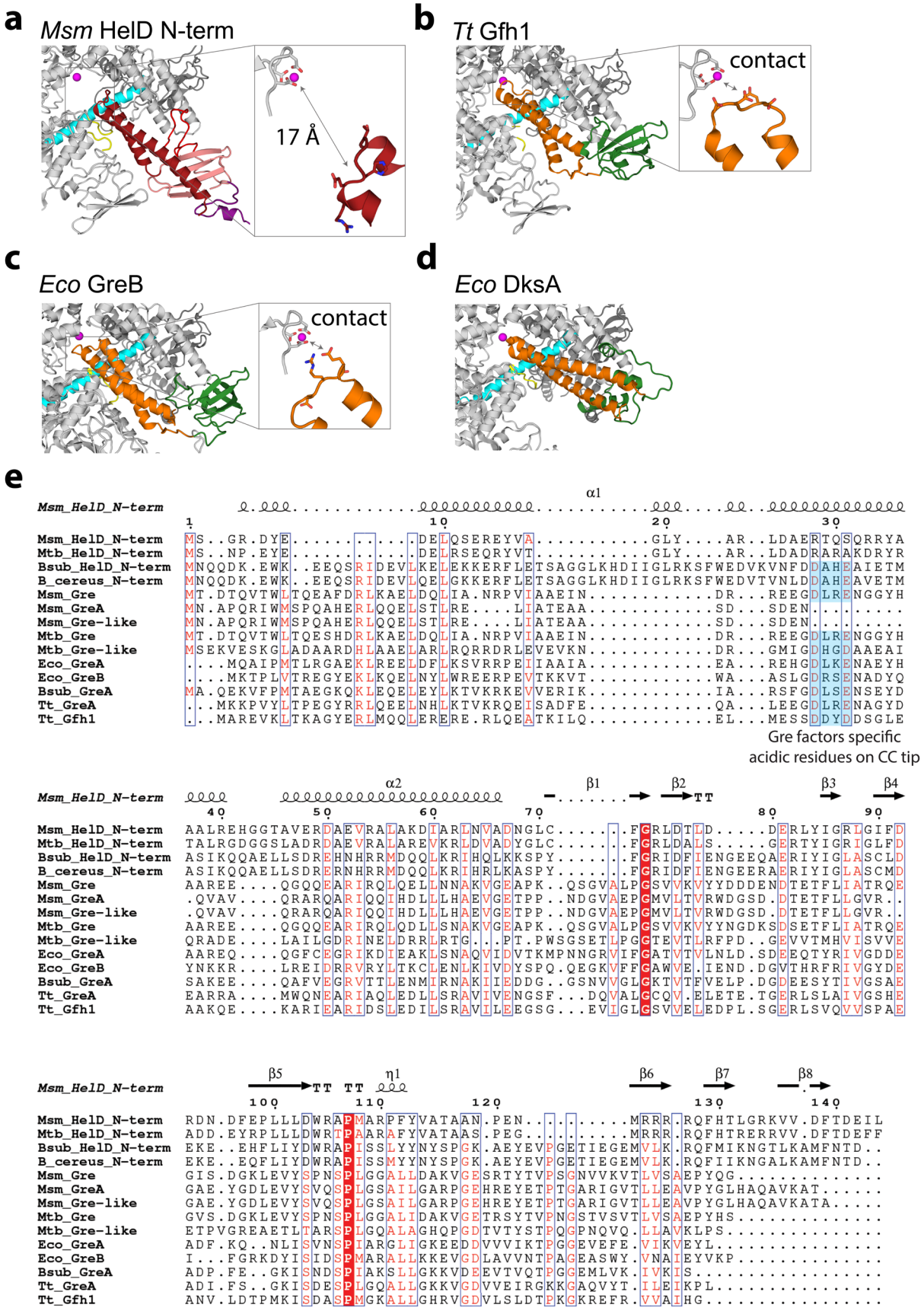
a
Msm HelD N-term
17 Å
b
Tt Gfh1
contact
c
Eco GreB
contact
d
Eco DksA
e
Msm_HelD_N-term
Msm_HelD_N-term MS..GR.DYE.....DELQSEREYVA.....GLY....AR..LDAERTQSQRRYA
Mtb_HelD_N-term MS..NP.EYE.....DELRSEQRYVT.....GLY....AR..LDADRARAKDRYR
Bsub_HelD_N-term MNQQDK.EWK..EEQSRIDEVLKELEKKERFLETSAGGLKHDIIGLRKSFWEDVKVNFDDAHEAIETM
B_cereus_N-term MNQQDK.EWK..EEQSRIDEVLQELGKKERFLETSAGGLKHDIIGLRKSFWEDVTVNLDDAHEAVETM
Msm_Gre MT.DTQVTWLTQEAFDRLKAELDQLIA.NRPVIAAEIN.....DR...REEGDLRENGGYH
Msm_GreA MN.APQRIWMSPQAHERLQQELSTLRE....LIATEAA.....SD...SDEN.....
Msm_Gre-like MN.APQRIWMSPQAHERLQQELSTLRE....LIATEAA.....SD...SDEN.....
Mtb_Gre MT.DTQVTWLTQESHDRLKAELDQLIA.NRPVIAAEIN.....DR...REEGDLRENGGYH
Mtb_Gre-like MSEKVESKGLADAARDHLAAELARLRQRRDRLEVEVKN.....DR...GMIGDHGDAAEAI
Eco_GreA ....MQAIPMTLRGAEKLREELDFLKSVRRPEIIAAIA.....EA...REHGDLKENAEYH
Eco_GreB ....MKTPLVTREGYEKLKQELNYLWREERPEVTKKVT.....WA...ASLGDRSENADYQ
Bsub_GreA MA.QEKVFPMTAEGKQKLEQELEYLKTVKRKEVVERIK.....IA...RSFGDLSENSEYD
Tt_GreA ...MKKPVYLTPEGYRRLQEELNHLKTVKRQEISADFE.....QA...LEEGDLRENAGYD
Tt_Gfh1 ...MAREVKLTKAGYERLMQQLERERE.RLQEATKILQ.....EL...MESSDDYDDSGLE
Gre factors specific
acidic residues on CC tip
Msm_HelD_N-term
Msm_HelD_N-term AALREHGGTAVERDAEVRALAKDTARLNVADNGLC.....FGRLDTLD.....DERLYIGRIGIFD
Mtb_HelD_N-term TALRGDGGSLADRDAEVRALAREVKRLDVADYGLC.....FGRLDALS.....GERTYIGRIGLFD
Bsub_HelD_N-term ASIKQQAELLSDREHNHRRMDQQLKRIHQLKKSPY.....FGRIDFIENGEEQAERIYIGLASCLD
B_cereus_N-term ASIKQQAELLSDRERNHRRMDQQLKRIHRLKASPY.....FGRIDFIENGEERAERIYIGLASCMD
Msm_Gre AAREE....QGQQEARIRQLQELLNNAKVGEAPK..QSGVALPGSVVKVYYDDDENDTETFLIATRQE
Msm_GreA .QVAV....QRARQARIQQIHDLLLHAEVGETPP..NDGVAEPGMVLTVRWDGSD.DTETFLLGVR..
Msm_Gre-like .QVAV....QRARQARIQQIHDLLLHAEVGETPP..NDGVAEPGMVLTVRWDGSD.DTETFLLGVR..
Mtb_Gre AAREE....QGQQEARIRQLQDLLSNAKVGEAPK..QSGVALPGSVVKVYYNGDKSDSETFLIATRQE
Mtb_Gre-like QRADE....LAILGDRINELDRRLRTG....PT.PWSGSETLPGGTEVTLRFPD..GEVVTMHVISVVE
Eco_GreA AAREQ....QGFCEGRIKDIEAKLSNAQVIDVTKMPNNGRVIFGATVTVLNLD.SDEEQTYRIVGDDE
Eco_GreB YNKKR....LREIDRRVRYLTKCLENLKIVDYSPQ.QEGKVFFGAWVE.IEND.DGVTHRFRIVGYDE
Bsub_GreA SAKEE....QAFVEGRVTTLENMIRNAKIIEDDG..GSNVVGLGKTVTFVELP.DGDEESYTIVGSAE
Tt_GreA EARRA....MWQNEARIAQLEDLLSRAVIVENGSF...DQVALGCQV.ELETE.TGERLSLAIVGSHE
Tt_Gfh1 AAKQE....KARIEARIDSLEDILSRAVILEEGSG...EVIGLGSVVELEDPL.SGERLSVQVVSPAE
Msm_HelD_N-term
Msm_HelD_N-term RDN.DFEPLLLDWRAPMARPFYVATAAN.PEN.....MRRR.RQFHTLGRKVV.DFTDEIL
Mtb_HelD_N-term ADD.EYRPLLLDWRTPAARAFYVATAAS.PEG.....MRRR.RQFHTRERRVV.DFTDEFF
Bsub_HelD_N-term EKE..EHFLIYDWRAPISSLYYNYSPGK.AEYEVPGETIEGEMVLK.RQFMIKNGTLKAMFNTD..
B_cereus_N-term EKE..EQFLIYDWRAPISSMYYNYSPGK.AEYEVPGETIEGEMVLK.RQFIIKNGALKAMFNTD..
Msm_Gre GIS.DGKLEVYSPNSPLGGALLDAKVGESRTYTVPSGNVVKVTLVSAEPYQG.....
Msm_GreA GAE.YGDLEVYSVQSPLGSAILGARPGEHREYETPTGARIGVTLLEAVPYGLHAQAVKAT.....
Msm_Gre-like GAE.YGDLEVYSVQSPLGSAILGARPGEHREYETPTGARIGVTLLEAVPYGLHAQAVKATA.....
Mtb_Gre GVS.DGKLEVYSPNSPLGGALIDAKVGETRSYTVPNGSTVSVTLVSAEPYHS.....
Mtb_Gre-like ETPVGREAETLTARSPLGQALAGHQPGDTVTYSTPQGPNQVQ.LLAVKLPS.....
Eco_GreA ADF.KQ..NLISVNSPIARGLIGKEEDDVVVIKTPGGEVEFE.VIKVEYL.....
Eco_GreB I...FGRKDYISIDSPMARALLKKEVGDLAVVNTPAGEASWY.VNAIEYVKP.....
Bsub_GreA ADP.FE..GKISNDSPIAKSLLGKKVDEEVTVQTPGGEMLVK.IVKIS.....
Tt_GreA ADI.FS..GKISDESPLGQALLGKKVGDVVEIRGKKGAQVYT.ILEIKPL.....
Tt_Gfh1 ANV.LDTPMKISDASPMGKALLGHRVGDVLSLDTPKGKREFR.VVAIHG.....

Supplementary Figure 8: Structural comparison of HelD and Gre-like transcription factors

a, **b**, **c**, and **d** Structural comparisons of (**a**) *Msm* HelD N-terminal domain and Gre-like transcription factors. HelD anchors into the RNAP secondary channel similarly to (**b**) *Tt* Gfh1 (PDB ID 3AOH) and (**c**) *Eco* GreB (PDB ID 6RI7) N-terminal CC (orange) and globular (green) domains. However, in contrast to GreB and Gfh1 CC domains, the tip of HelD NCC-domain does not reach to the AS (insets, MgA as magenta sphere). (**d**) *Eco* DksA interacts with the RNAP secondary channel in a similar fashion (PDB ID 5W1T). Graphics created with Pymol (Schrödinger, Inc.).

e, Sequence alignment of HelD homologs and Gre-like transcription factors. The mycobacterial HelD NCC-domain tip does not contain the conserved DXX(E/D) motif necessary for Gre factor-like endonuclease activity. Sequence alignment was performed using Clustal Omega[12] and the graphics was created in ESPript 3.0[10].

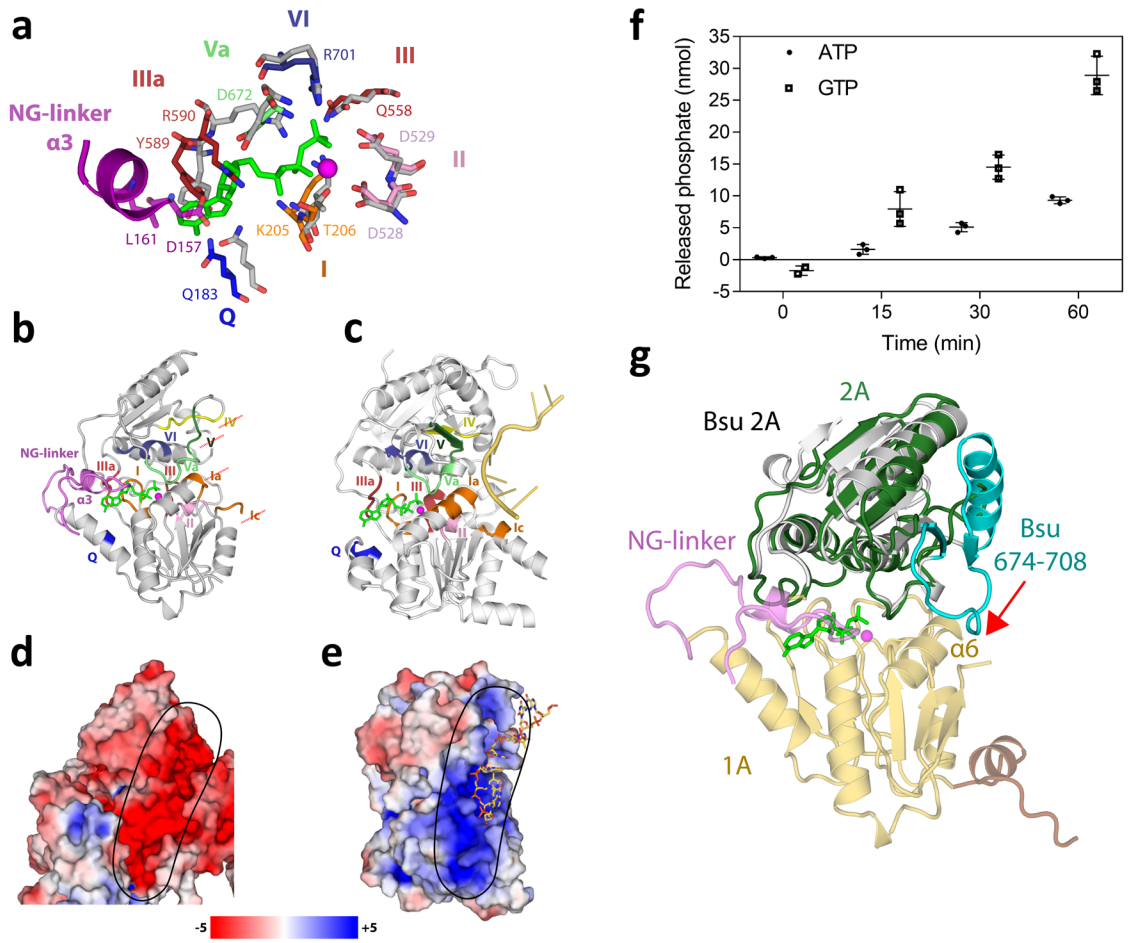

Supplementary Figure 9: *Msm* HelD 1A-2A heterodimer nucleotide binding site compared to UvrD; NTPase activity of *Msm* HelD; *Bsu* HelD CTD crystal structure.

a, Superposition of the HelD NTP-binding site (State I, color coded) and the UvrD ATP-bound state (grey, PDB ID 2IS4). Conserved residues from motifs Q (blue), I (orange), II (pink), ~III and IIIa (firebrick), Va (lightgreen) and VI (deepblue) are present but not in conformations compatible with NTP binding. The ordered NG-linker locks the conformation of Tyr589 (Van der Waals interactions with residues HelD/157, 160 and 161 of α3) and of Arg590 (Arg side chain links Asp157 and Glu672 of HelD) so that they would clash with the NTP base and ribose, probably making the NTP binding/hydrolysis in State I impossible.

b and **c**, Conserved nucleotide binding site motifs Q, I, II, III, IIIa, Va, and VI (color coded as in Figure 2d) as observed in HelD (a, b) in comparison to UvrD [(c),PDB ID 2IS4]. Residues responsible for ssDNA [pale yellow in (c)] binding in motifs Ia and Ic (orange), IV (yellow) and V (forest green) in UvrD are not present in HelD (red crossing).

d and **e**, Comparison of surface electrostatic potential of the HelD 1A-2A heterodimer and UvrD ssDNA-bound 1A-2A heterodimer, respectively. A prominent positively charged groove binds ssDNA (sticks in e) on the surface of UvrD (black oval). In contrast, a negatively charged groove is present in a similar area of HelD surface (black oval). Electrostatics surfaces were generated by APBS[13]within PyMol according to heat bar in k_BT/e units.

f, Hydrolyses of ATP and GTP were monitored and evaluated at 0, 15, 30 and 60 min intervals. Measurements were performed in 3 biological replicates for each time interval with separate background readings for each condition. The results are shown as mean values of the amounts of released phosphate in the reaction, with standard deviations shown as error bars. The symbols are individual replicates (n=3). The data were analysed and the graphics created with GraphPad Prism 7.02.

g, X-ray structure of the C-terminal domain of *Bsu* HelD compared with State I of *Msm* HelD. The C-terminal domain of *Bsu* HelD (residues 608-773) shown as secondary structure elements in grey superimposed by the SSM algorithm with the 2A domain of *Msm* HelD (colored as in Figure 1d); ATP (green sticks) and Mg^{2+} (magenta sphere) in positions as in the structure 2IS4 superimposed according to the NTP-binding site motifs in *Msm* HelD. The 2A domain structure of *Bsu* HelD corresponds to the Rossman fold of the RecA-like domain (central twisted 5-stranded β-sheet surrounded by 5 α-helices 611-620, 645-663, 674-687, 733-745, and 760-764); loop 624-630 was not localized. The domain is most similar to the crystal structure of the C-terminal domain of putative DNA helicase from *Lactobacillus plantarum* (PDB ID 3DMN, rmsd 1.23 Å, 151 aligned C^{α} atoms, 37.7% sequence identity) with identical fold and topology (PDBeFold server[14]). The structure aligns well with that of the 2A/2B domain of UvrD (PDB ID 2IS4, rmsd 1.6 Å, 149 aligned C^{α} atoms), with an almost perfect match of the secondary structure, however of significantly different topology (not shown). The C-terminal domain of *Bsu* HelD has a very similar localization of the amino acid residues forming the expected NTP-binding site (Arg608 corresponds to UvrD/Arg284 – part of motif IIIa, motif VI occurs as 741-TACTRAM-747, Arg745 very likely participating in NTP binding and cleavage, Glu716 is conserved in position of UvrD/Glu566, likely binding the NTP ribose moiety). In comparison with State I of *Msm* HelD the *Bsu* structure is more similar to the 2A domain (rmsd 2.2 Å, 92 aligned residues, sequence identity of the aligned parts 21.7%, alignment shown) than to 1A (2.7 Å, 102 residues aligned, 9.8%, alignment not shown). The helix-loop-strand motif 674-708 (cyan) of *Bsu* HelD does not match any element of 2A in *Msm* HelD and the region 695-699 of the loop would clash (red arrow) with α6 of domain 1A in *Msm* HelD.

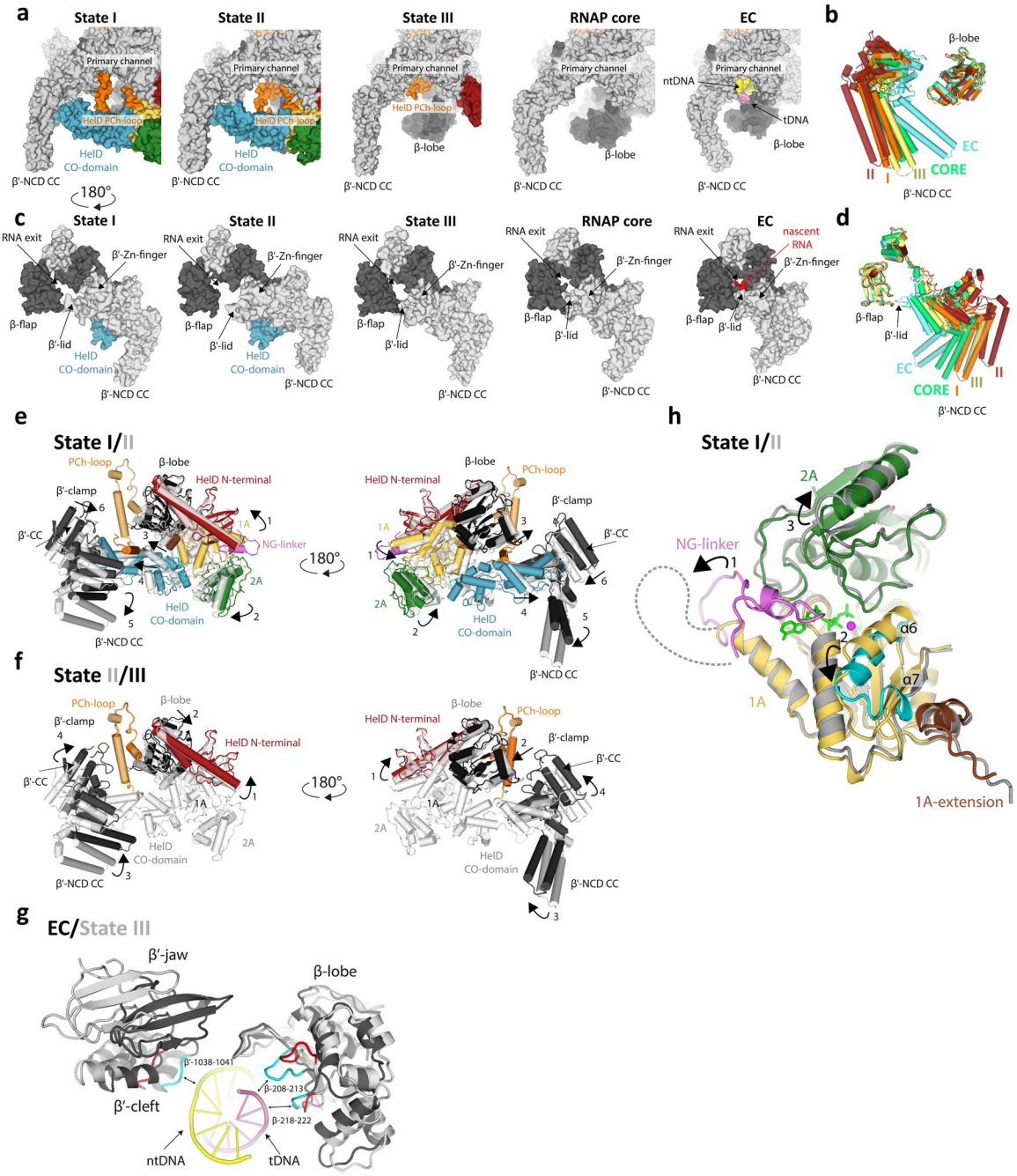

Supplementary Figure 10: The *Msm* HelD specific domain wedges into the RNAP primary channel; global domain changes in *Msm* HelD states.

a, Surface representation of HelD specific domain interaction with RNAP primary channel in State I, II, and III, compared to *Msm* RNAP core (PDB ID 6F6W) and model of *Msm* elongation complex according to PDB ID 2O5J. Color code as in Figure 1d, template DNA in pink, non-template in yellow.

b, Comparison of RNAP primary channel opening in RNAP complex with HelD in State I (orange), II (red), III (yellow), and without HelD in RNAP core (green) in EC (cyan).

c, Surface representation of RNA exit channel opening caused by HelD interaction with RNAP in State I, II, and III, compared to *Msm* RNAP core (PDB ID 6F6W) and model of *Msm* elongation complex according to PDB ID 2O5J. Color code as in Figure 1d, nascent RNA in red.

d, Comparison of RNAP RNA exit channel opening in RNAP complex with HelD in State I (orange), II (red), III (yellow), and without HelD in RNAP core (green) in EC (cyan).

e, Two views of State I and II superposition according to the RNAP core (β/430-738). The collapse of NG-linker in State II allows for 1A and 2A mutual reorientation (arrow 1 and 2). Concomitantly this causes a shift of 1A extension (arrow 3 in left panel) and β-lobe (arrow 3 in right panel). The reorientation of 1A-2A also causes a shift of the HelD CO-domain (arrow 4) and a further swing-out of β'-NCD CC (arrow 5). On the other hand the β'-CC shifts towards the HelD CO-domain (arrow 6). State I is colored as in Figure 1, State II is in light transparent grey. Only selected domains are displayed.

f, Two views of State II and III superposition according to the RNAP core (β/430-738). In State III, the HelD N-terminal domain slightly shifts within the RNAP secondary channel (arrow 1). The absence of 1A and 2A domains in State III allows relaxation of β-lobe, which shifts to a similar position as in State I (arrow 2), The absence of the HelD-specific domain allows closure of the β'-clamp (arrow 3 and 4). State III is colored as in Figure 1; State II is in light transparent grey as in (e). Only selected domains are displayed.

g, Superposition of State III (grey) with EC (black) according to the RNAP core (β/430-738), only selected domains are displayed. The HelD N-terminal domain insertion into the secondary channel induces changes in the RNAP primary channel that may destabilise the dwDNA interaction. Notice the shifts of both β-lobe and β'-jaw/cleft and changes in the loops contacting (double arrows) dwDNA in EC (cyan) and in the HelD presence (red).

h, Superposition of the 1A-2A heterodimer in State I (colored as in Figure 1) and State II (light grey) according to 1A-1 domain (1A-1 residues 174-259 superimposed by least squares on main chain, rmsd 2.37 Å). In state II, the disorder of NG-linker (arrow 1), rearrangement of α6 and formation of α7 (change from yellow to cyan, arrow 2), and shift of the 2A domain (arrow 3) altogether result in more open NTP-binding site (ATP in green, Mg^{2+} magenta sphere, modelled by superposition with UvrD ternary complex, PDB ID 2IS4).

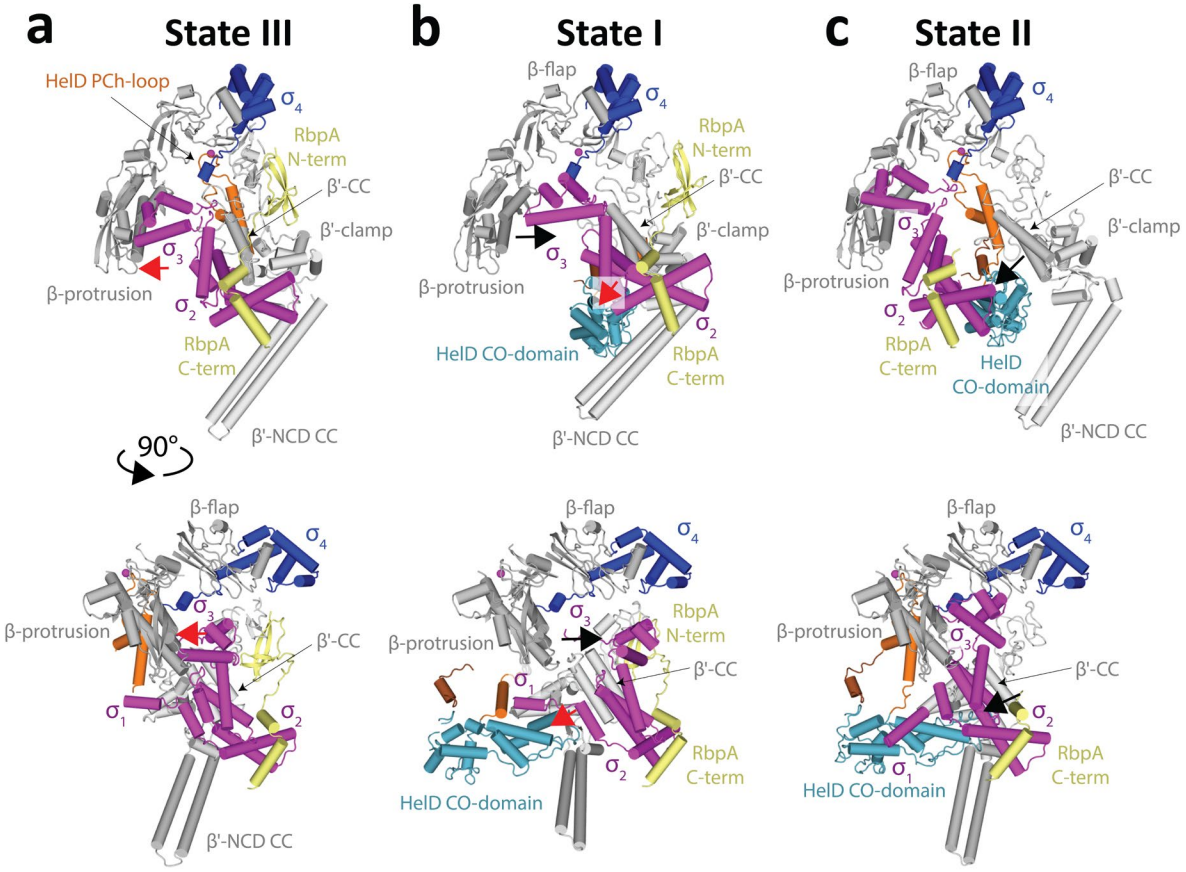

Supplementary Figure 11: Models of HelD, σ^A, and RbpA coexistence on RNAP.

a,**b**,**c** Three hypothetical coexistence modes (ordered according to the least adjustments needed) of HelD (only HelD-specific domains shown for clarity), σ^A, and RbpA in the RNAP primary channel in two perpendicular views. Color code as in Figure 1, domains σ^{1-3} in magenta, σ^4 in blue, RbpA in yellow.

a, The State III complex superimposed with PDB entries ID 6EYD and ID 5TW1 based on the RNAP core domain (β/430-738). In State III, the HelD CO-domain does not occupy the primary channel, and σ^2 can interact with the conserved binding site on the β'-clamp coiled-coil domain (β'-CC). The σ^3 domain clashes sterically with β-protrusion (also called β-domain 1, red arrow), however, a slight shift of σ^3 could accommodate the latter. The RbpA interaction with both σ^A and β'-clamp is preserved.

b, The State I complex superimposed with the PDB entries ID 6EYD and ID 5TW1 based on the RNAP β'-clamp (β'/6-404). In State I, the HelD CO-domain occupies the primary channel and σ^2 can interact with β'-CC if the CO-tip accommodates for σ^2 presence (red arrow) and σ^1 moves away. The opening of the RNAP clamp in State I causes σ^3 detachment from domain 1 (black arrow). The protein linker between σ^3 and σ^4 has to accommodate the RNAP clamp opening. The RbpA interaction with both σ^A and β'-clamp is preserved.

c, The State II complex superimposed with the PDB entry ID 5TW1 based on the RNAP core domain (β/430-738). In State II, the HelD CO-domain occupies the primary channel and moves

even further towards β'-CC, disallowing σ^2 to bind the β'-clamp. In this situation σ^3 and σ^4 hold only on the β-protrusion and β-flap and σ^2 detaches from the β'-clamp (black arrow). The resulting gap between σ^2 and β'-clamp may be filled with the HelD CO-domain.

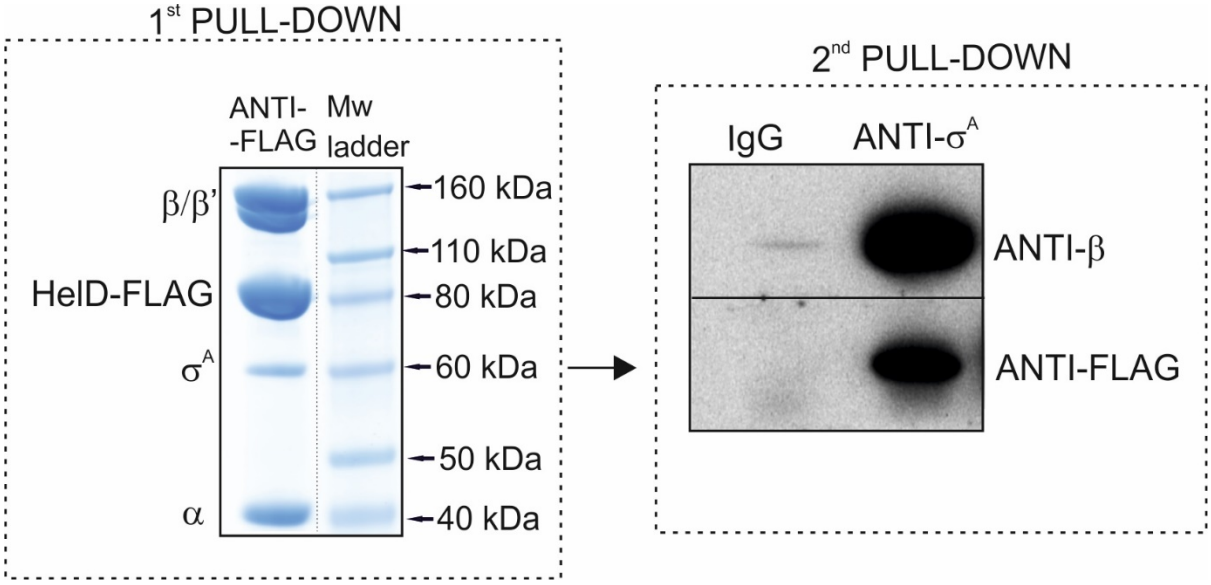

Supplementary Figure 12: HelD and σ^A can coexist on RNAP.

Double pull-down: The first pull-down was performed from *Msm* lysates (strain LK2590) with an antibody against the FLAG peptide (the same result as in Figure 4f). The Simply Blue-stained gel shows the resulting pulled-down proteins – first lane (ANTI-FLAG). The second lane shows Molecular weight (Mw) ladder. The two lanes were assembled electronically – marked with the dotted line. The protein mixture from the first pull-down was then used for the second pull-down with an antibody against σ^A and with IgG (negative control). The presence of HelD-FLAG (anti-FLAG) and RNAP (anti-β) was verified by Western blotting. The identities of the antibodies used for the detection are indicated next to the gel. The experiment was performed 2x with identical results.

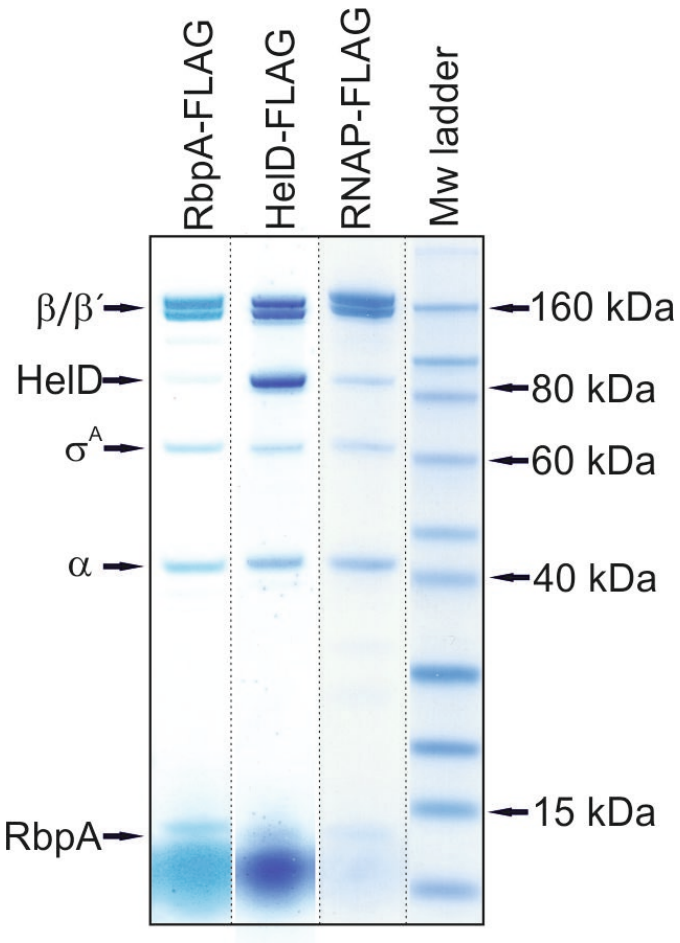

Supplementary Figure 13: RbpA is in complex with RNAP, σ^A, and HelD.

Simply Blue-stained SDS-PAGE of IPs of FLAG-tagged proteins from *Msm* (RbpA-FLAG, strain LK2541; HelD-FLAG, strain LK2590; RNAP-FLAG, strain LK1468). The identities of the FLAG-tagged proteins are indicated above the lanes. The identities of the pulled-down proteins are indicated with arrows (determined by mass spectrometry). The final gel was assembled electronically as indicated with the dotted lines. The experiment was performed 3x (biological replicates) with identical results.

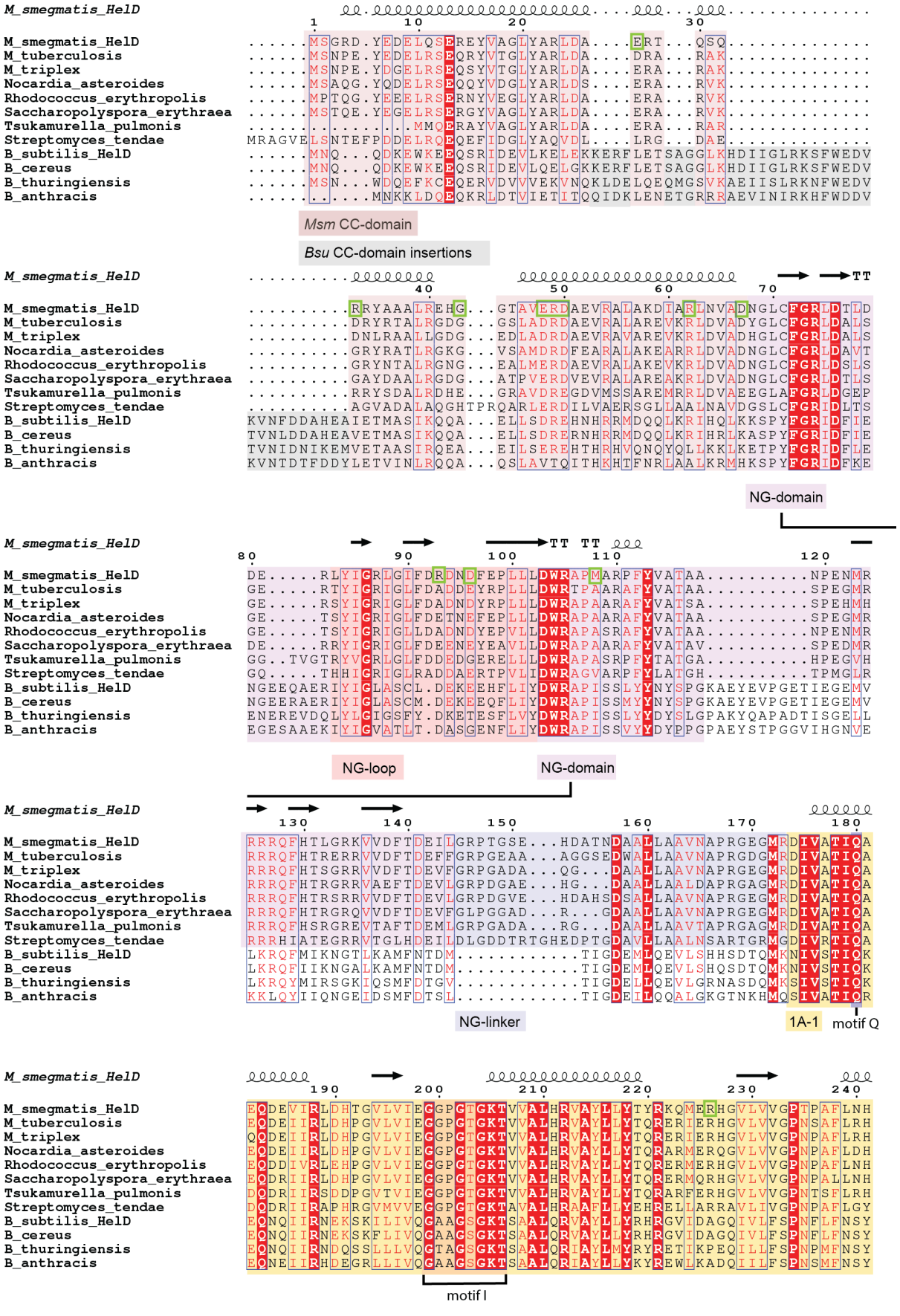
M_smegmatis_HelD
M_tuberculosis
M_triplex
Nocardia_asteroides
Rhodococcus_erythropolis
Saccharopolyspora_erythraea
Tsukamurella_pulmonis
Streptomyces_tendae
B_subtilis_HelD
B_cereus
B_thuringiensis
B_anthracis
Msm CC-domain
Bsu CC-domain insertions
NG-domain
NG-loop
NG-linker
1A-1
motif Q
motif I

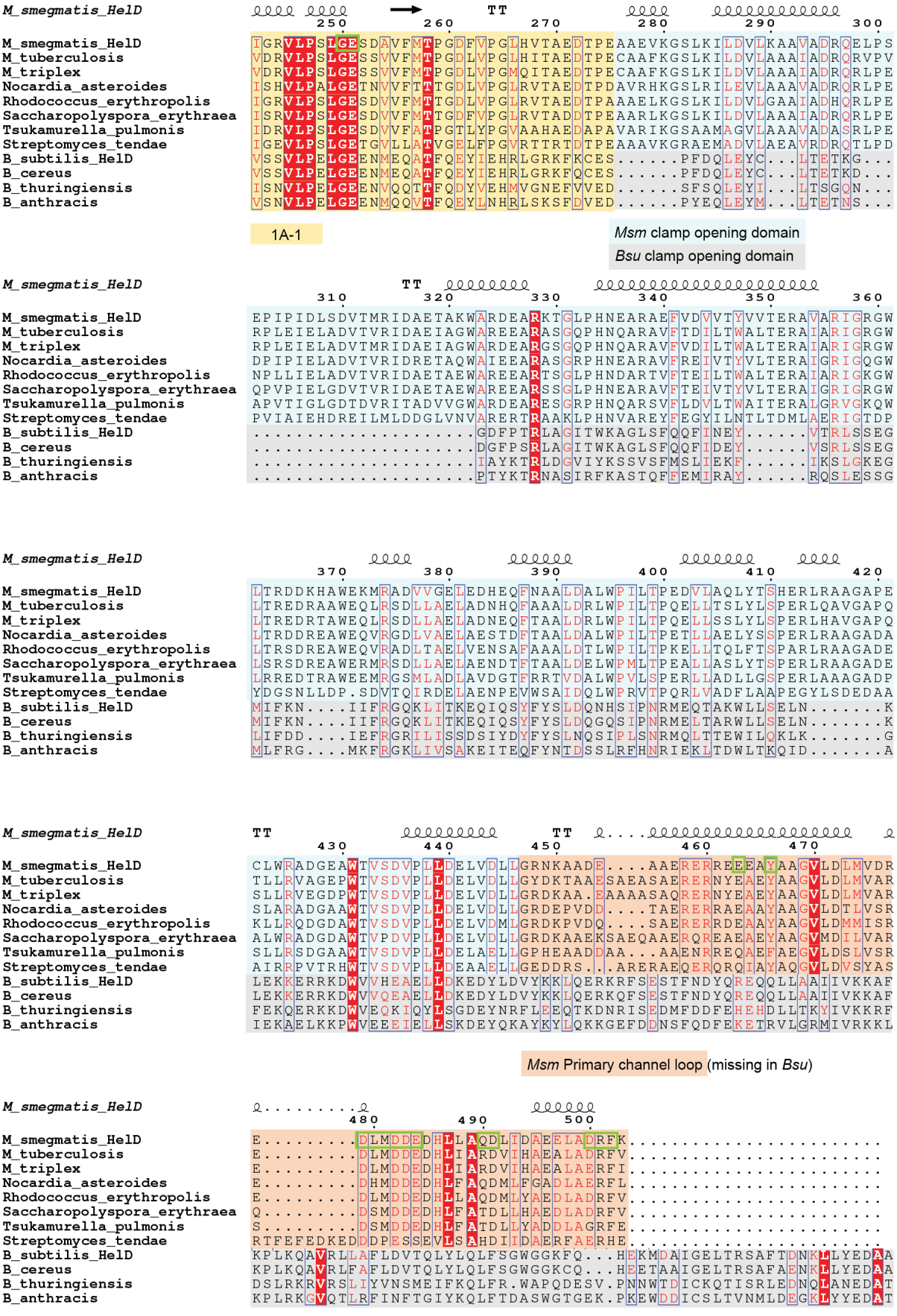
M_smegmatis_HelD
M_tuberculosis
M_triplex
Nocardia_asteroides
Rhodococcus_erythropolis
Saccharopolyspora_erythraea
Tsukamurella_pulmonis
Streptomyces_tendae
B_subtilis_HelD
B_cereus
B_thuringiensis
B_anthracis
1A-1
Msm clamp opening domain
Bsu clamp opening domain
Msm Primary channel loop (missing in Bsu)

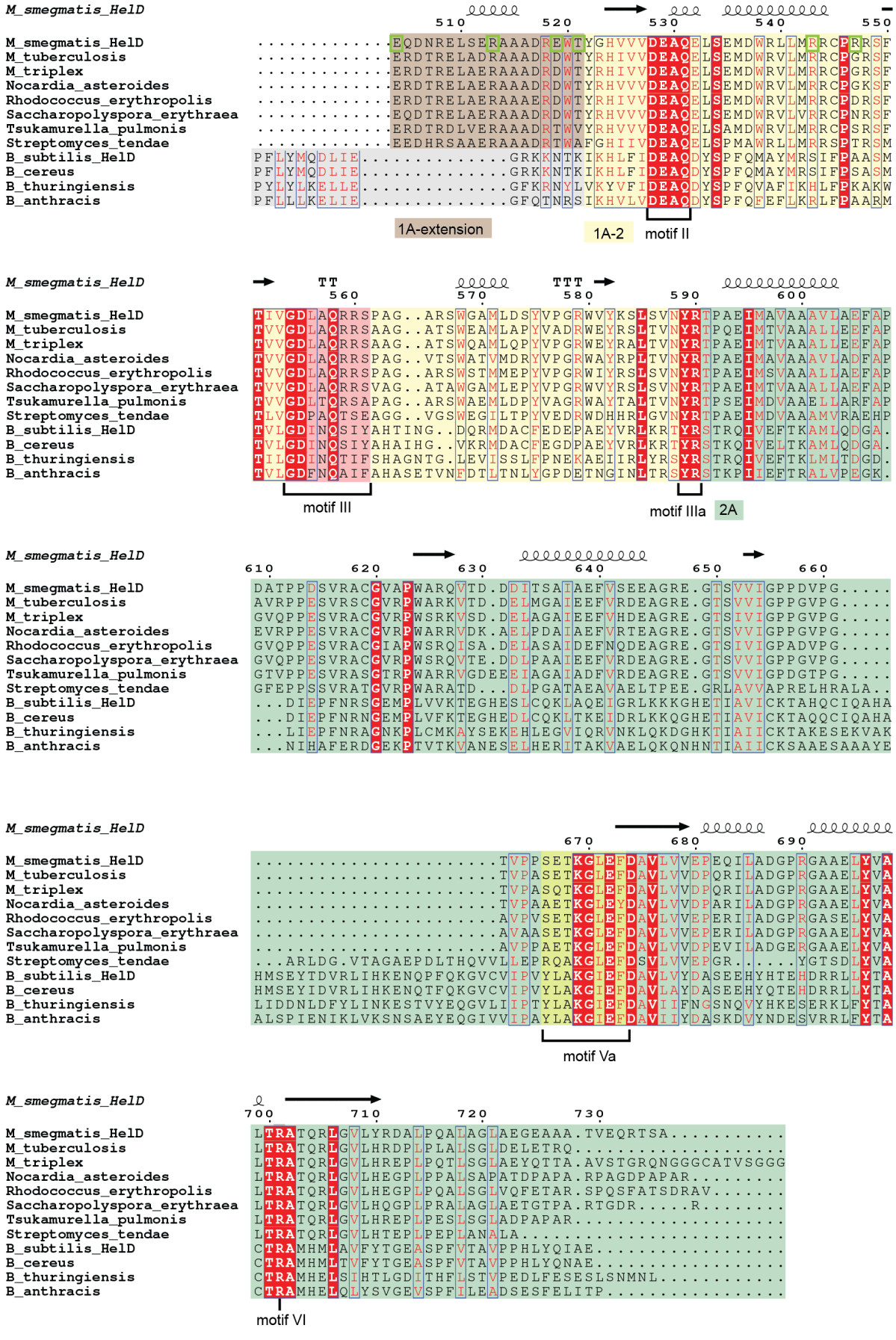
M_smegmatis_HelD
M_tuberculosis
M_triplex
Nocardia_asteroides
Rhodococcus_erythropolis
Saccharopolyspora_erythraea
Tsukamurella_pulmonis
Streptomyces_tendae
B_subtilis_HelD
B_cereus
B_thuringiensis
B_anthracis
1A-extension
1A-2
motif II
motif III
motif IIIa
2A
motif Va
motif VI

Supplementary Figure 14: Sequence alignment of HelD homologs.

Curated sequence alignment based on alignment generated by Clustal Omega software[12]. Amino acids in *Msm* HelD that make contacts with the RNAP core as observed in State II (Supplementary Tables 1-3) are marked with green rectangles. Secondary structure is denoted for *M. smegmatis* HelD. GeneBank codes of used sequences: *Msm* WP_003893549.1, *M. tuberculosis*: PLV44927.1; *M. triplex*: CDO88184.1, *Nocardia asteroides*: GAD85771.1, *Rhodococcus erythropolis*: WP_095971734.1, *Saccharopolyspora erythraea*: PFG97077.1, *Tsukamurella pulmonis*: WP_139061895.1; *Streptomyces tendae*: WP_150152972.1, *Bsu* WP_003244180.1, *Bacillus cereus* WP_095971734.1, *B. thuringiensis*: WP_074790911.1, *B. anthracis*: WP_071737252.1. The graphics was created using ESPript 3.0[15]

Supplementary Table 1: Hydrogen bonds and salt bridges between HelD N-terminal domain (State II) and RNAP β' subunit.

Interactions up to 4 Å distance according to the PDBe PISA server[14].

#	RNAP β' subunit	HelD residue
1	D:LYS 775	H:GLU 27
2	D:ASN 809	H:GLY 43
3	D:LYS 820	H:GLU 48
4	D:ARG 865	H:ASP 50
5	D:ARG 757	H:ASP 96
6	D:GLN 778	H:ARG 34
7	D:GLN1008	H:ARG 49
8	D:GLN1146	H:ARG 49
9	D:GLU 751	H:ARG 93
10	D:ASP 779	H:ARG 93
11	D:GLY 762	H:MET 108
12	D:ARG 865	H:ASP 50
13	D:ARG1086	H:ASP 67
11	D:GLU 771	H:ARG 62

Supplementary Table 2: Hydrogen bonds and salt bridges between HelD 1A domain (State II) and RNAP β-lobe and β'-jaw.

Interactions up to 4 Å distance according to the PDBe PISA server[14].

#	RNAP β subunit	HelD residue
1	C:LYS 188	H:THR 521
2	C:SER 185	H:ARG 513
3	C:GLU 187	H:ARG 226
4	C:GLU 187	H:ARG 513
5	C:LYS 209	H:GLU 519
6	C:ARG 210	H:GLU 519
7	C:ARG 210	H:ARG 543
8	C:LYS 209	H:THR 521
9	C:ASP 211	H:ARG 547
	RNAP β' subunit	
1	D:VAL1040	H:GLU 504
2	D:LYS1061	H:GLY 250
3	D:ARG1084	H:GLU 251

Supplementary Table 3: Hydrogen bonds and salt bridges between HelD primary channel loop (State I and II) and RNAP β and β' constituents of the primary channel.

Interactions up to 4 Å distance according to the PDBe PISA server[14].

State I		
#	RNAP β' subunit	HelD residue
1	D:ARG1205	H:ALA 467
State II		
#	RNAP β subunit	HelD residue
1	C:LYS 184	H:ASP 500
2	C:ARG 456	H:GLN 490
3	C:ARG 464	H:ASP 491
4	C:GLN 605	H:GLU 484
5	C:LYS 875	H:ASP 483
6	C:LYS 883	H:ASP 483
7	C:HIS1026	H:GLU 484
8	C:HIS1026	H:GLU 484
9	C:ARG1058	H:ASP 479
	RNAP β' subunit	
1	D:TYR 871	H:GLU 463
2	D:ARG 875	H:GLU 463
3	D:ARG 874	H:TYR 466
4	D:ARG 427	H:ASP 479
5	D:ARG 421	H:ASP 479
6	D:ARG 427	H:LEU 480
7	D:ARG 500	H:MET 481
8	D:GLN 540	H:MET 481
9	D:ALA 542	H:MET 481
10	D:ARG 500	H:ASP 482
11	D:ARG1039	H:PHE 502
12	D:ARG 874	H:TYR 466
13	D:ASP 878	H:TYR 466
14	D:ASP 539	H:ASP 483
15	D:ARG1012	H:ARG 501
16	D:ASP 868	H:ARG 501

Supplementary Table 4: Bacterial strains.

	Strain	Description/Notes	Source
E. coli			
RNAP *Msm*	LK1853		[16]
SigA(σ^A) *Msm*	LK1740	pET22b+ with C-terminal 6xHis SigA *Msm* BL21(DE3)	This work
HelD *Msm*	Mshe1	6xHis-HelD *Msm*, Lemo21 (DE3)	This work
RbpA *Msm*	LK1254	pET22b+ with C-terminal 6xHis RbpA *Msm*, BL21(DE3)	This work
M. smegmatis			
wt	LK865	*M. smegmatis* mc^2 155	Laboratory strain
RNAP-FLAG	LK1468 MR-sspB	kindly provided by D. Schnappinger, Weill Cornell Medical College, New York, USA	[17]
RbpA-FLAG	LK2541		This work
SigA-FLAG	LK2073		This work
HelD-FLAG	LK2590		This work

Supplementary Table 5: DNA oligonucleotides.

Primer	**Sequence *5'→ 3'***	
#1101	AAATCGGGCGGCGTCCCGGA	Primers for *Msm* DNA fragment for EMSA assays
#1146	ACGGAAGCTTGGCGAGGC	
#1155	GGAATTCCATATGGTGGCAGCGACAAAGGCA	Primers for σ^A (*MSMEG_2758*) cloning into pET22b
#1156	CCGCTCGAG GTCCAGGTAGTCGCGCAG	
#1182	CCGCTCGAGGCTTCCGGTTCCGCGCCG	Primers for *rbpA* (*MSMEG_3858*) cloning into pET22b
#1183	GGAATTCCATATGATGGCTGATCGTGTCCTG	
#2339	CTTCATATGGCAGCGACAAAGGCAAGCCCG	Primers for σ^A (*MSMEG_2758*) cloning into pTet-Int
#2340	CGTAAGCTTCTACTTGTCGTCGTCGTCCTTGTAGTCCAGGTAGTCGCGCAGCAC	
#2894	ATTCCATATGGCTGATCGTGTCCTGCGGGGC	Primers for *rbpA* (*MSMEG_3858*) cloning into pTet-Int
#3093	CGTAAGCTTCTACTTGTCGTCGTCGTCCTTGTAGTCGCTTCCGGTTCCGCGCCGCTT	
#3130	CATTCATATGTCAGGTCGGGACTACGAGGAC	Primers for *helD* (*MSMEG_2174*) cloning into pTetInt
#3131	CGTAAGCTTCTACTTGTCGTCGTCGTCCTTGTAGTCTGCCGACGTGCGCTGCTCGACCGT	

Supplementary Table 6. Cryo-EM data collection, refinement and validation statistics.

	Msm HelD-RNAP complex **State I**	*Msm* HelD-RNAP complex **State II**	*Msm* HelD-RNAP complex **State III**
Deposition	EMD-10996, PDB ID 6YXU	EMD-11004, PDB ID 6YYS	EMD-11026, PDB ID 6Z11
Data collection and processing			
Magnification	165,000	165,000	165,000
Voltage (kV)	300	300	300
Electron exposure (e^{-}/Å^2)	40-50	40-50	40-50
Defocus range (μm)	0.7-3.3	0.7-3.3	0.7-3.3
Pixel size (Å)	0.8311	0.8311	0.8311
Symmetry imposed	C1	C1	C1
Initial particle images (no.)	1,560,500	1,560,500	1,560,500
Final particle images (no.)	185,400	173,500	119,100
Map resolution (Å)	3.08	3.08	3.47
FSC threshold	0.143	0.143	0.143
Map resolution range (Å)	3.08-5.90	3.02-5.90	3.29-5.90
Estimated angular accuracy (°)	0.693	0.729	0.795
Efficiency score[2]	0.4	0.50	0.65
Sphericity[9]	0.938	0.919	0.916
Refinement			
Initial model used (PDB code)	6F6W[11]	6F6W	6F6W
Model resolution (Å)	3.2	3.2	3.5
FSC threshold	0.5	0.5	0.5
Model resolution range (Å)	3.09-5.90	3.02-5.90	3.05-5.90
Map sharpening *B* factor (Å^2)	-78.53	-81.37	-85.45
Model vs map cross correlation	0.81	0.79	0.81
Model composition			
Non-hydrogen atoms	27791	27930	23948
Protein residues	3583	3597	3077
Nucleotide residues	0	0	0
Ligands	3	3	3
B factors (Å^2)			
Protein	40.27	32.39	34.47
Ligand	61.69	47.49	46.56
R.m.s. deviations from ideal			
Bond lengths (Å)	0.006	0.005	0.005
Bond angles (°)	0.672	0.656	0.610
Validation			
MolProbity score	2.03	2.00	2.01
Clashscore	9.28	9.18	7.94
Poor rotamers (%)	0.00	0.00	0.04
Ramachandran plot			
Favored (%)	90.54	91.15	89.03
Allowed (%)	9.43	8.82	10.97
Disallowed (%)	0.03	0.03	0

Supplementary Table 7: Data collection and refinement statistic of the *B. subtilis* HelD C-terminal domain. Values in parentheses refer to the highest resolution shell.

PDB code	6VSX
Data collection	
X-ray source	Rigaku MicroMax 007 HF
Wavelength (Å)	1.54178
No. if oscillation images	1080
Total oscillation angle	1080
$\Delta\phi$ (°)	1
Crystal to detector distance (mm)	50
Average mosaicity (°)	1.4
Space group	$C2_1$
Cell dimensions	
a (Å)	106.96
b (Å)	38.81
c (Å)	44.43
β (º)	101.45
Resolution (Å)	25.0 – 2.0
No. of all observed reflections	245,968
No. of unique reflections	11,905
Average redundancy	20.7 (14.1)
Completeness (%)	96.7 (72.0)
$I/\sigma(I)$	60.1 (14.3)
Wilson B-factor (Å^2)	21.87
R-merge	0.044 (0.206)
CC1/2	(0.991)
CC*	(0.998)
SAD Phasing (S and P)	
Number of sites	10 (S) and 1 (P)
Figure of Merit	0.296
Refinement	
Resolution (Å)	25.0 – 2.0
No. of reflections used in refinement	11,869 (1,186)
R_{work}	0.1723 (0.1756)
R_{free}	0.2014 (0.2393)
No. of atoms	1,382
macromolecules	1,268
ligands	5
solvent	109
No. of protein residues	159
RMS deviations from ideal	
bond lengths (Å)	0.007
bond angles (°)	0.80
Clashscore (Molprobity)	5.92
Ramachandran plot, residues	
in favored region (%)	98.06
outliers (%)	0.0
Average B-factor (Å^2)	25.2
Macromolecules (Å^2)	24.6
Ligands (Å^2)	30.5
Solvent (Å^2)	32.9

Supplementary References

1 Zheng, S. Q. *et al.* MotionCor2: anisotropic correction of beam-induced motion for improved cryo-electron microscopy. *Nat Methods* **14**, 331-332, doi:10.1038/nmeth.4193 (2017).

2 Naydenova, K. & Russo, C. J. Measuring the effects of particle orientation to improve the efficiency of electron cryomicroscopy. *Nat Commun* **8**, 629, doi:10.1038/s41467-017-00782-3 (2017).

3 Rosenthal, P. B. & Henderson, R. Optimal determination of particle orientation, absolute hand, and contrast loss in single-particle electron cryomicroscopy. *J Mol Biol* **333**, 721-745 (2003).

4 Jakobi, A. J., Wilmanns, M. & Sachse, C. Model-based local density sharpening of cryo-EM maps. *Elife* **6**, doi:10.7554/eLife.27131 (2017).

5 Zivanov, J. *et al.* New tools for automated high-resolution cryo-EM structure determination in RELION-3. *Elife* **7**, doi:10.7554/eLife.42166 (2018).

6 Zivanov, J., Nakane, T. & Scheres, S. H. W. Estimation of high-order aberrations and anisotropic magnification from cryo-EM data sets in RELION-3.1. *IUCrJ* **7**, 253-267, doi:10.1107/S2052252520000081 (2020).

7 Pettersen, E. F. *et al.* UCSF Chimera--a visualization system for exploratory research and analysis. *J Comput Chem* **25**, 1605-1612, doi:10.1002/jcc.20084 (2004).

8 McNicholas, S., Potterton, E., Wilson, K. S. & Noble, M. E. Presenting your structures: the CCP4mg molecular-graphics software. *Acta Crystallogr D Biol Crystallogr* **67**, 386-394, doi:10.1107/S0907444911007281 (2011).

9 Tan, Y. Z. *et al.* Addressing preferred specimen orientation in single-particle cryo-EM through tilting. *Nat Methods* **14**, 793-796, doi:10.1038/nmeth.4347 (2017).

10 Robert, X. & Gouet, P. Deciphering key features in protein structures with the new ENDscript server. *Nucleic Acids Res* **42**, W320-324, doi:10.1093/nar/gku316 (2014).

11 Laskowski, R. A., Jablonska, J., Pravda, L., Varekova, R. S. & Thornton, J. M. PDBsum: Structural summaries of PDB entries. *Protein Sci* **27**, 129-134, doi:10.1002/pro.3289 (2018).

12 Madeira, F. *et al.* The EMBL-EBI search and sequence analysis tools APIs in 2019. *Nucleic Acids Res* **47**, W636-W641, doi:10.1093/nar/gkz268 (2019).

13 Jurrus, E. *et al.* Improvements to the APBS biomolecular solvation software suite. *Protein Sci* **27**, 112-128, doi:10.1002/pro.3280 (2018).

14 Krissinel, E. & Henrick, K. Inference of macromolecular assemblies from crystalline state. *J Mol Biol* **372**, 774-797, doi:10.1016/j.jmb.2007.05.022 (2007).

15 Le, T. T. *et al.* Mfd Dynamically Regulates Transcription via a Release and Catch-Up Mechanism. *Cell* **172**, 344-357 e315, doi:10.1016/j.cell.2017.11.017 (2018).

16 Kouba, T. *et al.* The Core and Holoenzyme Forms of RNA Polymerase from Mycobacterium smegmatis. *J Bacteriol* **201**, doi:10.1128/JB.00583-18 (2019).

17 Kim, J. H. *et al.* Protein inactivation in mycobacteria by controlled proteolysis and its application to deplete the beta subunit of RNA polymerase. *Nucleic Acids Res* **39**, 2210-2220, doi:10.1093/nar/gkq1149 (2011).

MANUSCRIPT VII

microorganisms

MDPI

Article

Effects of DNA topology on transcription from rRNA promoters in *Bacillus subtilis*

Petra Sudzinová[1], Milada Kambová[1], Olga Ramaniuk[1], Martin Benda[1], Hana Šanderová[1] and Libor Krásný[1]*

[1] Institute of Microbiology of the Czech Academy of Sciences, Prague, Czech Republic; petra.sudzinova@biomed.cas.cz (P.S.); mkambova@gmail.com (M.K.); ramaniuk@biomed.cas.cz (O.R.); mb.martin.benda@gmail.com (M.B.); sanderova@biomed.cas.cz (H.Š.)

* Correspondence: krasny@biomed.cas.cz

Received: date; Accepted: date; Published: date

Abstract: Expression of rRNA is one of the most energetically demanding cellular processes and as such, it must be stringently controlled. Here we report that DNA topology, *i. e.* the level of DNA supercoiling, plays a role in the regulation of *Bacillus subtilis* σ^A-dependent rRNA promoters in a growth phase-dependent manner. The more negative DNA supercoiling in exponential phase stimulates transcription from rRNA promoters, and DNA relaxation in stationary phase contributes to cessation of their activity. Novobiocin treatment of *B. subtilis* cells relaxes DNA and decreases rRNA promoter activity despite an increase in the GTP level, a known positive regulator of *B. subtilis* rRNA promoters. Comparative analyses of steps during transcription initiation then reveal differences between rRNA promoters and a control promoter, P*veg*, whose activity is less affected by changes in supercoiling. Additional data then show that DNA relaxation decreases transcription also from promoters dependent on alternative sigma factors σ^B, σ^D, σ^E, σ^F, and σ^H with the exception of σ^N where the trend is opposite. Finally, supercoiling also affects the ability of HelD, a transcriptional factor associating with RNAP, to stimulate recycling of RNAP. To summarize, this study identifies DNA topology as a factor important (i) for expression of rRNA in *B. subtilis* in response to nutrient availability in the environment, (ii) for transcription activities of *B. subtilis* RNAP holoenzymes containing alternative sigma factors, and (iii) for the capacity of *B. subtilis* HelD to stimulate transcription.

Keywords: *Bacillus subtilis*; transcription; ribosomal RNA; DNA topology

1. Introduction

Bacterial cells need to adapt to environmental changes. In nutrient-rich environments, cells grow and divide rapidly and this requires a large number of ribosomes to satisfy the need for new proteins. In nutritionally poor environments, the synthesis of new ribosomes virtually stops. As production of new ribosomes is energetically highly costly for the cell, it must be tightly regulated. The number of ribosomes in the cell is regulated mainly on the level of transcription initiation of ribosomal RNA (rRNA) [1].

Transcription initiation can be divided into several steps. First, when the RNA polymerase (RNAP) holoenzyme (contains the core RNAP subunits [$\alpha 2\beta\beta'\omega$] in complex with a σ factor) binds to specific DNA sequences, promoters, it forms the closed complex where DNA is still in the double-helical form [2]. The specificity of RNAP for promoter sequences is provided by the σ factor [3–6]. Subsequently, this complex isomerizes and forms the open complex where the two DNA strands are unwound and the transcription bubble is formed. At this stage, initiating nucleoside triphosphates NTPs (iNTPs) can enter the active site and transcription can begin. RNAP then leaves the promoter and enters the elongation phase of transcription [7].

In bacteria, the concentrations of iNTPs act as key regulators of transcription and directly affect RNAP at some promoters. These promoters form relatively unstable open complexes where the time window available to iNTPs to penetrate into the active site and initiate transcription is relatively short. The higher the concentration of the respective iNTP, the higher the chance that it penetrates into the active site while the transcription bubble is still open. Hence, increases in intracellular concentrations of iNTPs stimulate transcription whereas low levels of iNTPs result in inefficient transcription initiation [8–10].

Another important factor for transcription initiation in bacteria is the topological state of DNA, *e. i.* the levels of supercoiling. DNA is in the cells usually underwound and this results in negative supercoiling [11]. Negative supercoiling then helps RNAP to melt DNA in promoter regions. In general, bacterial cells display more pronounced negative supercoiling in exponential than in stationary phase of growth and initiation from a number of promoters is sensitive to this parameter [12–16].

rRNA promoters are prime examples of where transcription initiation is regulated by the concentration of the iNTP. In *Bacillus subtilis*, a model soil-dwelling, spore-forming gram-positive bacterium, the iNTP of the tandem rRNA promoters of all 10 (or 9, depending on the strain) rRNA operons is exclusively GTP [17]. The GTP level in *B. subtilis* is affected by (p)ppGpp, an alarmone that is produced at times of stress, such as amino acid starvation or heat shock. (p)ppGpp inhibits GuaB, the first enzyme in the de novo GTP biosynthesis pathway, which results in decreased GTP levels and increased ATP levels as more of the last common intermediate for the synthesis of both GTP and ATP, inosine monophosphate (IMP), is now available for ATP synthesis only [18,19]. By affecting the GTP level (p)ppGpp indirectly affects the activity of rRNA promoters in *B. subtilis* [20–22].

Here, we investigated how the activity of rRNA promoters in *B. subtilis* changes when the cells transition from exponential to stationary phase. These promoters depend on the primary σ factor, σ^A. We show that their activity decreases during the transition and this correlates with a decrease in the GTP concentration. Nevertheless, there is a point in the process where the level of GTP does not decrease any further but the activity of rRNA promoters does. We show that *B. subtilis* rRNA promoters are, besides [GTP], regulated by the level of their supercoiling, and we dissect the effects of supercoiling on the formation of closed and open complexes, thereby providing mechanistic insights into the process. Next, we show that supercoiled (SC) DNA is a more efficient template for transcription for all alternative σ factors tested with the exception of σ^N, a relatively newly discovered sigma factor, encoded on the pBS32 plasmid of the NCIB 3610 strain [23,24]. Finally, we show that transcriptional cycling dependent on the HelD protein that associates with RNAP [25–27] also depends on the DNA supercoiling level. In summary, a new updated model of *B. subtilis* promoter regulation is presented here.

2. Materials and Methods

2.1 Media and growth conditions

Cells were grown at 37°C, either in LB or in rich MOPS supplemented with 20 amino acids: 50 mM MOPS (pH 7.0), 1 mM $(NH_4)_2SO_4$, 0.5 mM KH_2PO_4, 2 mM $MgCl_2$, 2 mM $CaCl_2$, 50 μM $MnCl_2$, 5 μM $FeCl_3$, amino acids (50 μg/ml each), and 0.4 % glucose. Antibiotics used: ampicillin 100 μg/ml, chloramphenicol 5 μg/ml and MLS – linkomycin 0.5 μg/ml and erythromycin 2.5 μg/ml.

2.2 Bacterial strains and primers

Table 1. Bacterial strains used in a study.

Name	Original code	Nickname	Description	Reference
B. subtilis				
	RLG7554	BP1-lacZ	MO1099 *amyE*::Cm *rrnB* P1 (-39/+1)-*lacZ*	[17]

LK135	RLG7555	P*veg*-lacZ	MO1099 amyE::Cm Pveg (-38/-1, +1G)-lacZ	[17]
	RLG6943	RM-lacZ	MO1099 *amyE*::Cm *rrnO* P2 (-77/+50)-*lacZ*	[17]
LK1723	RLG7024	*wt* RNAP	C-ter. His10xβ' MH5636	[28]
LK1272	LK637	RNAPΔhelD	C-ter. His10xβ', *helD::MLS*	[25]
E. coli				
LK22		SigA		[29]
LK1207		SigB	C-ter. His6x sigB	This work
LK1187		SigD		[30]*
LK2580		SigE	C-ter. His6x sigE	This work
LK1425		SigF	C-ter. His6x sigF	This work
LK1208		SigH		This work
LK2531		SigN	His-SUMO-SigN in pBM05; BL21(DE3)	This work#
LK800		HelD	pHelD-His6x; BL21 (DE3)	[25]
		HelDΔN	MBP-HelDΔN; Lemo21 (DE3)	[31]
LK1177	RLG7558	P*veg*	pRLG770 with P*veg* (-38/+1) +1G; DH5α	[17]
LK1522	RLG7596	*rrn*B P1core	pRLG770 with *rrn*B P1 (-39/+1); DH5α	[17]
LK28	RLG6927	*rrn*B P1 P2	pRLG770 with *rrn*B P1 P2 (-248/+8); DH5α	[21]
LK17	RLG6916	*rrn*O P1 P2	pRLG770 with *rrn*O P1 P2 (-314/+9); DH5α	This work
LK1231		P*trxA*	pRLG770 with P*trxA* (-249/+11); DH5α	This work
LK1233		P*motA*	pRLG770 with P*motA* (-249/+11); DH5α	This work
LK2594		P*spoIIID*	pRLG770 with P*spoIIID* (-150/+10); DH5α	This work
LK1495		P*spoIIQ*	pRLG770 with P*spoIIQ* (-251/+9); DH5α	This work
LK1235		P*spoVG*	pRLG770 with P*spoVG* (-94/+11) DH5α	This work
LK2672		*sigN* P2 P3	pRLG770 with P*sigN* P2 P3 (-247/+159); DH5α	This work
LK2673		P*zpaB*	pRLG770 with P*zpaB* (-266/+175); DH5α	This work
LK2608		P*zpbY*	pRLG770 with P*zpbY* (-304/+155); DH5α	This work
LK2609		P*zpdG*	pRLG770 with P*zpdG* (-244/+170); DH5α	This work

* Thanks to Dr A. Gaballa for providing the strain.

Thanks to Dr D. Kearns for the pBM05 plasmid [24].

96 Table 2. List of primers.

Primer	Sequence 5′→ 3′	
#1001	GGAATTCCATATGAATCTACAGAACAACAAGG	Primers for *sigH* cloning into pET-22b(+)
#1002	CCGCTCGAGCTATTACAAACTGATTTCGCG	
#1004	GGAATTCCATATGACACAACCATCAAAAAC	Primers for *sigB* cloning into pET-22b(+)
#1006	CCGCTCGAGCATTAACTCCATCGAGGGATC	
#1069	CCGGAATTCATTCCGGAGTCATTCTTACGG	Primers for P*trxA* cloning into pRLG770
#1070	CCCAAGCTTCACTGTCATGTACTTTACCATG	
#1075	CCGGAATTCCTTTACACTTTTTTAAGGAGG	Primers for P*motA* cloning into pRLG770
#1076	CCCAAGCTTCTAGCTTGTCTATGGTTAATATC	
#1079	CCGGAATTCTTTATGACCTAATTGTGTAAC	Primers for P*spoVG* cloning into pRLG770
#1080	CCCAAGCTTATAAAAGCATTAGTGTATC	
#1309	GGAATTCCATATGGATGTGGAGGTTAAGAAAAAC	Primers for *sigF* cloning into pET-22b(+)
#1311	CCGCTCGAGGCCATCCGTATGATCCATTTG	
#1425	CCGGAATTCCATTCCATCCGGTCTTCAGG	Primers for P*spoIIQ* cloning into pRLG770
#1426	CCCAAGCTTCATCACCTCAGCAACATTCTG	
#2973	CAGTAACTTCCACAGTAGTTCACCAC	universal reverse primer for PE and qPCR
#2974	TCTAAGCTTCTAGGATCCCC	test RNA-specific forward primer for PE and qPCR
#2975	GTCGCTTTGAGAGAAGCACA	RM RNA-specific forward primer for PE and qPCR
#3109	GCGAATTCCGTGTCGGTCAACATAATAAAGG	Primers for *sigN* P2 P3 cloning into pRLG770
#3110	GCAAGCTTCGGCAAAAATCTTTCTCTCACC	
#3111	GCGAATTCGCGATGAATGAAGAGACACGG	Primers for P*zpaB* cloning into pRLG770
#3112	GCAAGCTTAGTCCATCTCGAAGATCTGGT	
#3113	GCGAATTCGACTCCAACATTTCTATTCC	Primers for P*zpbY* cloning into pRLG770
#3114	GCAAGCTTGGTCTTCTTCACTTAATTCA	
#3117	GCGAATTCTCAAAGATCTTCTAACTTGT	Primers for P*zpdG* cloning into pRLG770
#3118	GCAAGCTTGGCAGTAATCAATCAATTCT	
#3166	CGGCATATGTACATAGGCGGGAGTGAAGCC	Primers for *sigE* active form cloning into pET-22b(+)
#3167	CCGCTCGAGCACCATTTTGTTGAACTCTTTTC	
#3170	GGCGAATTCGCTTATTTCATTTTACAGGAG	

#3171	CCGAAGCTTTGTTAGGTTTGTAACAGTGT	Primers for P*spoIIID* cloning into pRLG770
PRIMER A	GGGAATTCATGGACATCAATGATATCTC	Primers for *rrn*O P1 P2 cloning into pRLG770
PRIMER B	GGAAGCTTTCAAAGCGACTACTTAATAG	

2.3 Determination of GTP concentrations

Wild-type (RLG7554, for *rrn*B P1 and RLG7555 for Pveg) were grown in the MOPS 20 AA medium supplemented with ^{32}P KH_2PO_4 (100 μCi/ml) until early exponential phase (OD_{600} ~ 0.3). Samples (100 μl) were pipetted into 100 μl 11.5 M formic acid, vortexed, left on ice for 20 min, and stored overnight at -80°C [32]. After microcentrifugation (5 min, 4 °C) to remove cell debris, the samples (5 μl) were spotted on TLC plates (Polygram®CEL 300 PEI purchased from Macherey-Nagel), developed in 0.85 M KH_2PO_4 (pH 3.4) and quantified by phosphorimaging. The identity of GTP was verified by comparison with commercial preparations of GTP run in parallel and visualized by UV shadowing [8].

2.4 Promoter activity monitored by quantitative primer extension (qPE)

Promoter constructs were fused to *lacZ* and activities were assayed by primer extension of the short lived lacZ mRNA that allows to observe rapid decreases in promoter activity in time. The experiments were conducted as described in [21]. Typically, 1 ml of cells was pipetted directly into 2ml phenol/chloroform (1:1) and 0.25 ml lysis buffer (50 mM Tris–HCl pH 8.0, 500 mM LiCl, 50 mM EDTA pH 8.0, 5% SDS). After brief vortexing, the RM was added. The RM RNA was made from *B. subtilis* strain RLG6943. This was followed by immediate sonication. Water was then added to increase the aqueous volume to 6 ml to prevent precipitation of salts, followed by two extractions with phenol/chloroform, two precipitations with ethanol, and suspension of the pellet in 20–50 ml 10 mM Tris–HCl, pH 8.0.

Primer extension was performed with M-MLV reverse transcriptase as recommended by the manufacturer (Promega) with 1-10 μl purified RNA. The ^{32}P 5'-labeled primer (#2973) hybridized 89 nt downstream from the junction of the promoter fragment used for the creation of the lacZ fusion. Samples were electrophoresed on 7 M urea 5.5 % or 9% polyacrylamide gels. The gels were exposed to screens. The screens were scanned with Molecular Imager FX (Bio-Rad) and were visualized and analysed using the Quantity One software (Bio-Rad), and normalized to cell number (OD_{600}) and RM.

2.5 Promoter activity monitored by RT–qPCR

*rrn*B P1 and P*veg* promoters were fused to the marker lacZ gene (RLG7554 and RLG7555), yielding identical transcripts. The strains were grown to exponential phase (OD_{600} ~ 0.5). Each culture was then divided into two flasks. Cells in one flask were treated with novobiocin (5 μg/ml) and cells in the other flask were left non-treated. At 0, 10, 20 and 30min, two ml of cells were withdrawn and treated with RNAprotect Bacteria reagent (QIAGEN), pelleted and immediately frozen. RNA was isolated with RNeasy Mini Kit (QIAGEN) and recovery marker RNA (RM RNA) was added at the time of extraction to control for differences in degradation and pipetting errors during extraction. The RM RNA was prepared from *B. subtilis* strain RLG6943 as for qPE. Finally, RNA was DNase treated according to manufacturers' instructions (TURBO DNA-free Kit, Ambion). Total RNA was then reverse transcribed to cDNA with reverse transcriptase (SuperScript™ III Reverse Transcriptase, Invitrogen) using primer #2973 that targets lacZ (both in the test mRNA and RM). This was followed by qPCR in a LightCycler 480 System (Roche Applied Science) containing LightCycler® 480 SYBR Green I Master and 0.5 μM primers (each). RM cDNA was amplified with primers #2974 and #2973, the test lacZ cDNA with primers #2975 and #2973. Sequences of primers were originally published in [21]. The final data were normalized to RM and the amount of cells (OD_{600}).

2.6 ^{3}H incorporation in total RNA

This experiment was conducted as described previously [33]. Briefly, strain RLG7554 was grown in LB medium to OD_{600} ~ 0.3 (early exponential phase). Newly synthesized RNA in the cells was labeled with ^{3}H-uridine (1 μCi/ml) (cold [non-radioactive] uridine was added to a final concentration of 100 μM). The bacterial culture was divided into three flasks – non-treated, treated with novobiocin (5 μg/ml), and treated with rifampicin (2 μg/ml), respectively. At 0, 5, 10, 20 and 30 min, 100 μl and 250 μl of cells were withdrawn to measure cell density and determine ^{3}H incorporation, respectively. The 250 μl cell sample was mixed with 1 ml of 10 % trichloroacetic acid (TCA) and kept on ice for at least 1 h. Thereafter, each sample was vacuum filtered, washed twice with 1 ml of 10% TCA and three times with 1 ml of ethanol. The filters were dried, scintillation liquid was added and the radioactivity was measured. The signal was normalized to cell density (OD_{600}).

2.7 RNAP levels in time

Cells (strain RLG 7554) were grown in LB rich medium to OD_{600} 0.3 (time point 0). Subsequently, every 30min 10ml of cells were pelleted and OD_{600} was measured. Pellets were washed with Lysis Buffer (20 mM Tris-HCl, pH 8, 150 mM KCl, 1 mM MgCl2) and frozen. Next day, pellets were resuspended in Lysis Buffer (100 – 500 μl, according to the size of pellet) and disrupted by sonication 2 x 1 min, with 1 min pause on ice between the pulses. After centrifugation (5 min, 4 °C) to remove cell debris, the amounts of proteins were measured with the Bradford protein assay and 5 μg was resolved by SDS-PAGE and analyzed by Western blotting, using mouse monoclonal antibodies against the β subunit of RNAP (clone name 8RB13, dilution 1:1000, Genetex) and anti-mouse secondary antibody conjugated with HRP (dilution 1:80 0000, Sigma). Subsequently, the blot was incubated for 5 min with SuperSignal™ West Femto PLUS Chemiluminiscent substrate (Thermo scientific), exposed on film and developed.

2.8 Proteins and DNA for transcription in vitro

2.8.1 Strain construction

Genes encoding SigB, SigE, SigF and SigH were amplified from genomic DNA (LK566) by PCR with Expand High Fidelity PCR System (Roche) with respective primers (Table 1, Material and Methods section) and cloned into pET22b(+) via *NdeI*/*XhoI* restriction sites and verified by sequencing. Primers for cloning of σ^{E} were designed for the active form of protein, as its first 27 AA are in the cell posttranslationally removed [34,35]. The resulting plasmids were transformed into expression strain BL21(DE3), yielding strains LK1207 (sigB), LK2580 (sigE), LK1425 (sigF), and LK1208 (sigH). His-SUMO-σ^{N} fusion protein in an expression plasmid pBM05 [24] was transformed to BL21(DE3), resulting in strain LK2531.

2.8.2 Protein purification

Wild type RNAP, containing a His10x-tagged β' subunit was purified from LK1723 as described [28]. RNAPΔHelD was purified from the strain LK1272 following the same protocol.

The **SigA** subunit of RNAP (LK22) was overproduced a purified as described [29].

σ^{B}, σ^{H}, σ^{E}, σ^{F} expression strains were grown to OD_{600} ~ 0.5 when IPTG was added to a final concentration of 0.8 mM. After 3 hours at room temperature, cells were harvested, washed and resuspended in P buffer (30 mM NaCl, 50 mM Na_2HPO_4, 3 mM β-mercaptoethanol). Cells were then disrupted by sonication and the supernatant was mixed with 1ml Ni-NTA agarose (Qiagen) and incubated for 1 h at 4 °C with gentle shaking. Ni-NTA agarose with the bound protein was loaded on a Poly-Prep® Chromatography Column (BIO-RAD), washed with P buffer and subsequently with the P buffer with the 30 mM imidazole. The protein was eluted with P buffer containing 400 mM imidazole and fractions containing σ factor were pooled together and dialyzed against storage buffer (50 mM Tris-HCl, pH 8.0, 100 mM NaCl, 50 % glycerol and 3mM β-ME). The proteins were stored at -20 °C.

σ^D was purified from inclusion bodies as described in [30].

Cells containing the plasmid for overproduction of **σ^N** were grown to OD_{600} ~ 0.5 and IPTG was added to final concentration 0.3 mM. After 3 hours, the cells were harvested, washed and resuspended in P buffer. All purification steps were done in P buffer, pH 9.5. Cells were then disrupted by sonication and the supernatant was mixed with 1ml Ni-NTA agarose (Qiagen) and incubated for 1 h at 4 °C with gentle shaking. Ni-NTA agarose with the bound His-SUMO-σ^N was loaded on a Poly-Prep® Chromatography Column (BIO-RAD), washed with P buffer and subsequently with the P buffer with the 30 mM imidazole. The protein was eluted with P buffer containing 400 mM imidazole and fractions containing His-SUMO-σ^N were pooled together and dialyzed against P buffer.

The SUMO tag was subsequently removed by using SUMO protease (Invitrogen). The cleavage reaction mixture was again mixed with the 1ml Ni-NTA agarose and allowed to bind for 1 h at 4 °C and centrifuged to pellet the resin. Supernatant was removed, the resin was washed once more with P buffer with 3 mM β-ME. The supernatants (containing σ^N) were pooled together and dialysed against storage buffer. The protein was stored at -20 °C.

HelD-His6x expression strain (LK800) was grown to OD_{600} ~ 0.5 when IPTG was added to a final concentration of 1 mM for 2 hours at room temperature. Subsequent purification was done according the same protocol mentioned above, in the section with alternative σ purification.

HelDΔN was purified by affinity chromatography as described in [31].

The purity of all proteins was checked by SDS-PAGE.

2.8.3 Promoter DNA construction

Promoter regions of alternative σ-dependent genes were amplified from genomic DNA LK566 of *B. subtilis* with primers listed in Table 2 (Material and Methods section) by PCR. All fragments were then cloned into p770 (pRLG770 [36]) using *EcoRI*/*HindIII* restriction sites and transformed into DH5*α*. All constructs were verified by sequencing.

Supercoiled plasmids (SC) were obtained using the Wizard® Plus Midipreps DNA Purification System, for higher yields Wizard® Plus Maxipreps DNA Purification System (both Promega) and subsequently phenol-chloroform extracted, precipitated with ethanol and dissolved in water. Aliquots of plasmids were linearized with the *PstI* restriction enzyme (TaKaRa), resulting in LIN, and again precipitated with ethanol to remove salts.

The state of DNA topology (linear, supercoiled) was checked on agarose gels.

2.9 Transcription in vitro

Transcription experiments were performed with the *B. subtilis* RNAP core reconstituted with a saturating concentration of σ^A (ratio 1:5) in storage buffer (50 mM Tris-HCl, pH 8.0, 0.1 M NaCl, 50% glycerol) for 15 min at 30°C. The 1:5 ratio was used also for σ^B, σ^D, σ^E, σ^F, and σ^H. For σ^N, the ratio was 1:8. Multiple round transcription reactions were carried out in 10 μl reaction volumes with 30 nM RNAP holoenzyme. The transcription buffer contained 40 mM Tris-HCl pH 8.0, 10 mM $MgCl_2$, 1 mM dithiothreitol (DTT), 0.1 mg/ml BSA and 150 mM KCl, and all four NTPs and 2 μM radiolabeled [α-^{32}P] UTP.

In K_{GTP} determination experiments, the amount of DNA (SC or LIN form) was 100 ng, ATP, CTP were 200 μM; UTP was 10 μM and GTP was titrated from 0 to 2,000 μM. To determine the affinity of RNAP to DNA, ATP, CTP were at 200 μM; UTP was 10 μM, GTP was 1,000 μM and DNA (SC/LIN) was titrated from 0 to 900 ng per reaction. In reactions with alternative σ, DNA (SC or LIN form) was 100 ng, CTP were at 200 μM; UTP was 10 μM and GTP/ATP was 1000 μM, depending on the identity of the base in the +1 position of the transcript. In reaction with HelD, HelD/HelDΔN were used in ratio 1:4 (RNAP:HelD), ATP, CTP were at 200 μM; UTP was 10 μM, GTP was 1,300 μM and DNA (SC or LIN form) was 100 ng.

All transcription reactions were allowed to proceed for 15 min at 30 °C and then stopped with equal volumes of formamide stop solution (95 % formamide, 20 mM EDTA, pH 8.0). Samples were loaded onto 7 M urea-7 % polyacrylamide gels and electrophoresed. The dried gels were scanned

with Molecular Imager FX (Bio-Rad) and were visualized and analysed using the Quantity One software (Bio-Rad).

3. Results

3.1 The activity of rrnB P1 decreases during entry into stationary phase

As the main model rRNA promoter, we selected the *rrn*B P1 promoter as it is one of the best-characterized rRNA promoters in *B. subtilis* that is regulated by [iNTP], [17,37–39]. Furthermore, the dynamic range of the activity of *rrn*B P1 is wide, which facilitated the design and interpretation of the experiments. As the main control promoter, we selected the strong P*veg* promoter that forms relatively stable open complexes and is saturated with a relatively low level of its iNTP. This promoter drives transcription of the *veg* gene that is involved in biofilm formation [40,41]. Promoter sequences are shown in Figure 1A.

To monitor promoter activities, we used promoter core promoter-lacZ fusions. The endogenous copy of P*veg* initiates transcription with ATP (+1A). Here, we used a +1G variant of P*veg* so that both transcripts (from *rrn*B P1-lacZ and P*veg*-lacZ) were identical, excluding any effects due to *e.g.* potentially differential decay of the transcripts. The +1G P*veg* promoter variant behaves identically with the +1A variant [17]. Throughout the study, promoter activity was determined by quantitative primer extension (qPE) or reverse transcription followed by quantitative PCR (RT-qPCR).

We used defined rich MOPS medium to grow the cells and measured (i) relative GTP level ([GTP]) and (ii) relative promoter activity (*rrn*B P1 and P*veg*) from early exponential phase till approximately two hours into stationary phase by qPE (Figure 1).

We detected a moderate decrease in [GTP] already during exponential phase (Fig. 2B). This moderate decrease was followed by a precipitous decline during the transition between the two phases. This correlated with a sharp spike in the (p)ppGpp level (Figure S1). However, early on in the stationary phase, [GTP] even slightly increased and then remained at the same level till the end of the experiment. The activities of both *rrn*B P1 and P*veg* decreased during the time course of the experiment; the activity of the former more than of the latter, consistent with the behavior of these promoters as reported in previous studies [10,17].

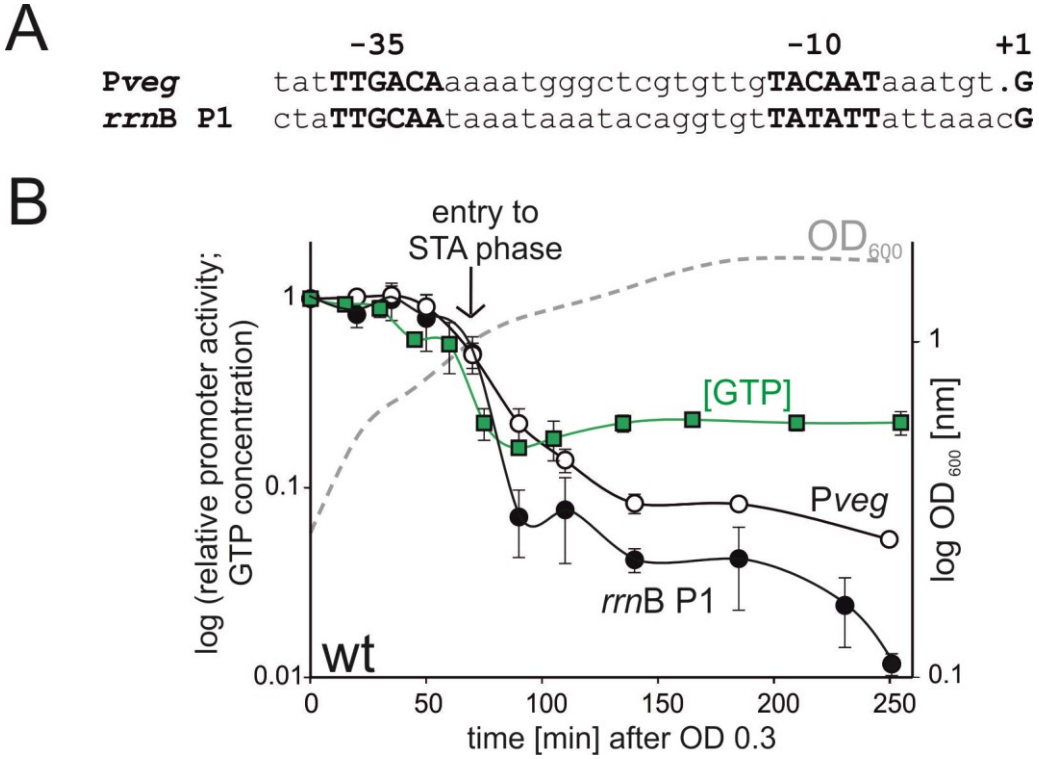

Figure 1. Correlation between GTP concentration and promoter activity after entry into the stationary phase. A) Sequences of P*veg* and *rrn*B P1. (B) Relative promoter activities of *rrn*B P1 (black

circles) and P*veg* promoters (open circles) after entry into stationary phase, relative GTP concentration (green squares), and optical density (dashed grey line). Promoter activities and GTP concentrations were normalized to 1 at time 0. Promoter activities were measured by qPE from *wt B. subtilis* strain: *rrn*B P1 (RLG7554), P*veg* (RLG7555). Promoter activities were calculated from three independent experiments, the error bars show ±SD. The GTP concentrations are from two independent experiments, showing the mean, and a representative bacterial growth curve is shown. The vertical arrow indicates the entry to stationary phase.

Surprisingly and interestingly, the activity *rrn*B P1 decreased even after the relative GTP concentration had been stabilized at a constant level. This strongly suggested that another mechanism, besides rRNA promoter regulation by [GTP], exists in the cell. DNA supercoiling is known to change between growth phases, typically the negative supercoiling from exponential phase becomes more relaxed in stationary phase [42]. Also, we noticed that the activity of P*veg* significantly decreased although the decrease was not as pronounced as that one of the ribosomal promoter. As DNA topology is an important factor for gene expression regulation, we decided to assess the potential of *B. subtilis* rRNA promoters to be regulated by the level of supercoiling.

3.2 Chromosome relaxation inhibits total RNA synthesis

To test whether DNA topology could affect rRNA expression *in vivo*, we used novobiocin. Novobiocin is an antimicrobial compound that binds to the β subunit of gyrase and blocks its function by inhibiting ATP hydrolysis [43–45]. Gyrase relieves tension in DNA caused by transcribing RNAPs or helicases by creating the DNA to be more negatively supercoiled. Hence, inhibition of gyrase causes DNA in the cell to be more relaxed [46].

In this experiment, we first used total RNA as a proxy for rRNA synthesis as in exponential phase most of RNA synthesis comes for rRNA operons (~80% of RNA in cell is rRNA and tRNA [32,47]). We treated early-exponentially growing cells (OD ~ 0.3) with novobiocin or mock-treated them, and measured the rates of total RNA synthesis by following incorporation of radiolabeled ^{3}H-uridine into RNA. As a positive control, where we expected cessation of RNA synthesis, we treated cells with rifampicin, a well-characterized inhibitor of bacterial RNAP.

Figure 2 shows that in the presence of novobiocin the synthesis of total RNA decreased/stopped, similarly as in the presence of rifampicin, suggesting that relaxation of the chromosome affects total RNA synthesis in the cell (Figure 2A).

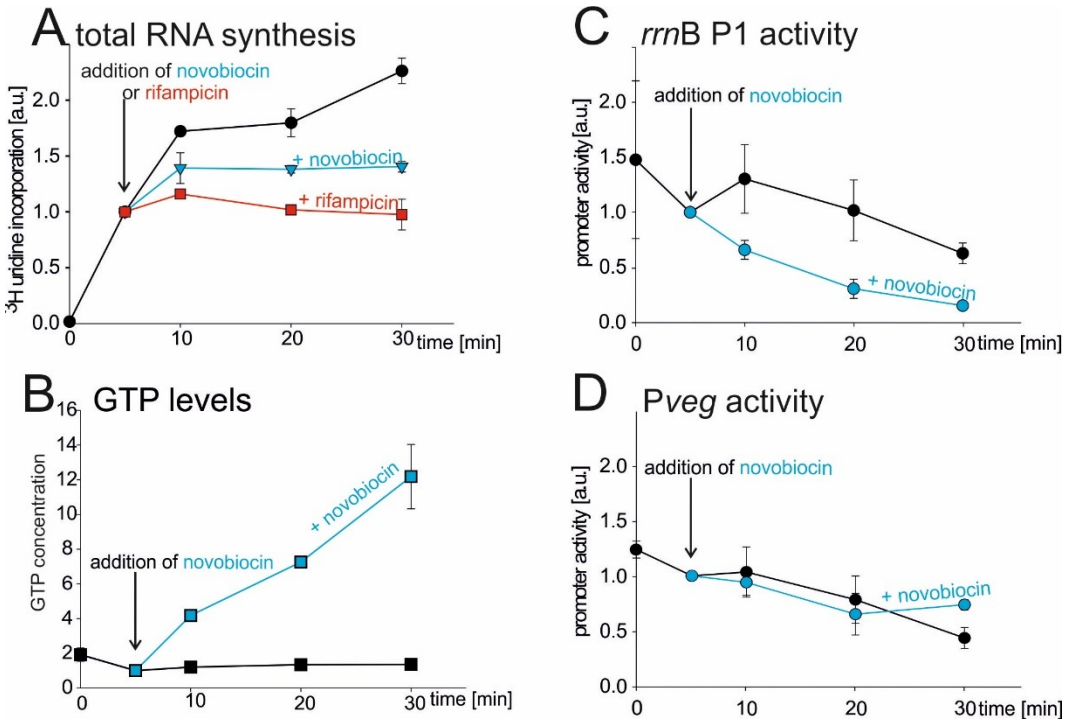

Figure 2. Effect of novobiocin-induced relaxation of chromosome on total RNA synthesis, GTP level and selected promoter activities. (A-D) Cells were grown to early exponential phase (OD_{600} ~ 0.3), and at time 5 min they were treated with novobiocin (5 μg/ml). (A) Total RNA synthesis after novobiocin treatment. After ^{3}H uridine had been added, the culture was divided into three flasks. At time 5 min the cells were treated with novobiocin or with rifampicin (2 μg/ml) as a control, or left untreated. The amount radiolabeled RNA at 5 min was set as 1. Black circles, mock-treated; blue triangles, treated with novobiocin; red squares, treated with rifampicin. The values are averages of three experiments with error bars (±SD). **(B)** GTP concentration after novobiocin treatment. Cells were grown in the presence of [^{32}P] H_3PO_4 and treated with novobiocin. Levels of GTP were determined by the TLC chromatography. GTP level at 5 min was set as 1. Results are averages from two measurements. The error bars show the range. **(C-D)** The activity of *rrn*B P1 and P*veg* promoters after novobiocin treatment. Cells were grown and at 5 min treated with novobiocin or not. RNA was extracted and determination of promoter activity was done by RT-qPCR. Promoter activities were set as 1 at time 0. The experiment was performed three times. The error bars show ±SD.

3.3 Novobiocin-induced relaxation of DNA affects the activity of rrnB P1 in vivo

Next, by RT-qPCR we monitored the response of *rrn*B P1 and P*veg* to novobiocin treatment, using the same conditions as in the previous experiment. We grew cells carrying the appropriate fusions [*rrn*B P1-lacZ (RLG7554) and P*veg*-lacZ (RLG7555)] to early-exponential phase (OD_{600} ~ 0.3) and either treated them with novobiocin or mock-treated them. In the case of *rrn*B P1, the promoter activity decreased after novobiocin treatment (as opposed to mock treatment), but in the case of P*veg*, the promoter activity displayed the same moderate decline regardless of the novobiocin treatment, suggesting that *rrnB* P1 is more sensitive to changes in DNA topology (Figure 2CD).

We also measured the GTP levels in novobiocin treated cells. We observed that novobiocin-induced relaxation resulted in an increase in the GTP level in cell (Figure 2C). The levels of ATP remained almost unchanged (Figure S2). Thus, the activity of *rrn*B P1 and the level of GTP became uncoupled.

3.4 Changes in DNA topology affect the affinity of RNAP for iNTP in vitro

We had speculated that the *in vivo* decrease in the activity of *rrn*B P1 during stationary phase and in response to novobiocin treatment could be due to altered affinity of RNAP for iGTP at this promoter (induced by changes in supercoiling levels): the GTP level does not change but the open promoter

becomes less stable, requiring more iGTP for maximal transcription. To address this hypothesis experimentally, we performed *in vitro* transcriptions with defined components. We used promoter core variants of *rrn*B P1 and P*veg* cloned in the p770 plasmid [17] (for details see Table 1 in Material and Methods section). The DNA templates were used in two different topological forms – in the negatively supercoiled plasmid form (SC), and in the relaxed form (LIN), using the same DNA construct but linearized with the *PstI* restriction enzyme (Figure S3).

We performed multiple round transcriptions *in vitro* with increasing [GTP] (Figure 3). The GTP concentration required for half-maximal transcription (K_{GTP}) was used as a measure of the affinity of RNAP for iGTP at the promoter. A characteristic of rRNA promoters is their requirement for relatively high levels of iGTP for maximal transcription (due to unstable open complexes), reflected in high values of K_{GTP} *in vitro*. P*veg*, to the contrary, has a low value of K_{GTP}.

Experiments with SC templates confirmed previously published results [48], the K_{GTP} for *rrn*B P1 was 275 ± 22 μM, and for P*veg* 35 ± 9 μM. Experiments with the LIN templates then revealed that K_{GTP} values for both promoters increased (*rrn*B P1 = 411 ± 35 μM, P*veg* = 510 ± 77 μM). In the case of *rrn*B P1 the K_{GTP} increased from SC to LIN ~1.5x, and in the case of P*veg* K_{GTP} ~14x. Surprisingly, the K_{GTP} value of LIN P*veg* was even higher than the value for *rrn*B P1 (Figure 2B). Furthermore, the experiments showed that the strength (the maximal level of transcription) of the *rrn*B P1 promoter dramatically decreased on the LIN template whereas in the case of P*veg* the maximal level of transcription was comparable for both types of the template.

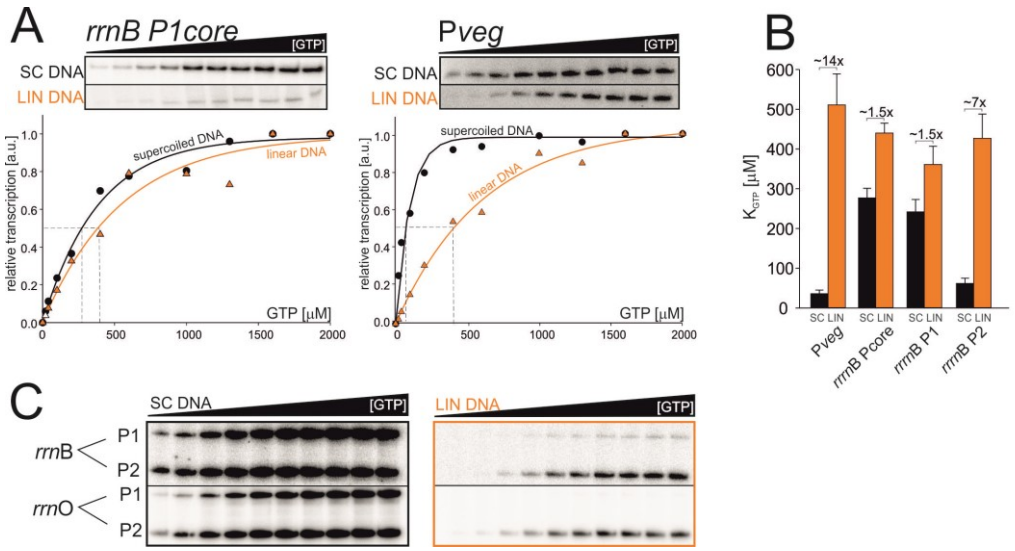

Figure 3. The affinity of RNAP for iNTP *in vitro* changes on different DNA templates. (A) Multiple-round transcriptions as a function of GTP concentration: representative primary data and their graphical comparison for *rrn*B P1core and P*veg*. The maximum signal was set as 1. (B) Graphical comparison of K_{GTP} values for SC and LIN DNA templates. The values are calculated from at least four experiments, the error bars show ±SD. (C) Low affinity for LIN *rrn*B P1 is conserved in all variants of *rrn* promoter variants. A representative primary data are shown.

As the preceding experiments were done with the core version of the *rrn*B P1 promoter, we also decided to use an extended version of the promoter region to assess whether the surrounding sequence has significant effects. Therefore, we used a DNA fragment containing both *rrn*B P1 and *rrn*B P2 promoters in their native tandem arrangement. Each of them contained by their respective native -60 to -40 regions encompassing the UP elements. UP elements are A/T-rich sequences that enhance promoter activity by binding the C-terminal domains of α-subunits of RNAP [49–51]. Although their stimulatory effect on rRNA promoters in *B. subtilis* [17] is less pronounced than *e. g.* in *E. coli* (~30x), it is still significant. Experiments with these promoter versions yielded virtually the same results as with the core version (Figure 3C). The K_{GTP} for *rrn*B P1 (from the tandem promoter

fragment) was 242 ± 31 μM for SC and 361 ± 46 μM for LIN. K_{GTP} for *rrn*B P2 was 62 ± 13 μM for SC and 427 ± 61 μM for LIN (see Table S1 and Figure S4AB). Similar results were obtained also with *rrn*O P1 and *rrn*O P2 promoters (Figure S4CD).

Hence, we concluded that for transcription from LIN templates higher concentrations of GTP are needed, regardless of the promoter. The increased K_{GTP} of P*veg* suggested that this change in RNAP affinity for the substrate iNTP might be responsible, at least in part, for the decrease in its activity during the transition from exponential to stationary phase. However, the moderate increase in K_{GTP} of *rrn*B P1 suggested that other factor(s) must be involved in the decrease of this promoter's activity *in vivo*. A likely candidate factor was the affinity of RNAP for promoter DNA, i. e. formation of the closed complex or/and the intracellular level of RNAP.

3.5 rRNA and Pveg promoter affinities for RNAP change with DNA relaxation

We tested the relative affinity of RNAP for promoter DNA by performing *in vitro* transcriptions as a function of increasing promoter DNA concentration. We used the tandem *rrn*B P1+P2 DNA fragment and P*veg*. The GTP concentration was set to 1 mM to ensure high efficiency of open complex formation for the tested promoters. Affinity for RNAP of both rRNA promoters was unchanged or slightly decreased on relaxed templates - higher levels of promoter DNA were required to reach a maximum activity(Figure 4 and Figure S5).

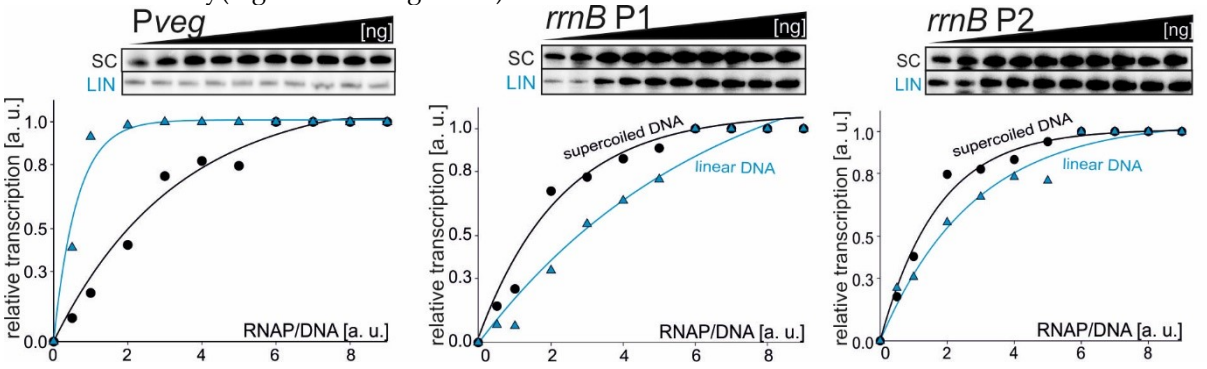

Figure 4. The affinity of RNAP for promoter DNA. Multiple-round transcriptions were carried as a function of the increasing DNA/RNAP ratio. The tested promoters were P*veg* and *rrn*B P1 and P2. Primary data are shown above the graphs. The maximum signal in the plateau phase was set as 1. SC – supercoiled and LIN – linear DNA templates. The experiments were conducted at least four times with the similar results. Representative primary data are shown.

The opposite trend was observed with P*veg*: a relatively low level of the relaxed promoter DNA was able to saturate RNAP compared to the supercoiled template. This behaviour could then explain why the activity of P*veg* decreased less than the activity of *rrnB* P1 during the experiment shown in Figure 1. Importantly, it was previously reported that the levels of RNAP subunits decrease from exponential to stationary phase [52,53] and we also observed this trend (Figure 5).

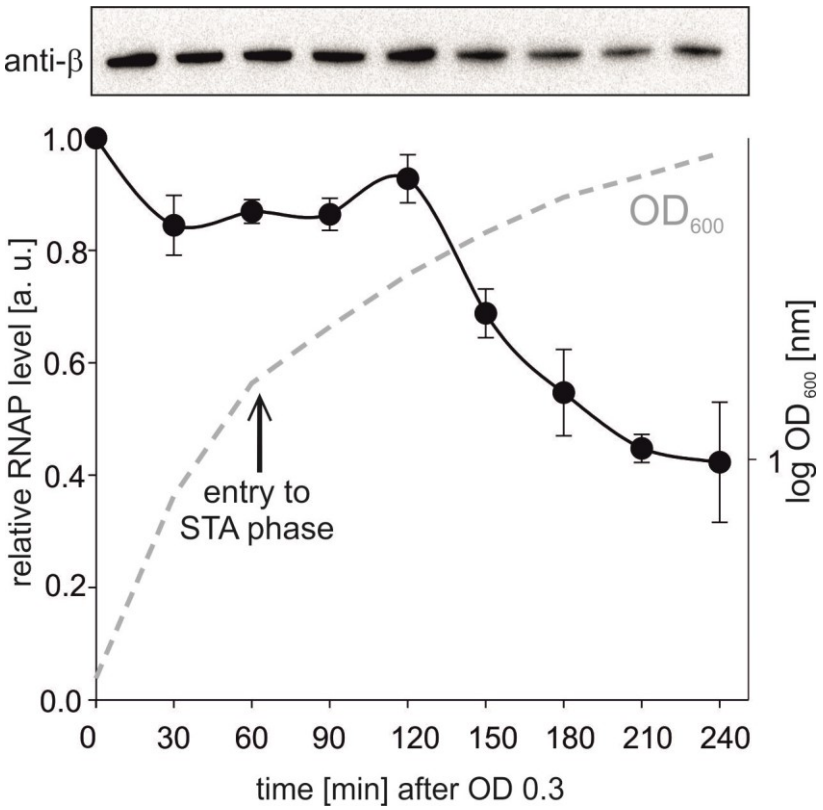

Figure 5. RNAP levels during bacterial growth.
Amounts of RNAP were detected by Western blotting from 5 μg of total protein per lane. Representative primary data are shown above the graph. The RNAP level from time point 1 was set as a 1. STA – stationary phase (indicated with arrow). The experiment was conducted in two independents replicas. The points are averages, the error bars show the range. The dashed line shows a representative bacterial growth.

3.6 The effect of supercoiling on transcription with alternative σ factors

To extend the study, we tested the effect of supercoiling on transcription from promoters dependent on alternative sigma factors: σ^B, σ^D, σ^E, σ^F and σ^H. σ^B is a general stress response sigma factor [54,55], σ^D transcribes genes linked with the cell motility and flagella formation [56]. σ^E and σ^F are sigma factors of early sporulation [57,58]. σ^H is responsible for transcription of early stationary genes [59].

We tested also σ^N (zpdN) is present only in the *B. subtilis* NCIB 3610 strain, which possesses a large, low-copy-number plasmid pBS32, which was lost during domestication of the commonly used laboratory strains [23,24,60]. pBS32 carries genes responsible for cell death after mitomycin C (MMC) treatment, and this effect is dependent on σ^N. MMC is an antitumor antibiotic that induces DNA strand scission, by DNA alkylation leading to crosslinking [61–63]. This DNA damage could lead to forming of linear DNA fragments.

Sequences of respective promoters are listed in Table S2. We performed transcriptions *in vitro* on SC and LIN DNA templates and in all but one cases it was the SC DNA that was the better template for transcription, similarly to what we observed with σ^A (Figure 6).

The exception was σ^N, which displayed about the same or higher activity on LIN DNA than on SC DNA, depending on the promoter (Figure 6B). To show that this effect was not due to some unknown properties of the plasmid DNA bearing these promoters, we also tested a longer *sigN* promoter construct (sigN P2+P3). This construct contains σ^A-dependent *sig*N P2 and σ^N-dependent *sig*N P3 promoters [24] and allowed us to test the effect of SC vs LIN topology for two sigmas with the same template. The results are shown in Figure 6C: σ^A-dependent P2 is more active on SC DNA whereas σ^N-dependent P3 prefers LIN DNA for efficient transcription.

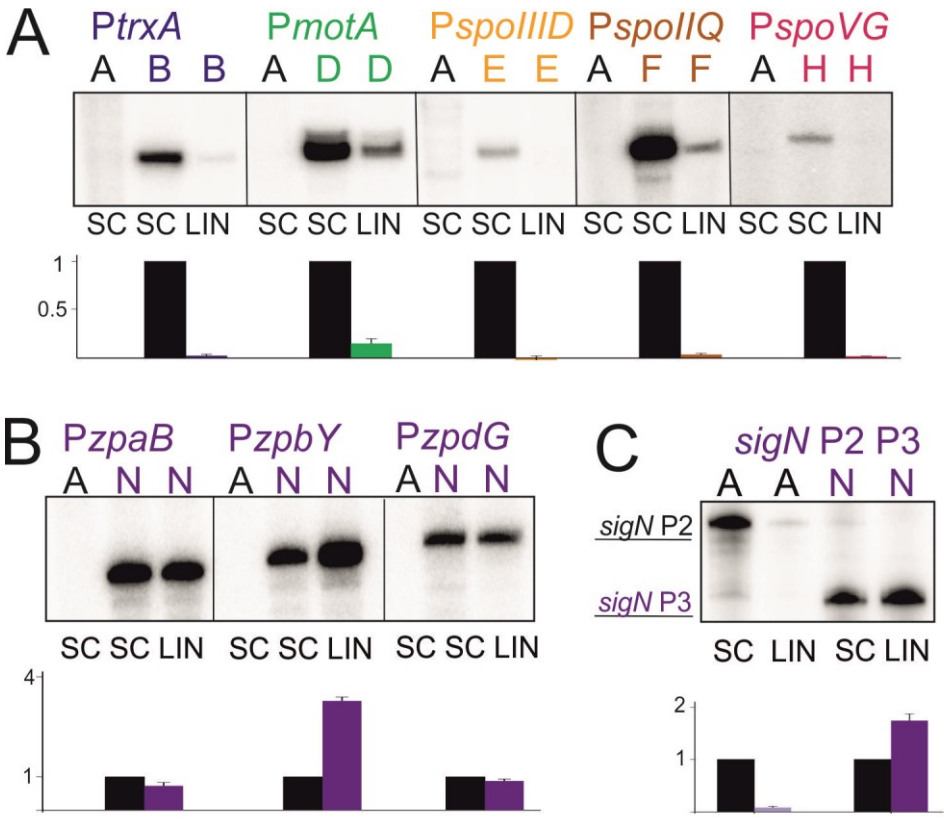

Figure 6. Transcription *in vitro* with alternative σ factors on different DNA templates. Representative primary data are shown (radioactively labelled transcripts resolved by polyacrylamide electrophoresis). SC stands for supercoiled promoter DNA, LIN for linear DNA. Letters above the gels indicate the sigma factor used – A for σ^A, B for σ^B *etc*. For each promoter three independent reactions were performed. The graphs show averages ±SD. The reactions with σ^A on all promoter fragments were used to show that the observed transcription was due to the addition of the specific Sigma factors and not due to (theoretical) contamination of the core with σ^A. A) Transcription *in vitro* on selected σ^B, σ^D, σ^E, σ^F and σ^H -dependent promoters. B) Transcription *in vitro* on σ^N-dependent promoters. C) Transcription *in vitro* using longer construct, *sigN* P2+P3. P2 is σ^A-dependent, P3 is σ^N-dependent.

3.7 The effect of DNA topology on termination of transcription HelD-dependent transcriptional cycling

Finally, we asked whether DNA topology could affect also other aspects of transcription besides initiation. So we decided to include in our studies the effects of HelD. HelD is a horseshoe-shaped helicase-like protein of 774 amino acids, a binding partner of RNAP, originally identified in *B. subtilis* ([26,27,31,64]and recently also in *Mycobacterium smegmatis* [65]. *B. subtilis* HelD binds to the RNAP core and stimulates transcriptional cycling by removing stalled transcriptional complexes from DNA and RNAP from nucleic acids post-termination. Its activity is stimulated by ATP or GTP hydrolysis [25,65].

We used multiple round transcriptions driven from the *rrn*B P1 and *rrn*B P2 promoters as in the previous experiments. The experiments were conducted in the absence/presence of HelD on supercoiled/relaxed templates. Figure 7 shows that on SC templates, similarly to previously published results [25], HelD stimulated transcription. On LIN templates, the stimulation was absent and even an inhibitory effect was detected. A mutant form of HelD (lacking the N-terminal domain), which had been previously shown to bind to RNAP but not provide the stimulatory effect [31], did not affect the reactions on either template. The same effect was observed with transcription from *rrn*O P1 and P2 (Figure S6). We concluded that the effect of HelD was strongly dependent on DNA topology.

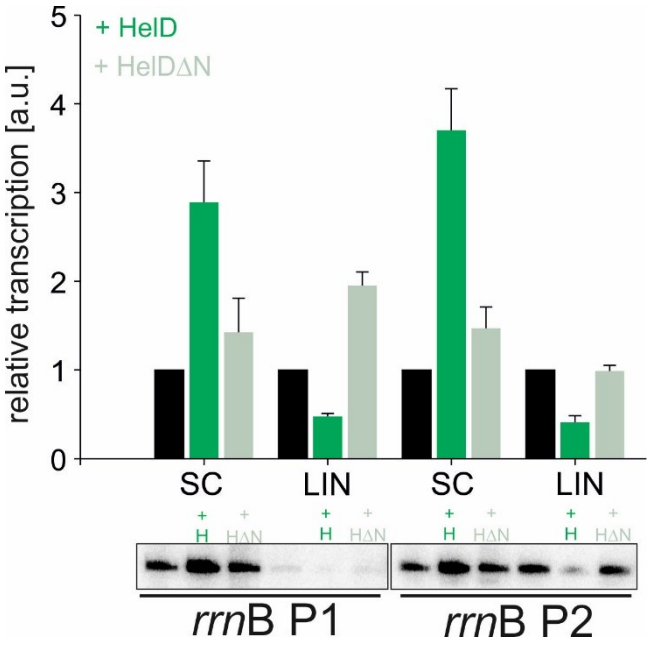

Figure 7. Effect of HelD on transcription *in vitro* from rRNA promoters. SC – supercoiled DNA, LIN – linear DNA. Transcription without HelD added was set as 1 (black bars). HelD was added in ratio 1:4 to RNAP (dark green; H), and HelDΔN also in 1:4 ratio (light green; HΔN). Graph shows mean from at least three independent experiments, with the corresponding SD. A representative primary data are shown below.

4. Discussion

In this study, we have identified the supercoiling level of DNA as a factor affecting the ability of *Bacillus subtilis* RNAP to transcribe from σ^A-dependent rRNA promoters as well as from selected promoters depending on alternative sigma factors. Lastly, supercoiling also influences the effects of HelD on RNAP.

4.1. rRNA promoters and Pveg

The more negatively supercoiled DNA in exponential phase contributes to the high activity of *B. subtilis* rRNA promoters. As this negative supercoiling becomes more relaxed when the cell transitions into stationary phase, this decreases the affinity of RNAP for rRNA promoters and GTP, and is affected by the concomitant decrease in the RNAP concentration. The decrease in the available RNAP pool is further exacerbated by association of the RNAP:σ^A holoenzyme with 6S-1 RNA that sequesters it in an inactive form in stationary phase [66]. The combined effect results in the shut-off of rRNA synthesis. This is similar but not identical to *E. coli* rRNA promoters where it is the decreased stability of the open complex that was identified as the main kinetic intermediate affected by supercoiling [67]. We note that supercoiling was also reported to be involved in rRNA expression in yeast although the mechanistic aspects of this regulation are less understood [68]. Interestingly, during novobiocin treatment the GTP level increases in *B. subtilis* and the changes in DNA topology override its stimulatory effect so that the net result is a decrease in the activity of *rrn*B P1. This is the first observation of a situation where the GTP level and rRNA promoter activity do not correlate in *B. subtilis*.

The activity of the control P*veg* promoter also decreases from exponential to stationary phase but the decrease is not as pronounced as in the case of *rrn*B P1. The decrease in the activity of P*veg* can be attributed, at least in part, to its increased requirement for the concentration of the iNTP when DNA supercoiling relaxes. Nevertheless, the affinity of P*veg* for RNAP seems to increase with DNA relaxation and this likely partially counteracts the negative effect on open complex formation.

4.2. Transcription with alternative σ factors, HelD

Transcription of promoters dependent on alternative σ factors revealed that linear templates are poorer substrates for the majority of them (σ^B, σ^D, σ^E, σ^F). This trend was reported also for RNAP:σ^H transcribing from the *spoIIA* promoter [69]. The exception is σ^N, where transcription (SC *vs* LIN) is either relatively unaffected or even increased on linear templates. This is likely physiologically important as mitomycin, which induces σ^N expression [23], causes also DNA relaxation and σ^N may have evolved to be most active under such conditions. The proficiency of RNAP:σ^N on linear templates then may stem from the relatively short spacers of σ^N dependent promoters (15 bp compared to 17 bp for σ^A, [70], analogously to σ^{70} and σ^S of *E. coli* where the different σ activities were proposed to be due to preferences for differently DNA supercoiled templates [71–73].

Supercoiling can affect not only transcription initiation but also other steps of transcription [74,75]. This is evident also for HelD where its stimulatory effect on transcription is lost on the linear rRNA template. This might explain the apparent absence of a differential effect for transcription from linear templates with/without Rho-independent terminators [25].

5. Conclusions

To conclude, our findings extend the current model of rRNA promoter regulation in *B. subtilis*, reveal the effect of supercoiling on transcription with alternative sigma factors, and the helicase-like protein, HelD.

Supplementary Materials: The following are available online at www.mdpi.com/xxx/s1, **Figure S1**: GTP and (p)ppGpp levels after entry into the stationary phase. **Figure S2:** Effect of novobiocin-induced relaxation of chromosome on ATP levels. **Figure S3:** SC and LIN promoter DNA on agarose gel. **Figure S4**: The affinity of RNAP for iNTP in vitro changes on different DNA templates. **Figure S5**: Graphical representation of RNAP affinity for DNA. **Figure S6**. Effect of HelD on transcription *in vitro* from rRNA promoters. **Table S1**: The K_{GTP} values for the promoters tested in the transcriptions *in vitro.* **Table S2**: Alternative σ factor-dependent promoters used in the study.

Author Contributions: LK supervised the project. LK and PS conceptualized the experiments. LK performed the qPE and TLC. PS performed novobiocin studies (RT-PCR, TLC), purified proteins and performed transcriptions *in vitro.* OR, MB and HŠ cloned and purified alternative σ factors and their respective promoters. MK cloned, purified and performed experiments with σ^N and its respective promoters. PS and LK wrote the manuscript. All authors have read and agreed to the published version of the manuscript.

Funding: This work was supported by 20-12109S to LK from the Czech Science Foundation.

Conflicts of Interest: The authors declare no conflict of interest. The funders had no role in the design of the study; in the collection, analyses, or interpretation of data; in the writing of the manuscript, or in the decision to publish the results.

References

1. Gourse, R.L.; Gaal, T.; Bartlett, M.S.; Appleman, J.A.; Ross, W. rRNA TRANSCRIPTION AND GROWTH RATE – DEPENDENT REGULATION OF RIBOSOME SYNTHESIS IN ESCHERICHIA COLI. **1996**.
2. Lee, J.; Borukhov, S. Bacterial RNA Polymerase-DNA Interaction-The Driving Force of Gene Expression and the Target for Drug Action. *Front. Mol. Biosci.* **2016**, *3*, 73, doi:10.3389/fmolb.2016.00073.
3. Helmann, J.D. Where to begin? Sigma factors and the selectivity of transcription initiation in bacteria. *Mol. Microbiol.* **2019**, *112*, 335–347, doi:10.1111/mmi.14309.
4. Gross, C.A.; Chan, C.; Dombroski, A.; Gruber, T.; Sharp, M.; Tupy, J.; Young, B. The functional and regulatory roles of sigma factors in transcription. In Proceedings of the Cold Spring Harbor Symposia on Quantitative Biology; 1998; Vol. 63, pp. 141–155.
5. Paget, M.S. Bacterial sigma factors and anti-sigma factors: Structure, function and distribution. *Biomolecules* **2015**, *5*, 1245–1265, doi:10.3390/biom5031245.
6. Feklistov, A.; Darst, S.A. Structural basis for promoter -10 element recognition by the bacterial RNA polymerase σ subunit. *Cell* **2011**, *147*, 1257–1269, doi:10.1016/j.cell.2011.10.041.

7. Mustaev, A.; Roberts, J.; Gottesman, M. Transcription elongation. *Transcription* **2017**, *8*, 150–161, doi:10.1080/21541264.2017.1289294.
8. Schneider, D.A.; Murray, H.D.; Gourse, R.L. Measuring Control of Transcription Initiation by Changing Concentrations of Nucleotides and Their Derivatives. *Methods Enzymol.* **2003**, *370*, 606–617, doi:10.1016/S0076-6879(03)70051-2.
9. Turnbough, C.L. Regulation of bacterial gene expression by the NTP substrates of transcription initiation. *Mol. Microbiol.* **2008**, *69*, 10–14, doi:10.1111/j.1365-2958.2008.06272.x.
10. Murray, H.D.; Schneider, D.A.; Gourse, R.L. Control of rRNA expression by small molecules is dynamic and nonredundant. *Mol. Cell* **2003**, *12*, 125–134, doi:10.1016/S1097-2765(03)00266-1.
11. Zechiedrich, E.L.; Khodursky, A.B.; Bachellier, S.; Schneider, R.; Chen, D.; Lilley, D.M.J.; Cozzarelli, N.R. Roles of topoisomerases in maintaining steady-state DNA supercoiling in Escherichia coli. *J. Biol. Chem.* **2000**, *275*, 8103–8113, doi:10.1074/jbc.275.11.8103.
12. Higgins, C.F.; Dorman, C.J.; Stirling, D.A.; Waddell, L.; Booth, I.R.; May, G.; Bremer, E. A physiological role for DNA supercoiling in the osmotic regulation of gene expression in S. typhimurium and E. coli. *Cell* **1988**, *52*, 569–584, doi:10.1016/0092-8674(88)90470-9.
13. Richardson, S.M.; Higgins, C.F.; Lilley, D.M. The genetic control of DNA supercoiling in Salmonella typhimurium. *EMBO J.* **1984**, *3*, 1745–1752, doi:10.1002/j.1460-2075.1984.tb02041.x.
14. McClure, W.R. Mechanism and control of transcription initiation in prokaryotes. *Annu. Rev. Biochem.* **1985**, *VOL. 54*, 171–204, doi:10.1146/annurev.bi.54.070185.001131.
15. Schnetz, K.; Wang, J.C. Silencing of the Escherichia Coli bgl Promoter: Effects of Template Supercoiling and Cell Extracts on Promoter Activity in vitro. *Nucleic Acids Res.* **1996**, *24*, 2422–2428, doi:10.1093/nar/24.12.2422.
16. Sioud, M.; Boudabous, A.; Cekaite, L. Transcriptional responses of Bacillus subtillis and thuringiensis to antibiotics and anti-tumour drugs. *Int. J. Mol. Med.* **2009**, *23*, 33–39, doi:10.3892/ijmm_00000098.
17. Krásný, L.; Gourse, R.L. An alternative strategy for bacterial ribosome synthesis: Bacillus subtilis rRNA transcription regulation. *EMBO J.* **2004**, *23*, 4473–4483, doi:10.1038/sj.emboj.7600423.
18. Bittner, A.N.; Kriel, A.; Wang, J.D. Lowering GTP Level Increases Survival of Amino Acid Starvation but Slows Growth Rate for Bacillus subtilis Cells Lacking (p)ppGpp. *J. Bacteriol.* **2014**, *196*, 2067–2076, doi:10.1128/JB.01471-14.
19. Kriel, A.; Bittner, A.N.; Kim, S.H.; Liu, K.; Tehranchi, A.K.; Zou, W.Y.; Rendon, S.; Chen, R.; Tu, B.P.; Wang, J.D. Direct regulation of GTP homeostasis by (p)ppGpp: A critical component of viability and stress resistance. *Mol. Cell* **2012**, *48*, 231–241, doi:10.1016/j.molcel.2012.08.009.
20. Henkin, T.M.; Yanofsky, C. Regulation by transcription attenuation in bacteria: How RNA provides instructions for transcription termination/antitermination decisions. *BioEssays* **2002**, *24*, 700–707, doi:10.1002/bies.10125.
21. Krásný, L.; Tišerová, H.; Jonák, J.; Rejman, D.; Šanderová, H. The identity of the transcription +1 position is crucial for changes in gene expression in response to amino acid starvation in Bacillus subtilis. *Mol. Microbiol.* **2008**, *69*, 42–54, doi:10.1111/j.1365-2958.2008.06256.x.
22. Natori, Y.; Tagami, K.; Murakami, K.; Yoshida, S.; Tanigawa, O.; Moh, Y.; Masuda, K.; Wada, T.; Suzuki, S.; Nanamiya, H.; et al. Transcription activity of individual rrn operons in Bacillus subtilis mutants deficient in (p)ppGpp synthetase genes, relA, yjbM, and ywaC. *J. Bacteriol.* **2009**, *191*, 4555–4561, doi:10.1128/JB.00263-09.
23. Myagmarjav, B.-E.; Konkol, M.A.; Ramsey, J.; Mukhopadhyay, S.; Kearns, D.B. ZpdN, a Plasmid-

Encoded Sigma Factor Homolog, Induces pBS32-Dependent Cell Death in Bacillus subtilis. *J. Bacteriol.* **2016**, *198*, 2975–2984, doi:10.1128/JB.00213-16.

24. Burton, A.T.; DeLoughery, A.; Li, G.W.; Kearns, D.B. Transcriptional regulation and mechanism of sigN (ZpdN), a pBS32-encoded sigma factor in bacillus subtilis. *MBio* **2019**, *10*, e01899-19, doi:10.1128/mBio.01899-19.
25. Wiedermannová, J.; Sudzinová, P.; Kovaľ, T.; Rabatinová, A.; Šanderová, H.; Ramaniuk, O.; Rittich, Š.; Dohnálek, J.; Fu, Z.; Halada, P.; et al. Characterization of HelD, an interacting partner of RNA polymerase from Bacillus subtilis. *Nucleic Acids Res.* **2014**, *42*, 5151–5163, doi:10.1093/nar/gku113.
26. Newing, T.; Oakley, A.; Miller, M.; Dawson, C.; Brown, S.; Bouwer, J.; Tolun, G.; Lewis, P. Molecular Basis for RNA Polymerase-Dependent Transcription Complex Recycling By The Helicase-like Motor Protein HelD. **2020**, doi:10.21203/rs.3.rs-40738/v1.
27. Wahl, M.; Pei, H.-H.; Hilal, T.; Chen, Z.; Huang, Y.-H.; Gao, Y.; Said, N.; Loll, B.; Rappsilber, J.; Belogurov, G.; et al. An energy charge sensor for balancing RNA polymerase recycling and hibernation. **2020**, doi:10.21203/rs.3.rs-40617/v1.
28. Qi, Y.; Hulett, F.M. PhoP~P and RNA polymerase sigma(A) holoenzyme are sufficient for transcription of Pho regulon promoters in Bacillus subtilis: PhoP~P activator sites within the coding region stimulate transcription in vitro. *Mol. Microbiol.* **1998**, *28*, 1187–1197, doi:10.1046/j.1365-2958.1998.00882.x.
29. Chang, B.-Y.; Doi, R.H. Overproduction, Purification, and Characterization of Bacillus subtilis RNA Polymerase SigA Factor. *J. Bacteriol.* **1990**, *172*, 3257–3263.
30. Chen, Y.-F.; Helmann, J.D. *The Bacillus subtilis Flagellar Regulatory Protein SigmaD: Overproduction, Domain Analysis and DNA-binding Properties*; 1995; Vol. 249;.
31. Kovaľ, T.; Sudzinová, P.; Perháčová, T.; Trundová, M.; Skálová, T.; Fejfarová, K.; Šanderová, H.; Krásný, L.; Dušková, J.; Dohnálek, J. Domain structure of HelD, an interaction partner of Bacillus subtilis RNA polymerase. *FEBS Lett.* **2019**, *593*, 996–1005, doi:10.1002/1873-3468.13385.
32. Paul, B.J.; Ross, W.; Gaal, T.; Gourse, R.L. rRNA Transcription in Escherichia coli. *Annu. Rev. Genet.* **2004**, *38*, 749–770, doi:10.1146/annurev.genet.38.072902.091347.
33. Panova, N.; Zborníková, E.; Šimák, O.; Pohl, R.; Kolář, M.; Bogdanová, K.; Večeřová, R.; Seydlová, G.; Fišer, R.; Hadravová, R.; et al. Insights into the Mechanism of Action of Bactericidal Lipophosphonoxins. *PLoS One* **2015**, *10*, e0145918, doi:10.1371/journal.pone.0145918.
34. Imamura, D.; Zhou, R.; Feig, M.; Kroos, L. Evidence that the Bacillus subtilis SpoIIGA protein is a novel type of signal-transducing aspartic protease. *J. Biol. Chem.* **2008**, *283*, 15287–15299, doi:10.1074/jbc.M708962200.
35. LaBell, T.L.; Trempy, J.E.; Haldenwang, W.G. Sporulation-specific σ factor σ29 of Bacillus subtilis is synthesized from a precursors protein, P31. *Proc. Natl. Acad. Sci. U. S. A.* **1987**, *84*, 1784–1788, doi:10.1073/pnas.84.7.1784.
36. Ross, W.; Thompson, J.F.; Newlands, J.T.; Gourse, R.L. E. coli Fis protein activates ribosomal RNA transcription in vitro and in vivo. *EMBO J.* **1990**, *9*, 3733–3742, doi:10.1002/j.1460-2075.1990.tb07586.x.
37. Deneer, H.G.; Spiegelman, G.B. Bacillus subtilis rRNA promoters are growth rate regulated in Escherichia coli. *J. Bacteriol.* **1987**, *169*, 995–1002, doi:10.1128/jb.169.3.995-1002.1987.
38. Samarrai, W.; Liu, D.X.; White, A.M.; Studamire, B.; Edelstein, J.; Srivastava, A.; Widom, R.L.; Rudner, R. Differential responses of Bacillus subtilis rRNA promoters to nutritional stress. *J. Bacteriol.* **2011**, *193*, 723–733, doi:10.1128/JB.00708-10.
39. Wellington, S.R.; Spiegelman, G.B. The kinetics of formation of complexes between Escherichia coli RNA

polymerase and the rrnB P1 and P2 promoters of Bacillus subtilis. Effects of guanosine tetraphosphate on select steps of transcription initiation. *J. Biol. Chem.* **1993**, *268*, 7205–7214.

40. Fukushima, T.; Ishikawa, S.; Yamamoto, H.; Ogasawara, N.; Sekiguchi, J. Transcriptional, functional and cytochemical analyses of the veg gene in Bacillus subtilis. *J. Biochem.* **2003**, *133*, 475–483, doi:10.1093/jb/mvg062.
41. Lei, Y.; Oshima, T.; Ogasawara, N.; Ishikawa, S. Functional Analysis of the Protein Veg, Which Stimulates Biofilm Formation in Bacillus subtilis. *J Bacteriol* **2013**, *195*, 1697–1705, doi:10.1128/JB.02201-12.
42. Dillon, S.C.; Dorman, C.J. Bacterial nucleoid-associated proteins, nucleoid structure and gene expression. *Nat. Rev. Microbiol.* **2010**, *8*, 185–95, doi:10.1038/nrmicro2261.
43. Alice, A.F.; Sanchez-Rivas, C. DNA supercoiling and osmoresistance in Bacillus subtilis 168. *Curr. Microbiol.* **1997**, *35*, 309–315, doi:10.1007/s002849900260.
44. Lewis, R.J.; Singh, O.M.P.; Smith, C. V; Skarzynski, T.; Maxwell, A.; Wonacott, A.J.; Wigley, D.B. The Nature of Inhibition of DNA Gyrase by the Coumarins and the Cyclothialidines Revealed by X-Ray Crystallography. *Embo J.* **1996**, *15*, 1412–1420, doi:10.1107/S0907444904011679.
45. Sugino, A.; Higginst, N.P.; Brownt, P. 0; Peeblesf, C.L.; Cozzarellitf, N.R. Energy coupling in DNA gyrase and the mechanism of action of novobiocin. *Biochemistry* **1978**, *75*, 4838–4842.
46. Gellert, M.; O'Dea, M.H.; Itoh, T.; Tomizawa, J.I. Novobiocin and coumermycin inhibit DNA supercoiling catalyzed by DNA gyrase. *Proc. Natl. Acad. Sci. U. S. A.* **1976**, *73*, 4474–4478, doi:10.1073/pnas.73.12.4474.
47. Dennis, P.P.; Bremer, H. Modulation of Chemical Composition and Other Parameters of the Cell at Different Exponential Growth Rates. *EcoSal Plus* **2008**, *3*, 1553– 1569, doi:10.1128/ecosal.5.2.3.
48. Sojka, L.; Kouba, T.; Barvík, I.; Šanderová, H.; Maderová, Z.; Jonák, J.; Krásný, L. Rapid changes in gene expression: DNA determinants of promoter regulation by the concentration of the transcription initiating NTP in Bacillus subtilis. *Nucleic Acids Res.* **2011**, *39*, 4598–611, doi:10.1093/nar/gkr032.
49. Estrem, S.T.; Gaal, T.; Ross, W.; Gourse, R.L. Identification of an UP element consensus sequence for bacterial promoters. *Proc. Natl. Acad. Sci. USA* **1998**, *95*, 9761–9766.
50. Meng, W.; Belyaeva, T.; Savery, N.J.; Busby, S.J.W.; Ross, W.E.; Gaal, T.; Gourse, R.L.; Thomas, M.S. UP element-dependent transcription at the Escherichia coli rrnB P1 promoter: Positional requirements and role of the RNA polymerase α subunit linker. *Nucleic Acids Res.* **2001**, *29*, 4166–4178, doi:10.1093/nar/29.20.4166.
51. Rao, L.; Ross, W.; Appleman, J.A.; Gaal, T.; Leirmo, S.; Schlax, J.P.; Record, M Thomas, J.; Gourse, R.L. Factor Independent Activation of rrnB P1: An "Extended" Promoter with an Upstream Element that Dramatically Increases Promoter Strength. *J. Mol. Biol.* **1994**, *235*, 1421–1435.
52. Klumpp, S.; Hwa, T. Growth-rate-dependent partitioning of RNA polymerases in bacteria. *Proc. Natl. Acad. Sci. U. S. A.* **2008**, *105*, 20245–20250, doi:10.1073/pnas.0804953105.
53. Liang, S.T.; Bipatnath, M.; Xu, Y.C.; Chen, S.L.; Dennis, P.; Ehrenberg, M.; Bremer, H. Activities of constitutive promoters in Escherichia coli. *J. Mol. Biol.* **1999**, *292*, 19–37, doi:10.1006/jmbi.1999.3056.
54. Haldenwang, W.G.; Losick, R. Novel RNA polymerase σ factor from Bacillus subtilis. *Proc. Natl. Acad. Sci. U. S. A.* **1980**, *77*, 7000–7004, doi:10.1073/pnas.77.12.7000.
55. Hecker, M.; Völker, U. General stress response of Bacillus subtilis and other bacteria. *Adv. Microb. Physiol.* **2001**, *44*, 35–91, doi:10.1016/S0065-2911(01)44011-2.
56. Jaehning, J.A.; Wiggs, J.L.; Chamberlin, M.J. Altered promoter selection by a novel form of Bacillus

subtilis RNA polymerase. *Proc. Natl. Acad. Sci. U. S. A.* **1979**, *76*, 5470–5474, doi:10.1073/pnas.76.11.5470.

57. Haldenwang, W.G.; Lang, N.; Losick, R. A sporulation-induced sigma-like regulatory protein from b. subtilis. *Cell* **1981**, *23*, 615–624, doi:10.1016/0092-8674(81)90157-4.
58. Partridge, S.R.; Foulger, D.; Errington, J. The role of σF in prespore-specific transcription in Bacillus subtilis. *Mol. Microbiol.* **1991**, *5*, 757–767, doi:10.1111/j.1365-2958.1991.tb00746.x.
59. Johnson, W.C.; Moran, C.P.; Losick, R. Two RNA polymerase sigma factors from Bacillus subtilis discriminate between overlapping promoters for a developmentally regulated gene. *Nature* **1983**, *302*, 800–804, doi:10.1038/302800a0.
60. Earl, A.M.; Losick, R.; Kolter, R. Bacillus subtilis genome diversity. *J. Bacteriol.* **2007**, *189*, 1163–1170, doi:10.1128/JB.01343-06.
61. Burby, P.E.; Simmons, L.A. A bacterial DNA repair pathway specific to a natural antibiotic. *Mol. Microbiol.* **2019**, *111*, 338–353, doi:10.1111/mmi.14158.
62. Lee, Y.J.; Park, S.J.; Ciccone, S.L.M.; Kim, C.R.; Lee, S.H. An in vivo analysis of MMC-induced DNA damage and its repair. *Carcinogenesis* **2006**, *27*, 446–453, doi:10.1093/carcin/bgi254.
63. Ueda, K.; Morita, J.; Komano, T. Phage inactivation and DNA strand scission activities of 7-N-(p-hydroxyphenyl)mitomycin C. *J. Antibiot. (Tokyo).* **1982**, *35*, 1380–1386, doi:10.7164/antibiotics.35.1380.
64. Delumeau, O.; Lecointe, F.; Muntel, J.; Guillot, A.; Guédon, E.; Monnet, V.; Hecker, M.; Becher, D.; Polard, P.; Noirot, P. The dynamic protein partnership of RNA polymerase inBacillus subtilis. *Proteomics* **2011**, *11*, 2992–3001, doi:10.1002/pmic.201000790.
65. Kouba, T.; Koval, T.; Sudzinová, P.; Pospíšil, J.; Brezovská, B.; Šanderová, H.; Janoušková, M.; Šiková, M.; Halada, P.; Barvík, I.; et al. Mycobacterial HelD is a nucleic acids-clearing factor for RNA polymerase. *bioRxiv* **2020**, 2020.07.20.211821, doi:10.1101/2020.07.20.211821.
66. Burenina, O.Y.; Hoch, P.G.; Damm, K.; Salas, M.; Zatsepin, T.S.; Lechner, M.; Oretskaya, T.S.; A. Kubareva, E.; Hartmann, R.K. Mechanistic comparison of Bacillus subtilis 6S-1 and 6S-2 RNAs-commonalities and differences. *RNA* **2014**, *20*, 348–359, doi:10.1261/rna.042077.113.
67. Glaser, G.; Sarmientos, P.; Cashel, M. Functional interrelationship between two tandem E. coli ribosomal RNA promoters. *Nature* **1983**, *302*, 74–76.
68. Schultz, M.C.; Brill, S.J.; Ju, Q.; Sternglanz, R.; Reeder, R.H. Topoisomerases and yeast rRNA transcription : negative supercoiling stimulates initiation and topoisomerase activity is required for elongation. *Genes Dev.* **1992**, *6*, 1332–1341, doi:10.1101/gad.6.7.1332.
69. Bird, T.; Burbulys, D.; Wu, J.J.; Strauch, M.A.; Hoch, J.A.; Spiegelman, G.B. The effect of supercoiling on the in vitro transcription of the spoIIA operon from Bacillus subtilis. *Biochimie* **1992**, *74*, 627–634, doi:10.1016/0300-9084(92)90134-Z.
70. Helmann, J.D. Compilation and analysus of Bacillus Subtilis σA-dependent promoter sequences: Evidence for extended contact between RNA polymerse and upstream promoter DNA. *Nucleic Acids Res.* **1995**, *23*, 2351–2360, doi:10.1093/nar/23.13.2351.
71. Typas, A.; Hengge, R. Role of the spacer between the -35 and -10 regions in sigmaS promoter selectivity in Escherichia coli. *Mol. Microbiol.* **2006**, *59*, 1037–1051, doi:10.1111/j.1365-2958.2005.04998.x.
72. Bordes, P.; Conter, A.; Morales, V.; Bouvier, J.; Kolb, A.; Gutierrez, C. DNA supercoiling contributes to disconnect σS accumulation from σS-dependent transcription in Escherichia coli. *Mol. Microbiol.* **2003**, *48*, 561–571, doi:10.1046/j.1365-2958.2003.03461.x.
73. Kusano, S.; Ding, Q.; Fujita, N.; Ishihama, A. Promoter Selectivity of Escherichia coli RNA Polymerase E and E Holoenzymes. *J. Biol. Chem.* **1996**, *271*, 1998–2004, doi:10.1074/jbc.271.4.1998.

700 74. Kim, S.; Beltran, B.; Irnov, I.; Jacobs-Wagner, C. Long-Distance Cooperative and Antagonistic RNA
701 Polymerase Dynamics via DNA Supercoiling. *Cell* **2019**, *179*, 106-119.e16, doi:10.1016/j.cell.2019.08.033.
702 75. Kotlajich, M. V.; Hron, D.R.; Boudreau, B.A.; Sun, Z.; Lyubchenko, Y.L.; Landick, R. Bridged filaments
703 of histone-like nucleoid structuring protein pause RNA polymerase and aid termination in bacteria. *Elife*
704 **2015**, *2015*, doi:10.7554/eLife.04970.
705
706

707

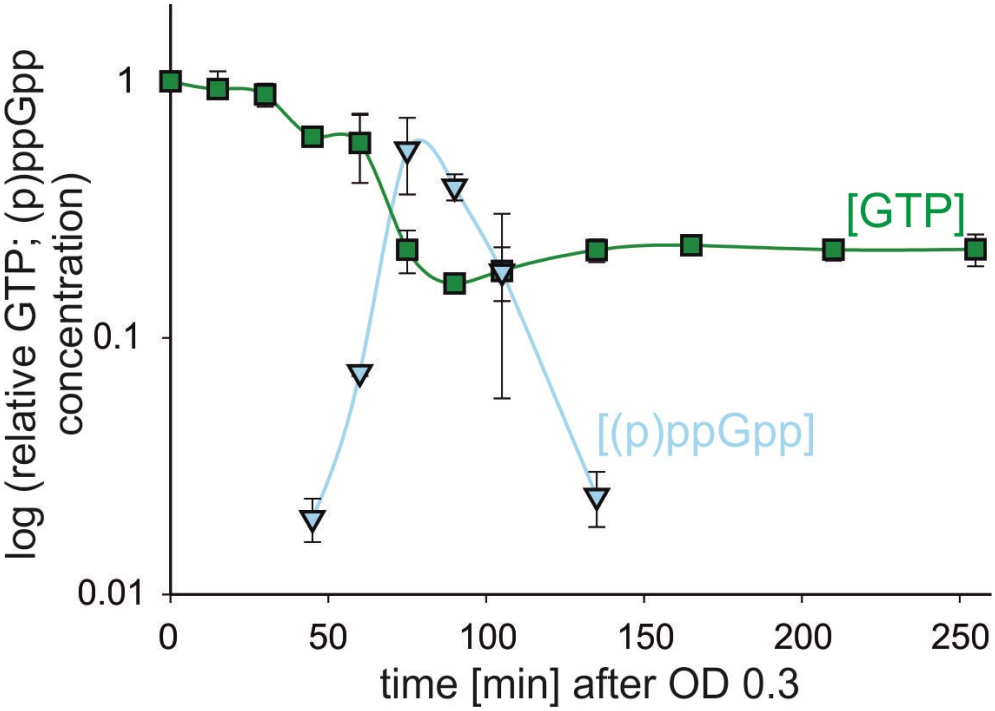

Figure S1. GTP and (p)ppGpp levels after entry into the stationary phase.

Relative GTP concentration (green squares) and relative (p)ppGpp concentration (blue triangles) in *wt* genetic background, after entry into stationary phase. GTP concentration is normalized to 1 at time 0. The GTP concentrations are from two independent experiments, showing the mean, and (p)ppGpp concentration are from the same experiments as GTP (Figure 1), normalized to the GTP.

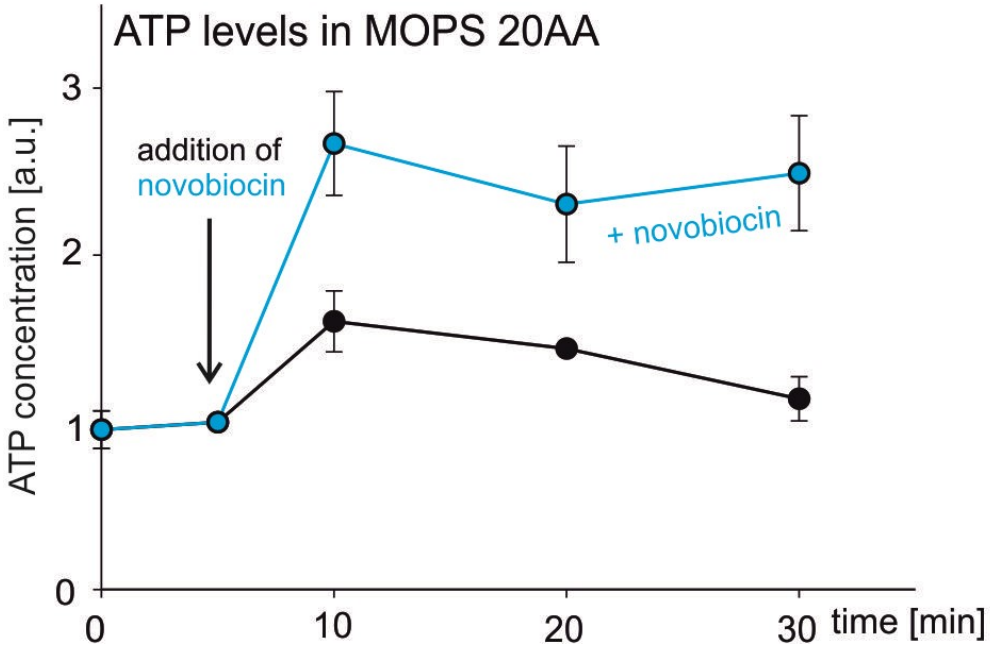

Figure S2. Effect of novobiocin-induced relaxation of chromosome on ATP levels.

Cells were grown in MOPS media supplemented with 20 amino acids in the presence of the [^{32}P] H_3PO_4 to early exponential phase (OD_{600} ~ 0.3), and at time 5 were treated with novobiocin (5 µg/ml). Levels of ATP were determined by the TLC chromatography from the same TLC plate as GTP levels in Figure 2. ATP level was set as 1 in time 5. Results are average from two measurements. Please note the different scale than in Figure 2.

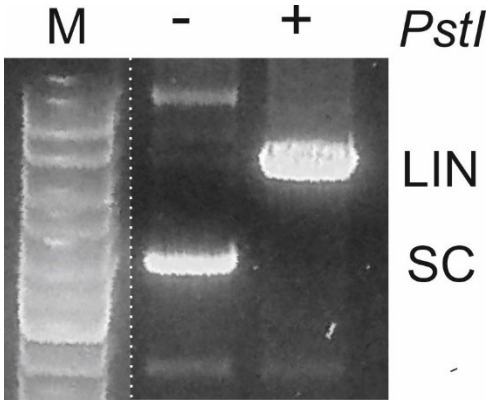

Figure S3. SC and LIN promoter DNA on agarose gel.

100ng of DNA resolved on 0.8 % agarose gel. M stays for marker, - and + for effect of restriction enzyme *Pst*I. DNA was stained with GelRed Marker was assembled electronically – marked with the dotted line.

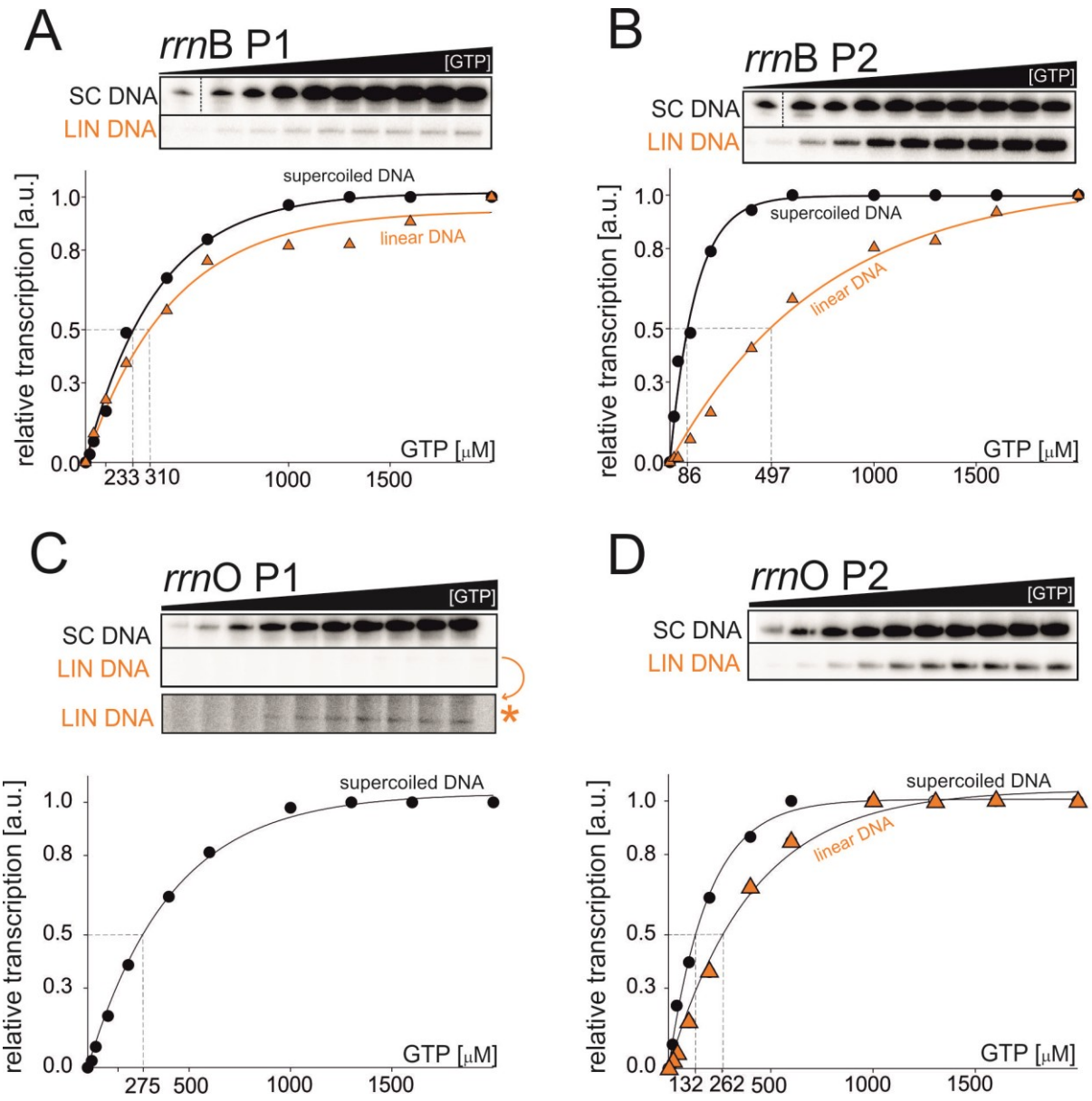

Figure S4. The affinity of RNAP for iNTP *in vitro* changes on different DNA templates.

Multiple-round transcriptions as a function of GTP concentration: representative primary data and their graphical comparison for *rrn*B P1 (A), *rrn*B P2 (B), *rrn*O P1 (C) and *rrn*O P2 (D). For LIN *rrn*O P1 were levels of transcript so close to the background, that were almost not detectable. The panel with asterics (*) was adjusted for better visibility. The K_{GTP} values are in Supplementary Table 1.

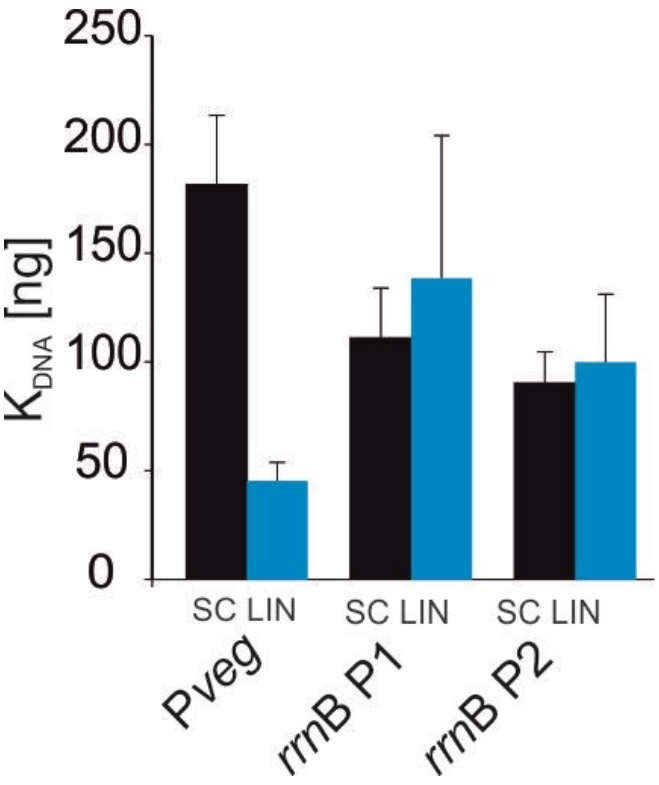

Figure S5. Graphical representation of RNAP affinity for DNA.

In case of Pveg, affinity for SC x LIN is changed to 30 %, for rrnB P1 P2 is the affinity change under error.

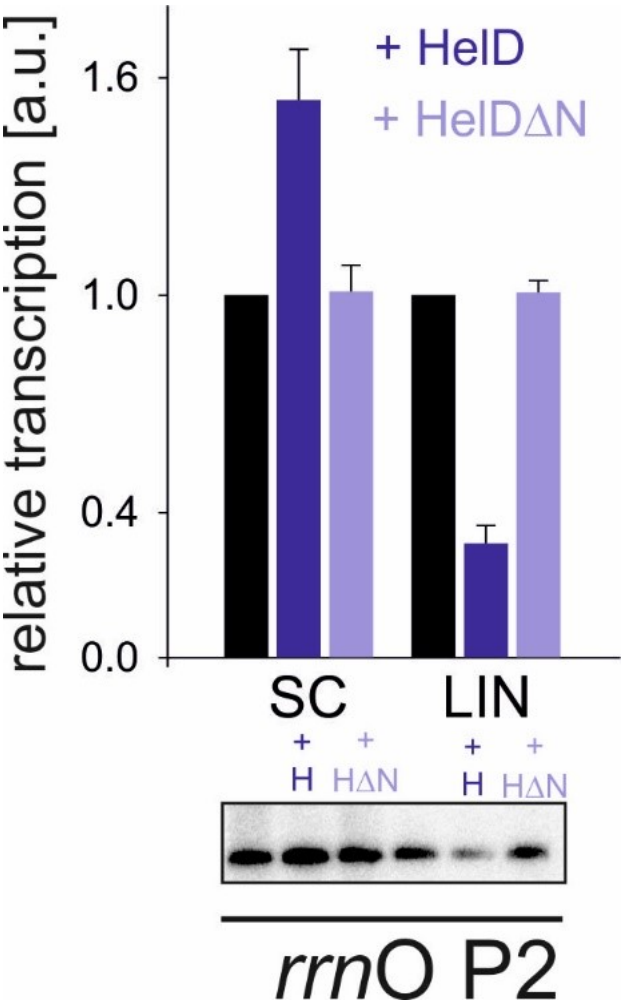

Figure S6. Effect of HelD on transcription *in vitro* from rRNA promoters. SC – supercoiled DNA, LIN – linear DNA. Transcription without HelD added was set as 1 (black bars). HelD was added in ratio 1:4 to RNAP (dark purple; H), and HelDΔN also in 1:4 ratio (light purple; HΔN). Graph show mean from at least three independent experiment using, with the corresponding SD. A representative primary data are shown below. For *rrn*O P1 were signals from LIN DNA to close to background.

Table S1: The K_{GTP} values for the promoters tested in the transcriptions *in vitro*.

The values were calculated at least from three independent experiments, showing the mean and ± SD.

K_{GTP} [µM]	**SC**	**LIN**	**Ratio SC/LIN**
P*veg*	36 ± 9	511 ± 78	~ 14x
*rrn*B P core	277 ± 24	440 ± 25	~ 1.5x
*rrn*B P1	242 ± 31	361 ± 46	~ 1.5x
*rrn*B P2	62 ± 13	427 ± 61	~ 7x
*rrn*O P1	240 ± 18	ND	
*rrn*O P2	98 ± 22	269 ± 8	~ 3x

Table S2. Alternative σ factor-dependent promoters used in the study.

σ factor	promoter	Product function*	Sequence of promoter	Reference
B	P*trxA*	Protection of proteins against oxidative stress	TCAG**GTTTTA**AAACAGCTCCGGCA**GGGCAT**GGTAAAGTAC**A**	[1]
D	P*motA*	Motility and chemotaxis	AATGTCCC**TAAA**GTTCCGGGCACCAAA**ACCGATAT**TAACCAT**A**	[2]
E	P*spoIIID*	Regulator of mother cell expression	ATATTCCCAAAAGAATGCTA**ATACAC**TGTTAC**A**	[3]
F	P*spoIIQ*	Forespore encasement by the spore coat	TT**GTATAT**ATTTTCAGAAAAGTGTT**CAGAATGT**TGCT**G**	[4]
H	P*spoVG*	Cell division, control of sporulation initiation	AAAAACGAGC**AGGATTT**CAGAAAAAATCGTG**GAAT**TGATACACT**A**	[5]
N	P*zpaB*	DNA gyrase#	**ATTTACGTTT**TAGAAAGACTA**GATATAA**AGATTAC**G**	[6]
N	P*zpbY*	unknown#	**ATTTACGTTT**TCAAAGGCACA**GATATAA**TAAC**A**	[6]
N	P*zpdG*	DNA pol III#	**ATTTACGTTT**TTGCCGGTCCA**GATATAA**ATACTTT**G**	[6]
N	*sigN* P3	Sigma factor#	TTTTCG**TTTACGTTT**CTATTTCTCTA**GATA**A**AA**TCATTAA**G**	[6]

*according to [7].

as published in [6].

1. Scharf, C.; Riethdorf, S.; Ernst, H.; Engelmann, S.; Völker, U.; Hecker, M. Thioredoxin is an essential protein induced by multiple stresses in Bacillus subtilis. *J. Bacteriol.* **1998**, *180*, 1869–1877, doi:10.1128/jb.180.7.1869-1877.1998.

2. Gilman, M.Z.; Wiggs, J.L.; Chamberlin, M.J. Nucleotide sequences of two bacillus subtilis promoters used by bacillus subtilis sigma-28 RNA polymerase. *Nucleic Acids Res.* **1981**, *9*, 5991–6000, doi:10.1093/nar/9.22.5991.

3. Kunkel, B.; Kroos, L.; Poth, H.; Youngman, P.; Losick, R. Temporal and spatial control of the mother-cell regulatory gene spoIIID of Bacillus subtilis. *Genes Dev.* **1989**, *3*, 1735–1744, doi:10.1101/gad.3.11.1735.

4. Amaya, E.; Khvorova, A.; Piggot, P.J. Analysis of Promoter Recognition In Vivo Directed by F of Bacillus subtilis by Using Random-Sequence Oligonucleotides. *J. Bacteriol.* **2001**, *183*, 3623–3630, doi:10.1128/JB.183.12.3623-3630.2001.

5. Haldenwang, W.G.; Losick, R. Novel RNA polymerase σ factor from Bacillus subtilis. *Proc. Natl. Acad. Sci. U. S. A.* **1980**, *77*, 7000–7004, doi:10.1073/pnas.77.12.7000.

6. Burton, A.T.; DeLoughery, A.; Li, G.W.; Kearns, D.B. Transcriptional regulation and mechanism of sigN (ZpdN), a pBS32-encoded sigma factor in bacillus subtilis. *MBio* **2019**, *10*, e01899-19, doi:10.1128/mBio.01899-19.

7. Zhu, B.; Stülke, J. SubtiWiki in 2018: From genes and proteins to functional network annotation of the model organism Bacillus subtilis. *Nucleic Acids Res.* **2018**, *46*, D743–D748, doi:10.1093/nar/gkx908.